Development of a Room Temperature Molecular Electronics: Direct vs. Indirect Metal Complex Synthesis

by Laura Cleary

Dublin City University
Ollscoil Chathair Bhaile Átha Cliath

A Thesis presented to Dublin City University

for the

Degree of Doctor of Philosophy

under the supervision of Professor Johannes G. Vos

School of Chemical Sciences

Dublin City University

March 2011

For anyone that left
And everyone who stayed.

Author's Declaration

I hereby certify that this material, which I now submit for assessment on the programme of study leading to the award Doctor of Philosophy by research and thesis is entirely my own work, that I have exercised reasonable care to ensure that the work is original, and does not to the best of my knowledge breach any law of copyright, and has not been taken from the work of others save and to the extent that such work has been cited and acknowledged within the text of my work.

Signed:_____

Laura Cleary

I.D. number: 52492393

Date:_____

Acknowledgements

Before anything else, I must thank Prof. J. G. Vos: for offering me the chance to work in his research group and for presenting me with the tools to stay there. Without his time, patience and constant help this project would not have reached completion.

Chapter 4 of this thesis includes a set of ligands kindly supplied by Dr. Sally Brooker of the University of Otago, NZ. I am so very grateful to Dr. Brooker for supplying me with these compounds as well as any information and useful discussion that was in her power to extend. Her expertise has been very much appreciated.

Another debt of gratitude is owed to Dr. W. R. Browne of the University of Groningen, NL for his inexhaustible knowledge, patience and spare bedroom. Wes, I don't know how you put up with the constant questions, insults and threats of tantrums, but you did. Thank you so, so much.

To everyone in the HVRG past or present, thanks for everything over the past four years.

The technicians working in DCU cannot go unacknowledged. Damien, Veronica, Ambrose, Vinny, Brendan, Mary and Catherine have all made my time in DCU so pleasant with their professionalism and sense of fun. A special thanks however has to go to John McLoughlin for his constant good humour when faced with stupid questions and/or pointless moaning. You can't teach that kind of patience!

A mention has to go to the counselling staff in DCU, particularly Ruan Kennedy, as well as the psychiatric staff at St. Brendan's hospital, Grangegorman. I wouldn't be here without the help you've given me.

Over the course of this project a lot has happened and many new definitions have been added to my dictionary. All of the friends I've made and lost and all of the family present or absent have lent their penny's worth to the last four years, and so I guess, this thesis is for you.

Finally, to Colm, this last year should have been impossible to live through. But it wasn't. And I think I have you to thank for that ☺

Table of Contents

Chapter 3: Synthesis and Characterisation of Novel $[M(bpy)_2(imphen)]^{2+}$ Type Metal Complexes

Chapter 4: Synthesis and Characterisation of Novel $[M(\text{-imphen})_2(bpy)]^{2+}$ Type Mononuclear Metal Complexes

Chapter 7: Conclusions and Future Work

Appendix A

Appendix B

Abstract

This thesis discusses the possibility of using molecular units as electronic devices as well as the synthesis of a number of such prototypes. This thesis also serves as a comparison between 'direct' (complexes as ligands/complexes as metals) and 'indirect' (on-complex) synthesis as a method of metal complex synthesis.

Chapter 1 introduces the theory behind molecular electronics and solar energy conversion as well as the applicability of transition metal complexes for this role. The target complexes to be synthesised as well as their methods of preparation are also introduced. The experimental methodology used to synthesize and characterize these complexes is detailed in chapter 2.

A number of ruthenium and osmium bis-bipyridyl metal complexes incorporating one phenanthroline type ligand have been synthesised using both direct and indirect synthetic methods and are discussed in Chapter 3. The synthesis of a series of ruthenium complexes containing two such ligands via an 'indirect' route is discussed in Chapter 4.
These complexes are fully characterized via ^{1}H-NMR, mass spectrometry and CHN with a discussion of their UV/vis and emission properties included.

The attempted synthesis of a series of dinuclear metal complexes, including two phenanthroline-thiophene type ligands (thimphen) using 3,5-bispyrid-2-yl-1,2,4-triazole as a bridging ligand is described in Chapter 5. A number of attempted synthetic routes for the dichloride starting material [Ru(thimphen)$_2$Cl$_2$] is also described.

The synthetic study of ruthenium(II) complexes containing the tetradentate ligands bis(2-pyridylmethyl)diiminoethane) (paen) and bis(2-pyridylmethyl)diiminopropane) (papn) is described in Chapter 6. A modified method for the synthesis of the starting materials [Ru(paen)Cl$_2$] and [Ru(papn)Cl$_2$] as well as a synthetic route for the metal

complexes $[Ru(paen)(P0P)Cl]^{+}$, $[Ru(paen)(P0P)_2]^{2+}$ and $[Ru(papn)(P0P)_2]^{2+}$ were developed. Again the complexes successfully synthesised are characterised by ^{1}H-NMR a discussion of their UV/vis and emission properties included.

Finally, the major conclusions drawn from this research and possible future work are also detailed.

Chapter 1: Introduction

Abstract

Chapter l introduces the concepts behind and reasons for this thesis. The first part of this chapter details the applicability of surface active transition metal complexes for use in practical purposes such as solar energy conversion and molecular electronics. The second part discusses different synthetic methods used in the synthesis of metal complexes suitable for these applications. Specifically direct synthesis (colloquially known as the "Complexes as Metals/Complexes as Ligands" approach) and modification of coordinated ligands (termed "Chemistry on the Complex") are discussed.

The purpose and scope of the thesis to follow is then outlined.

Introduction

As time progresses, so shall technology. In the quest to achieve a faster, cleaner and more efficient way of living, the tools and machinery used worldwide must follow suit. The demand for clean, renewable sources of fuel and therefore energy, is one of the main obstacles in this pursuit. Add to this the desire to continually improve the machines for which this fuel is required and a seemingly unscalable intellectual roadblock results. However, an extremely versatile class of transition metal complexes has emerged as a possible academic bulldozer.[1]

In the past two decades transition metal chemistry has exploded in growth to encompass a huge number of current research topics[2, 3, 4]. As a class of compounds transition metal complexes exhibit well-defined luminescent, photophysical and redox properties, which may be exploited for a number of significant uses, including, but not limited to artificial photosynthesis,[4, 5, 6] molecular machines and motors,[7, 8] molecular electronics, [9, 10] non-linear optics[11] and catalysis.[12, 13] Another attraction of transition metals for use in this sphere is their well-documented ability to be incorporated into well-ordered arrays.[14] These arrays still allow for communication between the constituents resulting in a device with a cumulative function while each of the components retains their individual properties.

This area of research is termed *supramolecular chemistry* and is discussed below in section 1.1.

1.1 Supramolecular Chemistry

Supramolecular chemistry may be defined as *chemistry beyond the molecule*[14]**.** This area focused originally on the non-covalent interactions between molecules, unlike many other, perhaps more conventional, areas in chemistry. The main goal of this branch of chemistry is the construction of supramolecular arrays; chemical arrangements composed of many components with discrete and well-defined properties, but when combined in a specific manner and pattern in a suitable matrix, these components, while retaining their individual properties, can act through non-covalent interactions to carry out a predetermined function. This greater function can be geared to mimic that of everyday machines and applicances, making the resulting supramolecular devices a potentially lucrative area of research.

As mentioned previously, supramolecular chemistry involves the organisation of molecules into a defined system in much the same way as atoms are organised into a molecule. But how can one tell the difference between a supramolecular array and a large molecule in which the building blocks are collected but not suitable to carry out a greater function? The answer lies in the electronic and energetic behaviour of the final product, shown schematically below in Figure 1.1.

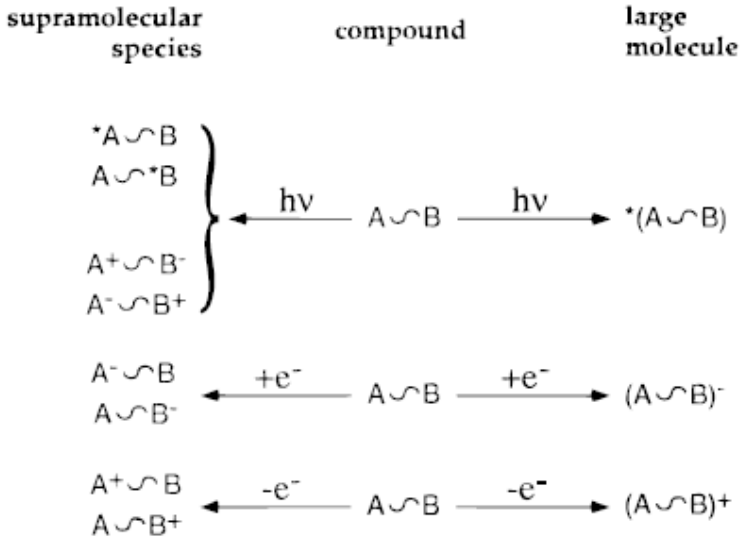

Figure 1.1: Schematic representation of the differences between supramolecular species and large molecules in terms of electronic and energetic behaviour[14]

As can be seen above when a supramolecular species is exposed to light, oxidised or reduced the change in energy or electron density is confined to one component of the array (in the case above A or B). In the case of a large molecule, the change in energy or electron density is delocalised over the entire system. This defining characteristic of supramolecular species is key to their value as a basis for molecular devices.

As a change in energy or electron density is located solely on one component or area of the array, conditions allowing, electron or energy transfer may occur from one component to another. One of the most lucrative industrial areas that this type of chemistry is suitable for is solar energy conversion, a topic which shall be discussed in detail below in section 1.2.

The metal complexes synthesised in this thesis also incorporate a group capable of coordination to electrode surfaces. As a result these complexes may be suitable for

applications as molecular electronics, a concept that shall also be discussed in section 1.4.

1.2 Transition Metal Complexes for Energy Production

For a number of years the fact that fossil fuels exist as a finite (and soon to be exhausted) source of energy has become more and more apparent. As a result a large amount of current research is ongoing in the area of energy conversion using natural resources. Synthetic chemists have taken a _molecular approach' in which compounds are synthesised targeted at the production of energy or alternative fuels at a molecular level. During the 1970's the idea of using surfactant layers of a derivative of the photoactive metal complex $[Ru(bpy)_3]^{2+}$ to split water using visible light was put forward[15]. This system however reported low efficiency with purified complexes[16] and as a result extensive research was carried out during the 1980's based on catalytic cycles including $[Ru(bpy)_3]^{2+}$ derivatives and methyl viologen (MV).[17] These cycles depended on an electron transfer type exchange between $[Ru(bpy)_3]^{2+}$ (acting as an electron donor) and MV (acting as the respective acceptor). This type of system is shown schematically below in Figure 1.2.[17]

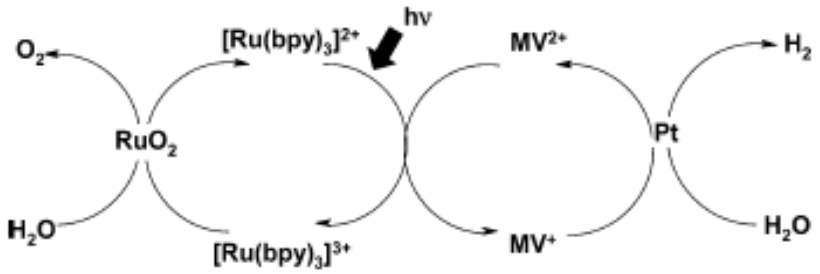

Figure 1.2: Catalytic cycle proposed for the splitting of water.

However, due to the fast back reaction between donor and acceptor, these models also exhibited low efficiencies. Despite numerous efforts to improve the efficiency of such systems, little progress was made. A different model was uncovered in the form of the dye sensitised solar cell (DSSC) designed by Grätzel and coworkers in the early 1990's[18]. These photovoltaic cells consisted of nanocrystalline TiO_2 surfaces modified with monolayers of ruthenium complexes. This basic model consisting of a dye-coated semiconductor electrode and a counter electrode with an electrolyte containing a redox mediator (A/A^-) arranged between them in a _sandwich' type fashion is now

one of the most viable methods of light harvesting available. Figure 1.3 below shows a schematic of such a system as well as the key reactions that take place.[19]

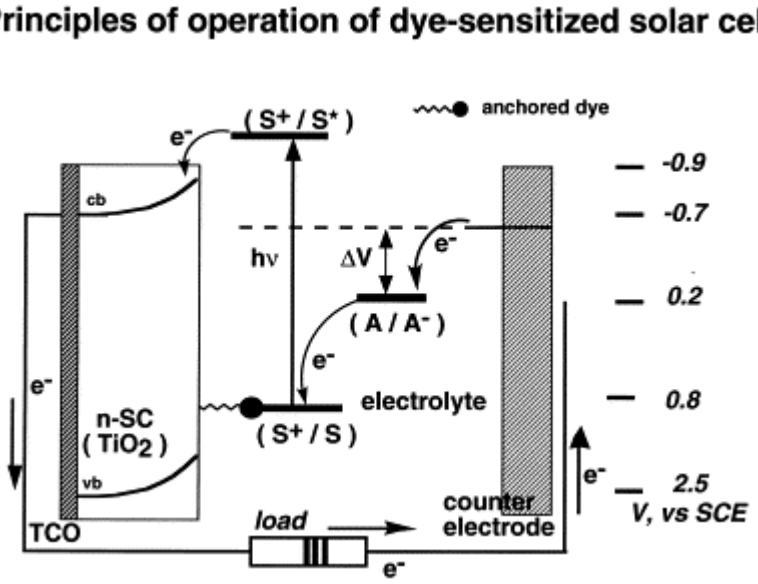

Figure 1.3: Schematic representation of a DSSC including the main reactions taking place therein[19]

Upon photoexcitation the dye undergoes electron transfer quenching, injecting electrons into the conduction band of the semiconductor.

$$S^* \rightarrow S^+ + e^-_{cb} \quad (1)$$

The oxidised dye is reduced by the electron donor present in the electrolyte.

$$S^+ + A^- \rightarrow S + A \quad (2)$$

The electrons now in the conduction band collect at the back collector electrode and pass through the external circuit to the counter electrode reversing the reaction concerning the redox mediator

$$A + e^- \rightarrow A^- \quad (3)$$

As a result the dye and the redox mediator are regenerated with the electron being driven through the external circuit, i.e. the sunlight absorbed is converted to an electric current. A structural representation of a Grätzel type solar cell is shown below in Figure 1.4.

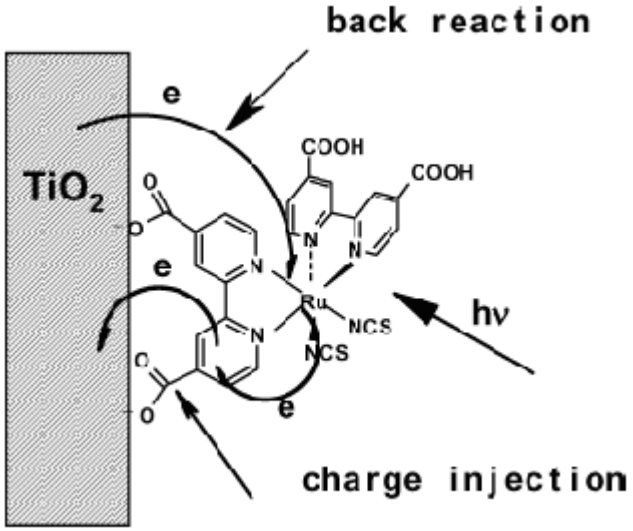

Figure 1.4: Structural representation of the electron transfer sequence in a Grätzel type solar cell

It is implied in the system shown above in Figure 1.4 that a direct chemical bond between the semiconductor surface and the molecular component is required, in this case through a carboxy group. However, it has been shown that for a dinuclear ruthenium/osmium compound injection from the osmium centre which is not attached directly, can take place via through space electron transfer.[20] The structure of this compound is shown below in Figure 1.5.

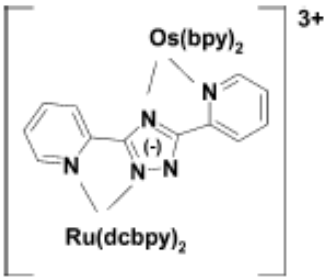

Figure 1.5: Structure of a dinuclear ruthenium/osmium compound (where dcbpy=4,4'-dicarboxybipyridyl)

Investigation of this compound in solution shows as expected that the emission is osmium based when excited at a characteristic absorbance wavelength for ruthenium. Therefore energy transfer occurs from the ruthenium to the osmium center (i.e. from an area of high energy to low energy). When attached to nanocrystalline TiO_2, however no emission is observed. Taking into account that electron transfer occurs only when the centre excited is bound to the TiO_2 surface and that the direction of energy transfer is away from the surface this appears impossible. It seems likely, however, that electron transfer does occur, not through the covalent bond to the TiO_2 surface but through space to a neighbouring nanoparticle.[22] As a *covalent* bond is therefore not necessary for the injection of electrons into a surface, the possibility of using self assembled monolayers on a conductor surface now reveals itself. This idea is applicable to both solar energy and molecular electronic applications and will be discussed further in section 1.3.

Another possible system for energy generation, distinct from DSSCs exists in the proposed mimicking of the most elegant system for energy production currently known: photosynthesis. The conversion of light to energy with the photocatalytic reduction of CO_2 and oxidation of water occurring in green plants and algae has received much attention in the last few decades, and a clear understanding of the manner in which the process occurs has been recently described.[21] In the natural photosynthetic process energy absorbed from sunlight is funnelled to a number of reaction centre chlorophylls which initiate a chain of multi-step electron transfer reactions. These reactions result finally in the transfer of an electron from the excited chlorophylls to an acceptor system, generating a separation of charge commonly termed _photoinduced charge separation‘.[22] It is this separation of charge which allows for the reduction of CO_2 and oxidation of water to form necessary carbohydrates for the organism‘s survival.

Any artificial assembly mimicking these reactions has been envisioned as a system in which intramolecular electron or energy transfer may occur, requiring a light harvesting unit and a catalytic centre.[23] This model is shown diagrammatically in Figure 1.6.

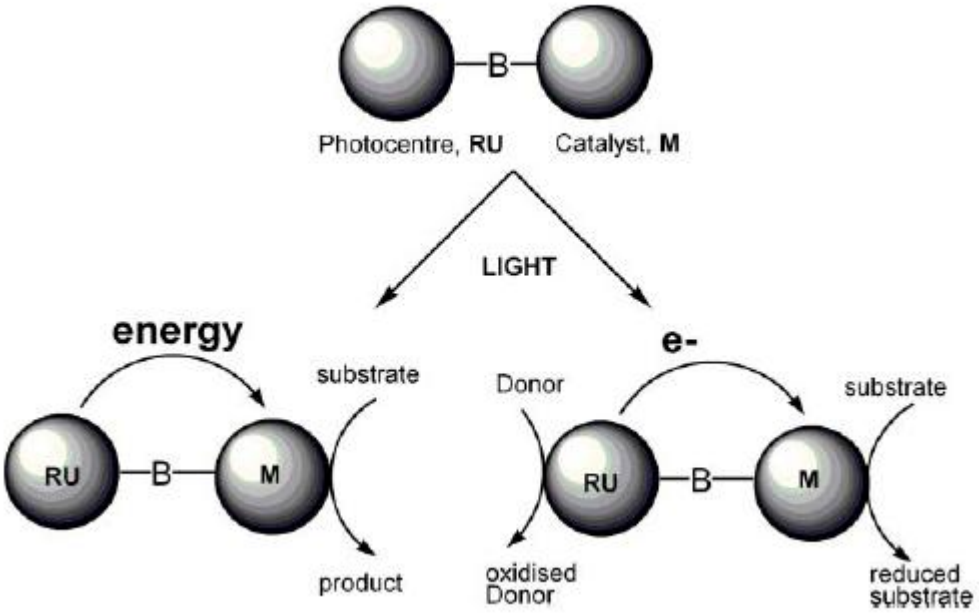

Figure 1.6: Schematic representation of an artificial photosynthetic array and the types of resulting reactions that may occur upon light absorption[23]

The system shown above in Figure 1.6 consists of three components, a light harvesting centre **Ru**, a bridging ligand **B** and a catalytic centre **M.** Light absorption occurs at the photoactive Ru centre, followed by electron or energy transfer to the catalytic centre M via the bridging ligand B. In the case of energy transfer, the Ru centre returns to its ground state while the excited catalytic center M donates its acquired energy to drive forward a catalytic reaction. In the case of electron transfer, the Ru centre is oxidised upon light absorption after which the removed electron is transferred to the catalytic centre which may then donate this electron to drive forward a reduction reaction. In order for the Ru centre to return to its ground state, a donor compound must undergo an oxidation reaction in which an electron is donated to the positively charged ruthenium centre. It is this type of system that is most pertinent with regard to the oxidation of water and reduction of CO_2 in potential catalytic assemblies.

Artificial photosynthetic systems consisting of linked ruthenium–manganese centers have been synthesized with a view to hydrogen production (water oxidation). The proposed electronic interactions occurring in one such complex is shown below in Figure 1.7.

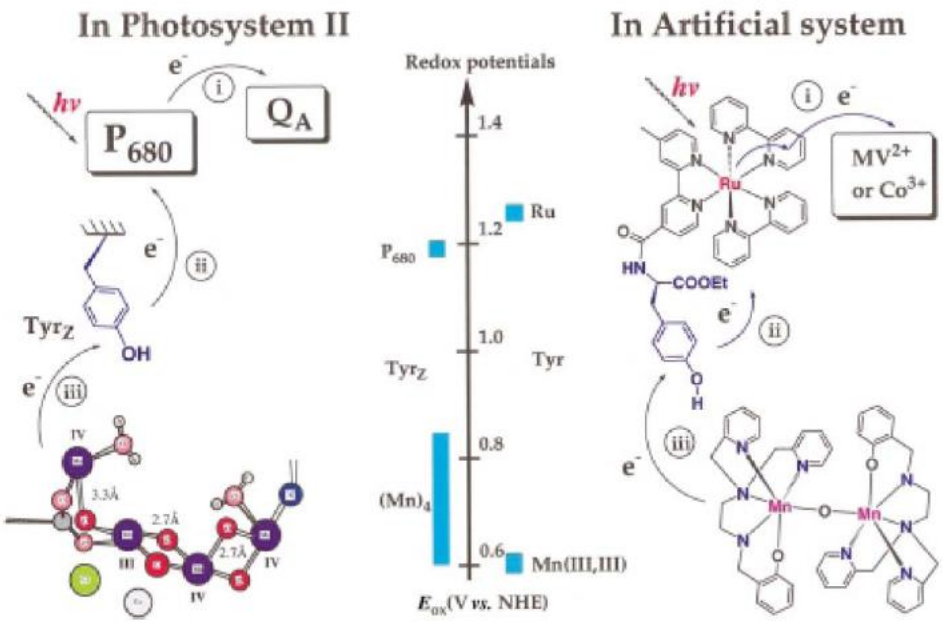

Figure 1.7: Comparison of electronic processes in natural and synthetic photosynthetic assemblies.[5]

These systems have displayed intramolecular electron transfer from the manganese centre to the ruthenium center oxidized upon light absorption as illustrated in Figure 1.7, but no related catalytic activity has been observed. [5]

Ruthenium based catalytic devices containing the ligand dppz (dipyrido[3,2-*a*:2,3-*c*]phenazine) have been found to be capable of storing up to four photogenerated electrons but until recently no catalytic systems had been reported.[24]

Ishitani *et al*. have developed a series of linked Ru(II)-Re(I) photoactive complexes capable of reducing CO_2 to CO[25], shown below in Figure 1.8.

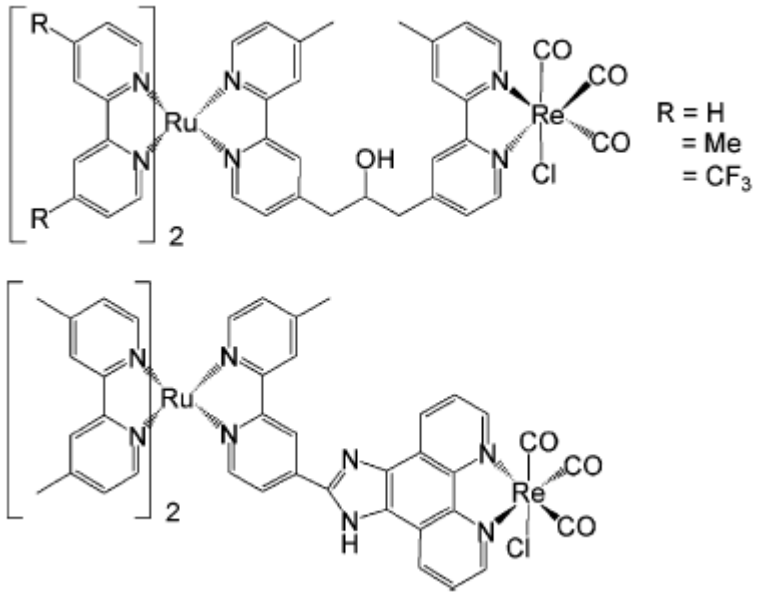

Figure 1.8: Structural representation of Ru(II)-Re(I) dinuclear complexes capable of CO_2 reduction.

Light absorption occurs at the ruthenium centre after which electron transfer occurs along the bridging ligand to the linked rhenium centre, which may react with CO_2 upon loss of a coordinated chloride. As the reduction of CO_2 requires two electrons, a second electron is assumed to follow a similar pathway.[26]

Sakai et al have investigated the ruthenium-platinum binuclear photocatalyst shown below in Figure 1.9 a as a suitable candidate for H_2 production using EDTA as a sacrificial donor. Only a small amount of photocatalytic H_2 production was observed however.[27] The related ruthenium-palladium complex shown in Figure 1.9 b showed a much larger H_2 production when irradiated with visible light ($\lambda \geq 450$ nm) in acetonitrile with triethylamine as a sacrificial donor.[28]

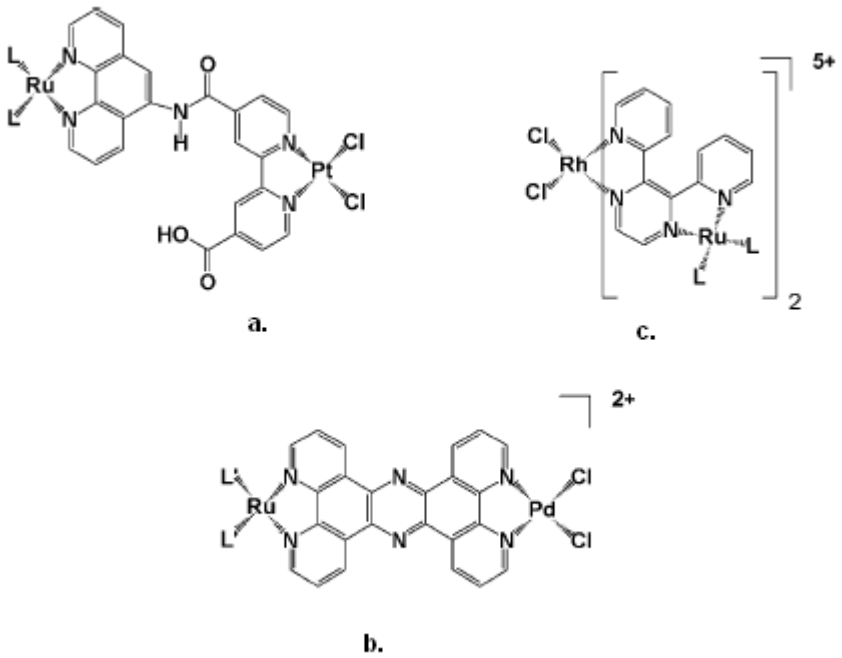

Figure 1.9 Heteronuclear complexes containing a light harvesting unit and a potential catalytic centre, L is 2,2_-bipyridine, L_ is 4,4_-di-t-butyl-2,2_-bipyridine.

Brewer *et al.* have reported the trinuclear metal complex shown in Figure 1.9 c containing two photoactive ruthenium centres and one catalytic Rh(III) centre. This complex has been shown to perform photocatalytic hydrogen production in acetonitrile: water mixtures with *N*,*N*-dimethylaniline as a sacrificial donor.[29] Unfortunately no detailed information on the amount of hydrogen produced or the underlying mechanisms are available.[30]

1.3 Molecular Electronics

Time slows for no man. In order to satisfy the insatiable market for newer, better, more productive machines, electronic constructions of increasing structural intricacy are envisioned, built from components of the smallest dimensions available.

The silicon-based electronic circuits used currently are reaching their physical limit in terms of size and if the current electronic miniaturisation trend is to continue (as predicted by Moore's law[31]) this method of fabrication may become obsolete. In answer to this possibility a number of groups have named molecular units as an elegant alternative.[32, 33]

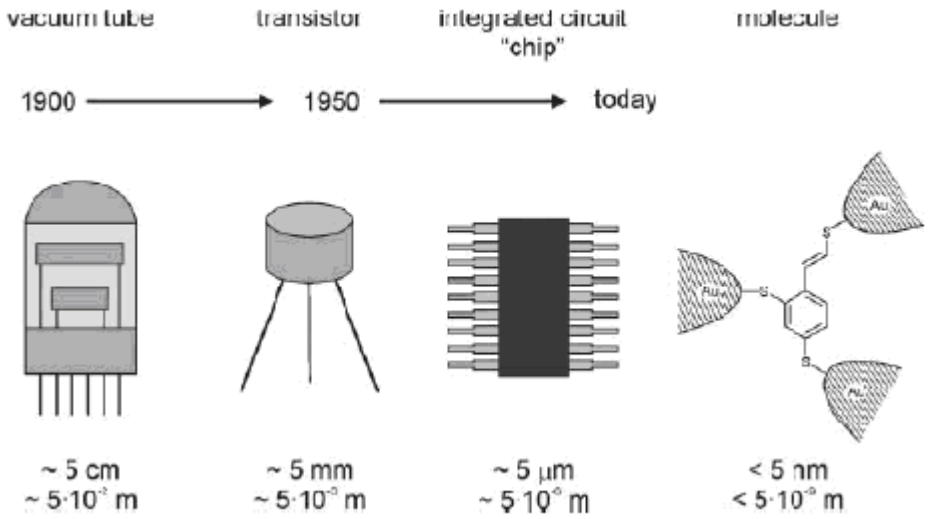

Figure 1.10: Miniaturisation of electronic components throughout the 20th and 21st centuries[34]

Figure 1.10 shows the miniaturisation of amplification devices used throughout the 20th and 21st centuries, from the vacuum tube to the transistor to currently used integrated microchips. The next hypothetical step shown is to a proposed single molecule interface for which interesting transport features have been calculated[35]. However, connecting such a molecule to three independent electrodes is still an unattained synthetic challenge.[34] In spite of this, a number of molecular device prototypes have been proposed including molecular diodes[36], molecular switches[37], molecular transistors[38] and approaches to circuits incorporating these elements[39] using

systems involving two or fewer electrode surfaces. The main limitation encountered in single molecule devices is that they often can only be brought to operate at cryogenic temperatures and/or at high vacuum.[36, 38] In order to be deemed useful for practical applications however, it is imperative that these components operate at room temperature under condensed matter conditions.

A large amount of research has been carried out around organic molecules as potential molecular electronics prototypes. Koo et al. have reported self assembled monolayers of organothiolates inserted between patterned Pt bottom electrode (30 nm) and Ti (5 nm)/Al (30 nm) top electrodes in crossbar array architectures.[40]

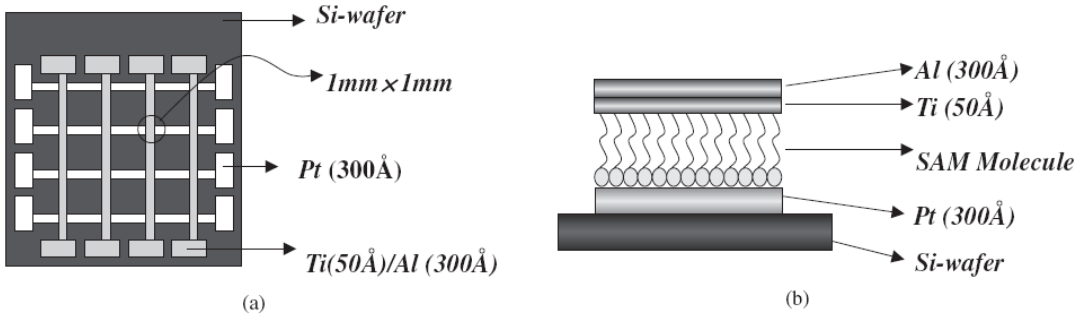

Figure 1.11: Organothiolate SAM between Pt and Ti electrodes (a) top view and (b) side view[40]

These monolayers display a molecular switching function, though it appears that the reliability of the results may be variable. Organothiolate monolayers have also been formed on gold substrates, with the first such model being put forward by Bell laboratories in 1983[41] A number of references further describing monolayers of this type are available in the literature though no sustainable molecular electronic properties have been identified[42].

Self assembled monolayers may also be formed on Si or SiO_2 with the formation of organic monolayers on SiO_2 from a solution of alkyltrichlorosilane having been introduced by Bigelow et al.[43] and developed further by Maoz and Sagiv.[44]

A schematic of organic SAM of this type deposited on Si substrate is shown below in Figure 1.12. The self-assembling molecule may be divided into three parts:

(i) *Head group, i.e. SiX_3*. Forms the chemical bond with surface atoms of the substrate resulting in binding of the molecule the substrate, Si.

(ii) *Alkyl chain, i.e.* $(CH_2)_n$. The inter-chain van der Waals interactions present in such a group could assist in formation of ordered molecular structure.

(iii) *Surface group, i.e. R*. This is the terminal group which may be replaced with different functional groups to obtain molecular electronics devices capable of different potential functions. A thin metal-layer (usually Al, Au or Hg-drop) is used on the top of the SAMs in order to measure their electrical properties and to fabricate molecular devices using them.[45]

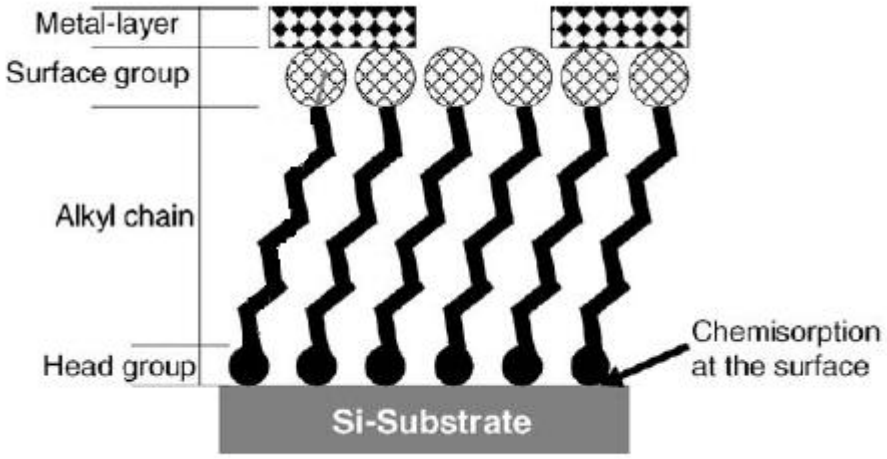

Figure 1.12: Schematic representation of an organothiolate monolayer immobilized on a Si substrate[45]

More pertinent to this thesis, a number of molecular electronics prototypes comprising of transition metal complexes have also been reported in recent years.[46, 47, 48] Transition metals exhibit many attractive properties making them suitable for incorporation into molecular electronics prototypes. These properties include well-defined electrochemistry and electron transfer chemistry as well as exhibition of stability in two or more distinct redox states. These properties will be discussed in more detail in Section 1.5.

Cobalt terpyridyl complexes for use as molecular transistors have been synthesised by McEuen and workers[46] and are shown below in Figure 1.13

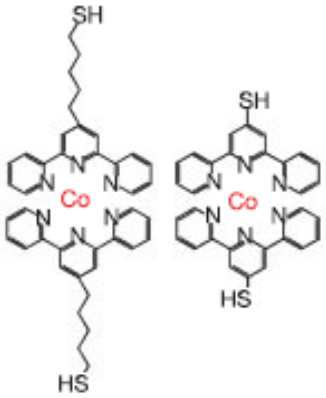

Figure 1.13: Molecular transistor prototypes as synthesised by McEuen and workers[46]

These complexes may be self-assembled on gold electrodes using the appended thiol group as a point of coordination. The level of conductance between the metal centre and the electrode was examined and moderated by synthetic control over the aliphatic linker connecting the anchoring thiol group to the coordinated terpyridine moiety. Cobalt is stable in both the Co(II) and Co(III) redox states and can be switched between these states electrochemically at low energy (~0.3 V *vs* Ag/AgCl). Upon electrochemical investigation it was found that a molecule of the type shown in Figure 1.13 incorporating shorter aliphatic chain allows for significantly larger conductance between the cobalt centre and the electrode surface as opposed to one incorporating a longer linker. Both complexes shown in Figure 1.13 however exhibit redox switching properties consistent with the model for single molecule transistors.[46]

A series of osmium polypyridine metal complexes have also been reported which display transistor-like behaviour (redox switching and amplification) at a near molecular level by Albrecht *et al*[48]. These systems, consisting of a monolayer of the complex in question formed on a gold or platinum surface, as shown in Figure 1.14, operate at room temperature and under condensed matter conditions and so are perfect model compounds for synthesis of novel molecular electronics prototypes.

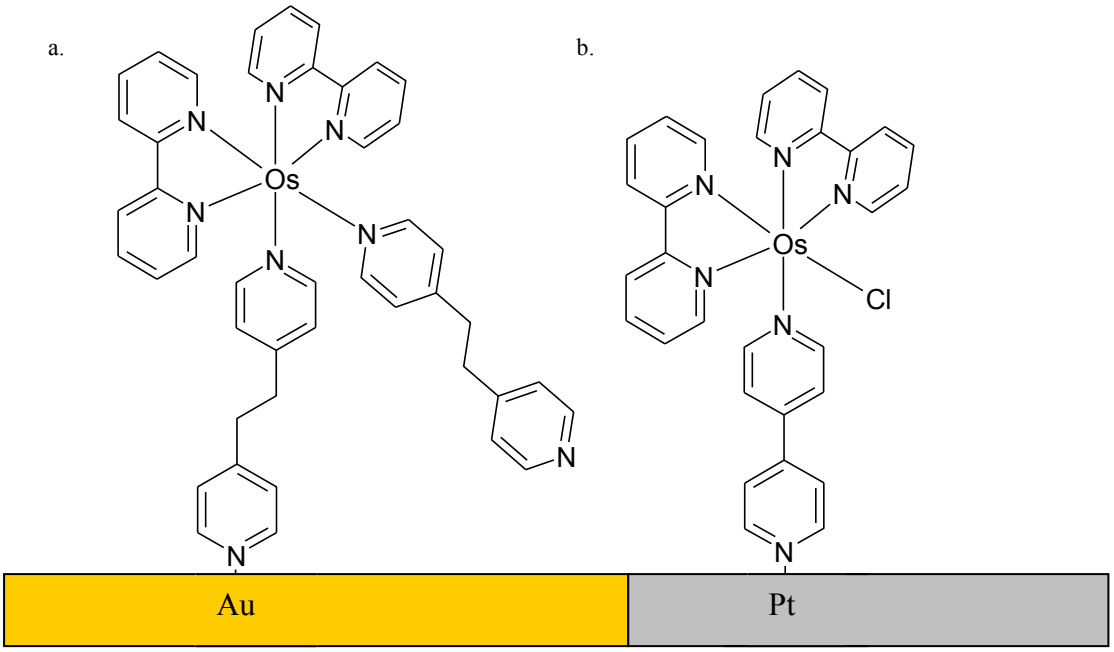

Figure 1.14: Scematic representation of (a) $Os(bpy)_2(p2p)^{2+}$ on a gold surface and (b) $[Os(bpy)_2(p0p)Cl]^+$ on a platinum surface[48, 49]

These results coupled with extensive research on both these and similar complexes carried out by Forster *et al* has cemented these types of osmium complexes as viable possibilities for molecular electronics prototypes[50, 51, 52] The researched complexes include the osmium complexes $[Os(bpy)_2(p2p)_2]^{2+/3+}$ and $[Os(bpy)_2(p0p)Cl]^{+/2+}$ (as shown above in Figure 1.14) as well as the cobalt complex $[Co(terpy)(terpy\text{-}O\text{-}(CH_2)_6\text{-}SAc]^{+/2+}$ where bpy is 2,2-bipyridine, p2p is 1,2-bis(4-pyridyl)ethane, p0p is 4,4-bipyridyl, terpy is 2,2‘,6, 2”-terpyridine and Ac is acetyl. Characterisation of the monolayers formed using these complexes by electrochemical techniques results in an almost ideal voltametric response. This implies that the electron transfer is mechanistically uncomplicated. The calculated surface coverages for the osmium complexes $[Os(bpy)_2(p2p)_2]^{2+/3+}$ and $[Os(bpy)_2(p0p)Cl]^{+/2+}$ suggest that assembly on a metal surface results in a close to a complete monolayer. Also, the electron transfer rate constant for the redox couple resulting from the complex $[Os(bpy)_2(p0p)Cl]^{+/2+}$ is in the range of 10^6 s^{-1} which is three orders of magnitude greater than the associated cobalt complex. This has been rationalised as resulting from the much stronger adiabatic electron coupling between the osmium complex and the associated electrode as compared to the cobalt complex monolayer.

The genesis of this thesis‘ project arose from the desire to synthesise a transition metal complex suitable for electrochemical study as a molecular electronics

prototype. Bis-bipyridyl complexes of ruthenium(II) and osmium (II) were settled on as the most suitable compounds to synthesise for this goals. Such complexes will allow electron transport within the molecule and will also absorb a portion of visible light due to their intrinsic photochemical properties. As a result, the target complexes may also be suitable for light harvesting applications such as those outlined in section 1.2. In order to better understand the design of the target molecules and its applicability to this function the general chemistry of transition metal (II) polypyridyl complexes shall be discussed below in section 1.4.

1.4 Chemistry of Metal (II) Polypyridyl Complexes

It has been mentioned previously in this introduction that ruthenium and osmium polypyridyl complexes are suitable to carry out an extensive list of diverse functions. One of the main reasons why these complexes are useful for such a wide number of different uses is due to a combination of functional properties that are not often found concurrently in other classes of compound. These properties include:

- Good stability of both the ground and excited state,
- Absorption in the visible region (due to intense MLCT bands),
- Highly emissive long lived excited states (due to the deactivation of the lowest lying MLCT excited state)
- Reversible metal centred oxidation and ligand centred reduction occurring at easily reached potentials[53]

The redox chemistry of these molecules is especially pertinent when applied to molecular devices. A molecular transistor controls the flow of current, switching between conducting and insulating properties on the application of an outside voltage. A molecular diode is a two terminal system displaying higher resistance in one direction than the other, allowing current to flow in one direction only. Naturally, it is the redox chemistry of the molecules in question which will dictate whether these functions may be carried out satisfactorily. In order to describe the suitability of ruthenium and osmium polypyridyl complexes for the applications described in sections 1.3 and 1.4, the ligand and metal orbitals of these systems shall be examined as well as any effect caused by coordination and/or use of different ligands within the

system (also termed ‗tuning' of the metal complex). The parent compounds $[Ru(bpy)_3]^{2+}$ and $[Os(bpy)_3]^{2+}$ shall then be introduced.

1.4.1 Electronic and Energetic processes for Ruthenium Polypyridyl Complexes

Ruthenium (II) is a d^6 system while polypyridine ligands possess σ donor orbitals localised on the nitrogen atoms with π donor and π* acceptor orbitals roughly situated on the aromatic rings.

For ruthenium(II) polypyridine complexes all the metal centred electrons are spin paired in the ground state.[54] This is shown schematically below in Figure 1.15.

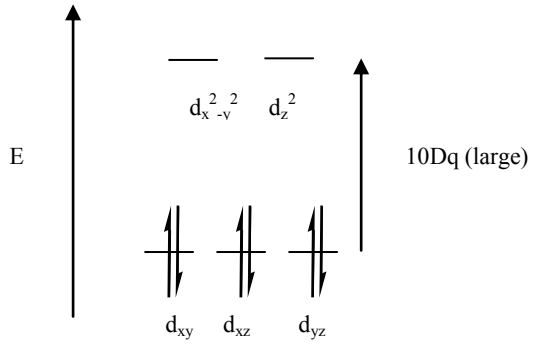

Figure 1.15: Diagrammatic representation of the electronic configuration of a d_6 low spin metal

The polypyridine ligands contain σ donor orbitals localised on the nitrogen atoms. These are the orbitals that form the coordination σ bonds to the metal. These σ donor orbitals interact with the empty metal centred orbitals of the e_g energy level, creating six σ bonds along the x, y and z axes, populated by the lone pair of electrons on each ligand nitrogen. In the case of $[Ru(bpy)_3]^{2+}$ which is octahedral, the coordination bonds that bind the ligands to the central metal atom are constructed as shown below in Figure 1.16.

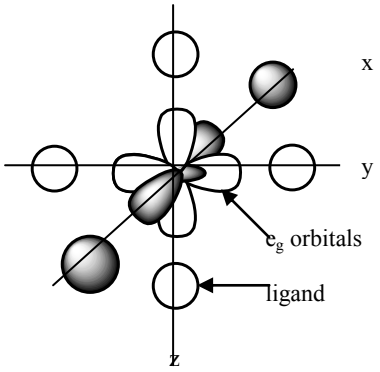

Figure 1.16: Schematic illustration of how coordination bonds are formed in octahedral metal complexes

The low energy σ bonds formed can create a high electron density on the metal. This state is unfavourable and so this excess is offloaded back onto the ligand through backbonding. The three filled t_{2g} orbitals on the metal are situated above and below the σ bond axes formed and so are available for π bonding with the ligand. The metal will form a π bond using the filled t_{2g} orbitals and offload any excess electron density into the empty π* antibonding orbitals. [54]

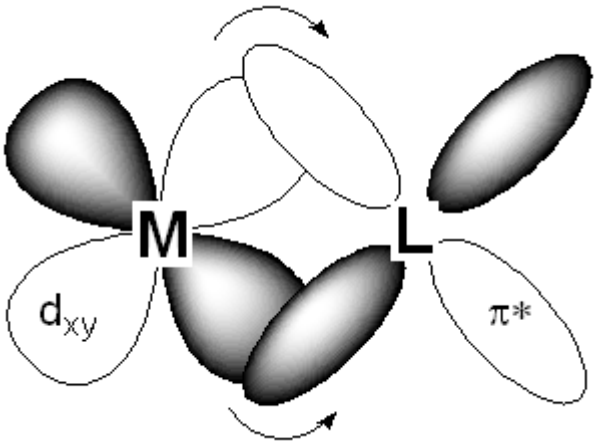

Figure 1.17: Schematic representation of d-p backbonding in metal complexes

This π bond that is formed is of higher energy than the initial σ coordination bond formed previously as well as the π bonds present in the ligand itself. However, the manner in which the remaining orbitals in the system are energetically organised depends entirely on the type of ligand coordinated as well as its energetic relationship to the metal. Three different possibilities for this organisation of metal and ligand orbitals are shown below in Figure 1.18.

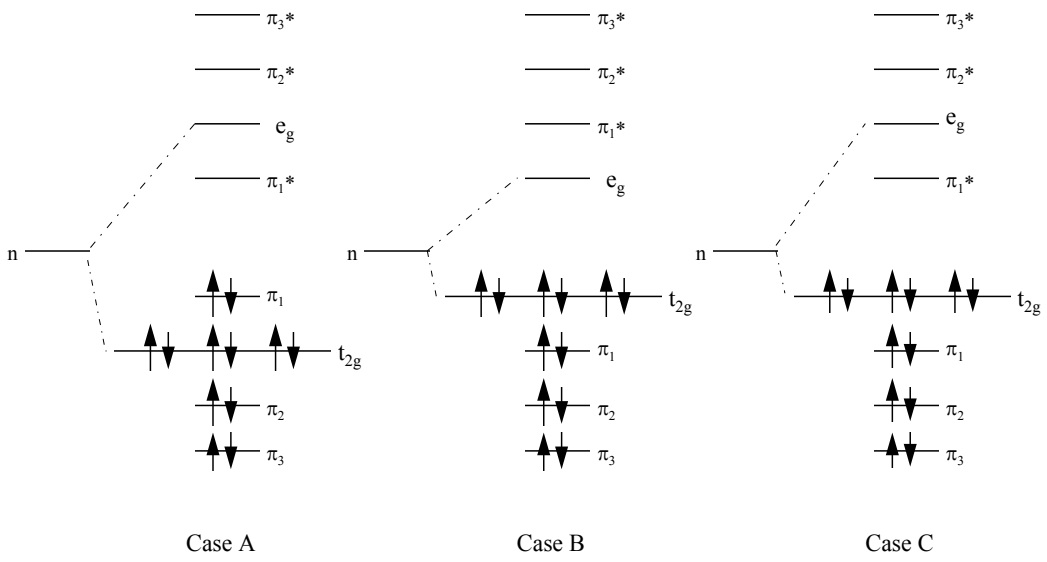

Figure 1.18: Schematic representation of orbital dispositions for d_6 metal (II) complexes

As shown above in Figure 1.18 three types of possible transitions are shown exhibiting different lowest-lying excited states in each case. Case A and B both display transitions between orbitals of the same nature, i.e. ligand to ligand transitions ($\pi \rightarrow \pi^*$) in Case A and metal to metal transitions ($d \rightarrow d^*$) in Case B. However it is the inter-orbital transitions ($d \rightarrow \pi^*$) shown in Case C which are of most relevance to this report. In this case the highest occupied molecular orbital (HOMO) is metal based (t_{2g}), while the lowest unoccupied molecular orbital (LUMO) is a ligand based anti-bonding orbital (π^*). An example of this kind of system is the molecule $[Ru(bpy)_3]^{2+}$. 2,2‘-bipyridine, which is a colourless molecule with an absorption spectrum showing a prominent $\pi \rightarrow \pi^*$ lowest lying excited state. However upon coordination to a ruthenium ion to form $[Ru(bpy)_3]^{2+}$, a whole new set of electronic transitions are observed which are neither purely ligand based nor metal based.[55] This intense transition band is charge transfer (CT) in nature and as in this case the charge is shifted from the metal to the ligand it is termed metal to ligand charge transfer (MLCT). This shift in electron density results in an excited state in which a ‗hole‘ is generated in the t_{2g} (HOMO) orbital set with the excited electron resting on the ligand, producing a different species to the ground state complex. The excitation energy now

possessed by the molecule can (i) be transferred to another molecule, (ii) return the promoted electron to the ground state thereby filling the hole (i.e. undergo reduction) or (iii) act as a reductant by transferring the promoted electron resting on the ligand to another species. It is these possible transitions that have engendered the immense research interest in metal (II) polypyridyl complexes over the past 40 years.

In the construction of supramolecular species for any function the possible electronic transitions that may occur must be carefully considered. As discussed above the transitions may vary depending on the HOMO and LUMO arrangements of the metal ion and the ligand(s) coordinated. Therefore careful selection of the components used in such systems is essential. This is best illustrated through examination of specific examples, in this case the parent complexes for the novel complexes discussed in this thesis: $[Ru(bpy)_3]^{2+}$ and $[Os(bpy)_3]^{2+}$.

1.4.2 Properties of $[Ru(bpy)_3]^{2+}$ and $[Os(bpy)_3]^{2+}$

$[Ru(bpy)_3]^{2+}$ has been one of the most widely studied compounds since the late 1950's.[56] It displays well defined photophysical properties and has become the benchmark for all other ruthenium(II) diimine complexes. [57, 58, 59, 60, 61]

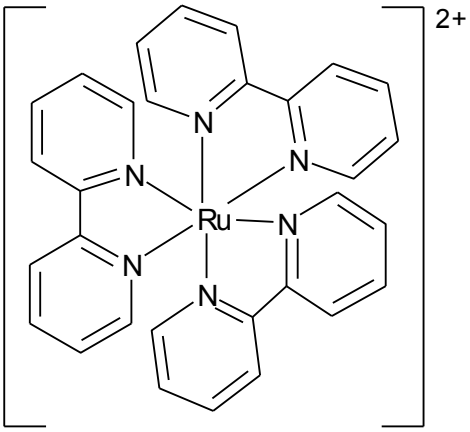

Figure 1.19: Structure of $[Ru(bpy)_3]^{2+}$

As mentioned previously, it is the photophysical and electrochemical properties displayed by $[Ru(bpy)_3]^{2+}$ and $[Os(bpy)_3]^{2+}$ that drive interest into both these and their related complexes. As discussed above the lowest energy transitions occurring within

the free ligand bpy are π-π^* in nature, whereas upon coordination to a ruthenium ion a new set of spectral possibilities are created which are neither metal or ligand localized. As shown in Figure 1.18 (Case C) a situation now exists in which the HOMO is the metal based (t_{2g}) and the LUMO is the ligand based (π^*). This means that upon absorption of a photon an electron is promoted from the t_{2g} orbital localized on the Ru(II) metal centre to the π^* orbital present within the 2,2‘-bipyridine system. This species is chemically different from its ground state and potentially possesses different properties. As mentioned before the excitation energy resulting from light absorption can be (i) transferred to another molecule, (ii) undergo reduction (refilling the _hole‘) or (iii) act as a reductant by transferring the promoted electron to another species. These properties have a number of potential uses, including light harvesting and molecular electronics as discussed earlier. However, $[Ru(bpy)_3]^{2+}$ is in possession of other properties which render it unsuitable for such practical applications.

Figure 1.20 depicts the most important photophysical properties of $[Ru(bpy)_3]^{2+}$. Light absorption results in a metal to ligand charge transfer (MLCT) transition populating the singlet ^{1}MLCT energy level. Fast intersystem crossing (ISC) from singlet to triplet states occurs with an efficiency of unity quickly populating the ^{3}MLCT level. Emission from the triplet state to the ground state (k_r) or radiationless deactivation (k_{nr}) to the ground state may occur but another deactivation pathway is provided by population of the nearby metal centred excited state (^{3}MC) which leads to radiationless deactivation or to photodecomposition of the complex.[62,63,64,65]

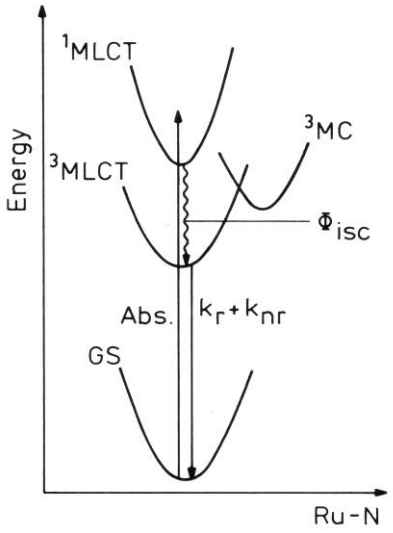

Figure 1.20: Potential Energy diagram showing the relative positions of the excited states of $[Ru(bpy)_3]^{2+}$

Any excited state transitions between the ^{1}MLCT energy level and the ground state are very quick to occur and therefore allow no time for any further electron or energy transfer, rendering the complex useless for any practical functions. In the case that the ^{3}MLCT energy level is populated by ISC (as is the case for $[Ru(bpy)_3]^{2+}$) radiative or non-radiative decay back to the ground state becomes formally forbidden creating a possibility of further electronic transitions. However is the case of $[Ru(bpy)_3]^{2+}$, the nearby ^{3}MC state (i.e. the e_g of the metal centre) is inevitably populated by ISC from the ^{3}MLCT level. The photochemistry of $[Ru(bpy)_3]^{2+}$ therefore arises mostly from the ^{3}MC excited state which can at best lead to non radiative decay, but can also lead to ligand loss photochemistry. The reason for this is the lengthening and therefore weakening of the Ru-N bond, which is the result of population of the ^{3}MC state. The ^{3}MC state has considerable e_g orbital character and as electron density is placed in it, electron density is thereby placed between the ruthenium centre and the nitrogen donor atoms. The resulting loss of backbonding from the t_{2g}-π^* orbital weakens the Ru-N bond and often leads to ligand loss. [66, 67, 68]

A secondary weakness associated with the $[Ru(bpy)_3]^{2+}$ complex is its failure to efficiently utilize the solar spectrum, only absorbing within a very narrow spectral range. Consequently investigations have been carried out to develop a system capable

of demonstrating photo-properties based on those of the parent complex $[Ru(bpy)_3]^{2+}$ without the related disadvantages. By substituting one or more of the 2,2-bipyridine ligands it is possible to improve the parent complex and generate a system which may undergo more efficient intra- and intermolecular processes. This substitution can result in altering the energy gap between the ^{3}MLCT excited state and the ^{3}MC state, thereby reducing the deactivation pathways available within the system.

The photo-redox properties of $[Ru(bpy)_3]^{2+}$ are also of interest. Normally oxidation of $[Ru(bpy)_3]^{2+}$ occurs within a metal centered orbital, resulting in a decrease in the metal‘s oxidtation state generating Ru(III) which is inert to ligand substitution. The oxidation potential of $[Ru(bpy)_3]^{2+}$ falls in a narrow range around +1.25V vs. SCE, with the reduction potential at around -1.35V vs. SCE. However, substitution of one or more of the bpy ligands in $[Ru(bpy)_3]^{2+}$ can dramatically alter these redox potentials.

In terms of redox behaviour, the orbital orientation shown in Figure 1.18 Case C will result in oxidation being localised on the metal and reduction being localised on the ligands. While many metal complexes are prone to decomposition following oxidation or reduction, Ru-polypyridine complexes are usually stable in both oxidised and reduced form: the metal centred oxidation leads to the formation of stable Ru(III) complexes (low spin t_{2g}^5 configuration). [14]

$$[Ru^{II}(L)_3]^{2+} \rightarrow [Ru^{III}(L)_3]^{3+} + e^- \quad (4)$$

Reduction takes place on the low-lying π* orbital of one of the coordinated ligands as shown in Figure 1.15. Therefore the reduced complex retains a low spin t_{2g}^6 configuration rendering it stable. [14]

$$[Ru^{II}(L)_3]^{2+} + e^- \rightarrow [Ru^{II}(L)_2(L^-)]^+ \quad (5)$$

The electrochemical properties of Ru(II) complexes may be tuned by choosing appropriate ligands for coordination, with the redox chemistry of the final complex being governed by the σ-donor and π-acceptor properties of the ligands used.[69]

σ-donor ligands donate electron density to the metal centre, which lowers the complex‘s oxidation potential and creates more negative reduction potentials. π-

acceptors however, remove electron density from the metal centre, stabilising the full metal orbitals resulting in higher oxidation potentials and lower reduction potentials.
An ideal metal complex for use as a molecular electronics prototype must display accessible oxidation and reduction potentials while ensuring that all processes remain reversible and the complex remains stable in all oxidation states.
Incorporating strong π-accepting ligands such as 2,2‘-bipyrazine, 2,2‘-bipyrimidine and 2,2‘-biquinoline results in a less negative reduction potential for the ensuing complex. However, strong π-acceptors tend to be weak field ligands, resulting in smaller ligand field splitting of the Ru(II) orbitals resulting in an increase in oxidation potential for the metal centre as well as increasing the possibility of the LUMO being metal centred.[70]
Incorporating strong σ-donor ligands such as imidazole, pyrazole and 1,2,4-triazole lower the oxidation potential of the metal centre. However, as these ligands are not strong π acceptors their π* orbitals are higher in energy than for bpy, resulting in unfavourably negative reduction potentials.

By combining the two systems, a model containing two π-acceptor ligands (such as bpy) and one σ-donor (a triazole) should display a ligand based LUMO on account of bpy being present while the coordinated triazole will lower the oxidation potential.
The presence of a strong σ-donating ligand within the complex increases the electron density on the metal centre through back-bonding thereby lowering the oxidation potential / raising the reduction potential. The presence of π acceptors ligands lower the π* orbitals of the resulting metal complex ensuring reduction is ligand centred. [71]

$$[Ru(bpy)_3]^{2+} + e^- \rightarrow [Ru(bpy)_3]^{+} \qquad E^0 = -1.35\ V \qquad (6)$$

$$[Ru(bpy)_3]^{+} + e^- \rightarrow [Ru(bpy)_3]^{2+} \qquad E^0 = +1.26\ V \qquad (7)$$

$$[Os(bpy)_3]^{2+} + e^- \rightarrow [Os(bpy)_3]^{+} \qquad E^0 = -1.28\ V \qquad (8)$$

$$[Os(bpy)_3]^{+} + e^- \rightarrow [Os(bpy)_3]^{2+} \qquad E^0 = +0.83V \qquad (9)$$

$[Os(bpy)_3]^{2+}$ and its related complexes provide better options in terms of photo-redox properties due to their lower lying oxidation potentials. As a result osmium polypyridyl complexes can be more readily used on surfaces such as gold or platinum. Seeing as how immobilisation on surfaces has been described as the method in which

molecular electronics are most efficiently arranged into supramolecular _circuitry', the research surrounding the formation and utilization of self-assembled monolayers is outlined hereafter.

1.4.3 Self Assembled Monolayers

As discussed previously the methods used at present for fabrication of solid-state electronics are classed as a _top down' approach: etching silicon crystals using laser technology to form electronics and circuits. If the miniaturisation of electronics continues as predicted (the amount of devices per circuit doubling every 18-24 months) the intricacy and delicacy of the _top down' fabrication approach must increase, dragging the cost of production with it. Molecular synthesis however, is a _bottom-up' approach using atoms to construct nanometer-sized structures that may then be arranged further to form supramolecular circuitry.[33] Molecular components may be assembled with a high level of organisation in a number of different ways. This level of organisation may be achieved on semiconductor or electrode surfaces using self-assembly[72]. Similarly, this concept may be applied to DSSCs in which light harvesting molecules are arranged on a suitable conductor surface. Self-assembly is a well-documented area of supramolecular chemistry allowing for construction of highly ordered films of molecules on a solid matrix.[42(c)] These self-assembled monolayers (SAMs) present a number of advantages when applied to the field of molecular electronics. These advantages include:

- Self assembly is a parallel process. This allows for the fabrication of many circuits simultaneously, increasing cost effectiveness.
- Self assembly generates highly ordered monolayers, often with sub-nanometer precision.
- Self assembly also allows for fabrication of 3-D architectures.
- External forces and geometric constraints can affect the result of a self-assembly process. Therefore, systems may be reconfigured if desired.[72]

As a result a large number of devices may be _grown' in one batch allowing for rapid, cost effective, high yielding processes.

Traditional microchip fabrication allows for construction of devices on the micrometer scale. However, molecular units may be arranged in tightly packed

structures at the nanometer level resulting in potential structures of density much greater than presently attainable with solid state devices. This would satisfy the demand for increasingly tiny, dense circuitry plaguing the electronics industry.

As mentioned previously, formation of self assembled monolayers is an effective method of organisation to form supramolecular arrays. It has also been pointed out that covalent bonds are not necessary for electron injection into a conductor/semiconductor. Therefore formation of self assembled monolayers is an elegant method for the construction of molecular electronics prototypes.
For a molecule to be used effectively for monolayer formation it must contain a group capable of coordination to conductor/semiconductor surfaces. Groups of this kind include thiol (-SH) groups, for use on gold surfaces[73], triethoxysilane (-$SiOEt_3$) for use on ITO surfaces[74], pyridine groups for use on platinum surfaces[48] and thiophene groups for use on gold surfaces[75] An illustrative example of this diversity is shown below in Figure 1.21, depicting two similar supramolecular species, one of which is anchored onto an ITO surface[74], while the other is bound to a gold electrode[76].

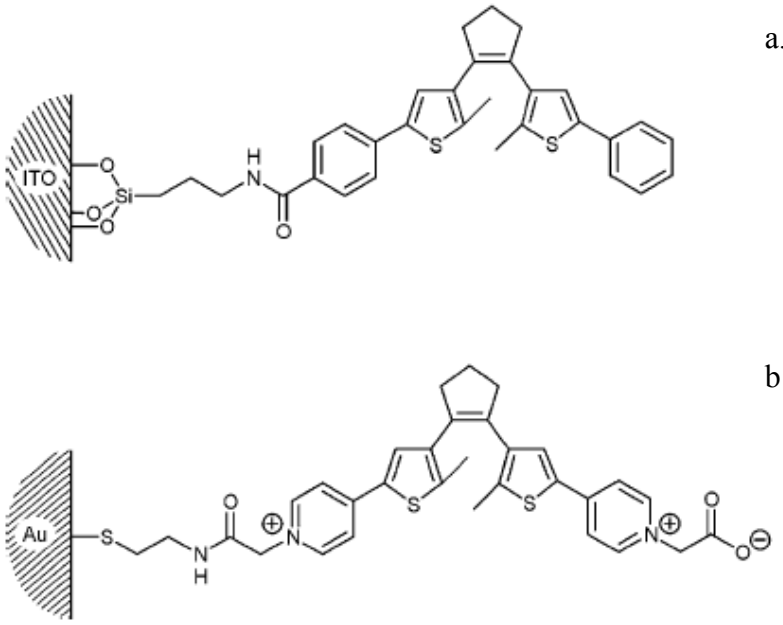

Figure 1.21: Schematic representation of a molecular switch prototype anchored to a substrate using different surface active groups[34]. Compound a is anchored on an ITO

surface through an SiO_3 group[74], while compound b is anchored on a gold electrode via a thiol[76]

Thiol groups have proven very attractive as anchors for surface modification as they readily form well organised monolayers. Mayor et al have prepared a number of organothiol compounds for monolayer formation[73, 77, 78, 79] with a view to use as molecular devices. Many of these compounds employ a protected -SOAc functional group as opposed to the conventional –SH group used in thiols for monolayer formation. This acetyl thiol derivative is quite easily attainable by synthetic means and is not as labile as the –SH thiol functionality. Also, the synthetic pathway leading to these acetyl thiol compounds proceeds via a tert butyl thiol precursor[80], a group which can withstand relatively harsh synthetic conditions thereby increasing the synthetic possibilities for molecules of this type.

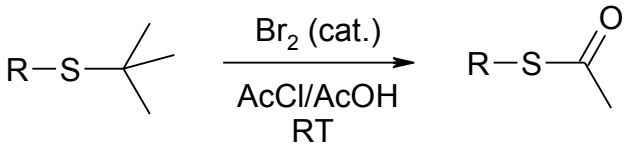

Figure 1.22: General reaction scheme for conversion of tert-butyl thiol to its acetyl derivative[80]

Also, when used to form a monolayer, the acetyl group is removed *in situ* allowing for coordination of the S group with no complications.[73] An example of one such system is shown below in Figure 1.23.

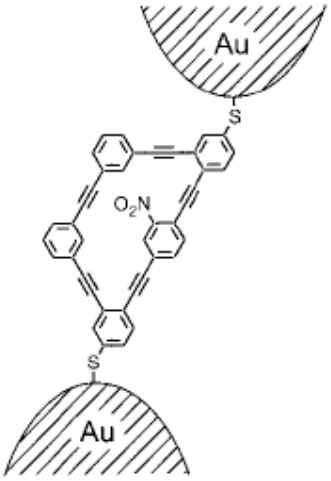

Figure 1.23 Schematic representation of a molecular electronics prototype as synthesised by Mayor et al. The molecule is anchored to two separate electrodes via acetyl thiol groups which are converted to thiols during attachment to the electrode surface.[73]

Thiol groups have also been employed as anchor groups for transition metal complexes. An $[Ru(bpy)_3]^{2+}$ derivative has been synthesised with two appended thiol anchor groups.[81] These groups are synthesised through reaction of thiourea with a bromoprecursor. The product complex readily forms monolayers on gold.[81]

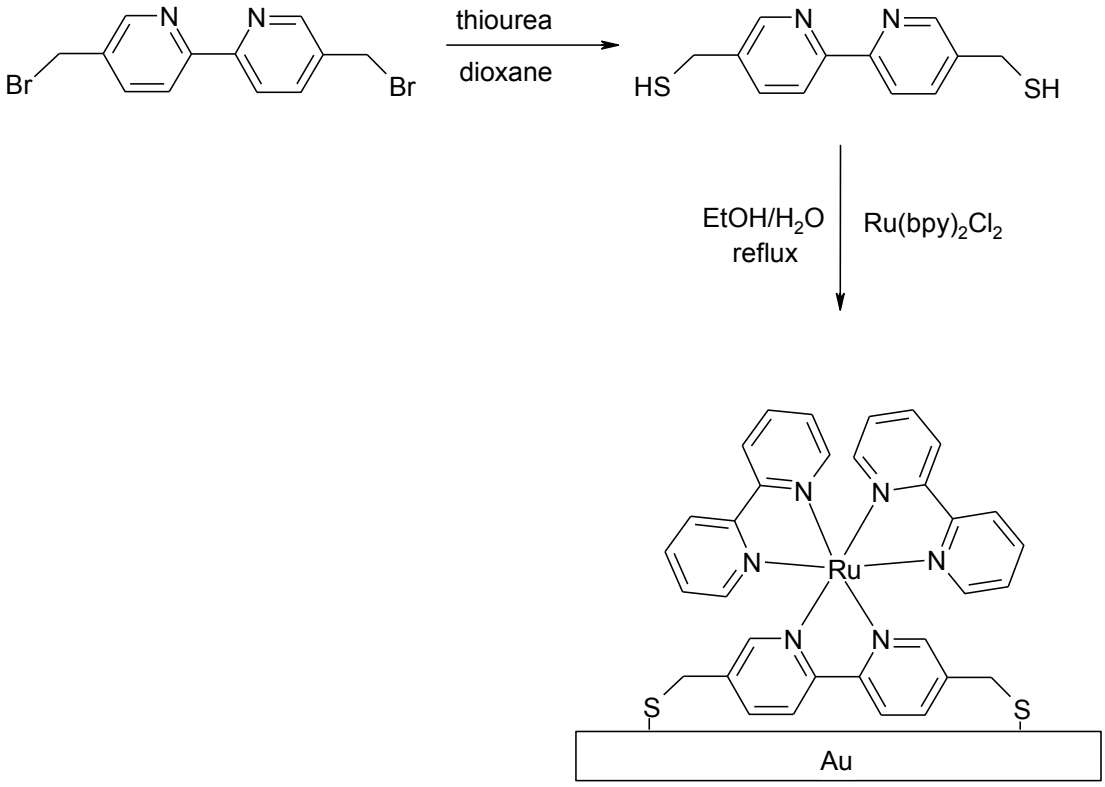

Figure 1.24: Schematic representation of synthesis of $Ru(bpy)_2(bpySH)$ and its coordination to a gold surface[81]

As shown previously in Figure 1.14 pyridine is also a suitable group for surface coordination. Pyridine groups have also been used by Forster et al. for monolayer formation on platinum with osmium complexes of similar structure[82]

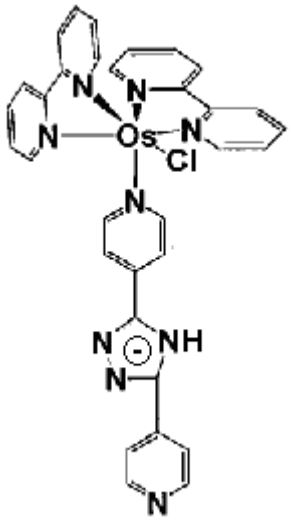

Figure 1.25: Structure of $[Os(bpy)_2(4,4'\text{-}bpy)](PF_6)_2$, used for coordination to platinum[82]

Pyridine has also been employed as an anchoring group for ruthenium and osmium based polymers used to modify electrode surfaces. The polymer $[Ru(PVP)_{10}Cl]Cl$ (the structure of which is shown below in Figure 1.26) has been used for electrochemical photolysis experiments when immobilised on an electrode surface.

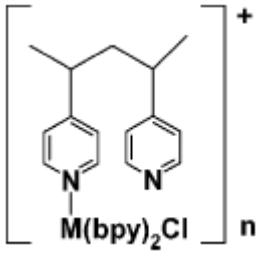

Figure 1.26: General structure of redox polymers where M is Ru or Os and N is 5, 10, 15 and 25 representing the ratio between the polymer units and metal centres present.

Upon recording the cyclic voltammogram of the polymer $[Ru(PVP)_{10}Cl]Cl$ under continuous irradiation, the original redox couple (observed at 640 mV) is replaced by a second signal occurring at 840 mV as shown below in Figure 1.27.

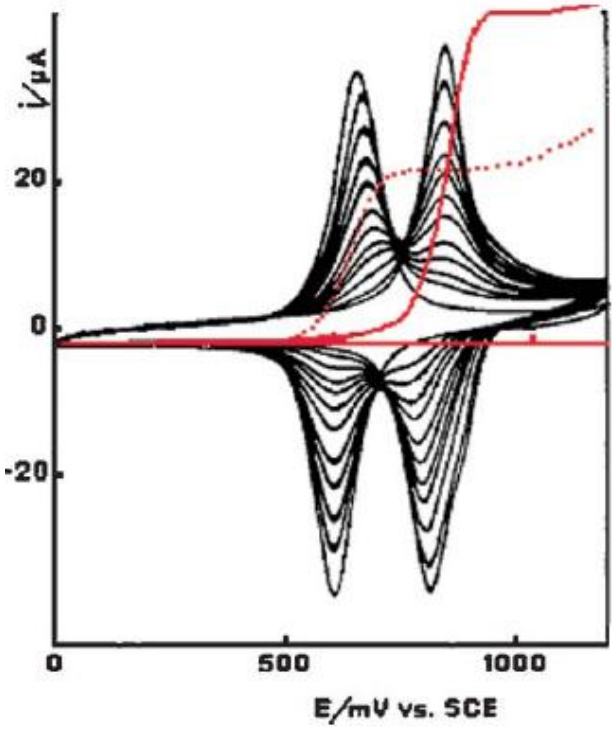

Figure 1.27: Cyclic Voltametric analysis of photolysis experiment on electrode modified with $Ru(bpy)_2(PVP)_{10}Cl]Cl$. Black: effect of photolysis on electrochemical properties. Red: limiting current obtained for the oxidation of Fe(II) using a rotating disc electrode. Dotted line before and solid line after photolysis.[83]

These changes are indicative of the photolytic exchange process shown in Equation 10.

$$[Ru(bpy)_2(PVP)_{10}Cl]^+ + H_2O \rightarrow [Ru(bpy)_2(PVP)_{10}H_2O]^{2+} + Cl^- \quad (10)$$

The osmium analogues of these polymers do not exhibit any ligand loss photolysis upon monolayer irradiation and so have been subjected to extensive studies.[1] Electrochemical studies on the effect of temperature, electrolyte concentration, crosslinking, layer thickness *etc.* have been carried out and a detailed understanding has been obtained of the charge transport properties of thin layers of these materials. An extensive review of this research is available in reference 1.

Thiophene has also been used for monolayer formation of gold. Molecular thiophene was found to form a monolayer following vacuum deposition on gold.[84] Sako et al have observed monolayer formation also after extended soaking of a gold electrode in an ethanolic solution of thiophene.[75] However, following further analysis the adsorbed species was found to be an aliphatic thiolate. Even so, this evidence is very encouraging with respect to use of thiophene for monolayer formation.

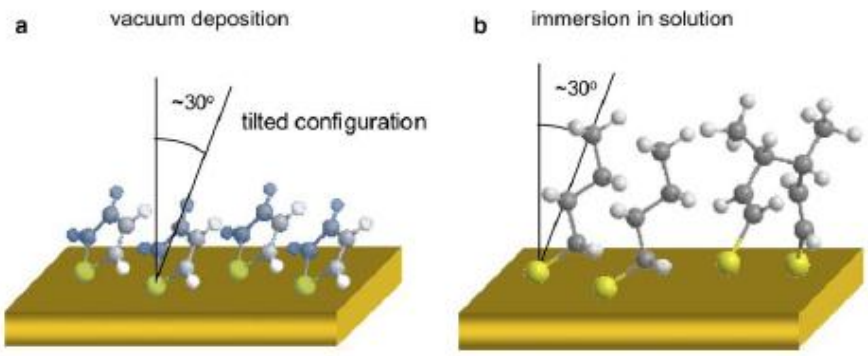

Figure 1.28: Schematic illustration of the structural models for the adsorbed thiophene on Au(111), (a) prepared by vacuum deposition and (b) by immersion in ethanol solution.[75]

It can be seen from the information discussed in Section 1.4 and 1.5 that transition metal complexes containing osmium and a group suitable for coordination to an electrode surface are perfect candidates for a molecular electronics prototype. Of the surface active units discussed above (thiol, pyridine and thiophene groups) pyridine and thiophene groups are the most synthetically viable as metal complexes

incorporating thiol groups have shown a number of synthetic difficulties in the past.[85] The target complexes for synthesis in this thesis are introduced below in section 1.6.

1.5 Target Complexes

The aim of this project has been to successfully synthesise and characterise mono-and dinuclear transition metal complexes capable of exhibiting molecular electronic type properties at room temperature and atmospheric pressure.

The desired final product is a dinuclear system capable of diode type behaviour (i.e. ‗directing' an applied current in one direction only) built from units used to construct the transistor type mononuclear model complexes.

The mononuclear (transistor) complexes envisioned incorporate a bis-bipyridyl metal complex fabricated with a phenanthroline unit from which a surface active group is appended. The target molecules are shown below in Figure 1.29.

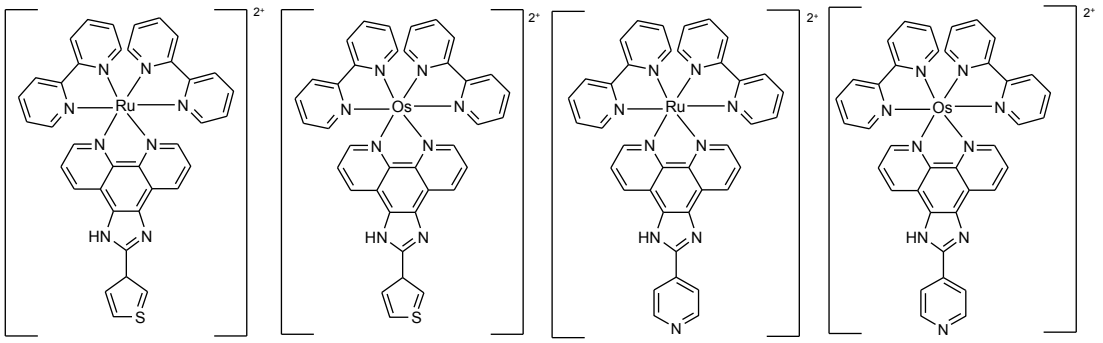

Figure 1.29: Target mononuclear complexes later discussed in Chapter 3. From left to right: $[Ru(bpy)_2(thimphen)]^{2+}$, $[Os(bpy)_2(thimphen)]^{2+}$, $[Ru(bpy)_2(pyrphen)]^{2+}$, $[Os(bpy)_2(pyrphen)]^{2+}$

As shown in Figure 1.29 the analogous ruthenium complexes for each mixed ligand system are envisioned as well as the osmium. These have been included as coordination of certain ligands may alter the redox potential of the system from the expected +1.3 V, *vs* SCE (observed for $[Ru(bpy)_3]^{2+}$) to a lower potential which will allow for monolayer formation on an electrode surface and allow conductivity to be measured in aqueous electrolyte: two imperative prerequisites for the fabrication of a molecular electronics prototype. $[Os(bpy)_3]^{2+}$ on the other hand exhibits oxidation potentials at approximately +0.9 V *vs* SCE rendering it and its related complexes ideal for molecular electronics applications. These molecules should also allow for vertical

coordination to electrode surfaces, maximising the possible surface coverage of modified electrodes.

The synthesis of a second type of mononuclear complex has also been attempted in collaboration with the University of Otago, New Zealand. These complexes are ruthenium based, incorporating a tetradentate unit as well as surface active 4,4‘-bipyridyl units as shown below in Figure 1.30.

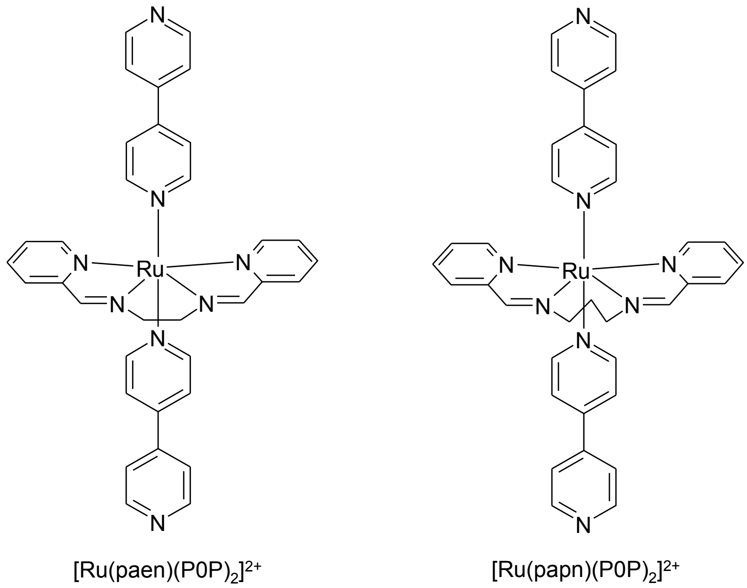

Figure 1.30: Target mononuclear complexes later discussed in Chapter 6.

As mentioned for the mononuclear metal complexes shown in Figure 1.29 the ligands used may pull the oxidation potential of the complexes shown in Figure 1.30 low enough to form monolayers on electrode surfaces and to operate in aqueous media.

Dinuclear systems incorporating the novel phenanthroline based ligands shown in Figure 1.29 are also targeted for synthesis in this project.

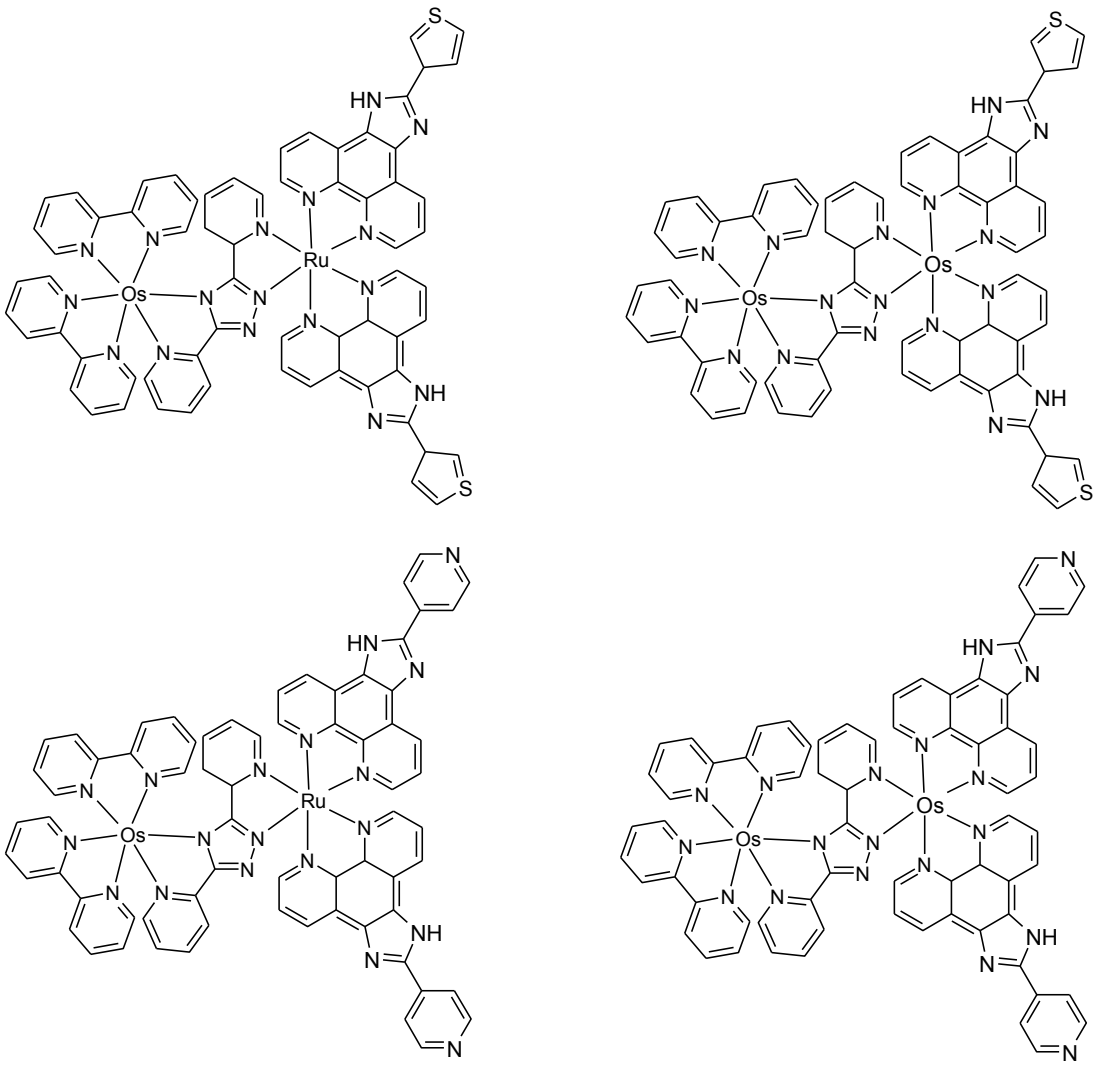

Figure 1.31: Structures for possible dinuclear complexes, synthetic approaches for which are outlined in Chapters 4 and 5

All of the dinuclear complexes shown above in Figure 1.31 consist of two metal centres linked via a Hbpt bridging ligand. Hbpt has been shown to be an effective mediator of electron transfer between metal centres[86]. The method of electron transfer has been rationalised as arising from strong coupling between the linked metal centres due to mixing of the dπ orbitals present on the metal with the π orbitals present on the bridging ligand.[87] Dinuclear molecules such as those shown in Figure 1.31 are envisioned as molecular diode prototypes. A diode is defined as an electronic component allowing current to flow in one direction only[32]. This model may be achieved in a molecular sense by synthesising a system in which two metal centres of

differing oxidation potential are linked using a bridge which will allow electronic communication. This may be achieved using completely different metal centres (e.g. the RuOs type heterodinuclear complexes shown in Figure 1.31) or by using identical metal centres which have been _tuned' to different oxidation potentials by virtue of their appended ligands (e.g. the RuRu and OsOs homodinuclear complexes shown in Figure 1.31). By applying a voltage which will cause the centre of higher potential to oxidise, electron transfer should occur via the bridging ligand to the centre of lower oxidation potential. However, by applying voltage causing the centre of lower potential to oxidise electron transfer should theoretically not occur. This is due to the fact that electrons which require a high potential applied to effect oxidation are higher in energy than those which require a lower potential to incur oxidation and electron transfer cannot occur from an area of low energy to an area of high energy. This design is shown schematically below in Figure 1.32.

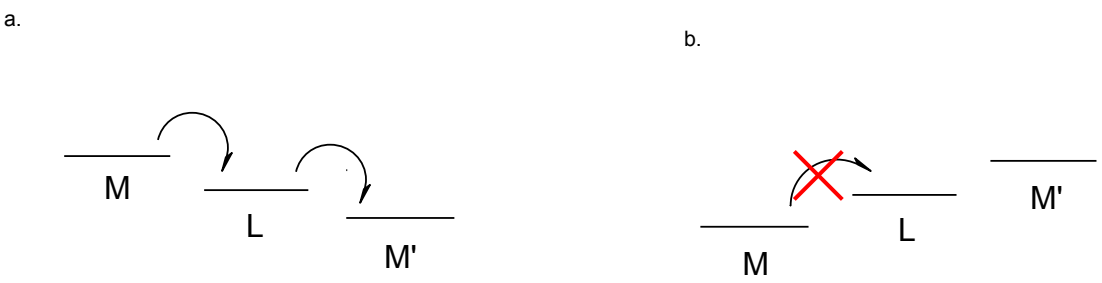

Figure 1.32: Schematic representation of a system in which M and M' are electrochemically different metal centres and L is a bridging ligand allowing electronic communication. Theoretical electron transfer upon oxidation of M is shown where appropriate where M is (a) higher in oxidation potential than M' and (b) lower in oxidation potential than M'

The necessity of low oxidation potentials for the formation of self assembled monolayers has already been discussed in section 1.4.3 with osmium polypyridyl complexes being identified as the most suitable candidates for this role. Therefore a successful diode prototype suitable for surface coordination will contain an osmium centre to which surface active ligand are coordinated. The remaining metal centre may be ruthenium or osmium based.

Molecules of this type are synthesised using a series of documented organic and inorganic synthetic methods. These methods as well as work performed using them heretofore shall be the focus of the next section of this chapter.

1.6 Synthetic Strategies for the Preparation of Transition Metal Complexes

Direct Synthesis vs. Modification of Metal Complexes

This thesis deals with synthesis of metal complexes via two different methods, *Direct* and *Indirect* synthesis. The main manner in which transition metal complexes are synthesised is using the *"Complexes as Metals/Complexes as Ligands"* approach or *Direct Synthesis*.[14,88]. In this approach mononuclear complexes are formed according to the following equation (6), where M is the free metal and L is the free ligand.

$$M + nL = M(L)_n \qquad (6)$$

When constructing these complexes, the central metal is not available as a pure element. These reactions are carried out with neutral complexes of ruthenium or osmium containing easily replaced ligands (usually Cl.)

A metal complex in which all of the ligands present are identical, is termed a homoleptic metal complex.[89] These complexes are of limited synthetic and practical value, and so more synthetically complicated metal complexes are required.

Metal complexes containing two or more different types of ligand are termed heteroleptic complexes.[89] This type of complex is synthesised in the same manner as shown in equation (6) but in the place of M a metal complex containing two or more types of ligand is used, one more easily replaced than the other.

where:

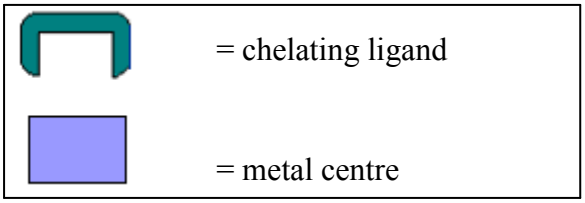

Figure 1.33: Diagrammatic representation of the synthesis of a mononuclear complex via the Complexes as Metals/Complexes as Ligands approach

One of the most frequently used of these starting materials is $[Ru(bpy)_2Cl_2].2H_2O$[90]. In this case, the chloride ligands are easily replaced when heated in the presence of a slight excess of ligand L. This type of synthesis is a widely used method for the preparation of mononuclear heteroleptic complexes.[14]

If the coordinating ligand L contains one or more coordination sites other than that used to form the $[Ru(bpy)_2L]^{n+}$ complex, this product molecule may take the place of L in equation (6) which may then react with another metal starting material, containing (a) the same metal centre (e.g. a second molecule of $[Ru(bpy)_2Cl_2]$ resulting in a homodinuclear complex, or (b) a different metal centre (e.g. $[Os(bpy)_2Cl_2]$) creating a heterodinuclear complex.

As can be seen from Figure 1.34, in order to synthesise a homodinuclear complex, the bridging ligand may be reacted with two stoichiometric equivalents of the metal starting material. However, in the case of the heterodinuclear complex shown there are two separate steps that must be undertaken. In the first step equal equivalents of the first metal starting material and the bridging ligand are reacted. This will form the desired mononuclear complex shown in Figure 1.34 b**.** Care must be taken in order to avoid formation of the homodinuclear complex shown in Figure 1.34 a. There shall most likely be a certain amount of homonuclear complex present as an impurity but this may be removed using column chromatography. The purified mononuclear complex may then be reacted with the second metal starting material, yielding the desired heterodinuclear complex.

This strategy has been employed popularly for the formation of large numbers of dinuclear, polynuclear and dendritic complexes[14].

However, this method of synthesis has proven unsuitable for a variety of different metal complexes.

For example, the heterodinuclear complex shown above in Figure 1.34 employs a symmetrical bridging ligand. This allows for the formation of two possible products, the homodinuclear complex $[(bpy)_2Ru(bpt)Ru(bpy)_2]^{3+}$ and the heterodinuclear complex $[(bpy)_2Ru(bpt)Os(bpy)_2]^{3+}$.

a.

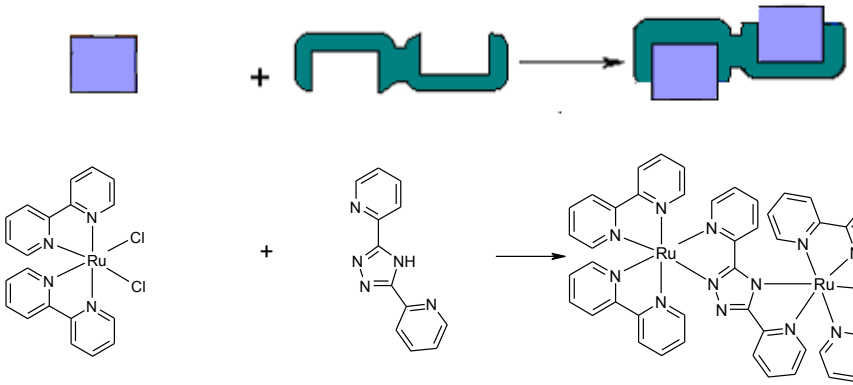

b.

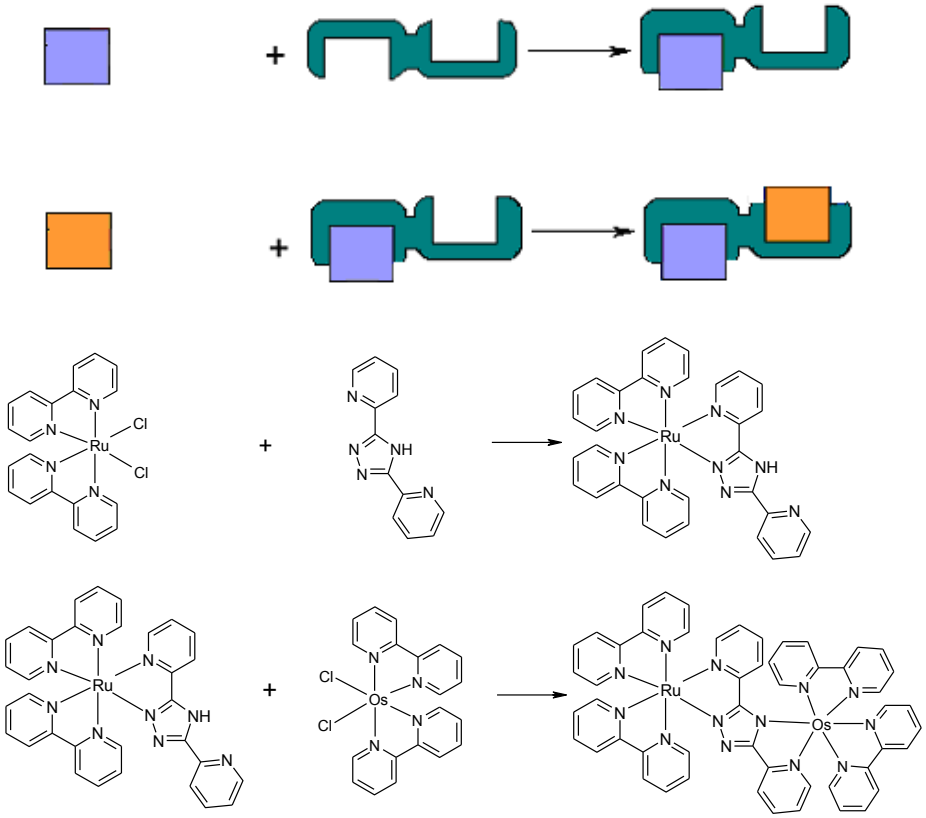

where:

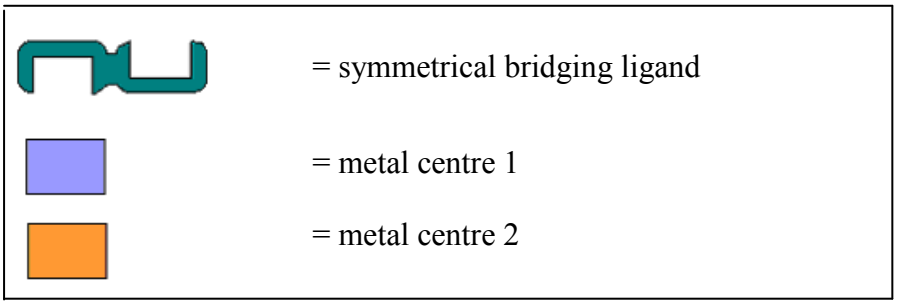

Figure 1.34: Diagrammatic representation of the preparation of homodinuclear (a) and heterodinuclear complexes(b) using a symmetrical bridging ligand[14]

However, if an asymmetrical bridging ligand is introduced in place of the symmetrical one shown above, the number of potential products increases.

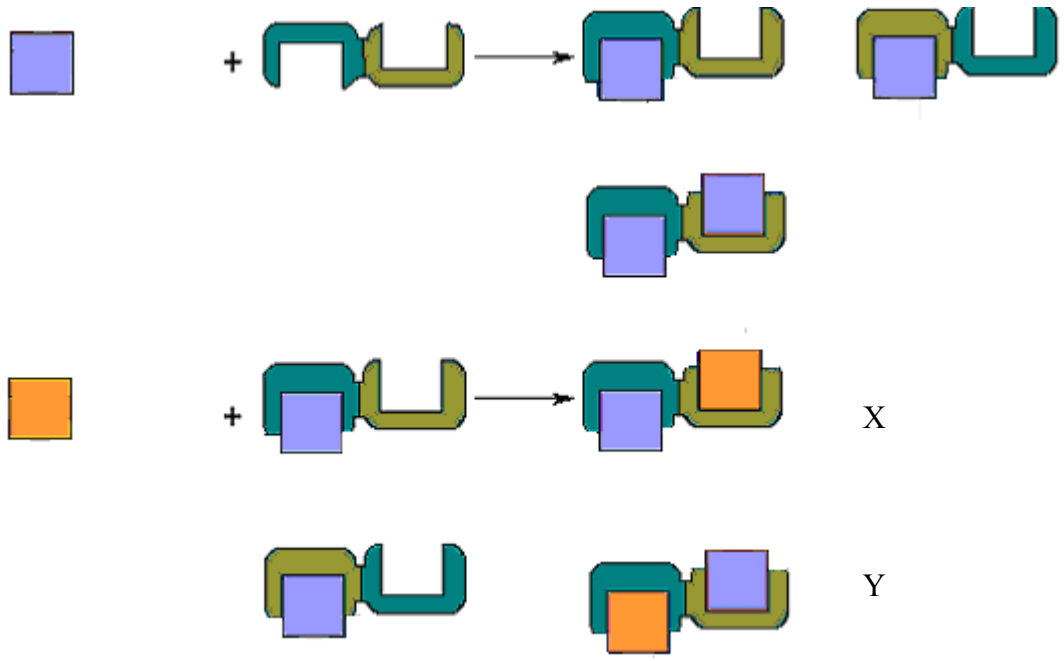

Where:

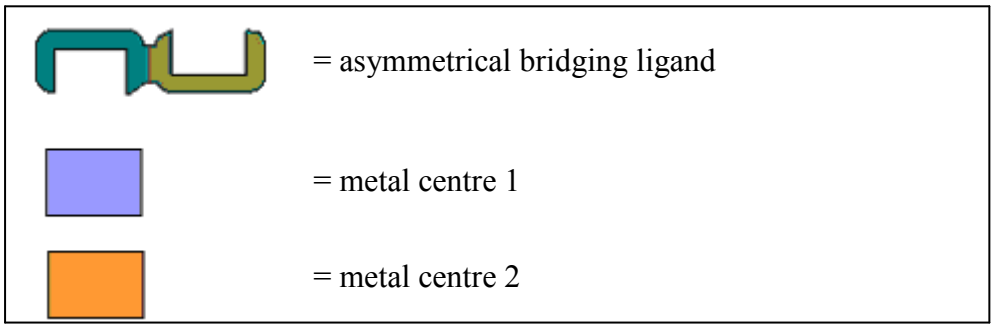

Figure 1.35: Diagrammatic representation of the preparation of heterodinuclear complex using an asymmetrical bridging ligand[91]

As shown in Figure 1.35, the first step of the synthesis resulting in the coordination of the first metal centre now yields three different products as opposed to the two products formed when employing a symmetrical bridging ligand. As there are two different coordination sites present on this bridging ligand the formation of two different mononuclear precursors is unavoidable. Though these complexes are chemically different their similar structure and electronic configuration makes separation very difficult.

If the mononuclear precursor is reacted further to yield the heterodinuclear complex a mixture of two different isomers (X and Y) will result. These complexes are often difficult to separate, and the reaction carried out in this manner is very low yielding (as it results in a number of competing products).

The idea of *'Chemistry on the Complex"* is a way to circumvent issues of this type. In the case of preparing dinuclear complexes, this technique involves first synthesising a mononuclear metal complex using a ligand with only one chelating site. This (usually straightforward and high yielding) reaction product may then be further functionalised, creating a second chelating site, which may be coordinated to a second metal centre. This method avoids the formation of undesired by-products and so increases the purity and yield of the products formed.

These processes are usually carried out via cross coupling reactions, such as Negishi coupling[92], Sonigashira coupling[93], Suzuki coupling[91] and Stille coupling[94]. Sauvage et al. have published results detailing the synthesis of a multi-component ruthenium system via Suzuki cross-coupling.[95] Suzuki cross coupling is a boron mediated catalytic process resulting in carbon-carbon bond formation between a halide functionalised starting material (R-X) and a boronic acid starting material (R'-$B^-(OH)_3$). In the synthetic pathway detailed by Sauvage et al. two homodinuclear ruthenium(II) complexes are constructed using functionalized mononuclear complexes as building blocks with a difunctionalized aromatic spacer. The reaction scheme for this reaction is shown below in Figure 1.36.

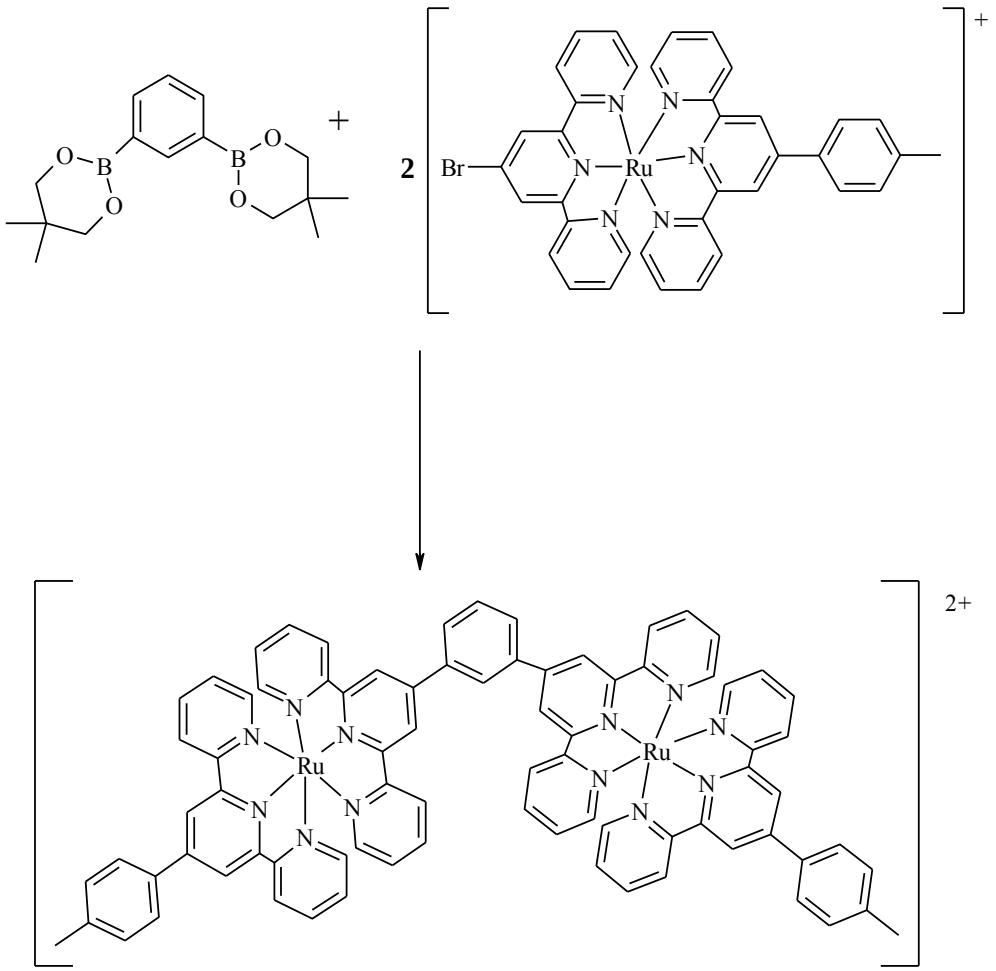

Figure 1.36: Reaction scheme for the formation of a homodinuclear ruthenium complex via Suzuki cross-coupling[91,95]

Kumada (nickel mediated) cross coupling has also been used to build dinuclear species using functionalised starting materials. This type of coupling involves carbon-carbon bond formation between two bromo-functionalised starting materials in the presence of a nickel catalyst. The first reported use of Ni(0) catalyzed coupling reactions in inorganic chemistry was by Vos et al.[96] in the synthesis of dinuclear ruthenium triazole type complexes as shown below in Figure 1.37.[96, 97]

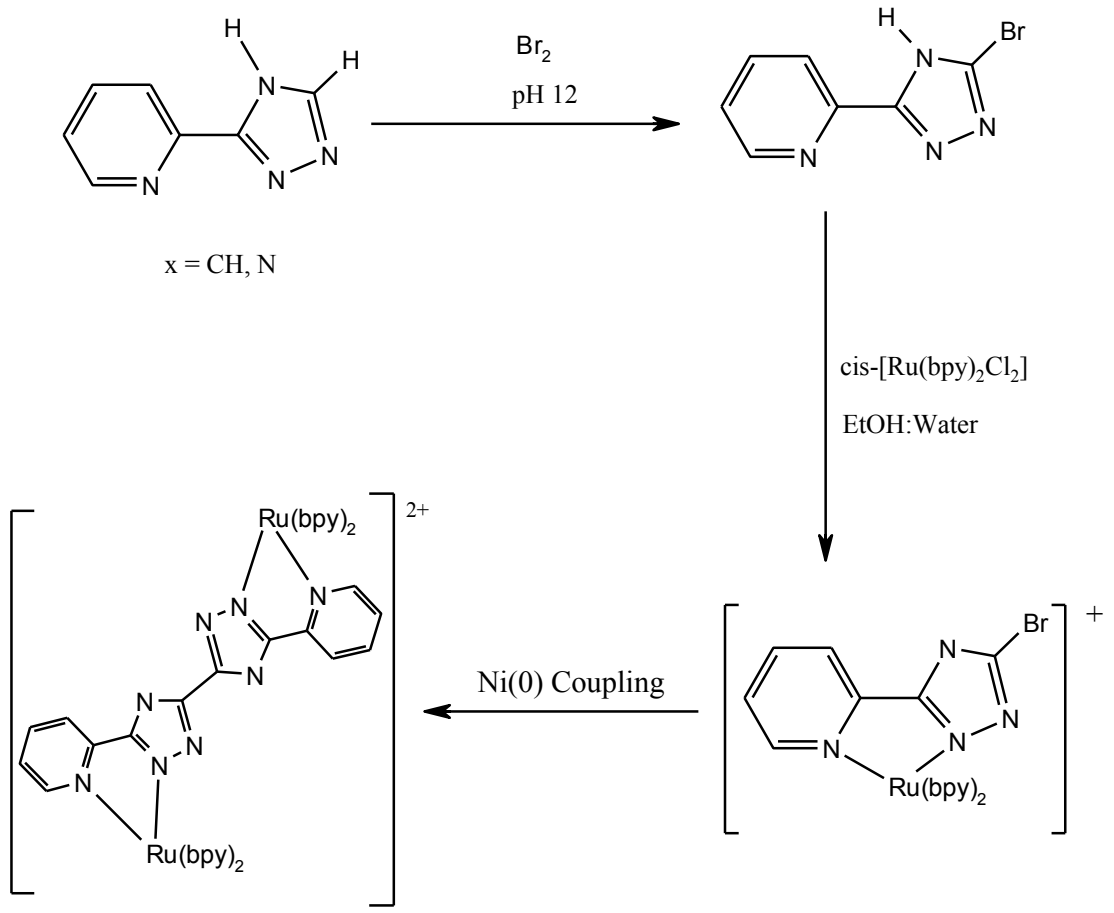

Figure 1.37: Synthetic scheme employed by Vos and co-workers in the formation of $[Ru(bpy)_2(pytr\text{-}pytr)Ru(bpy)_2]^{2+}$ [97,98]

"Chemistry on the Complex" techniques are also applicable to mononuclear complexes. Hanan et al. have developed a method of preparation for the synthetically elusive cyano- complex $[Ru(4\text{-cyanoterpyridine})_2](PF_6)_2$[98]. No viable method has been found for the synthesis of a 4-cyano funtionalised ruthenium bis terpyridine complex. Hanan et al therefore have used a transition metal catalysed approach, which allows conversion of a chloro- precursor complex to the desired cyano- derivative, shown below in Figure 1.38.

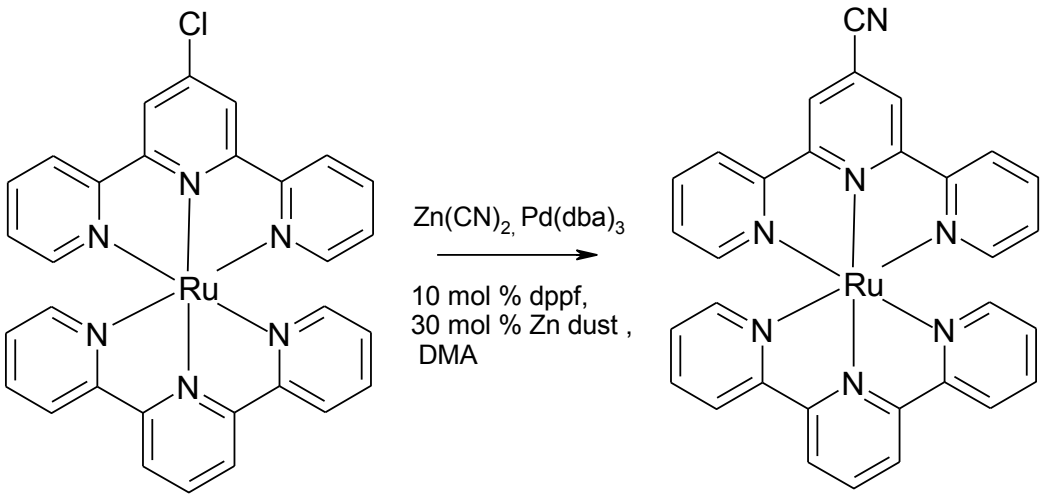

Figure 1.38: On-Complex method for Palladium catalysed cyanation of Ru(II) complexes of 4-choroterpyridine[98]

This type of method may prove effective for the preparation of metal complexes containing ligands with labile groups that may not withstand the harsh conditions used in complexation reactions.

The acylation of the noncoordinated hydroxyl group of [Co(dhpta)]- (where dhpta = 1,3-diamino-2-hydroxypropane-N,N,N',N'-tetraacetate ion) by reaction with a series of acid anhydrides in the presence of 4-(dimethylamino)pyridine has also been reported[99] The reaction scheme for these findings is shown below in Figure 1.39.

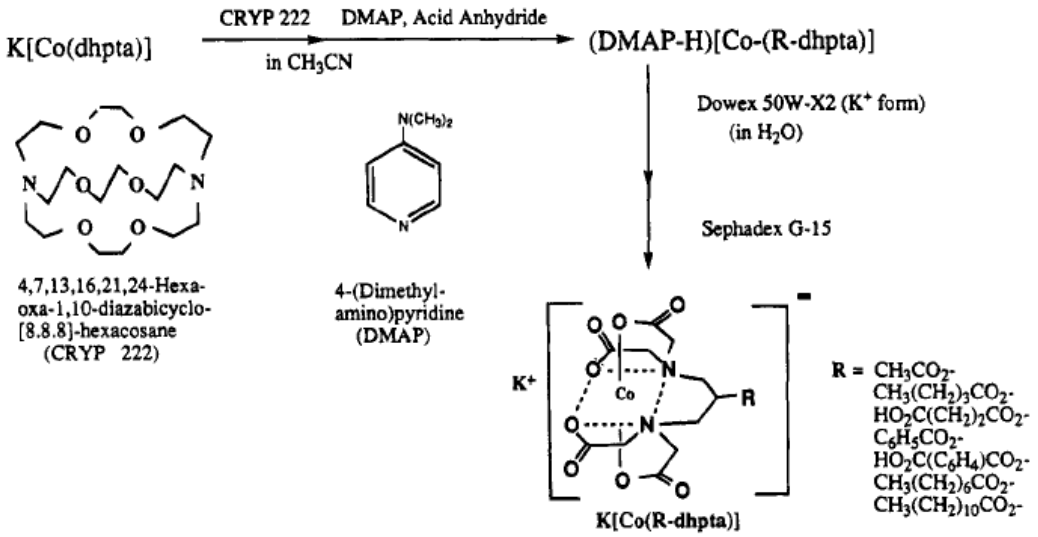

Figure 1.39: Reaction scheme for the acylation of [Co(dhpta)][99]

Relatively high yields (38%-95% depending on the ester formed) were reported while keeping the coordination sphere intact.

Lastra and workers have also reported a modification of a transition metal complex to generate a range of products.[100] A range of hydridotris(pyrazolyl)borate ruthenium (II) complexes containing new phosphane ligands are described, and are formed by electrophilic attack to a coordinated 1,3,5-triaza-7-phosphatricyclo[3.3.1.13,7]decane ligand. This is shown diagrammatically below in Figure 1.40.

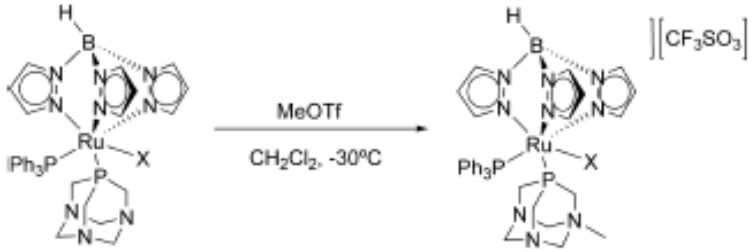

Figure 1.40: Reaction scheme for the formation of hydridotris(pyrazolyl)borate ruthenium (II) complexes containing new a phosphane ligand by modifying a coordinated ligand[100]

Direct synthesis, being the least complicated of these two methods has been the default method used for synthesis of the metal complexes described in this thesis. However, upon encountering a number of labile groups as well as ligands that were difficult to synthesise in their free state, indirect synthesis has provided a viable and in some cases, the only method for synthesis of certain metal complexes described hereafter. As a result this thesis provides somewhat of a comparison between the two methods as viable approaches for preparation of the target complexes shown in section 1.6. The specifics of these approaches and indeed all of the synthetic work attempted during this project is outlined below in section 1.7.

1.7 Scope of Thesis

The aim of this project has been to successfully synthesise and characterise mono- and dinuclear transition metal complexes for use as molecular electronics prototypes. These complexes must be capable of coordination to an electrode surface and consist of units known to result in complexes capable of exhibiting transistor or diode type electrochemical behaviour as part of a self assembled monolayer on an electrode surface.

Chapter 1 has provided an introduction to supramolecular chemistry and the manner in which surface active metal complexes arranged in supramolecular arrays may be used to solve some major commercial issues taking up research interest at present. The synthetic approaches to be used in this report have also been introduced. The next sections of this thesis describe the synthesis and characterisation of mononuclear ruthenium(II) and osmium(II) polypyridyl complexes containing surface active ligands. A number of attempts to synthesis an associated heterodinuclear species are also described. Chapter 2 details the experimental methodology used in the synthesis, purification and characterisation of these complexes. The synthesis of all starting materials are described also.

The first series of mononuclear metal complexes are encountered in Chapter 3. The novel ligand included in the metal-bisbipyridyl system is a phenanthroline imidazole type molecule incorporating either a thiophene or pyridine group for surface coordination. Both direct synthesis (complexes as ligands/complexes as metals strategy) and on-complex methods have been used in the synthesis of these complexes. While the direct synthetic route is identical to the reaction types outlined in section 1.7, the on-complex method used involves a novel ligand being built on the complex from a bisbipyridyl-phenanthroline base.

This type of _on-complex' approach is also described in Chapter 4 for the synthesis of a series of ruthenium complexes containing two novel ligands of the type synthesised in Chapter 3. Again, the ligands in question consist of a phenanthroline base to which a thiophene or pyridine group is appended for surface coordination. These complexes are all synthesised by an _indirect' route in which the two surface active ligands are synthesised simultaneously on the metal complex by modification of a bis-phenanthroline type complex.

Chapter 5 describes the attempted synthesis of a series of homodinuclear and heterodinuclear metal complexes, using 3,5-bispyrid-2-yl-1,2,4-triazole as a bridging ligand as well as incorporating two thiophene groups as a point of coordination to electrode surfaces. A number of attempted synthesic routes for the dichloride starting material $[Ru(thimphen)_2Cl_2]$ (in which ‗thimphen' is a thiophene containing phenanthroline-imidazole ligand synthesised previously in Chapter 3) is also described.

A second type of mononuclear complex is encountered in Chapter 6, which describes the synthetic study of the a ruthenium(II) complex containing the tetradentate ligand bis(2-pyridylmethyl)diiminoethane) (paen) and 4,4'-bipyridyl as a point of surface coordination.

Chapter 7 details major conclusions drawn from the research outlined in Chapters 1-6 as well as setting out a number of different possible routes which future work stemming from this research may take.

1.8 Bibliography

[1] J.G. Vos, J. M. Kelly, *Dalton Trans.*, 2006, 4869

[2] M.W. Cooke, G.S. Hanan, *Chem. Soc. Rev.* 2007, **36**, 1466

[3] L. De Cola, P.Belser; A. von Zelerwsky, F. Vogtle, *Inorg. Chim. Acta,* 2006, **360**, 775

[4] J.H. Alstrum—Acevedo, M.K. Brennaman, T.J. Meyer; *Inorg. Chem.*, 2005, **44**, 6802

[5] L. Sun, L. Hammarström, B. Äkermark, S. Styring; *Chem. Soc. Rev*; 2001, **30,** 36

[6] L. Hammarström; *Curr. Opin. Chem. Bio*., 2003, **7,** 666

[7] S. Bonnet; J.P. Collin, M. Koizumi, P. Mobian, J.P. Sauvage; *Advanced Mater.*; 2006, **18,** 1239

[8] J.P Collin; V Heitz; J.P. Sauvage; *Molec. Mach. Topics in Curr. Chem.,* 2005, **262**, 29

[9] R. Ziessel, M. Hissler, A. El-ghayoury, A. Harriman; *Coord. Chem. Rev,* 1998, **178,** 1251

[10] B. Coe, N. Curati; *Comm. On. Inorg. Chem.,* 2004, **25**, 147

[11] J.N Demas, B.A. DeGraff; *Coord. Chem. Rev.,* 2001, **211**, 317

[12] M.H.S.A. Hamid, P.A. Slatford, J.M.J. Williams, *Adv. Synth. & Cat.,* 2007 **349**, 1555

[13] V. Dragutan, I, Dragutan, L. Delaude, A. Demonceau; *Coord. Chem. Rev.,* 2007, **251**, 765

[14] V. Balzani, A, Juris, M, Venturi, S. Campagna, S. Serroni; *Chem. Rev.*, 1996, **96,** 759

[15] G. Sprintschnik, H. W. Sprintschnik, P. P. Kirsch, D. G. Whitten, *J. Am. Chem. Soc.*, 1976, **98**, 2337

[16] G. Sprintschnik, H.W. Sprintschnik, P. P. Kirsch, D. G.Whitten, *J. Am. Chem. Soc.*, 1977, **99**, 4949.

[17] K. Kalyanasundaram, M. Grätzel, *Angew. Chem., Int. Ed. Engl.*, 1979, **18**, 781.

[18] B. O'Regan, M. Grätzel, *Nature*, 1991, **353**, 737

[19] K. Kalyanasundaram, M.Grätzel, *Coord. Chem. Rev.,* 1998, **177**, 347

[20] A.C. Lees, C. J. Kleverlaan, C. A. Bignozzi, J. G. Vos, *Inorg. Chem.*, 2001, **40**, 5343.

[21] J. Barber, B. Andersson, *Nature*, 1994, **370**, 31

[22] Bignozzi; Schoonover; Scandola; *"Molecular Level Artificial Photosynthetic Materials-Progress in Inorganic Chemistry"*; Volume Editor: Meyer, J, 1997 **44,** 2

[23] S. Rau, D. Walther, J. G. Vos: *Dalton. Trans.*, 2007, 915

[24] R. Konduri, H. Ye, F. M. MacDonnell, S. Serroni, S. Campagna, K. Rajeshwar, *Angew. Chem., Int. Ed.*, 2002, **17**, 3185.

[25] B. Gholamkhass, H. Mametsuka, K. Koike, T. Tanabe, M. Furue, O. Ishatani, *Inorg. Chem.*, 2005, **44**, 2326.

[26] K. Koike, H. Hori, M. Ishizuka, J. R. Westwell, K. Takeuchi, T. Ibusuki, K. Enjouji, H. Konno, K. Sakamoto O. Ishitani, *Organometallics*, 1997, **16**, 5724

[27] H. Ozawa, M.-A. Haga, K. Sakai, *J. Am. Chem. Soc.*, 2006, **128**, 4926.

[28] S. Rau, B. Schäfer, D.Gleich, E. Anders, M. Rudolph, M. Friedrich, H.Görls, W. Henry, J. G. Vos, *Angew. Chem., Int. Ed.*, 2006, **45**, 6215;

[29] M. Elvington, K. J. Brewer, *Inorg. Chem.*, 2006, **45**, 5242.

[30] K. J. Brewer, M. Elvington, US 20060120954A1, 2006.

[31] M. Lundstrom *Science* 2003, **299**, 210

[32] P.J. Low *Dalton Trans.* 2005, 2821

[33] J. M. Tour *Acc. Chem. Res.* 2000, **33**, 791

[34] N. Weibel, S. Grunder, M. Mayor, *Org. Biomol. Chem.* 2007, **5**, 2343

[35] D.M. Cardamone, C. A. Stafford, S. Mazumdar, *Nano Lett.*, 2006, **6**, 2422.

[36] M. Elbing, R. Ochs, M. Koentopp, M. Fischer, C. von Hänisch, F. Weigend, F. Evers, H. B. Weber, M. Mayor, *PNAS*, 2005, **102**, 8815

[37] S. Grunder, R. Huber, V. Horhoiu, M. T. Gonzalez, C. Schönenberger, M. Calame, M. Mayor, *J. Org. Chem.* 2007, **72**, 8337

[38] J. Park, A. N. Pasupathy, J. I. Goldsmith, C. Chang, Y. Yaish, J. R. Petta, M. Rinkoshi, J. P. Sethna, H. D. Abruña, P. L. McEuan, D. C. Ralph, *Nature,* 2002, **417**, 722

[39] K. Nørgaard, T. Bjørnholm, *Chem. Commun.*, 2005, 1812

[40] J-R Koo, S-W. Pyo, J-H Kim, H-K Lee, Y. K. Kim, *Jpn. J. Appl. Phys*., 2005, **44**, *1B*, 566

[41] R.G. Nuzzo, D.L. Allara, *J. Am. Chem. Soc*. 1983, **105**, 4481.

[42] [(a)]A. Ulman, *Chem. Rev.* 1996, **96** 1533 [(b)]L.H. Dubois, R.G. Nuzzo, *Annu. Rev. Phys. Chem.* 1992, **43,** 437 [(c)] F. Schreiber, *Prog. Surf. Sci.* 2000, **65,** 151. [(d)]F.

Schreiber, *J. Phys.: Condens. Matter* 2004, **16**, 881. [(e)]J.C. Love, L.A. Estroff, J.K. Kriebel, R.G. Nuzzo, G.M. Whitesides, *Chem. Rev*. 2005, **105**, 1103.

[43] W.C. Bigelow, D.I. Pickett, W.A. Zisman, *J. Colloid Sci*. 1946, **1,** 513.

[44] R. Maoz, J. Sagiv, J. Colloid *Interf. Sci*. 1984, **100,** 465.

[45] D.K. Aswal, S. Lenfant, D. Guerin, J.V. Yakhmi, D. Vuillaume, *Analytica Chimica Acta*, 2006, **568**, 84

[46] J, Park, A. N. Pasupathy, J. I. Goldsmith, C. Change, Y. Yashi, J. R. Petta, M. Rinkoshi, J. P. Sethna, H. D. Abruna, P. L. McEuen, D. C. Ralph, *Nature*, 2002, **417**, 722.

[47] R. L. Carroll, C. B. Gorman, *Angew. Chem. Int. Ed,* 2002, **41**, 4379

[48] T. Albrecht, A. Guckian, J. Ulstrup, J. G. Vos, *Nano Lett.* 2005, **5**, 1451

[49] T. Albrecht, A. Guckian, A. M. Kuznetsov, J. G. Vos, J. Ulstrup, *J. Am. Chem. Soc.* 2006, **128**, 17132

[50] R. J. Forster, L. R. Faulkner, *J. Am. Chem. Soc.* 1994**, 116**, 5444.

[51] R. J. Forster, E. Figgemeier, A. Lees, J. Hjelm, J. G. Vos, *Langmuir*, 2000, **16**, 7867

[52] R. J. Forster, J. P. O'Kelly, *J. Electrochem. Soc.,* 2001, **148**, 31

[53] S. Serroni, S. Campagna, F, Puntoriero, C. Di Pietro, N.D. McClenaghan, F. Loiseau; *Chem. Soc. Rev.,* 2001, **30**, 367

[54] H. B. Gray *"Chemical Bonds: An Introduction to Atomic and Molecular Structure"(1st ed.)* 1994 University Science Books

[55] D. M. Klassen, G. A. Crosby, *J. Chem. Phys.,* 1968**, 48**, 1853

[56] G. A. Crosby, R. J. Watts, D.W. Carstens, *Science*, 1970, **170**, 1195

[57] B. Durham, J. V. Casper, J. K. Nagle, J. Meyer, *J. Am. Chem. Soc*., 1982, **104**, 4803.

[58] R. Watts, *J. Chem. Ed*., 1983, **60**, 834.

[59] J. V. Casper, T. J. Meyer, *J. Am. Chem. Soc*., 1983, **105**, 5583

[60] N. H. Damrauer, G. Cerullo, A. Yeh, T. R. Boussie, C. V. Shank, J. K. McCusker, *Science*, 1997, **275**, 54

[61] C. Li, M. Z. Hoffman, *Inorg. Chem*., 1998, **37**, 830

[62] J. Van Houten, R. J. Watts, *J. Am. Chem. Soc*., 1975, **97**, 3843

[63] J. N. Demas, G. A. Crosby, *J. Am. Chem. Soc*., 1971, **93**, 2841

[64] J. N. Demas, G. A. Taylor, *Inorg. Chem.,* 1979**, 18**, 3177

[65] E. M. Kober, T. J. Meyer, *Inorg. Chem.,* 1984, **23**, 3877

[66] E. M. Kober, T. J. Meyer, *Inorg. Chem.,* 1982, **21,** 3967.

[67] E. M. Kober, T. J. Meyer, *Inorg. Chem.,* 1983, **22,** 1614.

[68] Kober E. M., Meyer T.J., *Inorg. Chem.,* 1984, **23**, 3877.

[69] A. Guckian, *PhD Thesis*, Dublin City University 2002

[70] M. Gerloch, E. Constable *"Transition metal chemistry : the valence shell in d-block chemistry" (1st ed.)* 1994, Weinheim ; Cambridge

[71] R. Hage, A. H. J. Dijkhuis, J. G. Haasnoot, J. Pron, J. Reedijk, B. E. Buchanan, J. G. Vos, *Inorg. Chem*., 1988, **27**, 2185

[72] B. Parvis, *IEEE transactions on Advanced Packing,* 2003, **26**, 233

[73] A. Blaszczyk, M. Chadim, C. von Hänisch, M. Mayor, *Eur. J. Org. Chem.* 2006 3809

[74] J. Areephong, W. R. Browne, N. Katsonis, B. L. Feringa, *Chem. Commun.* 2006 3930

[75] E. O. Sako, H. Kondoh, I. Nakai, A. Nambu, T. Nakamura, T. Ohta, *Chem. Phys. Lett.,* 2005, **413**, 267

[76] R. Baron, A. Onopriyenko, E. Katz, O. Lioubashevski, I. Willner, S. Wang, H. Tian, *Chem. Commun,* 2006, 2147

[77] Z. Li, B. Han, G. Meszaros, I. Pobelov, Th. Wandlowski, A. Blaszczyk, M. Mayor, *Faraday Discuss.* 2006, **131**, 121

[78] A. Blaszczyk, M. Fischer, C. von Hänisch, M. Mayor, *Helvetica Chimica Acta,* 2006, **89**, 1986

[79] A. Shaporenko, M. Elbing, A. Blaszczyk, C. von Hänisch, M. Mayor, M. Zharnikov, *J. Phys. Chem. B*, 2006, **110**, 4307

[80] A. Blaszczyk, M. Elbing, M. Mayor, *Org. Biomol. Chem.* 2004, **2**, 2722

[81] P. Bertoncello, E. T. Kefalas, Z. Piramenou, P. R. Unwin, R. J. Forster, *J. Phys. Chem. B* 2006, **110**, 10063

[82] R. J. Forster, J. G. Vos, T. E. Keyes, *Analyst*, 1998, **123**, 1905

[83] O. Haas, M.Kriens, J.G. Vos, *J. Am. Chem. Soc.*, 1981, **103**, 1318.

[84] A. Nambu, H. Kondoh, I. Nakai, K. Amemiya, T. Ohta, *Surf. Sci.*, 2003, **530,** 101

[85] S. Tasca, *PhD Thesis,* Dublin City University, 2006

[86] Y. Halpin, *PhD Thesis,* Dublin City University, 2009.

[87] J. H. van Diemen, R. Hage, J.G. Haasnoot, H.E.B. Lempers, J. Reedijk, J.G. Vos, L. DeCola, F. Barigelletti, V. Balzani, *Inorg. Chem.* **1992**, 31, 3518

[88] G. Denti, S. Campagna, S, Serroni, M. Ciano, V. Balzani, *J. Am. Chem. Soc.*, 1992, **144**, 2944

[89] L. Spiccia, G. Deacon, C. Kepert; *Coord. Chem. Rev.* 2004, **248**, 1329

[90] D. Husek, Y. Inoue, S.R.L. Everitt, H. Ishida, M. Kumeda, M.G.B. Drew. *Inorg. Chem.,* 2000, **39**, 308.

[91] L. Cassidy *PhD Thesis* Dublin City University 2008

[92] Y.-Q. Fang, M.I. Polson, G. S. Hanan, *Inorg. Chem.,* 2003, **42**, 5

[93] D. Tzalis, Y. Tor, *J. Am. Chem. Soc*, 1997, **119**, 852

[94] S. J. Dunne, E. C. Constable, *Inorg. Chem. Commun.* 1998, **1**, 167

[95] S. Chodorowski-Kimmes, M. Beley, J. P. Collin, J. P. Sauvage, *Tet. Lett.*, 1996, **37**, 2963

[96] C. Di Pietro, S. Serroni, S. Campagna, M. T. Gandolfi, R. Ballardini, S. Fanni, W. R. Browne, J. G. Vos, *Inorg. Chem*., 2002, **41**, 2871

[97] S. Fanni, C. Di Pietro, S. Serroni, S. Campagna, J.G. Vos, *Inorg. Chem. Comm*., 2000, **3**, 42

[98] J. Wang, Y-Q, Fang, G. S. Hanan, F. Loiseau, S. Campagna, *Inorg. Chem.,* 2005, **45**, 5

[99] S. Yano, J. M. Kato, J. K. Tsukahara, M. Sato, J. T. Shibahara, K. Lee, Y. Sugihara, M. Iida, K. Goto, S. Aoki, Y. Shibahara, H. Nakahara, S. Yanagisawa, H. Miyagawa, *Inorganic Chemistry,* 1994, **33**, 5030

[100]A. García-Fernández, J. Díez, M. P. Gamasa, E. Lastra, *Inorganic Chemistry*, 2009, **48**, 2471

Chapter 2: General Instrumental and Synthetic Methods

Abstract

This chapter details the instrumental methods used for the identification of the compounds synthesised hereafter. The methods of characterization used to detail the properties of these compounds are mass spectrometry, ^{1}H-NMR and elemental analysis while UV-Visible absorption and emission were recorded to detail the properties of these compounds. HPLC information has also been used to describe the relative purity of reaction mixtures, and also to monitor several reactions' progress. As a result the systems used are described in this chapter.

The syntheses for starting materials used in further chapters are also detailed.

2.1 Instrumental Methods

2.1.1 Structural Characterisation

Nuclear Magnetic Resonance (NMR) Spectroscopy

^{1}H NMR (400 MHz) spectra were obtained on a Bruker Advance 400 NMR Spectrometer in deuteriated solvents with either TMS or residual solvent peaks as reference. Free induction decay (FID) profiles were processed using an XWIN-NMR software package. 2-D correlated spectroscopy (COSY) experiments performed involved the accumulation of 128 FIDs of 16 scans. In certain cases, usually for samples of weak concentration, ^{1}H NMR spectra (600 MHz) were obtained on a Bruker Advance 600 NMR Spectrometer, again in deuterated solvents with either TMS or residual solvent peaks as reference. Any 600 MHz spectra included in this report are highlighted as such. The solvent used for metal complexes was mainly deuterated acetonitrile, acetone or dimethyl sulphoxide. Deuterated dimethyl sulphoxide and chloroform were used for ligands.

Mass Spectrometry

Mass spectrometry was recorded with a Bruker-EsquireLC_00050 with the assistance of Mr. Damien McGuirk. This system is an electrospray ionization mass spectrometer which record spectra at positive polarity with cap-exit voltage of 167 V. Spectra were recorded in the scan range of 50-2200 m/z with an acquisition time of between 300 and 900 μs and a potential of between 30 and 70 V. Each spectrum was recorded by the summation of 20 scans. ESI is a soft ionization technique, resulting in protonated, sodiated species in positive ionisation mode.

Elemental Analysis

Carbon, hydrogen and nitrogen (CHN) elemental analyses were carried out on an Exador Analytical CE440 by the Microanalytical Department, University College Dublin.

Ultra Violet/Visible Spectroscopy (UV/Vis)

UV−vis absorption spectra were recorded on a Shimadzu 3100 UV-vis/NIR instrument with 1 cm quartz cells interfaced with an Elonex-466 PC using UV-vis data manager software. Measurements were carried out in aerated spectroscopic grade CH_3CN. Absorption maxima are ±2 nm with molar absorptivities ±10 %.

Emission spectra

Emission spectra at room temperatures were obtained in spectroscopic grade solvents on a Perkin-Elmer LS50B luminescence spectrometer equipped with a red sensitive Hamamatsu R928 detector: this was interfaced with an Elonex-466 PC using Windows based fluorescence software. Measurements at room temperature were carried out in 1 cm quartz cells. The error associated with the emission spectra is ±5 nm.

Acid-Base Titration Data

pH titration was employed to determine the ground and excited state pK_as which were carried out in Britton-Robinson buffer (0.04 M boric acid, 0.04 M acetic acid, 0.04 M phosphoric acid) and monitored by UV-vis spectroscopy using a Jasco V-670 spectrophotometer. The pH was adjusted by adding concentrated NaOH or concentrated H_2SO_4 and measured using a Corning 240 digital pH meter, the error associated with which is ±0.005 pH units.

HPLC Analysis

HPLC chromatography was carried out using a Varian Prostar photodiode array HPLC system along with Varian Star software, a Varian 230.01 pump, a 20 μl injector loop and strong cation exchange Luna SCX column (25 cm x 4.6 nm). A mobile phase of 75: 20: 5 acetonitrile: water: methanol 0.1M KNO_3 was used, with all solvents used being of HPLC grade.

2.2 General Synthetic Materials

Column chromatography was performed using neutral activated aluminum oxide (150 mesh) or silicon oxide (35–70 μm).

All synthetic reagents were of commercial grade and no further purification was employed. The compounds 2,2'-bipyridine (bpy) and $[RuCl_3].xH_2O$ were purchased from Aldrich and used without further purification

2.2.1 Synthesis of Starting Materials

Synthesis of Ligands

Preparation of 1,10-phenanthroline-5,6-dione

This ligand was synthesised using an established literature approach[6].1.00 g (5.04 mmol) 1,10-phenanthroline and 5.10 g (50 mmol) sodium bromide was stirred at 5^0C. 20 cm^3 cold concentrated sulphuric acid was added to the reaction mixture followed by 10 cm^3 concentrated nitric acid, added dropwise along the sides of the flask. The resulting solution was cooled to room temperature and heated to boiling point until the bromine vapours were eliminated. The reaction mixture was cooled to room temperature and poured onto 400 cm^3 ice cold water. The solution was made neutral by the addition of potassium bicarbonate and extracted with dichloromethane. The solvent was removed from the organic phase *in vacuo* to yield 1,10-phenantholine-5,6-dione as a yellow powder.

Yield: 0.98 g (88%) ^{1}H NMR ($CDCl_3$): 9.13 (d, H), 8.55 (d, H), 7.60 (t, 2H).

Synthesis of Deuterated Ligands

Where appropriate the deuterated analogues of peripheral ligands have been synthesised in order to obtain simplified spectra of metal complexes. The most useful of this type of ligand is deuterated 2,2'-bipyridyl. The synthesis for a second compound is also shown below.

All deuteriation reactions were carried out using a Teflon Cup contained in a general purpose dissolution Bomb P/N 4744 from Scientific Medical products. Percentage deuteration was determined by comparison of the ^{1}H NMR spectra of analogous deuterated and non-deuterated compounds as described in section 2.2.3.

d_8-2,2'-bipyridyl

This ligand was synthesised using an established literature approach[7]

2g (12.8 mmol) 2,2'-bipyridine was placed in 20 cm^3 D_2O with 50 mg 10% Pd/C catalyst and heated to 200^0C in the set-up outlined above for 3 days. The system was cooled and the mixture was filtered. The catalyst was washed with 2 x 50 cm^3 diethyl ether to remove any residual deuterated material. The aqueous filtrate was extracted with CH_2Cl_2 and the organic extract and ether washings were evaporated to dryness to yield the deuterated product.

In order to obtain a high level of deuteration this procedure was repeated twice for the same sample.

Yield: 1.58 g (75%)

Percentage deuteration: 99%

Synthesis of Metal Complex Starting Materials

cis-$[Ru(bpy)_2Cl_2].2H_2O$

This procedure has been modified slightly to that described by Meyer *et al.* [8]

A suspension containing $RuCl_3.3H_2O$ (3.90 g, $1.5x10^{-2}$ mol), 2, 2' bipyridine (4.68g, $3x10^{-2}$ mol) and LiCl (4.30 g, 0.10 mol) was heated at reflux in dimethylformamide (25 cm^3). After 8 hours the mixture was allowed to cool to room temperature and 125 cm^3 of acetone was added. This was left at 0^0C for 24 hours. The resulting violet precipitate was filtered and the isolated solid washed with water until the filtrate was no longer coloured. The solid was washed with diethyl ether and dried to yield 6.11 g microcrystalline solid.

Yield: 6.11 g, 87%

^{1}H NMR (d^{6}-DMSO, 298K) δ; 10.00 (2H, d), 8.65 (2H, d), 8.48 (2H, d), 8.05 (2H, t), 7.75 (2H, t), 7.65 (2H, t), 7.5 (2H, d), 7.1 (2H, d).

cis-[Ru(d_8-bpy)$_2$Cl$_2$].2H$_2$O

This procedure has been modified slightly to that described for the non-deuterated analogue, by Meyer *et al.* [8]

A suspension containing $RuCl_3.3H_2O$ (3.90 g, $1.5x10^{-2}$ mol), d_8-2, 2' bipyridine (4.68 g, $3x10^{-2}$ mol) and LiCl (4.30 g, 0.10 mol) were heated at reflux in dimethylformamide (25 cm^3). After 8 hours the mixture was allowed to cool to room temperature and 125 cm^3 of acetone was added. This was left at 0^0C for 24 hours. The resulting violet precipitate was filtered and the isolated solid washed with water until the filtrate was no longer coloured. The solid was washed with diethyl ether and dried to yield 5.79 g microcrystalline solid.

Yield: 5.79 g, 80 %

cis-[Os(bpy)$_2$Cl$_2$].2H$_2$O [9]

K_2OsCl_6 (300 mg, 0.6 mmol) and 2,2'-bipyridine (203 mg, 1.31 mmol) were heated to reflux in 3 cm^3 ethylene glycol with constant stirring. The resulting solution was allowed to cool to room temperature and 5 cm^3 of a saturated aqueous solution of sodium dithionite ($Na_2S_2O_4$) was added. The resulting solid was isolated by filtration and washed with water until the filtrate was colourless. The solid was further washed with diethyl ether and placed in a desiccator overnight.

Yield: 283 mg, 80%

^{1}H NMR (d^{6}-DMSO, 298K) δ; 9.61 (2H, d), 8.50 (2H, d), 8.35 (2H, d), 7.61 (2H, dd), 7.55 (2H, dd), 7.30 (4H, m), 6.80 (2H, dd).

cis-[Os(d_8-bpy)$_2$Cl$_2$].2H$_2$O

This procedure has been modified slightly to that described for the non-deuterated analogue.[9]

K_2OsCl_6 (500 mg, 1.04 mmol) and d_8-2,2' bipyridine (340 mg, 2.18 mmol) were heat to reflux in 3 cm^3 ethylene glycol with constant stirring. The resulting solution was allowed to cool to room temperature and 5 cm^3 of a saturated aqueous solution of sodium dithionite ($Na_2S_2O_4$) was added. The resulting solid was isolated by filtration and washed with water until the filtrate was colourless. The solid was further washed with diethyl ether and placed in a dessicator overnight.

Yield: 326 mg, 53%

[Ru(bpy)$_2$(phen)](PF$_6$)$_2$

0.346 g (1.9 mmol) 1,10-phenanthroline and 0.75 g (1.6 mmol) Ru(bpy)$_2$Cl$_2$.2H$_2$O were refluxed in 30 cm^3 2:1 ethanol: water for 5 hr. The ethanol was removed from the solution by rotary evaporation, and the resulting mixture was allowed to cool to room temperature. A saturated aqueous solution of NH_4PF_6 was added and the mixture was filtered yielding an orange solid which was then recrystallised from CH_3CN: H_2O 50:50.

Yield: 1.04 g, 75%

^{1}H NMR: ^{1}H DMSO δ: 8.88-8.79 (m, 6H), 8.39 (s, 2H), 8.22 (t, 2H), 8.15-8.09 (m, 4H), 7.70-7.57 (m, 4H), 7.36 (t, 2H)

[Os(bpy)$_2$(phen)](PF$_6$)$_2$

300 mg (0.51 mmol) [Os(bpy)$_2$Cl$_2$].2H$_2$O and 110 mg (0.61 mmol) 1,10-phenanthroline was refluxed in 20 cm^3 ethylene glycol for 4 hr. This mixture was cooled to room temperature and was added to 150 cm^3 saturated aqueous NH_4PF_6 solution. This mixture was refrigerated at 5^0C overnight and filtered and the resulting solid was recrystallised from CH_3CN: H_2O 50:50.

Yield: 371 mg, 73%

^{1}H NMR: ^{1}H DMSO δ: 8.86-8.80 (m, 4H), 8.58 (d, 2H), 8.37 (s, 2H), 8.06-7.99 (m, 4H), 7.90 (t, 2H), 7.84-7.80 (m, 2H), 7.76 (d, 2H), 7.50-7.45 (m, 4H), 7.24 (t, 2H,)

$[Ru(phen)_2(bpy)](PF_6)_2$

500 mg (0.94 mmol) $[Ru(phen)_2Cl_2.]2H_2O$ and 175 mg (1.13 mmol) 2,2'-bipyridyl were refluxed in 15 cm^3 2:1 ethanol: water for 3 hr. The resulting mixture was cooled to room temperature and the ethanol was removed in vacuo. A saturated solution $KPF_{6\ (aq)}$ was added to precipitate the product, which was removed by vacuum filtration. The resulting solid was recrystallised from acetone: water.
Yield: 72% (598 mg)
^{1}H NMR: ^{1}H d_6-acetone δ: 8.75-8.72 (m, 4H), 8.62 (d, 2H), 8.44 (d, 2H), 8.32-8.26 (q, 4H), 8.15 (d, 2H), 8.07 (t, 2H), 7.92 (d, 2H), 7.88-7.85 (m, 2H), 7.64-7.60 (m, 2H), 7.33 (t, 2H)

$[Ru(phen)_2(dmbpy)](PF_6)_2$

300 mg (0.53 mmol) $[Ru(phen)_2Cl_2.]2H_2O$ and 117 mg (0.63 mmol) 4,4'-dimethyl-2,2'-bipyridine were refluxed in 20 cm^3 2:1 ethanol: water for 3 hr. The resulting mixture was cooled to room temperature and the ethanol was removed in vacuo. A saturated solution $KPF_{6\ (aq)}$ was added to precipitate the product, which was removed by vacuum filtration. The resulting solid was recrystallised from acetone: water.
Yield: 83% (428 mg)
^{1}H NMR: ^{1}H d_6-acetone δ: 8.86 (d, 2H), 8.75-8.73 (m, 4H), 8.57 (d, 2H), 8.45-8.38 (q, 4H), 8.27 (d, 2H), 8.02-7.98 (m, 2H), 7.83 (d, 2H) 7.76-7.72 (m, 2H), 7.30 (d, 2H)

$[Ru(phen)_2(Mepytr)](PF_6)$

500 mg (0.94 mmol) $[Ru(phen)_2Cl_2.]2H_2O$ and 169 mg (1.06 mmol) 2-methyl-2'-pyrid-2-yl-triazole were refluxed in 20 cm^3 2:1 ethanol: water for 3 hr. The resulting mixture was cooled to room temperature and the ethanol was removed in vacuo. A saturated solution $KPF_{6\ (aq)}$ was added to precipitate the product, which was removed by vacuum filtration. The resulting solid was recrystallised from acetone: water.
Yield: 65% (541 mg)
^1H NMR: ^1H d_6-acetone δ: 8.76-8.73 (m, 2H), 8.67 (d, 1H), 8.60 (d, 1H), 8.37-8.28 (m, 5H), 8.09 (d, 1H), 8.05-7.88 (m, 6H), 7.78-7.70 (m, 1H), 7.64-7.60 (m, 1H), 7.44 (d, 2H), 7.11 (t, 1H), 1.12 (s, 3H)

$[Ru(phen)_2(Ppytr)](PF_6)$
500 mg (0.94 mmol) $[Ru(phen)_2Cl_2.]2H_2O$ and 236 mg (1.06 mmol) 2-phenyl-2'-pyrid-2-yl-triazole were refluxed in 20 cm^3 2:1 ethanol: water for 3 hr. The resulting mixture was cooled to room temperature and the ethanol was removed in vacuo. A saturated solution $KPF_{6\ (aq)}$ was added to precipitate the product, which was removed by vacuum filtration. The resulting solid was recrystallised from acetone: water.
Yield: 76% (674 mg)
^1H NMR: ^1H d_6-acetone δ: 8.77-8.74 (m, 2H), 8.69 (d, 1H), 8.64 (d, 1H), 8.39-8.30 (m, 5H), 8.16-8.10 (m, 4H), 8.04 (d, 1H), 8.01-7.94 (m, 3H), 7.83-7.80 (m, 2H), 7.76-7.72 (m, 1H), 7.69-7.66 (m, 1H), 7.48 (d, 1H), 7.31-7.28 (m, 2H), 7.25-7.23 (m, 1H), 7.18-7.14 (m, 1H)

Synthesis of $[Ru(phen)_2(bpt)](PF_6)$
This complex was synthesised according to a modified literature approach[10]. 416 mg (1.87 mmol) 2,2'-bipyrid-2-yl-triazole was heated to reflux in 20 cm^3 2:1 ethanol: water. 500 mg (0.94 mmol) $[Ru(phen)_2Cl_2.]2H_2O$ in 10 cm^3 2:1 ethanol: water was added slowly to the reaction mixture over 45 min. The reaction mixture was then heated at reflux for 5 hr. The resulting mixture was evaporated to dryness and redissolved in 15 cm^3 water. One drop conc. NH_4OH was added to the solution before the metal complex

was precipitated through addition of a saturated solution $KPF_{6\ (aq)}$. The resulting solid was removed from the mixture by vacuum filtration and the collected solid purified by column chromatography on neutral alumina using acetonitrile as eluent. The principal red band was collected and the solvent removed *in vacuo.* The resulting solid was recrystallised from acetone: water.

Yield: 46% (346 mg)

^{1}H NMR: ^{1}H d_6-acetone δ: 8.75-8.66 (m, 3H), 8.60 (d, 1H), 8.56 (d, 1H), 8.39-8.36 (m, 5H), 8.25-8.19 (m, 4H), 8.02-7.90 (m, 5H), 7.78-7.74 (m, 2H), 7.70 (t, 1H), 7.69-7.66 (m, 1H), 7.18-7.14 (m, 2H)

2.2.2 ^{1}H NMR of Deuterated Ligands

^{1}H NMR is the primary tool used in this report to determine the percentage deuteration of treated ligands as well as a measure of the samples' purity.

The spectrum for d_8-bpy is an illustrative example for the effect of deuteration on a sample's ^{1}H NMR spectrum.

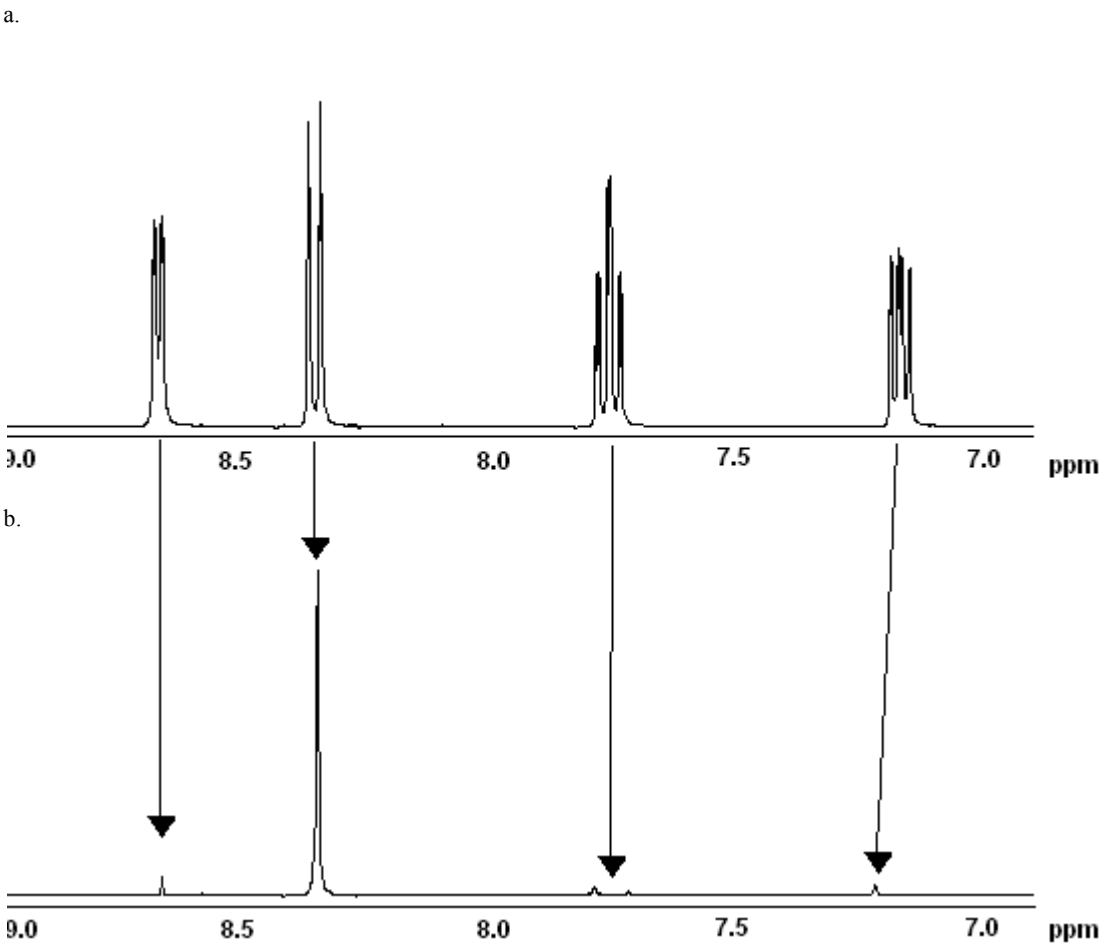

Figure 2.1: ^{1}H NMR spectra of (a) 2,2'-bipyridyl and (b) d_8-2,2'-bipyridyl measured in d_6-DMSO

As can be seen in Figure 2.1 each of the bpy signals collapses to a singlet and decreases dramatically in intensity with respect to the DMSO peak (which is kept constant and integrated as a standard amount in both spectra).

For NMR analysis an equal mass of both the deuterated and non-deuterated samples are prepared in equal volumes of solvent. As the amount of DMSO is kept constant in both spectra and all sample peaks are integrated with respect to the solvent peak the percentage deuteriation may be calculated as the difference between two corresponding

integrations taken as a fraction of the non-deuterated integration of the peak in question, as shown below in equation (7).

$$\frac{\text{(Integration non-deut. peak-Integration deut. peak)}}{\text{Integration non-deut. Peak}} \times \frac{100}{1} = \%\ \text{Deuteriation} \quad (1)$$

2.3 Bibliography

[1] A. E. Kaifer, M. Gomez-Kaifer, *Supramolecular Electrochemistry*, Wiley-VCH, Weinheim, Germany, 1999

[2] V. V. Pavlishchuk, A. W. Addison, *Inorg. Chim. Acta*, 2000, **298**, 97

[3] S. Rau, B. Schafer, A. Grussing, S. Schebeta, K. Lamm, J. Vieth, H. Gorls, D. Walther, M. Rudolph, U. W. Grummt, E. Birkner, *Inorg. Chim. Acta.*,, 2004, **357**, 4496

[4] M. A. Bennett, G. Wilkinson, *Chem. Ind*., 1959, 1516

[5] T. B. Hadda, H. Le Bozec, *Polyhedron,* 1988, **7**, 575

[6] K.R. Rupesh, S. Deepalatha, M. Krishnaveni, R. Venkatesan, S. Jayachandran, European Journal of Medicinal Chemistry, 2006, **41**, 1494

[7] W. R. Browne, C. M. O'Connor, J. S. Killeen, A. L. Guckian, M. Burke, P. James, M. Burke, J. G. Vos, *Inorg. Chem.,* 2002, **41**, 4245

[8]B. P. Sullivan, D. J. Salmon, T. J. Meyer, *Inorg. Chem.,* 1978, **17**, 3334

[9]P. Lay, A.M. Sargeson, H. Taube, M. H. Chou, C. Creutz, *Inorg. Syn.*, 1986, 24, *John Wiley and Sons (Publishers)*

[10] L. Cassidy, *PhD Thesis,* Dublin City University, 2008

Chapter 3: Synthesis and Characterisation of Novel $[M(bpy)_2(imphen)]^{2+}$ Type Metal Complexes

Abstract:

*Chapter 3 describes the synthesis of novel mononuclear metal complexes using the conventional "complexes as metals / complexes as ligands" strategy (**direct synthesis**) as well as a different "on-the-complex" approach (**indirect synthesis**). The complexes described in this chapter have been synthesised as prototypes for molecular transistors. They incorporate a 'surface active' group, allowing for monolayer formation on electrode surfaces.*

The chapter includes characterisation of the complexes synthesized using mass spectrometry, nuclear magnetic resonance, deuteration, UV/vis spectroscopy and elemental analysis. The absorbance and emission properties of the ruthenium complexes synthesised under varying pH conditions are also investigated.

3.1 Introduction

As mentioned in chapter 1, electronic constructions of greater and greater structural intricacy are required in order to meet with the demand for faster, smaller, more efficient machines.

Moore‟s law predicts not only the miniturization of electronics currently in use[1], it has also predicted the insustainable nature of the current technology used for electronics manufacture and fabrication. Photolithography, the technology used to manufacture computer chips currently has been refined to construct structures smaller than 100 nanometers, but the processes used are very difficult, expensive and inconvenient. The technology faces two main limitations. The first is that the shortest wavelength of ultraviolet light currently used in production processes is about 190 nanometers. Trying to make structures smaller than half of that spacing is like trying to read print that is too tiny: diffraction causes the features to blur and meld together. The second limitation follows on from the first: because it is technically difficult to make such small structures using light, it is also very expensive to do so. The photolithographic tools that will be used to make chips with features below 100 nanometers will each cost tens of millions to hundreds of millions of dollars[2]

Molecular units may be considered as an elegant alternative to this methodology[3, 4] with atoms being used to construct nanometer-sized structures that may then be arranged further to form circuitry.[4] A number of molecular device prototypes have been proposed including molecular diodes[5], molecular switches[6], molecular transistors[7] and approaches to circuits incorporating these elements[8]. The main limitation encountered in single molecule devices is that they often can only be brought to operate at cryogenic temperatures and/or at high vacuum.[5, 7] However, it is imperative that these components operate at room temperature and under condensed matter conditions in order to be useful for practical applications. It has emerged that a class of compounds capable of surmounting these limitations may exist within the realm of transition metal chemistry. A series of mononuclear osmium polypyridine metal complexes have been reported which display transistor-like behaviour (redox switching and amplification) at a near single molecule level.[9] These systems, consisting of a monolayer of the complex in question on a gold or platinum surface operate at room temperature and under condensed matter conditions and so are perfect model compounds for synthesis of novel molecular electronics prototypes.

In this chapter a series of new complexes expected to display transistor type properties are introduced. These mononuclear complexes contain pyridine and thiophene groups for surface coordination and have been spectroscopically characterised and investigated electrochemically for monolayer formation. Two different methods of synthesis were developed for effective preparation of the complexes: one consisting of a direct „complexes as metals/complexes as ligands" type strategy, the other involving synthesis of the ligand in question „on the complex". Reaction schemes illustrating these methods are shown below in Figure 3.1

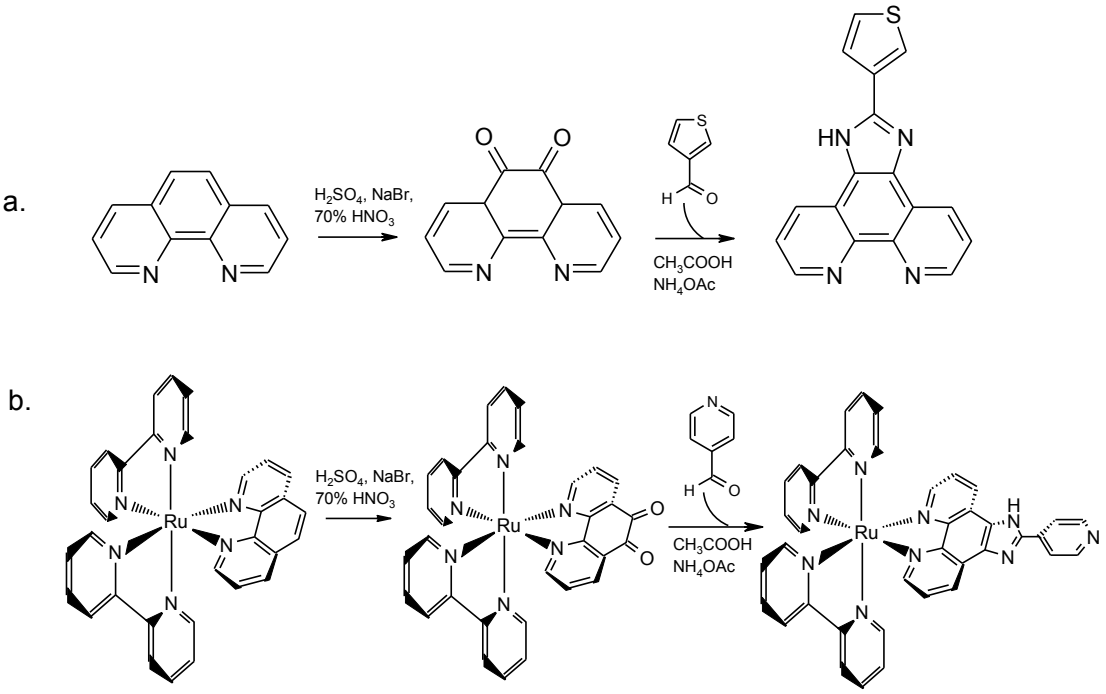

Figure 3.1: Reaction scheme for formation of the ligand 'thimphen' (a) and the reaction scheme for the formation of the ligand 'pyrphen' on a ruthenium complex

The reason for developing these two separate methods of synthesis is based around ligand stability. The ligand shown above in Figure 3.1 (a), thimphen, was synthesised successfully in high yield and then coordinated to the appropriate metal centre. However, upon attempting this reaction for the pyridine analogue of this ligand (pyrphen) a number of synthetic challenges were encountered, the main result of which being that the free ligand pyrphen could not be successfully synthesised. Instead the indirect approach shown above in Figure 3.1 (a) was devised, proving to be successful. Although the imidazole formation shown in Figure 3.1 (b) has not been attempted on a ruthenium complex to date, the starting material [Ru(bpy)$_2$(phendione)]$^{2+}$ has been used by other groups in similar „on complex" type

reactions. Ohno *et al* have synthesised both the mononuclear complex $[Ru(bpy)_2(tpbpz)]^{2+}$ and the dinuclear metal complex $[Ru(bpy)_2(tpbpz)Os(bpy)]^{2+}$ (as shown below in Figure 3.2) using $[Ru(bpy)_2(phendione)]^{2+}$ as a starting material[10].

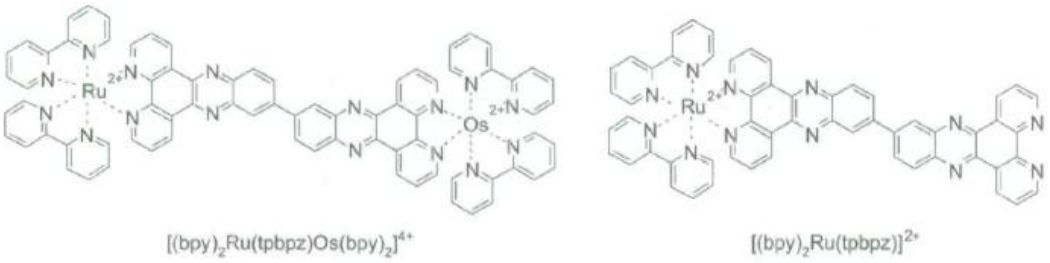

Figure 3.2: Structures of $[Ru(bpy)_2(tpbpz)]^{2+}$ and $[Ru(bpy)_2(tpbpz)Os(bpy)]^{2+}$ as synthesised on the complex from the starting material $[Ru(bpy)_2(phendione)]^{2+}$

Turro and workers have also employed this approach to synthesise a series of mononuclear ruthenium complexes suitable for DNA intercalation.[11] The ligands which were built up from the dione group present on the starting material $[Ru(bpy)_2(phendione)]^{2+}$ are shown below in Figure 3.3.

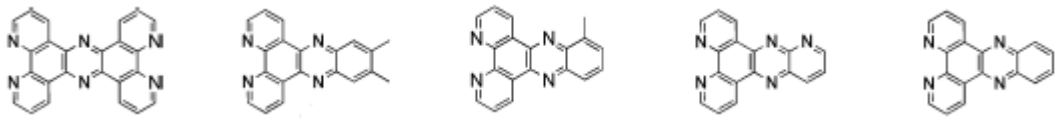

Figure 3.3: Ligands which were built 'on the complex' by modification of the dione group present in the starting material $[Ru(bpy)_2(phendione)]^{2+}$ by Turro et al[11]

Koike et al have also synthesised a series of similar complexes in the same way, this time for photosensitisation of nanocrystalline TiO_2.[12] The complexes synthesised in this work are shown below in Figure 3.4.

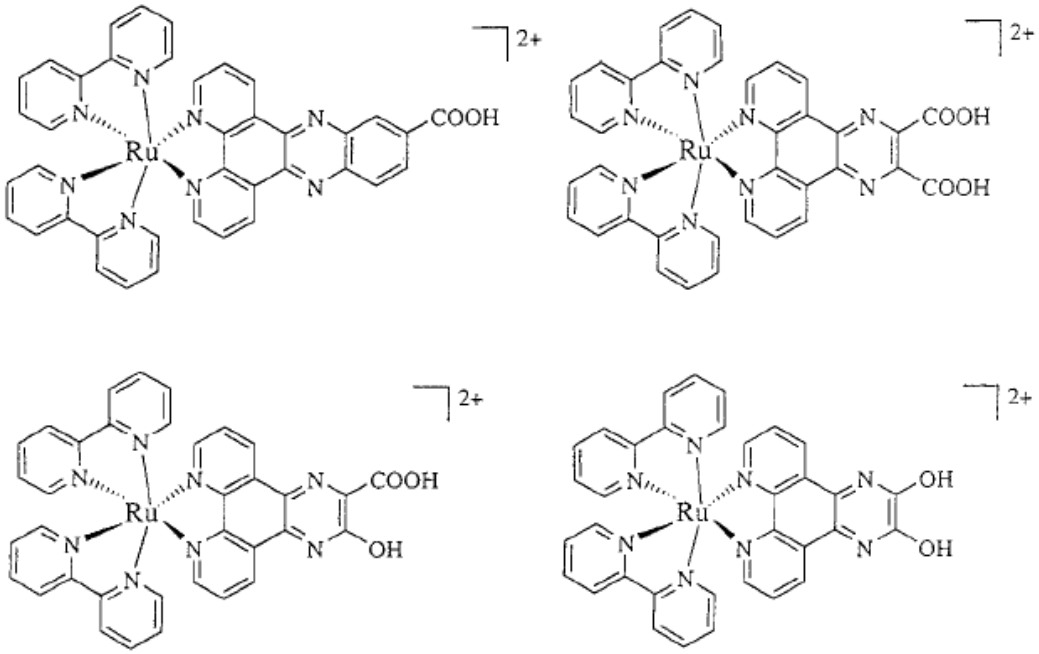

Figure 3.4: Structures of the ruthenium bis-bipyridyl complexes synthesised by Koike et al by modification of the precursor $[Ru(bpy)_2(phendione)]^{2+}$ (reference 12)

This approach was also used in the synthesis of a series of ruthenium polypyridyl complexes for anticancer studies. The synthesised compounds showed selective cytotoxicity against certain cancer types and also showed greater efficiency than cis-platin. The structures of the ligands built up on the complex using $[Ru(bpy)_2(phendione)]^{2+}$ as a precursor are shown in Figure 3.5 below.[13]

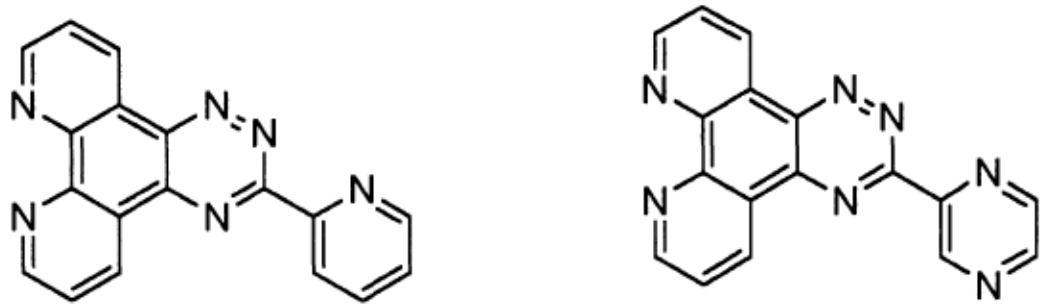

Figure 3.5: Structures of the ligands built up on the complex for anticancer studies using $[Ru(bpy)_2(phendione)]^{2+}$ as a precursor

Section 3.2 discusses the differences in and reasons for the two different synthetic approaches taken to synthesise the target compounds shown below in Figure 3.6.

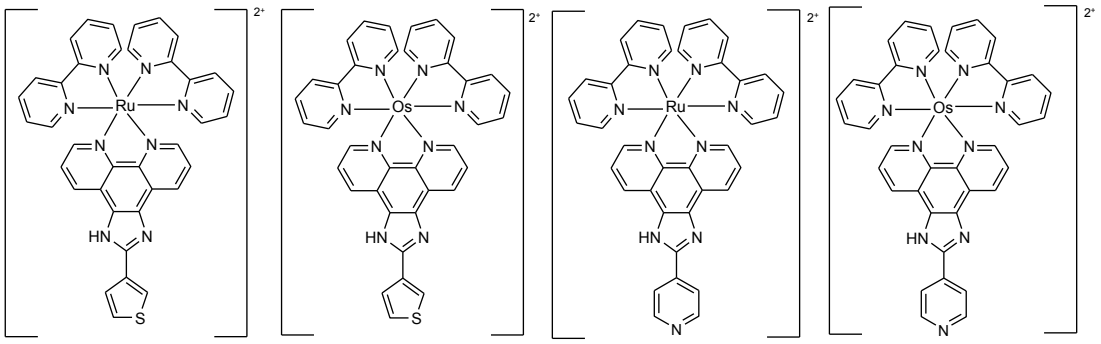

Figure 3.6: Target mononuclear complexes in this chapter. From left to right: $[Ru(bpy)_2(thimphen)]^{2+}$, $[Os(bpy)_2(thimphen)]^{2+}$, $[Ru(bpy)_2(pyrphen)]^{2+}$, $[Os(bpy)_2(pyrphen)]^{2+}$

3.2. Results and Discussion

The approaches taken to synthesize the novel metal complexes suggested in section 3.1 are outlined hereafter along with characterisation of the novel ligands and complexes constructed.

3.2.1 Synthetic Considerations

The synthesis of the mononuclear complexes $[Ru(bpy)_2(thimphen)]^{2+}$ and $[Os(bpy)_2(thimphen)]^{2+}$ are shown schematically in Figure 3.7 below.

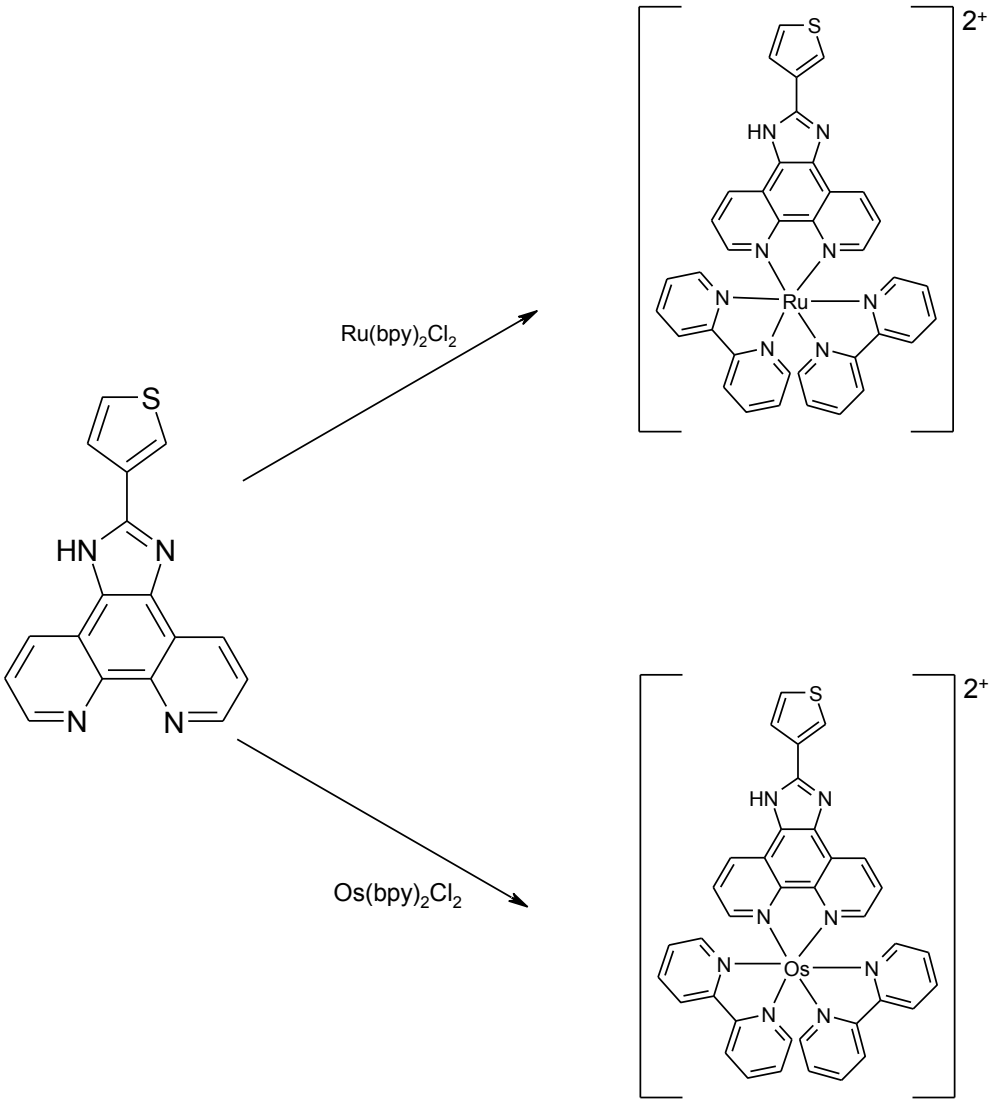

Figure 3.7: Formation of $[Ru(bpy)_2(thimphen)]^{2+}$ and $[Os(bpy)_2(thimphen)]^{2+}$

The ligand shown in Figure 3.7 was synthesised in acceptable yield using a modified literature procedure[14]. This procedure details a multistep synthesis firstly involving a Schiff base formation between the phenanthroline dione moiety and ammonium acetate. The imidazole is then formed from the resulting diimine and the suitable aldehyde. The reaction mechanism is shown in *Figure 3.8*

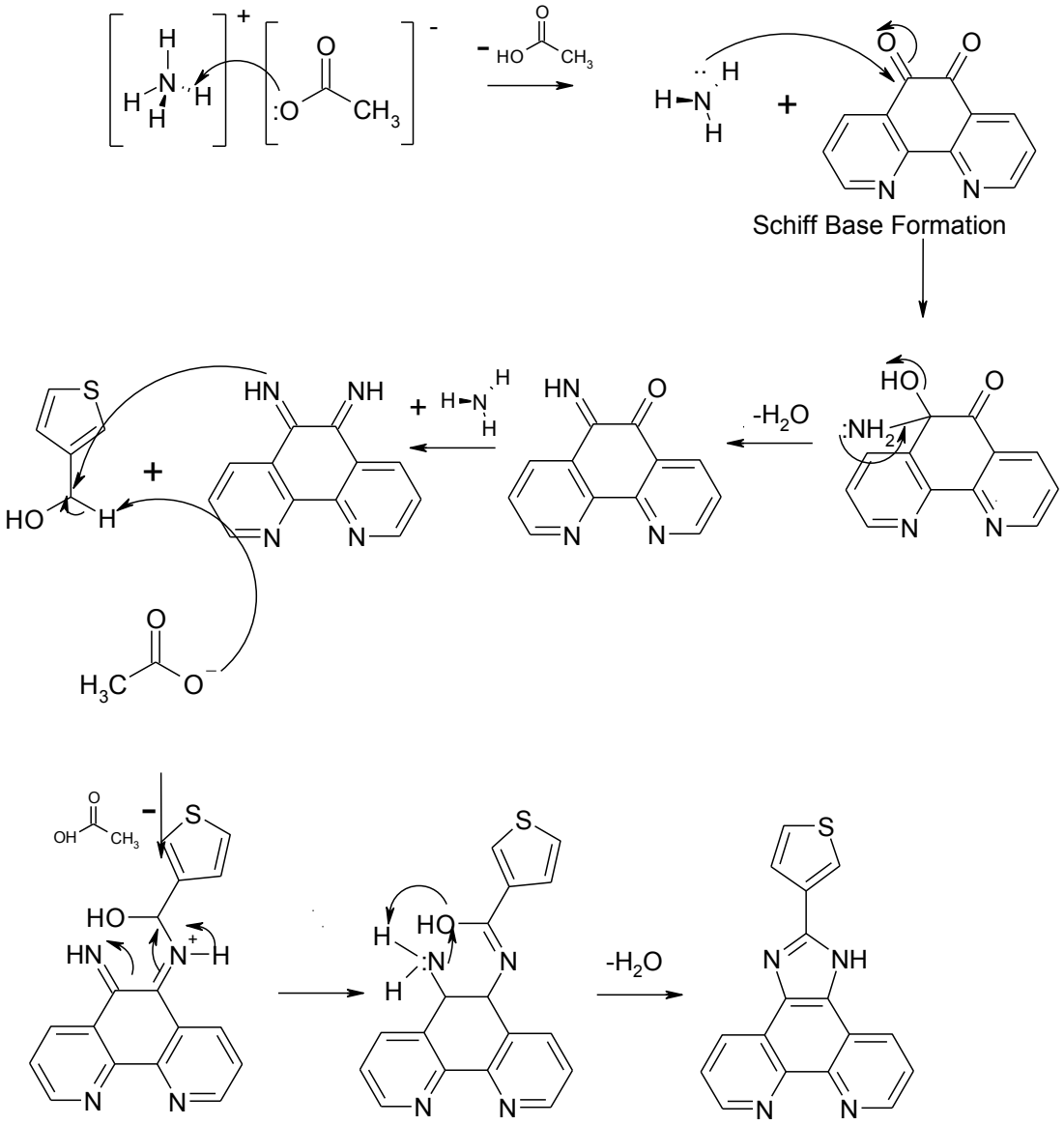

Figure 3.8: Reaction mechanism for the formation of thimphen [15]

The ligand was then reacted with the appropriate ruthenium or osmium bipyridyl precursor to yield the complexes shown in Figure 3.7. This method follows the well-established complexes as metals/complexes as ligands strategy.[16] This method involves heating the metal bipyridyl precursor at reflux (e.g. $[Ru(bpy)_2Cl_2].2H_2O$) in a slight excess of the ligand to be coordinated in a suitable solvent (for ruthenium a mixture of ethanol and water is usually sufficient, but for osmium higher reaction temperatures are needed, therefore ethylene glycol is more suitable). The resulting complexes were purified using column chromatography.

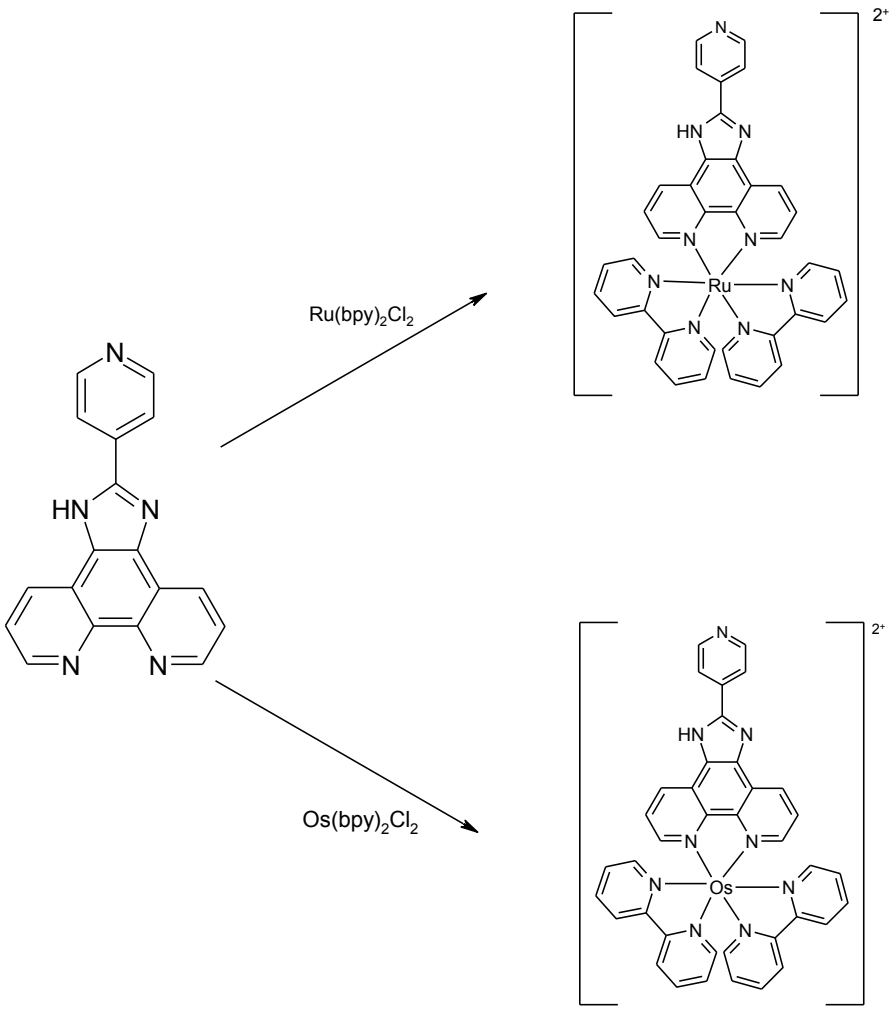

Figure 3.9: Proposed formation of $[Ru(bpy)_2(pyrphen)]^{2+}$ and $[Os(bpy)_2(pyrphen)]^{2+}$

As thimphen had been synthesised with relative ease, it was assumed that the corresponding pyridine analogue could be synthesised in a similar manner. However, when this synthesis was attempted using the same conditions, the desired ligand was not formed following neutralisation of the cooled reaction mixture as for thimphen[15]. Instead a yellow solid precipitated from the reaction solution before completion of the reaction time employed for the synthesis of thimphen (*c.f.* Section 3.4). The ^{1}H NMR of the product obtained displayed four doublets of equal intensity, contrasting starkly with the five signal ^{1}H NMR expected. The predicted spectrum should also include a triplet corresponding to H_3 and H_8 of the phenanthroline moiety. These ^{1}H NMR results are shown and discussed in Section 3.3.2

A number of different reaction conditions for the synthesis of pyrphen were tested and are shown in Table 3.1

Exp.	**Equivalents** (aldehyde:dione :acetate)	**Solvent**	**Reaction Time**	**Solvent Dried**	**Reference**	**Successful**
1	1:1:2.5	Acetic Acid	5 hrs	No	14	No
2	1:1:30	Acetic Acid	3 hrs	No	17	No
3	1:1:2.5	Ethanol	3 hrs	No	18	No
4	1:1:20	Acetic Acid	1.5 hrs	Yes	19	No
5	1:1:20	Acetic Acid	1 hr	Yes	8 (modified)	Yes

Table 3.1: Attempted syntheses for pyrphen ligand

The ^{1}H NMR spectrum obtained for reaction 4 showed a mixture of components, one appearing to be the desired product (displaying four doublets and a triplet all of equal intensity). This indicated that decreasing the reaction time further as well as using dry glacial acetic acid could yield the desired product.

Reaction 5 as shown in Table 3.1 was attempted on a 100 mg scale, and was found to have a yield of 25%. Attempts were then made at increasing the scale of the reaction, a summary of which is shown below in Table 3.2.

Experiment	**Scale (dione starting material)**	**Solvent Volume**	**Successful**	**Yield**
6	100 mg	4 cm^3	Yes	25%
7	200 mg	6 cm^3	Yes	29%
8	1 g	20 cm^3	No	-
9	500 mg	8 cm^3	No	-

Table 3.2: Summary of attempts at scale-up of pyrphen synthesis

Pyrphen synthesis was found to be effective only on a 100-200mg scale. Also small amount of impurity was visible in the ^{1}H NMR spectra of the synthesised ligand.

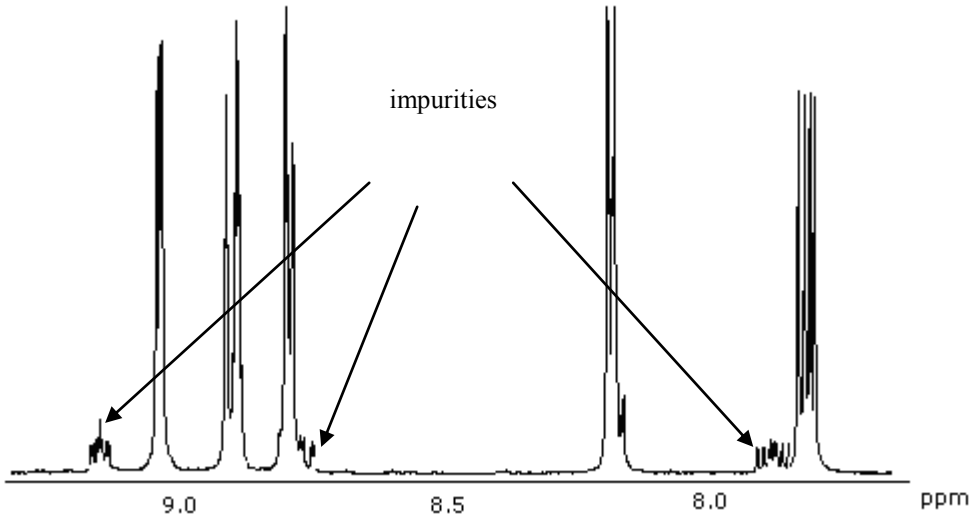

Figure 3.10: ^{1}H NMR spectrum of pyrphen ligand, impurities highlighted

However, when purification was attempted, the ligand appeared to degrade. Following recrystallisation from hot ethanol a change in the peaks corresponding to the sample was observed and the previously seen impurities were still present. This is shown below in Figure 3.11.

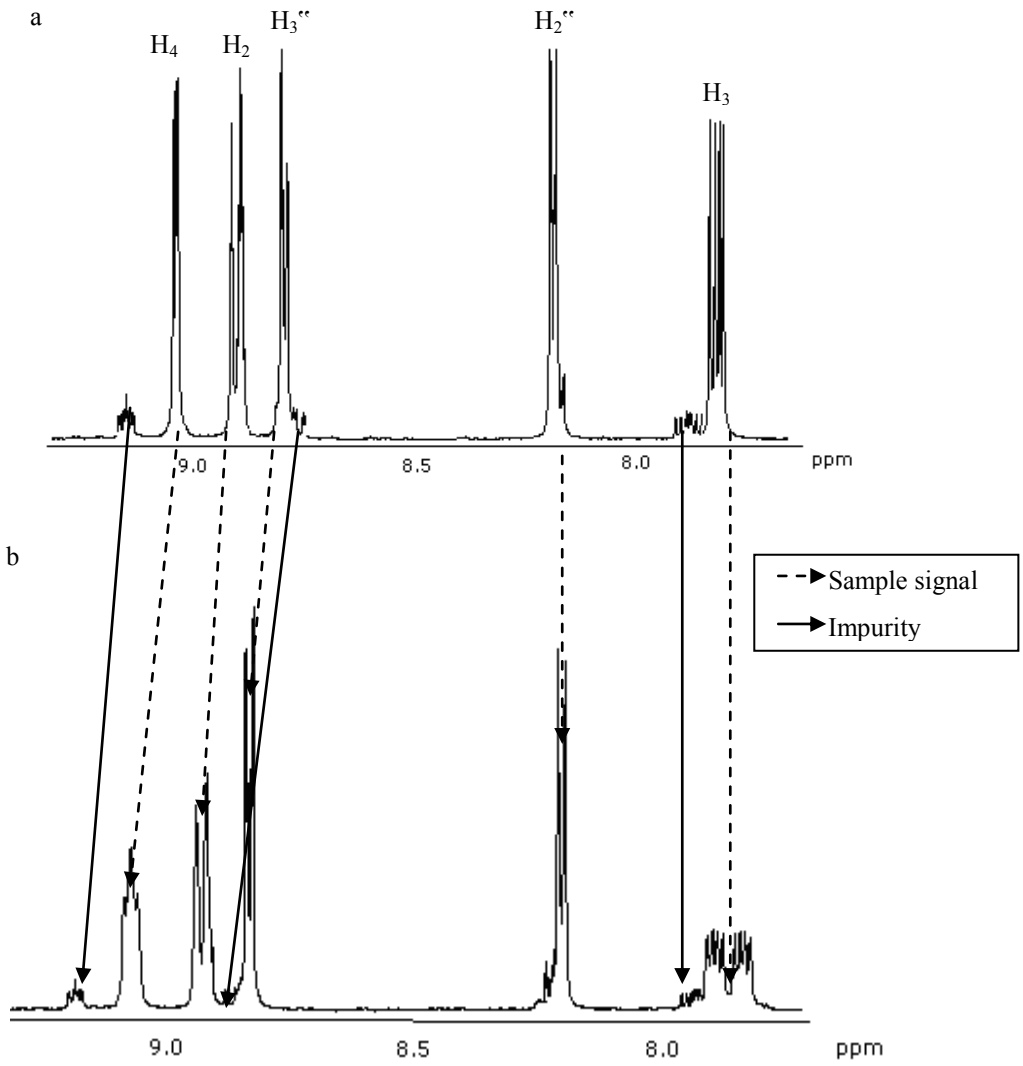

Figure 3.11: ^1H NMR spectrum of pyrphen ligand in d_6-DMSO (a) before recrystallisation and (b) after recrystallisation. Corresponding peaks are marked

Column chromatography was also attempted on neutral alumina using acetonitrile as eluent. However, though a decrease in the impurities present was observed, one of the peaks corresponding to the ligand disappeared from the spectrum, leading to the conclusion that the ligand also degrades during column chromatography.

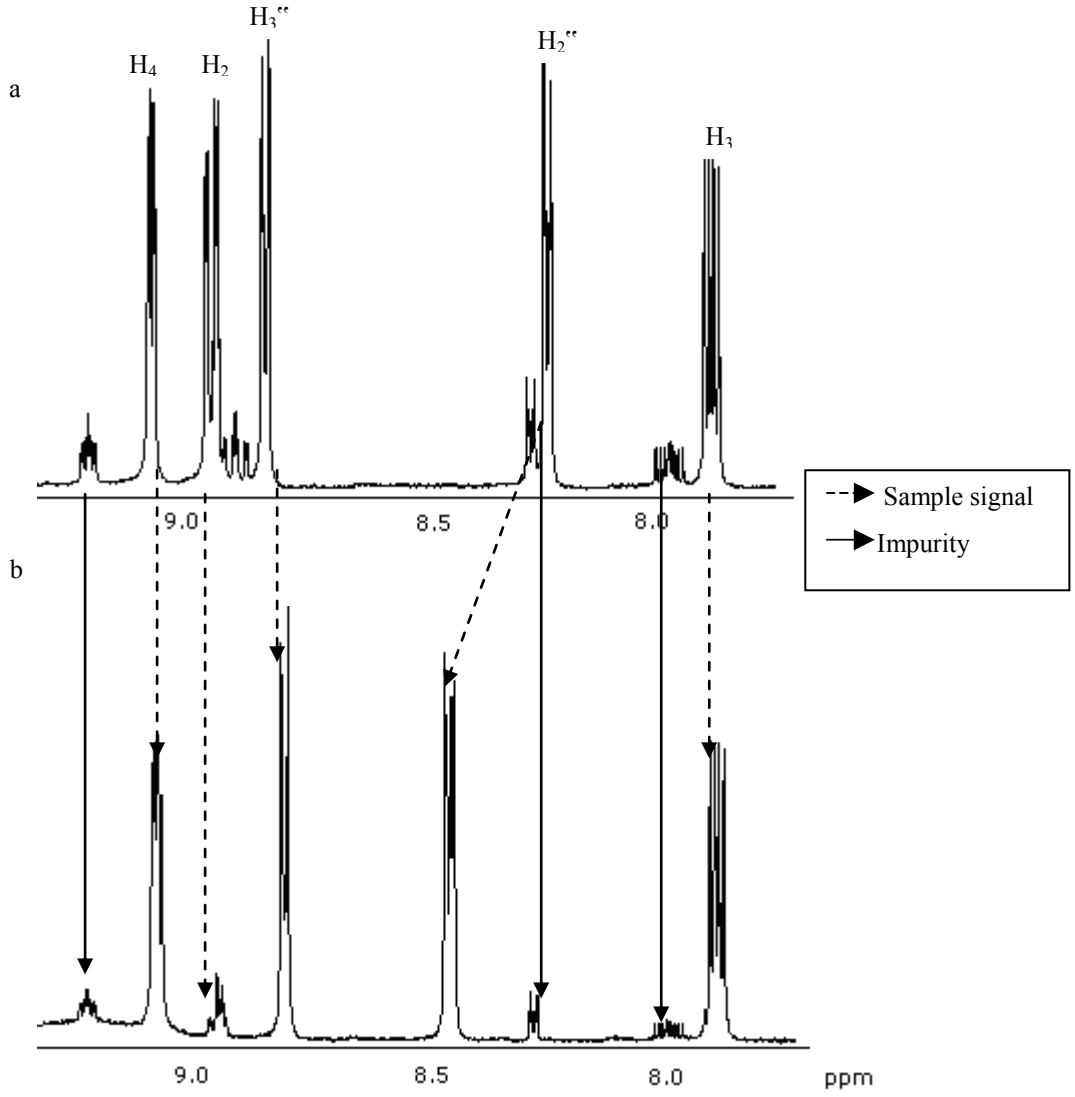

Figure 3.12: ^{1}H NMR spectrum of pyrphen ligand in d_6-DMSO (a) before and (b) after column chromatography. Corresponding peaks are marked.

It was therefore concluded that the complexes as metals/complexes as ligands strategy was not a viable method to synthesise the metal complexes $[Ru(bpy)_2(pyrphen)]^{2+}$ and $[Os(bpy)_2(pyrphen)]^{2+}$. Instead, a method involving modification of precursor complexes was developed.

A method to synthesise a ruthenium bipyridyl complex of 1,10-phenanthroline-5,6-dione was found[20]. A possible problem with the free ligand synthesis was that the ligand itself appeared to be soluble in most solvents that could be used in the synthesis (water, ethanol, methanol, diethyl ether and ethyl acetate). If the ligand could be synthesised „on the complex" these solubility issues may not be such an important factor.

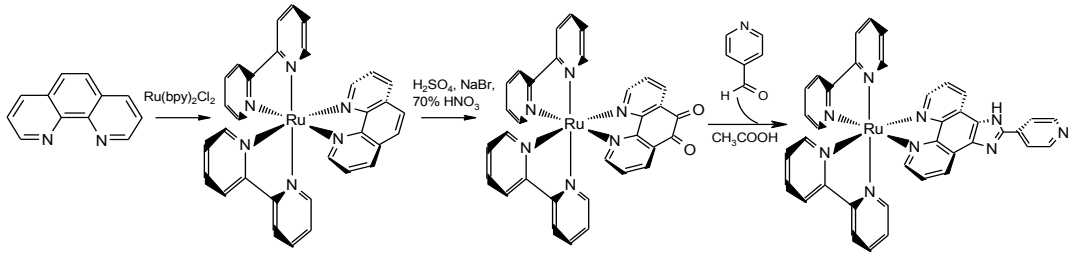

Figure 3.13: Reaction scheme for the 'on-complex' synthesis of the metal complex $[Ru(bpy)_2(pyrphen)]^{2+}$

The $[Ru(bpy)_2(phendione)]^{2+}$ starting material was synthesised satisfactorily and was used to synthesise the $[Ru(bpy)_2(pyrphen)]^{2+}$ complex using method 5 as outlined in Table 3.1. The obtained complex was still water soluble as a PF_6 salt but was easily precipitated by addition to diethyl ether. The complex was then purified by column chromatography, resulting in a 25% pure yield.

The analogous osmium complex was synthesised taking the same approach.

3.2.2 ^{1}H NMR Analysis

3.2.2.1 ^{1}H NMR of Ligands

The ^{1}H NMR data obtained experimentally will be compared to that for the standard compounds imphen (imidazo-[f] 1,10-phenanthroline) and phenimphen (2-phenylimidazo-1,10-phenanthroline)[21]. The structures of these molecules as well as the numbering of the protons present are shown in Figure 3.14.

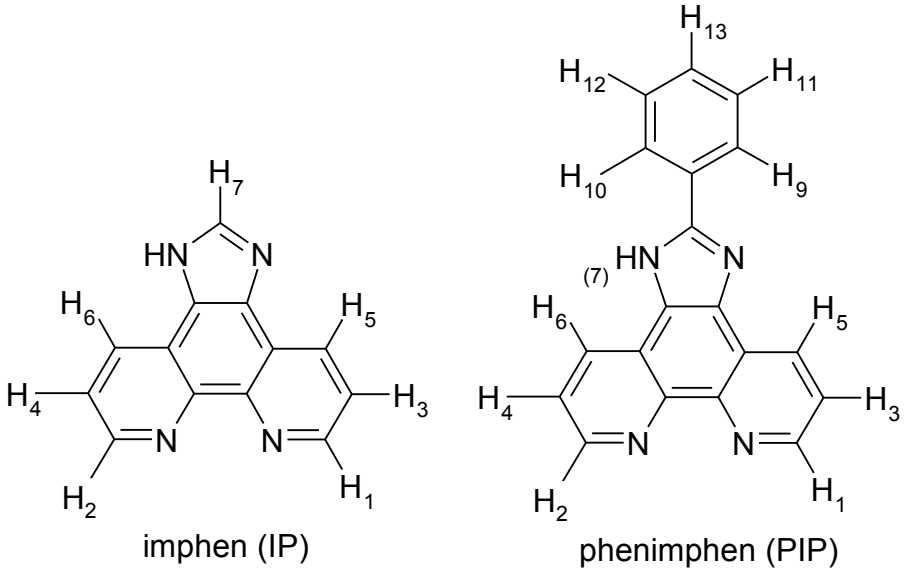

Figure 3.14: Structure and numbering of reference compounds imphen and phenimphen [21]

These ligands show C_{2V} symmetry in solution and so H_1 and H_2, H_3 and H_4, H_5 and H_6, H_9 and H_{10} and $H_{11}$and H_{12} respectively are chemically equivalent. This results in these pairs of protons appearing as one signal in the ^{1}H NMR spectrum showing an integration value of two.[21] Pyrphen incorporates a phenyl type group and so shall be compared to phenimphen. Thimphen however incorporates a five membered ring and so is deemed more applicable to compare with the imphen model ligand. The chemical shifts of corresponding protons are shown in Table 3.3.

Proton	**Imphen δ (ppm)**	**Thimphen δ (ppm)**	**Phenimphen δ (ppm)**	**Pyrphen δ (ppm)**
H_1/H_2	8.79 (d)	8.84 (d)	8.90 (d)	8.89 (d)
H_3/H_4	7.75 (dd)	7.81-7.76 (m)	7.70 (dd)	7.83-7.80 (dd)
H_5/H_6	9.05 (dd)	9.00 (d)	9.04 (dd)	9.03 (d)
H_7	8.30 (s)	N/A	N/A	N/A
H_9	N/A	8.29 (s)	8.31 (d)	8.78 (d)
H_{10}	N/A	7.87 (d)	8.31 (d)	8.78 (d)
H_{11}	N/A	7.81-7.76 (m)	7.49 (dd)	8.18 (d)
H_{12}	N/A	N/A	7.49 (dd)	8.18 (d)
NH	13.54 (broad)	Not present	13.41 (broad)	Not present

Table 3.3: Chemical shifts of the ligands thimphen and pyrphen protons as measured by ^1H NMR in d_6-DMSO as compared to literature compounds imphen (IP) and phenimphen (PIP) measured in d_6-DMSO[21].

The numbering system used to identify the protons in these molecules is shown below in Figure 3.15.

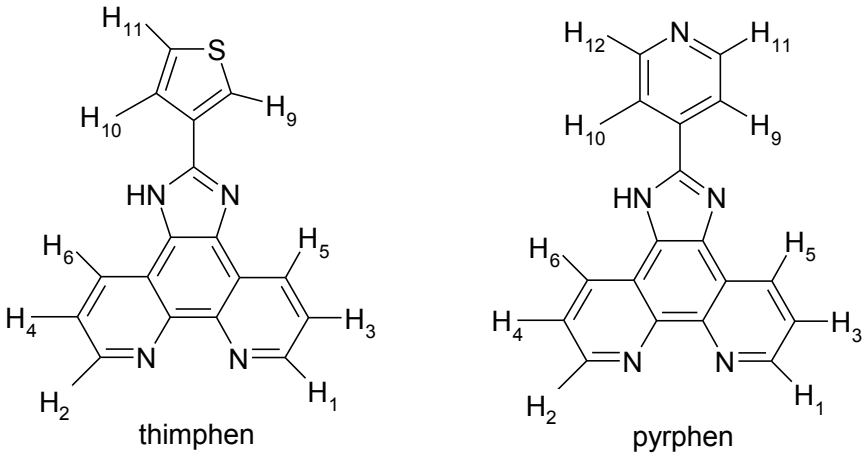

Figure 3.15: Labelling scheme used for assignment of ^1H NMR protons of ligands thimphen and pyrphen

The signals shown in the spectra for these ligands (as shown below in Figure 3.16 and Figure 3.18) were assigned by comparison with the spectra of the literature compounds imphen and phenimphen as well as through use of 2D COSY spectra.

Thimphen

The ^{1}H NMR spectrum of thimphen is shown below in Figure 3.16.

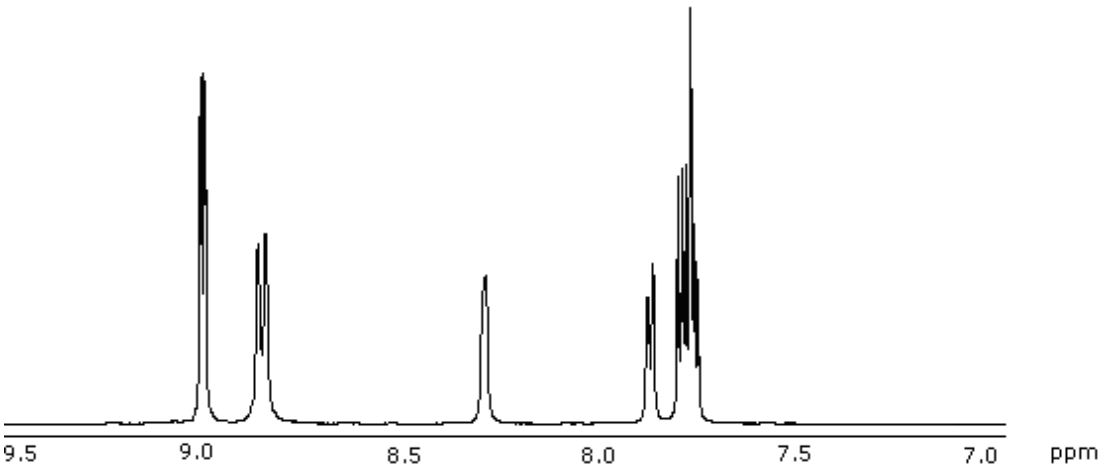

Figure 3.16: ^{1}H NMR spectrum of thimphen ligand in d_6-DMSO

Table 3.3 above shows that the imidazole (-NH) proton does not appear in the spectrum for thimphen. This is due to the highly acidic nature of this proton. It is extremely difficult to obtain a completely dry sample for ^{1}H NMR analysis (i.e. containing no residual water in the sample *or* in the solvent used) and as a result the imidazole proton dissociates easily from the compound causing the associated ^{1}H NMR signal (appearing at approximately 15 ppm) to broaden into the baseline.
The ^{1}H COSY spectrum of thimphen is shown below in Figure 3.17.

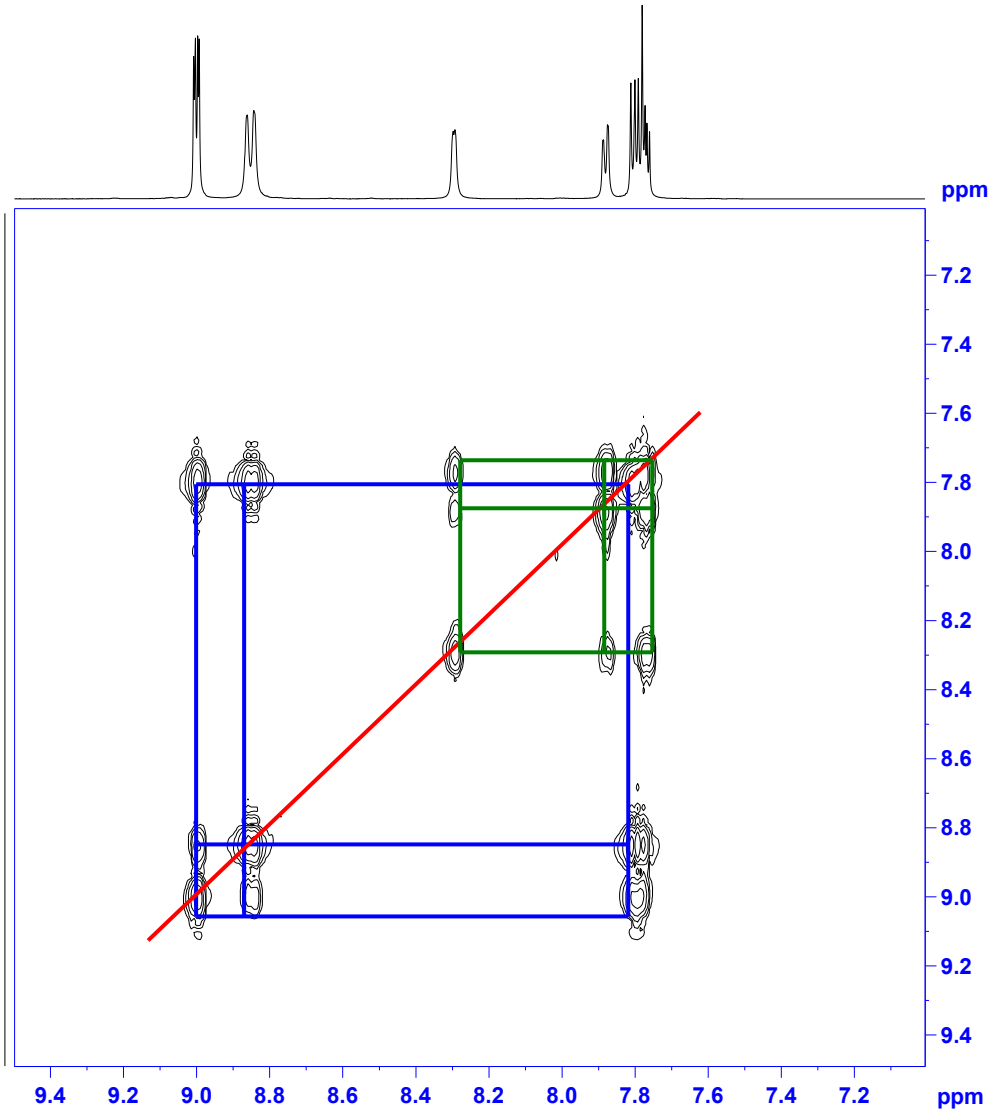

Figure 3.17: 2D COSY spectrum for thimphen as measured in d_6-DMSO showing the correlation between adjacent phenanthroline (blue) and thiophene (green) protons

Examining the ^{1}H COSY spectrum shown in Figure 3.17 the signals shown may be sorted into those corresponding to the phenanthroline moiety of the ligand and those corresponding to the appended thiophene. The singlet appearing at 8.29 ppm can be identified as the proton H_9 situated on the thiophene group as this is the only proton present in the molecule without an adjacent hydrogen atom. It is visible from the COSY spectrum that two other protons present in the molecule interact with this proton via long range coupling. These two signals (a doublet present at 7.87 ppm and a portion of the multiplet situated between 7.81-7.76 ppm) also couple strongly with each other and therefore can be identified as the remaining two thiophene protons H_{10} and H_{11}. H_{10} has been identified as the further downfield of the two at 7.87 ppm as it

is adjacent to the imidazole moiety which contains a more electronegative N than the S atom adjacent to H_{11} (therefore defined as part of the multiplet shown between 7.81 and 7.76 ppm).

The remaining three signals couple very strongly with each other and show no interaction with the H_9 singlet at 8.29 ppm. These signals at 8.84 ppm, 9.00 ppm and another signal present in the multiplet at 7.81-7.76 ppm are therefore attributable to the phenanthroline portion of the molecule. These values compare favourably with the corresponding chemical shift values for the reference compound imphen (IP). On the basis of this, as shown in Table 3.3 the protons $H_{1\text{-}6}$ may be assigned.

There is very little difference in the chemical shift of the corresponding protons of thimphen and imphen. From this it can be inferred that the thiophene group does not affect the phenanthroline moeity in electronic terms.

Pyrphen

The ^{1}H NMR spectrum of pyrphen is shown below in Figure 3.18.

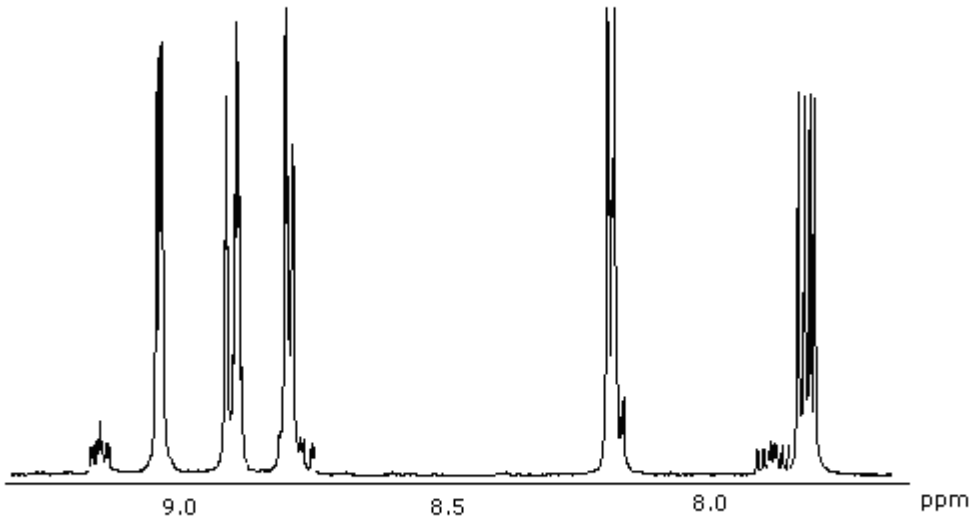

Figure 3.18: ^{1}H NMR spectrum of pyrphen ligand as measured in d_6-DMSO

Again, the imidazole proton H_5 is not visible in the spectrum.

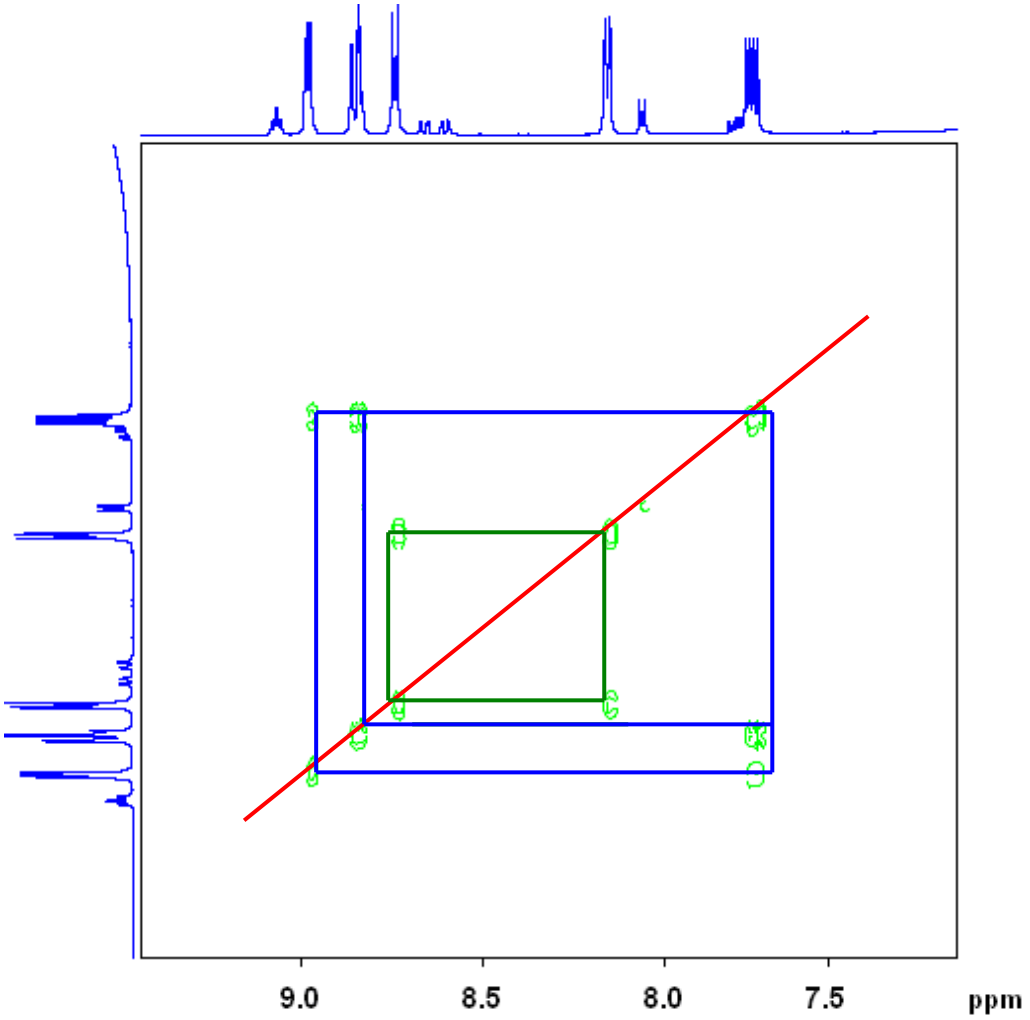

Figure 3.19: 2D COSY spectrum for pyrphen as measured in d_6-DMSO showing the correlation between adjacent phenanthroline (blue) and pyridine (green) protons

It can be seen that the doublet present at 8.78 ppm and the doublet present at 8.18 ppm couple strongly to each other and not to any other signal in the spectrum. It can therefore be assumed that these peaks relate to the pyridine moiety of the molecule. The more upfield of the signals at 8.78 ppm relates to the protons adjacent to the pyridine nitrogen, H_{10} and H_{11}. The signal at 8.18 ppm therefore relates to H_8 and H_9. The remaining three signals represent the phenanthroline protons present in the molecule. It is evident that these protons couple to each other, with each of the remaining doublets (present at 9.03 ppm and 8.89 ppm) coupling to the triplet at 7.82 ppm. This triplet therefore can be assumed to relate to H_3 and H_4. In order to assign the remaining two signals pyrphen may be compared to the literature compound phenimphen (PIP) as shown in Table 3.3. From this information the remaining two

signals can be easily identified, the doublet visible at 8.89 ppm relating to H_1 and H_2 and the doublet visible at 9.03 ppm relating to H_5 and H_6.

3.2.2.2 ^{1}H NMR of Mononuclear Metal Complexes: Direct Synthesis Approach

Here, as in the previous section, full assignment of ^{1}H-NMR spectra have been made using a combination of 1-dimensional and 2-dimensional studies.

To allow for accurate assignment of signals, the deuterated bipyridyl analogues of these complexes have also been synthesised. Removal of the bpy signals leads to a simplified spectrum and allows for much more accurate assignment of the coordinated ligand protons.

Ru(bpy)$_2$(thimphen)$^{2+}$/Os(bpy)$_2$(thimphen)$^{2+}$

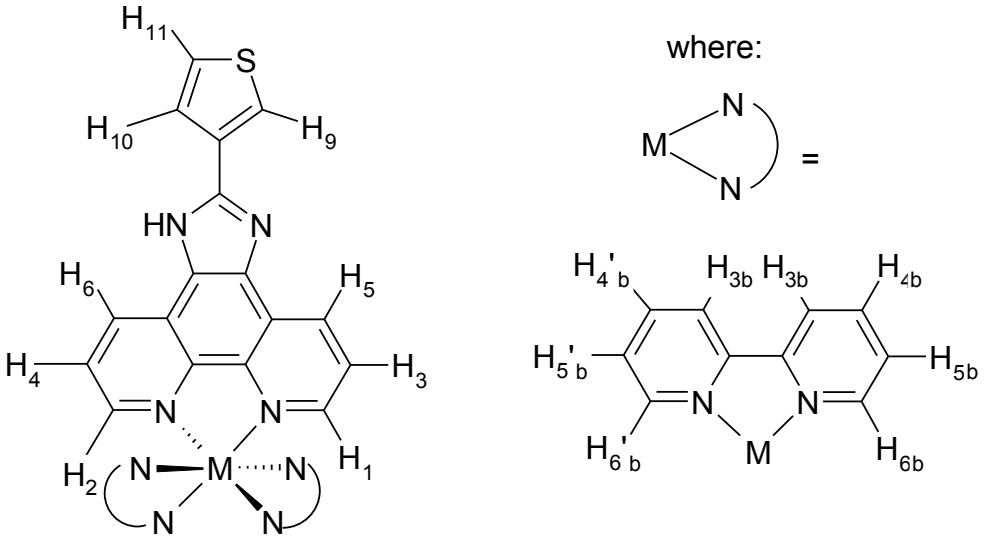

Figure 3.20: Labelling scheme used for assignment of ^{1}H NMR protons of [Ru(bpy)$_2$(thimphen)]$^{2+}$ and [Os(bpy)$_2$(thimphen)]$^{2+}$

The ^{1}H NMR spectra for (a) [Ru(bpy)$_2$(thimphen)](PF$_6$)$_2$ and (b) [Os(bpy)$_2$(thimphen)](PF$_6$)$_2$ are shown below in Figure 3.21.

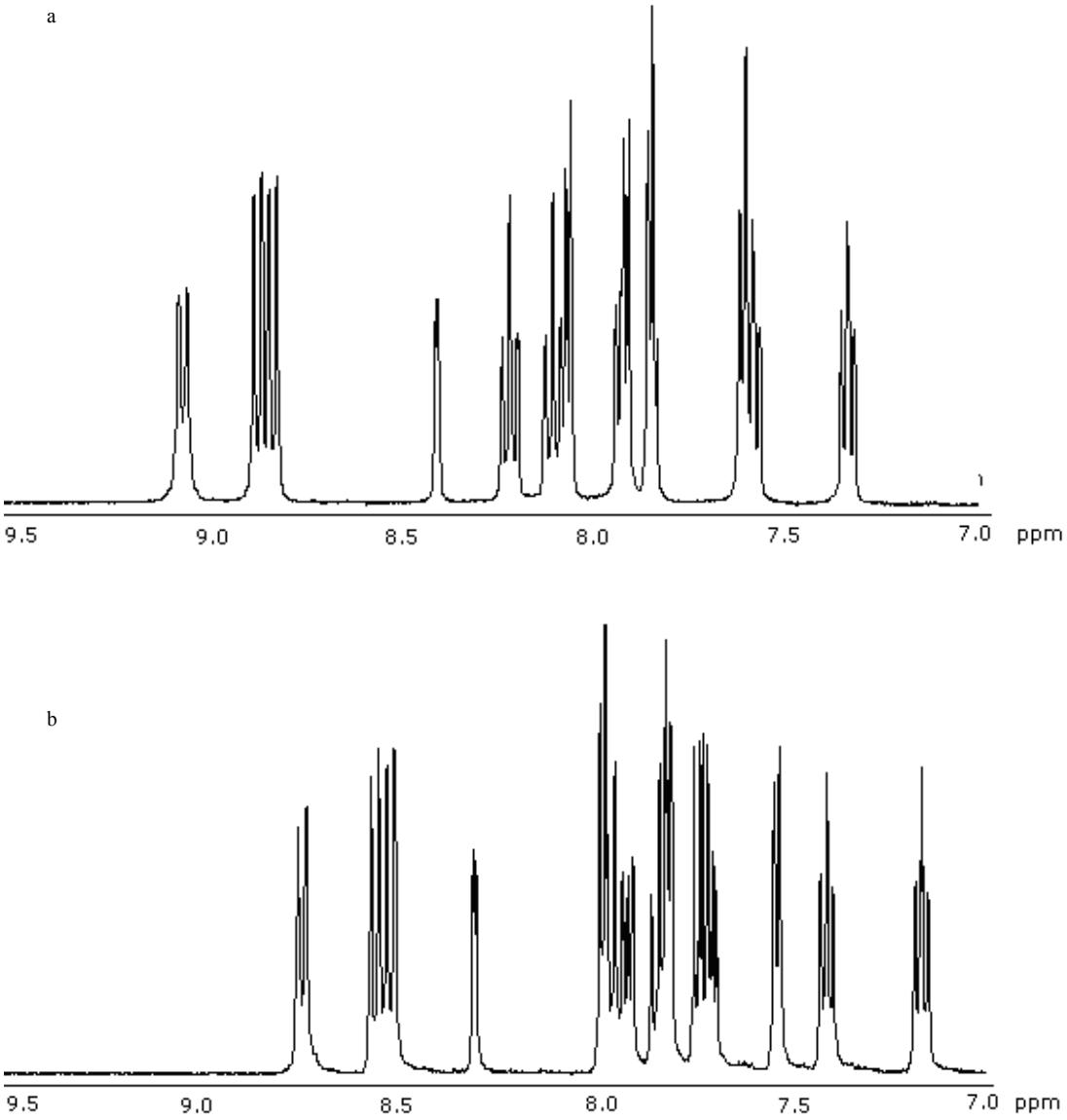

Figure 3.21: ^1H NMR spectrum of (a) $[Ru(bpy)_2(thimphen)]^{2+}$ and (b) $[Os(bpy)_2(thimphen)]^{2+}$ as measured in d_6-DMSO

Use of the ^{1}H NMR spectra of the deuterated analogues of these complexes as well as 2D COSY spectra were instrumental in the assignment of the ^{1}H NMR spectra obtained throughout this chapter. A direct comparison between (a) the free ligand thimphen, (b) the deuterated complex $[Ru(d_8\text{-bpy})_2(thimphen)]^{2+}$ and (c) the non-deuterated metal complex $[Ru(bpy)_2(thimphen)]^{2+}$ is shown below in Figure 3.22.

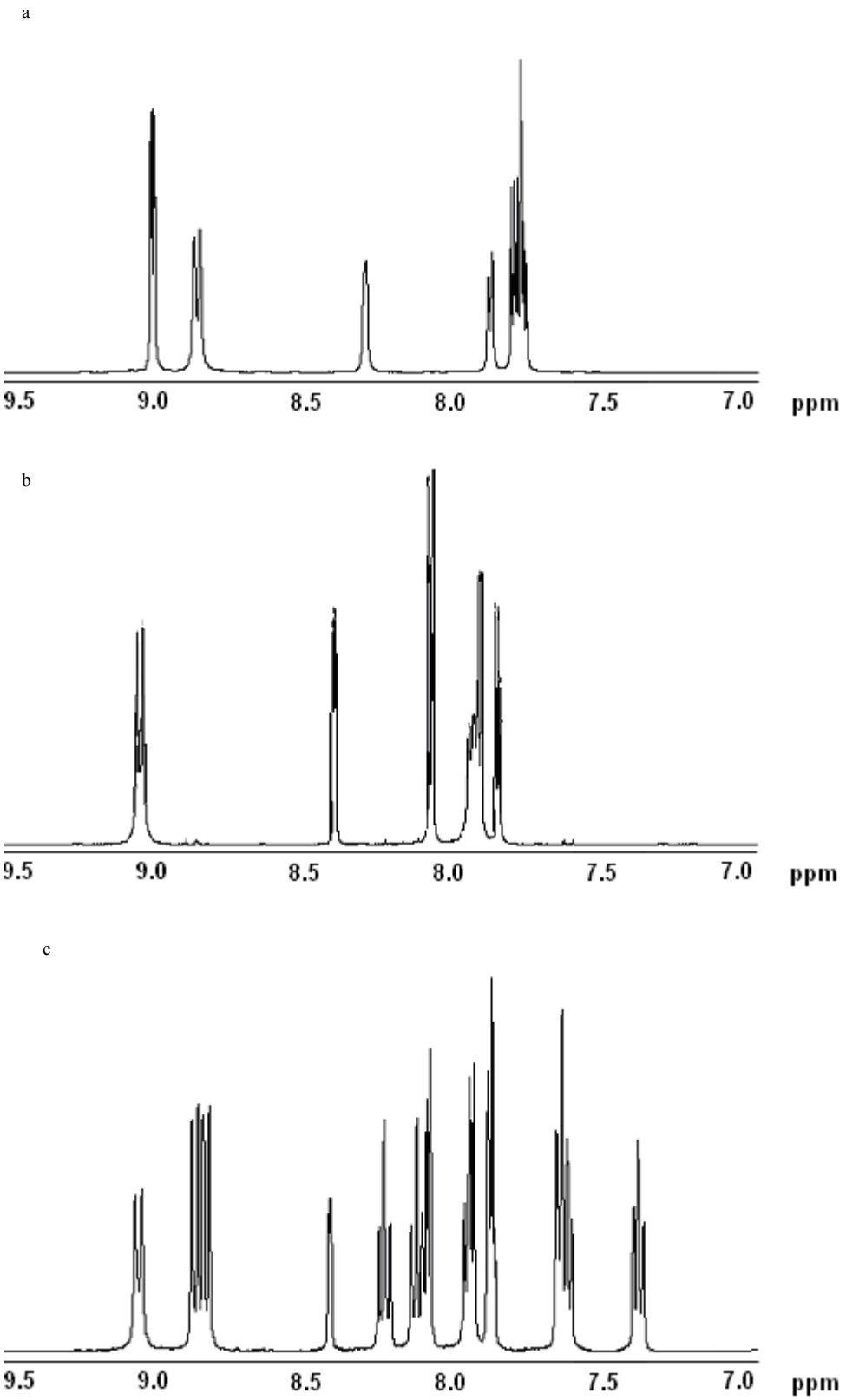

Figure 3.22: ^1H NMR spectrum of (a) thimphen (b) $[Ru(d_6\text{-}bpy)_2(thimphen)]^{2+}$ and (c) $[Ru(bpy)_2(thimphen)]^{2+}$ as measured in d_6-DMSO

The signals that should be affected least by metal complexation are those corresponding to the thiophene protons present in thimphen. By comparing spectrum (a) with spectrum (b) as shown in Figure 3.22 it is obvious that the singlet corresponding to H_9 at 8.39 ppm as well as the two doublets corresponding to H_{10} and H_{11} at 7.93 and 7.85 ppm respectively appear at the same chemical shift when complexed as for the free ligand. The peak corresponding to H_4 also remains at the same chemical shift value when complexed as for the free ligand, also being situated too far away from the metal coordination site.

The values for the thimphen portion of the metal complexes $[Ru(bpy)_2(thimphen)](PF_6)_2$ and $[Os(bpy)_2(thimphen)](PF_6)_2$ as compared to the chemical shift values of the free ligand thimphen are shown below in Table 3.4.

$[Ru(bpy)_2(thimphen)](PF_6)_2$			
Proton	**δ (complex) ppm**	**δ (free ligand) ppm**	**Difference**
H_1/H_2	8.05 (d)	8.84 (d)	-0.79
H_3/H_4	7.93-7.89 (m)	7.78 (m)	~0.13
H_5/H_6	9.03 (d)	9.00 (dd)	0.03
H_9	8.39 (dd)	8.29 (d)	0.10
H_{10}	7.93-7.89 (m)	7.89 (d)	~0.02
H_{11}	7.93-7.85 (m)	7.81 (m)	~0.10
$[Os(bpy)_2(thimphen)](PF_6)_2$			
Proton	**δ (complex) ppm**	**δ (free ligand) ppm**	**Difference**
H_1/H_2	7.97-7.89 (m)	8.84 (d)	~(-0.91)
H_3/H_4	7.73-7.68 (m)	7.78 (m)	~(-0.07)
H_5/H_6	8.74 (d)	9.00 (dd)	-0.26
H_9	8.29 (t)	8.29 (d)	0
H_{10}	7.97-7.89 (m)	7.89 (d)	~(-0.04)
H_{11}	7.73-7.68 (m)	7.81 (m)	~(-0.10)

Table 3.4: Comparison between the thimphen ligand protons of the ruthenium/osmium complex and the free ligand

It is unclear which signals correspond to H_3 and H_4. At this point, the use of 2D COSY spectra is particularly helpful.

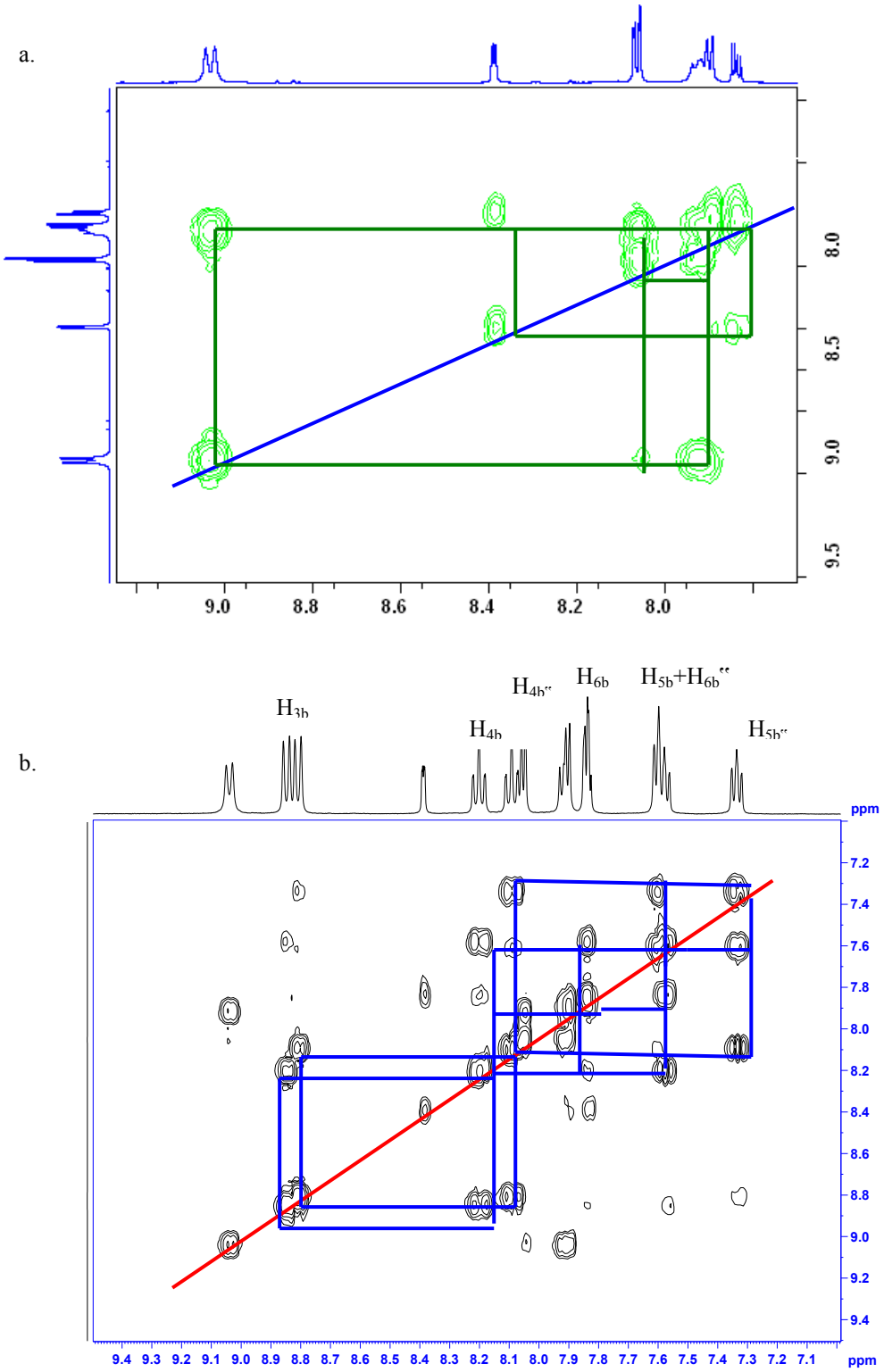

Figure 3.23: 2D COSY NMR spectra for (a) $[Ru(d_8\text{-}bpy)_2(thimphen)]^{2+}$ highlighting coupled phenanthroline protons and (b) $[Ru(bpy)_2(thimphen)]^{2+}$ highlighting coupled biypydriyl protons as measured in d_6-DMSO

Figure 3.23 (a) shows the 2D COSY NMR spectrum for $[Ru(bpy)_2(thimphen)]^{2+}$, and therefore the signals shown correspond only to the protons present in the thimphen portion of the molecule. The signal corresponding to H_9 is easily identifiable as the only peak integrating for one proton. This is the peak appearing at 8.39 ppm. This peak displays some long range coupling to the peaks appearing at 7.90 and 7.83 ppm, signifying the nearby protons H_{10} and H_{11}. As in the case for the free ligand, the further downfield of the signals corresponds to H_{10} as it is situated adjacent to the imidazole group, which is more electronegative than the sulphur atom neighbouring H_{11}.

The remaining signals correspond therefore to the phenanthroline protons. As for the free ligand the signal corresponding to H_3 and H_4 appears at 7.90 ppm and the signal corresponding to H_5 and H_6 appears at 9.03 ppm.

The doublet appearing at 8.05 ppm therefore signifies the phenanthroline protons H_1 and H_2. This signal is shifted 0.79 ppm upfield with respect to the corresponding signal in the free thimphen spectrum. Upon complexation, H_1/H_2 is placed above the bpy ring system and as a result is shielded from the magnetic field by the electronic field of the bpy ring system.

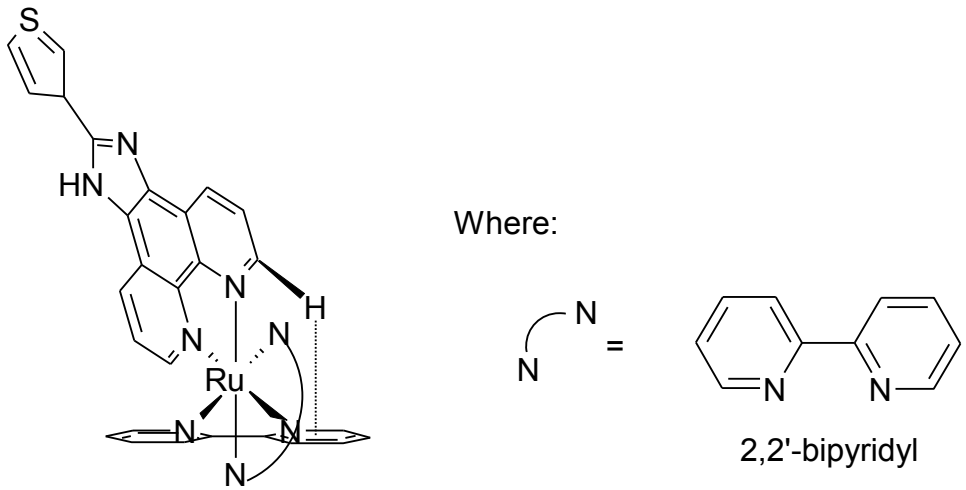

Figure 3.24: Illustration of positioning of proton H_2 of thimphen group upon complexation with $Ru(bpy)_2$

This results in the upfield shift observed when the complex spectrum is compared to that of the free ligand. This effect may be observed for all complexes of this type synthesised.

There is a minor downfield shift observed for the remaining ligand protons, perhaps due to a slight electron withdrawing effect introduced by the metal centre, but the magnitude of the effect is negligible.

The bipyridyl protons were then assigned on the basis of the 2D COSY spectrum for $[Ru(bpy)_2(thimphen)]^{2+}$, shown above in Figure 3.23 (b). The doublet of doublets visible at 8.84 ppm corresponds to H_{3b}. All four H_{3b} protons are in an identical environment, therefore showing in the spectrum as one peak. Also they are situated adjacent to the interconnecting C-C bond between the two pyridyl rings which act as a more electronegative force than the aromatic C-C bonds making up the rest of the molecule. It can also be noted that because of the steric proton-proton repulsion between nearby H_{3b} protons in space will result in reducing the electron density present on them. This accounts for the high chemical shift value for H_{3b} compared to the other bipyridyl protons present. It can be seen from the COSY spectrum shown in Figure 3.23 (b) that this multiplet couples strongly to two triplets occurring at 8.20 ppm and 8.09 ppm, implying that these two signals correspond to the protons H_{4b} and $H_{4b''}$. The further downfield of these two triplets (assigned as H_{4b}) couples strongly to multiplet shown in Figure 3.23 (b) between 7.61 and 7.56 ppm. This implies that this multiplet contains the signal corresponding to the proton H_{5b}. This multiplet in turn couples to a second multiplet present at 7.85-7.83 ppm, implying that this multiplet contains the signal corresponding to H_{6b}. Returning to the triplet at 8.09 ppm corresponding to $H_{4b''}$, strong coupling between $H_{4b''}$ and the triplet present at 7.34 ppm is evident in Figure 3.23 (b). The triplet at 7.34 ppm may therefore be assigned as $H_{5b''}$. This triplet, in turn, couples with the multiplet at 7.61-7.56 ppm, already containing the signal for H_{5b}. Therefore, this multiplet also contains the signal corresponding to $H_{6b''}$.

The chemical shift values assigned to the relevant protons as explained above are shown below in Table 3.6.

Proton	**Chemical Shift (ppm) $[Ru(bpy)_2(thimphen)]^{2+}$**	**Chemical Shift (ppm) $[Os(bpy)_2(thimphen)]^{2+}$**
H_1 /H_2	8.05 (d)	7.97-7.89 (m)
H_3 /H_4	7.93-7.89 (m)	7.73-7.68 (m)
H_5 /H_6	9.03 (d)	8.74 (d)
H_9	8.39 (dd)	8.29 (t)
H_{10}	7.93-7.89 (m)	7.97-7.89 (m)
H_{11}	7.85-7.83 (m)	7.73-7.68 (m)
$H_{3b/3b''}$	8.82 (dd)	8.53 (dd)
H_{4b}	8.20 (t)	7.97-7.89 (m)
$H_{4b''}$	8.09 (t)	7.84-7.79 (m)
H_{5b}	7.61-7.56 (m)	7.39 (m)
$H_{5b''}$	7.34 (t)	7.15 (m)
H_{6b}	7.85-7.83 (m)	7.84-7.79 (m)
$H_{6b''}$	7.61-7.56 (m)	7.52 (d)

Table 3.5: Chemical shifts of $[Ru(bpy)_2(thimphen)]^{2+}$ and $[Os(bpy)_2(thimphen)]^{2+}$ protons as measured by ^1H NMR in d_6-DMSO

3.2.2.3 ^{1}H NMR of Mononuclear Metal Complexes: Modification of Complex Starting Materials Approach

The ^{1}H NMR data for the products obtained for all reactions carried out using an „on-complex" approach is discussed below.

$[Ru/Os(bpy)_2(pyrphen)]^{2+}$

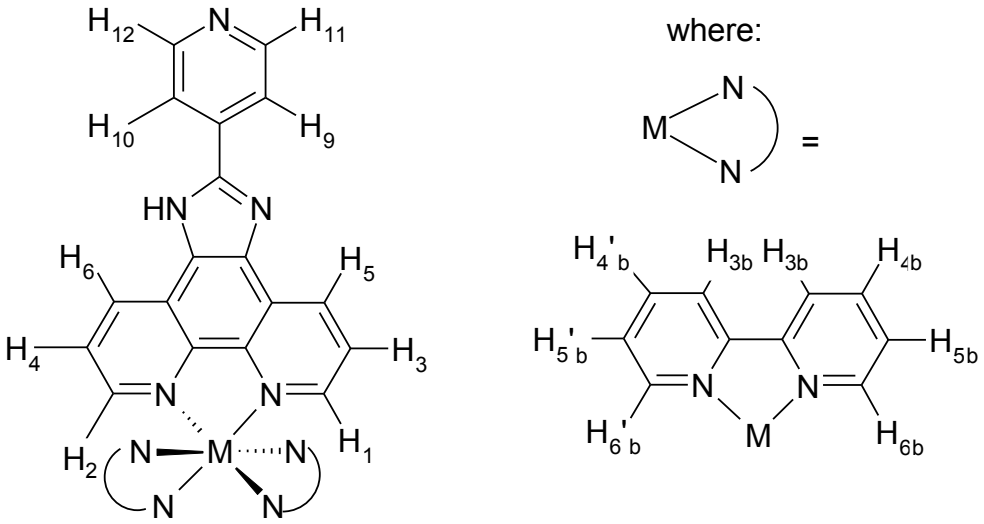

Figure 3.25: Labelling scheme used for assignment of ^{1}H NMR protons of the ruthenium and osmium complexes of pyrphen.

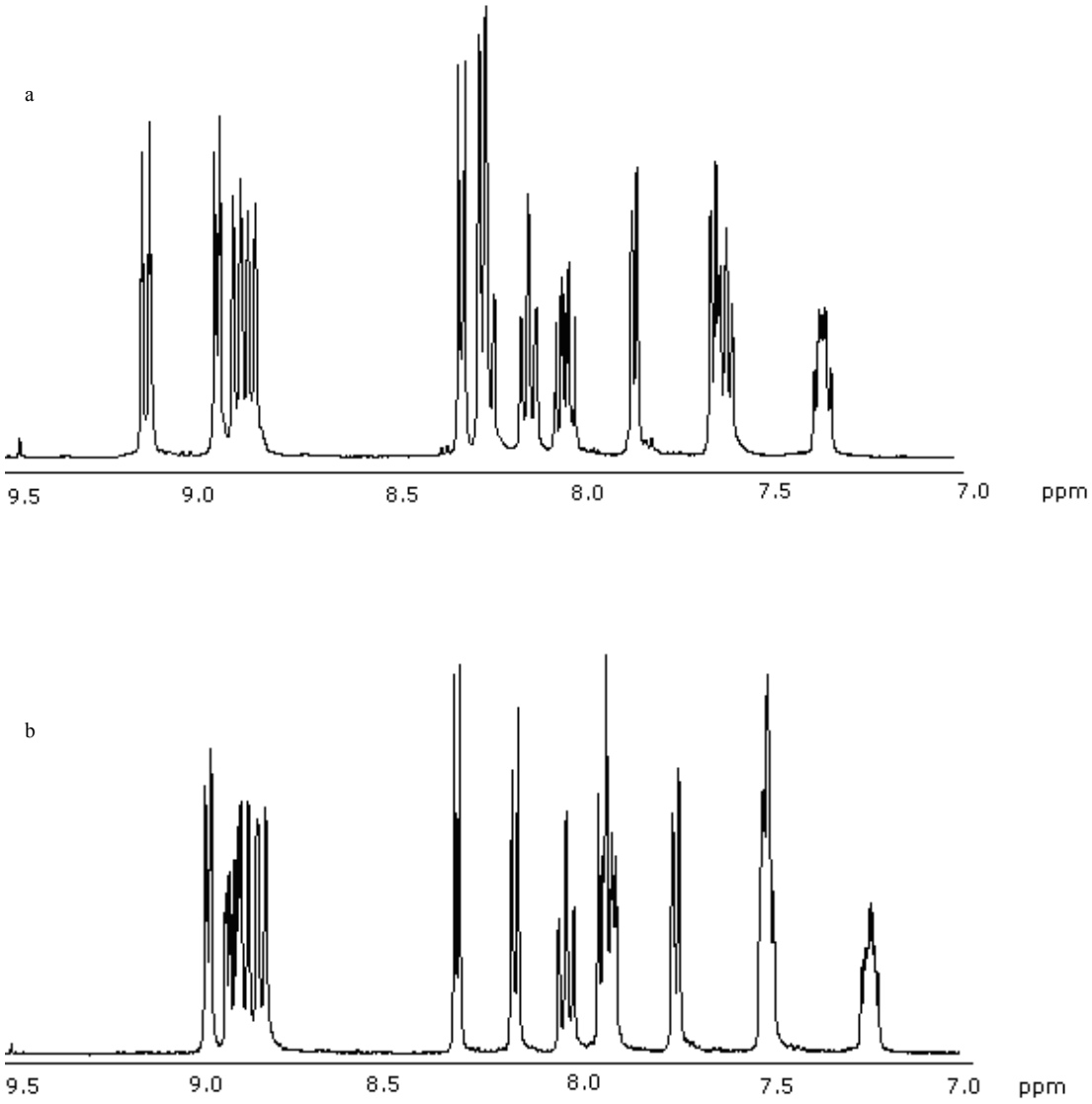

Figure 3.26: ^1H NMR spectrum of (a) $[Ru(bpy)_2(pyrphen)]^{2+}$ and (b) $[Os(bpy)_2(pyrphen)]^{2+}$ as measured in d_6-DMSO

As for the thimphen metal complexes discussed in section 3.2.2.2, the ^{1}H NMR spectra of the deuterated analogues of the metal complexes $[Ru(bpy)_2(pyrphen)](PF_6)_2$ and $[Os(bpy)_2(pyrphen)](PF_6)_2$ have also been measured. Figure 3.27 shows a direct comparison between (a) the free ligand pyrphen, (b) the deuterated complex $[Ru(d_8\text{-}bpy)_2(pyrphen)]^{2+}$ and (c) the non-deuterated metal complex $[Ru(bpy)_2(pyrphen)]^{2+}$.

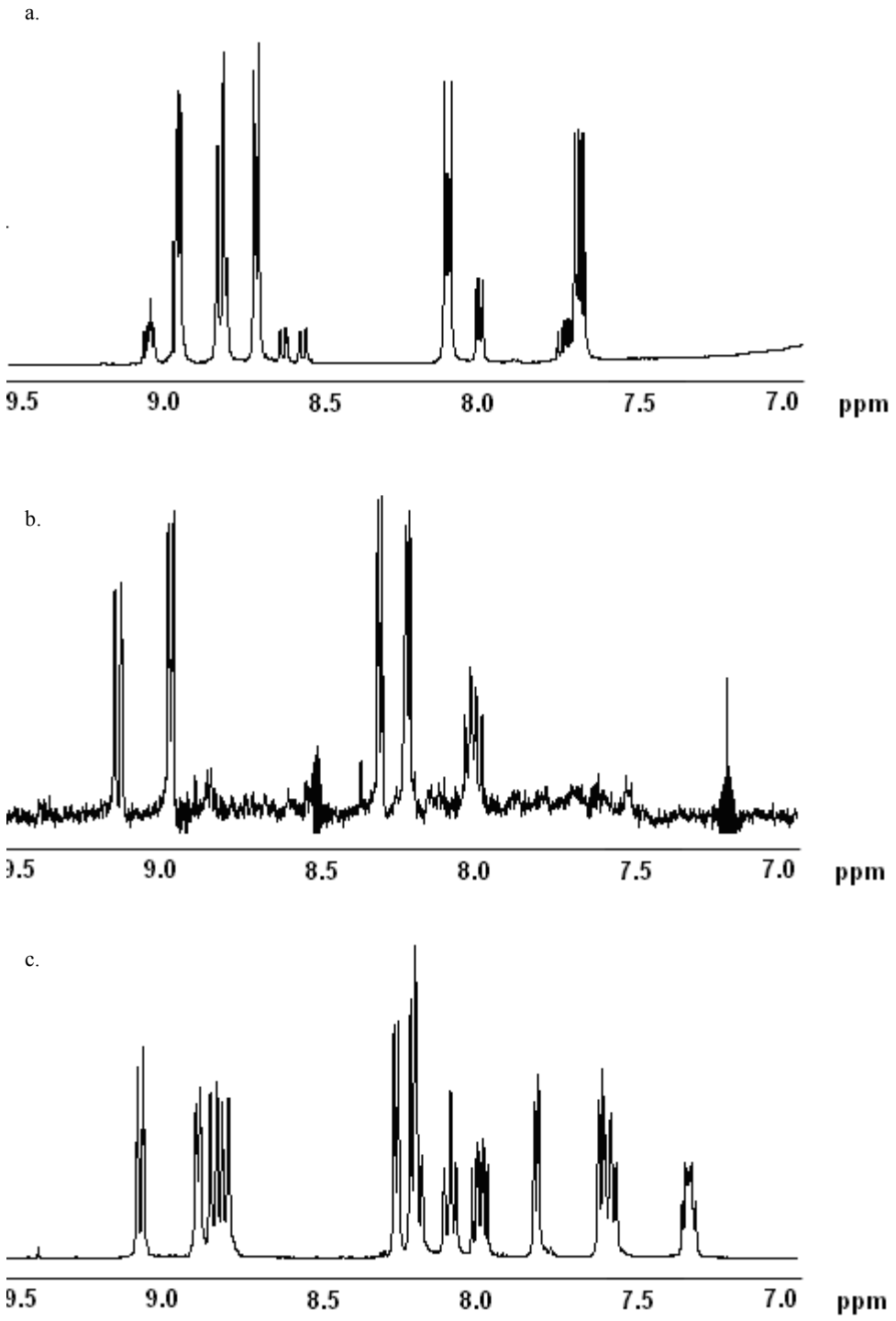

Figure 3.27: ^{1}H NMR spectrum of (a) pyrphen (b) [Ru(d_8-bpy)$_2$(pyrphen)]$^{2+}$ and (c) [Ru(bpy)$_2$(pyrphen)]$^{2+}$ as measured in d_6-DMSO

As for the complexes of the ligand thimphen, the main pyrphen based signal that shall be affected by complexation is the doublet relating to H_1/H_2. Comparing the spectrum shown in Figure 3.27 (a) to Figure 3.27 (b) it can be plainly seen that the doublet

present at 8.89 ppm in the free ligand (Figure 3.27 (a)) shifts to the lower chemical shift of 8.21 ppm upon complexation.

$[Ru(bpy)_2(pyrphen)]^{2+}$			
Proton	**δ (complex) ppm**	**δ (free ligand) ppm**	**Difference**
H_1/H_2	8.24-8.21 (m)	8.89 (d)	~(-0.67)
H_3/H_4	8.02 (dd)	7.82 (dd)	0.20
H_5/H_6	9.13 (d)	9.03 (d)	0.10
H_9/H_{10}	8.93 (d)	8.78 (d)	0.15
H_{11}/H_{12}	8.30 (d)	8.18 (d)	0.12
$[Os(bpy)_2(pyrphen)]^{2+}$			
Proton	**δ (complex) ppm**	**δ (free ligand) ppm**	**Difference**
H_1/H_2	8.16 (d)	8.89 (d)	-0.73
H_3/H_4	7.95-7.90 (m)	7.82 (dd)	~0.11
H_5/H_6	8.99 (d)	9.03 (d)	-0.04
H_9/H_{10}	8.96-8.81 (m)	8.78 (d)	~0.17
H_{11}/H_{12}	8.32 (d)	8.18 (d)	0.14

Table 3.6: Chemical shifts of $[Ru(bpy)_2(pyrphen)]^{2+}$ and $[Os(bpy)_2(pyrphen)]^{2+}$ ligand protons compared to the free ligand as measured by ^1H NMR in d_6-DMSO

In order to assign the $[Ru(bpy)_2(pyrphen)]^{2+}$ bipyridyl protons it is necessary to examine the 2D COSY spectrum of the non-deuterated $[Ru(bpy)_2(pyrphen)]^{2+}$. This is shown below in Figure 3.28.

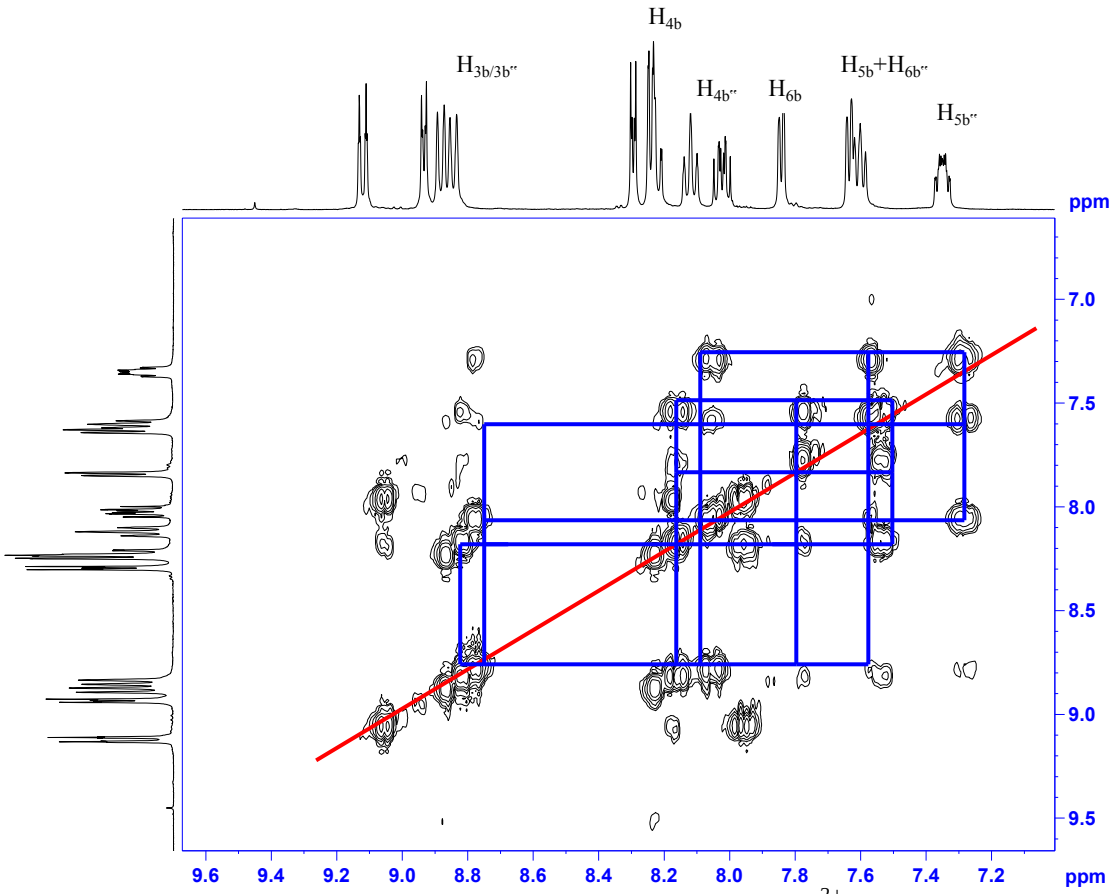

Figure 3.28: 2D COSY NMR spectrum for $[Ru(bpy)_2(pyrphen)]^{2+}$ highlighting coupled biypydriyl protons as measured in d_6-DMSO

The bipyridyl protons appear in this spectrum in the same order and in very similar position as for $[Ru(bpy)_2(thimphen)]^{2+}$. The coupling patterns observed are the same also.

The chemical shift values assigned to these protons are shown below in Table 3.9.

Proton	**δ (ppm) $[Ru(bpy)_2(pyrphen)]^{2+}$**	**δ(ppm) $[Os(bpy)_2(pyrphen)]^{2+}$**
H_1/H_2	8.24-8.21 (m)	8.16 (d)
H_3/H_4	8.02 (dd)	7.95-7.90 (m)
H_5/H_6	9.13 (d)	8.99 (d)
H_9/H_{10}	8.93 (d)	8.96-8.81 (m)
H_{11}/H_{12}	8.30 (d)	8.32 (d)
$H_{3b/3b''}$	8.89-8.84 (dd)	8.96-8.81 (m)
H_{4b}	8.24-8.21 (m)	8.03 (t)
$H_{4b''}$	8.12 (t)	7.95-7.90 (m)
H_{6b}	7.84 (d)	7.75 (d)
$H_{6b''}$	7.64-7.59 (m)	7.56-7.51 (m)
H_{5b}	7.64-7.59 (m)	7.56-7.51 (m)
$H_{5b''}$	7.37-7.32 (m)	7.26-7.22 (m)

Table 3.7: Chemical shifts of $[Ru(bpy)_2(pyrphen)]^{2+}$, $[Os(bpy)_2(pyrphen)]^{2+}$ as measured in d_6-DMSO

3.2.3 Elemental Analysis

The ligands thimphen and pyrphen were analysed by elemental analysis, providing a decisive insight into the molecular makeup of each compound. The observed and calculated values for the ligand thimphen are shown below in Table 3.8. A number of possible compositions are shown to account for the difference between the calculated and observed values.

Thimphen ligand: $C_{17}N_4H_{10}S$: calculated: %C: 67.5, %H: 3.34, %N: 18.5

Observed: %C: 57.3, %H: 4.5, %N: 16.8

Proposed compound	Calculated values
$C_{17}N_4H_{10}S.3H_2O$	%C: 57.4, %H: 4.4, %N: 15.7
$C_{17}N_4H_{10}S.2H_2O.½NH_4OH$	%C: 57.4, %H: 4.5, %N: 17.7

Table 3.8: Elemental analysis data for the ligand thimphen

The closest overall calculated value to the observed value is for the compound $[C_{17}N_4H_{10}S.2H_2O.½NH_4OH.½CH_3OH]$. However, this composition appears quite

complex and unlikely. The presence of ammonium hydroxide and methanol also are not visible in the ligand ^{1}H NMR spectrum shown below in Figure 3.29.

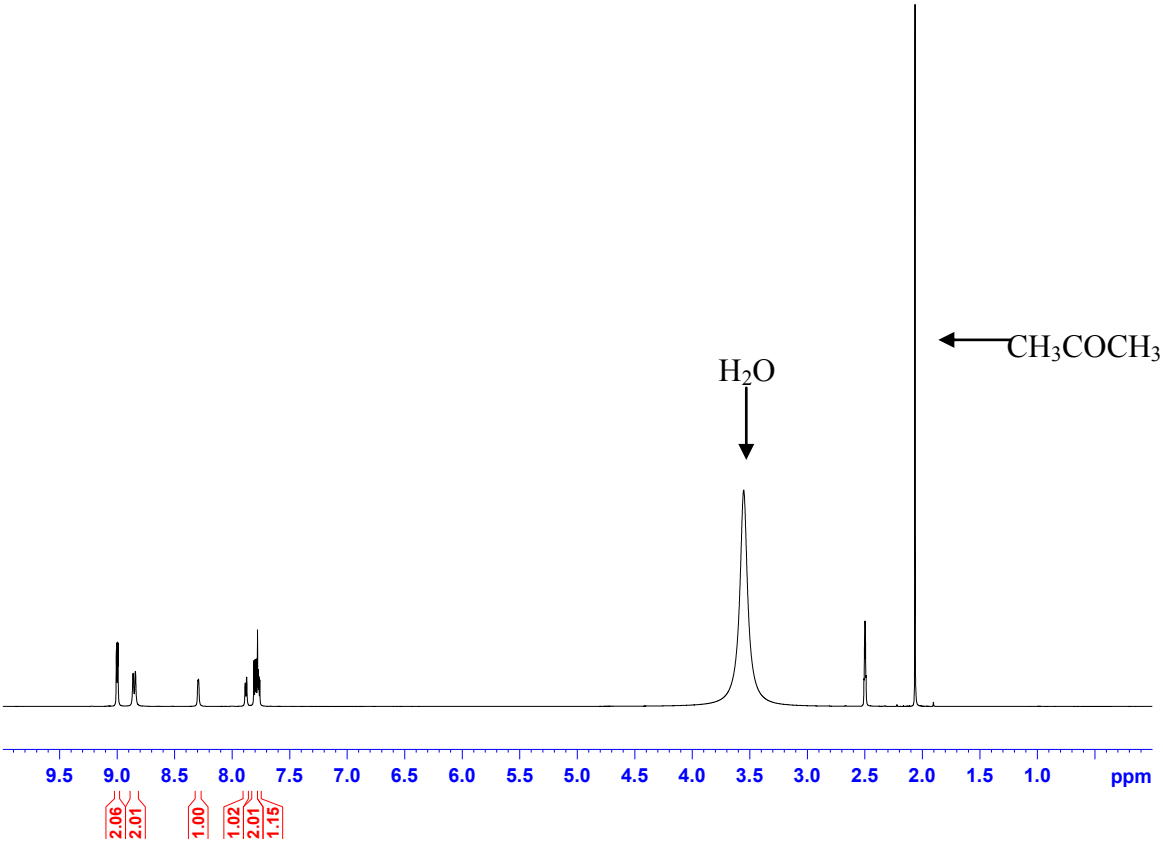

Figure 3.29: ^{1}H NMR spectrum of thimphen measured in d_6-DMSO

It is obvious from the spectrum shown in Figure 3.29 that water (s, 3.55 ppm)[22] and acetone (2.06 ppm)[22] are present in the ^{1}H NMR sample. There is no evidence of the presence of methanol (s, 3.16; s, 4.01)[22] and the three singlets at approximately 7.0 ppm attributable to the ammonium ion are also not present in this spectrum. As shown in Table 3.8, the presence of three water molecules in the structure of thimphen will yield the elemental analysis result %C: 57.4, %H: 4.4, %N: 15.7. This result shows a comparable figure for percentage carbon and percentage hydrogen to the respective observed values (%C: 57.3, %H: 4.5) each contributing a difference of ±0.1%. The difference between the calculated and observed nitrogen values is more considerable (calculated %N: 15.7, observed %N: 16.8) displaying a difference of 1.1%. The addition of one acetone molecule to the thimphen.3H_2O model results in the nitrogen value 16.9% which compares much more favourably with the observed value of 16.8%. The substitution of one water molecule in thimphen.3H_2O with an acetone molecule brings the nitrogen value to 13.5%, increasing the difference between the

calculated and observed values further. As the calculated value for % nitrogen in the molecule thimphen.$3H_2O$ is lower than the observed value, addition of more water or acetone molecules will further reduce the calculated % nitrogen value and increase the discrepancy between the calculated and observed values. This, coupled with the fact that the ^{1}H NMR spectrum of the ligand (see Figure 3.29 and Figure 3.16) as well as its mass spectrum (see Figure 3.32) show little impurity the elemental makeup of the ligand thimphen was decided to be $C_{17}N_4H_{10}S.3H_2O$.

As for thimphen, the observed and calculated values for the ligand pyrphen are shown below in Table 3.9. Again, a number of possible compositions are shown to account for the difference between the calculated and observed values.

Pyrphen ligand: $C_{18}N_5H_{11}$: calculated: %C: 72.7, %H: 3.7, %N: 23.6

Observed: %C: 57.93, %H: 3.71, %N: 16.33

Proposed compound	Calculated values
$C_{18}N_5H_{11}.2CH_3COOH$	%C: 63.6, %H: 4.1, %N: 16.8
$C_{18}N_5H_{11}.4H_2O$	%C: 58.5, %H: 5.2, %N: 18.9
$C_{18}N_5H_{11}.2CH_3COOH.NH_4OH$	%C: 56.4, %H: 5.2, %N: 17.9

Table 3.9: Elemental analysis data for the ligand pyrphen

As the ligand pyrphen was only synthesised in small amounts which were not purified successfully, it is probable that its elemental anaylsis will provide little conclusive information. In order to justify the compounds proposed in Table 3.9 and to investigate for further possible solvent based impurities the ^{1}H NMR spectrum of pyrphen is shown below in Figure 3.30.

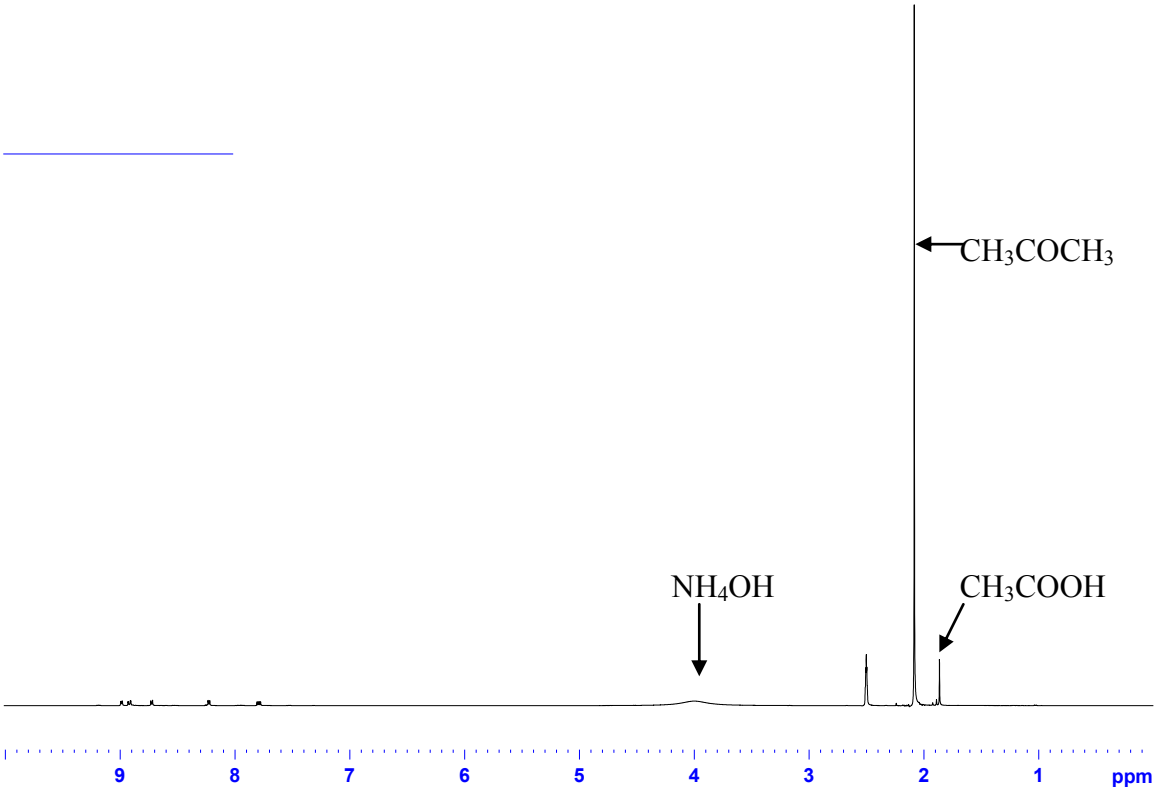

Figure 3.30: ^1H NMR spectrum of pyrphen in d_6-DMSO

Examining the above ^1H NMR spectrum shown in Figure 3.30, acetone is visible (s, 2.06 ppm)[22] as well as acetic acid (s, 1.91 ppm)[22]. A broad singlet is also visible at approximately 4 ppm. This is indicative of an –OH type proton, with the –OH proton of ethanol (s, 4.63 ppm) and methanol (s, 4.01 ppm)[22] occurring at approximately the same chemical shift. The only reagent used in the synthesis of pyrphen containing a hydroxy proton is ammonium hydroxide used to neutralise the reaction mixture. Factoring acetic acid and ammonium hydroxide the calculated percentages for the molecule become more favourable with respect to the observed values: %C: 56.4, %H: 5.2, %N: 17.9. However, the values for %H and %N are a little too high with respect to the observed values and the value for %C is a little low. The fact that so much solvent based impurity is contained in this ligand, which has proven particularly difficult to purify, renders the use of elemental analysis as a method of characterisation extremely limited. The use of elemental analysis to characterise $[Ru(bpy)_2(pyrphen)](PF_6)_2$ in which the ligand has been built on the complex shall be much more pertinent to this chapter.

The metal complexes synthesised from the above ligands were also characterised by elemental analysis, the observed and calculated values for the metal complexes

$[Ru(bpy)_2(thimphen)](PF_6)_2$ and $[Os(bpy)_2(thimphen)](PF_6)_2$ are shown below in Table 3.10 and Table 3.11 respectively. Again, a number of possible compositions are shown to account for the difference between the calculated and observed values.

$[Ru(bpy)_2(thimphen)](PF_6)_2$: $[C_{37}H_{26}N_8SRu](PF_6)_2$:

Calculated :%C: 44.2, %H:2.6 , %N: 11.1

Observed: %C: 45.0, %H: 3.3, %N: 11.1

Proposed compound	**Calculated values**
$[C_{37}H_{26}N_8SRu](PF_6)_2$	%C: 44.2, %H:2.6 , %N: 11.1
$[C_{37}H_{26}N_8SRu](PF_6)_2.½H_2O$	%C: 43.8, %H: 2.7, %N: 11.0
$[C_{37}H_{26}N_8SRu](PF_6)_2.½\ CH_3CN$	%C: 44.4, %H: 2.8, %N: 11.6

Table 3.10: Elemental analysis data for the metal complex $[Ru(bpy)_2(thimphen)](PF_6)_2$

In the case of $[Ru(bpy)_2(thimphen)](PF_6)_2$, the calculated and observed values may be reconciled satisfactorily with addition of half an acetonitrile molecule (the solvent used to purify the metal complex by column chromatography). This brings each calculated value to within ±0.5% of the observed values.

$[Os(bpy)_2(thimphen)](PF_6)_2$: $[C_{37}H_{26}N_8SOs](PF_6)_2$:

Calculated: %C: 40.6, %H: 2.4, %N: 10.2

Observed: %C: 38.8, %H: 2.3, %N: 8.8

Proposed compound	**Calculated values**
$[C_{37}H_{26}N_8SOs](PF_6)_2.2H_2O$	%C: 39.2, %H:2.7 , %N: 9.9

Table 3.11: Elemental analysis data for the metal complex $[Os(bpy)_2(thimphen)](PF_6)_2$

There appears to be more discrepancy between the calculated and observed values for $[Os(bpy)_2(thimphen)](PF_6)_2$. Examining the ^1H NMR spectrum for $[Os(bpy)_2(thimphen)](PF_6)_2$ shown below in Figure 3.31 may provide further insight into the elemental composition of the complex.

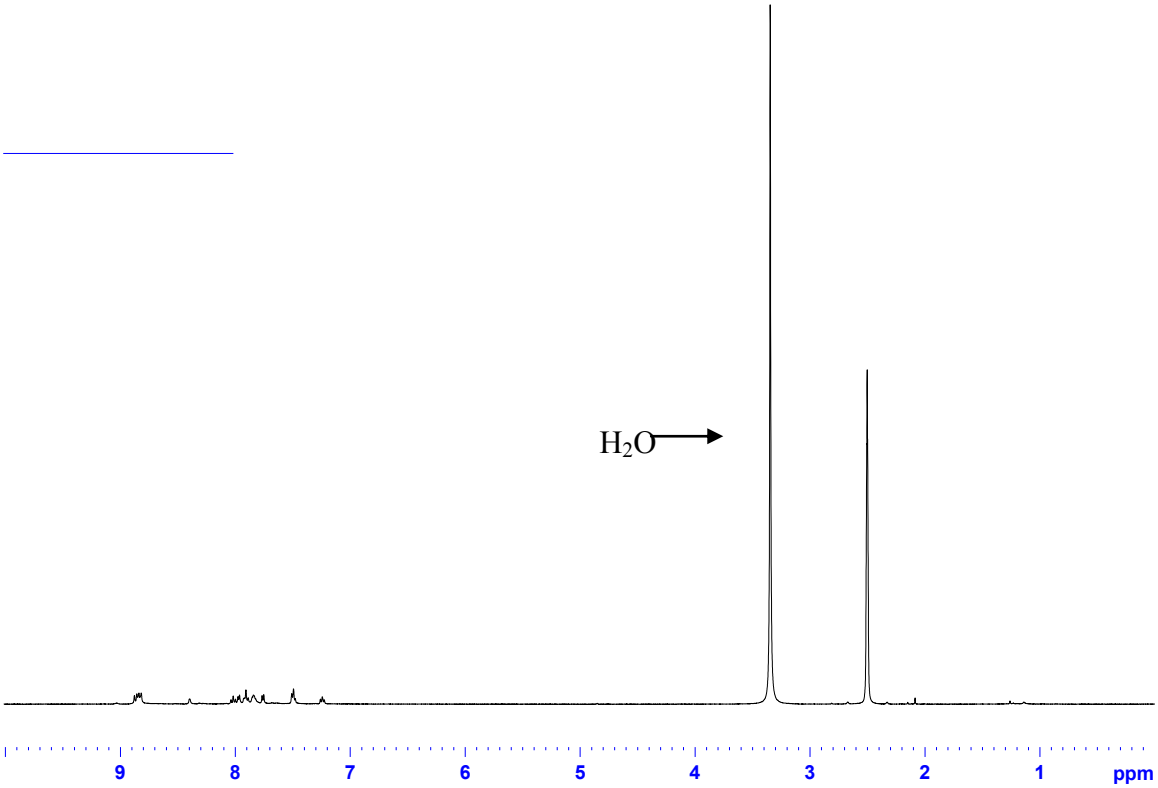

Figure 3.31: ^1H NMR spectrum of $[Os(bpy)_2(thimphen)](PF_6)_2$ in d_6-DMSO

Examining Figure 3.31, it can be easily seen that the only solvent impurity present is water (s, 3.33 ppm)[22]. Addition of two water molecules to the elemental composition of the complex brings the calculated values to %C: 39.2, %H: 2.7, %N: 9.9. The values for %C and %H here are within ±0.5% of the observed values. The %N value however is 1.1% higher than the observed value. Introduction of a third water molecule to the complex‟s composition however brings the %C and %H values out of the preferred range when compared to the observed values and also does not reduce the %N value sufficiently to warrant its inclusion. As the ^1H NMR spectrum (as shown in Figure 3.31 and Figure 3.21b) and the mass spectrum (as shown in Figure 3.36) show that the metal complex is formed with minimal to no impurity the discrepancy between the calculated and observed %N values has been deemed an anomaly, attributable perhaps to the method of analysis used.

The elemental analysis data for the ruthenium and osmium complexes of the ligand pyrphen, $[Ru(bpy)_2(pyrphen)](PF_6)_2$ and $[Os(bpy)_2(pyrphen)](PF_6)_2$ is shown below in Table 3.12 and Table 3.13 respectively.

$[Ru(bpy)_2(pyrphen)](PF_6)_2$: $[C_{38}H_{27}N_9Ru](PF_6)_2$:

Calculated :%C: 45.6, %H:2.7 , %N: 12.6

Observed: %C: 44.0, %H: 2.6, %N: 10.6

Proposed compound	**Calculated values**
$[C_{38}H_{27}N_9Ru](PF_6)_2.2H_2O$	%C: 44.0, %H:3.0 , %N: 12.1

Table 3.12: Elemental analysis data for the metal complex $[Ru(bpy)_2(pyrphen)](PF_6)_2$

$[Os(bpy)_2(pyrphen)](PF_6)_2$: $[C_{38}H_{27}N_9Os](PF_6)_2$:

Calculated :%C: 41.9, %H:2.5 , %N: 11.56

Observed: %C: 41.9, %H: 3.2, %N: 8.19

Proposed compound	**Calculated values**
$[C_{38}H_{27}N_9Os](PF_6)_2.2H_2O$	%C: 40.5, %H:2.8 , %N: 11.1

Table 3.13: Elemental analysis data for the metal complex $[Os(bpy)_2(pyrphen)](PF_6)_2$

In the elemental analysis of both of these metal complexes the observed %N value is much lower than the calculated value, while the observed %C and %H values are both relatively close to their respective calculated counterparts. As a result, addition of two water molecules brings the calculated %C and %H values in excellent agreement with the observed values for both complexes, but the calculated %N values remain 2% or more greater than the observed values. In an effort to reduce the overall %C, H and N in both molecules, ½ a KPF_6 molecule may be added as it is the only component used in the synthesis of these complexes that contains no carbon, hydrogen or nitrogen. It is possible that this residual KPF_6 may have survived the acetone: water recrystallisation following the precipitation of the final products $[Ru(bpy)_2(pyrphen)](PF_6)_2$ and $[Os(bpy)_2(pyrphen)](PF_6)_2$ or may have been introduced to the complexes during the precipitation of the precursor complexes $[Ru(bpy)_2(phendione)](PF_6)_2$ and $[Os(bpy)_2(phendione)](PF_6)_2$. In order to then reconcile the lowered %C and %H values, acetone (used in the synthesis of these complexes prior to their precipitation from their respective reaction mixtures with diethyl ether) molecules (two in the case of the ruthenium complex, three for the osmium) must also been taken into account in the complexes‟ overall makeup. In the case of $[Ru(bpy)_2(pyrphen)](PF_6)_2$ this brings the calculated values within agreeable range of the observed values, while in the case of $[Os(bpy)_2(pyrphen)](PF_6)_2$ the calculated %N value will remain higher than the

observed value, but introduction of a fourth acetone molecule would push the calculated %C and %H values out of acceptable range of the observed values.
It is obvious however, that examining the ^{1}H NMR data for these complexes as shown in section 3.2 and the mass spectrometry data shown in section 3.4 this level of impurity is not present in these samples, and so it has been concluded that there is two water molecules present in both pyrphen complexes as for $[Os(bpy)_2(thimphen)](PF_6)_2$.

A trend can be observed throughout almost all of the above elemental analyses displaying low %N values. A number of different batches of samples has been analysed for %N, with similarly low values appearing each time. Heretofore the researcher has been unable to account for this discrepancy in the results, but due to the encouraging results obtained via ^{1}H NMR analysis, UV/vis analysis and mass spectroscopy there is little doubt as to the identity of the samples analysed being that of the target complexes. It has been thereby concluded that the low %N values are due to a common analysis error.

3.2.4 Mass Spectrometry of Ligands

Mass spectrometry as an analytical method provides reliable qualitative information in an accurate, easily obtained manner. At its most basic level it is a method of measuring the molecular weight of the analyte. The mass spectrometer ionises the sample, producing charged particles that consist of both the parent ion and smaller fragments of the parent molecule. These ions are then detected in sequence according to their mass/charge ratio. The presence of fragment ions is significant in that it is possible to gain structural information about the molecule by analysing the mass of the fragments produced. Several mechanisms of fragmentation are known and may be applied to various systems.[23]

The method of mass spectrometry used here is electrospray mass spectrometry. In this method an aerosol is achieved by passing a dilute solution of the analyte through a fine needle held at 47 eV at 80^0C. The droplets produced divide into progressively smaller droplets until the sample enters the gas phase as an ion. The detected spectra are measured in the positive mode. This implies that the number of charged species

normally observed reflect the number of basic sites on a molecule that can be protonated at under acidic conditions. Electrospray mass spectrometry is an example of a soft ionization technique. Soft ionisation often leaves the complex intact and so the full molecular weight is detected.

Ruthenium has seven stable isotopes ranging in atomic mass from 95.9 to 103.9 as shown in Table 3.14. The relative abundances of each isotope are also included. These isotopes, coupled with the isotope present for carbon and nitrogen produce a molecular ion with a unique fingerprint for each metal complex.

Ru Isotope	**Relative Abundance (%)**
95.9	18
97.9	6
98.9	40
99.9	40
100.9	54
101.9	100
103.9	59

Table 3.14: The seven isotopes of ruthenium and their corresponding relative abundances[24]

The data found by mass spectrometry for the ligands thimphen and pyrphen are shown below in Table 3.15. The ligands in question are of neutral charge and so the theoretical m/z value is equal to the molecular weight. Also the observed m/z value is often one mass unit greater than the value expected.[25] This is due to the nature of detection employed. The ions intercepted by the detector are analysed in the „positive mode" as mentioned above. This implies that all of the detected ions are protonated and so have a charge of +1 and are one mass unit heavier.

Ligand	**Molecular Weight**	**Observed (m/z + H)**	**Other peaks**
Thimphen	303.4	303.2	414.7
Pyrphen	297.4	298.3	321.2

Table 3.15: Mass spectrometry data for the ligands thimphen and pyrphen

The mass spectra of these ligands are shown in the Figures below.

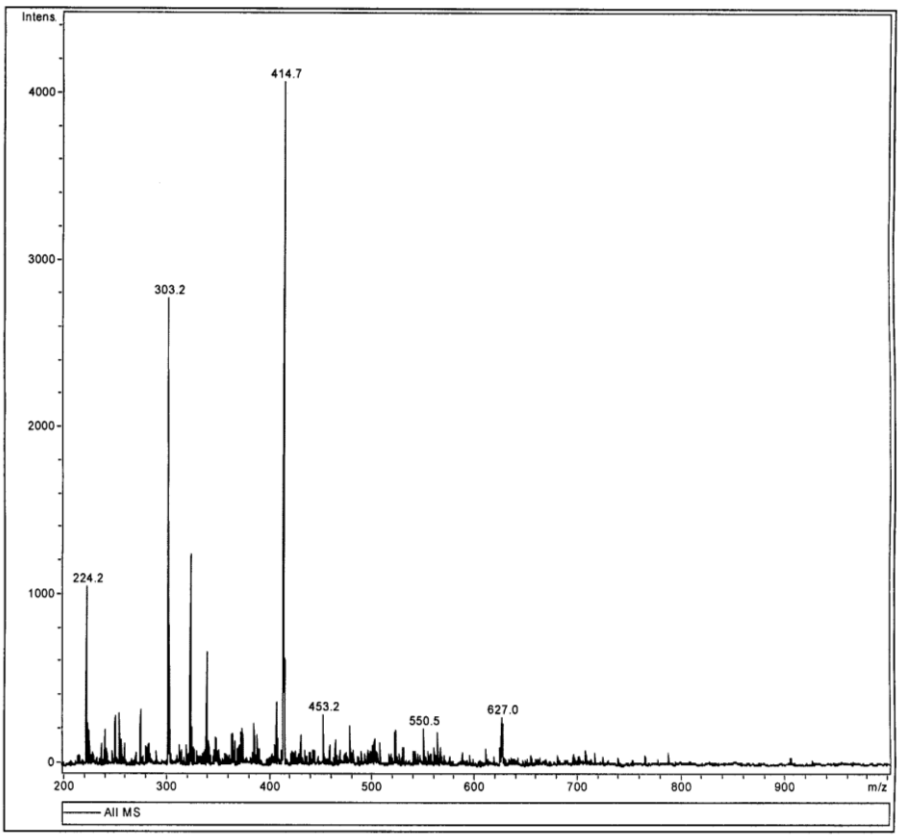

Figure 3.32: Mass spectrum of 'thimphen' ligand

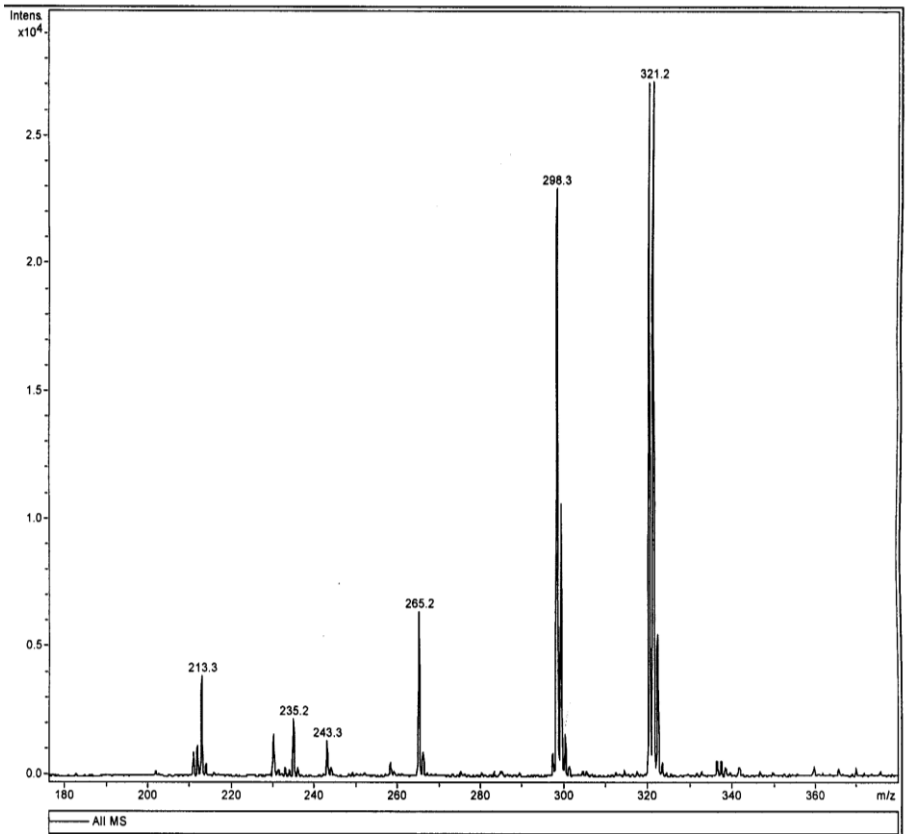

Figure 3.33: Mass spectrum of' pyrphen' ligand

Figure 3.32 shows the mass spectrum of thimphen. The molecular ion is visible at 303.2 mass units but is not the base peak of the spectrum. The peak visible at 414.7 mass units may be a side product of this reaction, involving the reaction of two phenanthroline dione groups with ammonium acetate resulting in the formation of a bis-phenanthroline compound.

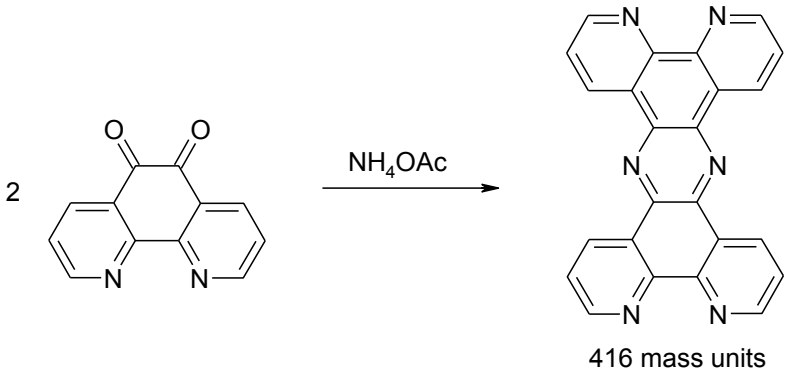

Figure 3.34: Proposed synthetic pathway for bis phenanthroline side product in 'thimphen' ligand synthesis

This compound is not visible in the ^{1}H NMR spectrum for this ligand (see section 3.3.4) nor is it visible in the mass or ^{1}H NMR spectra for pyrphen. It is therefore

possible that it is merely a contaminant present in the sample shown here. This is compounded by the fact that this compound is known to be extremely insoluble[26] and so would most likely be removed from the reaction solution before precipitation of the final product. This compounds the suggestion that the proposed compound is merely a small contaminant present in the sample analysed.

Another possibility is mentioned above in Section 3.3.2. The ^1H NMR spectrum shown in Figure 3.29 shows that acetone and water are present in the NMR sample of thimphen. The mass of the collective molecule thimphen.$3H_2O.CH_3COCH_3$ is 414.5. It is possible that the solvent molecules present are so strongly bound to the ligand that a portion of the analyte that reaches the detector still contains the co-crystallised solvent molecules.

Figure 3.33 shows the mass spectrum of pyrphen. The molecular ion is visible at 298.3 mass units. The second peak visible at 321 is attributable to the sodium salt of the complex, which may form upon injection into the mass spectrometer. There is no peak present in this spectrum at 416 mass units corresponding to the side product shown in Figure 3.34. However, as the method used to synthesise pyrphen employs a shorter reaction time it may provide a lower chance for side products to form.

3.2.5 Mass Spectrometry of Metal Complexes

The data found by mass spectrometry for the six mononuclear complexes $[Ru(bpy)_2(thimphen)]^{2+}$, $[Os(bpy)_2(thimphen)]^{2+}$, $[Ru(bpy)_2(pyrphen)]^{2+}$, $[Os(bpy)_2(pyrphen)]^{2+}$ are shown below in Table 3.16

Complex	**Calculated m/z**	**Observed (m/z + H)**	**Other peaks**
$[Ru(bpy)_2(thimphen)]^{2+}$	357.5	358.1	714.9
$[Os(bpy)_2(thimphen)]^{2+}$	402	403.3	805.2
$[Ru(bpy)_2(pyrphen)]^{2+}$	355	356.4	857.4
$[Os(bpy)_2(pyrphen)]^{2+}$	399.5	401.4	947.4

Table 3.16: Mass spectrometry data for the mononuclear ruthenium and osmium complexes of thimphen and pyrphen

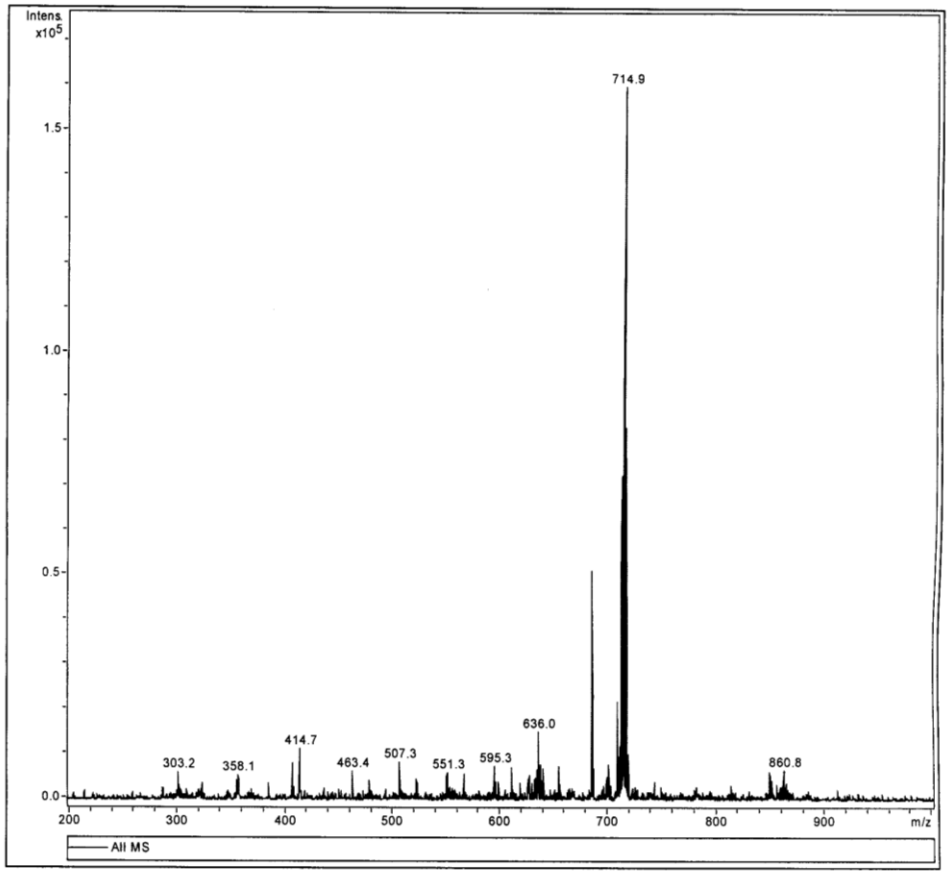

Figure 3.35: Mass spectrum for $[Ru(bpy)_2(thimphen)]^{2+}$

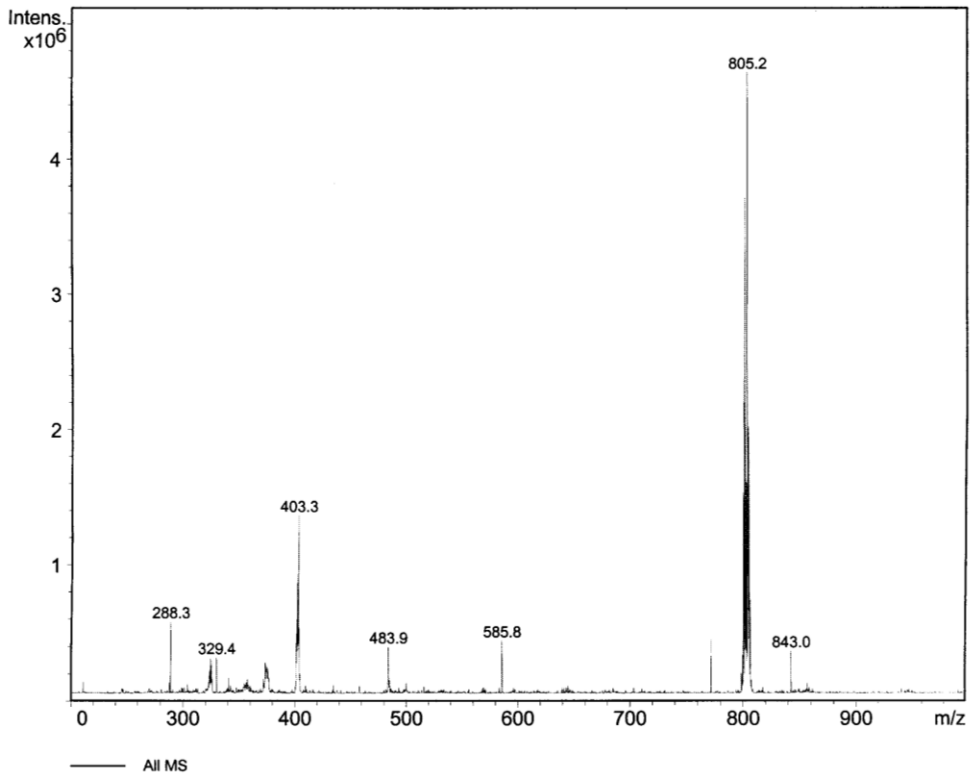

Figure 3.36: Mass spectrum for $[Os(bpy)_2(thimphen)]^{2+}$

The mass spectra of $[Ru(bpy)_2(thimphen)](PF_6)_2$ and $[Os(bpy)_2(thimphen)](PF_6)_2$ are shown in Figure 3.35 and Figure 3.36 respectively. As displayed in Table 3.16 the expected mass to charge ratio (m/z) values (i.e. the molecular mass of the compound in question divided by the molecular charge of +2) for the ruthenium and osmium complexes are 357.9 and 402.5 respectively. The molecular weight of $[Ru(bpy)_2(thimphen)]^{2+}$ is 715.8 while that of $[Os(bpy)_2(thimphen)]^{2+}$ is 805.0. When divided by the applicable charge of +2 the resulting m/z values match those stated above. These peaks are present, but are not present as the base peak of the spectrum. Instead, the most intense peak in both spectra relate directly to the value for the mass of the molecule, not taking its charge of +2 into account, in the case of $[Ru(bpy)_2(thimphen)]^{2+}$ this is 714.9 and for $[Os(bpy)_2(thimphen)]^{2+}$ 805.2. The only explanation for this is that the sample at the time of measurement possesses a charge of +1 and not +2.

The imidazole NH proton present on the ligand thimphen is potentially acidic in nature and can dissociate from the rest of the molecule in the presence of water. If this occurs the molecule is left with an extra negative charge that will reduce the molecule"s original charge of +2 (arising from the central metal"s oxidation state of +2) to +1. As electrospray mass spectrometry is a „soft" ionisation technique, there is minimal fragmentation observed in these spectra. As a result, other peaks present are most likely due to impurities present in the sample. For example, in the spectrum shown above of $[Ru(bpy)_2(thimphen)]^{2+}$ the peak visible at 303.3 relates to the uncoordinated ligand thimphen (mol wt=302 g/mol).

In the $[Ru(bpy)_2(thimphen)]^{2+}$ spectrum the peak visible at 860.8 mass units relates to the molecule $[Ru(bpy)_2(thimphen)](PF_6)^+$.

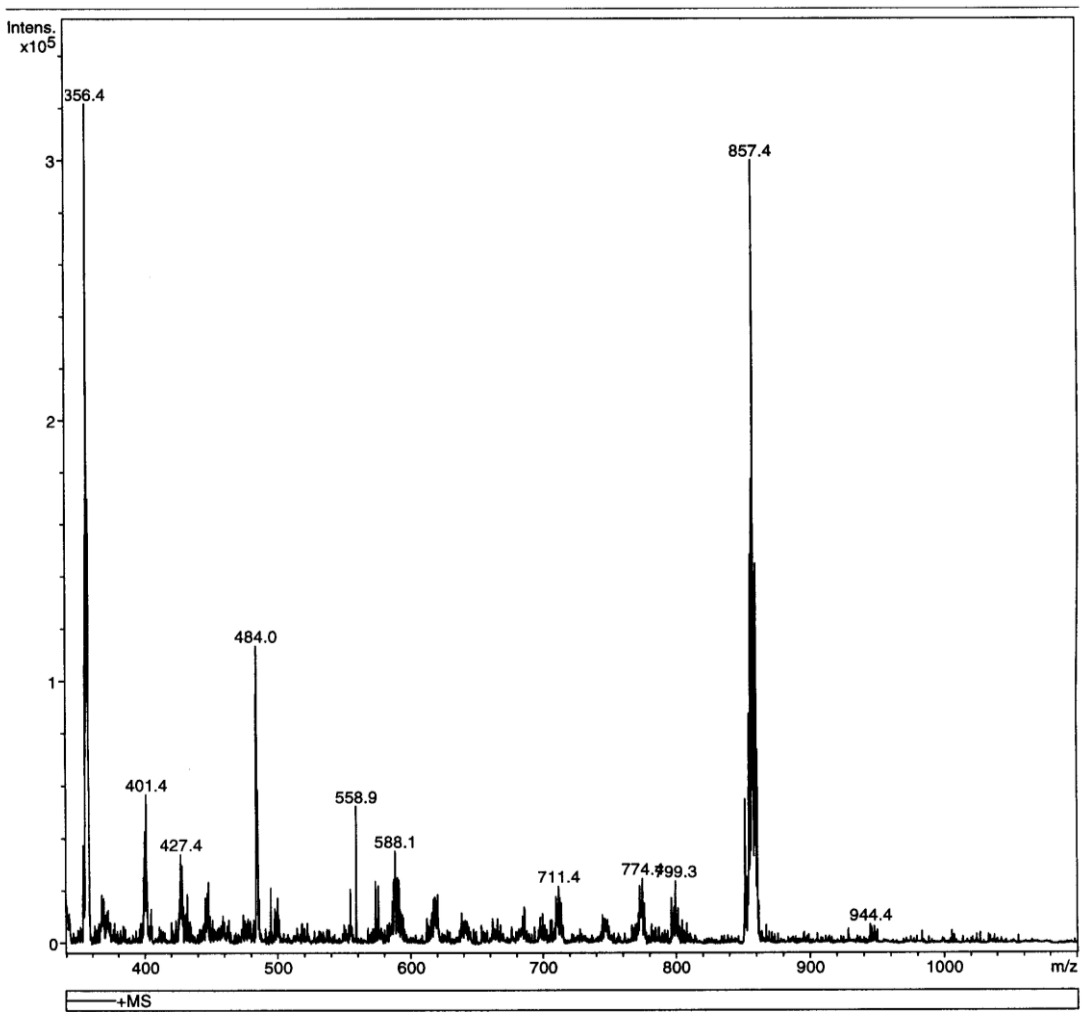

Figure 3.37: Mass spectrum for $[Ru(bpy)_2(pyrphen)](PF_6)_2$

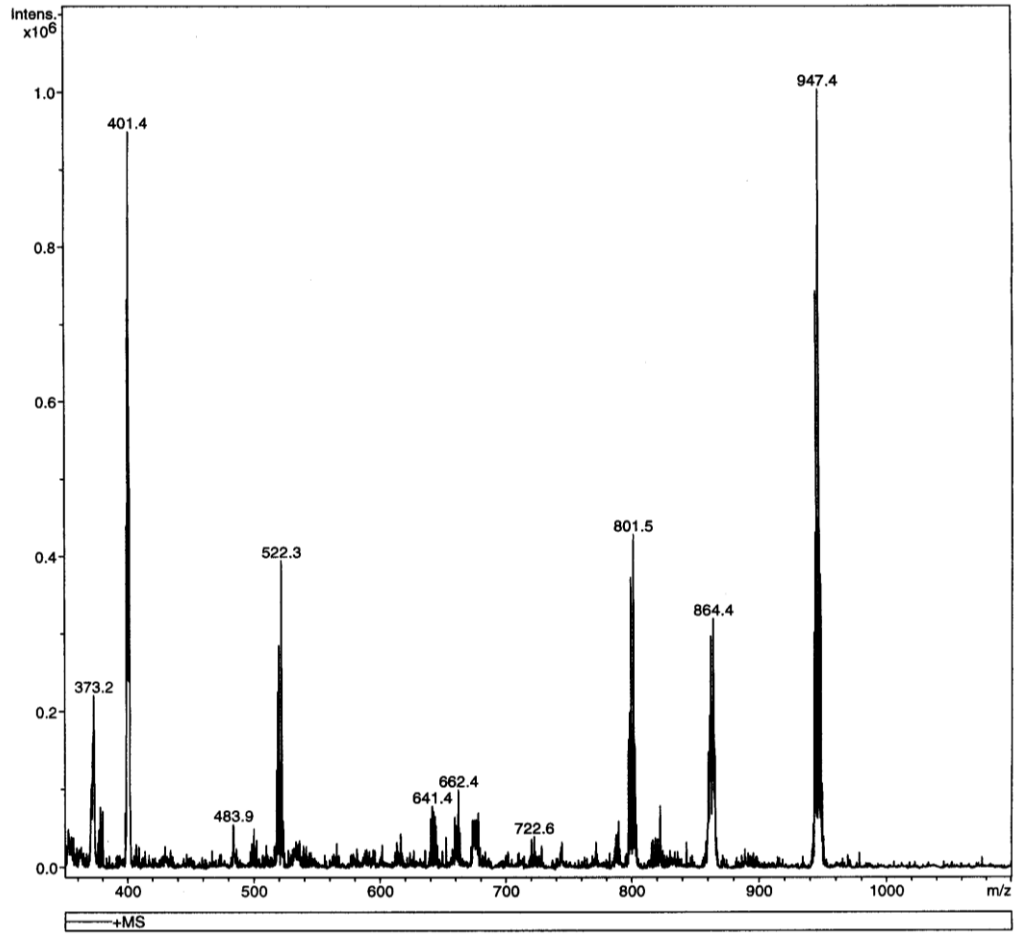

Figure 3.38: Mass spectrum for $[Os(bpy)_2(pyrphen)](PF_6)_2$

The mass spectra of $[Ru(bpy)_2(pyrphen)](PF_6)_2$ and $[Os(bpy)_2(pyrphen)](PF_6)_2$ are shown above in Figure 3.37 and Figure 3.38 respectively. As before, the peaks relating to the expected m/z value are present; for $[Ru(bpy)_2(pyrphen)]^+$ the expected m/z value is 355 seen here as 356.4 mass units while for $[Os(bpy)_2(pyrphen)]^{2+}$ the expected m/z value is 399.5, seen here as 401.4 mass units. There is also a peak present in both spectra relating to the complex with a charge of +1 instead of +2; For $[Ru(bpy)_2(pyrphen)]^+$ the calculated m/z value is 710 and is visible in the spectrum at 711.4 mass units, while for $[Os(bpy)(pyrphen)]^+$ the expected m/z value is 800 and is visible in the spectrum at 801.5 mass units. This is attributable again to the loss of the acidic imidazole NH proton in both cases. The peaks corresponding to the singly charged species (i.e. the complex minus the imidazole proton) of $[Ru(bpy)_2(pyrphen)]^+$ and $[Os(bpy)_2(pyrphen)]^+$ are much lower in intensity when compared to the corresponding peaks present in the spectra of $[Ru(bpy)_2(thimphen)](PF_6)_2$ and $[Os(bpy)_2(thimphen)](PF_6)_2$. This implies that there

is a greater tendency for the imidazole proton to dissociate when the „direct synthesis" route is taken as opposed to the „on-complex" approach. This is most likely due to the greater volumes of water incorporated in the „direct synthesis" approach when compared to synthesis on the complex. There is an intense peak present in each spectrum instead relating to the complex $[M(bpy)_2(pyrphen)](PF_6)^+$ where M is ruthenium (m/z=857.4) or osmium (m/z=947.4). This is due to one $(PF_6)^-$ counterion detaching from the complex upon injection.

3.2.6 UV/Vis Absorbance and Emission Spectroscopy of the Mononuclear Ruthenium (II) and Osmium (II) Complexes.

The UV-vis absorbance properties of the ruthenium and osmium metal complexes of the ligands synthesised are shown below in Figure 3.39 and Figure 3.39.

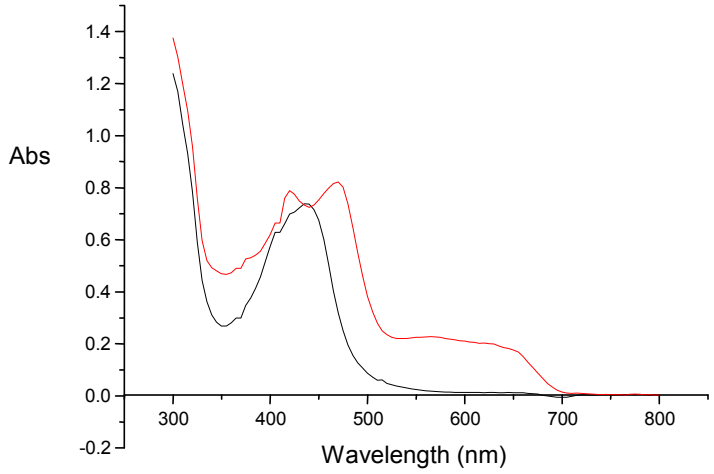

Figure 3.39: Absorbance spectra of the mononuclear complexes $[Ru(bpy)_2(thimphen)]^{2+}$ 0.04 mM (black) and $[Os(bpy)_2(thimphen)]^{2+}$ 0.04 mM (red) in acetonitrile.

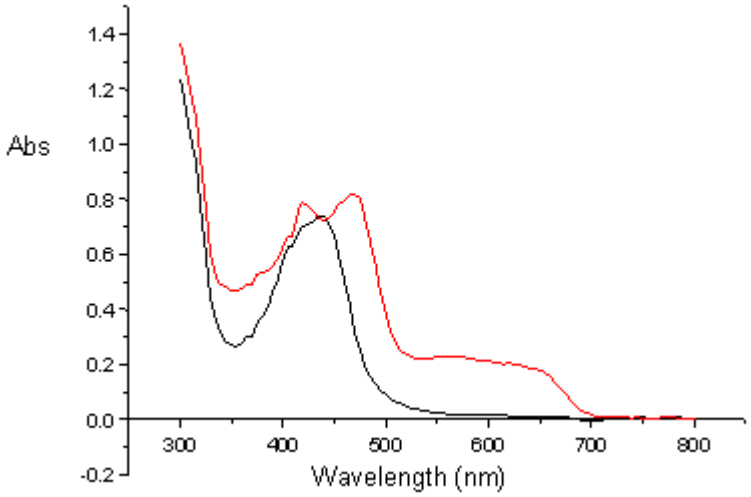

Figure 3.40: Absorbance spectra of the mononuclear complexes $[Ru(bpy)_2(pyrphen)]^{2+}$ 0.04mM (black) and $[Os(bpy)_2(pyrphen)]^{2+}$ 0.04mM (red) in acetonitrile

Complex	**Absorption λ_{max} (nm)**	**Extinction Coefficient (ε) ($M^{-1}cm^{-1}$)**
$[Ru(bpy)_2(thimphen)]^{2+}$	424	18677
$[Ru(bpy)_2(pyrphen)]^{2+}$	435	19221
$[Ru(bpy)_2]^{3+}$	450	11500 [24]
$[Os(bpy)_2(thimphen)]^{2+}$	440	16780
$[Os(bpy)_2(pyrphen)]^{2+}$	469	15604
$[Os(bpy)_2]^{3+}$	468	11100 [24]

Table 3.17: Absorbance properties of $[Ru(bpy)_2(thimphen)]^{2+}$, $[Ru(bpy)_2(pyrphen)]^{2+}$, $[Ru(bpy)_3]^{2+}$, $[Os(bpy)_2(thimphen)]^{2+}$, $[Os(bpy)_2(pyrphen)]^{2+}$ and $[Os(bpy)_3]^{2+}$ in acetonitrile at 293K.

The UV-vis spectra of the four mononuclear complexes shown in Figure 3.39 and Figure 3.40 are dominated by intense absorbance in the visible region at 424 nm and 435 nm for the ruthenium complexes and 440 nm and 469 nm for the osmium complexes. These bands are attributed to dπ-π* metal to ligand charge transfer (^{1}MLCT) transitions as explained previously in Chapter 1.

The osmium complexes display further, less intense absorbance at 570 nm which are due to a formally forbidden triplet dπ-π* (^{3}MLCT) transition. The increase in spin orbit coupling observed for osmium complexes as compared to ruthenium allows for a greater mixing of the singlet and triplet states, resulting in a breakdown in the selection rules prohibiting changes in spin. (*c.f.* Chapter 1)

Any changes in the wavelength at which the ^{1}MLCT absorbance occur when compared to the parent compound $[Ru(bpy)_3]^{2+}$ is attributable to the coordinated ligand(s).[16] π-acceptor ligands will cause a red shift (i.e. a shift to longer wavelength) as its interaction with the metal dπ orbitals (through backbonding) stabilises the metal orbitals resulting in a greater energy difference between the t_2g and π* energy levels[27]. However, introduction of σ-donor ligands will cause a blue shift as ligands of this type will donate electron density to the metal, further destabilising the t_2g and so makes the dπ-π* transition more energetically favourable (by decreasing the energy gap between them).

In the case of the complexes measured here there is little difference observed when compared to the literature complexes $[Ru(bpy)_3]^{2+}$ and $[Os(bpy)_3]^{2+}$.

The room temperature emission spectral data of the ruthenium and osmium metal complexes of the ligands synthesised are shown below in Figure 3.41 and Figure 3.37.

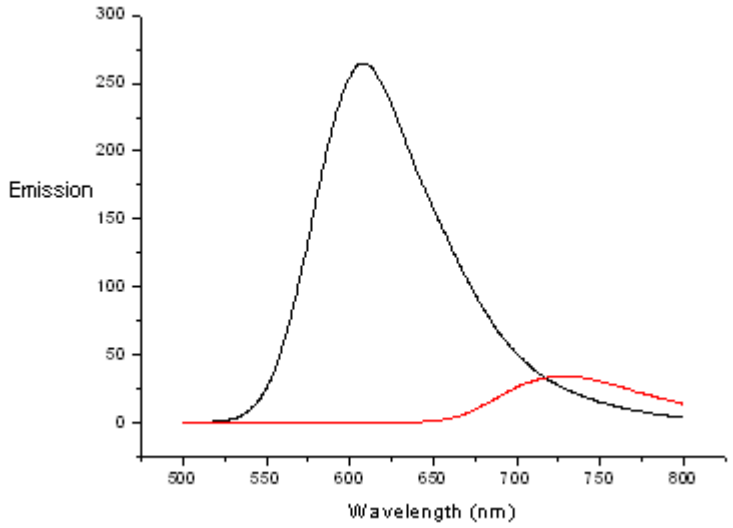

Figure 3.41: Emission spectra of the mononuclear complexes $[Ru(bpy)_2(thimphen)]^{2+}$ 1.0 mM (black) and $[Os(bpy)_2(thimphen)]^{2+}$ 1.0 mM (red) in acetonitrile at 293K

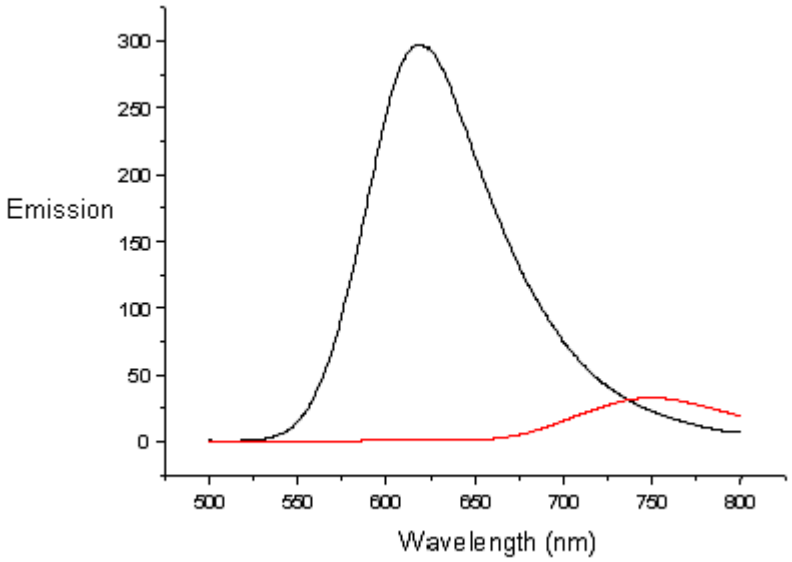

Figure 3.42: Emission spectra of the mononuclear complexes $[Ru(bpy)_2(pyrphen)]^{2+}$ 1.0 mM (black) and $[Os(bpy)_2(pyrphen)]^{2+}$ 1.0 mM (red) in acetonitrile at 293K.

Complex	**Emission λ_{max} (nm)**
$[Ru(bpy)_2(thimphen)]^{2+}$	607
$[Ru(bpy)_2(pyrphen)]^{2+}$	618
$[Ru(bpy)_3]^{2+}$	615[24]
$[Os(bpy)_2(thimphen)]^{2+}$	726
$[Os(bpy)_2(pyrphen)]^{2+}$	748
$[Os(bpy)_3]^{2+}$	732[24]

Table 3.18: Emission properties of $[Ru(bpy)_2(thimphen)]^{2+}$, $[Ru(bpy)_2(pyrphen)]^{2+}$, $[Ru(bpy)_3]^{2+}$, $[Os(bpy)_2(thimphen)]^{2+}$, $[Os(bpy)_2(pyrphen)]^{2+}$ and $[Os(bpy)_3]^{2+}$ in acetonitrile at 278K

The four mononuclear complexes display luminescence at room temperature originating from the ^{3}MLCT. Their emissive properties are shown above in Table 3.18. As seen for the absorbance properties there is little difference when compared to the parent complexes, which can be attributed to experimental error.

3.2.7 Acid/Base Properties of Mononuclear Complexes

All of the complexes described here contain a labile proton, present at the imidazole group of the –imphen type ligand. As the removal of this proton results in a decrease in charge, it also represents a potential change in the electronic behaviour of the parent complex. There has been extensive research in this area in recent years[28, 29] particularly for use as pH responsive „on/off switches".[30, 31] In similar complexes to those discussed in this chapter, the protonation state of the imidazole group has been shown to modify the complexes" luminescence behaviour[32] The presence or absence of this proton is invariably pH dependent and so it was deemed necessary to investigate the effect of pH on the UV/vis properties of the complexes.

The effect of changing pH in a Britton-Robson buffer on the UV-vis and emission spectra of $[Ru(bpy)_2(thimphen)]^{2+}$ is shown in Figures 3.33-3.36

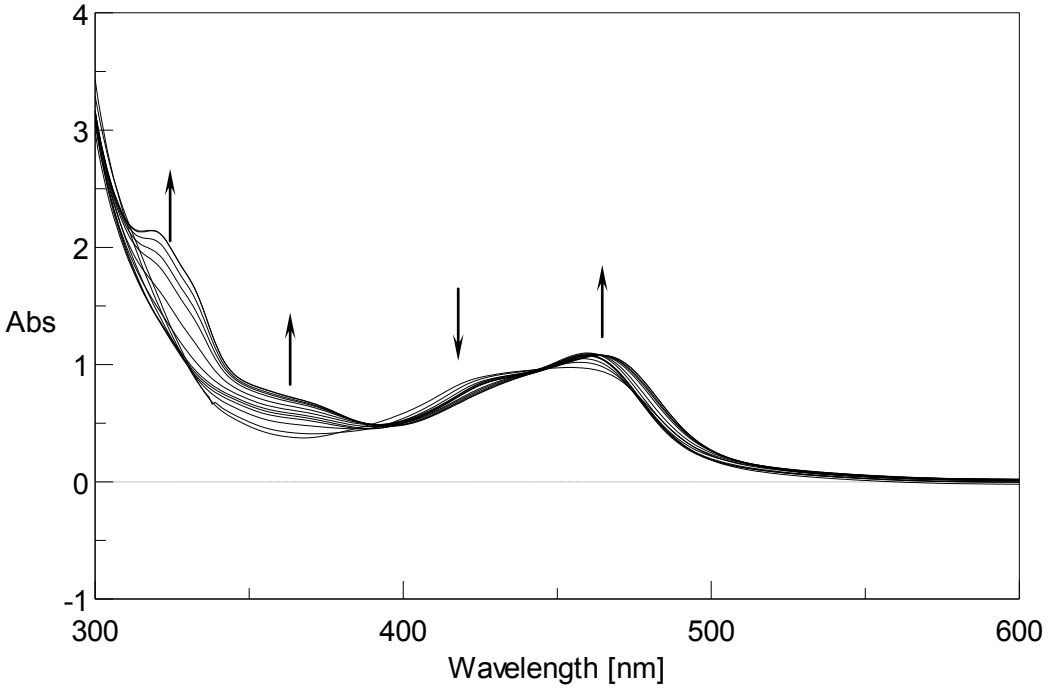

Figure 3.43: UV-vis absorbance spectra of $[Ru(bpy)_2(thimphen)](PF_6)_2$ recorded between pH 2 and 12 showing the direction of pH related change in each spectral region.

Minor changes are observed in these spectra with changing pH though no change is seen in the λ_{max} of the spectra. One such change occurs at 367 nm between pH 1 and 5 and is shown below in Figure 3.44.

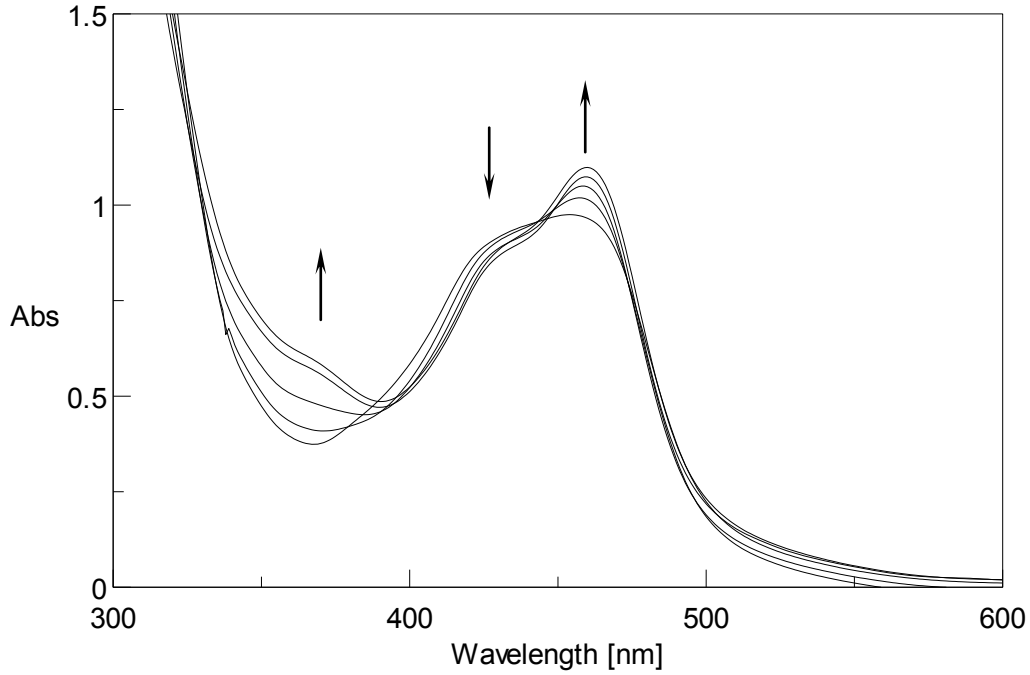

Figure 3.44: UV spectra of $[Ru(bpy)_2(thimphen)](PF_6)_2$ at between pH 1 and 5 showing the direction of pH related spectral changes

This change in intensity may be plotted against pH to yield a titration curve, as shown in Figure 3.45.

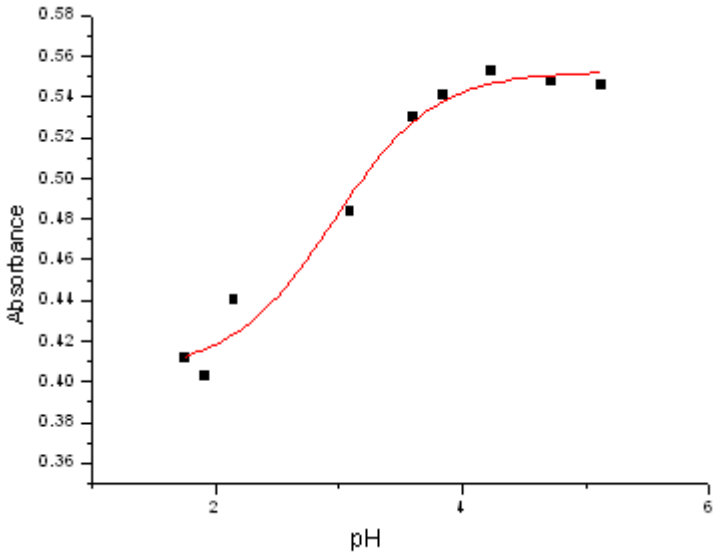

Figure 3.45: Titration plot for $[Ru(bpy)_2(thimphen)](PF_6)_2$ at 350 nm between pH 2 and 5

This titration curve places the pK_a of $[Ru(bpy)_2(thimphen)](PF_6)_2$ at 3.06.
A similar change in absorbance is seen at the same wavelength between pH 5 and 12, and also at 486 nm within the same pH range. Both of these changes are shown below in Figure 3.46.

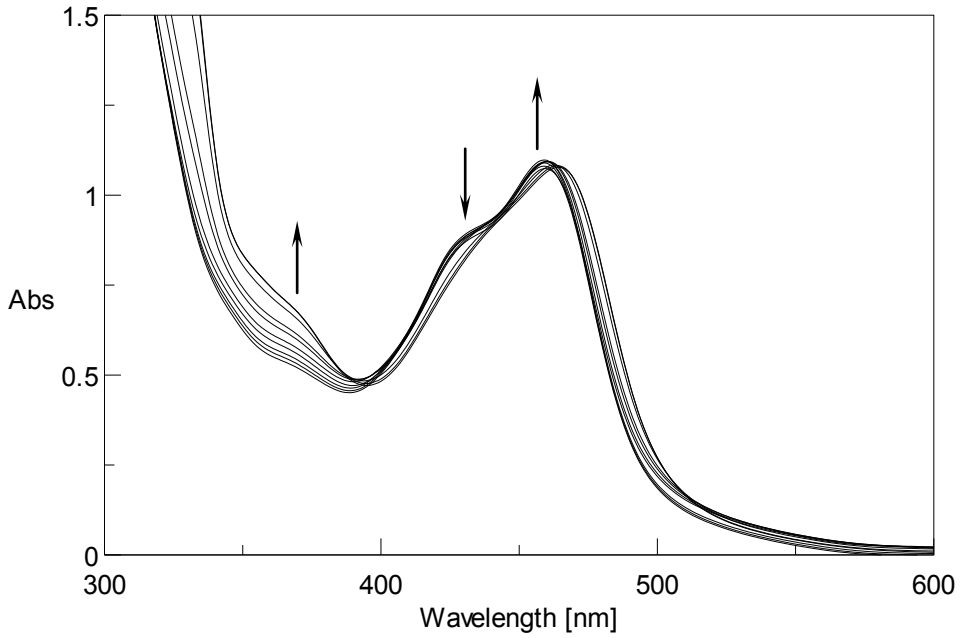

Figure 3.46: UV spectra of $[Ru(bpy)_2(thimphen)](PF_6)_2$ between pH 5 and 12 showing the direction of pH related spectral changes

As is visible in Figure 3.46 three main changes are visible between pH 5 and 12, an increase in absorbance intensities at 367 nm and 486 nm. A decrease is visible at 432 nm as well as a minor red shift for the λ_{max} of the complex between pH 10 and 12. The changes in absorbance visible at 367nm and 486 nm were plotted against pH to yield the titration curves shown below in Figure 3.47 (367 nm) and Figure 3.48 (486 nm).

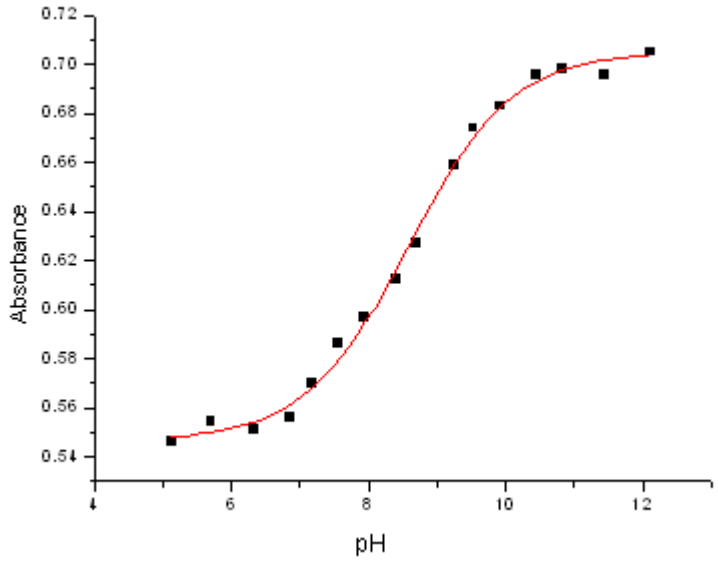

Figure 3.47: Titration plot for $[Ru(bpy)_2(thimphen)](PF_6)_2$ using absorbance data at 367 nm between pH 5 and 12

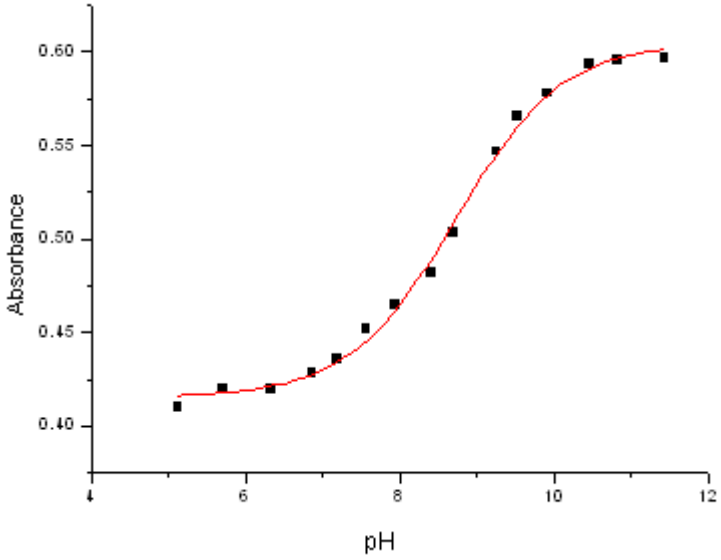

Figure 3.48: Titration plot for $[Ru(bpy)_2(thimphen)](PF_6)_2$ using absorbance data at 486 nm between pH 5 and 12

Both of these titration curves place the pK_a of $[Ru(bpy)_2(thimphen)](PF_6)_2$ at 9.02. In a system such as this, one would expect three separate protonation states, $M(L)_2(H_2L^{4+})$, $M(L)_2(LH^{3+})$ and $M(L)_2(L^{2+})$; where L is 2,2′-bipyridine and L^{2+} is thimphen. These three protonation states are shown diagrammatically below in Figure 3.49.

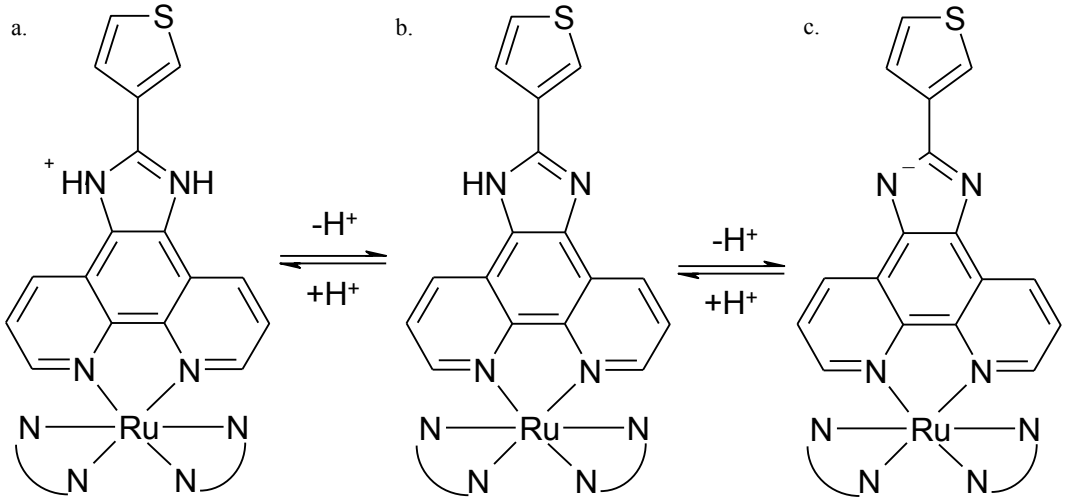

Figure 3.49: Structural representation of the protonation states of $[Ru(bpy)_2(thimphen)]^{2+}$ where (a) is $M(L)_2(H_2L'^{+})$, (b) is $M(L)_2(HL')$ and (c) is $M(L)_2(L'^{-})$

The pK_a value of 3.06 must relate to the first deprotonation step in which the complex $M(L)_2(LH^{+}\text{-}H^{+})$ is singly deprotonated and converted to $M(L)_2(H_2L'^{+})$. The second deprotonation step shown in Figure 3.49 (c) may then be signified by the pK_a value of 9.02. This is however at odds with the fact that the pK_a of free imidazole is 14.5[33]. In this experiment, pH 14 or higher was not measured as upon reaching approximately pH 12.5 the amounts of base needed to increase the pH resulted in the concentration of the overall solution to change. As this would have introduced an unacceptable level of error to the results obtained, the experiment was stopped at this point.

In order to better understand the ground state pK_a value obtained above, the above pH monitoring experiment was also attempted on the free ligand. Upon reaching pH 5 however, the solution became cloudy, which is consistent with the neutralisation method of precipitation of the ligand from reaction solution[15]. As a result any measurements recorded over a pH gradient was deemed unfeasible for the free ligand thimphen.

However, comparing the pK_a values obtained for the metal complex $[Ru(bpy)_2(thimphen)]^{2+}$ to literature values a level of similarity may be observed. For example, similar pK_a values were obtained by Gao *et al* in their ground state pH studies on the ruthenium-phenanthro-imidazo complexes $[Ru(bpy)_2(pipipH_2)]^{2+}$, $[Ru(bpy)_2(dpipipH_2)]^{2+}$ and $[Ru(bpy)_2(bpibH_2)]^{2+}$ shown in Figure 3.50 below.

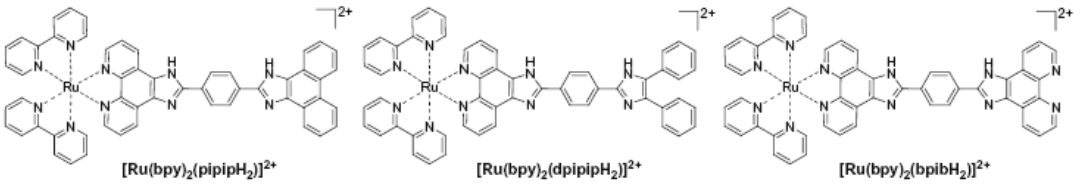

Figure 3.50: Chemical structures for 3 ruthenium phenanthro-imidazole complexes investigated for pH responsive behaviour by Gao et al[34]

These complexes each display three distinct pK_a values: one at pH ~0.7, one at pH ~5 and a third at pH ~11. The latter two approximate pK_a values obtained by Gao et al are comparable to those obtained for $[Ru(bpy)_2(thimphen)]^{2+}$.

Two distinct isosbestic points are also visible for the absorbance of $[Ru(bpy)_2(thimphen)]^{2+}$ across a particular pH range. The first, shown below in Figure 3.51, is present at 387 nm for the pH range 6-12.

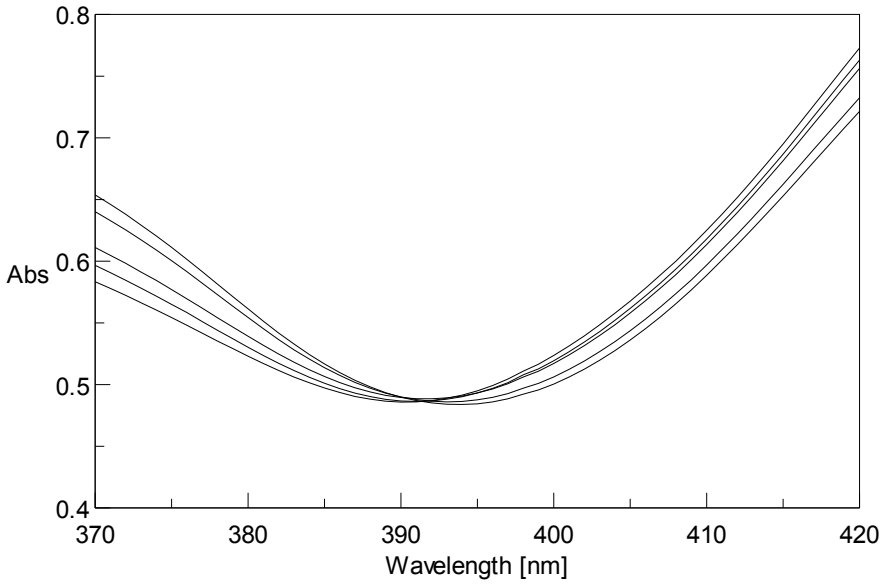

Figure 3.51: Isosbestic Point visible at 387 nm for $[Ru(bpy)_2(thimphen)]^{2+}$ between pH 6 and 12

A second isosbestic point is also visible for $[Ru(bpy)_2(thimphen)]^{2+}$ within the same pH range, at 465 nm. This is shown below in Figure 3.52.

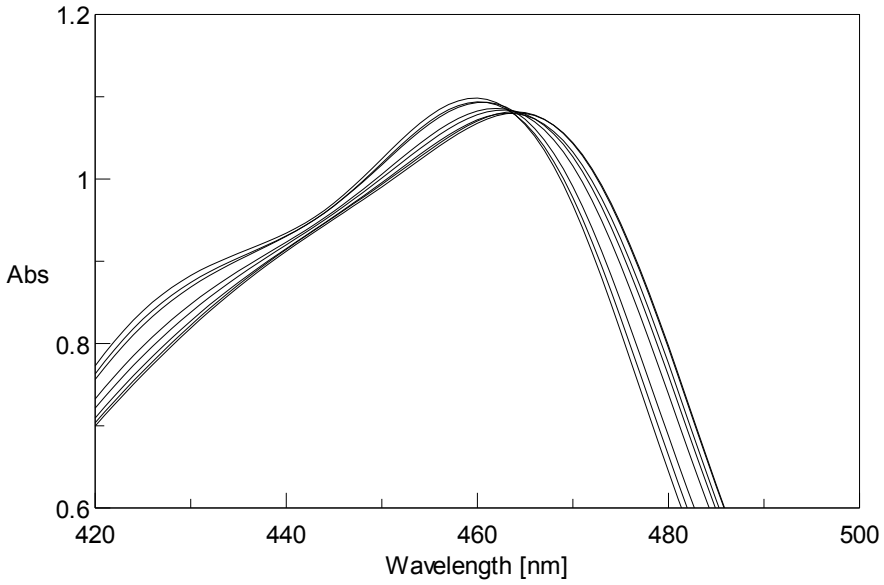

Figure 3.52: Isosbestic point visible at for [Ru(bpy)$_2$(thimphen)]$^{2+}$ 465nm between pH 6 and 12

Emission data was obtained for [Ru(bpy)$_2$(thimphen)]$^{2+}$ using these isosbestic points as excitation wavelengths. The emission data obtained for [Ru(bpy)$_2$(thimphen)]$^{2+}$using 387 nm as an excitation wavelength between pH 6 and 12 is shown below in Figure 3.53.

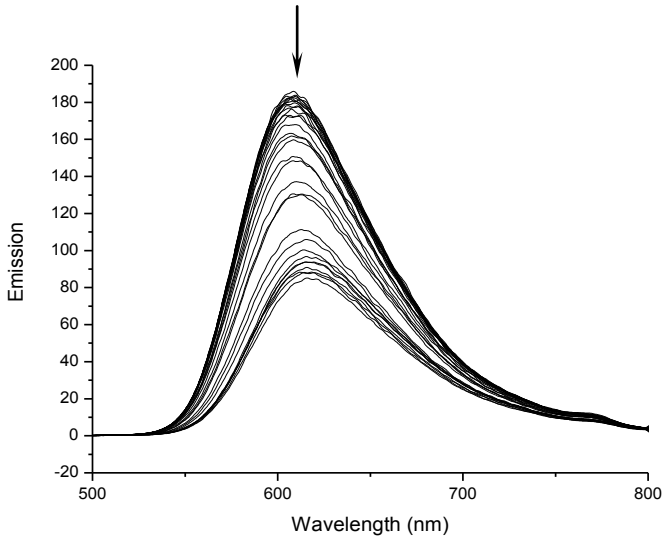

Figure 3.53: Emission spectra of Ru[(bpy)$_2$(thimphen)]$^{2+}$ at 387 nm excitation between pH 6 and 12 showing the direction of pH related spectral changes.

A visible change in emission intensity is plainly seen over this pH range, and a resultant titration curve may be easily plotted, as shown below in Figure 3.54.

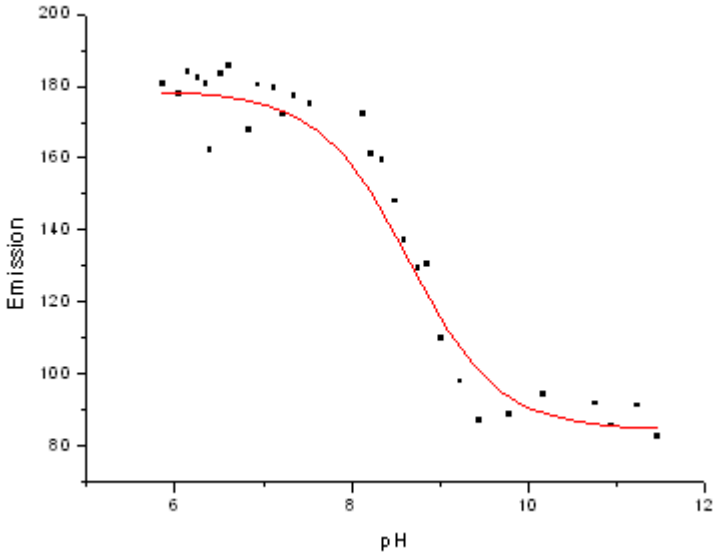

Figure 3.54: Titration plot for $[Ru(bpy)_2(thimphen)](PF_6)_2$ using emission data employing 387 nm as an excitation wavelength

Similar data was collected for the emission of the same complex using 465 nm as an excitation wavelength. A similar range of emissions was obtained, shown below in Figure 3.55

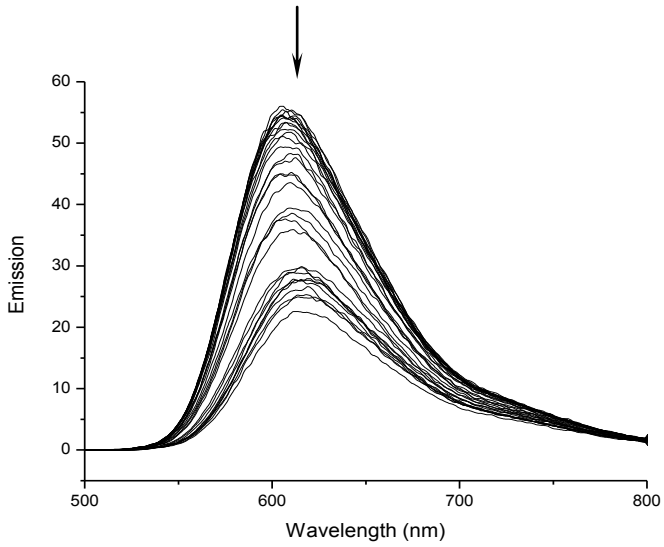

Figure 3.55: Emission spectra of $Ru[(bpy)_2(thimphen)]^{2+}$ at 465 nm excitation between pH 6 and 12 showing the direction of pH related spectral changes

Again, a titration curve was plotted using this information and is shown below in Figure 3.56.

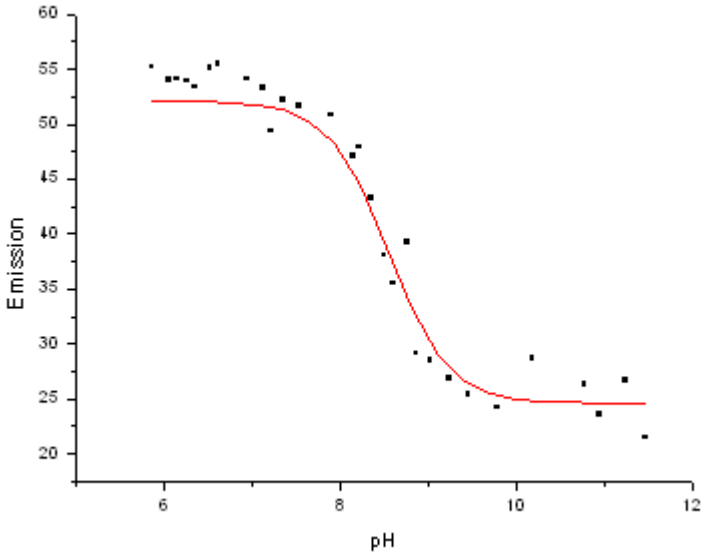

Figure 3.56: Titration plot for $[Ru(bpy)_2(thimphen)](PF_6)_2$ using emission data employing 465 nm as an excitation wavelength

Both of these titration curves shown in Figure 3.54 and Figure 3.56 place the excited state pK_a of $[Ru(bpy)_2(thimphen)](PF_6)_2$ at 8.52. This is comparable with the ground state pK_a of 9.02, indicating that this excited state pK_a is representative of the deprotonation step shown in Figure 3.49 (c). Again this value is comparable for the values of ~11.5 obtained for the excited state pK_as of the complexes shown in Figure 3.50 by Gao *et al.*[34] There is no clear isosbestic point visible in the absorbance data shown above within the pH range 1-5. This is not to say there is no excited state pK_a corresponding to this pH range, it is possible however that the changes observed for this pH range are so minute that clear measurements cannot be made for an excited state pK_a here.

The effects of pH in Britton-Robson buffer on the UV-vis absorption and emission spectra of $[Ru(bpy)_2(pyrphen)](PF_6)_2$ has also been investigated. The UV-vis absorption spectra recorded across the pH range 2.0 to 13.5 is shown below in Figure 3.57.

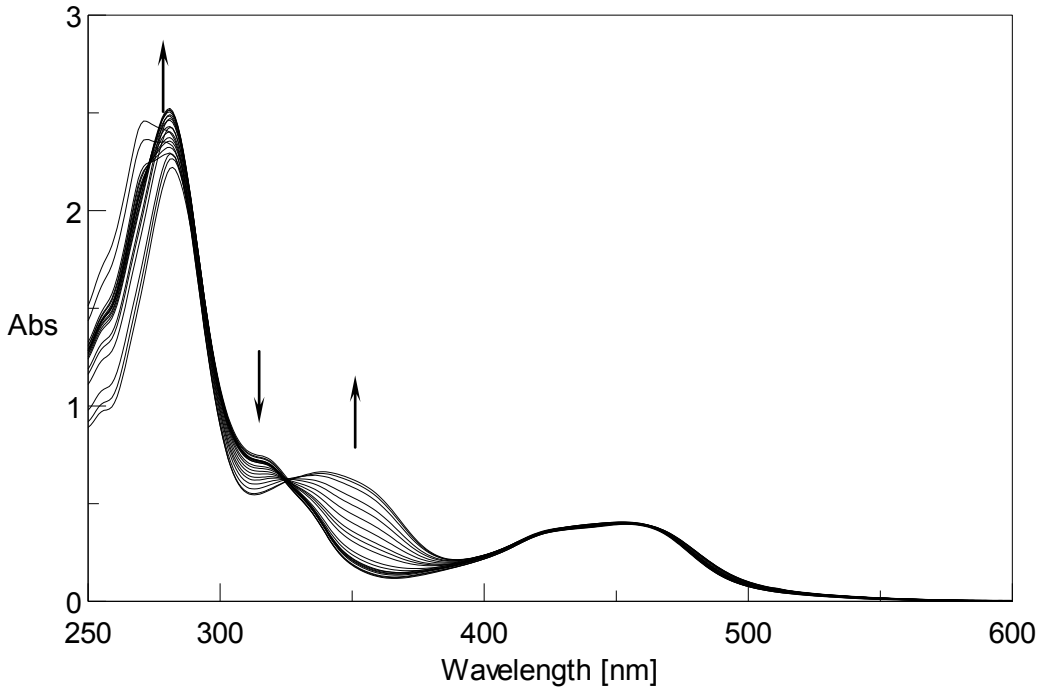

Figure 3.57: UV-vis absorbance spectra of $[Ru(bpy)_2(pyrphen)]^{2+}$ recorded between pH 2.0 and 13.5

In contrast to the spectra of $[Ru(bpy)_2(thimphen)]^{2+}$ across a similar pH range as shown in Figure 3.43, there are some dramatic changes in absorbance visible for $[Ru(bpy)_2(pyrphen)]^{2+}$. Two main wavelengths were chosen at which changes in absorbance intensity were observed. The first of which is 280 nm, shown below in Figure 3.58, in which the change in intensity is seen between pH 2.35 and 3.64.

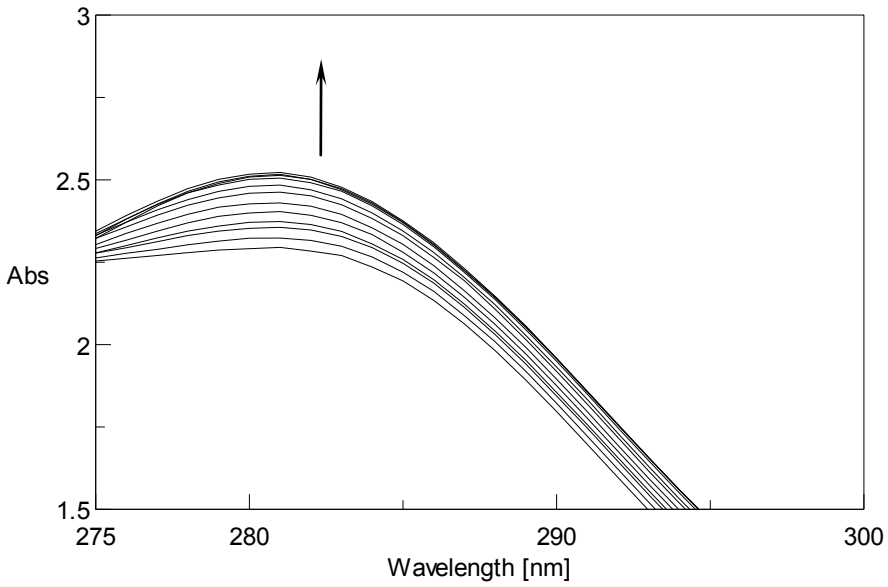

Figure 3.58: UV spectra for $[Ru(bpy)_2(pyrphen)]^{2+}$ between pH 2.35 and 3.64 showing related pH spectral changes.

A titration plot was attempted using this data, but the changes observed did not allow for the construction of a sigmoidal type curve. Therefore the information regarding pK_a assignment shall be taken from the second wavelength at which a visible change in absorbance intensity occurred: 350 nm. This change in absorbance also occurred over the pH range 2.35-3.64 and is shown below in Figure 3.59.

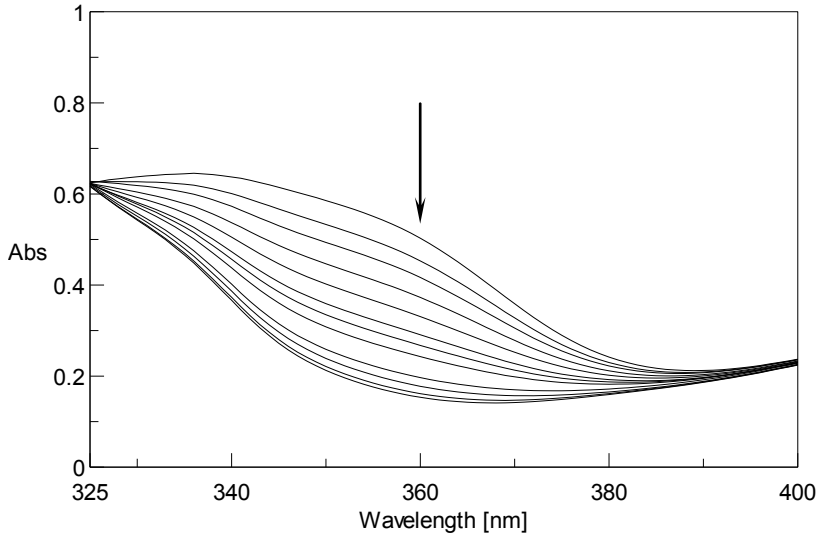

Figure 3.59: UV spectra for $[Ru(bpy)_2(pyrphen)]^{2+}$ between pH 2.35 and 3.64 showing related pH spectral changes.

The information from this range of data allowed for the creation of a successful titration curve, shown below in Figure 3.60.

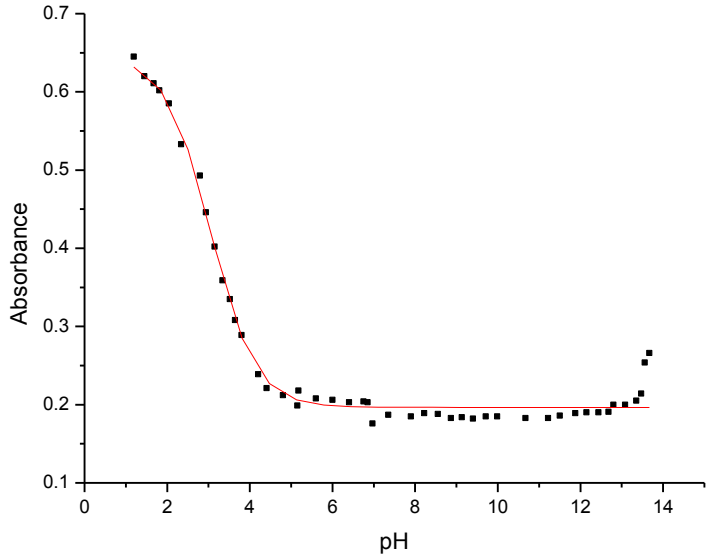

Figure 3.60: Titration plot for $[Ru(bpy)_2(pyrphen)](PF_6)_2$ using absorbance data at 350 nm

This titration curve places the pK_a of $[Ru(bpy)_2(pyrphen)]^{2+}$ at 3.16. This is comparable to the value of 3.06 obtained for $[Ru(bpy)_2(thimphen)]^{2+}$. However, the incline of the curve shown in Figure 3.60 is much steeper than that corresponding to the same process in $[Ru(bpy)_2(thimphen)](PF_6)_2$ shown in Figure 3.45. In order to explain this difference in character between the two spectra, it is necessary to examine the differences in potential protonations between the two metal complexes.

In the case of $[Ru(bpy)_2(thimphen)]^{2+}$ there are three possible protonation states, signifying two possible protonation/deprotonation steps. This has been illustrated previously in Figure 3.49. However, $[Ru(bpy)_2(pyrphen)]^{2+}$ provides a fourth possible protonation state by virtue of its appended pyridine group. As the pyridine moiety may be protonated also, the complex $M(L)_2(LH^{+}\text{-}(H^{+})_2)$ may be formed at low pH and so is added to the list of previously discussed imidazole based protonation states $M(L)_2(LH^{+}\text{-}H^{+})$, $M(L)_2(LH^{+})$ and $M(L)_2(L^{-})$.

These four protonation states and the three associated protonation/deprotonation steps are shown schematically in Figure 3.61 below.

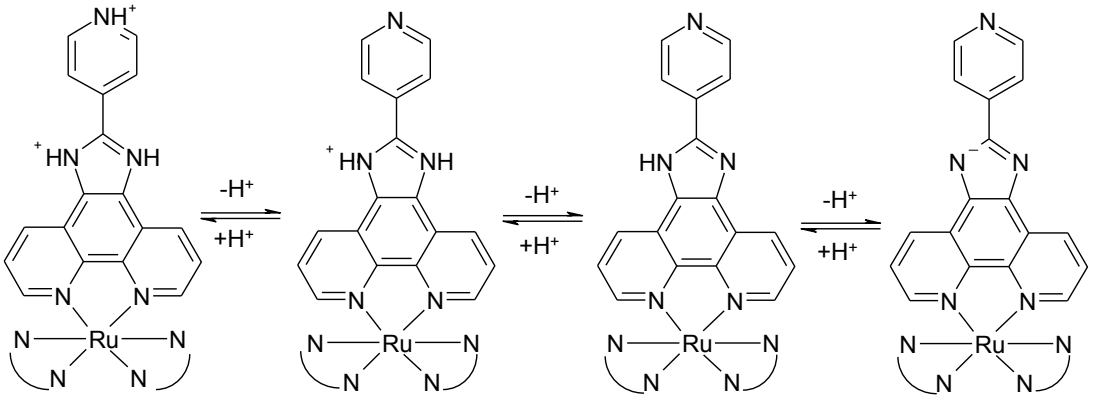

Figure 3.61: Structural representation of the protonation states of $[Ru(bpy)_2(pyrphen)]^{2+}$ where (a) is $M(L)_2(LH'\text{-}(H^+)_2)$, (b) is $M(L)_2(LH'\text{-}H^+)$, (c) is $M(L)_2(LH')$ and (d) is $M(L)_2(L^-)$

The pK_a of free pyridine is 5.14[35] As a result it may be postulated that the deprotonation signified by this pK_a of 3.16 is attributable to the deprotonation of the pyridine group as well as the first imidazole protonation as explained above for $[Ru(bpy)_2(thimphen)](PF_6)_2$.

As for $[Ru(bpy)_2(thimphen)]^{2+}$, $[Ru(bpy)_2(pyrphen)]^{2+}$ displays a number of isosbestic points across certain pH ranges. There are isosbestic points visible at 277 nm and 364 nm between pH 2.35 and 3.64. These are shown below in Figure 3.62 and Figure 3.63.

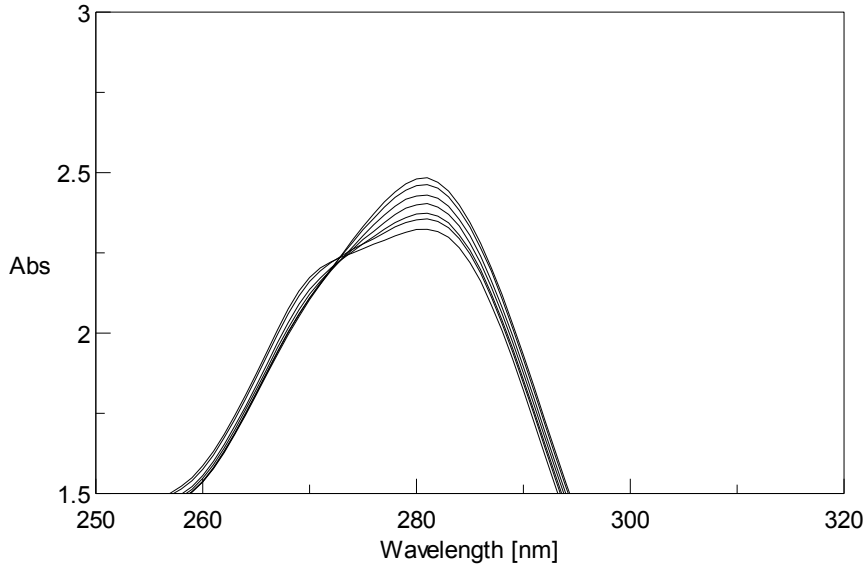

Figure 3.62: Isosbestic point visible for $[Ru(bpy)_2(pyrphen)]^{2+}$ at 277nm between pH 2.35 and 3.52

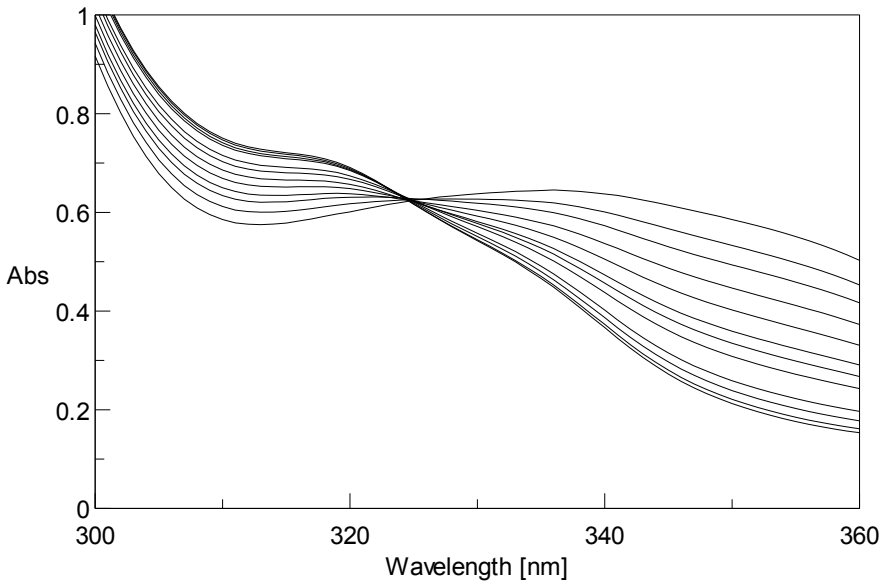

Figure 3.63: Isosbestic point visible for $[Ru(bpy)_2(pyrphen)]^{2+}$ at 324nm between pH 2.35 and 3.64.

As before the emission of the metal complex was measured using these isosbestic wavelengths as the point of excitation. The resulting emission spectra are shown below in Figure 3.64 and Figure 3.65.

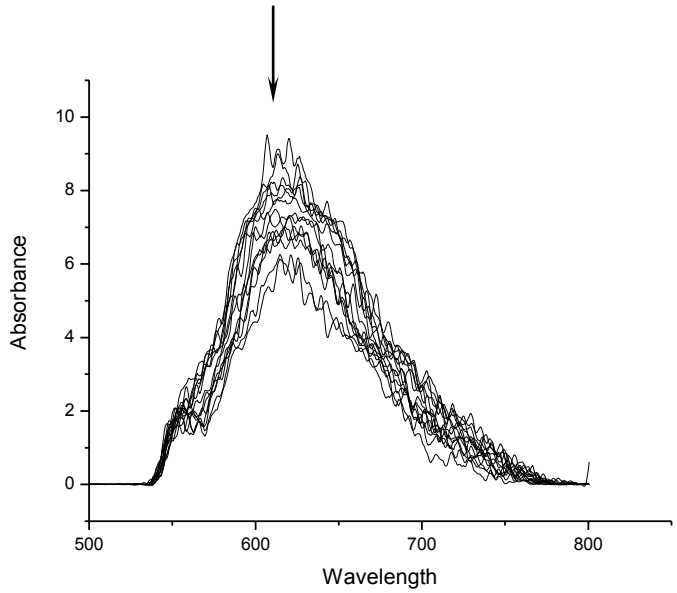

Figure 3.64: Emission spectra of Ru[(bpy)$_2$(pyrphen)]$^{2+}$ at 277 nm excitation between pH 2.35 and 3.64 showing the direction of pH related spectral changes

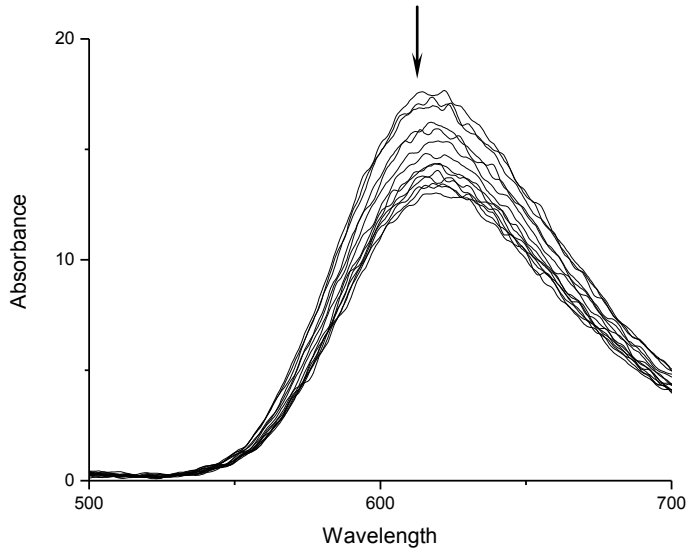

Figure 3.65: Emission spectra of Ru[(bpy)$_2$(pyrphen)]$^{2+}$ at 364 nm excitation between pH 2.35 and 3.64 showing the direction of pH related spectral changes.

Attempts were made to construct titration plots from the data provided in these spectra, but neither wavelength provided a sigmoidal type curve. The attempted titration curves are shown below in Figure 3.66 and Figure 3.67.

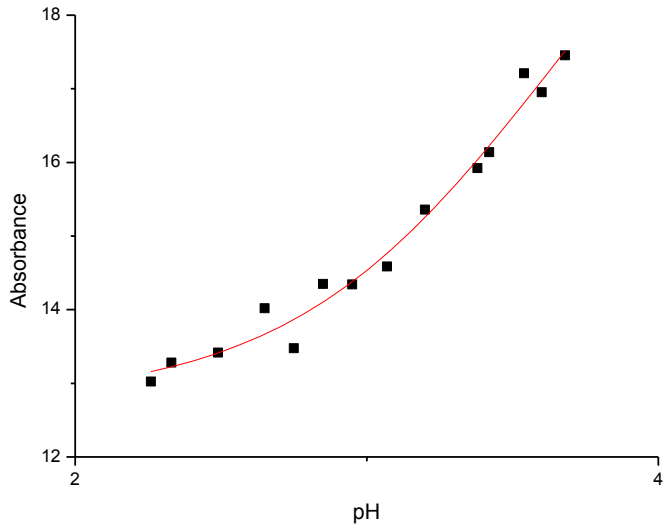

Figure 3.66: Titration plot for $[Ru(bpy)_2(pyrphen)](PF_6)_2$ using emission data employing 277 nm as an excitation wavelength

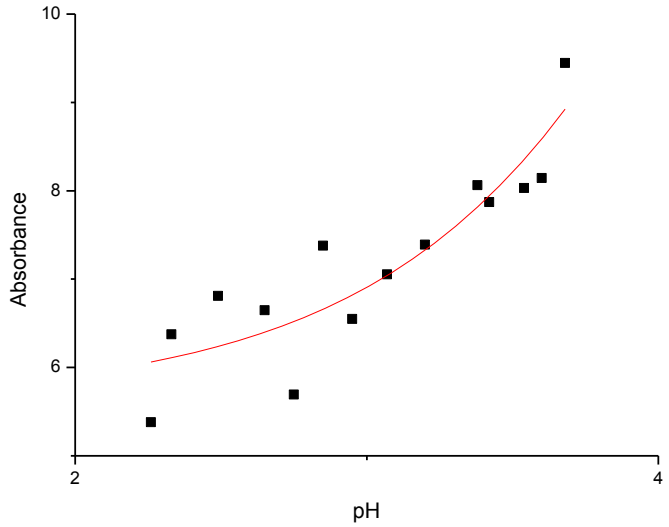

Figure 3.67: Titration plot for $[Ru(bpy)_2(pyrphen)](PF_6)_2$ using emission data employing 365 nm as an excitation wavelength

It is possible that the highly visible deprotonation of the pyridine group in the $[Ru(bpy)_2(pyrphen)](PF_6)_2$ molecule so dwarfs any metal based changes, which even in the case of $[Ru(bpy)_2(thimphen)_2](PF_6)_2$ are extremely minute, that they are not visible and so cannot be plotted accurately in a titration type curve.

The fact that the changes in pH display such a small influence on the behaviour of the metal based behaviour of the complexes measured, it may be assumed that pH

conditions and possible protonation states of the –imphen type ligands in these complexes exerts no noticeable effect on the electronic or photophysical behaviour of the complexes.

3.3 Conclusion

Chapter 3 detailed the synthesis of four mononuclear metal complexes and their deuterated analogues as prototypes for molecular transistors. Two different methods of synthesis have been used, direct and indirect synthesis. The free ligand „thimphen" was synthesised using the established method first used by Steck and Day[15]. Its related mononuclear metal complexes were then synthesised successfully using the direct *"complexes as metals / complexes as ligands"* method. The novel complexes $[Ru(bpy)_2(thimphen)]^{2+}$ and $[Os(bpy)_2(thimphen)]^{2+}$ as well as their deuterated analogues were synthesized in this manner. These complexes were characterised by ^1H NMR, mass spectrometry and CHN analysis. Their absorption and emission properties were obtained also. While the ^1H NMR, mass spectrometry, absorbance and emission analyses all produced satisfactory results proving successful synthesis of the target complexes, the elemental analysis results obtained display %N values that do not correspond with the calculated value. Considering the agreement and reliability of the other analytical information received for these complexes, the low %N value obtained has been termed an anomaly perhaps linked to the method of analysis.

The same direct method of synthesis was attempted for the preparation of the ligand „pyrphen" and its related ruthenium and osmium complexes. However this approach was found to be unsuitable due to degradation issues discovered with the free ligand pyrphen. Instead an *"on-the-complex"* method was used, with the pyrphen ligand being built from a ruthenium phenanthroline starting material. This method was found to be successful for the synthesis of the mononuclear complexes $[Ru(bpy)_2(pyrphen)]^{2+}$ and $[Os(bpy)_2(pyrphen)]^{2+}$. These complexes were also characterised by ^1H NMR, mass spectrometry and CHN analysis, with their absorption and emission properties being recorded also. As for $[Os(bpy)_2(thimphen)]^{2+}$ the elemental analysis of both $[Ru(bpy)_2(pyrphen)]^{2+}$ and $[Os(bpy)_2(pyrphen)]^{2+}$ display a low %N value as compared to the calculated value,

but as for the related thimphen complexes this has been termed a possible error linked to the method of analysis.

In an effort to better understand the electronic properties of the metal complexes, spectroscopic titration experiments were carried out on the ruthenium complexes of thimphen and pyrphen. pK_a values for the metal complexes $[Ru(bpy)_2(thimphen)]^{2+}$ and $[Ru(bpy)_2(pyrphen)]^{2+}$ have been identified, but the changes seen over varying pH were found to be minute, making definitive measurement of the pK_a for both complexes difficult. Due to the small nature of these changes with the absorbance spectra recorded however it was concluded that the protonation state of the metal complex has little impact on the electronic behaviour of the complex.

3.4 Experimental

Materials

Materials

1,10-phenanthroline-5,6-dione[36], $[Ru(bpy)_2Cl_2].2H_2O$[37], $[Os(bpy)_2Cl_2].2H_2O$[38], $[Ru(d_8\text{-}bpy)_2Cl_2].2H_2O$, $[Os(d_8\text{-}bpy)_2Cl_2].2H_2O$, $[Ru(bpy)_2(phen)](PF_6)_2$[39], $[Os(bpy)_2(phen)](PF_6)_2$ were synthesised according to established literature procedures as described in Chapter 2. All other chemicals were purchased from Sigma-Aldrich and used without further purification. All synthetic solvents used were of reagent grade. All solvents used for spectroscopic measurements were of HPLC grade.

3.4.1 Synthesis of Ligands

Thimphen

2-(3-thio)imidazo[f]-1,10-phenanthroline

Thimphen was synthesised using an established literature approach [40, 14]. 3.50 g (17 mmol) 1,10-phenanthroline-5,6-dione and 11.55 g (150 mmol) ammonium acetate were dissolved in 150 cm^3 glacial acetic acid. This mixture was warmed and 1.56 cm^3 (17 mmol) 3-thiophene carboxaldehyde was added dropwise. The resulting mixture was heated to 90^0C for 5 hours, cooled to room temperature, poured onto 500 cm^3

H_2O and neutralised with conc. ammonia. The resulting brown precipitate was filtered, washed with water and dried with diethyl ether. This crude product was recrystallised from hot methanol.

Yield: 50% (2.60g)

^1H NMR: d_6-DMSO ^1H δ 9.00 (dd, 2H, H_5+H_6, J=2.4Hz), 8.84 (d, 2H, H_1+$_2$, J=7.2Hz), 8.293 (d, 1H, H_9, J=1.6 Hz), 7.87 (d, 1H, H_{10}, J=5.2Hz), 7.81-7.76 (m, 3H, H_3+H_4+H_{11})

Mass spec: Observed m/z: 303.2 $[M^+]$

Calc m/z = 302.37

Elemental Analysis: $C_{17}N_4H_{10}S.3H_2O$: Observed: %C: 57.3, %H: 4.5, %N: 16.8

Calculated:%C: 57.4, %H: 4.4, %N: 15.7

Pyrphen

2-(4-pyridyl)imidazo[f]-1,10-phenanthroline

This ligand was synthesised using a modified literature approach.[40,14]

200mg (0.95 mmol) 1,10-phenanthroline-5,6-dione and 1.47g (19.04 mmol) ammonium acetate were dissolved in 6 cm^3 dry glacial acetic acid at 100^0C. 0.08 cm^3 (0.95 mmol) 4-pyridyl carboxaldehyde was added dropwise to the mixture, which was heated at 100^0C for 1 hr. The hot solution was then poured into a beaker and allowed to stand for 1 hr. The yellow precipitate formed was filtered off and allowed to dry under vacuum.

Yield: 25% (72 mg)

^1H NMR: DMSO ^1H δ: 9.03 (dd, 2H, H_5+H_6, J=2.4Hz), 8.89 (dd, 2H, H_1+H_2, J=2.8Hz), 8.78 (d, 2H, H_{11}+H_{12}, J=6Hz), 8.18 (d, 2H, H_9+H_{10}, J=6.4Hz), 7.82 (dd, 2H, H_3+H_4, J=3.6Hz)

Mass spec: Observed m/z: 298.3 $[M+1^+]$

Calc m/z = 297

Elemental Analysis: $C_{18}N_5H_{11}.2CH_3COOH$: Observed: %C: 57.9, %H:3.7, %N: 16.3

Calculated: %C: %C: 63.6, %H: 4.1, %N: 16.8

3.4.2 Synthesis of Metal Complexes

Method A: Direct synthesis

$[Ru(bpy)_2(thimphen)](PF_6)_2$

374 mg (1.2 mmol) thimphen ligand was dissolved in 25 cm^3 2:1 ethanol:water and heated to reflux temperature. 500 mg (0.96 mmol) $Ru(bpy)_2Cl_2.2H_2O$ in 55 cm^3 2:1 ethanol:water was added to the reaction mixture over 1 hr. The resulting mixture was heated at reflux for 5 hours. The ethanol was removed from the mixture by rotary evaporation. The remaining solution was allowed to cool to room temperature and a saturated aqueous solution of NH_4PF_6 was added. The orange mixture was left at 5^0C overnight, filtered and the resulting solid was columned on alumina with CH_3CN and recrystallised from acetone:water 50:50.

Yield: 33% (318.9 mg)

^1H NMR: DMSO ^1H δ= 9.03 (d, 2H, H_5+H_6), 8.82 (dd, 4H, H_{3b}, J=7.6Hz), 8.39 (dd, H_9, J=4.0Hz), 8.20 (t, 2H, H_{4b}, J=8.0 Hz), 8.09 (t, 2H, $H_{4b''}$, J=8.4Hz) 8.05 (d, 2H, H_1+H_2), 7.93-7.89 (m, 3H, H_3+H_4+H_{10}), 7.85-7.83 (m, 3H, H_{11}+H_{6b}), 7.61-7.56 (m, 4H, H_{5b}+$H_{6b''}$), 7.34 (t, 2H, $H_{5b''}$, J=4.4 Hz)

Mass spec: Observed m/z: 358

Calc m/z = 357.92

Elem. Anal: $[C_{37}H_{26}N_8SRu](PF_6)_2.½CH_3CN$.:

Observed: %C: 45.0, %H: 3.3, %N: 11.1

Calculated: %C: 44.4, %H: 2.8, %N: 11.6

$[Os(bpy)_2(thimphen)](PF_6)_2$

61 mg (0.20 mmol) thimphen was dissolved in 5 cm^3 ethylene glycol at 100^0C.

100 mg (0.17 mmol) [Os(bpy)2Cl2].$2H_2O$ was added to the reaction in 6 cm^3 ethylene glycol over 1 hr. The resulting mixture was refluxed for 4 hr, cooled to room temperature and added slowly to 50 cm^3 saturated NH_4PF_6 aqueous solution. The resulting black/green solid was filtered and columned on alumina using 50:50 $CHCl_3$: CH_3CN and recrystallised from acetone: water 50:50.

Yield: 43.26% (80 mg)

^1H NMR: ^1H DMSO δ: 8.74 (d, 2H, H_5+H_6, J=8 Hz), 8.53 (dd, 4H, H_{3b}, J=8 Hz), 8.29 (t, 1H, H_9, J=1.2 Hz), 7.97-7.89 (m, 5H, H_1+H_2+H_{10}+H_{4b}), 7.84-7.79 (m, 4H,

$H_{4b''}$+H_{6b}), 7.73-7.68 (m, 3H, H_3+H_4+H_{11}), 7.52 (d, 2H, $H_{6b''}$, J=5.2 Hz), 7.39 (m, 2H, H_{5b}, J=4.4), 7.15 (dt, 2H, $H_{5b''}$, J=4.4Hz)

Mass spec: Observed m/z: 403.3

Calc m/z = 402.48

Elem. Anal: $[C_{37}H_{26}N_8SOs](PF_6)_2.2H_2O$:

Observed: %C: 38.8, %H: 2.3, %N: 8.8

Calculated: %C: 39.2, %H:2.7 , %N: 9.9

Method B: Modification of Precursor Complex

$[Ru(bpy)_2(pyrphen)](PF_6)_2$

Step 1: $[Ru(bpy)_2(phendione)](PF_6)_2$

This step was carried out according to a literature procedure.[20] 300 mg (0.34 mmol) $[Ru(bpy)_2(phen)](PF_6)$ was dissolved in 7 cm^3 H_2SO_4 with stirring. 349 mg (3.39 mmol) NaBr was added, followed by 5.5 cm^3 70% HNO_3. The resulting mixture was heated to 110^0C for 20 min, cooled to room temperature and poured onto 50 cm^3 cold saturated $KPF_{6\ (aq)}$ solution. This mixture was left at 5^0C overnight, filtered and washed with water. This solid was difficult to dry fully and so was assumed to form in quantitative yield and used in the next step

Step 2: $[Ru(bpy)_2(pyrphen)](PF_6)_2$

312 mg (0.34 mmol) $[Ru(bpy)_2(phendione)](PF_6)_2$ was dissolved in 9 cm^3 dry glacial acetic acid with 523 mg (6.78 mmol) ammonium acetate. This mixture was heated to 100^0C and 0.03 cm^3 (0.34 mmol) 4-pyridyl carboxaldehyde was added dropwise. The resulting mixture was heated to 100^0C for 1 hr. After cooling to room temperature 20 m^3 acetone was added and the resulting solution was added to approximately 300 cm^3 diethyl ether with vigorous stirring. The resulting suspension was filtered and the orange solid was dissolved in a small volume of acetone. This solution was diluted to twice its volume with water and the product was precipitated by addition of a saturated aqueous solution of KPF_6. This crude product was filtered, dried at the pump and purified by column chromatography on alumina using acetonitrile as an eluent, followed by recrystallisation from 1:1 acetone: water.

Yield: 153 mg (45.1%)

^{1}H NMR: DMSO ^{1}H δ: 9.13 (2H, d, H_5+H_6), 8.93 (2H, d, H_9+H_{10}), 8.89-8.84 (4H, dd, H_{3b}, J=7.6 Hz), 8.30 (2H, d, H_{11}+H_{12}), 8.24-8.21 (4H, m, H_1+H_2+H_{4b}), 8.12(2H, t, $H_{4b''}$, J=7.6), 8.02 (dd, 2H, H_3+H_4), 7.84 (2H, d, H_{6b}, J=4.8), 7.64-7.59 (4H, m, $H_{6b''}$+H_{5b}), 7.37-7.32 (2H, m, H_{5b})

Mass spec: Observed m/z: 356

Calc m/z = 355.40

Elem. Anal: $[C_{38}H_{27}N_9Ru](PF_6)_2.2H_2O$:

Observed: %C: 44.0, %H: 2.6, %N: 10.6

Calculated:%C: 44.0, %H: 3.0, %N: 12.1

$[Os(bpy)_2(pyrphen)](PF_6)_2$

Step 1: $[Os(bpy)_2(phendione)](PF_6)_2$

This reaction was carried out as for $[Ru(bpy)_2(phendione)](PF_6)_2$, using 500 mg $[Os(bpy)_2(phen)](PF_6)_2$ (0.51 mmol) and 529 mg NaBr (5.14 mmol) in 7.5 cm^3 H_2SO_4 and 5.5 cm^3 70% HNO_3. This reaction was also assumed to occur in quantitative yield and was used immediately in the next reaction.

Step 2: $[Os(bpy)_2(pyrphen)](PF_6)_2$

515 mg (0.51 mmol) $[Os(bpy)_2(phendione)](PF_6)_2$ was dissolved in 15 cm^3 dry glacial acetic acid with 792 mg (10.28 mmol) ammonium acetate. This mixture was heated to 100^0C and 0.049 cm^3 (0.51 mmol) 4-pyridyl carboxaldehyde was added dropwise. The resulting mixture was heated to 100^0C for 1 hr. After cooling to room temperature 40 cm^3 acetone was added and the resulting solution was added to a large amount of diethyl ether with stirring. The resulting suspension was filtered and the black/green solid was dissolved in a small volume of acetone. This solution was diluted to twice its volume with water and the product was precipitated by addition of a saturated aqueous solution of KPF_6. This crude product was filtered, dried at the pump and purified by column chromatography on alumina using acetonitrile as an eluent followed by recrystallisation from 1:1 acetone: water.

Yield: 33mg (29.5%)

^{1}H NMR: DMSO ^{1}H δ: 8.99 (2H, d, H_5+H_6), 8.96-8.81 (6H, m, H_9+H_{10}+H_{3b}), 8.32 (2H, d, H_{11}+H_{12}), 8.16 (2H, d, H_1+H_2), 8.03 (2H, t, H_{4b}, J=4.8 Hz), 7.95-7.90 (4H, m, H_3+H_4+$H_{4b''}$), 7.75 (2H, d, H_{6b}, J=5.2), 7.56-7.51 (4H, m, $H_{6b''}$+H_{5b}), 7.26-7.22 (2H, m, $H_{5b''}$)

Mass spec: Observed m/z: 947 $[M(PF_6)^+]$

Calc m/z = 944.94

Also present: Observed: 801 $[M]^+$; 401 $[M]^{2+}$

Calculated:799 $[M]^+$; 399.5 $[M]^{2+}$

Elem. Anal$[C_{38}H_{27}N_9Os](PF_6)_2.2H_2O$:

Observed: %C: 41.9, %H: 3.2, %N: 8.2

Calculated:%C: 40.5, %H: 2.8, %N: 11.1

3.5 Bibliography

[1] M. Lundstrom *Science* 2003, **299**, 210

[2] G. M. Whitesides, J. C. Love. "The Art of Building Small." Scientific American Reports Sep. 2007, 13

[3] P.J. Low *Dalton Trans.* 2005, 2821

[4] J. M. Tour *Acc. Chem. Res.* 2000, **33**, 791

[5] M. Elbing, R. Ochs, M. Koentopp, M. Fischer, C. von Hänisch, F. Weigend, F. Evers, H. B. Weber, M. Mayor, *PNAS*, 2005, **102**, 8815

[6] S. Grunder, R. Huber, V. Horhoiu, M. T. Gonzalez, C. Schönenberger, M. Calame, M. Mayor, *J. Org. Chem.* 2007, **72**, 8337

[7] J. Park, A. N. Pasupathy, J. I. Goldsmith, C. Chang, Y. Yaish, J. R. Petta, M. Rinkoshi, J. P. Sethna, H. D. Abruña, P. L. McEuan, D. C. Ralph, *Nature,* 2002, **417**, 722

[8] K. Nørgaard, T. Bjørnholm, *Chem. Commun.*, 2005, 1812

[9] T. Albrecht, K. Moth-Poulsen, J. B. Christensen, A. Guckian, T. Bjørnholm, J. G. Vos, J. Ulstrup, *Faraday Discuss.* 2006, **131**, 265

[10] Z. A. Siddique, K. Miyawaki, T. Ohno, *Croatia Chemica Acta,* 2008, **81**, 477

[11] Y. Sun, D. A. Lutterman, C. Turro, *Inorg. Chem.* 2008, **47**, 6427

[12] B Gholamkhass, K. Koike, N. Negishi, H. Hori, K. Takeuchi, *Inorg. Chem.* 2001, **40**, 756

[13] J. Liu, X-H. Zou, Q.-L. Zhang, W.-J. Mei, J-Z. Liu, L-N. Ji, *Metal Based Drugs,* 2000, **7**, 343

[14] T. Cardineals, J. Ramaekers, D. Guillon, B. Donnio, K. Binnemans, *J. Am. Chem. Soc.* 2005, **127**, 17602

[15] E. Steck, A. Day, *J. Am. Chem. Soc.* 1943, **65**, 452

[16] V. Balzani, A, Juris, M.Venturi, *Chem. Rev.* 1996, **2**, 759

[17] P. Lenearts, A. Storms, J. Mullens, J. D'Ἤaen, C. Gorller-Walrand, K. Binnemans, K. Driesen; *Chem. Mater.* 2005, **17**, 5194

[18] B. Gholamkhass, H. Mametsuka, K. Koike, T. Tanabe, M. Furue, O. Ishitani, *Inorg. Chem.* 2005, **44**, 2326

[19] J. -Z. Wu, B. -H. Ye, L. Wang, L. –N. Ji, J. –Y. Zhou, R. –H. Li, Z. –Y. Zhou, *J. Chem. Soc. Dalton Trans.* 1997, 1395

[20] S. D. Bergman, M. Koi, *Inorg. Chem.* 2005, **44**,1647

[21] J.-Z. Wu, L. Li, T.-X. Zeng, L.-N. Ji, J.-Y. Zhou, T. Luo, R.-H. Li. *Polyhedron,* 1997, **16**, 103

[22] H. E. Gottlieb, V. Kotlyar, A. Nudelman, J. Org. Chem. 1997**, 62**, 7512

[23] Willard, H. H: Merritt, L. L Jr: Dean, J. A: Settle, F. A. Jr., *Instrumental Methods of Analysis*, 7th Ed, Wadsworth, 1988

[24] L. Cassidy, *PhD Thesis,* Dublin City University, 2008

[25] D. Mulhern, *PhD Thesis,* Dublin City University, 2005

[26] S. Rau, D. Walther, J.G. Vos, *Dalton Trans*, 2007, 915

[27] H. B. Gray *"Chemical Bonds: An Introduction to Atomic and Molecular Structure"(1st ed.)* 1994 University Science Books

[28] V. Balzani, F. Scandola, *Supramolecular Photochemistry*, Horwood, Chichester, 1991.

[29] V. Balzani, M. Venturi, A. Credi, *Molecular Devices and Machines,* Wiley-VCH, Weinheim, 2003.

[30] T. Gunnlaugsson, J. P. Leonard, K. Sénéchal, A. J. Harte, *J. Am. Chem. Soc.* 2003, **125**, 12062

[31] Y. Diaz-Fernandez, F. Foti, C. Mangano, P. Pallavicini, S. Patroni, A. Perez-Gramateges, S. Rodriguez-Calvo, *Chem. Eur. J.*, 2006, **12**, 921

[32] A. Quaranta, F. Lachaud, C. Herrero, R. Guillot, M.-F. Charlot, W. Leibl, A. Aukauloo, *Chem. Eur. J.*, 2007, **13**, 8201

[33] M. S. Silberberg *Chemistry*, 5th edition, McGraw-Hill 2009

[34] F. Gao, X. Chen, F. Zhou, L-T. Guo, M. Chen, H. Chao, L-N. Ji, *Inorg. Chim. Acta*, 2009, **362**, 4960

[35] H.C. Brown, E.A. in Braude, F.C. Nachod *Determination of Organic Structures by Physical Methods*, Academic Press, New York, 1955

[36] K.R. Rupesh, S. Deepalatha, M. Krishnaveni, R. Venkatesan, S. Jayachandran, European Journal of Medicinal Chemistry, 2006, **41**, 1494

[37] B. P. Sullivan, D. J. Salmon, Meyer T. *J., Inorg. Chem.* 1978, **17,** 3334

[38] D. A. Buckingham, F. P. Dwyer, H. A. Goodwin, A. M. Sargeson, *Aust. J. Chem.* 1964, **17**, 325.

[39] W.Huang, T. Ogawa, *Polyhedron,* 2006, **25**, 1379

[40] J-Z. Wu, L. Li, T-X. Zeng, L-J. Ji, J-Y. Zhou, T. Luo, R-H. Li, *Polyhedron*, 1997, **16**, 103

Chapter 4: Synthesis and Characterisation of Novel $[M(\text{-imphen})_2(bpy)]^{2+}$ Type Mononuclear Metal Complexes

Abstract:

Chapter 4 describes the synthesis of mononuclear metal complexes containing two novel ligands of the type discussed in Chapter 3. These complexes have been built exclusively using an 'on-complex' synthetic approach as potential prototypes for molecular transistors. This chapter also includes the attempted synthesis of the metal complexes $[Ru(pyrphen)_2(bpt)]^{2+}$ and $[Ru(thimphen)_2(bpt)]^{2+}$ which are possible precursors for dinuclear systems containing ligands suitable for surface coordination.

The chapter includes characterization of the complexes synthesized using mass spectrometry, nuclear magnetic resonance, deuteration, UV/vis spectroscopy and elemental analysis.

4.1 Introduction

In this chapter the idea of a molecular transistor prototype consisting of a metal complex containing two surface active ligands is discussed. As in Chapter 3, thiophene and pyridine are employed as surface active groups in the complexes whose synthesis is targeted in this chapter. Both derivatives are synthesised using the 'on-complex' approach used to synthesise the complex [Ru(bpy)$_2$(pyrphen)](PF$_6$)$_2$ in Chapter 3. Reaction schemes illustrating the synthetic pathway for these complexes are shown below in Figure 4.1.

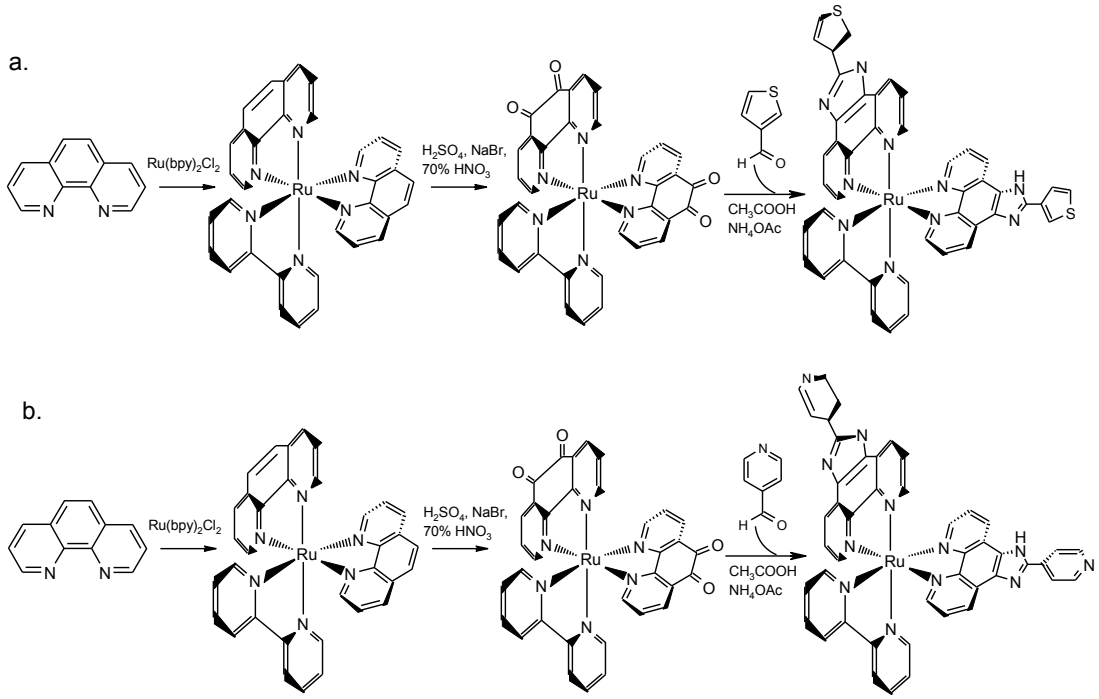

Figure 4.1: Reaction scheme for the synthesis of (a) [Ru(thimphen)$_2$(bpy)]$^{2+}$ and (b) [Ru(pyrphen)$_2$(bpy)]$^{2+}$ using the 'on complex' synthetic approach outlined in Chapter 3.

The idea of 'Chemisty of the Complex' has been explored to some extent in Chapter 3, detailing it as an invaluable method for tuning the properties of metal complexes as well as carrying out synthetic reactions that are not feasible through traditional organic or metal complex synthesis.

Hanan et al. have used this type of 'on-complex' approach to synthesise a series of ruthenium bis-terpyridine ([Ru(tpy)$_2$]$^{2+}$) complexes in an effort to increase the short luminescence lifetime of the parent complex [Ru(tpy)$_2$]$^{2+}$.[1] This range of complexes is shown below in Figure 4.2.

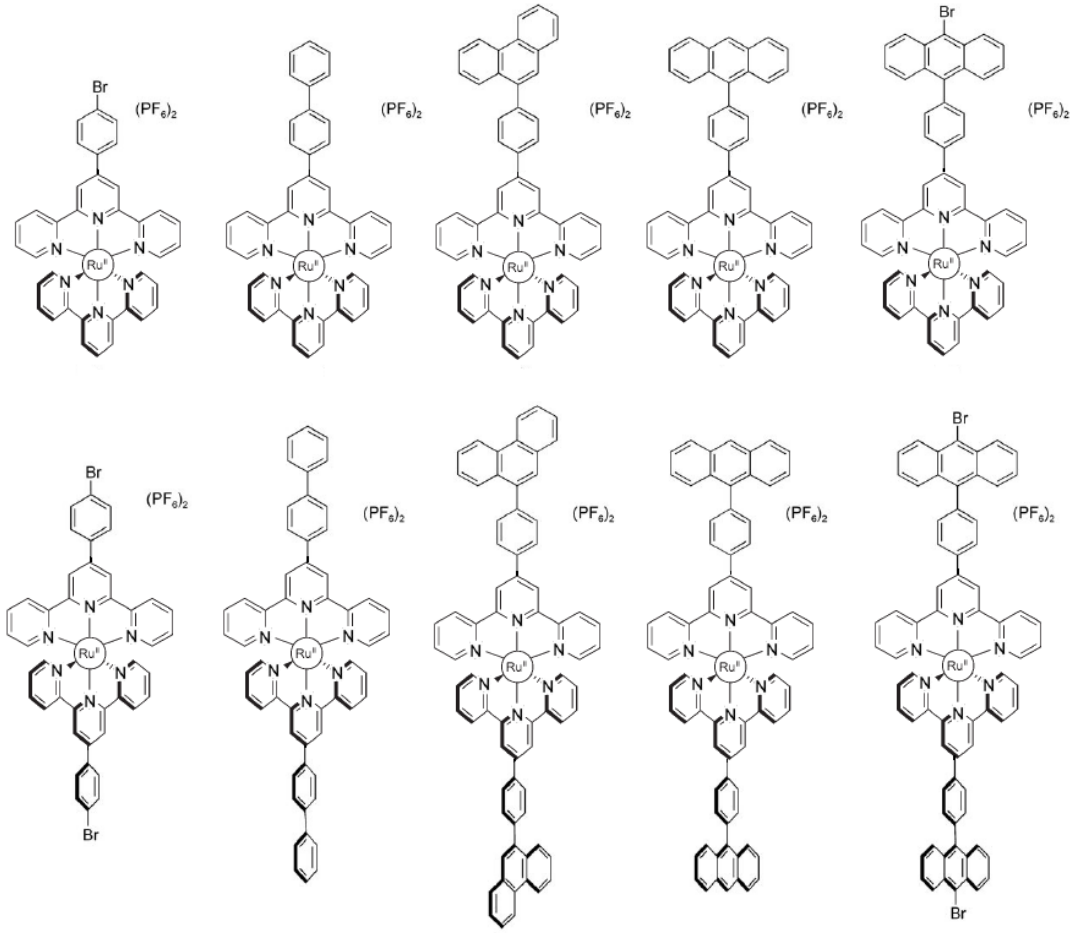

Figure 4.2: Structural illustration of the series of complexes synthesised by Hanan et al using an 'on-complex' approach[1]

Instead of preparing a lengthy series of ligands and attaching them one by one to the ruthenium centre, all of the above complexes were synthesised by modification of the bromo starting material $[Ru(tpy)(Br\text{-}tpy)](PF_6)_2$

A similar series of Ru(tpy) type complexes have also been synthesised by Hanan and Campagna and workers, this time using a chloride type ruthenium terpyridine precursor.[2] These complexes are pictured below in Figure 4.3.

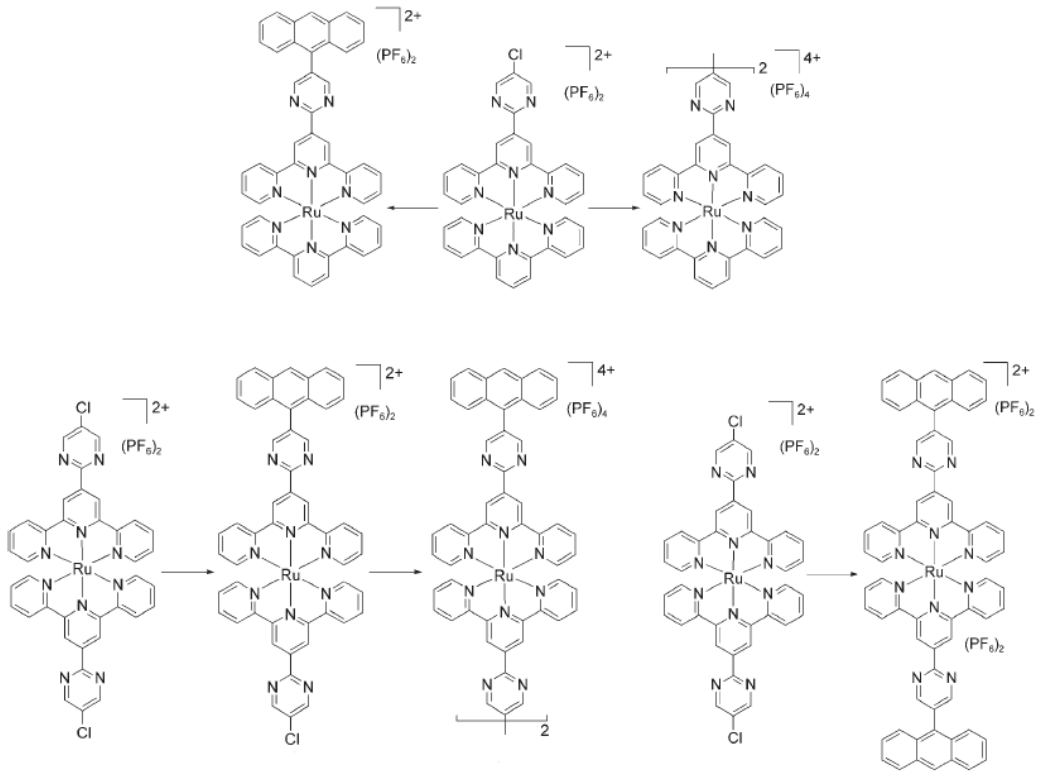

Figure 4.3: Series of complexes synthesised by Campagna and workers using an on-complex approach[2]

This series of complexes also illustrates how 'chemistry on the complex' may be used to build metal complexes of increasing intricacy and magnitude using a modular approach. The reaction type employed here is a Suzuki type coupling, with the reaction occurring between 9-anthrylboronic acid and reactive chloro-groups present on precursor complexes. Suzuki coupling is an extremely popular method of complex modification and has been since its discovery[3] in the 1970's. This type of coupling is palladium catalysed and occurs between a halide (usually a chloro or bromo group) and a boronic acid group, both of which may be appended to metal complex precursors. The reaction yields a C-C bond in place of the two reactive groups, linking the two precursor molecules.

Welter *et al*. have also used this approach to synthesise a series of ruthenium complexes from one bromo type precursor.[4] In this case a number of rod-like dinuclear ruthenium complexes were synthesized containing phenylene spacers of varying length. The reaction scheme for the coupling type reaction performed on the complex precursor is shown below in Figure 4.4.

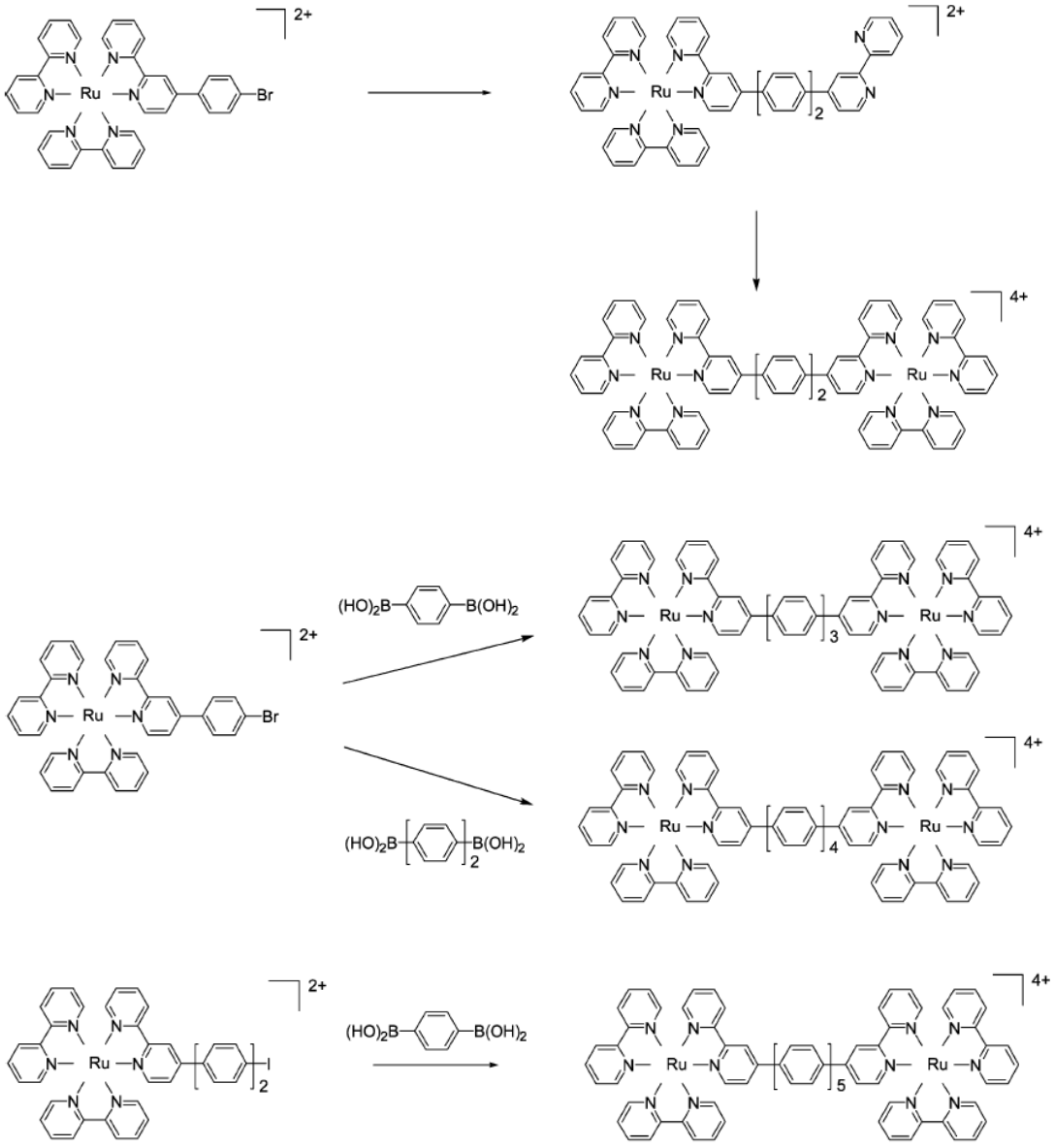

Figure 4.4: Synthetic routes used by Welter et al. for the preparation of a series of dinuclear ruthenium complexes containing varying phenylene spacers[4]

A similar approach has been used by Rau *et al* for the formation of ruthenium complexes containing derivatives of the ligand dipyrido[3,2-a:2',3'-c]phenazine (dppz) as shown below in Figure 4.5.[5] Ruthenium complexes of (dppz) are extensively investigated due to the multiple applications arising from such a strongly luminescent complex, varying from luminescent DNA sensors [6] to reversible electron carriers.[7]

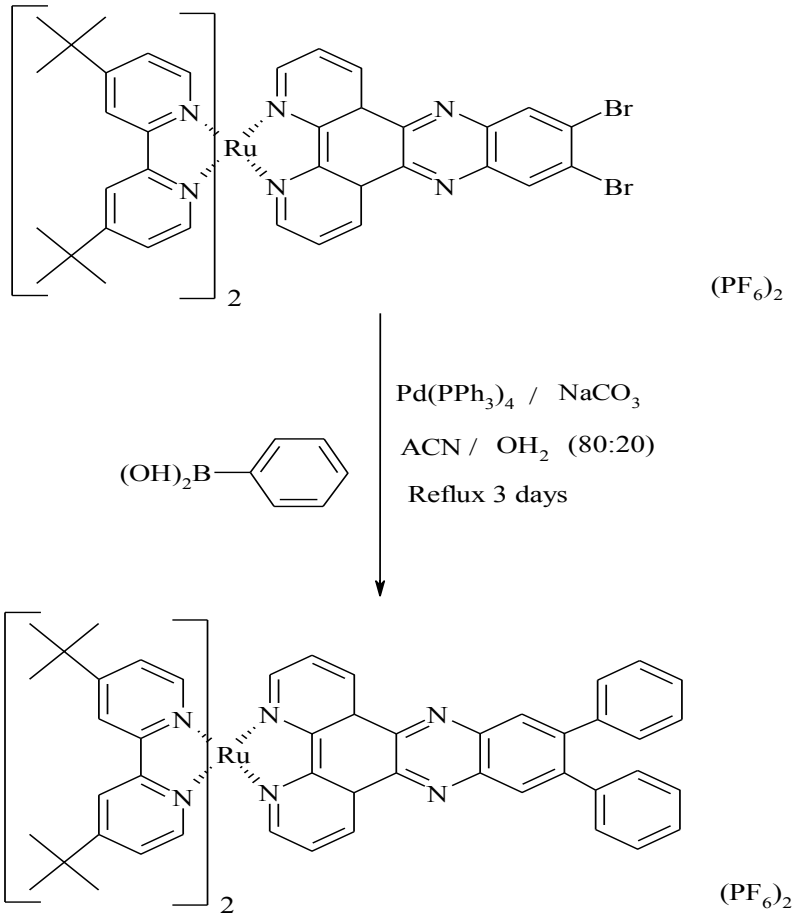

Figure 4.5: Ruthenium complex based Suzuki reaction as carried out by Rau and workers.[5]

Castellano *et al* used a similar coupling approach to synthesise a dinuclear rhenium-gold dimer: (fac-Re(phenCtCAuPPh_3)$(CO)_3$-Cl) for photophysical studies. The gold containing precursor was found to be exceptionally unstable, and not suitable to withstand a number of metal coordination reactions.[8] As a result a coupling reaction conducted on the complex was used to yield the dinuclear complex shown below in Figure 4.6.

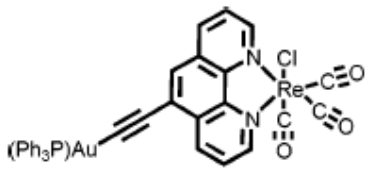

Figure 4.6: Structure of the dinuclear species synthesised by Castellano et al using 'on complex' coupling methods[8]

Another type of coupling reaction termed Ni(0) catalyzed coupling reactions has also been used to modify metal complexes, one such example being carried out by Vos[9] and co-workers in the synthesis of multinuclear ruthenium triazole containing complexes featuring proton controlled intramolecular communication, as shown in Figure 4.9

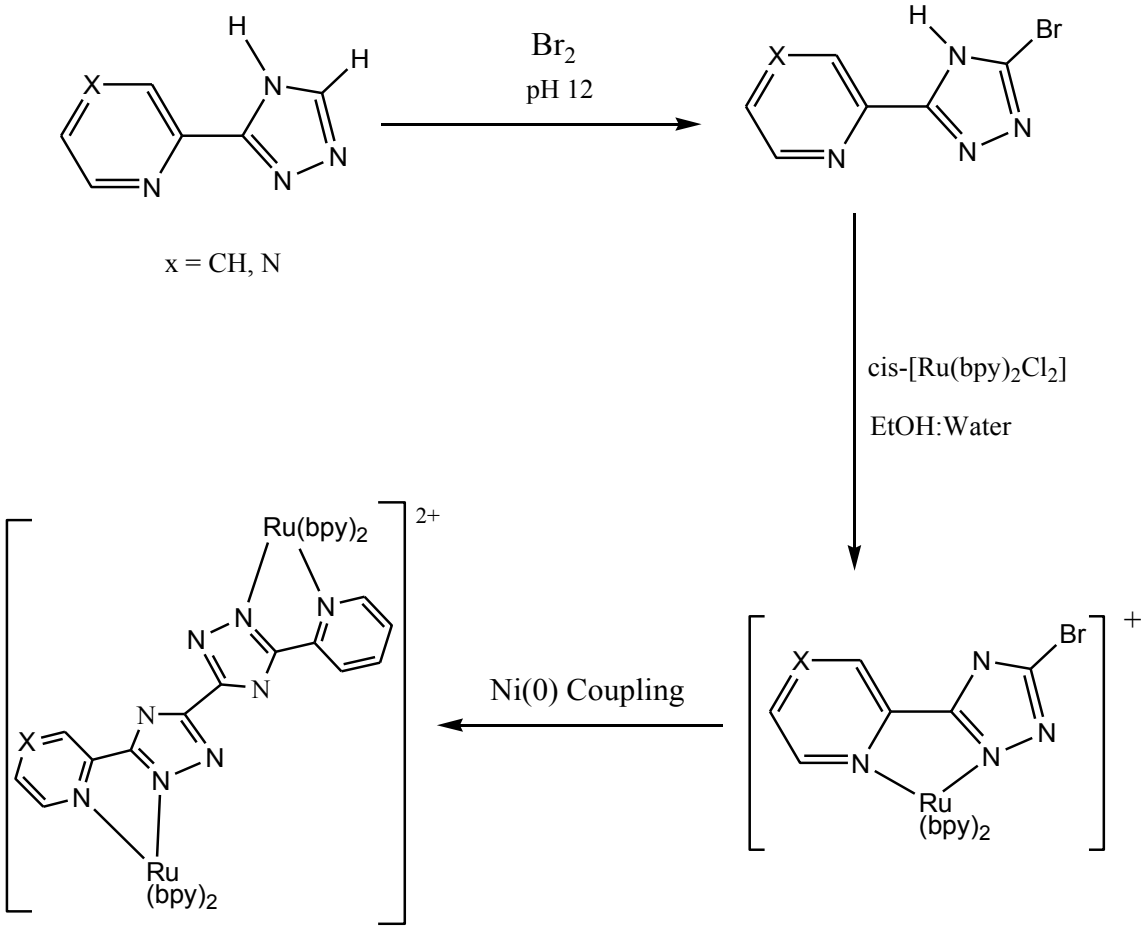

Figure 4.9: Synthetic scheme employed by Vos and co-workers in the formation of $[Ru(bpy)_2(pytr\text{-}pytr)Ru(bpy)_2]^{2+}$. [9]

This method was used to avoid the formation of many different coordination isomers and to allow for a single well-defined product to be obtained. By using the *"complexes as metals / complex as ligands"* strategy (introduced in chapter 1) fourteen possible isomers would be obtained from the reaction, 5 dinuclear complexes and 9 mononuclear complexes.[10] Therefore by use of this coupling procedure the formation of by-products is eliminated.

A very similar method was subsequently used by Hanan *et al*[11, 12, 13] to prepare new polynucleating ligands for symmetrical and asymmetrical pyridylpyrimidine dimers. The nickel-catalyzed coupling of a ruthenium ortho-chloroimine complex, shown in figure 5.7, creates a new vacant bidentate binding site suitable for generating higher nuclearity ruthenium complexes.[14]

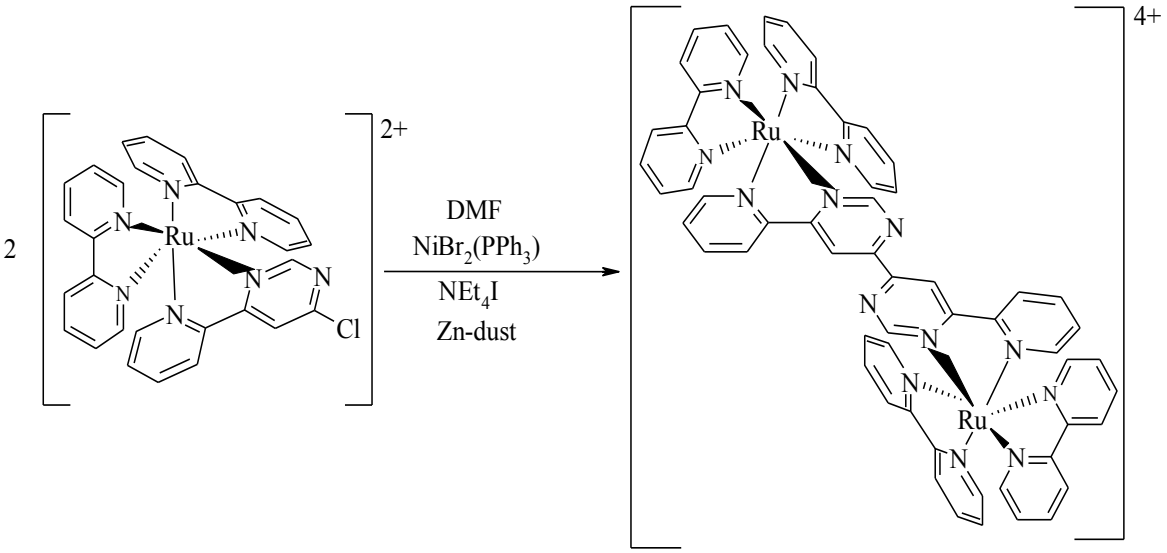

Figure 4.7: Synthetic scheme used by Hanan et al for the formation of the novel ruthenium dinuclear complex.[14]

This method was used to create new binding sites in order to rapidly increase ion content in metallodendrimers.

The starting material [Ru(phendione)$_2$(bpy)]$^{2+}$ employed in this chapter has also been used by Zou *et al* in the synthesis of molecular light sensors for DNA intercalation[15].

In these experiments a triazine ring is formed from a condensation reaction between the dione moiety and an amidrazone, shown below in Figure 4.8.

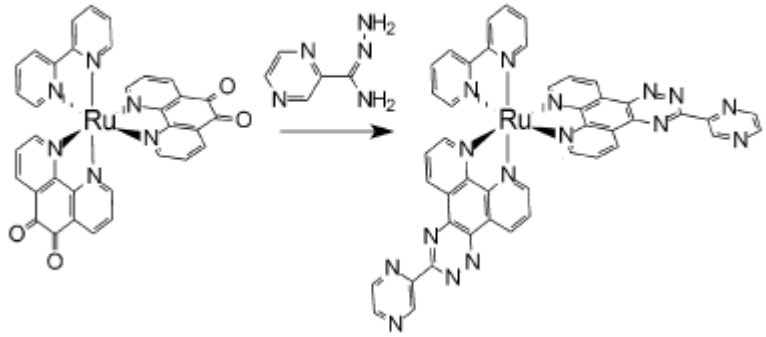

Figure 4.8: Reaction scheme for formation of the complex $[Ru(pztp)_2(bpy)]^{2+}$ as carried out by Zou et al[15]

Macdonnell and workers have also used a similar reaction type to form pyrazine bridged bisphenanthroline ligands on the complex through the reaction scheme shown below in Figure 4.9.[16]

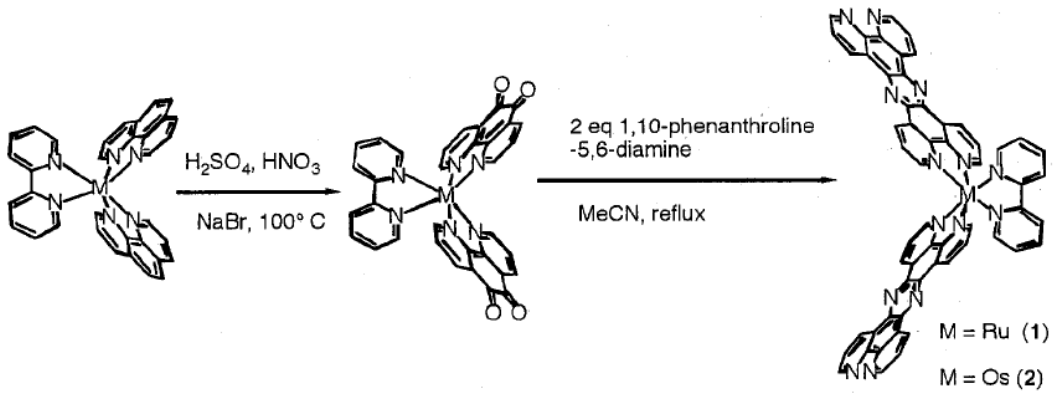

Figure 4.9: Reaction scheme for formation of the complexes $[(bpy)Ru(tpphz)_2]^{2+}$ and $[(bpy)Os(tpphz)_2]^{2+}$ as carried out by Macdonell et al[16]

There is yet to be published any on-complex chemistry involving the imidazole formation type reaction shown in Figure 4.1. The synthesis of a series of complexes using this type of unexamined method has been attempted with all products characterized by ^1H NMR, UV-vis spectroscopy, mass spectrometry and elemental analysis. The complexes synthesized are shown in Figure 4.10 below.

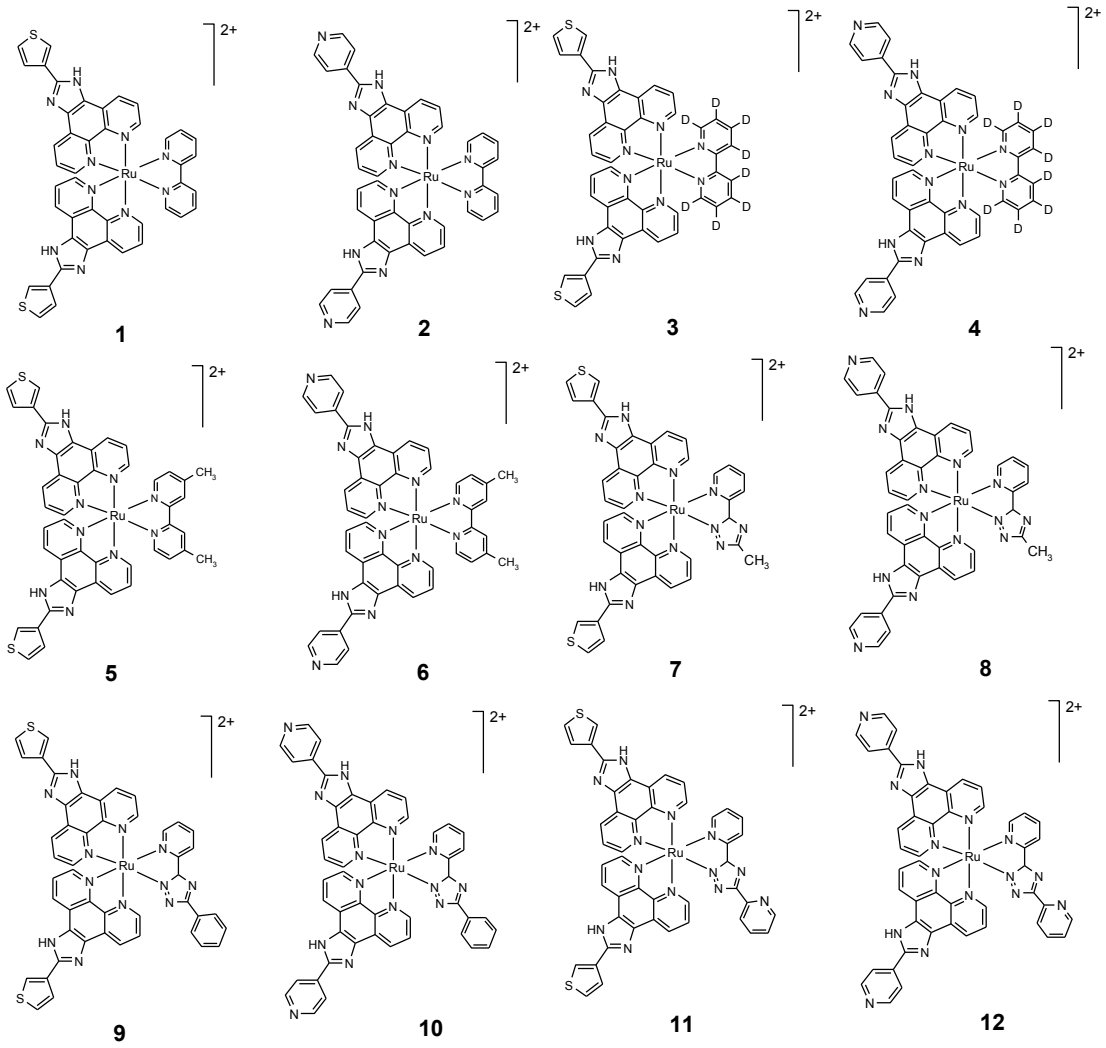

Figure 4.10: Structures of compounds 1-14, the syntheses of which are attempted in this chapter

As outlined in chapters 1 and 3, metal complexes incorporating surface active ligands such as the imidazole type ligands shown in Figure 4.10 are theoretically suitable for implementation as molecular electronics. The series of complexes synthesised in both this chapter and Chapter 3 falls into this category and may be termed molecular transistor prototypes (*c.f.* Chapter 1/Chapter 3). But what merit do the complexes shown in Figure 4.10 have over those synthesised in Chapter 3?

Examining complexes 11 and 12 in Figure 4.10 a second area for metal ion coordination is apparent. As a result, these complexes are suitable precursors for dinuclear systems that may be used as molecular diode prototypes as explained in

chapter 1. Figure 4.11 below shows four possible structures for these dinuclear species.

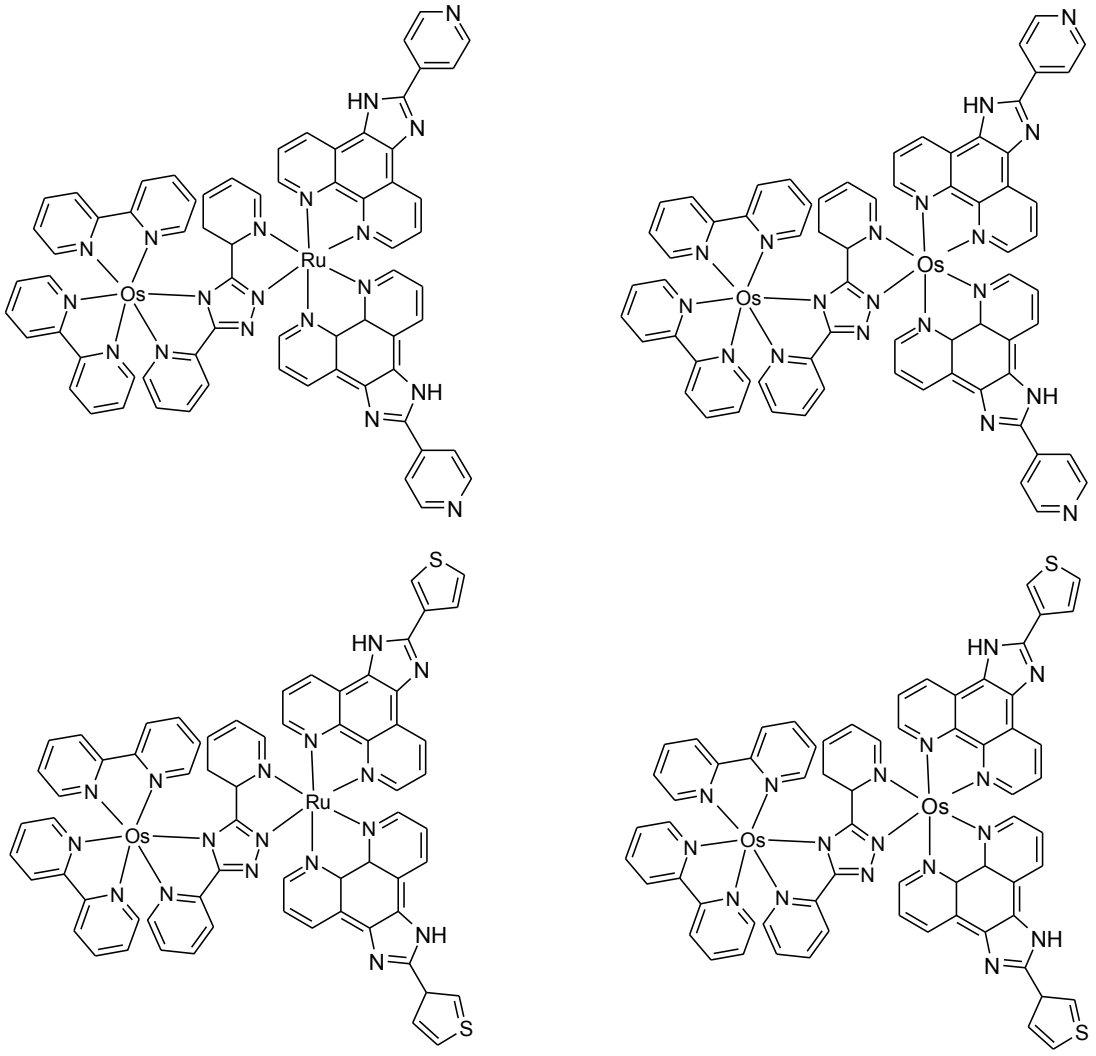

Figure 4.11: Structures for possible dinuclear complexes incorporating surface-active ligands for use as molecular diode prototypes.

As mentioned in Chapter 1 the bridging ligand Hbpt has been shown to be an effective mediator of electron transfer between metal centres[17] and so dinuclear complexes containing metal centres of different oxidation potential will allow the directional current necessary for a diode type device. So, complexes 11 and 12 may be treated as precursors for the complexes shown above in Figure 4.11 (the methods used to synthesise complexes 11 and 12 theoretically should also allow for synthesis of the osmium analogues). Also, the 'on-complex' method discussed in this chapter may also be used to attach surface active groups to dinuclear complexes containing two

free phenanthroline groups. This possible future approach shall be discussed in more detail in Chapter 7.

The synthesis and characterisation of the mononuclear 'model' complexes shown in Figure 4.10 are discussed below in Section 5.2.

4.2 Results and Discussion

4.2.1 Synthetic Considerations

The mononuclear complexes 1, 2, 3, 4 and 6 as shown in Figure 4.12 were synthesised in acceptable yield using the procedure for modification of precursor complexes as outlined in Chapter 3.

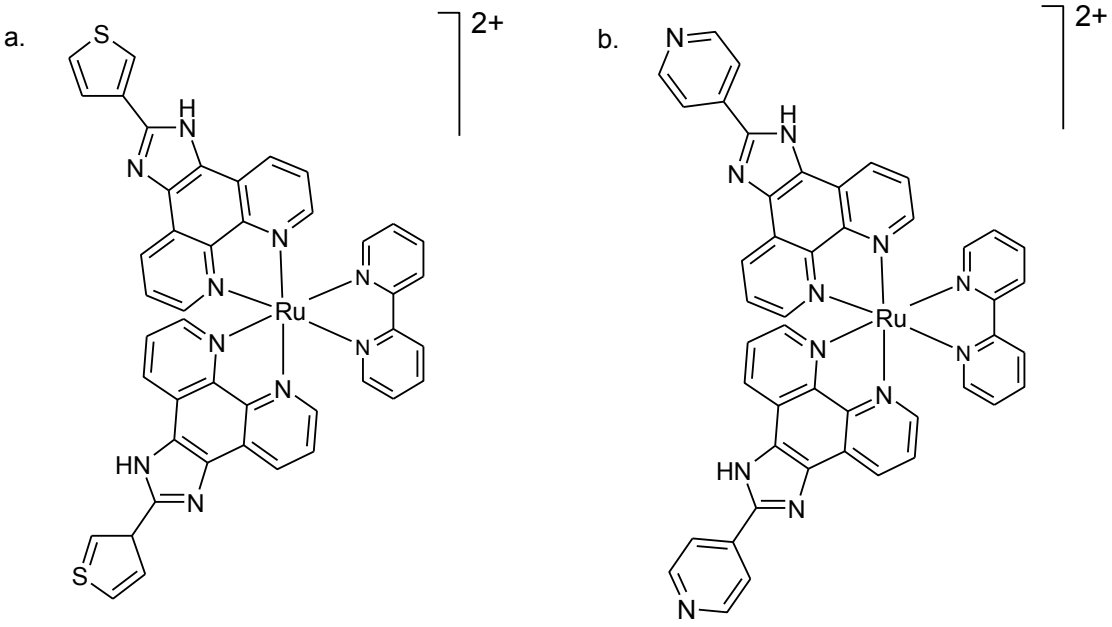

Figure 4.12: Chemical structure of the mononuclear complexes (a) [Ru(thimphen)$_2$(bpy)]$^{2+}$(complex 1) and (b) [Ru(pyrphen)$_2$(bpy)]$^{2+}$ (complex 2)

The first reaction step undertaken was the creation of two reactive phenanthroline dione groups within the starting complex [Ru(phen)$_2$Cl$_2$] using a modified version of the method outlined for the synthesis of [Ru(bpy)$_2$(phendione)]$^{2+}$ [18] The formation of the bis-(phenanthroline dione) intermediate complex takes place in concentrated acid conditions [18, 23]. As a result, the reaction to form the dichloride [Ru(phendione)$_2$Cl$_2$] from [Ru(phen)$_2$Cl$_2$] was attempted after considerable hesitation as the labile chloride ligands were expected to disscociate in the harsh acidic conditions. An opportunity to prove or disprove this assumption was not provided as the final product

[Ru(phendione)$_2$Cl$_2$] could not be precipitated from the reaction mixture using the KPF_6 salt formation detailed in the experimental section 6.4 below. Addition of acetone (as used to precipitate the analogous dichloride complex [Ru(bpy)$_2$Cl$_2$] from a DMF reaction mixture) was attempted but was found to result in an extremely vigorous reaction between the acidic reaction mixture and the organic solvent added and was thus deemed too hazardous to use as a method of product isolation. The acidic reaction mixture was neutralised with $KHCO_3$[18] to eliminate this risk and acetone added as for [Ru(bpy)$_2$Cl$_2$] but no precipitation was observed. Instead, the N_6 complex [Ru(phen)$_2$(bpy)](PF$_6$)$_2$ was modified, the 2,2'-bipyridyl ligand being much more stable in acidic conditions of this type[23] as seen in Chapter 3. This is shown schematically below in Figure 4.13.

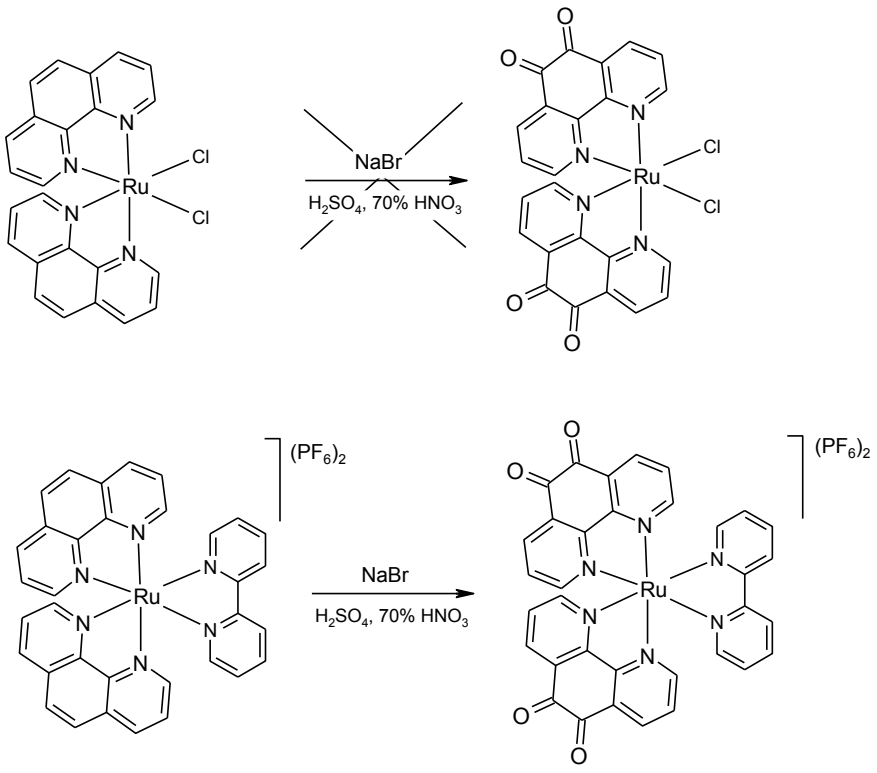

Figure 4.13: Schematic representation of (a) the unfeasible conversion of Ru(phen)$_2$Cl$_2$ to Ru(phendione)$_2$Cl$_2$ and (b) the successful conversion of [Ru(phen)$_2$(bpy)](PF$_6$)$_2$ to [Ru(phendione)$_2$(bpy)](PF$_6$)$_2$

A key consideration in the synthesis of the bis-dione type complex shown in Figure 4.13 (b) was the use of fresh NaBr in the reaction. It was found that use of NaBr in excess of six months old resulted in little or no conversion of the bis-phenantholine starting material whereas use of NaBr within a few months of purchase resulted in yields of between 75% and 35% of the desired product. In the case of the bpy and d_8-

bpy bis-phenanthroline complexes, conversion to the bis-phenanthroline dione complexes was achieved using the same method as for the mono-phenanthroline dione complexes synthesised in Chapter 3. In the case of [Ru(phen)$_2$(dmbpy)](PF$_6$)$_2$ and [Ru(phen)$_2$(bpt)](PF$_6$) precipitation was only achieved following neutralisation of the reaction mixture using $KHCO_3$[18]. Upon reaching neutral pH any solid residue was removed by filtration and the desired bis-phenanthroline dione complex was precipitated using KPF_6. This type of conversion, employing both neutralisation and non neutralisation techniques was used for the attempted synthesis of [Ru(phendione)$_2$(Mepytr)](PF$_6$)$_2$ and [Ru(phendione)$_2$(Ppytr)](PF$_6$)$_2$. In the case of both metal complexes no precipitation was observed from the reaction solution using either method.

The conversion of the successfully synthesised bis-phenanthroline dione complexes to the desired bis-thiophene or bis-pyridine imidazole analogues involves a Schiff base formation between the phenanthroline dione moiety of the complex and ammonium acetate present in the reaction mixture as described previously in Chapter 3. The imidazole is then formed from the resulting diimine and a suitable aldehyde. By keeping the ammonium acetate used in the reaction in excess and doubling the amount of aldehyde added as well as doubling the reaction time employed, modification of both phenanthroline groups present in the molecule to yield the desired molecule was successful. A reaction time of two hours was sufficient for synthesis of the successfully synthesised [Ru(pyrphen)$_2$(L)](PF$_6$)$_2$ (where L=bpy, d_8-bpy, and dmbpy) type complexes, while for the [Ru(thimphen)$_2$(L)](PF$_6$)$_2$ analogues of these complexes proved much more difficult to synthesise. In the case of [Ru(thimphen)$_2$(bpy)](PF$_6$)$_2$ (Complex 1) an extended reaction time of 3 hr was found to be effective. However, for the metal complex [Ru(thimphen)$_2$(dmbpy)](PF$_6$)$_2$ (Complex 5) even overnight reflux yielded the broad spectrum shown below in Figure 4.14.

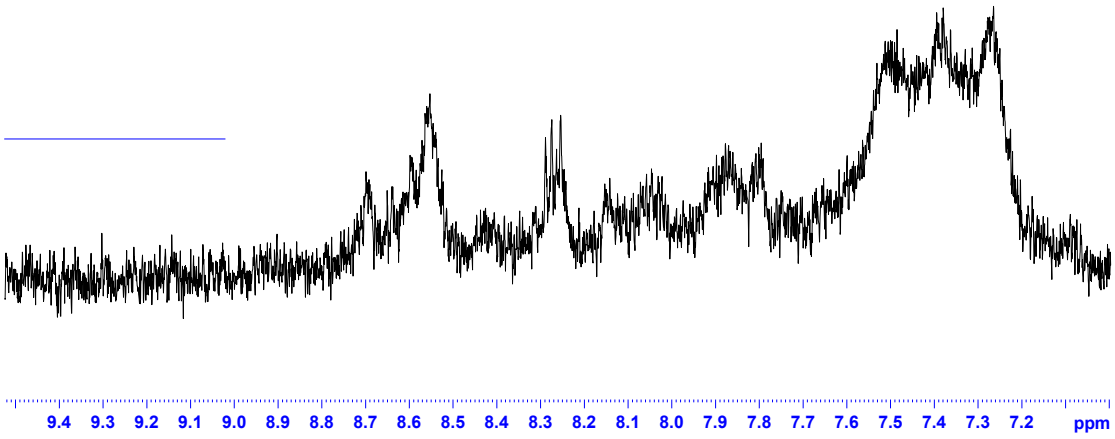

Figure 4.14: ^{1}H NMR spectrum for the small amount of solid obtained for the attempted synthesis of [Ru(thimphen)$_2$(dmbpy)](PF$_6$)$_2$ measured on a 600 MHz instrument using d$_6$-acetone as solvent at 295K.

This product was analysed by HPLC methods also in order to ascertain whether any of the desired complex was synthesised. The HPLC chromatogram for the metal complex [Ru(thimphen)$_2$(dmbpy)]$^{2+}$ (complex 5) is shown below in Figure 4.15.

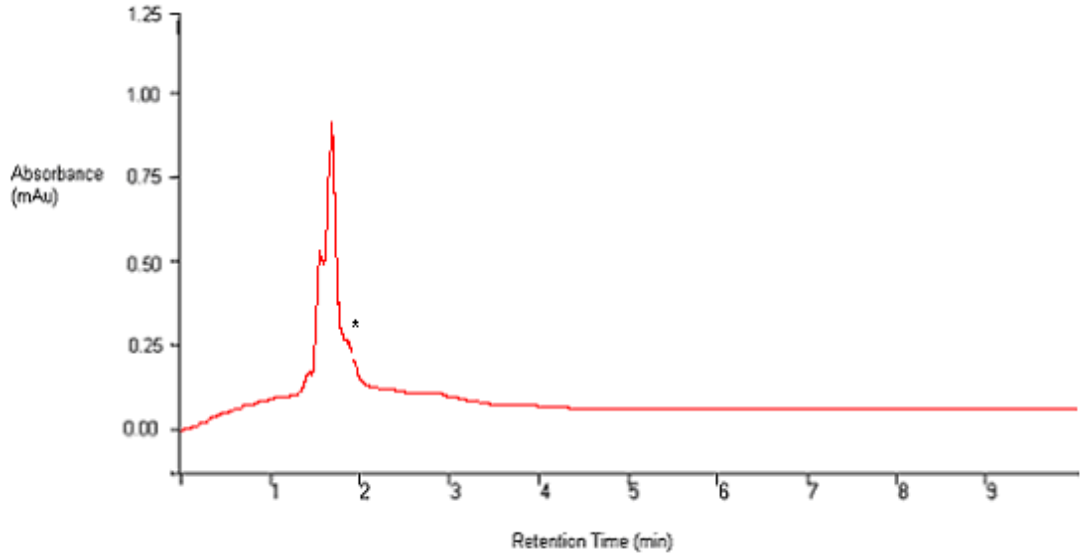

Figure 4.15: HPLC chromatogram of the solid obtained from the attempted [Ru(thimphen)$_2$(dmbpy)]$^{2+}$ (complex 5) reaction

The clarity of the above spectrum not ideal but the presence of a ruthenium complex has been detected. Two main overlapping peaks are visible at 1.7 min and 1.8 min

displaying only organic material, perhaps residual aldehyde or reaction solvent (glacial acetic acid). The shoulder appearing at 2.1 min in Figure 4.15 marked with a * shows a different type of absorbance shown below in Figure 4.16.

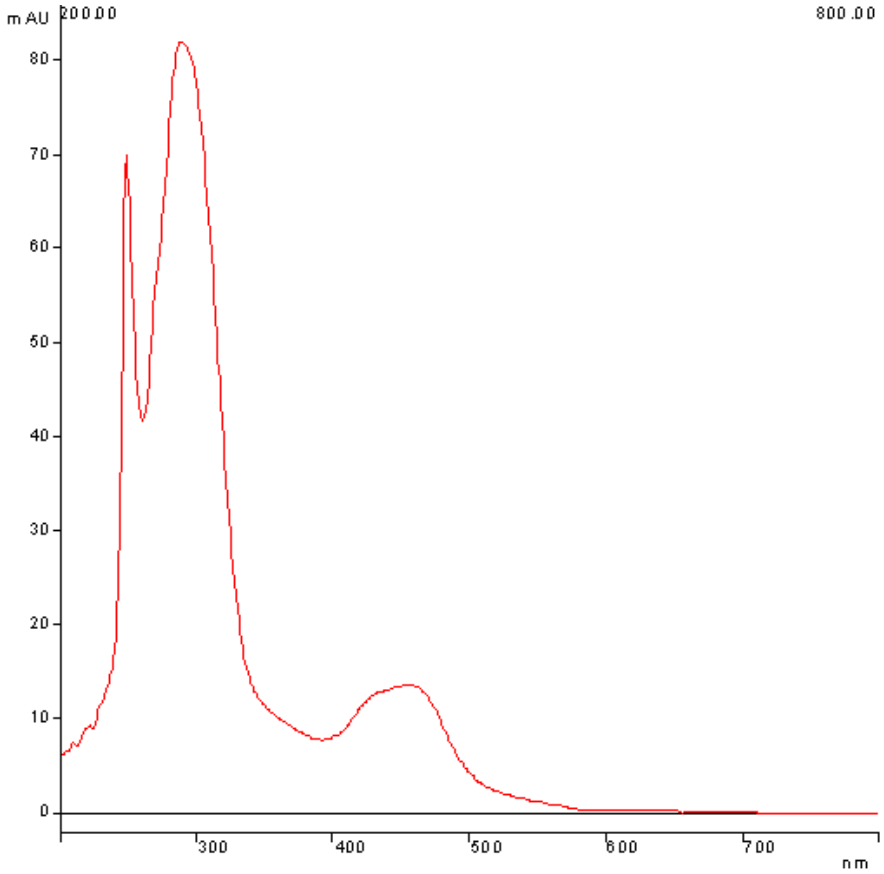

Figure 4.16: Absorbance spectrum for both peaks shown at 2.1 min in Figure 4.15

The absorbance observed at 450 nm indicates the presence of an N_6 ruthenium metal complex. However, as there is no conclusive ^1H NMR information available for this fraction it cannot be ascertained whether this absorbance relates to the starting material $[Ru(phendione)_2(dmbpy)]^{2+}$ or the desired product $[Ru(thimphen)_2(dmbpy)]^{2+}$. UV/vis analysis and HPLC analysis have been deemed insufficient to prove or disprove the presence of $[Ru(thimphen)_2(dmbpy)]^{2+}$ due to the structural similarity between it and the starting material $[Ru(phendione)_2(dmbpy)]^{2+}$. As a result further research into a more effective method of purification must be undertaken in order to ascertain whether or not the metal complex (5) $[Ru(thimphen)_2(dmbpy)]^{2+}$ can be synthesised using this method.

Conclusive ^1H NMR data was not obtained for the complexes $[Ru(thimphen)_2(bpt)]^+$ or $[Ru(pyrphen)_2(bpt)]^+$ either. These complexes were therefore also analysed by

HPLC methods with the chromatogram for [Ru(thimphen)$_2$(bpt)]$^+$ (complex 11) shown below in Figure 4.17.

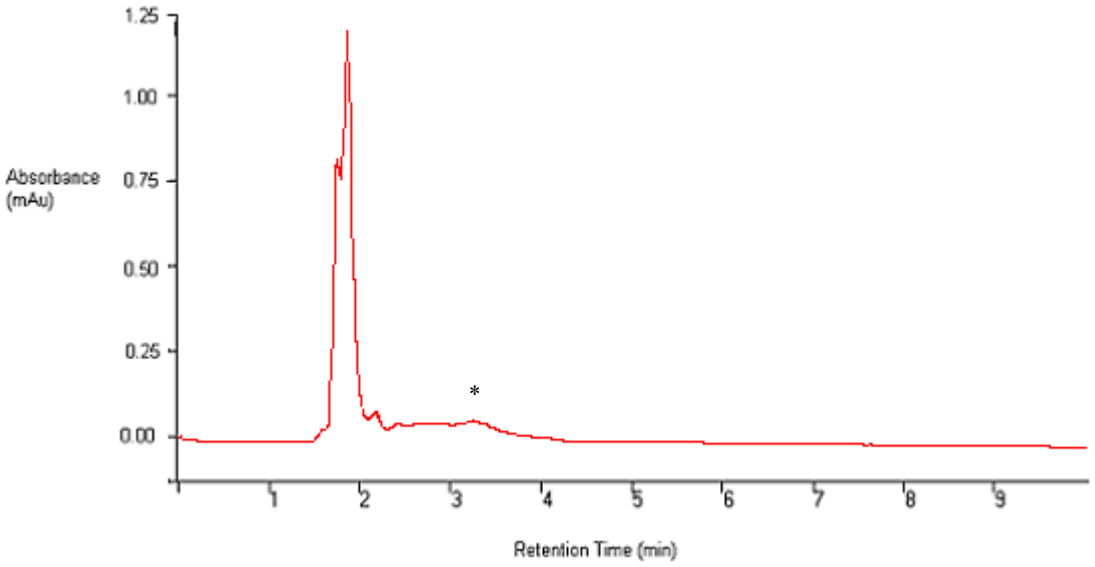

Figure 4.17: HPLC chromatogram of the solid obtained from the attempted [Ru(thimphen)$_2$(bpt)]$^+$ (complex 11) reaction

Again two main overlapping peaks are visible at 1.7 min and 1.8 min, the UV/vis spectra for each showing organic materials only.

A weak peak is visible at 2.2 min in Figure 4.17 which yields an inconclusive UV/vis spectrum however a second peak, marked with a * is visible at 3.3 min. The associated UV/vis spectrum for this peak displays an absorbance maximum at 420 nm and is shown below in Figure 4.18.

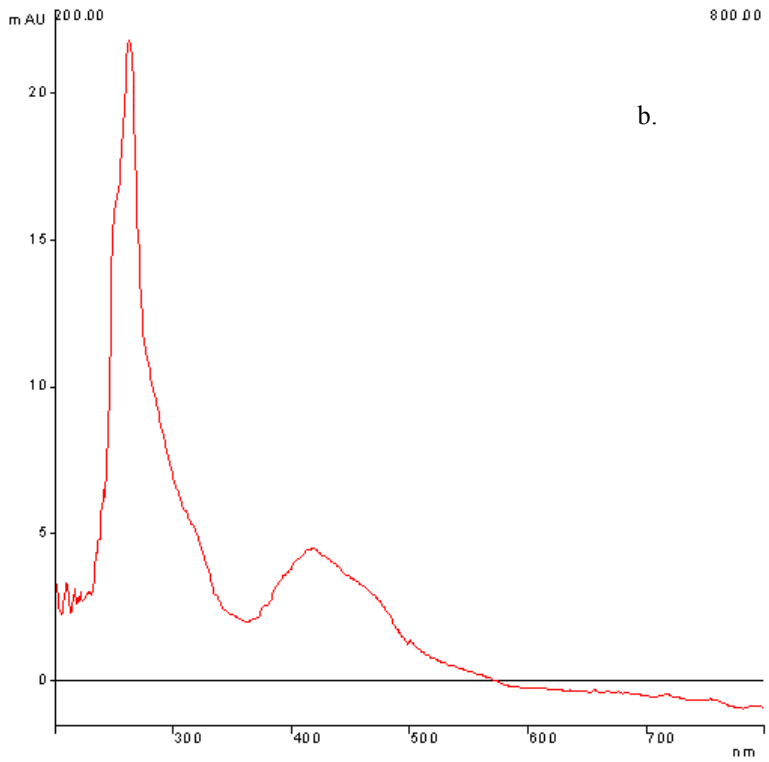

Figure 4.18: Absorbance spectrum for the peak shown at 3.3 min in Figure 4.17

This spectrum bears a certain resemblance to the UV/vis spectrum obtained for the overall $[Ru(thimphen)_2(bpt)]^+$ (complex 11) sample discussed in Section 5.2.3 but again, due to the structural similarity between $[Ru(thimphen)_2(bpt)]^+$ and its bis-phenanthroline dione starting material there is no way to prove that the spectrum shown here is defeinitely that of $[Ru(thimphen)_2(bpt)]^+$. Therefore it was concluded for $[Ru(thimphen)_2(bpt)]^+$ as for $[Ru(thimphen)_2(dmbpy)]^{2+}$ that further experimental research must be carried out on this synthetic method in order to ascertain if it is suitable for the successful synthesis of this complex.

The crude product obtained from the attempted $[Ru(pyrphen)_2(bpt)]^+$ (complex 12) reaction was also analysed by HPLC methods. The HPLC chromatogram for this solid is shown below in Figure 4.19.

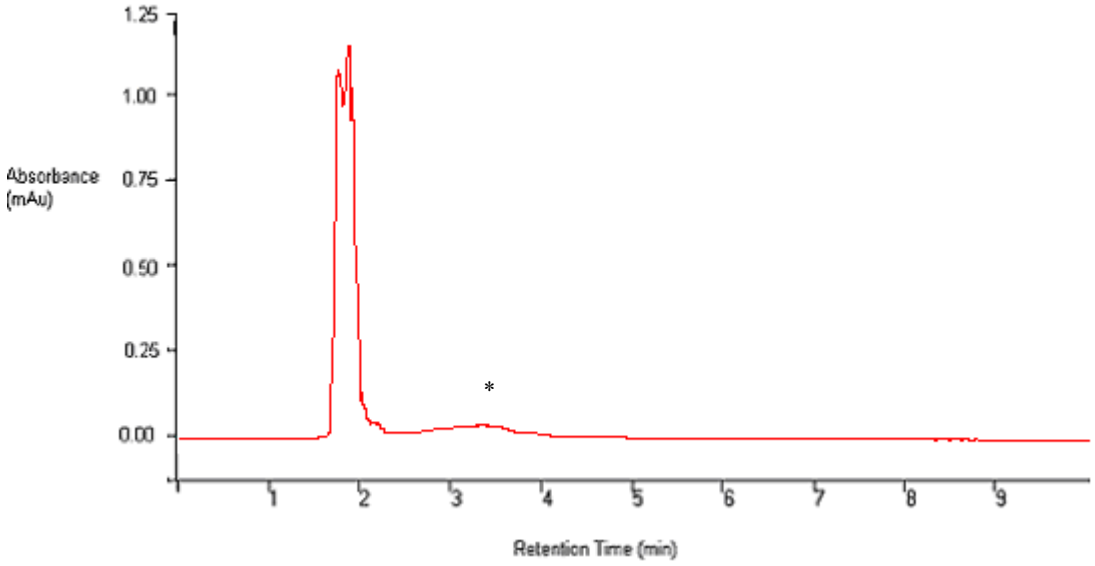

Figure 4.19: HPLC chromatogram of the solid obtained from the attempted [Ru(pyrphen)$_2$(bpt)]$^+$ reaction

The HPLC chromatogram shown in Figure 4.19 for [Ru(pyrphen)$_2$(bpt)]$^+$ bears much similarity to the chromatogram shown in Figure 4.17 for [Ru(thimphen)$_2$(bpt)]$^+$. Again two overlapping peaks are visible between 1.7 min and 1.8 min, both of which display no metal complex absorbance, only an intense organic absorbance as before. A third peak is visible at 3.3 min marked in Figure 4.19 with a *. Both the retention time and the absorbance spectrum of this peak are identical to those of the fourth peak eluting at 3.3 min in the chromatogram for [Ru(thimphen)$_2$(bpt)]$^+$. The absorbance spectrum for the peak present at 3.3 min in the chromatogram shown in Figure 4.19 for [Ru(pyrphen)$_2$(bpt)]$^+$ are shown below in Figure 4.20.

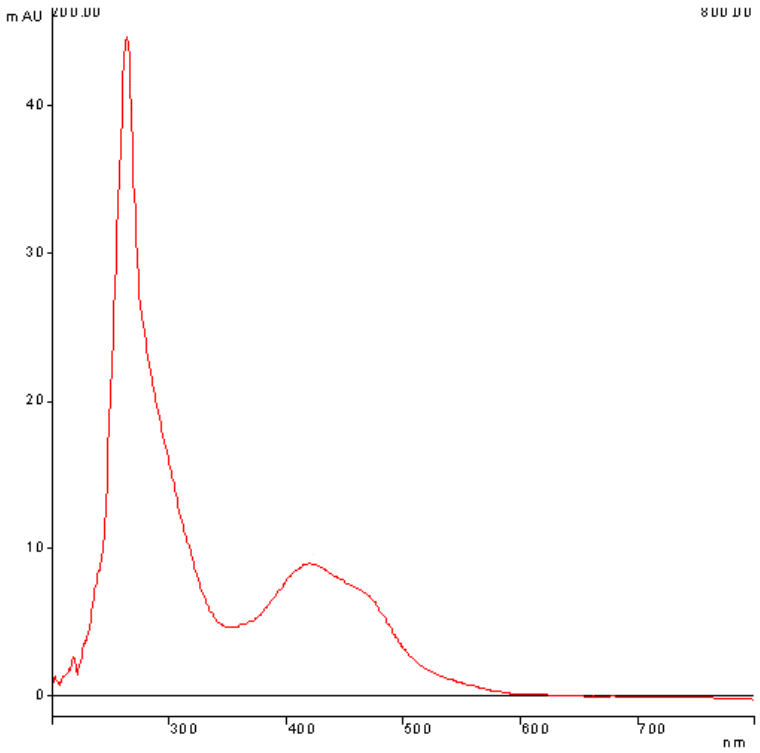

Figure 4.20: Absorbance spectra for the peak shown at 3.3 min in Figure 4.19

As in the case of [Ru(thimphen)$_2$(bpt)]$^+$ the spectrum shown in Figure 4.20 bears some resemblance to the UV/vis spectrum obtained for the overall [Ru(pyrphen)$_2$(bpt)]$^+$ sample discussed in Section 5.2.3 but again there is no solid proof that this spectrum refers to [Ru(pyrphen)$_2$(bpt)]$^+$ and not [Ru(phendione)$_2$(bpt)]$^+$. Therefore it was concluded for [Ru(pyrphen)$_2$(bpt)]$^+$ as for [Ru(thimphen)$_2$(bpt)]$^+$ and [Ru(thimphen)$_2$(dmbpy)]$^{2+}$ that further experimental research must be carried out on this synthetic method in order to ascertain if it is suitable for the successful synthesis of this complex.

The full characterisation of the complexes successfully synthesised follows in the next sections.

4.2.2 ^{1}H NMR Analysis

As mentioned in previous chapters ^{1}H NMR is an invaluable tool in assigning the structural attributes of a novel compound as well as ascertaining its purity. In this series of reactions the use of ^{1}H NMR is particularly pertinent. As a series of intermediate metal complexes are synthesised, ^{1}H NMR can be used to build a comprehensive map of the synthetic pathway. The following subsections describe the ^{1}H NMR characterisation of the successfully synthesised complexes $[Ru(pyrphen)_2(bpy)](PF_6)_2$ (2), $[Ru(thimphen)_2(bpy)](PF_6)_2$ (1), $[Ru(pyrphen)_2(d_8\text{-}bpy)](PF_6)_2$ (4), $[Ru(thimphen)_2(d\text{-}_8bpy)](PF_6)_2$ (3), $[Ru(pyrphen)_2(dmbpy)](PF_6)_2$ (6) including the precursor complexes leading to their formation.

4.2.2.1 ^{1}H NMR of $[Ru(phen)_2L](PF_6)_2$ precursor complexes

This section relates to characterisation of the precursor complexes $[Ru(phen)_2(bpy)](PF_6)_2$ and $[Ru(phen)_2(dmbpy)]$ by ^{1}H NMR methods. The numbering schemes for $[Ru(phen)_2(bpy)](PF_6)_2$ and $[Ru(phen)_2(dmbpy)](PF_6)_2$ are shown below in Figure 4.21.

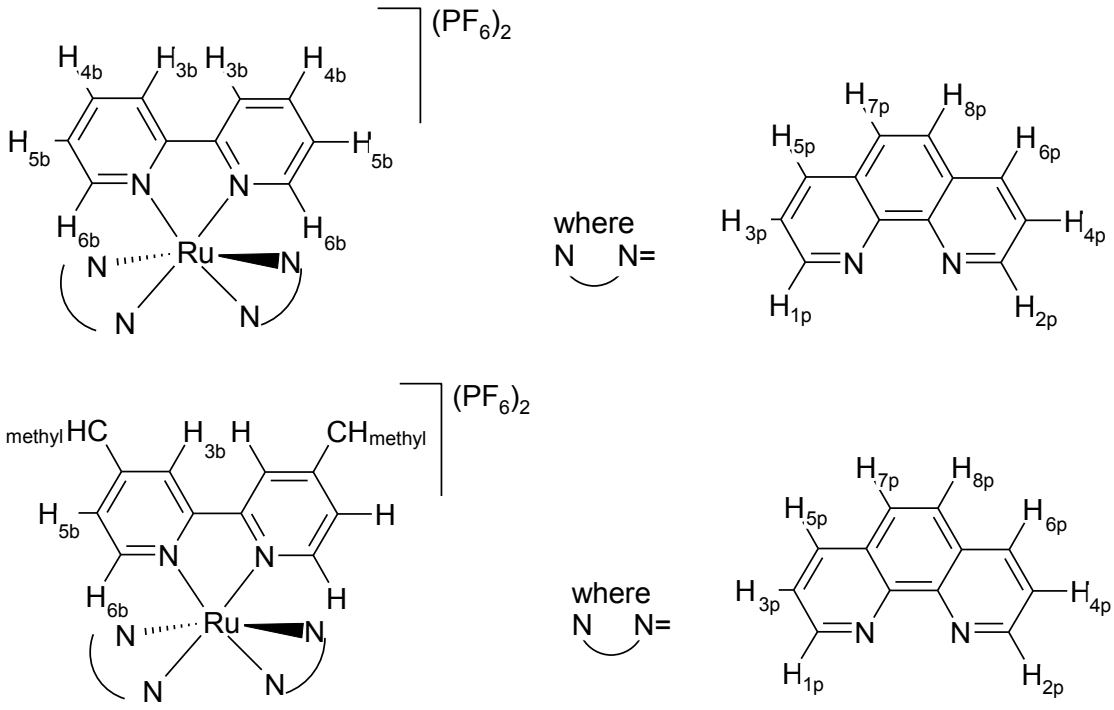

Figure 4.21: Proton numbering scheme for the ^{1}H NMR interpretation of the metal complexes $[Ru(phen)_2(bpy)](PF_6)_2$ and $[Ru(phen)_2(dmbpy)](PF_6)_2$

$[Ru(phen)_2(bpy)](PF_6)_2$

The first complex synthesised, $[Ru(phen)_2(bpy)](PF_6)_2$, is the starting point for both of the novel compounds $[Ru(thimphen)_2(bpy)](PF_6)_2$ and $[Ru(pyrphen)_2(bpy)](PF_6)_2$. As in Chapter 3 the deuterated bipyridyl analogues of these complexes were synthesised as an aid to ^1H NMR interpretation.

The ^1H NMR spectra of the deuterated and non-deuterated metal complexes $[Ru(phen)_2(bpy)](PF_6)_2$ and $[Ru(phen)(d_8\text{-bpy})](PF_6)_2$ are shown below in Figure 4.22.

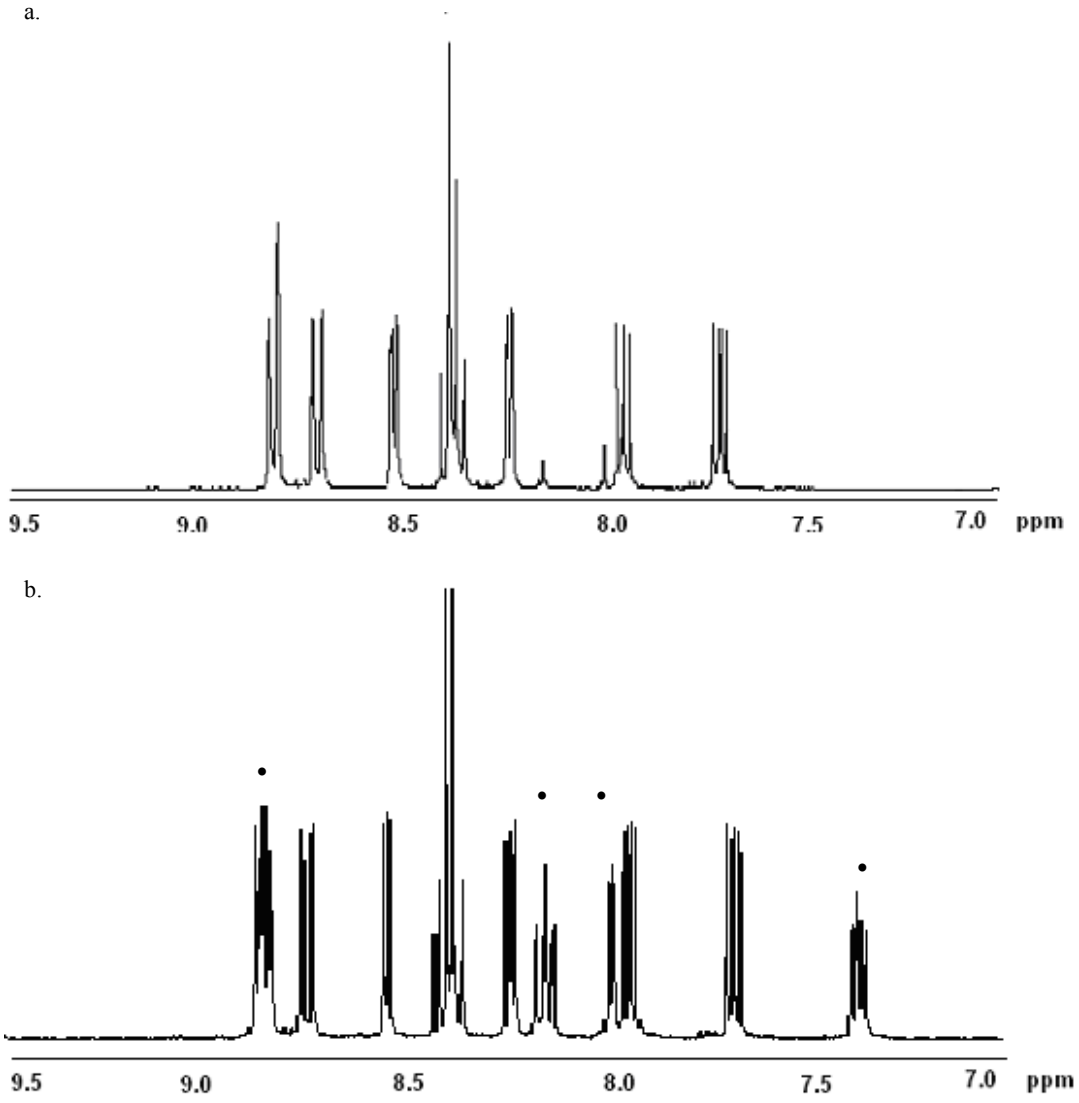

Figure 4.22: ^1H NMR spectra of (a) $[Ru(phen)_2(d_8\text{-bpy})](PF_6)_2$ and (b) $[Ru(phen)_2(bpy)](PF_6)_2$ in d_6-acetone

From the above spectra it can be seen that the peaks present at 8.75-8.72 ppm, 8.06 ppm, 7.91 ppm and 7.33 ppm (marked with a •) appear only in Figure 4.22 (b) (i.e. the non-deuterated spectrum) and therefore are attributable to the 2,2'-bipyridyl portion of the molecule. Note that a peak appears at 8.75-8.72 ppm in both spectra but the signal appearing in Figure 4.22 (b) displays twice the intensity of the peak appearing in the same place in Figure 4.22 (a). Therefore the peak appearing at 8.75-8.72 ppm in Figure 4.22 (b) consists of two overlapping signals, one corresponding to a phenanthroline signal the other to a bipyridyl signal. These bipyridyl peaks follow the usual order for symmetrical 2,2'- bipyridyl complexes, with four separate signals appearing (two doublets and two triplets) each corresponding to two identical protons. In order to better assign these signals the COSY spectrum of [Ru(phen)$_2$(bpy)](PF$_6$)$_2$ is shown below in Figure 4.23.

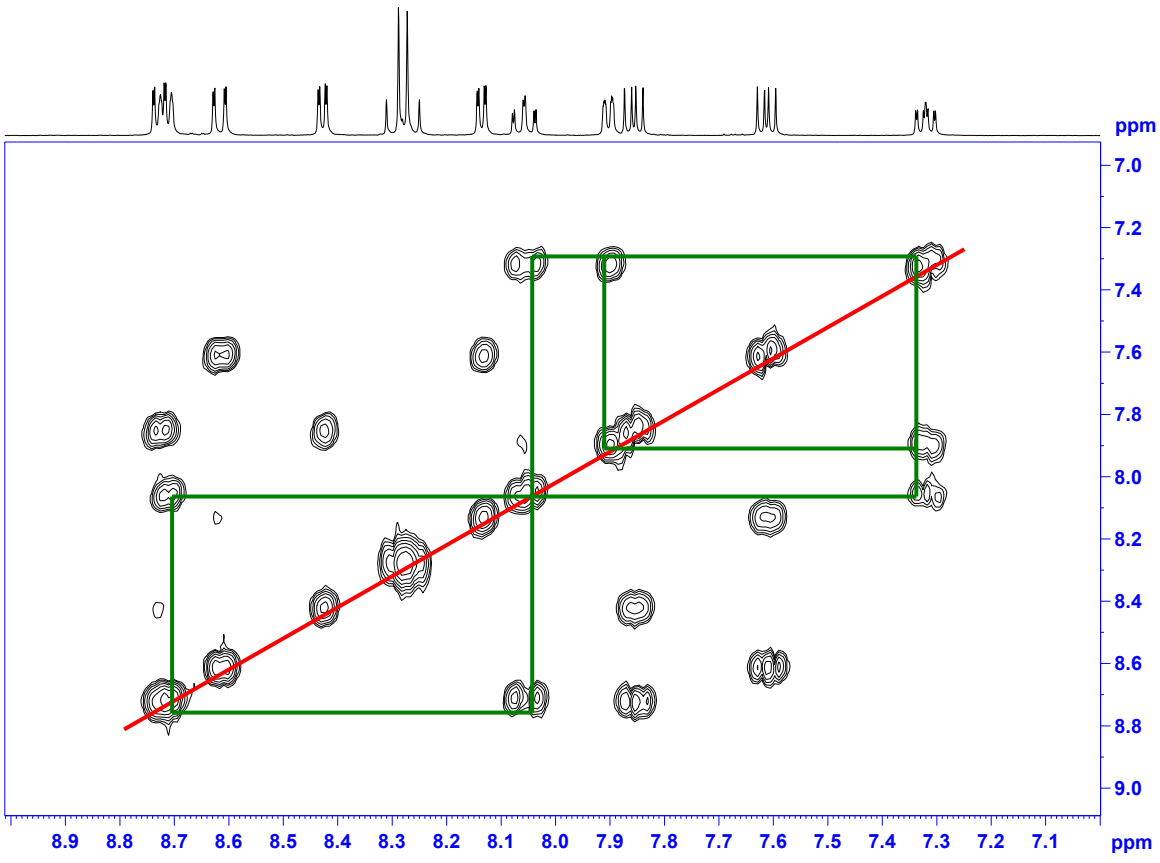

Figure 4.23: ^{1}H COSY spectrum for [Ru(phen)$_2$(bpy)](PF$_6$)$_2$ as measured in d_6-acetone highlighting coupling bipyridyl protons

From the COSY spectrum shown above it can be seen that the triplet present at 7.33 ppm couples with the doublet present at 7.91 ppm. These signals must relate to the protons H$_{5b}$ and H$_{6b}$ respectively. These protons are situated over the aromatic system

of the adjacent phenanthroline ligands. The shielding provided by the aromatic system results in the upfield position of these signals. This effect is shown below in Figure 4.24.

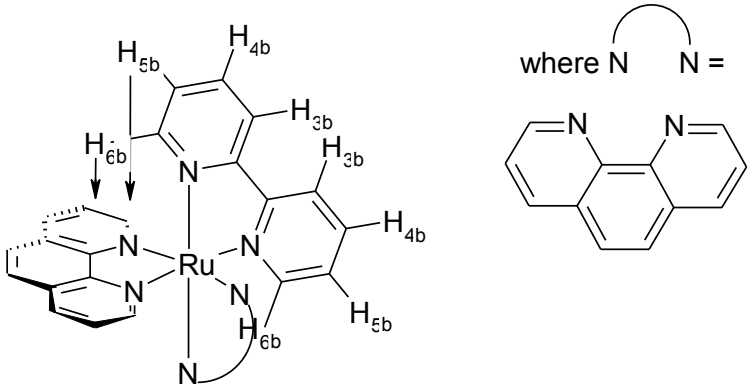

Figure 4.24: Diagrammatic representation of the positioning of the protons H_{5b} and H_{6b} in $[Ru(phen)_2(bpy)](PF_6)_2$

The triplet at 7.33 ppm also couples with the triplet present at 8.09 ppm, confirming that the triplet at 7.34 ppm corresponds to H_{5b} and also shows that the triplet at 8.09 ppm corresponds to H_{4b}. The triplet at 8.09 ppm also couples with the multiplet present between 8.75 and 8.72 ppm, intimating that this multiplet contains the signal for H_{3b}. The downfield position of this signal is characteristic for H_{3b} in a bipyridyl molecule[19].

The remaining phenanthroline based signals may be assigned based on the coupling pattern shown in Figure 4.25.

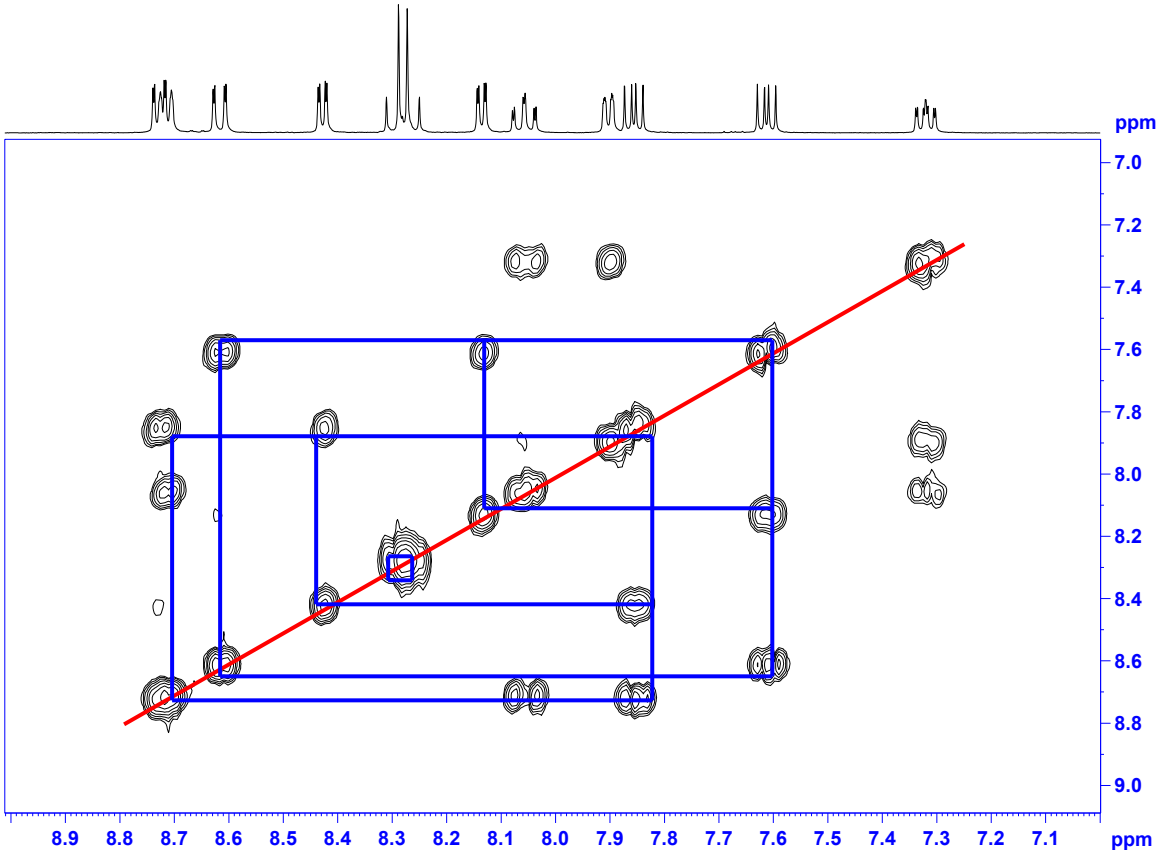

Figure 4.25: ^1H COSY spectrum for $[Ru(phen)_2(bpy)](PF_6)_2$ as measured in d_6-acetone highlighting coupling phenanthroline protons

It can be seen from the spectrum for $[Ru(phen)_2(d_8\text{-bpy})](PF_6)_2$ shown in Figure 4.22 that there are six distinct phenanthroline signals present in the spectrum, each displaying an integration value corresponding to two protons apiece as well as a multiplet displaying an integration value corresponding to four protons. This multiplet present at 8.32-8.26 ppm does not couple with any other peak in the spectrum as can be seen in Figure 4.25, and therefore it may be assumed that this signal corresponds to a number of adjacent protons in a very similar environment, coupling only to each other. Examining the structure of the phenanthroline portion of the molecule it was inferred that this signal (present at 8.32-8.26 ppm) corresponds to the protons H_{7p} and H_{8p}.

H_{3p} and H_{4p} are the only protons in the phenanthroline portion of the molecule situated adjacent to two CH groups and so will be the only signals to appear as triplets in the spectrum. Examining the COSY spectrum as shown in Figure 4.25 there are two doublets of doublets visible at 7.62 ppm and 7.88-7.85 ppm each integrating for two protons and each coupling with two other signals in the spectrum. The further upfield

of the signals has been attributed to H_{3p}. As seen before with the bipyridyl protons present in this molecule, H_{3p} and H_{1p} are situated above the aromatic system of the adjacent phenanthroline ligand. As a result the ^1H NMR signals corresponding to these protons will appear further upfield than the peaks signifying the chemically similar protons H_{2p} and H_{4p}, as H_{2p} and H_{4p} are situated over the adjacent bipyridyl ligand which does not feature a conjugated π system like that of the fused-ring aromatic phenanthroline structure. This effect is shown diagrammatically below in Figure 4.26.

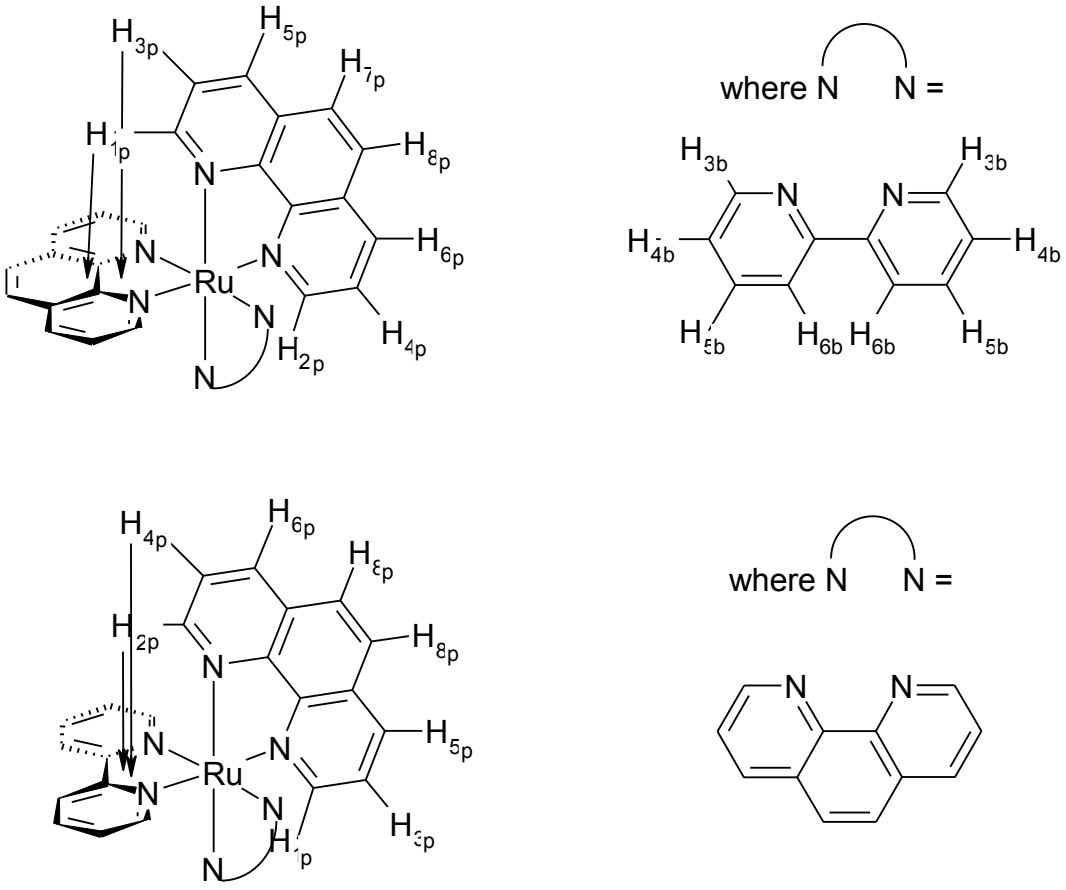

Figure 4.26: Diagrammatic representation of the position of H_{1p} and H_{3p} as well as H_{1p} and H_{3p} in the molecule $[Ru(phen)_2(bpy)](PF_6)_2$

This further upfield signal corresponding to H_{3p} couples with the doublet present at 8.62 ppm as well as a second doublet present at 8.15 ppm. H_{1p} are subject to the same shielding effect as H_{3p} and therefore will appear further upfield of the signal corresponding to H_{5p}. Therefore the doublet present at 8.15 ppm corresponds to H_{1p}

while the doublet present at 8.62 ppm represents H_{5p}. The doublet of doublets present at 7.88-7.85 ppm was earlier identified as H_{4p}. This signal also couples to two doublets, one at 8.44 ppm, the other at 8.75-8.72 ppm. These signals correspond to H_{2p} and H_{6p} respectively. As mentioned previously, the protons H_{2p} are situated over the adjacent 2,2'-bipyridyl ligand, which does not provide as much electronic shielding as 1,10-phenanthroline, explaining why H_{2p} appear at higher chemical shift than $H_{1p.}$ However, when comparing H_{2p} to H_{6p} the adjacent bipyridyl ligand supplies enough electronic shielding to force the signal corresponding to H_{2p} to appear further upfield when compared to the signal representing H_{6p}. The values for this assignment are tabulated below in Table 4.1.

[Ru(phen)$_2$(dmbpy)](PF$_6$)$_2$

The second precursor complex synthesised was [Ru(phen)$_2$(dmbpy)](PF$_6$)$_2$, this time using 4,4'-dimethyl-2,2'-bipyridine (dmbpy) as an ancillary ligand instead of 2,2'-bipyridine. The ^{1}H NMR spectrum of [Ru(phen)$_2$(dmbpy)](PF$_6$)$_2$ is shown below in Figure 4.27.

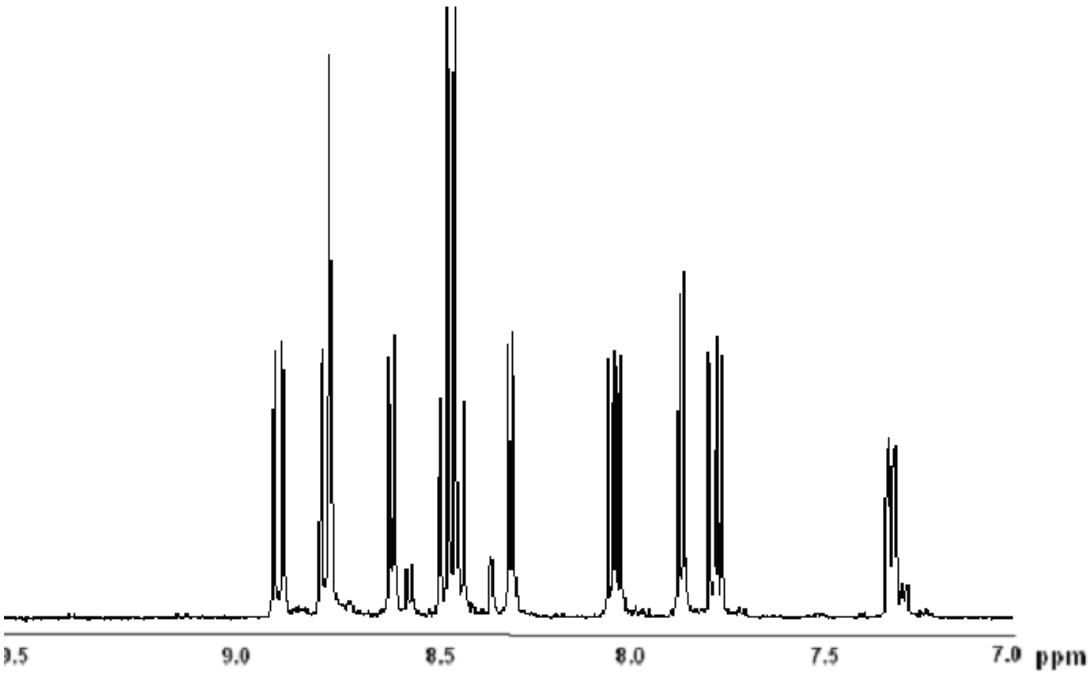

Figure 4.27: ^{1}H NMR spectrum for [Ru(phen)$_2$(dmbpy)](PF$_6$)$_2$ as measured in d_6-acetone

This spectrum is as expected: almost identical to that of [Ru(phen)$_2$(bpy)](PF$_6$)$_2$, missing only the signal corresponding to H_{4b} in the spectrum of

$[Ru(phen)_2(bpy)](PF_6)_2$ as shown in Figure 4.22 (b). This similarity is compounded by the coupling pattern encountered in the COSY spectrum for this complex, shown below in Figure 4.28.

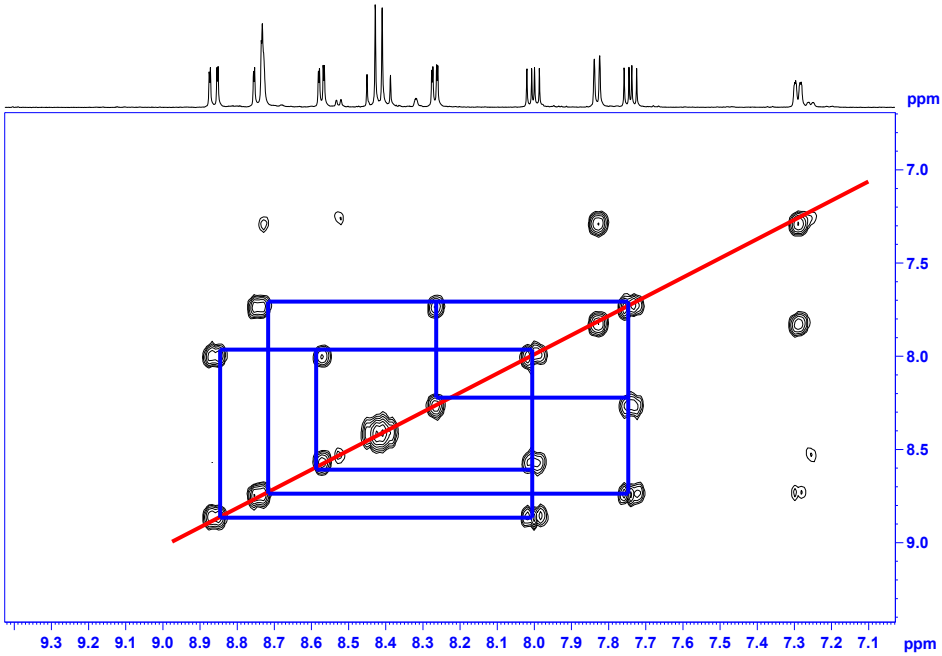

Figure 4.28: COSY spectrum of $[Ru(phen)_2(dmbpy)](PF_6)_2$ highlighting coupling phenanthroline protons as measured in d_6-acetone

Due to the similarity between the chemical shift, multiplicity and coupling pattern of $[Ru(phen)_2(dmbpy)](PF_6)_2$ as compared to $[Ru(phen)_2(bpy)](PF_6)_2$ the interpretation of the spectra shown in Figure 4.27 and Figure 4.28 has been omitted (see Appendix A) with the final assignment shown below in Table 4.2.

4.2.2.2 $[Ru(phendione)_2(L)](PF_6)_2$ intermediate complexes

The next set of complexes synthesised were the intermediate complexes $[Ru(phendione)_2(bpy)](PF_6)_2$ and $[Ru(phendione)_2(dmbpy)]$. This section relates the characterisation of these intermediates by ^1H NMR methods.

$[Ru(phendione)_2(bpy)](PF_6)_2$

The complexes described in Chapter 3 containing one phenanthroline-dione group were found to yielded broad, uneven spectra that provided little to no information about the complex being analysed. However, following extensive drying, the metal complexes $[Ru(bpy)(phendione)_2](PF_6)_2$ and $[Ru(d_8\text{-}bpy)(phendione)_2](PF_6)_2$ yielded the sharp, relatively clean spectra shown below in Figure 4.29. It has therefore been

assumed that ruthenium-phenanthroline dione complexes may have an increased propensity to hold excess water, which may in turn yield to the broadening observed for this type of complex in Chapter 3.

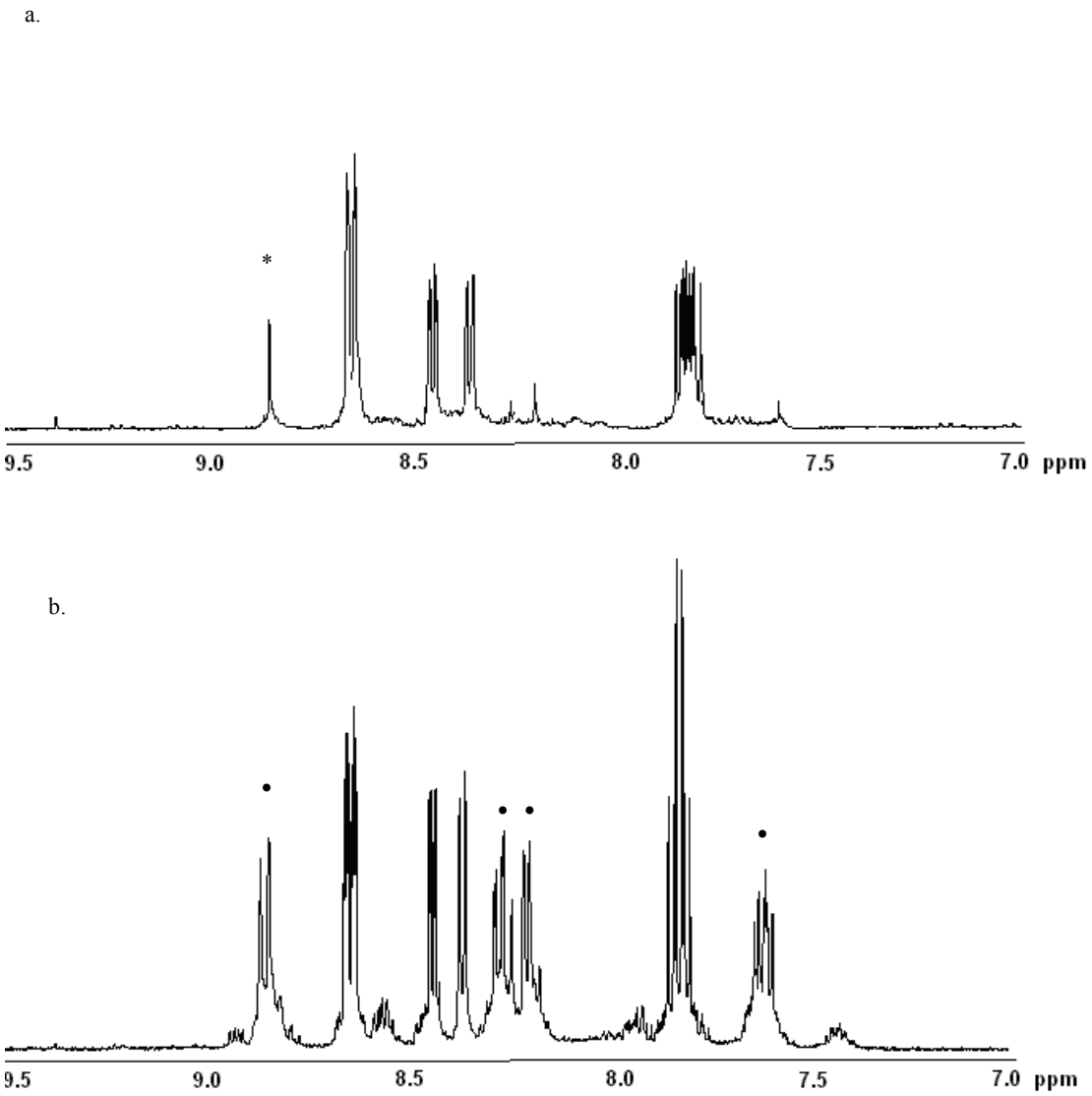

Figure 4.29: ^1H NMR spectra for the metal complexes (a) [Ru(d_8-bpy)(phendione)$_2$](PF$_6$)$_2$ and (b) [Ru(bpy)(phendione)$_2$](PF$_6$)$_2$ in d_6-acetone

Comparing Figure 4.29 (a) ([Ru(phendione)$_2$(bpy)](PF$_6$)$_2$) with Figure 4.29 (b) ([Ru(phendione)$_2$(bpy)](PF$_6$)$_2$) it can be seen that the peaks visible at 8.84 ppm, 8.26 ppm, 8.19 ppm and 7.64-7.56 ppm appear only in Figure 4.29 (b) (the non-deuterated spectrum) and are therefore attributable to the bipyridyl protons present in the molecule. These signals are marked with a •. It may be noted that there is a singlet present at 8.84 ppm in the deuterated spectrum Figure 4.29 (a) marked above with a *.

This does not imply that this signal is phenanthroline based, in fact this is a deuterated bipyridyl signal that has most likely been partially rehydrogenated by the harsh acidic conditions used in this reaction. The bipyridyl signals identified in the spectrum above may be more accurately assigned through examination of the COSY spectrum for [Ru(phendione)$_2$(bpy)](PF$_6$)$_2$, shown below in Figure 4.30.

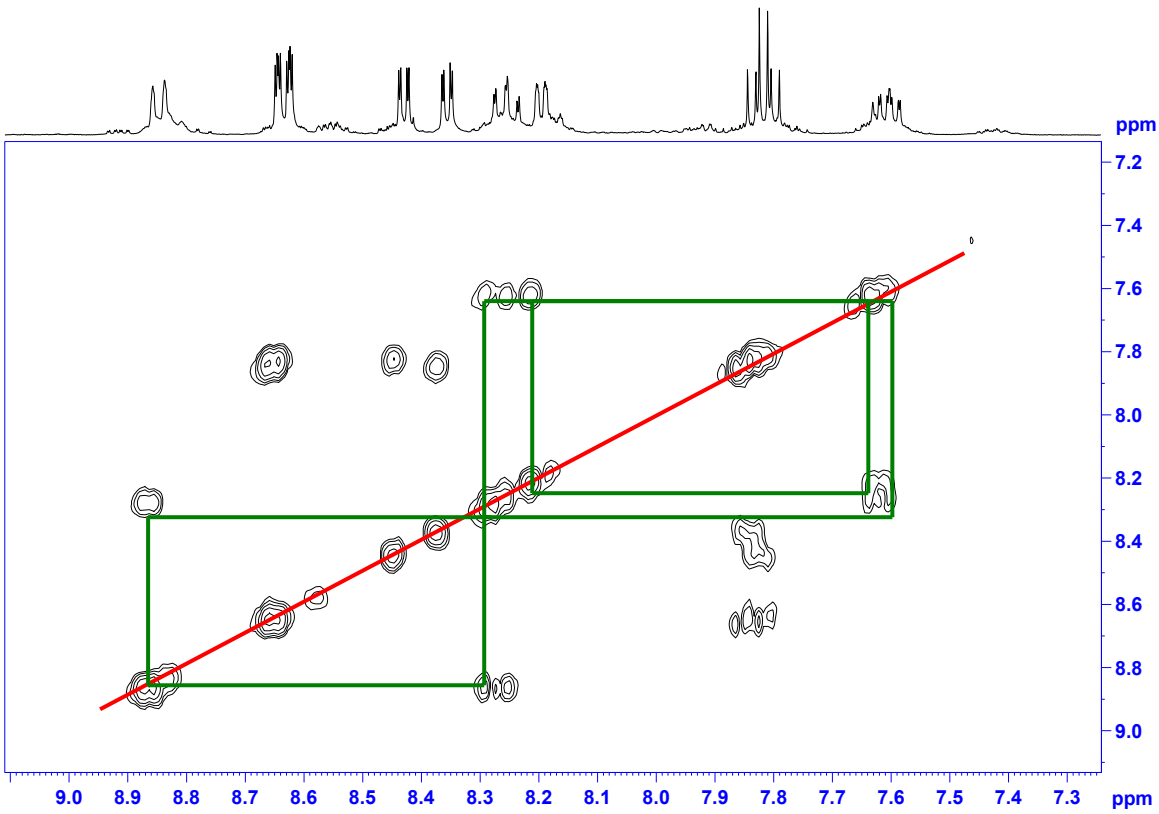

Figure 4.30: COSY spectrum of [Ru(phendione)$_2$(bpy)](PF$_6$)$_2$ as measured in d_6-acetone at 295 K, highlighting coupling bipyridyl signals.

Of the four bipyridyl signals highlighted in Figure 4.30, the most downfield signal may be attributed to H$_{5b}$, keeping in line with the bipyridyl type arrangement seen previously in Chapter 3. This multiplet at 7.64-7.56 ppm couples to a doublet present at 8.19 ppm and a triplet present at 8.26 ppm. These signals correspond to the adjacent protons H$_{6b}$ and H$_{4b}$ respectively, H$_{6b}$ appearing as a doublet as H$_{5b}$ is its only adjacent proton while H$_{4b}$ appears as a tripet as it also couples with H$_{3b}$. This coupling is evident in Figure 4.30, with the triplet corresponding to H$_{4b}$ coupling to the H$_{5b}$ multiplet as well as a doublet appearing at 8.84 ppm which therefore corresponds to H$_{3b}$. It is worth noting that there is a recovery of symmetry in the bipyridyl portion of the molecule, both H$_{3b}$ protons yield one signal, as does H$_{4b}$, H$_{5b}$ and H$_{6b}$.

By comparing the spectrum shown in Figure 4.22 (a) ([Ru(phen)$_2$(d$_8$-bpy)](PF$_6$)$_2$) to that shown in Figure 4.29 (a) ([Ru(phendione)$_2$(d$_8$-bpy)](PF$_6$)$_2$) it can be seen that there is some change in the positioning and multiplicity of the phenanthroline peaks in the spectrum for [Ru(phendione)$_2$(bpy)](PF$_6$)$_2$ as compared to [Ru(phen)$_2$(bpy)](PF$_6$)$_2$. The peak present at approximately 8.40 ppm integrating for four protons in Figure 4.22 (a) does not appear in the related dione spectrum shown in Figure 4.29 (a) and so must correspond to the phenanthroline protons H_{7p} and H_{8p} which are oxidised to form four identical carbonyl groups. Further comparison of the two spectra shows that there are some other differences between them, most notably the amalgamation of the two doublets seen at 8.84 ppm and 8.73 ppm in Figure 4.22 (a) into one multiplet visible at 8.66-8.62 ppm in Figure 4.29 (a) and a similar joining of the two triplets seen at 7.74 ppm and 7.98 ppm in Figure 4.22 (a) to form the multiplet present at 7.86-7.78 ppm in Figure 4.29 (a). The integrations of the overlapping peaks present in Figure 4.29 (a) are double that of each single peak at similar chemical shift in Figure 4.22 (b), confirming that the amalgamated signals present in the [Ru(phendione)$_2$(d$_8$-bpy)](PF$_6$)$_2$ spectrum represent two overlapping signals. The assignment of these and the remaining phenanthroline signals in the ^{1}H NMR spectrum may be explained through examination of the COSY spectrum shown below in Figure 4.31, highlighting coupling phenanthroline signals.

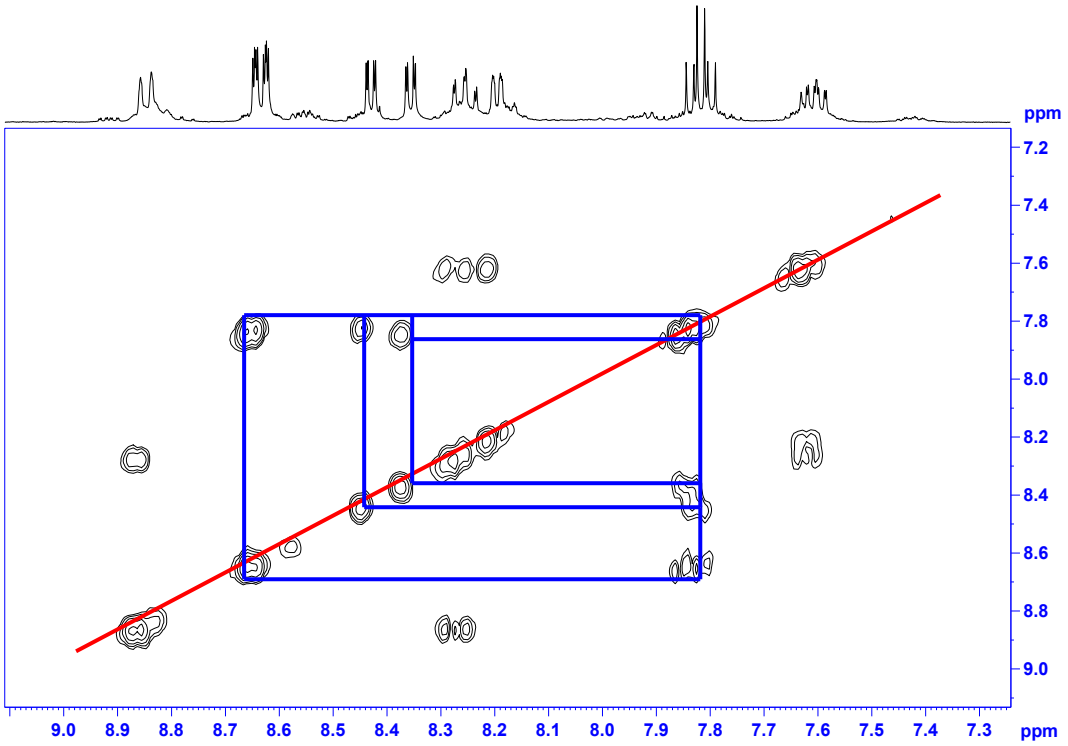

Figure 4.31: COSY spectrum of $[Ru(phendione)_2(bpy)](PF_6)_2$ as measured in d_6-acetone at 295 K, highlighting coupling phenanthroline signals.

Examining the COSY spectrum shown in Figure 4.31 it can be seen that the multiplet occurring at 7.86-7.78 ppm corresponding to H_{3p} and H_{4p} couples to the multiplet present between 8.66 ppm and 8.62 ppm as well as to the two remaining doublets, one appearing at 8.44 ppm, the other at 8.36 ppm. The multiplet present at 8.66-8.62 ppm has already been identified as corresponding to H_{5p} and H_{6p}, so the two remaining doublets must relate to H_{1p} and H_{2p}. Examining the interpretation of $[Ru(phen)_2(bpy)](PF_6)_2$ shown above it has been shown that H_{1p} appears further upfield that H_{2p}, so by virtue of this the doublet present at 8.36 ppm has been identified as corresponding to H_{1p} while the further downfield doublet present at 8.44 ppm relates to H_{2p}.

$[Ru(phendione)_2(dmbpy)](PF_6)_2$

As in the case of $[Ru(phen)_2(bpy)](PF_6)_2$ the next complex synthesised was the bis-phenanthroline dione complex $[Ru(phendione)_2(dmbpy)](PF_6)_2$, the ^{1}H-NMR spectrum for which is shown below in Figure 4.32.

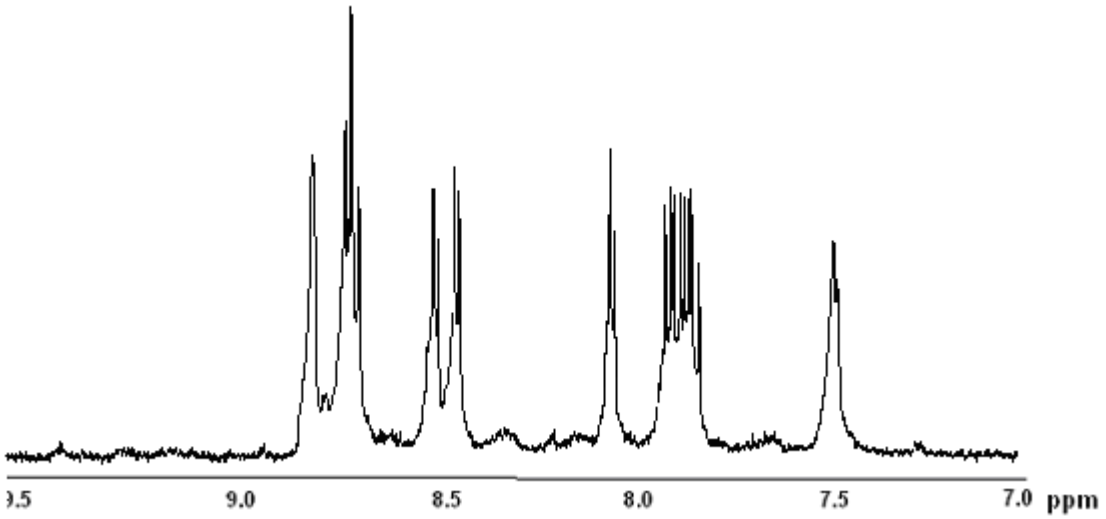

Figure 4.32: ^{1}H NMR spectrum for [Ru(phendione)$_2$(dmbpy)](PF$_6$)$_2$ as measured in d_6-acetone

As for [Ru(phendione)$_2$(bpy)](PF$_6$)$_2$ the spectrum shown in Figure 4.32 for [Ru(phendione)$_2$(dmbpy)](PF$_6$)$_2$ displays a conspicuous absence of the multiplet shown in Figure 4.27 corresponding to H_{7p} and H_{8p} indicating that these protons have been replaced by the desired dione moiety. The remaining signals have shifted somewhat with respect to their original position in the [Ru(phendione)$_2$(dmbpy)](PF$_6$)$_2$ spectrum shown in Figure 4.27. This is most likely due to residual acid in the sample arising from the reaction conditions used. The coupling pattern for these signals is shown below in the COSY spectra shown in Figure 4.33.

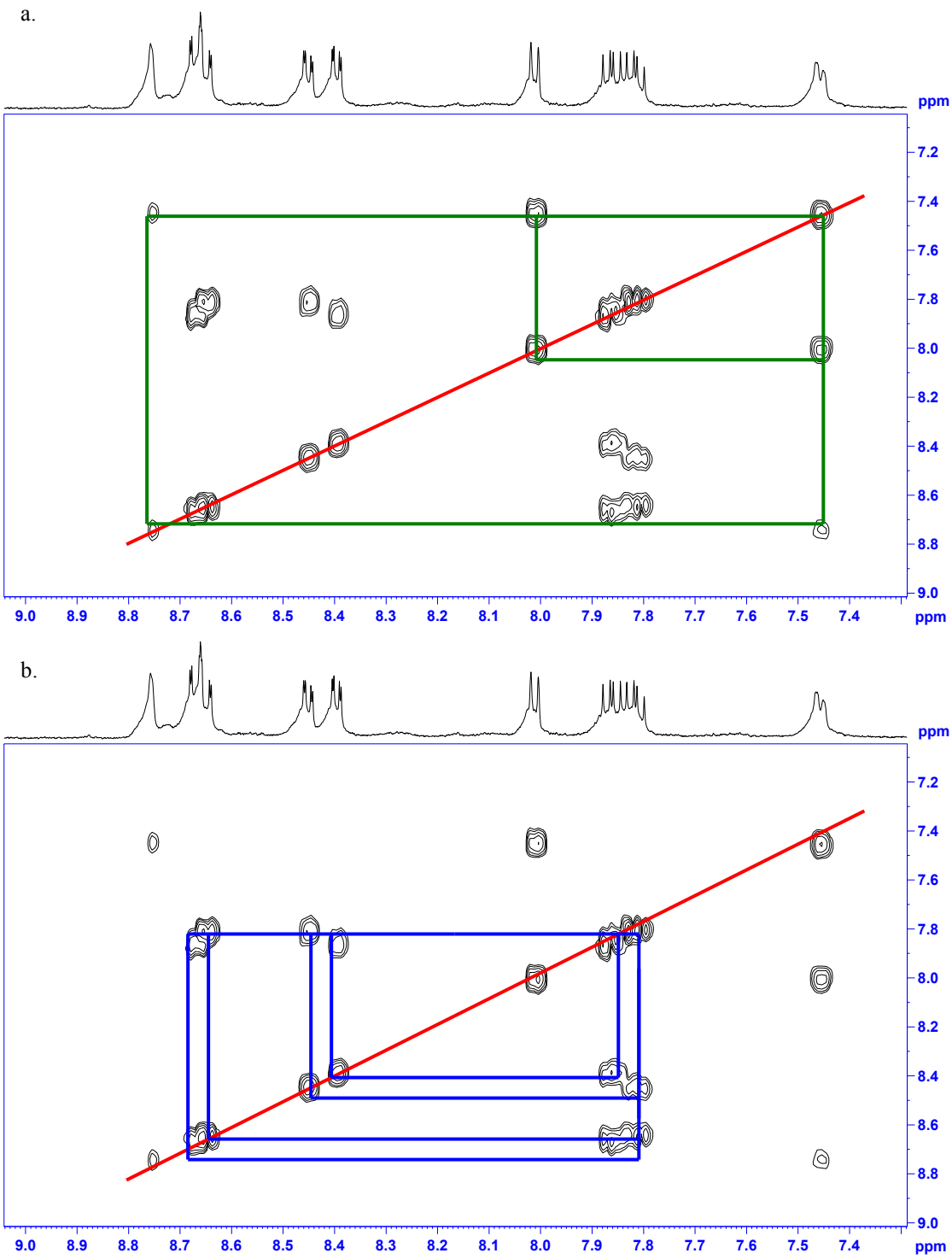

Figure 4.33: ^1H COSY spectrum for $[Ru(phendione)(dmbpy)](PF_6)_2$ as measured in d_6-acetone showing (a) coupling dmbpy protons and (b) coupling phenanthroline protons

The coupling patterns shown above in Figure 4.33 are identical to those described above for $[Ru(phendione)_2(bpy)](PF_6)_2$. As a result the explanation of the coupling

pattern has been omitted with the final assignment given in Table 4.2. The full explanation of these assignments is given in appendix 1.

4.2.2.3 [Ru(pyrphen)$_2$L](PF$_6$)$_2$

At this point in the synthetic pathway, two different metal complexes may be built. Depending on the type of aldehyde used in the final reaction, as outlined above in Section 5.2.1, a pyridine- or thiophene-imidazole group may be appended to the phenanthroline groups present in the molecule. As this type of 'on-complex' synthetic method was used for the synthesis of the metal complex [Ru(bpy)$_2$(pyrphen)](PF$_6$)$_2$ in Chapter 3, the analogous metal complexes [Ru(pyrphen)$_2$(bpy)](PF$_6$)$_2$ and [Ru(pyrphen)$_2$(dmbpy)](PF$_6$)$_2$ will be examined first.

[Ru(pyrphen)$_2$(bpy)](PF$_6$)$_2$ (Complex 2)

The numbering scheme for the assignment of the protons present in this molecule is shown below in Figure 4.34.

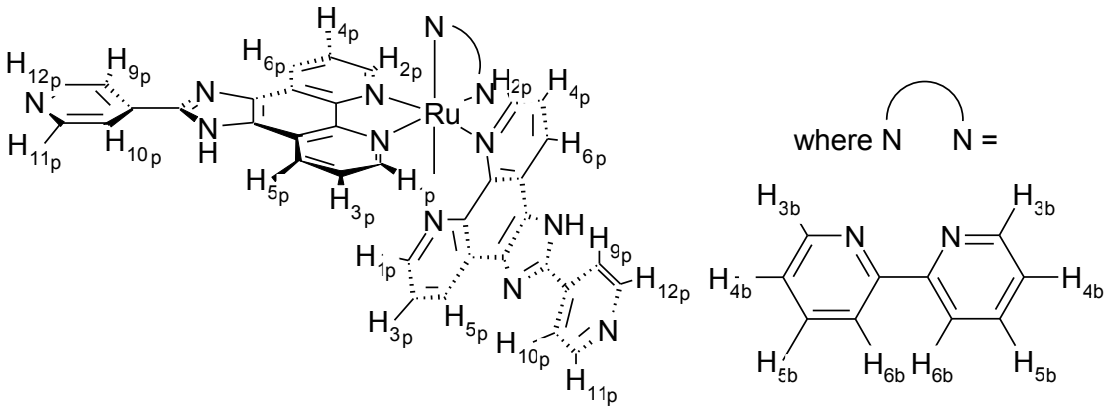

Figure 4.34: Numbering system for the assignment of protons in the ^{1}H NMR analysis of [Ru(pyrphen)$_2$(bpy)](PF$_6$)$_2$

The ^{1}H NMR spectra for the metal complexes [Ru(pyrphen)$_2$(bpy)](PF$_6$)$_2$ and [Ru(pyrphen)$_2$(d$_8$-bpy)](PF$_6$)$_2$ are shown below in Figure 4.35.

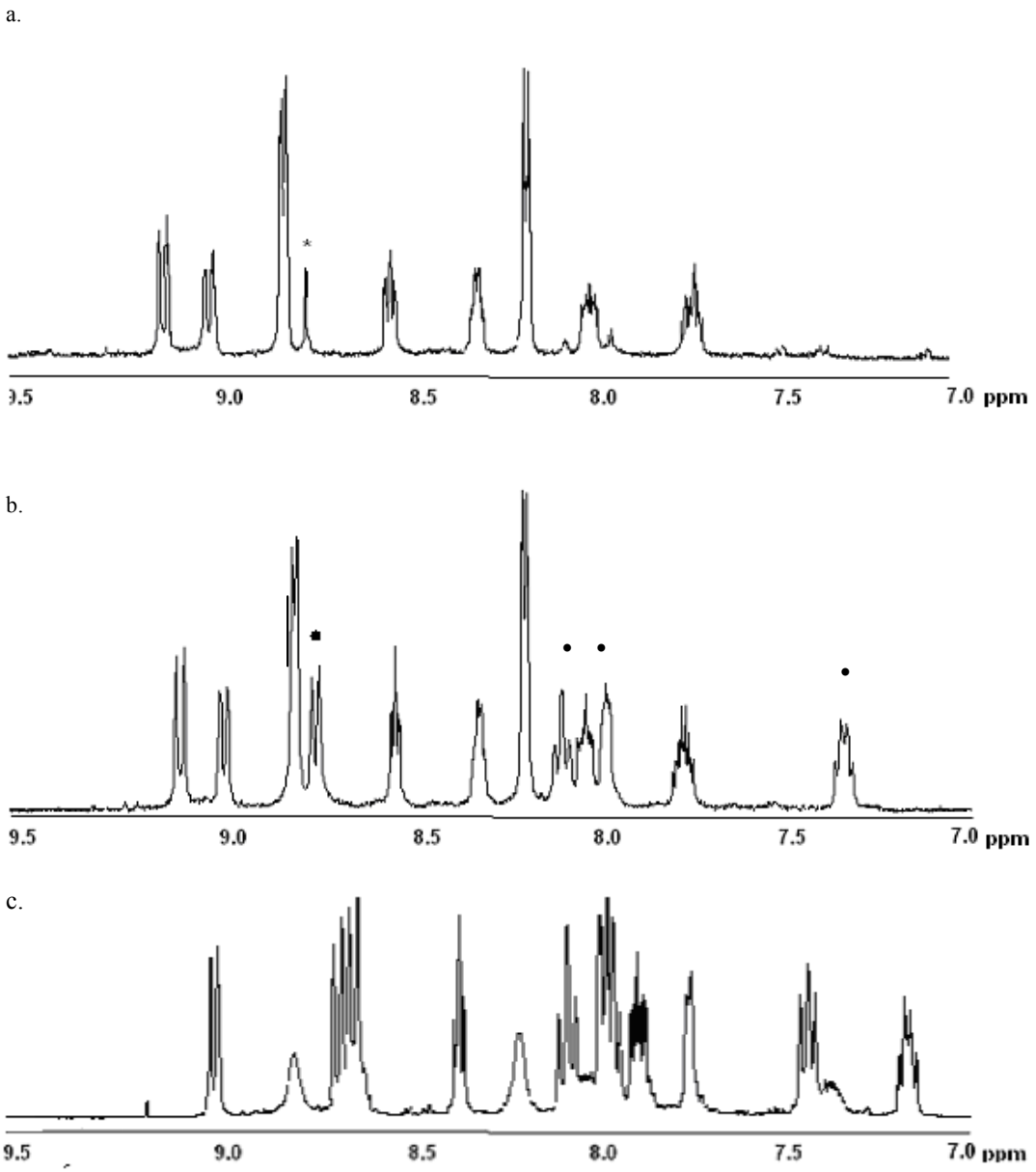

Figure 4.35: ^1H NMR spectra of (a) $[Ru(pyrphen)_2(d_8\text{-}bpy)](PF_6)_2$ (b) $[Ru(pyrphen)_2(bpy)](PF_6)_2$ and (c) $[Ru(bpy)_2(pyrphen)](PF_6)_2$ as measured in d_6-acetone

The spectrum for $[Ru(bpy)_2(pyrphen)](PF_6)_2$ is shown for clarity in Figure 4.35. The $[Ru(bpy)_2(pyrphen)](PF_6)_2$ sample measured here is identical to that used for the spectrum shown in Figure 3.25 (a) (*c.f.* Chapter 3) The solvent used in Chapter 3 was d_6-DMSO which yielded the clear, sharp spectrum shown in Figure 3.25. However, upon changing this to d_6-acetone here in order that the spectrum be comparable to the others shown in this chapter, broadening is observed for the peaks present at 7.54

ppm, 8.35 ppm and 8.87 ppm. This implies that any broadening observed in the spectra for $[Ru(pyrphen)_2(d_8\text{-bpy})](PF_6)_2$ and $[Ru(pyrphen)_2(bpy)](PF_6)_2$ (shown in Figure 4.35 a and b respectively) occurs as a result of the solvent used and not any impurity in the sample. There is a measure of similarity between the spectra for $[Ru(bpy)_2(pyrphen)](PF_6)_2$ and $[Ru(pyrphen)_2(bpy)](PF_6)_2$ as shown in Figure 4.35 c and b, with a number of corresponding peaks appearing at similar chemical shift in the two spectra. These consist of a doublet occurring at 9.07 ppm in Figure 4.35 c corresponding to H_{5p} and H_{6p} of $[Ru(bpy)_2(pyrphen)](PF_6)_2$ which is comparable with the doublets occurring at 9.00 ppm and 9.12 ppm in Figure 4.35 b which are assigned to H_{5p} and H_{6p} of $[Ru(pyrphen)_2(bpy)](PF_6)_2$ in Table 4.1. Also the multiplet occurring from 8.75-8.67 ppm in Figure 4.35 c corresponding to H_{3b} and $H_{3b'}$ in $[Ru(bpy)_2(pyrphen)](PF_6)_2$ is also comparable to the doublet occurring at 8.75 ppm in Figure 4.35 b corresponding to H_{3b} as assigned in Table 4.1. The broad singlets corresponding to the appended pyridine group in Figure 4.35 c are also comparable to the related signals for the same group in Figure 4.35 b. The former occur at 8.85 ppm and 8.27 ppm for $H_{9p/10p}$ and $H_{11p/12p}$ respectively while the latter occur at 8.81 ppm and 8.21 ppm for the same respective protons. All other peaks shown in Figure 4.35 b display small shifts (approximately 0.5 ppm) with respect to the corresponding signals present in Figure 4.35 c and are tabulated in Table 4.1. The fact that there are is no major shift (i.e. greater than 0.5 ppm) for these peaks implies that the structural similarity shown below in Figure 4.36 between the two molecules is intact.

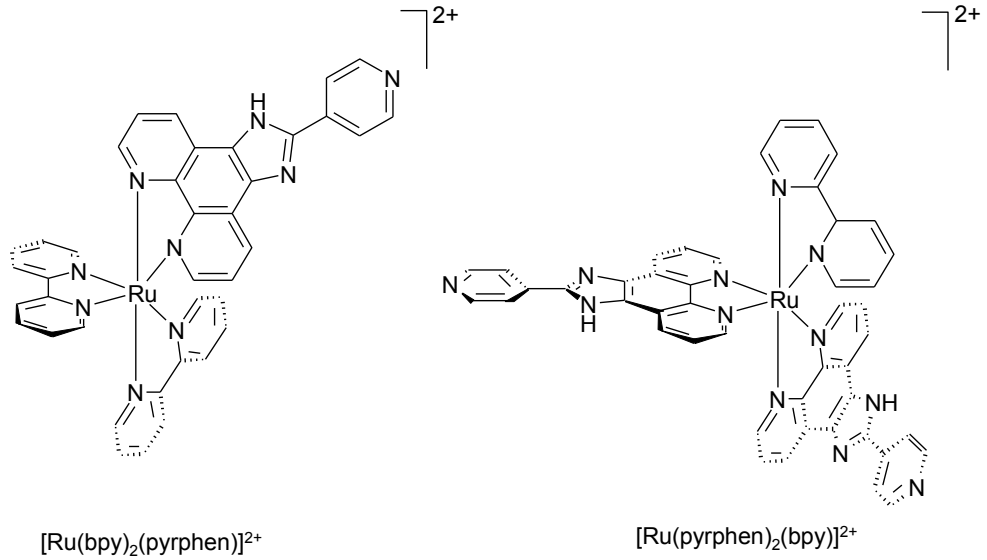

$[Ru(bpy)_2(pyrphen)]^{2+}$ $[Ru(pyrphen)_2(bpy)]^{2+}$

Figure 4.36: Structural representation of the differences in positioning of ligands in the molecules $[Ru(bpy)_2(pyrphen)]^{2+}$ and $[Ru(pyrphen)_2(bpy)]^{2+}$

However, as these small discrepancies are visible when comparing Figure 4.35 b and c, it has been deemed more appropriate to assign the signals in the ^{1}H NMR spectrum of [Ru(pyrphen)$_2$(bpy)]$^{2+}$ through comparison of the deuterated and non-deuterated spectra shown in Figure 4.35 a and b as well as 2-D COSY spectroscopy methods. Examining these two spectra, the peaks present in Figure 4.35 (a) at 7.34 ppm, 8.10 ppm and 8.59 ppm as well as part of the multiplet between 7.71 ppm and 7.88 ppm are attributable to the bipyridyl protons present in the molecule as they are not present in the deuterated-bipyridyl spectrum shown in Figure 4.35 (a). As before these signals are marked with a • in Figure 4.35 (a). In order to assign the bipyridyl protons identified above more accurately, the COSY spectrum of [Ru(pyrphen)$_2$(bpy)](PF$_6$)$_2$ is pictured below in Figure 4.37.

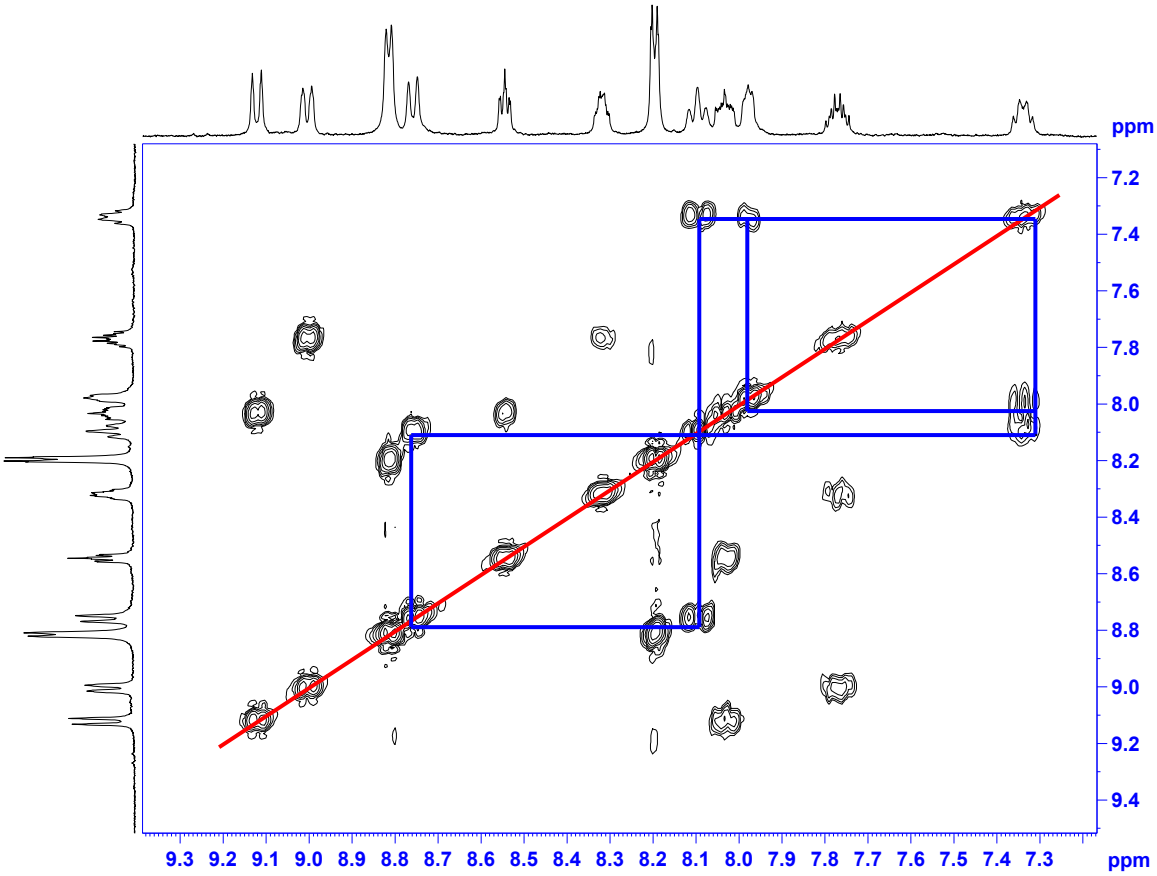

Figure 4.37: COSY spectrum for [Ru(pyrphen)$_2$(bpy)](PF$_6$)$_2$ as measured in d_6-acetone with coupling bpy protons highlighted

From the COSY spectrum shown above it can be seen that the bipyridyl signals present in the molecule appear at almost identical chemical shift to the bipyridyl protons in the parent complex [Ru(phen)$_2$(bpy)](PF$_6$)$_2$ as well as displaying the same coupling pattern. The triplet present at 7.34 ppm couples with the peak masked within

the multiplet occurring between 7.71 ppm and 7.88 ppm implying that these signals must relate to the protons H_{5b} and H_{6b} respectively. The triplet at 7.34 ppm also couples with the triplet present at 8.10 ppm, confirming that the triplet at 7.34 ppm corresponds to H_{5b} and also shows that the triplet at 8.10 ppm corresponds to H_{4b}. The triplet at 8.10 ppm also couples with the doublet at 8.59 ppm, intimating that this doublet at 8.59 ppm corresponds to H_{3b}.

Shown below in Figure 4.38 is the COSY spectrum of [Ru(pyrphen)$_2$(bpy)](PF$_6$)$_2$ with the coupled pyrphen protons highlighted.

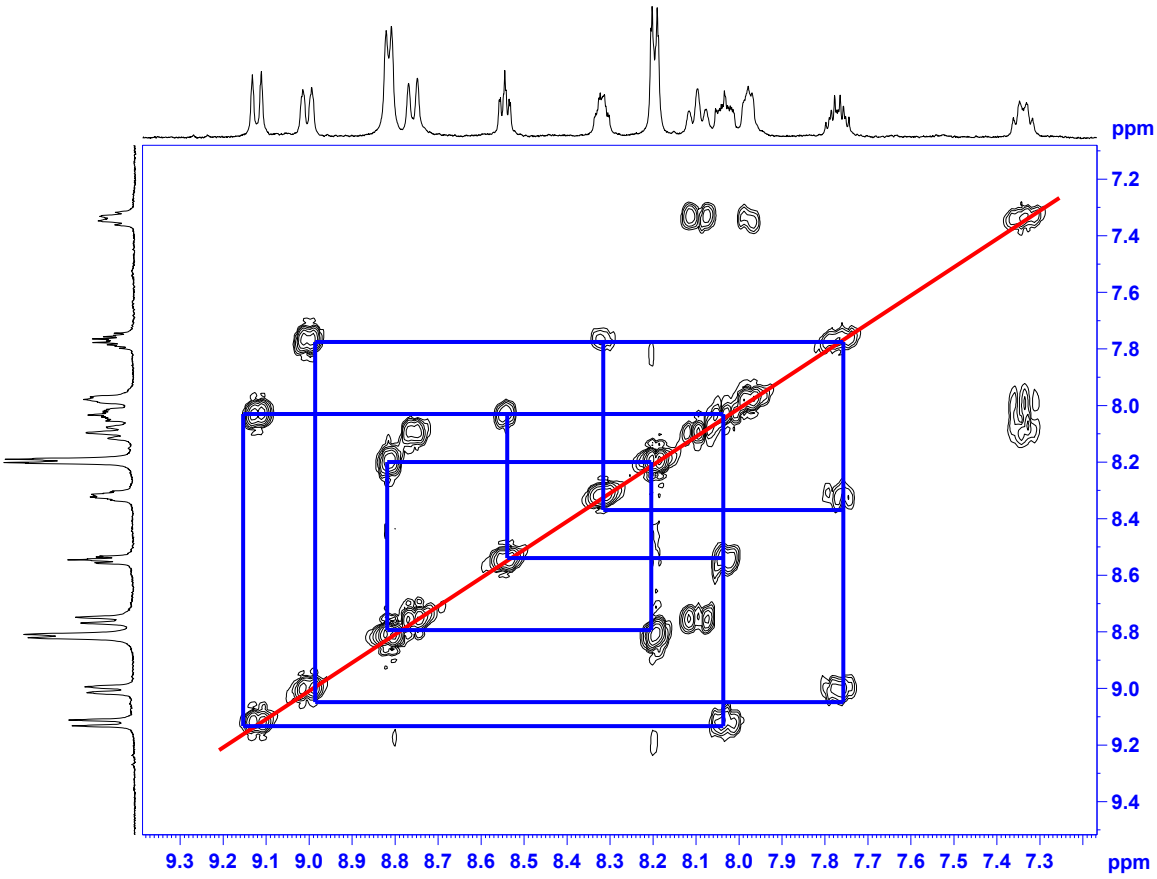

Figure 4.38: COSY spectrum for [Ru(pyrphen)$_2$(bpy)](PF$_6$)$_2$ as measured in d_6-acetone with coupling pyrphen protons highlighted

Of the signals highlighted in Figure 4.38, two doublets dominate the spectrum: one at 8.81 ppm and one at 8.20 ppm. These peaks couple strongly with each other and the peak at 8.81 ppm couples to nothing else in the spectrum, implying that these peaks relate to the pyridine protons $H_{9p,}$ $H_{10p,}$ $H_{11p}$and H_{12p}.The doublet at 8.81 ppm relates to four equivalent protons confirming that this peak relates only to four pyridine protons, in this case the H_{11p} and H_{12p} protons present in the

$[Ru(pyrphen)_2(bpy)](PF_6)_2$ molecule. The high chemical shift of this peak as compared to the other pyridine doublet in the spectrum at 8.20 ppm may be explained by the close proximity of the H_{11p} and H_{12p} protons to the electronegative pyridine nitrogen.

Discounting these signals it can be seen that there are six distinct phenanthroline signals present in the spectrum, each displaying an integration value corresponding to two protons apiece. Therefore there is an individual peak corresponding to each phenanthroline proton: H_{1p}, H_{2p}, H_{3p}, H_{4p}, H_{5p} and H_{6p}, as seen for the parent complex $[Ru(phen)_2(bpy)](PF_6)_2$.

H_{3p} and H_{4p} are the only protons in the phenanthroline portion of the molecule situated adjacent to two CH groups and so, as mentioned for $[Ru(phen)_2(bpy)](PF_6)_2$, will be the only two signals to couple with two other peaks in the spectrum. Examining the COSY spectrum as shown in Figure 4.38 it can be seen that the phenanthroline signal present within the multiplet between 7.74 ppm and 7.79 ppm as well as the signal present at 8.05-8.01 ppm both couple to two other phenanthroline peaks present in the spectrum, indicating that these are the peaks relating to H_{3p} and H_{4p}. The more upfield of these signals may be attributed to H_{3p} for the electronic shielding seen for $[Ru(phen)_2(bpy)](PF_6)_2$.

This further upfield signal corresponding to H_{3p} couples with the multiplet present between 8.33 ppm and 8.30 ppm and the doublet present at 9.00 ppm. The more upfield of these signals may be attributed to H_{1p} as a result of aromatic shielding while, the further downfield signal present between 9.00 ppm may then be attributed to H_{5p}.

The multiplet present at 8.05-8.01 ppm therefore represents H_{4p}. This signal couples with a triplet present at 8.54 ppm and the doublet visible at 9.13 ppm. As for the metal complex $[Ru(bpy)_2(pyrphen)](PF_6)_2$ upon complexation the proton adjacent to the complexed nitrogen atom, in this case H_{2p}, appears at a comparatively low chemical shift when contrasted with the signal corresponding to the proton bonded to the carbon adjacent to the imidazole group, in this case H_{6p}. The chemical shift values for each of the protons present in the molecule $[Ru(pyrphen)_2(bpy)](PF_6)_2$ as well as the chemical shift values for the parent complexes $[Ru(phen)_2(bpy)](PF_6)_2$ and $[Ru(phendione)_2(bpy)](PF_6)_2$ are tabulated below in Figure 4.1.

Proton	**Chemical shift δ (ppm) $[Ru(phen)_2(bpy)]^{2+}$**	**Chemical shift δ (ppm) $[Ru(phendione)_2(bpy)]^{2+}$**	**Chemical shift δ (ppm) $[Ru(pyrphen)_2(bpy)]^{2+}$**	**Chemical shift δ (ppm) $[Ru(pyrphen)_2bpy)]^{2+}$**
H_{1p}	8.15 (d)	8.36 (d)	8.33-8.30 (m)	8.08-8.01 (m)
H_{2p}	8.44 (d)	8.44 (d)	8.54 (t)	8.08-8.01 (m)
H_{3p}	7.62 (dd)	7.86-7.78 (m)	7.79-7.74 (m)	7.98-7.92 (m)
H_{4p}	7.88-7.85 (t)	7.86-7.78 (m)	8.05-8.01 (m)	7.98-7.92 (m)
H_{5p}	8.62 (d)	8.66-8.62 (m)	9.00 (d)	9.07 (d)
H_{6p}	8.75-8.72 (dd)	8.66-8.62 (m)	9.12 (d)	9.07 (d)
H_{7p}	8.32-8.26 (m)	-	-	-
H_{8p}	8.32-8.26 (m)	-	-	-
H_{9p}	-	-	8.20 (d)	8.27 (br s)
H_{10p}	-	-	8.20 (d)	8.27 (br s)
H_{11p}	-	-	8.81 (d)	8.85 (br s)
H_{12p}	-	-	8.81 (d)	8.85 (br s)
H_{3b}	8.75-8.72 (dd)	8.84 (d)	8.75 (d)	8.86-8.67 (m)
H_{4b}	8.06 (t)	8.26 (t)	8.10 (t)	H_{4b} 8.42 (t) $H_{4b'}$ 8.14 (t)
H_{5b}	7.33 (t)	7.64-7.56 (m)	7.36-7.32 (m)	H_{5b} 7.49 (t) $H_{5b'}$ 7.28-7.24 (m)
H_{6b}	7.91 (d)	8.19 (d)	7.97 (m)	H_{6b} 8.08-8.01 (m) $H_{6b'}$ 7.82 (d)

Table 4.1: Chemical shifts for the proton signals present in ^1H NMR spectrum for the molecules $[Ru(phen)_2(bpy)](PF_6)_2$, $[Ru(phendione)_2(bpy)](PF_6)_2$ and $[Ru(pyrphen)_2(bpy)](PF_6)_2$ as measured in d-acetone.

$[Ru(pyrphen)_2(dmbpy)](PF_6)_2$ (Complex 6)

The numbering scheme for the assignment of the protons present in this molecule is shown below in Figure 4.39.

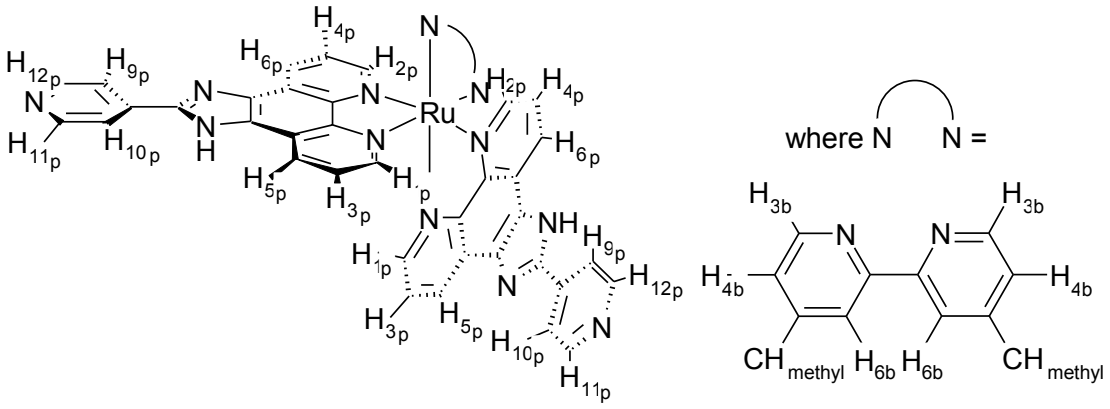

Figure 4.39: Numbering system for the assignment of protons in the ^1H NMR analysis of $[Ru(pyrphen)_2(dmbpy)](PF_6)_2$

The ^1H NMR spectra for the metal complex $[Ru(pyrphen)_2(dmbpy)](PF_6)_2$ is shown below in Figure 4.40.

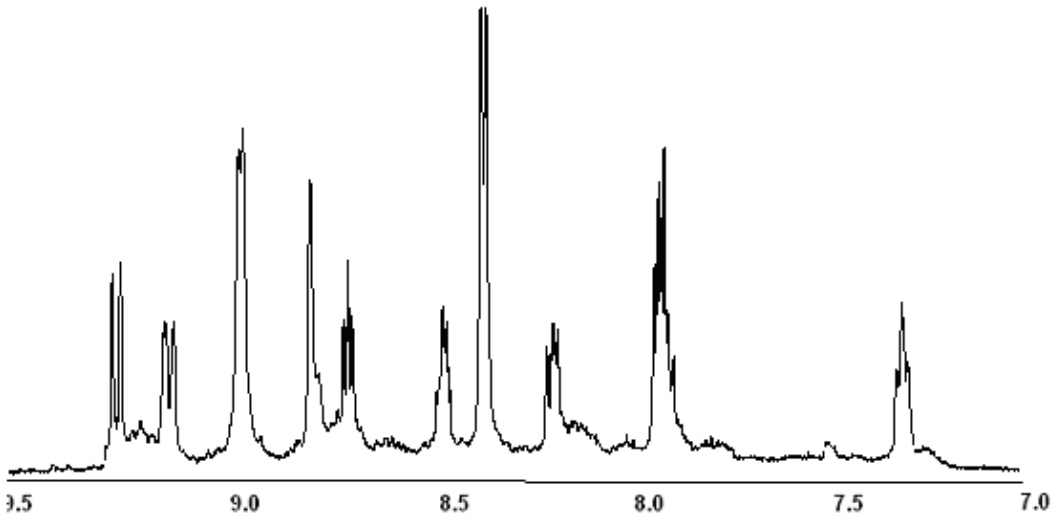

Figure 4.40: ^1H NMR spectra of $[Ru(pyrphen)_2(dmbpy)](PF_6)_2$ as measured in d_6-acetone

As before, the chemical shift values and coupling patterns for $[Ru(pyrphen)_2(dmbpy)](PF_6)_2$ are very similar to those seen for $[Ru(pyrphen)_2(bpy)](PF_6)_2$ and so the interpretation of the spectrum shown in Figure 4.40 and its related COSY spectrum have been omitted with the final assignment shown in Table 4.2. The omitted characterisation is included in Appendix A.

Proton	**Chemical shift δ (ppm) $[Ru(phen)_2(dmbpy)]^{2+}$**	**Chemical shift δ (ppm) $[Ru(phendione)_2(dmbpy)]^{2+}$**	**Chemical shift δ (ppm) $[Ru(pyrphen)_2(dmbpy)]^{2+}$**
H_{1p}	8.27 (d)	8.39 (d)	8.46-8.42 (m)
H_{2p}	8.57 (d)	8.49 (d)	8.67 (m)
H_{3p}	7.74 (dd)	7.89-7.75 (dd)	7.91-8.86 (m)
H_{4p}	8.00 (t)	7.89-7.75 (dd)	8.19-8.15 (m)
H_{5p}	8.74 (m)	8.76-8.66 (d)	9.11 (d)
H_{6p}	8.86 (dd)	8.76-8.66 (d)	9.23 (d)
H_{7p}	8.45-8.39 (m)	-	-
H_{8p}	8.45-8.39 (m)	-	-
H_{9p}	-	-	8.33 (d)
H_{10p}	-	-	8.33 (d)
H_{11p}	-	-	8.94 (d)
H_{12p}	-	-	8.94 (d)
H_{3b}	8.74 (m)	8.88 (s)	8.79 (s)
H_{5b}	7.29 (t)	7.46 (dd)	7.30 (t)
H_{6b}	7.83 (d)	8.01 (d)	7.91-7.86 (m)
CH_{methyl}	2.57 (s)	3.01 (s)	2.57 (s)

Table 4.2: Chemical shifts for the complexes $[Ru(phen)_2(dmbpy)](PF_6)_2$, $[Ru(phendione)_2(dmbpy)](PF_6)_2$ and $[Ru(pyrphen)_2(dmbpy)](PF_6)_2$

4.2.2.4 $[Ru(thimphen)_2(L)](PF_6)_2$

The only compound synthesised successfully which follows the $[Ru(thimphen)_2L](PF_6)_2$ model was $[Ru(thimphen)_2(bpy)](PF_6)_2$ (Complex 1). The numbering scheme for the assignment of the protons present in this molecule is shown below in Figure 4.41.

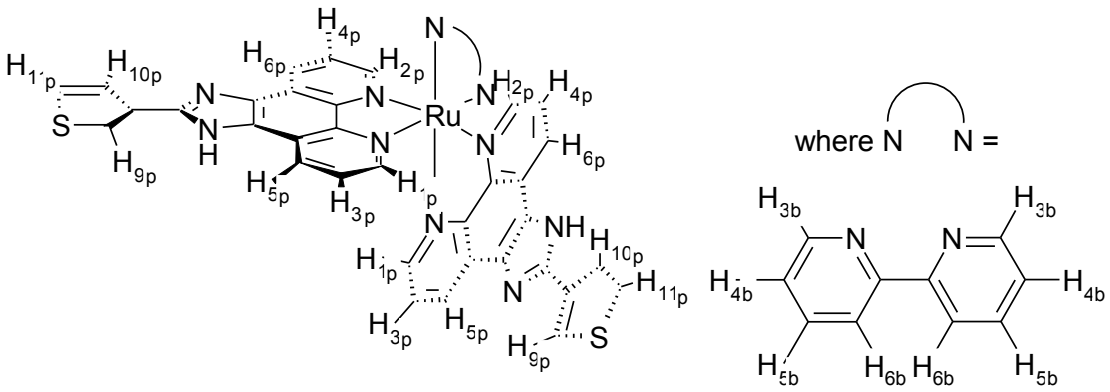

Figure 4.41: Numbering system for the assignment of protons in the ^1H NMR analysis of $[Ru(thimphen)_2(bpy)](PF_6)_2$

The ^1H NMR spectra for the metal complexes $[Ru(thimphen)_2(bpy)](PF_6)_2$ and $[Ru(thimphen)_2(d_8\text{-bpy})](PF_6)_2$ are shown below in Figure 4.42.

Examining the spectrum shown in Figure 4.42 (c) and comparing it with the other two spectra shown in this figure, it is evident that there is broadening of the signals present at approximately 9.0 ppm in each spectrum. As mentioned above this has been attributed to solvent-sample interactions arising from the use of d_6-acetone as solvent here as an identical sample when analysed using d_6-DMSO yielded the sharp spectrum shown in Figure 3.20 in Chapter 3. As in the case of $[Ru(pyrphen)_2(bpy)]^{2+}$ discussed previously, a number of related signals present in Figure 4.42 (b) and (c) occur at similar chemical shift including all three thiophene signals: H_{9p} appearing at 8.27 ppm in Figure 4.42 (c) and 8.20 ppm in Figure 4.42 (b); H_{10p} appearing at 7.84-7.78 ppm in Figure 4.42 (c) and 7.78 ppm in Figure 4.42 (b); and H_{11p} appearing at 7.65-7.54 ppm in Figure 4.42 (c) and 7.64 ppm-7.61 ppm in Figure 4.42 (b). However, as in the case of $[Ru(pyrphen)_2(bpy)]^{2+}$, due to the fact that a number of signals are shifted as well as the loss of equivalence for certain phenanthroline signals upon introduction of a second thimphen ligand, 2-D COSY techniques as well as comparison of the deuterated and non-deuterated spectra shown in Figure 4.42 (a) and (b) have been used to assign the ^1H NMR signals shown in Figure 4.42 (b) for $[Ru(thimphen)_2(bpy)]^{2+}$.

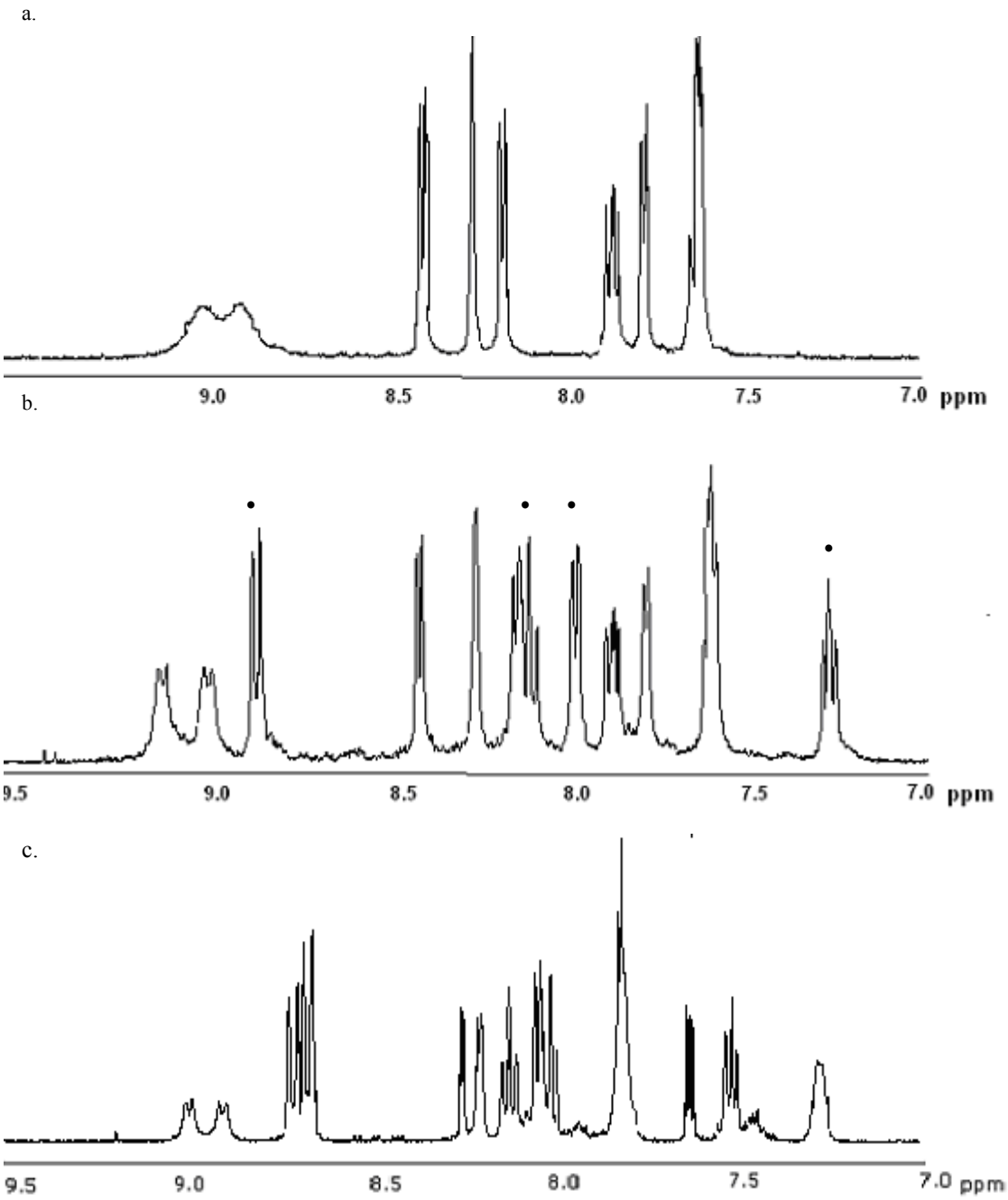

Figure 4.42: ^1H NMR spectra of (a) $[Ru(thimphen)_2(d_8\text{-}bpy)](PF_6)_2$ (b) $[Ru(thimphen)_2(bpy)](PF_6)_2$ and (c) $[Ru(bpy)_2(thimphen)](PF_6)_2$ as measured in d_6-acetone

Comparing the Figure 4.42 (a) and (b), the bipyridyl protons present in the molecule $[Ru(thimphen)_2(bpy)](PF_6)_2$ can be identified as the signals present at 7.96 ppm, 7.33

ppm, 8.74 ppm. There is also a reduction in integration of the multiplet at 8.11-8.05 ppm going from Figure 4.42 (b) to Figure 4.42 (a), indicating that this multiplet in the non-deuterated spectrum Figure 4.42 (b), contains both a bipyridyl and a thimphen signal. As before these signals have all been marks with •. The order in which these bipyridyl protons occur is identical to that in which they have appeared in both the parent complexes [Ru(phen)$_2$(bpy)](PF$_6$)$_2$ and [Ru(phendione)$_2$(bpy)](PF$_6$)$_2$ as well as the analogous [Ru(pyrphen)$_2$(bpy)](PF$_6$)$_2$. H$_{3b}$ appears furthest downfield as a doublet at 8.74 ppm. H$_{4b}$ occurs within the multiplet at 8.11-8.05 ppm. H$_{5b}$ occurs as a triplet at characteristically low chemical shift: 7.33 ppm, and H$_{6b}$ occurs as a doublet at 7.96 ppm. This assignment is compounded by the coupling pattern shown below in Figure 4.43.

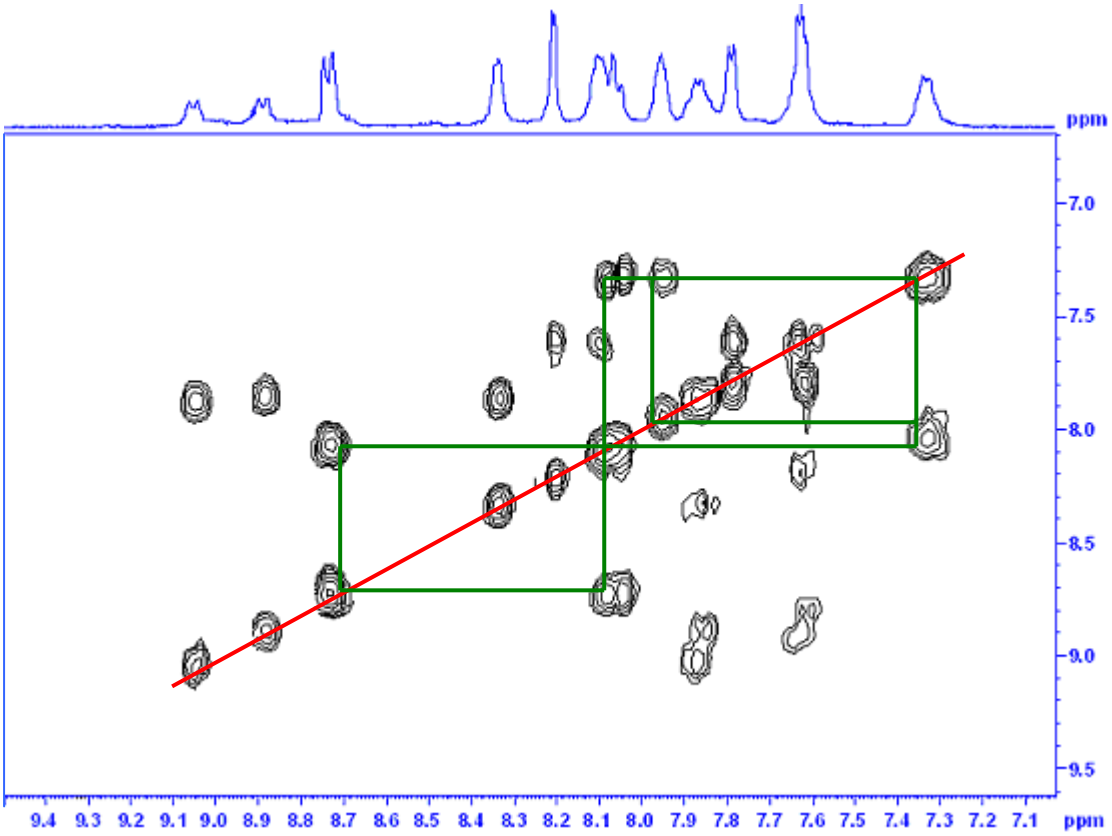

Figure 4.43: COSY spectrum for [Ru(thimphen)$_2$(bpy)](PF$_6$)$_2$ as measured in d_6-acetone with coupling bipyridyl protons highlighted

The downfield signal for H$_{3b}$ at 8.74 ppm couples to the multiplet at 8.11-8.05 ppm, confirming that this multiplet contains the signal for H$_{4b}$. This multiplet, in turn couples to the triplet appearing at 7.33 ppm confirming that this signal represents H$_{5b}$.

Finally, this triplet also couples with a doublet at 7.96 ppm, confirming that this is the signal corresponding to H_{6b}.

In order to assign the phenanthroline signals in the spectrum, the COSY spectrum for $[Ru(thimphen)_2(bpy)](PF_6)_2$ is shown again below, this time highlighting the coupling thimphen signals.

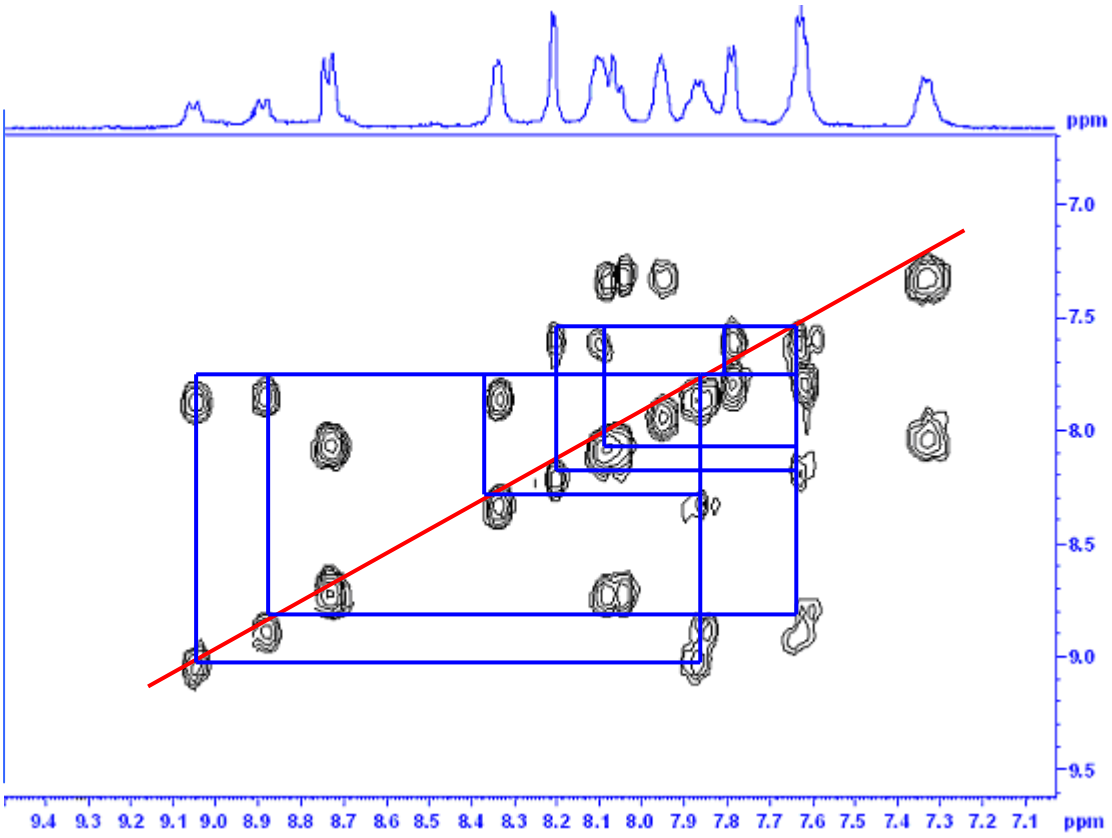

Figure 4.44: COSY spectrum for $[Ru(thimphen)_2(bpy)](PF_6)_2$ as measured in d_6-acetone with coupling thimphen protons highlighted

The spectrum for $[Ru(thimphen)_2(d_8\text{-bpy})](PF_6)_2$ shown in Figure 4.42 (a) shows that there are eight signals in total corresponding to the nine thimphen protons in the molecule. The thiophene protons are the simplest to identify as H_{9p} is the only proton to result in a singlet peak, appearing here at 8.20 ppm. Examining the COSY spectrum shown in Figure 4.44 it can be seen that this singlet couples slightly with the multiplet visible at 7.64-7.61 ppm. This multiplet in turn couples with a doublet at 7.78 ppm. The doublet in question at 7.78 ppm relates to H_{10p} while the thiophene signal contained in the multiplet at 7.64-7.61 ppm corresponds to H_{11p}. H_{10p} appears further downfield with respect to H_{11p} on account of its closer proximity to the electronegative imidazole ring. As for $[Ru(phen)_2(bpy)](PF_6)_2$ the signals relating to

H_{3p} and H_{4p} will be the only two of the remaining unassigned thimphen protons to couple to two other signals. As expected, two such signals are seen in the COSY spectrum shown in Figure 4.44, one occurring at 7.88-7.85 ppm as a broad triplet, the other contained in the multiplet at 7.64-7.61 ppm. The further upfield of these signals corresponds to H_{3p}, as it is affected by the ring shielding effect shown in Figure 4.26. This signal couples with two doublets, one at 8.85 ppm, the other contained in the multiplet occurring at 8.11-8.05 ppm. The further upfield of these signals corresponds to H_{1p} as it is affected by the same electronic shielding as H_{3p}. This assignment implies that the doublet present at 8.85 ppm relates to H_{5p}. The broad triplet (representing H_{4p}) present at 7.88-7.85 ppm couples to two doublets also, one occurring at 8.89 ppm, the other at 8.34 ppm. The doublet at 8.34 ppm corresponds to H_{2p}, its chemical shift further upfield than that of H_{6p} on account of the electronic shielding incurred by the adjacent bipyridyl ring. Therefore the final unassigned doublet at 8.89 ppm relates to H_{6p}. These values are tabulated below in Table 4.3.

Proton	**Chemical shift δ (ppm) $[Ru(phen)_2(bpy)]^{2+}$**	**Chemical shift δ (ppm) $[Ru(phendione)_2(bpy)]^{2+}$**	**Chemical shift δ (ppm) $[Ru(thimphen)_2(bpy)]^{2+}$**	**Chemical shift δ (ppm) $[Ru(bpy)_2(thimphen)]^{2+}$**
H_{1p}	8.15 (d)	7.98 (d)	8.11-8.05 (m)	8.23 (d)
H_{2p}	8.44 (d)	7.67-7.60 (t)	8.34 (d)	8.23 (d)
H_{3p}	7.62 (dd)	7.67-7.60 (t)	7.64-7.61 (m)	7.84-7.78 (m)
H_{4p}	7.88-7.85 (t)	8.07 (d)	7.88-7.85 (t br)	7.84-7.78 (m)
H_{5p}	8.62 (d)	8.55-8.52 (m)	8.85 (dd)	9.05-8.94 (br d)
H_{6p}	8.75-8.72 (dd)	8.55-8.52 (m)	8.96 (d)	9.05-8.94 (br d)
H_{7p}	8.32-8.26 (m)	-	-	-
H_{8p}	8.32-8.26 (m)	-	-	-
H_{9p}	-	-	8.20 (s)	8.27 (s)
H_{10p}	-	-	7.78 (d)	7.84-7.78 (m)
H_{11p}	-	-	7.64-7.61 (m)	7.65-7.54 (m)
H_{3b}	8.75-8.72 (dd)	8.55-8.52 (m)	8.74 (d)	8.76-8.70 (m)
H_{4b}	8.06 (t)	8.12 (t)	8.11-8.05 (m)	H_{4b} 8.14 (t) $H_{4b'}$ 8.10-8.01 (m)
H_{5b}	7.33 (t)	7.45 (t)	7.33 (t)	H_{5b} 7.51 (t) $H_{5b'}$ 7.28 (br s)
H_{6b}	7.91 (d)	7.86 (d)	7.96 (d)	H_{6b} 8.10-8.01 (m) $H_{6b'}$ 7.84-7.78 (m)

Table 4.3: Chemical shifts for the proton signals present in ^1H NMR spectrum for the molecules $[Ru(phen)_2(bpy)](PF_6)_2$, $[Ru(phendione)_2(bpy)](PF_6)_2$ and $[Ru(thimphen)_2(bpy)](PF_6)_2$ as measured in d_6-acetone.

4.2.3 Elemental Analysis

The predicted and actual elemental analyses of the metal complexes $[Ru(pyrphen)_2(bpy)](PF_6)_2$, $[Ru(thimphen)_2(bpy)](PF_6)_2$ and $[Ru(pyrphen)_2(dmbpy)](PF_6)_2$ are tabulated in Table 4.4 below.

Compound Name	**Chemical Formula**	**Predicted values**	**Observed values**
$[Ru(pyrphen)_2(bpy)](PF_6)_2$	$[C_{44}H_{30}N_{12}Ru](PF_6)_2$	%C: 47.3 %H: 2.7 %N: 15.0	%C: 2.5 %H: 4.0 %N: 1.1
$[Ru(thimphen)_2(bpy)](PF_6)_2$	$[C_{42}H_{28}N_{10}SRu](PF_6)_2$	%C: 44.7 %H: 2.5 %N: 12.4	%C: 39.0 %H: 2.2 %N: 8.3
$[Ru(pyrphen)_2(dmbpy)](PF_6)_2$	$[C_{48}H_{34}N_{12}Ru](PF_6)_2$	%C: 49.3 %H: 2.9 %N: 14.4	%C: 42.3 %H: 2.4 %N: 9.7

Table 4.4: Predicted and actual elemental analyses of the metal complexes $[Ru(pyrphen)_2(bpy)](PF_6)_2$, $[Ru(thimphen)_2(bpy)](PF_6)_2$ and $[Ru(pyrphen)_2(dmbpy)](PF_6)_2$

Examining Table 4.4 it can be seen that while the observed values for $[Ru(thimphen)_2(bpy)](PF_6)_2$ and $[Ru(pyrphen)_2(dmbpy)](PF_6)_2$ are encouragingly close to their respective predicted values, there is a large difference visible between the predicted and observed values for $[Ru(pyrphen)_2(bpy)](PF_6)_2$. Looking more closely at these values, a ratio of 17.5: 1: 5.6 C:H:N is observed for the predicted values while a ratio of 0.23: 1: 0.27 C:H:N is observed for the observed values. The fact that the observed values shown appear lower than the corresponding calculated values implies that there is a non-CHN type substance present, decreasing the overall percentages of carbon, hydrogen and nitrogen to below 5%. This substance is most likely residual KPF_6 present in the sample which has not been removed by the washing and recrystallisation steps outlined in Section 5.4 below. The observed percentage hydrogen and nitrogen values for $[Ru(pyrphen)_2(bpy)](PF_6)_2$ are also higher in ratio than the observed percentage carbon value for the complex. This may

be due to residual acetonitrile present in the sample following column chromatography using this solvent as eluent (see Section 5.4). Again, if this is the case, this residual solvent has survived recrystallisation from acetone: water and drying prior to submission for elemental analysis. Due to time constraints synthesis of a second sample for a duplicate analysis has not been conducted.

The elemental analysis results obtained for the metal complexes [Ru(thimphen)$_2$(bpy)](PF$_6$)$_2$ and [Ru(pyrphen)$_2$(dmbpy)](PF$_6$)$_2$ are discussed below.

[Ru(thimphen)$_2$(bpy)](PF$_6$)$_2$: [$C_{42}H_{28}N_{10}SRu$](PF$_6$)$_2$

Calculated :%C: 44.7, %H: 2.5, %N: 12.4

Observed: %C: 39.0, %H: 2.2, %N: 8.3

Proposed compound	**Calculated values**
[$C_{42}H_{28}N_{10}SRu$](PF$_6$)$_2$.KPF$_6$	%C: 38.4, %H:2.2 , %N: 10.7

Table 4.5: Elemental analysis data for the complex [Ru(thimphen)$_2$(bpy)](PF$_6$)$_2$

Table 5.5 above attempts to rationalise the discrepancy between the predicted and observed CHN values for [Ru(thimphen)$_2$(bpy)](PF$_6$)$_2$ identified in Table 4.4. It has been proposed that excess KPF$_6$ present in the [Ru(pyrphen)$_2$(bpy)](PF$_6$)$_2$ sample submitted is partially responsible for the undesirable results obtained. In the case of [Ru(thimphen)$_2$(bpy)](PF$_6$)$_2$, excess KPF$_6$ is also responsible for the disagreement between the predicted and observed values. Inclusion of one KPF$_6$ molecule into the molecular formula of the complex brings the observed and calculated values within ±0.6 agreement. The nitrogen value observed however remains low when compared to the calculated values shown. This discrepancy has also been encountered in chapter 3 and has been assumed to be a result of the method of measurement employed.

[Ru(pyrphen)$_2$(dmbpy)](PF$_6$)$_2$: [$C_{48}H_{34}N_{12}Ru$](PF$_6$)$_2$

Calculated :%C: 49.3, %H: 2.9, %N: 14.4

Observed: %C: 42.4, %H: 2.4, %N: 9.4

Proposed compound	**Calculated values**
[$C_{48}H_{34}N_{12}Ru$](PF$_6$)$_2$.KPF$_6$	%C: 42.6, %H: 2.5 , %N: 12.4

Table 4.6: Elemental analysis data for the complex [Ru(pyrphen)$_2$(dmbpy)](PF$_6$)$_2$

As for $[Ru(thimphen)_2(bpy)](PF_6)_2$ there is a discrepancy visible between the calculated and observed CHN values for the metal complex $[Ru(pyrphen)_2(dmbpy)](PF_6)_2$. Again, as for $[Ru(thimphen)_2(bpy)](PF_6)_2$ this discrepancy may be explained by incorporation of one KPF_6 molecule into the molecular formula for the complex. Inclusion of this fragment brings the %C and %H calculated and observed values to within ±0.6 agreement. As before, the observed %N value for the complex is still low as compared to the calculated value but again, as this has been a common feature to all of the compounds analysed by this method in this thesis, the appearance of this discrepancy has been termed an analytical anomaly.

4.2.4 UV/vis Analysis

The UV/vis absorbance spectra of $[Ru(pyrphen)_2(bpy)](PF_6)_2$ (2) and $[Ru(thimphen)_2(bpy)](PF_6)_2$ (1) are shown below in Figure 4.45.

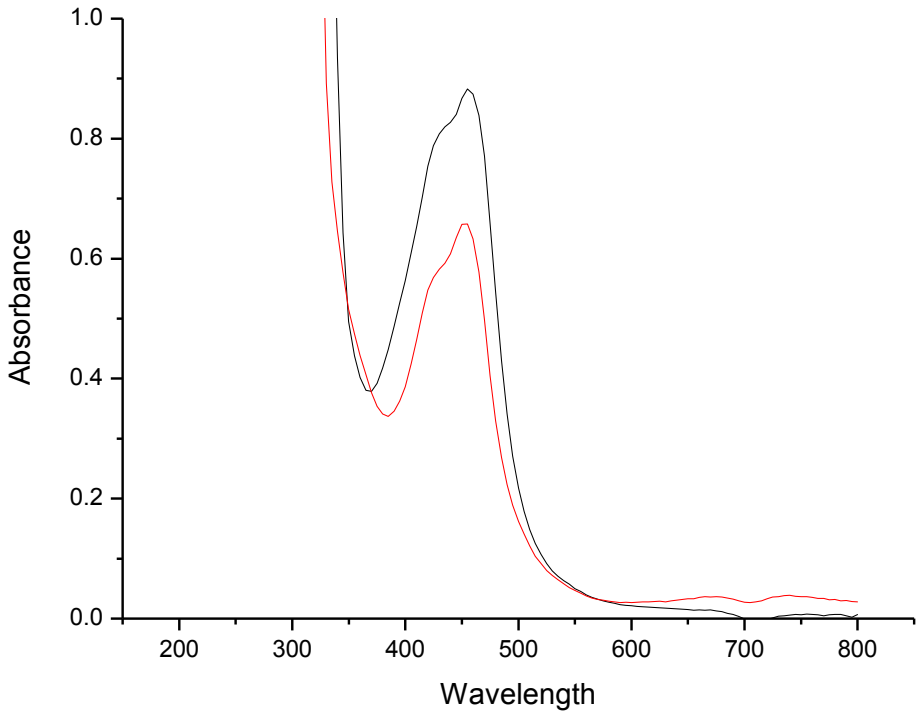

Figure 4.45: UV/vis absorbance spectra of $[Ru(pyrphen)_2(bpy)](PF_6)_2$ 0.03 mM (black) and $[Ru(thimphen)_2(bpy)](PF_6)_2$ 0.03 mM (red) as measured in acetonitrile at 293K

Complex	Absorption λ_{max} (nm)	Extinction Coefficient (ε) ($M^{-1}cm^{-1}$)
$[Ru(pyrphen)_2(bpy)](PF_6)_2$	455	4800
$[Ru(thimphen)_2(bpy)](PF_6)_2$	450	21487
$[Ru(bpy)_2(pyrphen)]^{2+}$	435	19221
$[Ru(bpy)_2(thimphen)]^{2+}$	424	18677
$[Ru(bpy)_3]^{2+}$	450	11500[19]

Table 4.7: Absorbance data for the metal complexes $[Ru(pyrphen)_2(bpy)](PF_6)_2$ and $[Ru(thimphen)_2(bpy)](PF_6)_2$ and related complexes as measured in acetonitrile at 293K

The UV/vis spectra of the metal complexes $[Ru(pyrphen)_2(bpy)](PF_6)_2$ and $[Ru(thimphen)_2(bpy)](PF_6)_2$ are dominated by intense bands at 455 nm and 450 nm respectively. These bands may be attributed to dπ-π* metal to ligand charge transfer (^{1}MLCT) transitions as discussed for the related complexes in Chapter 3. These values exhibit a shift of approximately 20 nm when compared to the λ_{max} values for the corresponding mononuclear complexes $[Ru(bpy)_2(thimphen)]^{2+}$ and $[Ru(bpy)_2(pyrphen)]^{2+}$. This cements the fact that the shift observed when comparing the λ_{max} of $[Ru(bpy)_2(thimphen)]^{2+}$ and $[Ru(bpy)_2(pyrphen)]^{2+}$ to that of the parent complex $[Ru(bpy)_3]^{2+}$ is within experimental error. Incorporation of two –imphen type ligands has spectra almost identical to that of $[Ru(bpy)_3]^{2+}$ so it may be assumed that complexes incorporating any feasible number of ligands of this type will lead to similar photochemical behaviour. As a result, it may be assumed that when incorporated into the proposed molecular diode structures postulated in Section 5.1 the portion of the molecule examined here (i.e. containing the ligands thimphen or pyrphen) will exhibit similar electronic behaviour to that of the parent complex $[Ru(bpy)_3]^{2+}$. However, these properties may be 'tuned' through incorporation of a ligand with σ-donor properties as opposed to the π-donating 2,2'-bipyridine used currently as discussed in Chapter 1.

Finally, the low extinction coefficient value of 4800 $M^{-1}cm^{-1}$ displayed in Table 4.7 for the complex $[Ru(pyrphen)_2(bpy)]^{2+}$ is a result of the excess of co-crystallised KPF_6 and solvent present in this sample as identified in section 5.2.3. Again, due to time constraints synthesis of a duplicate sample of $[Ru(pyrphen)_2(bpy)]^{2+}$ was not prepared.

Similar UV/vis spectra are visible below for [Ru(pyrphen)$_2$(dmbpy)](PF$_6$) (6) and [Ru(thimphen)$_2$(dmbpy)](PF$_6$)$_2$ (5) in Figure 4.46. Even though conclusive ^{1}H NMR spectra could not be obtained for the complex [Ru(thimphen)$_2$(dmbpy)](PF$_6$)$_2$, clean UV/vis spectra were obtained and so these results are reported below.

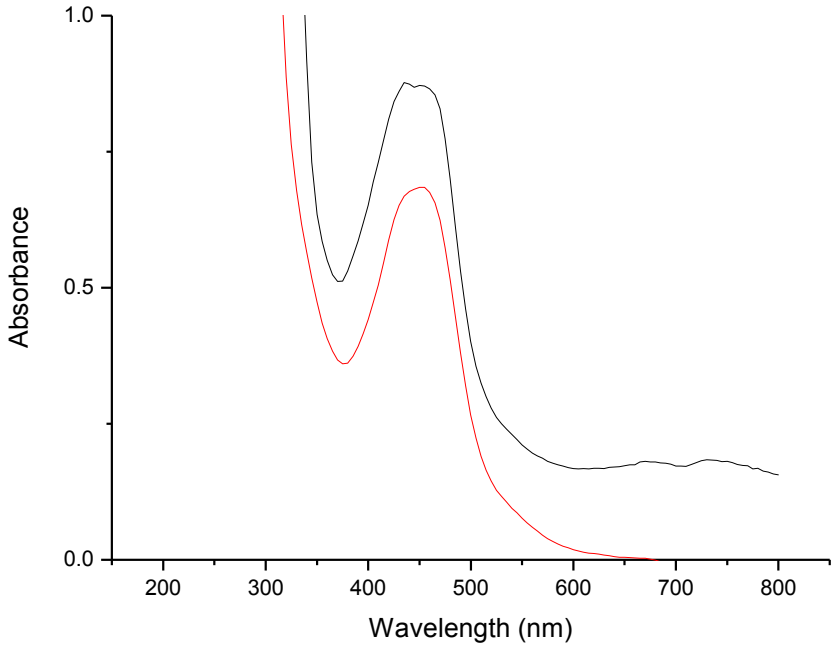

Figure 4.46: UV/vis absorbance spectra of [Ru(pyrphen)$_2$(dmbpy)](PF$_6$)$_2$ 0.03 mM (black) and [Ru(thimphen)$_2$(dmbpy)](PF$_6$)$_2$ 0.03 mM (red) as measured in acetonitrile at 293K

The spectra for [Ru(pyrphen)$_2$(dmbpy)](PF$_6$)$_2$ and [Ru(thimphen)$_2$(dmbpy)](PF$_6$)$_2$ display similar ^{1}MLCT transitions to those seen for [Ru(pyrphen)$_2$(bpy)](PF$_6$)$_2$ and [Ru(thimphen)$_2$(bpy)](PF$_6$)$_2$ leading to identical conclusions drawn on their photochemical behaviour.

Complex	**Absorption λ_{max} (nm)**	**Extinction Coefficient (ε) ($M^{-1}cm^{-1}$)**
$[Ru(pyrphen)_2(dmbpy)](PF_6)_2$	455	8500
$[Ru(thimphen)_2(dmbpy)](PF_6)_2$	450	2400
$[Ru(bpy)_2(pyrphen)]^{2+}$	435	19221
$[Ru(bpy)_2(thimphen)]^{2+}$	424	18677
$[Ru(bpy)_3]^{2+}$	450	11500

Table 4.8: Absorbance data for the metal complexes $[Ru(pyrphen)_2(dmbpy)](PF_6)_2$ and $[Ru(thimphen)_2(dmbpy)](PF_6)_2$ as measured in acetonitrile at 293K

According to the information shown in Table 4.8 the extinction coefficient of $[Ru(thimphen)_2(dmbpy)](PF_6)_2$ is much lower than that of $[Ru(pyrphen)_2(dmbpy)](PF_6)_2$. However, experimentally, much less material available for use to measure the extinction coefficient value of $[Ru(thimphen)_2(dmbpy)](PF_6)_2$ when compared to the amount of material used to measure the extinction coefficient of $[Ru(pyrphen)_2(dmbpy)](PF_6)_2$. This practical difference between the two measurements is most likely the reason for the difference visible between the two values.

The UV/vis spectra for $[Ru(pyrphen)_2(bpt)]PF_6$ (12) and $[Ru(thimphen)_2(bpt)]PF_6$ (11) are also reported even though conclusive ^1H NMR data could not be obtained. The spectra shown in Figure 4.47 exhibit some subtle differences to the spectra discussed previously.

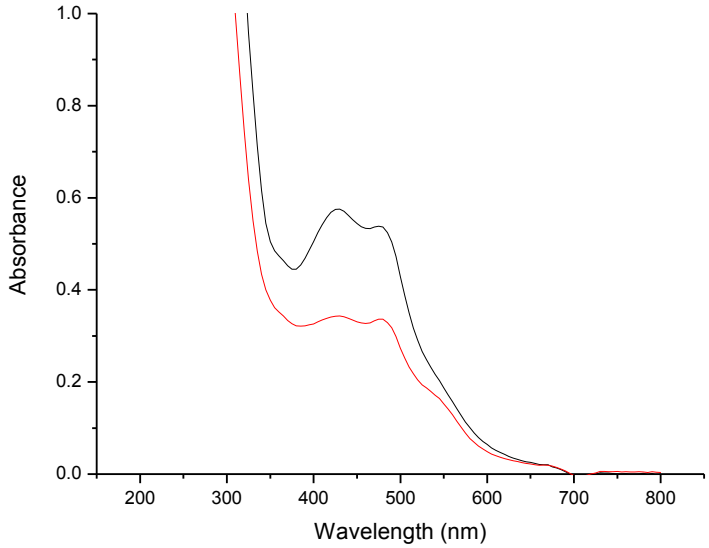

Figure 4.47: UV/vis absorbance spectra of $[Ru(pyrphen)_2(bpt)]PF_6$ 0.025 mM (black) and $[Ru(thimphen)_2(bpt)]PF_6$ 0.025 mM (red) as measured in acetonitrile at 293K

Both spectra in Figure 4.47 display two separate absorbencies, one at 430 nm, the other at 480 nm. The maximum absorbances and extinction cooeffiecients for both complexes are tabulated below in Table 4.9. Due to its marginally higher absorbance, extinction coefficients have been measured using 430 nm as the point of absorbance.

Complex	**Absorption λ_{max} (nm)**	**Extinction Coefficient (ε) ($M^{-1}cm^{-1}$)**
$[Ru(pyrphen)_2(bpt)]^+$	430, 480	2100
$[Ru(thimphen)_2(bpt)]^+$	430, 480	3800
$[Ru(bpy)_2(bpt)]^+$	420, 460	11300[19]
$[Ru(bpy)_2(pyrphen)]^{2+}$	435	19221
$[Ru(bpy)_2(thimphen)]^{2+}$	424	18677
$[Ru(bpy)_3]^{2+}$	450	11500[19]

Table 4.9: Absorbance data for the metal complexes $[Ru(pyrphen)_2(bpt)]PF_6$ and $[Ru(thimphen)_2(bpt)]PF_6$ as measured in acetonitrile at 293K

Again, the calculated extinction coefficient values calculated are low when compared to those of the related complexes listed in Table 4.9. This has been attributed to the level of probable impurity present in the sample as confirmed by ^1H NMR analysis. However, as these impurities do not appear to affect the absorbance properties of the complexes their photochemical behaviour may be discussed. For comparison, the absorbance spectrum for $[Ru(bpy)_2(bpt)]^{2+}$ is shown below in Figure 4.48.

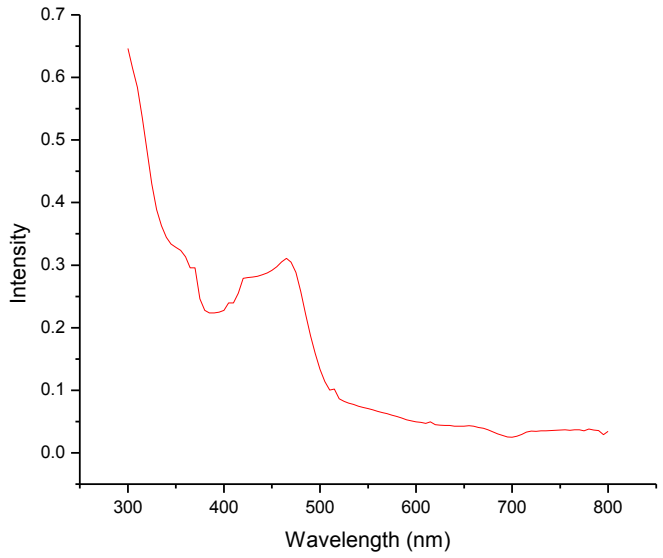

Figure 4.48: UV/vis absorbance spectra of $[Ru(bpy)_2(bpt)]^+$ as measured in acetonitrile at 293K[19]

Comparing the λ_{max} values for $[Ru(pyrphen)(bpt)]^+$ and $[Ru(thimphen)(bpt)]^+$ with that of $[Ru(bpy)_2(bpt)]^+$ it can be seen that the maximum of the two dominant absorbencies seen for $[Ru(pyrphen)(bpt)]^+$ and $[Ru(thimphen)(bpt)]^+$ occurs at 430 nm while for $[Ru(bpy)_2(bpt)]^+$ the maximum absorbance occurs at 460 nm. The fact that a blue shift of 30 nm is visible for the complexes $[Ru(pyrphen)(bpt)]^+$ and $[Ru(thimphen)(bpt)]^+$ with respect to $[Ru(bpy)_2(bpt)]^+$ suggests that thimphen and pyrphen are stronger σ-donors than bpy (*c.f.* Chapter 1), enhancing the σ-donor effect of bpt. This effect may be augmented by substituting the ruthenium ion present in the molecule with osmium, which should allow for ^{3}MLCT transitions as well as ^{1}MLCT transitions by further stabilising the excited state as previously outlined in Chapter 1 This effect may be overturned by substituting the ruthenium ion present in the molecule with osmium, which should allow for ^{3}MLCT transitions as well as ^{1}MLCT transitions by further stabilising the excited state as previously outlined in Chapter 1.

4.2.5 Emission Analysis

The emission spectra of [Ru(pyrphen)$_2$(bpy)]$^{2+}$, [Ru(thimphen)$_2$(bpy)]$^{2+}$, [Ru(pyrphen)$_2$(bpy)]$^{2+}$ and [Ru(thimphen)$_2$(bpy)]$^{2+}$ are shown below in Figure 4.49.

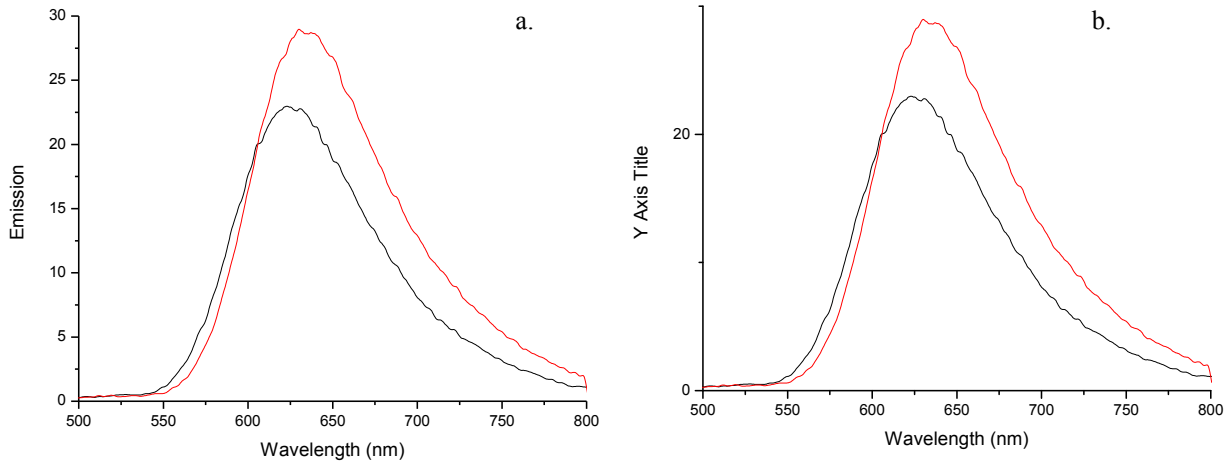

Figure 4.49: UV/vis absorbance spectra of (a) [Ru(pyrphen)$_2$(bpy)]$^{2+}$ 0.03 mM (black) and [Ru(thimphen)$_2$(bpy)]$^{2+}$ 0.03 mM (red) and (b) [Ru(pyrphen)$_2$(dmbpy)]$^{2+}$ 0.03 mM (black) and [Ru(thimphen)$_2$(dmbpy)]$^{2+}$ 0.03 mM as measured in acetonitrile at 293K

Complex	**Emission λ_{max} (nm)**
[Ru(pyrphen)$_2$(bpy)]$^{2+}$	625
[Ru(thimphen)$_2$(bpy)]$^{2+}$	630
[Ru(pyrphen)$_2$(dmbpy)]$^{2+}$	620
[Ru(thimphen)$_2$(dmbpy)]$^{2+}$	635
[Ru(bpy)$_2$(thimphen)]$^{2+}$	607
[Ru(bpy)$_2$(pyrphen)]$^{2+}$	618
[Ru(bpy)$_3$]$^{2+}$	615[19]

Table 4.10: Absorbance data for the metal complexes [Ru(pyrphen)$_2$(bpy)]$^{2+}$, [Ru(thimphen)$_2$(bpy)]$^{2+}$, [Ru(pyrphen)$_2$(dmbpy)]$^{2+}$ and [Ru(thimphen)$_2$(dmbpy)]$^{2+}$ as measured in acetone at 293K

Due to the noticeable similarity between the absorbance spectra of [Ru(pyrphen)$_2$(bpy)]$^{2+}$, [Ru(thimphen)$_2$(bpy)]$^{2+}$, [Ru(pyrphen)$_2$(bpy)]$^{2+}$ and [Ru(thimphen)$_2$(bpy)]$^{2+}$ they have been shown together in Figure 4.49. These complexes all show a small red shift in maximum emission wavelength when compared to their analogous complexes [Ru(bpy)$_2$(pyrphen)]$^{2+}$ and

$[Ru(bpy)_2(thimphen)]^{2+}$ as well as the model complex $[Ru(bpy)_3]^{2+}$. A blue shift compared to $[Ru(bpy)_3]^{2+}$ is desired for novel ruthenium complexes as it implies that the complexes synthesized possess electronic properties closer to that of the photostable model complex $[Os(bpy)_3]^{2+}$ (λ_{max} 732 nm *c.f.* Chapter 1). However, the red shift of approximately 20 nm observed here for $[Ru(pyrphen)_2(bpy)]^{2+}$, $[Ru(thimphen)_2(bpy)]^{2+}$, $[Ru(pyrphen)_2(dmbpy)]^{2+}$ and $[Ru(thimphen)_2(dmbpy)]^{2+}$ is not sufficient to bring their emission maxima within tolerable range of the emission maximum of 732 nm observed for $[Os(bpy)_3]^{2+}$. As a result it has been surmised that these complexes may be deemed as displaying similar emissive behaviour to that of the parent complex $[Ru(bpy)_3]^{2+}$. This is also in agreement with the conclusions drawn above for these complexes' absorbance behaviour. The complexes $[Ru(thimphen)_2(bpt)]^{+}$ and $[Ru(pyrphen)_2(bpt)]^{+}$ however, exhibit slightly different emission behaviour as shown below in Figure 4.50.

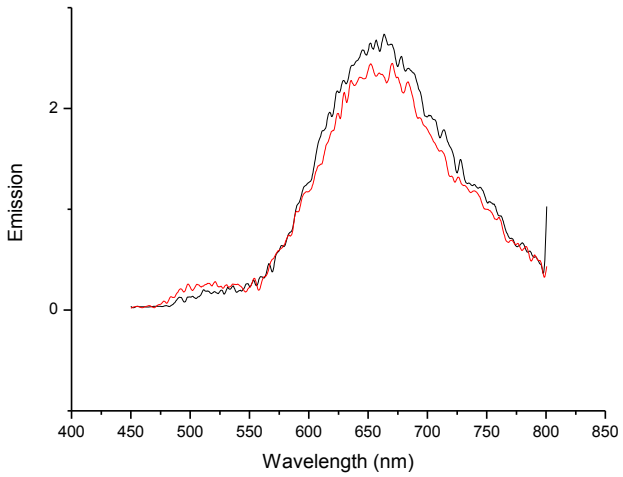

Figure 4.50: UV/vis absorbance spectra of $[Ru(pyrphen)_2(bpt)]^{+}$ 0.025 mM (black) and $[Ru(thimphen)_2(bpy)]^{+}$ 0.025 mM (red) measured in acetonitrile at 293 K

Complex	**Emission λ_{max} (nm)**
$[Ru(pyrphen)_2(bpt)](PF_6)$	665
$[Ru(thimphen)_2(bpt)](PF_6)$	650
$[Ru(phen)_2(bpy)](PF_6)_2$	600
$[Ru(bpy)_3]^{2+}$	615
$[Os(bpy)_3]^{2+}$.	725

Table 4.11: Absorbance data for the metal complexes $[Ru(pyrphen)_2(bpt)]^{+}$, $[Ru(thimphen)_2(bpt)]^{+}$ as measured in acetone at 293K

Examining the spectra shown in Figure 4.50 as well as the data shown in Table 4.11 there is a more sizeable red shift visible in the emission maxima for the complexes $[Ru(pyrphen)_2(bpt)]^+$ and $[Ru(thimphen)_2(bpt)]^+$ as compared to $[Ru(bpy)_3]^{2+}$ than for the complexes corresponding to the spectra shown in Figure 4.50. This renders these complexes theoretically more suitable for molecular electronics applications as it appears that as the complexes' photochemical properties are beginning to approach those of the complex $[Os(bpy)_3]^{2+}$. For reasons outlined in Chapter 1, this is most desirable in the formulation of a molecular electronics prototype. There is a distinct difference in the intensity of the spectra shown in Figure 4.50 when compared to those shown in Figure 4.49. This has been termed a result of the level of impurity present in the sample (mentioned in the HPLC analysis of both samples outlined in section 5.2.1) the concentration of metal complex present in the sample analysed is markedly less than the concentration of the overall sample.

4.3 Conclusion

Chapter 4 has detailed the successful synthesis of six mononuclear metal complexes including two deuterated bipyridyl type analogues as prototypes for molecular transistors. The method used for the synthesis of these complexes is identical to that used for construction of the metal complexes $[Ru(bpy)_2(pyrphen)]^{2+}$ and $[Os(bpy)_2(pyrphen)]^{2+}$ as outlined in Chapter 3. This method of synthesis, involving the modification of a bis-phenanthroline precursor to append surface active groups, was found to be effective for the appending of both a pyridine and thiophene group in the case of the novel metal complexes $[Ru(pyrphen)_2(bpy)]^{2+}$ and $[Ru(thimphen)_2(bpy)]^{2+}$ as well as their deuterated bipyridyl analogues. However in the case of the precursor complex $[Ru(phen)_2(dmbpy)]^{2+}$ only a pyridine group could be successfully appended and for the precursor complex $[Ru(phen)_2)(bpt)]^+$ though encouraging results were obtained indicating the attachment of a pyridine group, conclusive characterisation of the complex was not achieved, most likely due to a level of impurity still present in the sample. These reactions, though successful in producing the desired compounds were not high yielding and in the case of $[Ru(pyrphen)_2(bpy)]^{2+}$ a large amount of KPF_6 and solvent used in purification methods were found to co-crystallise with the metal complex. Therefore further synthetic work is needed in this area to investigate maximisation of yields as well as

identifying more effective methods of purification. Also, as encouraging HPLC, UV/vis and emission spectroscopic data was obtained for the crude samples of [Ru(thimphen)$_2$(dmbpy)]$^{2+}$, [Ru(thimphen)$_2$(bpt)]$^{2+}$ and [Ru(pyrphen)$_2$(bpt)]$^{2+}$ further synthetic research to modify the methods of synthesis used is also needed in order to prepare pure samples of the aforementioned complexes.

The complexes successfully synthesised here (i.e. [Ru(bpy)$_2$(pyrphen)]$^{2+}$, [Ru(thimphen)$_2$(bpy)]$^{2+}$ and [Ru(pyrphen)$_2$(dmbpy)]$^{2+}$) were characterised by ^{1}H NMR and CHN analysis, with their absorption and emission properties being recorded also. Being ruthenium complexes displaying electronic data very similar to that of [Ru(bpy)$_3$]$^{2+}$ these compounds are not suitable candidates for molecular electronics prototypes (*c.f.* Chapter 1). However, replacing the ruthenium ion with osmium may render complexes synthesised in the manner outlined in this chapter suitable for molecular electronics prototypes[20].

The synthesis of the novel metal complexes [Ru(pyrphen)$_2$(mepytr)]$^{2+}$, [Ru(thimphen)$_2$(mepytr)]$^{2+}$, [Ru(pyrphen)$_2$(ppytr)]$^{2+}$ and [Ru(pyrphen)$_2$(ppytr)]$^{2+}$ were also attempted, but all reactions were unsuccessful.

It was found throughout the synthetic portion of this chapter that attaching a thiophene group to the phenanthroline moiety of any of the precursor complexes was much more difficult than attaching a pyridine group, with only two thiophene type complexes being synthesised successfully as opposed to twice as many successfully synthesised pyridine type complexes. As a result, a second ***direct*** method of synthesis for [Ru(thimphen)$_2$(L)]$^{2+}$ type complexes was attempted. This approach is outlined in Chapter 5.

4.4 Experimental

Materials

$[Ru(phen)_2Cl_2].2H_2O$[21] and d_8-2,2'-bipyridyl[22] were synthesised according to established literature procedures. All other chemicals were purchased from Sigma-Aldrich and used without further purification. All synthetic solvents used were of reagent grade. All solvents used for spectroscopic measurements were of HPLC grade.

4.4.1 Synthesis of Metal Complexes (Successful)

Complex 1: $[Ru(thimphen)_2(bpy)](PF_6)_2.KPF_6$

Step 1: Synthesis of $[Ru(phendione)_2(bpy)](PF_6)_2$

This synthesis was based on a literature procedure.[23] 300 mg (0.30 mmol) $Ru(phen)_2(bpy)](PF_6)_2$ was stirred in 7.5 cm^3 H_2SO_4 until dissolved. 307 mg (3.01 mmol) was added to the reaction mixture followed by 5.5 cm^3 70% HNO_3. This mixture was then heated to 110 ^{0}C for 40 min. The reaction mixture was then cooled to room temperature and poured onto 50 cm^3 cold $KPF_{6\ (aq)}$ saturated solution. The resulting brown/orange suspension was kept at 5 ^{0}C for 2 hr. The brown solid was collected by vacuum filtration, washed with 25 cm^3 cold water and dried at the pump overnight.

Yield: 75.8%

^{1}H NMR: d_6-acetone ^{1}H δ: 8.84 (2H, d, H_{3b}, J=7.6 Hz), 8.66-8.62 (4H, m, H_{5p}+H_{6p}), 8.44 (2H, d, H_{2p} J=7.2 Hz), 8.36 (2H, d, H_{1p} J=6.8 Hz), 8.26 (2H, t, H_{4b}, J=8 Hz), 8.19 (2H, t, H_{6b}, J=6.8 Hz),7.86-7.78 (4H, m, H_{3p}+H_{4p}), 7.64-7.56 (2H, m, H_{5b})

Step 3: Synthesis of $[Ru(thimphen)_2(bpy)_2](PF_6)_2.KPF_6$

150 mg (0.14 mmol) $[Ru(phendione)_2(bpy)](PF_6)_2$ was placed in 8 cm^3 dry glacial acetic acid with 218 mg (2.84 mmol) ammonium acetate and heated to 100 ^{0}C. 12 µl (0.28 mmol) 3-thiophene carboxaldehyde was added to the reaction mixture, which was then heated at 100 ^{0}C for 3 hr. The resulting dark orange solution was cooled to

room temperature, and 10 cm^3 acetone was added. This mixture was then added dropwise to 400 cm^3 diethyl ether with vigorous stirring. The resulting suspension was filtered and the collected orange solid was purified by column chromatography on neutral alumina using acetonitrile as eluent. The main orange band was collected, and the solvent removed. The orange solid obtained was dissolved in 5 cm^3 H_2O and precipitated by addition of a saturated solution $KPF_{6\ (aq)}$. The orange precipitate was collected by vacuum filtration and recrystallised from acetone: water.

Yield: 14.6 % (10 mg)

^1H NMR: d_6-acetone ^1H δ: 8.96 (2H, d, H_{6p}, J=8 Hz), 8.85 (2H, dd, H_{5p}, J=6.8 Hz), 8.74 (2H, d, H_{3b}, J=8.4 Hz), 8.34 (2H, d, H_{2p}, J=5.2 Hz), 8.20 (2H, s, H_{9p}), 8.11-8.05 (4H, m, H_{1p}+H_{4b}), 7.96 (2H, d, H_{6b}, J=5.2 Hz), 7.88-7.85 (2H, t br, H_{4p}), 7.78 (2H, d, H_{10p}, J=4.4 Hz), 7.64-7.61 (4H, m, H_{11p}+H_{3b}), 7.33 (2H, t, H_{5b}, J=6.4 Hz)

Elem. Anal$[C_{42}H_{28}N_{10}Ru](PF_6)_2.KPF_6$

Observed: %C: 39.0, %H: 2.2, %N: 8.3

Calculated:%C: 38.4, %H: 2.2, %N: 10.7

Complex 2: $[Ru(pyrphen)_2(bpy)](PF_6)_2$

Step 1: Synthesis of $[Ru(phendione)_2(bpy)](PF_6)_2$

This procedure was carried out in an identical manner to that described for *Step 2* in the synthesis of $[Ru(thimphen)_2(bpy)](PF_6)_2$.

Step 2: Synthesis of $[Ru(pyrphen)_2(bpy)_2](PF_6)_2$

100 mg (0.09 mmol) $[Ru(phendione)_2(bpy)](PF_6)_2$ was placed in 8 cm^3 dry glacial acetic acid with 144 mg (1.89 mmol) ammonium acetate and heated to 100 ^0C. 18 µl (0.19 mmol) 4-pyridine carboxaldehyde was added to the reaction mixture, which was then heated at 100 ^0C for 2 hr. The resulting dark orange solution was cooled to room temperature, and 10 cm^3 acetone was added. This mixture was then added dropwise to 400 cm^3 diethyl ether with vigorous stirring. The resulting suspension was filtered and the collected orange solid was purified by column chromatography on neutral alumina using acetonitrile as eluent. The main orange band was collected, and the solvent removed. The orange solid obtained was dissolved in 5 cm^3 H_2O and precipitated by addition of a saturated solution $KPF_{6\ (aq)}$. The orange precipitate was collected by vacuum filtration and recrystallised from acetone: water.

Yield: 12.9% (13 mg)*

^{1}H NMR: d_6-acetone ^{1}H δ: 9.12 (2H, d, H_{6p}, J=8.4 Hz), 9.00 (2H, d, H_{5p}, J=8 Hz), 8.81 (4H, d, H_{12p}+H_{11p}, J=4.8 Hz), 8.75 (2H, d, H_{3b}, J=8 Hz), 8.54 (2H, d, H_{2p}, J=4.8 Hz), 8.33-8.30 (2H, m, H_{1p}), 8.20 (4H, d, H_{9p}+H_{10p}, J=4.8 Hz), 8.10 (2H, t, H_{4b}, J=8 Hz), 8.05-8.01 (2H, m, H_{4p}), 7 .97 (2H, m, H_{6b}), 7.80-7.74 (2H, m, H_{3p}), 7.36-7.32 (2H, m, H_{5b})

Observed: %C: 2.52, %H: 4.0, %N: 1.1*

Calculated:%C: 47.3, %H: 2.7, %N: 15.0

*Final yield contains excess KPF_6 and column chromatography solvent. See Section 5.2.3

Complex 6: [Ru(pyrphen)$_2$(dmbpy)](PF$_6$)$_2$.KPF$_6$

Step 1: Synthesis of [Ru(phendione)$_2$(dmbpy)](PF$_6$)$_2$

This synthesis was based on a literature procedure. 200 mg (0.21 mmol) [Ru(phen)$_2$(dmbpy)](PF$_6$)$_2$ was stirred in 5 cm^3 H_2SO_4 until dissolved. 212 mg (2.06 mmol) was added to the reaction mixture followed by 3.5 cm^3 70% HNO_3. This mixture was then heated to 110 ^{0}C for 40 min. The reaction mixture was then cooled to room temperature and neutralised by addition of solid potassium bicarbonate. The resulting suspension was filtered and the residue washed with H_2O. The product was precipitated through addition of solid KPF_6 to the filtrate, which was then left uncovered overnight to maximise precipitation. The resulting brown solid was collected by vacuum filtration, washed with 25 cm^3 cold water and dried at the pump overnight.

Yield: 35% (69 mg)

^{1}H NMR: d_6-acetone ^{1}H δ: 8.88 (2H, s, H_{3b}), 8.76-8.66 (4H, m, H_{5p}+H_{6p}), 8.49 (2H, d, H_{2p}, J=4.4 Hz), 8.39 (2H, d, $H_{1p,}$ J=4 Hz), 8.01 (2H, d, H_{6b}, J=6 Hz), 7.89-7.89 (4H, m, H_{3p}+H_{5p}), 7.46 (2H, d, H_{5b}, J=6 Hz), 3.01 (6H, s, CH_{methyl})

Step 2: Synthesis of [Ru(pyrphen)$_2$(dmbpy)](PF$_6$)$_2$.KPF$_6$

70 mg (0.07 mmol) [Ru(phendione)$_2$(bpy)](PF$_6$)$_2$ was placed in 8 cm^3 dry glacial acetic acid with 100 mg (1.36 mmol) ammonium acetate and heated to 100 ^{0}C. 13 µl (0.14 mmol) 4-pyridine carboxaldehyde was added to the reaction mixture, which was

then heated at 100 ^{0}C for 2 hr. The resulting dark orange solution was cooled to room temperature, and 10 cm^3 acetone was added. This mixture was then added dropwise to 300 cm^3 diethyl ether with vigorous stirring. The resulting suspension was filtered and the collected orange solid was purified by column chromatography on neutral alumina using acetonitrile as eluent. The main orange band was collected, and the solvent removed. The orange solid obtained was dissolved in 5 cm^3 H_2O and precipitated by addition of a saturated solution $KPF_{6\ (aq)}$. The orange precipitate was collected by vacuum filtration and recrystallised from acetone: water.

Yield: 15.3% (12.5 mg)

^{1}H NMR: d_6-acetone ^{1}H δ: 9.23 (2H, d, H_{6p}, J=7.2 Hz), 9.11 (2H, d, H_{5p}, J=6 Hz), 8.94 (4H, d, H_{11p}+H_{12p}, J=4.4 Hz), 8.79 (2H, s, H_{3b}), 8.67 (2H, m, H_{2p}), 8.46-8.42 (2H, m, H_{1p}), 8.33 (4H, d, H_{9p}+H_{10p}, J=5.2 Hz), 8.19-8.15 (2H, m, H_{4p}), 7.91-8.86 (4H, m, H_{3p}+H_{6b}), 7.30 (2H, t, H_{5b}, J=5.2 Hz), 2.57 (6H, s, CH_{methyl})

Elem. Anal$[C_{44}H_{24}N_{12}Ru](PF_6)_2.KPF_6$

Observed: %C: 42.4, %H: 2.4, %N: 9.4

Calculated:%C: 42.6, %H: 2.6, %N: 12.5

4.4.2 Synthesis of Metal Complexes (Unsuccessful)

Complex 5: $[Ru(thimphen)_2(dmbpy)](PF_6)_2$

Step 1: Synthesis of $[Ru(phendione)_2(dmbpy)](PF_6)_2$

This procedure was carried out in an identical manner to that described for *Step 2* in the synthesis of Complex 6: $[Ru(pyrphen)_2(dmbpy)](PF_6)_2$.

Step 2: Synthesis of $[Ru(thimphen)_2(dmbpy)](PF_6)_2$

100 mg (0.09 mmol) $[Ru(phendione)_2(dmbpy)](PF_6)_2$ was placed in 8 cm^3 dry glacial acetic acid with 150 mg (1.94 mmol) ammonium acetate and heated to 100 ^{0}C. 17 µl (0.19 mmol) 3-thiophene carboxaldehyde was added to the reaction mixture, which was then heated at 100 ^{0}C for 3 hr. The resulting dark orange solution was cooled to room temperature, and 10 cm^3 acetone was added. This mixture was then added dropwise to 300 cm^3 diethyl ether with vigorous stirring. The resulting suspension was filtered and the collected orange solid was purified by column chromatography on neutral alumina using acetonitrile as eluent. The main orange band was collected, and the solvent removed. The orange solid obtained was dissolved in 5 cm^3 H_2O and

precipitated by addition of a saturated solution $KPF_{6\ (aq)}$. The orange precipitate was collected by vacuum filtration and recrystallised from acetone: water. A conclusive ^1H NMR spectrum was not obtained and thus the reaction was deemed unsuccessful.

Complex 9: [Ru(thimphen)$_2$(Mepytr)](PF$_6$) &

Complex 10: [Ru(pyrphen)$_2$(Mepytr)](PF$_6$)

Step : Synthesis of [Ru(phendione)$_2$(Mepytr)](PF$_6$)

This synthesis was based on a literature procedure. 100 mg (0.11 mmol) $Ru(phen)_2(Mepytr)](PF_6)_2$ was stirred in 3 cm^3 H_2SO_4 until dissolved. 109 mg (1.06 mmol) was added to the reaction mixture followed by 2.5 cm^3 70% HNO_3. This mixture was then heated to 110 ^{0}C for 40 min. The reaction mixture was then cooled to room temperature and poured onto 50 cm^3 cold $KPF_{6\ (aq)}$ saturated solution. The resulting brown mixture was kept at 5 ^{0}C for overnight. The solution was then left uncovered in a fumehood for 48 hours. No precipitate was formed and thus the reaction was termed unsuccessful. This rendered attempted synthesis of the metal complexes $[Ru(thimphen)_2(Mepytr)](PF_6)_2$ and $[Ru(pyrphen)_2(Mepytr)](PF_6)_2$ impossible.

Complex 11: [Ru(thimphen)$_2$(Ppytr)](PF$_6$) &
Complex 12: [Ru(pyrphen)$_2$(Ppytr)](PF$_6$)

Step 1: Synthesis of [Ru(phendione)$_2$(Ppytr)](PF$_6$)

This synthesis was based on a literature procedure. 100 mg (0.10 mmol) $Ru(phen)_2(Ppytr)](PF_6)_2$ was stirred in 3.5 cm^3 H_2SO_4 until dissolved. 102 mg (0.10 mmol) was added to the reaction mixture followed by 2.5 cm^3 70% HNO_3. This mixture was then heated to 110 ^{0}C for 40 min. The reaction mixture was then cooled to room temperature and poured onto 50 cm^3 cold $KPF_{6\ (aq)}$ saturated solution. The resulting brown/orange suspension was kept at 5 ^{0}C overnight. No precipitate was formed and thus the reaction was termed unsuccessful. This rendered attempted synthesis of the metal complexes $[Ru(thimphen)_2(Ppytr)](PF_6)_2$ and $[Ru(pyrphen)_2(Ppytr)](PF_6)_2$ impossible.

Complex 13: [Ru(thimphen)$_2$(bpt)](PF$_6$)

Step 1: Synthesis of [Ru(phendione)$_2$(bpt)](PF$_6$)

This synthesis was based on a literature procedure. 100 mg (0.10 mmol) [Ru(phen)$_2$(bpt)](PF$_6$) was stirred in 3 cm^3 H_2SO_4 until dissolved. 102 mg (1.00 mmol) was added to the reaction mixture followed by 2.5 cm^3 70% HNO_3. This mixture was then heated to 110 ^{0}C for 40 min. The reaction mixture was then cooled to room temperature and poured onto 50 cm^3 cold $KPF_{6\ (aq)}$ saturated solution. The resulting suspension was collected by vacuum filtration and dried at the pump. A conclusive ^{1}H NMR spectrum was not obtained. As a result the solid obtained from this reaction was treated as an intermediate and used directly in the next reaction.

Step 2: Synthesis of [Ru(thimphen)$_2$(bpt)](PF$_6$)

50 mg (0.05 mmol) [Ru(phendione)$_2$(bpy)](PF$_6$) was placed in 5 cm^3 dry glacial acetic acid with 75 mg (1.00 mmol) ammonium acetate and heated to 100 ^{0}C. 10 µl (0.10 mmol) 3-thiophene carboxaldehyde was added to the reaction mixture, which was then heated at 100 ^{0}C for 2 hr. The resulting dark orange solution was cooled to room temperature, and 10 cm^3 acetone was added. This mixture was then added dropwise to 300 cm^3 diethyl ether with vigorous stirring. The resulting suspension was filtered and the collected orange solid was purified by column chromatography on neutral alumina using acetonitrile as eluent. The main orange band was collected, and the solvent removed. The orange solid obtained was dissolved in 5 cm^3 H_2O and precipitated by addition of a saturated solution $KPF_{6\ (aq)}$. A definite ^{1}H NMR spectrum was not obtained for the solid obtained, and so the reaction was termed inconclusive.

Step 1: Synthesis of [Ru(phendione)$_2$(bpt)](PF$_6$)

This procedure was carried out in an identical manner to that described for *Step 1* in the synthesis of Complex 5: [Ru(thimphen)$_2$(bpt)](PF$_6$).

Step 2: Synthesis of [Ru(pyrphen)$_2$(bpt)](PF$_6$)

55 mg (0.05 mmol) [Ru(phendione)$_2$(bpt)](PF$_6$) was placed in 5 cm^3 dry glacial acetic acid with 80 mg (1.00 mmol) ammonium acetate and heated to 100 ^{0}C. 10 µl (0.11 mmol) 4-pyridine carboxaldehyde was added to the reaction mixture, which was then

heated at 100 ^{0}C for 2 hr. The resulting dark orange solution was cooled to room temperature, and 10 cm^3 acetone was added. This mixture was then added dropwise to 300 cm^3 diethyl ether with vigorous stirring. The resulting suspension was filtered and the collected orange solid was purified by column chromatography on neutral alumina using acetonitrile as eluent. The main orange band was collected, and the solvent removed. The orange solid obtained was dissolved in 5 cm^3 H_2O and precipitated by addition of a saturated solution $KPF_{6\ (aq)}$. The orange precipitate was collected by vacuum filtration and recrystallised from acetone: water. A definite ^{1}H NMR spectrum was not obtained for the solid obtained, and so the reaction was termed inconclusive.

4.4.3 Synthesis of Deuterated Metal Complexes

Complex 3: [Ru(thimphen)$_2$(d$_8$-bpy)](PF$_6$)$_2$

Step 1: Synthesis of [Ru(phen)$_2$(d$_8$-bpy)](PF$_6$)$_2$

This procedure was carried out in an identical manner to that described for *Step 1* in the synthesis of [Ru(thimphen)$_2$(bpy)](PF$_6$)$_2$, using 184 mg (1.12 mmol) d$_8$-2,2'-bipyridyl in place of 2,2'-bipyridyl in the original procedure.

Yield: 70% (584 mg)

Step 2: Synthesis of [Ru(phendione)$_2$(d$_8$-bpy)](PF$_6$)$_2$

This procedure was carried out in an identical manner to that described for *Step 2* in the synthesis of [Ru(thimphen)$_2$(bpy)](PF$_6$)$_2$, using 450 mg (0.49 mmol) [Ru(phen)$_2$(d$_8$-bpy)](PF$_6$)$_2$, 502 mg (4.92 mmol) NaBr, 9 cm^3 H_2SO_4 and 6 cm^3 70% HNO_3. A percentage yield was not calculated for this reaction as the washed, dried product signified a yield higher than 100%. This is most likely due to excess KPF_6 still present in the sample.

Step 3: Synthesis of [Ru(thimphen)$_2$(d$_8$-bpy)](PF$_6$)$_2$

This procedure was carried out in an identical manner to that described for *Step3* in the synthesis of [Ru(thimphen)$_2$(bpy)](PF$_6$)$_2$, using 300 mg (0.31 mmol) [Ru(phendione)$_2$(d$_8$-bpy)](PF$_6$)$_2$, 55 µl (0.62 mmol) 3-thiophene carboxaldehyde, 474 mg (6.15 mmol) ammonium acetate and 7 cm^3 dry glacial acetic acid. Also, this

reaction was heated for 3 hr as opposed to 1 hr in the case of $[Ru(thimpen)_2(bpy)](PF_6)_2$

Yield: 6.9% (24.4 mg)

Complex 4: $[Ru(pyrphen)_2(d_8\text{-bpy})](PF_6)_2$

Step 1: Synthesis of $[Ru(phen)_2(d_8\text{-bpy})](PF_6)_2$

This procedure was carried out in an identical manner to that described for *Step 1* in the synthesis of $[Ru(pyrphen)_2(bpy)](PF_6)_2$, using 184 mg (1.12 mmol) d_8-2,2'-bipyridyl in place of 2,2'-bipyridyl in the original procedure.

Yield: 70% (584 mg)

Step 2: Synthesis of $[Ru(phendione)_2(d_8\text{-bpy})](PF_6)_2$

This procedure was carried out in an identical manner to that described for *Step 2* in the synthesis of $[Ru(pyrphen)_2(bpy)](PF_6)_2$, using 450 mg (0.49 mmol) $[Ru(phen)_2(d_8\text{-bpy})](PF_6)_2$, 502 mg (4.92 mmol) NaBr, 9 cm^3 H_2SO_4 and 6 cm^3 70% HNO_3. A percentage yield was not calculated for this reaction as the washed, dried product signified a yield higher than 100%. This is most likely due to excess KPF_6 still present in the sample.

Step 3: Synthesis of $[Ru(pyrphen)_2(d_8\text{-bpy})](PF_6)_2$

This procedure was carried out in an identical manner to that described for *Step3* in the synthesis of $[Ru(pyrphen)_2(bpy)](PF_6)_2$, using 300 mg (0.31 mmol) $[Ru(phendione)_2(d_8\text{-bpy})](PF_6)_2$, 54.4 µl (0.62 mmol) 4-pyridine carboxaldehyde, 474 mg (6.15 mmol) ammonium acetate and 7 cm^3 dry glacial acetic acid.

Yield: 6.1% (23.2 mg)

4.5 Bibliography

[1] E. A. Medlycott, G. S. Hanan, F. Loiseau, S. Campagna, *Chem. Eur. J*., **13**, (2007), 2837

[2] J. Wang, Y-Q. Fang, L. Bourget-Merle, M. I. J. Polson, G. S. Hanan, A. Juris, F. Loiseau, S. Campagna, *Chem. Eur. J*. **12**, (2006), 8539.

[3] N. Miyaura, A. Suzuki, A., *Chem. Rev*., **95**, (1995), 2457

[4] S. Welter, N. Salluce, A. Benetti, N. Rot, P. Belser, P. Sonar, A. C. Grimsdale, K. Müllen, M. Lutz, A. L. Spek, L. De Cola, *Inorg. Chem*., **44**, (2005), 4706

[5] B. Schafer, H. Gorls, M. Presselt, M. Schmitt, J. Popp, W. Henry, J. G. Vos, S. Rau, *Dalton Trans*., (2006) 2225

[6] J. K. Barton, A. T. Danishefsky, J. M. Goldberg, *J. Am. Chem. Soc*., **106**, (1984) 2172

[7] D. A. McGovern, A. Selmi, J. E. O'Brien, J. M. Kelly, C. Long, *Chem. Comm*., (2005) 1402

[8] I. E. Pomestchenko, D. E. Polyansky, F. N. Castellano, *Inorg. Chem.*, **44**, *10*, (2005) 3412

[9] C. Di Pietro, S. Serroni, S. Campagna, M. T. Gandolfi, R. Ballardini, S. Fanni, W. R. Browne, J. G. Vos, *Inorg. Chem*., **41**, (2002) 2871

[10] B. D. J. R. Fennema, R. Hage, J. G. Haasnoot, J. Reedijk, *Inorg. Chimica. Acta*, **171**, (1990), 223

[11] M. I. J. Polson, J. A. Lotoski, K.O. Johansson, N. J. Taylor, G. S. Hanan, B. Hasenknopf, R. Thouvenot, F. Loiseau, R. Passalaqua, S. Campagna, *Eur. J. Inorg. Chem,* (2002), 2549

[12] E. A. Medlycott., G. S. Hanan, *Chem. Soc. Rev*, **34**, (2005) 133

[13] F. Loiseau, R. Passalacqua, S. Campagna, M. I. J. Polson, Y. Q. Fang, G. S. Hanan, *Photochem. Photobiol. Sci.,* **1,** (2002) 982

[14] K. O. Johansson, J. A. Lotoski, C. C. Tong, G. S. Hanan, *Chem. Comm*., (2000), 819

[15] X-H. Zou, B-H. Ye, H. Li, Q-L. Zhang, H. Chao, J-G. Liu, L-N. Ji, X-Y. Li, *J. Biol. Inorg. Chem.* **6**, (2001) 143

[16] M. M. Ali, F. M. MacDonnell, *J. Am. Chem. Soc.* **122**, (2000) *46* 11527

[17] Y. Halpin, *PhD Thesis,* Dublin City University, 2009.

[18] K.R. Rupesh, S. Deepalatha, M. Krishnaveni, R. Venkatesan, S. Jayachandran, European Journal of Medicinal Chemistry, 2006, **41**, 1494

[19] L. Cassidy, *PhD Thesis,* Dublin City University, 2008

[20] T. Albrecht, A. Guckian, A. M. Kuznetsov, J. G. Vos, J. Ulstrup, *J. Am. Chem. Soc.* 2006, **128**, 17132

[21] B. P. Sullivan, D. J. Salmon, Meyer T. *J., Inorg. Chem.* **17**, (1978), *17*, 3334

[22] W. R. Browne, C. M. O'Connor, J. S. Killeen, A. L. Guckian, M. Burke, P. James, J. G. Vos, *Inorg. Chem.,* **41**, (2002) 4245-4251

[23] S. D. Bergman. M. Koi, *Inorg. Chem.,* **44**, (2005) 1647-1654

Chapter 5: Approaches to Dinuclear Systems incorporating two Surface Active Ligands

Abstract:

Chapter 5 details attempts made towards the development of a dinuclear metal species containing two novel ligands of the type discussed in Chapter 3.

The attempted synthesis of dinuclear metal complexes containing two 'thimphen' ligands as a potential means of surface coordination is described. By modifying the well-known [Ru(bpy)$_2$Cl$_2$] dichloride synthesis[17] and replacing 2,2'-bipyridyl with thimphen, synthesis of the novel dichloride [Ru(thimphen)Cl$_2$] was attempted. This starting material was reacted with the mononuclear metal complex [Ru(bpy)$_2$(bpt)]$^{2+}$ where bpt is 3,5-bis(pyridin-2-yl)1,2,4-triazole. The products obtained and attempts at their purification are discussed. Characterisation of the complexes synthesised using nuclear magnetic resonance, HPLC and UV/vis absorption spectroscopy is also reported.

5.1 Introduction

As mentioned previously in Chapter 3, the demand for increasingly elaborate electronic constructions, while still allowing for the incessant shrinking of appliances they are used to build, is a conundrum currently plaguing the electronics industry. The current 'top-down' approach that uses macroscopic materials and techniques to create circuitry that is fast becoming microscopic in scale is sure to become obsolete within a very short time. One fact is extremely clear: an alternative method must be found. As outlined in Chapter 3, the 'bottom-up' approach of molecular synthesis may potentially allow for the construction of nanometer sized devices that may be arranged into circuits.[1, 2] The type of compounds suitable for use as molecular electronics prototypes that shall be discussed in this report will be restricted to metal complexes of ruthenium and osmium. Osmium polypyridyl metal complexes have been shown to display transistor-like behaviour when arranged as a monolayer on a gold or platinum surface.[3]

Chapter 3 detailed the synthesis of molecular transistor prototypes containing one –imphen type ligand (the ligands thimphen and pyrphen). This chapter will contain the synthesis of similar transistor prototypes containing two of these novel ligands in order to investigate their suitability for this role.

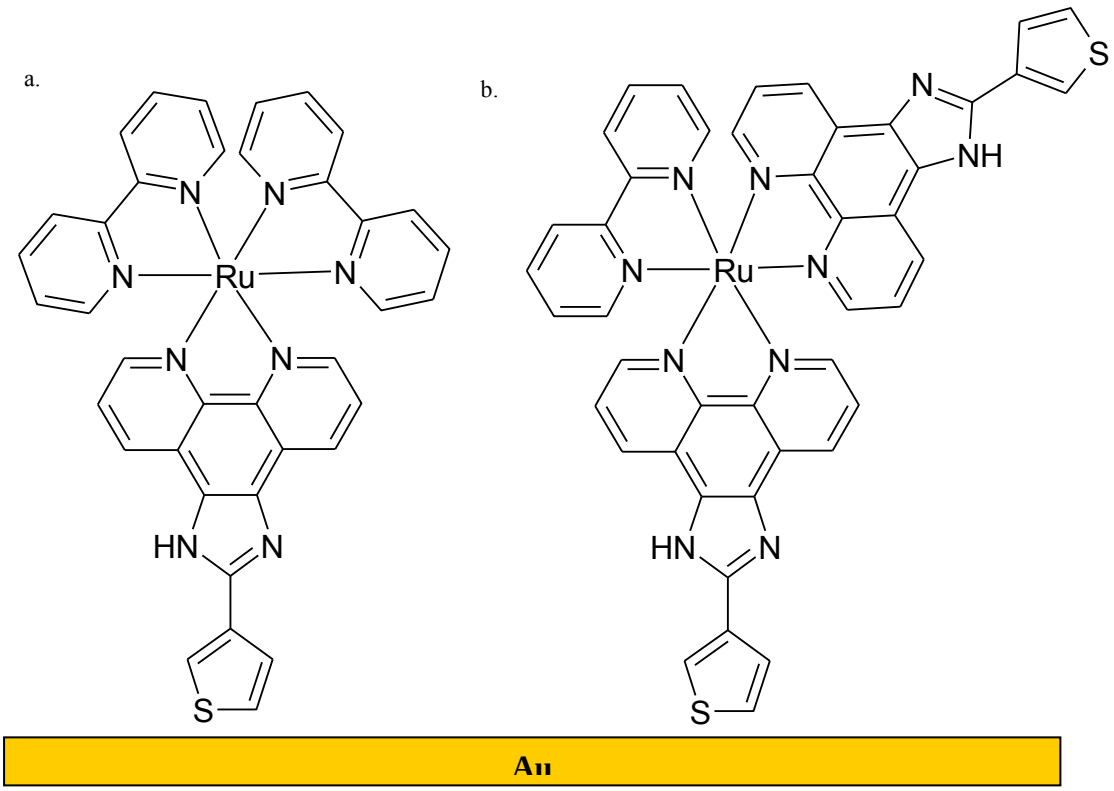

Figure 5.1: Diagrammatic representation of the metal complexes (a) $[Ru(bpy)_2(thimphen)]^{2+}$ (Chapter 3) and (b) $[Ru(thimphen)_2(bpy)]^{2+}$ (Chapter 4) as bound to a gold surface

The synthesis of these materials also serves a second function as they may also serve as model complexes for possible diode prototypes based on the above 'imphen' type ligands. A diode may be termed an electronic device that allows current to flow in one direction only. Molecular devices of this type are theoretically possible, based on metal complexes of different oxidation potential as discussed previously in section 1.5 of Chapter 1. The synthetic chemistry involved in synthesis of mononuclear building blocks for dinuclear complex synthesis is well known and extensively documented[4] (*c.f.* Chapter 1).

However, the incorporation of surface active ligands instead of the ubiquitous bis-bipyridyl system discussed in Chapter 1 is a much greater synthetic challenge. Chapter 4 has described a modification type method in which the desired surface active ligands are built up on precursor complexes using a multistep synthesis. While this appears to be the only option for synthesis of surface active dinuclear metal complex incorporating the novel ligand pyrphen (*c.f.* Chapter 3/4) a less complex method may be possible for the synthesis of mono- and dinuclear complexes

including the novel ligand 'thimphen' as a point of surface coordination. This is doubly attractive considering the difficulties met with when synthesising the thimphen analogues of the novel metal complexes $[Ru(pyrphen)_2(dmbpy)]^{2+}$ and $[Ru(pyrphen)_2(bpt)]^{2+}$ as encountered in Chapter 4. Unlike pyrphen, thimphen may be synthesised as a free ligand (see Chapter 3). As a result it is theoretically possible to replace thimphen for 2,2'-bipyridyl in the synthesis of the dichloride precursor $[Ru(bpy)_2Cl_2].2H_2O$. Incorporating the resulting dichloride starting material $[Ru(thimphen)_2Cl_2]$ a simpler reaction scheme than that outlined in Chapter 4 for the construction of a surface active dinuclear complex reveals itself. A reaction scheme for one such pathway is shown below in Figure 5.2.

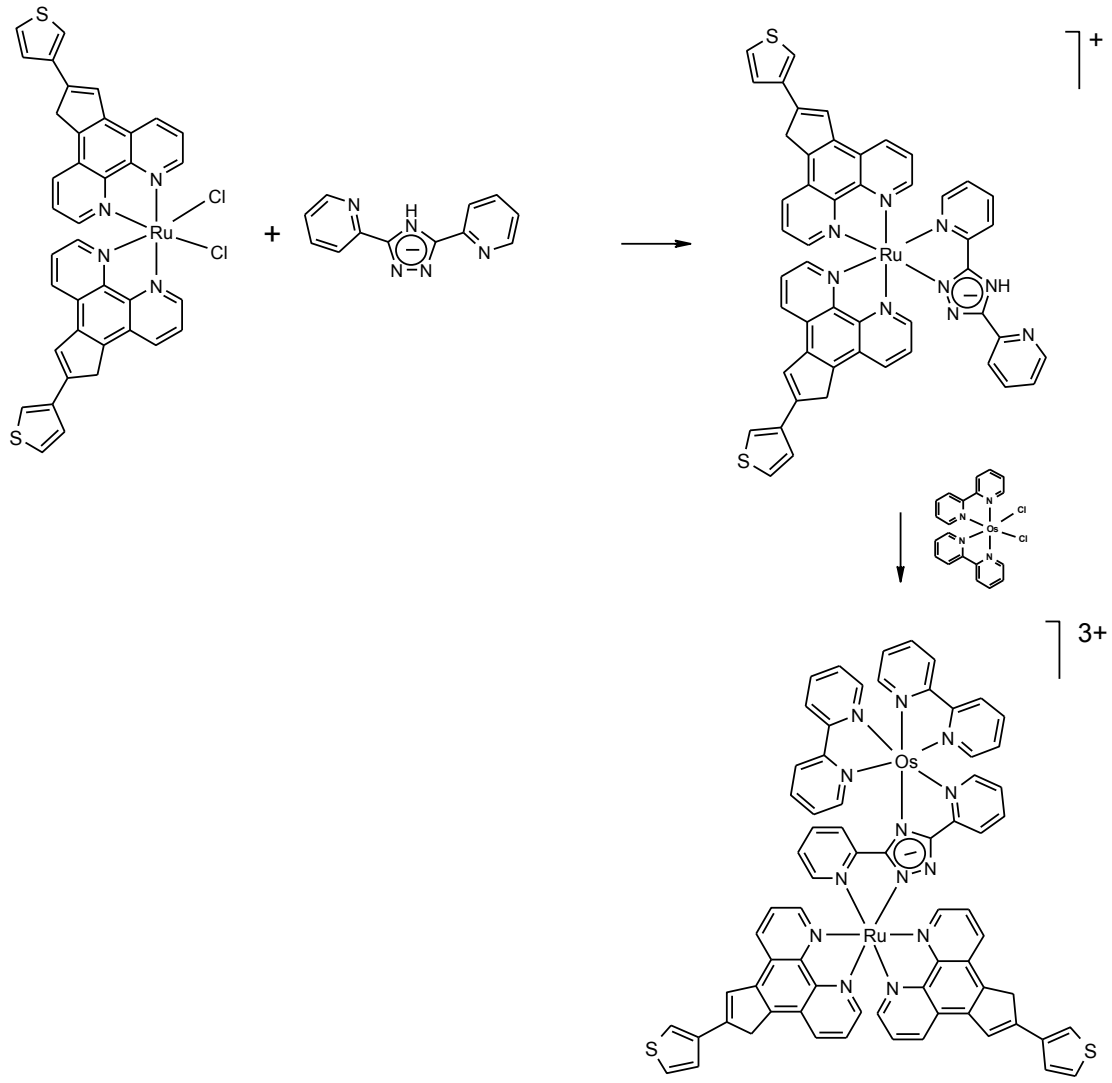

Figure 5.2: Theoretical synthetic pathway for construction of a molecular diode based on the surface active thimphen ligands described in Chapters 3 and 4

Examining Figure 5.2 it can be seen that the main area of novelty (and therefore challenge) lies in the incorporation of the dichloride material $[Ru(thimphen)_2Cl_2]$. A similar structure, $[Ru(pip)_2Cl_2]$ shown below in Figure 5.3, has been successfully by Mei *et al*[5].

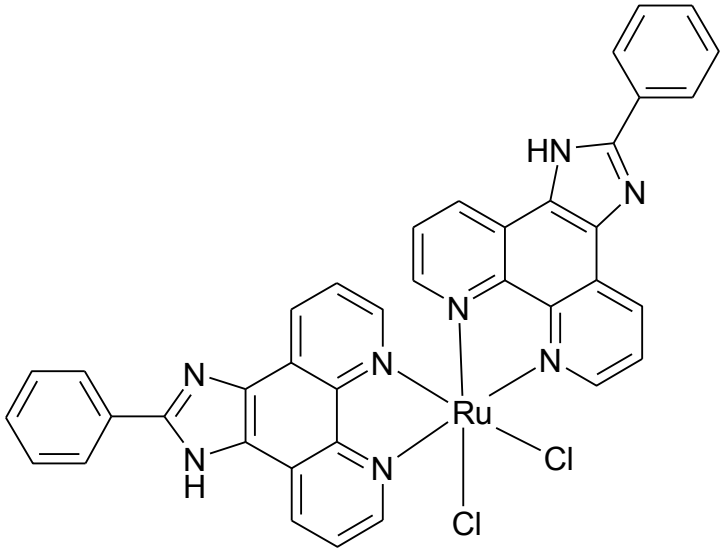

Figure 5.3: Structure of the metal complex $[Ru(pip)_2Cl_2]$[5]

Synthesis of $[Ru(pip)_2Cl_2]$ was carried out using the same reaction conditions as for the widely used starting material $[Ru(bpy)_2Cl_2]$ (*c.f.* Chapter 2) substiituting the ligand pip for bpy in the reaction. The successfully synthesised $[Ru(pip)_2Cl_2]$ was then used to synthesise a dinuclear metal complex containing a zinc porphyrin as a model complex for photodynamic therapy[6]

Jiang et. al have also used this starting material to synthesise a series of phenanthroline based ruthenium complexes for non-linear optics applications[7] as shown below in Figure 5.4.

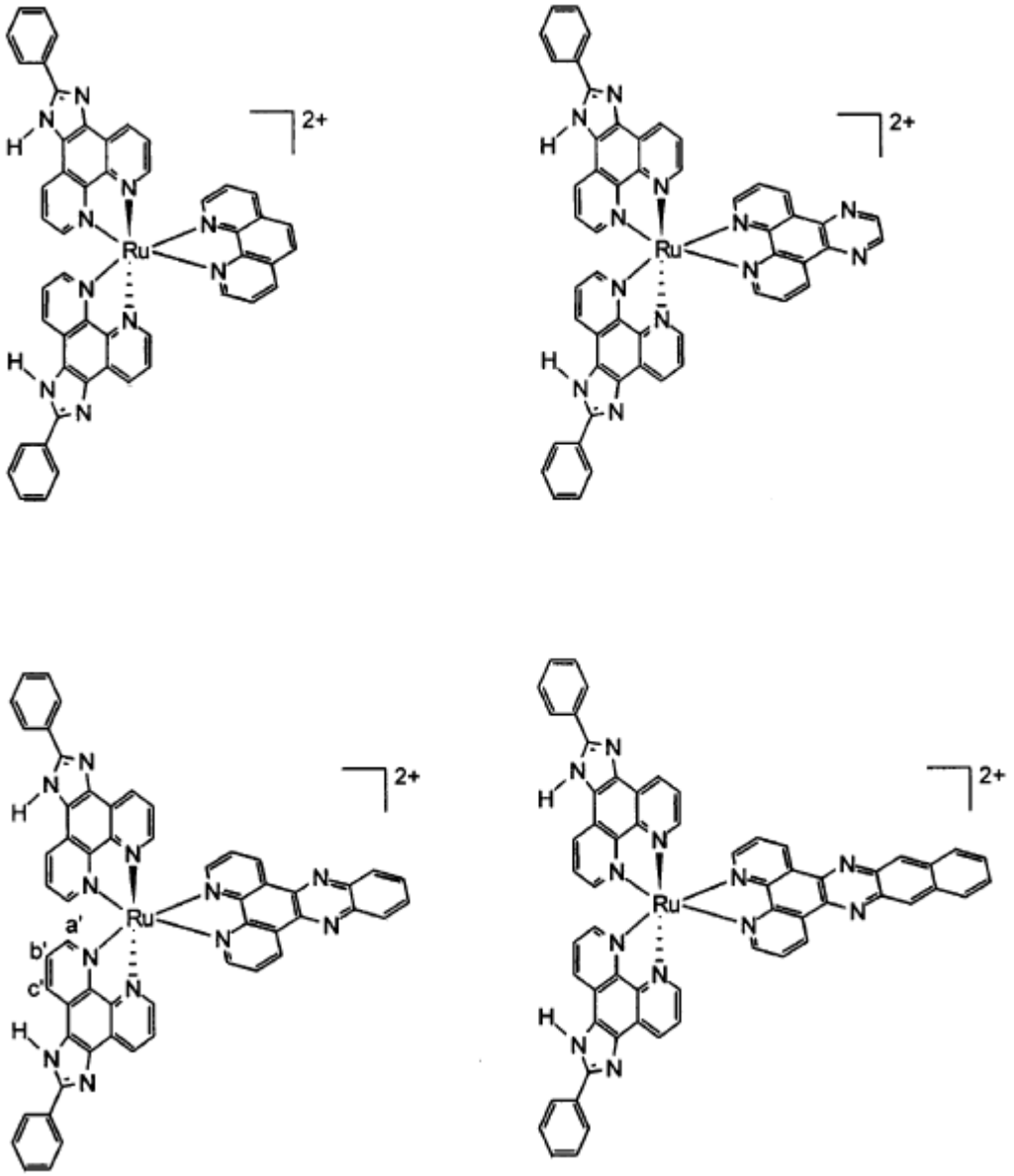

Figure 5.4: Structures for the series of ruthenium complexes containing the group $[Ru(pip)_2(phen)]^{2+}$ *as synthesised be Jiang et al*[7]

This chapter details the attempted synthesis of dinuclear complexes containing ruthenium and osmium using the starting material $Ru(thimphen)_2Cl_2$. Analysis of products obtained was carried out using ^1H NMR and UV/vis spectroscopy as well as HPLC methods.

5.2 Results and Discussion

5.2.1 Synthetic Considerations

This set of reactions follows a well-documented area of inorganic chemistry. It follows the classic "*complexes as metals* / *complexes as ligands"* strategy. [8, 9, 10] This is a type of 'structurally directed' synthesis [11] in which mononuclear 'building blocks' containing a free coordination site and/or labile ligands (most often chlorides) to form di/polynuclear compounds. When using a symmetrical bridging ligand a relatively straightforward series of reactions, as discussed in Chapter 1, may be followed to yield the desired dinuclear product.

As can be seen in Chapter 1 this strategy is suitable for the synthesis of both homo- and heterodinuclear metal complexes. As a series of homo- and heterodinuclear complexes are desired in this case, examples of which are shown below in Figure 5.5, this was the synthetic strategy adopted.

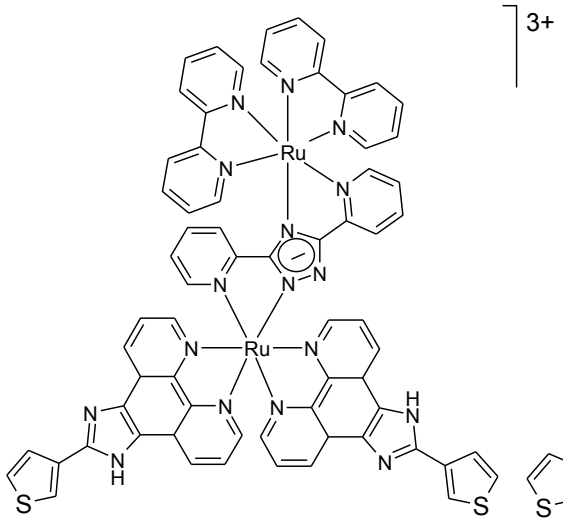

$[Ru(thimphen)_2(bpt)Ru(bpy)_2]^{3+}$

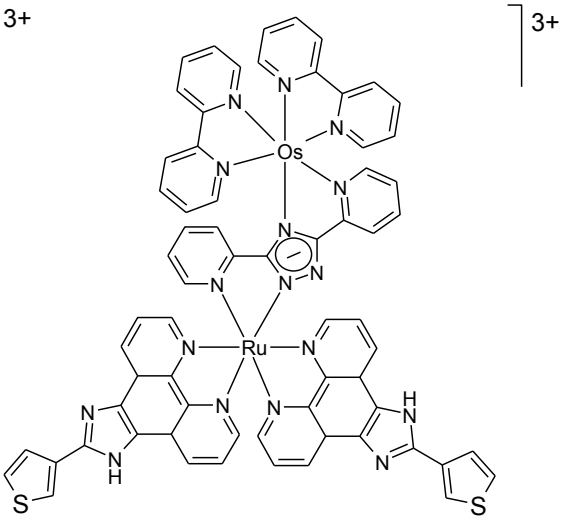

$[Ru(thimphen)_2(bpt)Os(bpy)_2]^{3+}$

Figure 5.5: Molecular structures for the homo- and heterodinuclear metal complexes the synthesis of which were attempted in this chapter

The first step attempted was the synthesis of a dichloride starting material containing two surface active ligands which shall be discussed below.

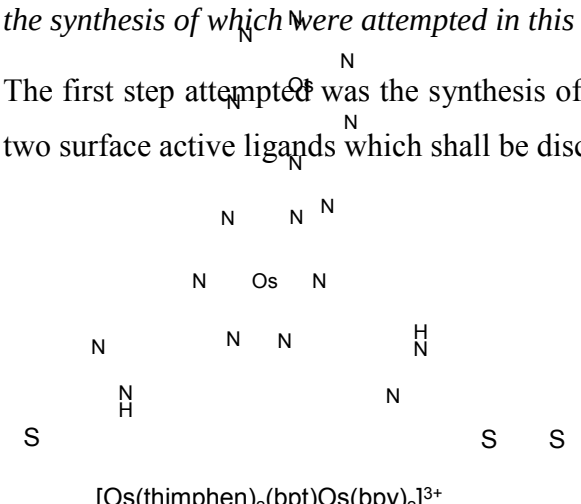

$[Os(thimphen)_2(bpt)Os(bpy)_2]^{3+}$

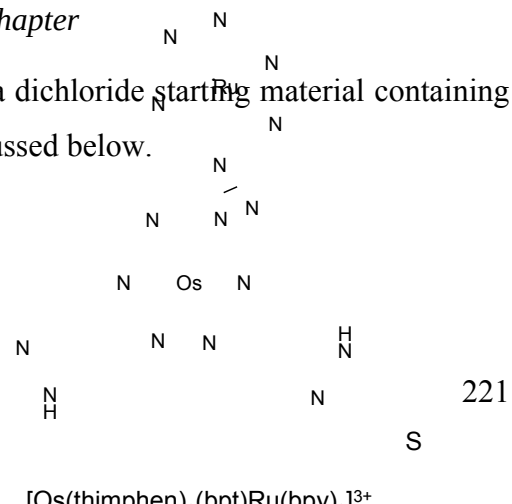

$[Os(thimphen)_2(bpt)Ru(bpy)_2]^{3+}$

5.2.1.1 Synthesis of the starting material $Ru(thimphen)_2Cl_2$

$Ru(bpy)_2Cl_2$ Method[17]

As mentioned previously the thiophene containing ligand 'thimphen' was chosen for synthesis of a ruthenium-dichloride starting material as it can be synthesised in its entirety as a free ligand (as opposed to the pyridine containing ligand 'pyrphen that must be built on the complex *c.f.* Chapter 3). The reaction type employed for this dichloride synthesis follows the same system as for the well known starting material $[Ru(bpy)_2Cl_2].2H_2O$[17]. In this procedure, commercially available $Ru(III)Cl_3$ is refluxed with two equivalents 2,2'-bipyridyl and an excess of LiCl in DMF. The reaction scheme for this procedure is shown schematically below in Figure 5.6.

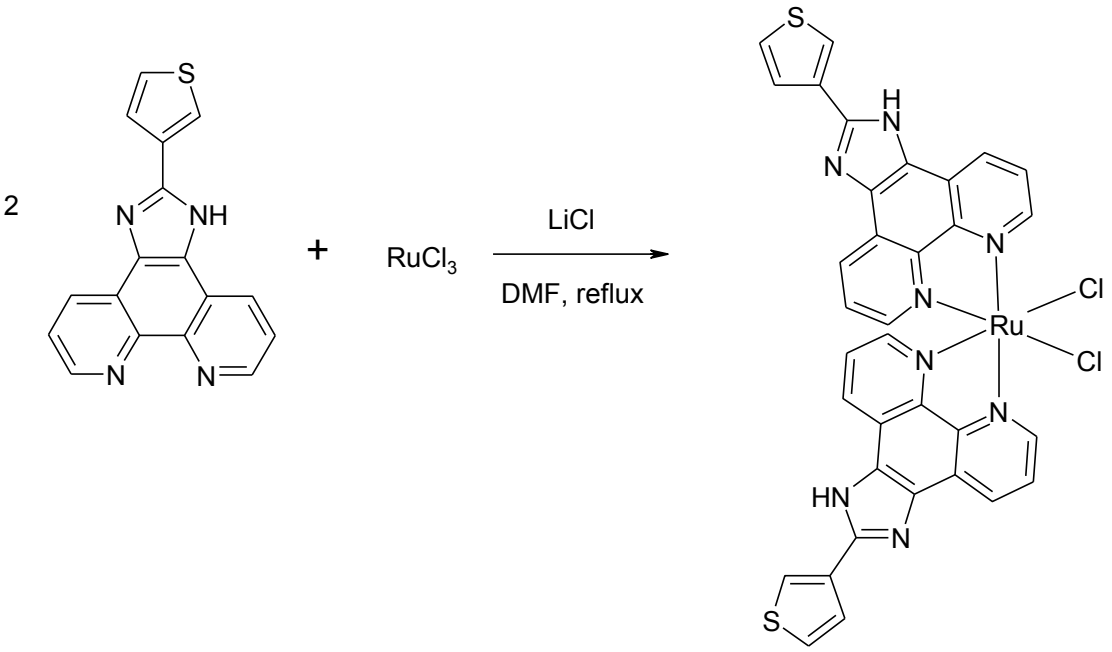

Figure 5.6: Reaction scheme for the formation of the starting material $Ru(thimphen)_2Cl_2$

The solid obtained from this reaction was submitted for ^1H NMR analysis, yielding a broad, uneven spectrum shown below in Figure 5.7.

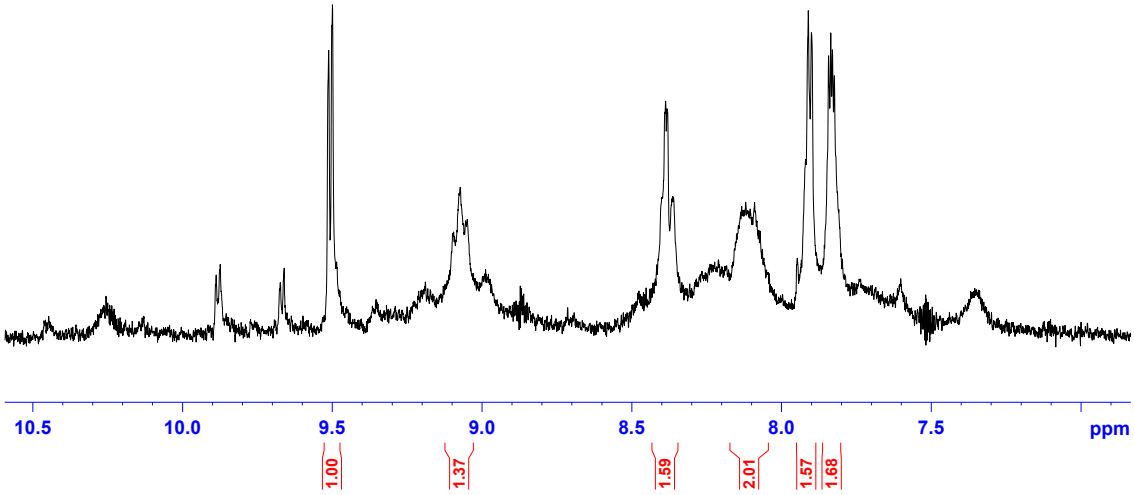

Figure 5.7: ^{1}H NMR spectra of $Ru(thimphen)_2Cl_2$ in d_6-DMSO

Recrystallisation from hot acetone was carried out in an attempt at purification, but this did not improve the ^{1}H NMR spectrum. Therefore, different methods of synthesis were considered, as discussed below.

$[Ru(bpy\text{-}CO_2Et_2)_2Cl_2]$ Method[12]

A similar method for $[Ru(L)_2Cl_2]$ synthesis where L is a bidentate ligand has been used by Han et al. for the synthesis of $[Ru(bpy\text{-}CO_2Et_2)_2Cl_2]$.[12] This method involves the reflux of $RuCl_3.3H_2O$ and a bidentate ligand (in the case of reference 12 [bpy-CO_2Et_2]) in ethanol for 3 days in an N_2 atmosphere. The resulting dichloride is then precipitated by addition of diethyl ether. This method employs much milder reaction conditions than the conventional $Ru(L)_2Cl_2$ synthetic method discussed above, the reaction proceeding at a much lower reflux temperature due to the substitution of ethanol for DMF. This reduction in reflux temperature allows for the synthesis of a ruthenium dichloride containing a labile ester group as described in reference 12. Therefore, as it is possible that the broad ^{1}H NMR spectrum shown in Figure 5.7 is a result of ligand decomposition caused by the harsh reaction conditions used, this method may result in a sharper spectrum and cleaner product.

Upon attempting the reaction between $RuCl_3.2H_2O$ and thimphen using ethanol as solvent a brown suspension was obtained. This suspension was filtered to yield a brown solid and orange filtrate. Diethyl ether was added to this filtrate, yielding a yellow solid, collected by filtration. Both these submitted for ^{1}H NMR analysis. The resulting spectra are shown below in Figure 5.8.

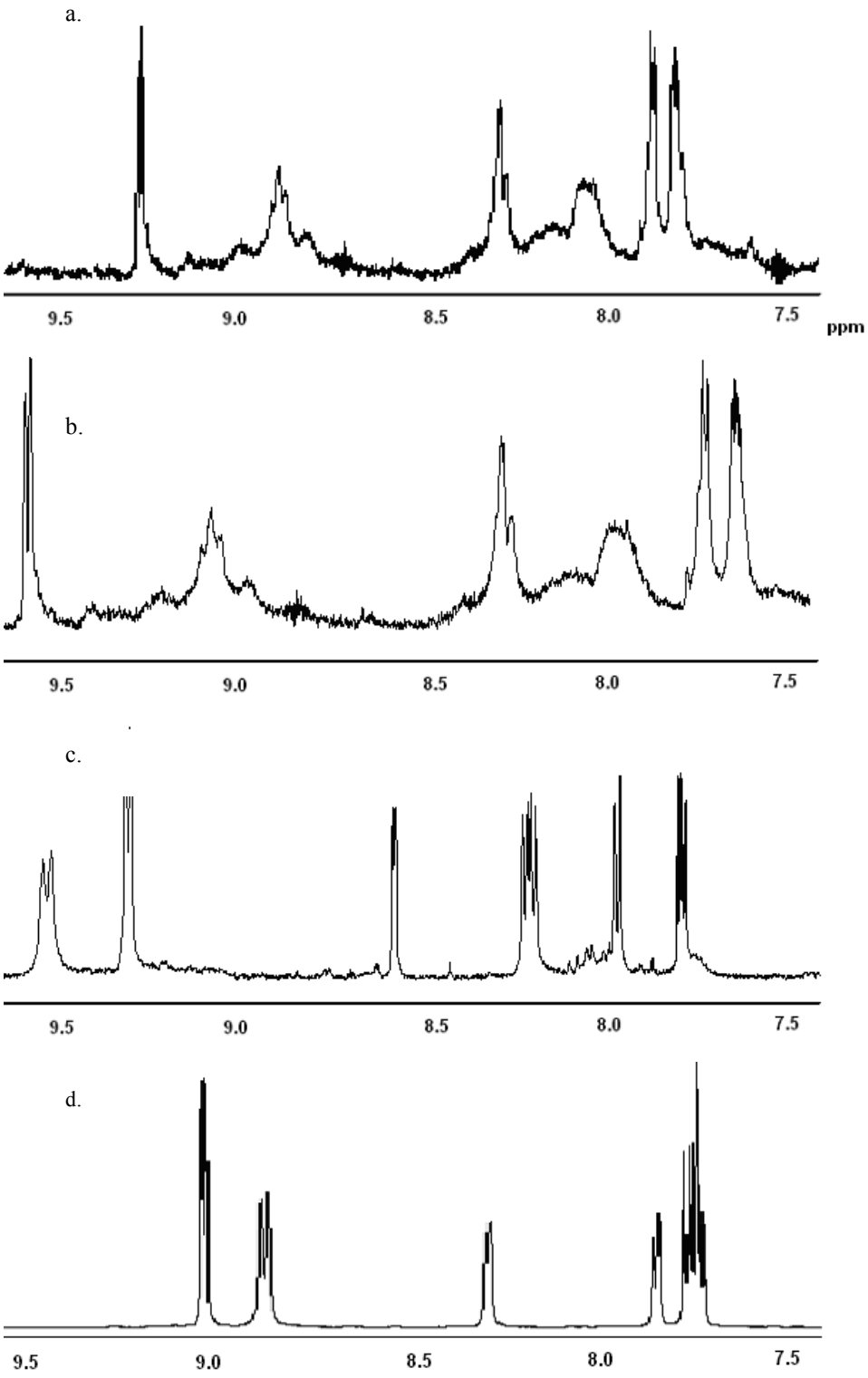

Figure 5.8: ^{1}H NMR spectra of (a) $Ru(thimphen)_2Cl_2$ obtained from DMF/LiCl reaction, (b) brown solid obtained from filtration of EtOH $Ru(thimphen)_2Cl_2$ reaction mixture, (c) yellow solid obtained from the filtered EtOH $Ru(thimphen)_2Cl_2$ reaction mixture and (d) pure thimphen as measured in d_6-DMSO

Comparing the spectra shown in Figure 5.8 a and b it can be seen that there is very little difference between the two spectra other than some minor shifts in Figure 5.8 b with respect to Figure 5.8 a, possibly as a result of the different reaction solvents used to synthesise the two different solids. In any case it is obvious from these spectra that the material formed in both reactions is the same. Comparing the spectra shown in Figure 5.8 c and d it can be seen that there is a large similarity between the spectrum of the yellow solid obtained from the reaction mixture discussed above (Figure 5.8 c) and the spectrum of the free ligand thimphen (Figure 5.8 d). However, there is a large associated shift observed for all signals present in Figure 5.8 c with respect to Figure 5.8 d, implying that though the integration and splitting of the spectral peaks shown in Figure 5.8 c match those of the signals present in Figure 5.8 d, the chemical shift values for the signals corresponding to the yellow solid obtained from the [Ru(bpy-$CO_2Et_2)_2Cl_2$] type reaction detailed here is not made up of free ligand.

It is possible that this yellow solid, the spectrum for which is shown in Figure 5.8 c, may be a mono-,bis- or poly-carbonyl complex in which one or more C=O groups are coordinated to the ruthenium centre along with one or more thimphen ligands. Carbonyl coordination resulting from the degredation of solvent and/or incorporation of atmospheric carbon dioxide is encountered in the synthesis of the ruthenium-dichloride complex $[Ru(bpy)_2Cl_2]$[17] and so it is possible that a similar process has occurred here. In order to assess whether or not this complex is present an IR spectrum was run using a thin film of the complex deposited on KCl plates using acetone as solvent. Following the sample's dissolution in acetone, the resulting solution was deposited onto an analysis plate and the solvent allowed to evaporate off before the spectrum was recorded. As the purpose of recording the spectrum was to ascertain the presence of a carbonyl group, a blank spectrum was also run using evaporated acetone to ensure that no vital peaks were masked by residual solvent. These spectra are shown below in Figure 5.9.

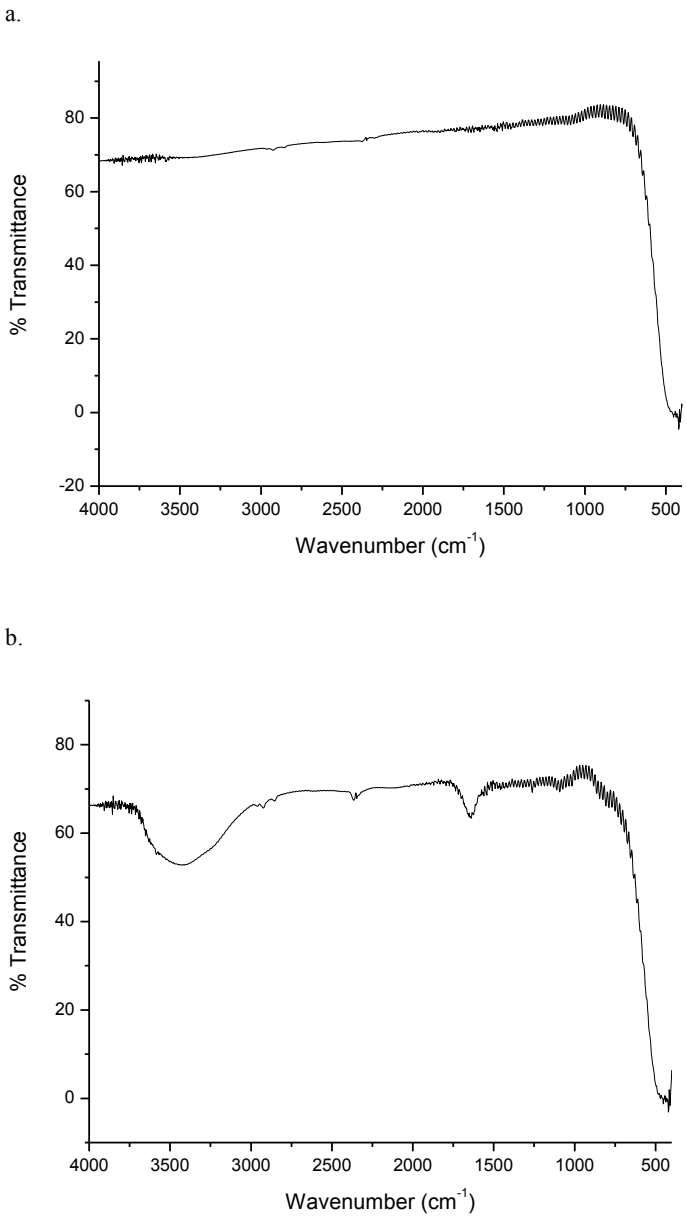

Figure 5.9: Infra-Red spectra of (a) blank containing only evaporated acetone and (b) acetone deposited thin-film of yellow solid obtained from Et_2O addition to $[Ru(thimphen)_2Cl_2]$ reaction mixture using method outlined in reference 14

Comparing spectrum a to spectrum b as shown in Figure 5.9 it can be seen that the only peak present in both the blank and the $[Ru(thimphen)_2Cl_2]$ (yellow solid) sample is the strong peak present at approximately 415 cm^{-1} in both spectra. There are however three other spectral features prominent in Figure 5.9 b that cannot be seen in Figure 5.9 a, namely a weak absorbance present at 1640 cm^{-1}, a very weak absorbance at 2350 cm^{-1} and finally a broad medium strength absorbance present at 3400 cm^{-1}. A carbonyl group will almost always absorb strongly in the region 1700-1750 cm^{-1} [13]

and the absence of such an absorbance is conspicuous in the spectrum shown in Figure 5.9 b. The absorbencies observed may be attributed to the amine/imine character of the thimphen as well as the presence of the sulphur component in this molecule. The absorbance present at 1640 cm^{-1} may be attributed to either C=S thiocarbonyl bond stretching and/or C=N imine bond vibrations. The weak absorbance present at 2350 cm^{-1} is also attributable to the sulphur component present in the molecule as weak absorbances in this region are characteristic of mercaptans and thiophenol type compounds[13]. The broad peak visible at 3400 cm^{-1} is most likely a result of the amine portion of the thiophene imidazole, though it may also be attributable to residual ethanol from the reaction solution present within the sample.[13] Due to the absence of any carbonyl type absorbance in Figure 5.9 b it was concluded that a carbonyl complex was not formed in this instance.

It is possible that the compound yielding the spectrum shown in Figure 5.8 c is the tris-thimphen complex $[Ru(thimphen)_3]^{2+}$. In order to explore this possibility a reaction to prepare this material involving reflux of excess thimphen with $[Ru(III)Cl_3].2H_2O$ in 2:1 ethanol: water was carried out. A yellow solid precipitated from solution spontaneously after approximately three hours reflux. When sent for ^1H NMR analysis, the spectrum shown below in Figure 5.10 was obtained.

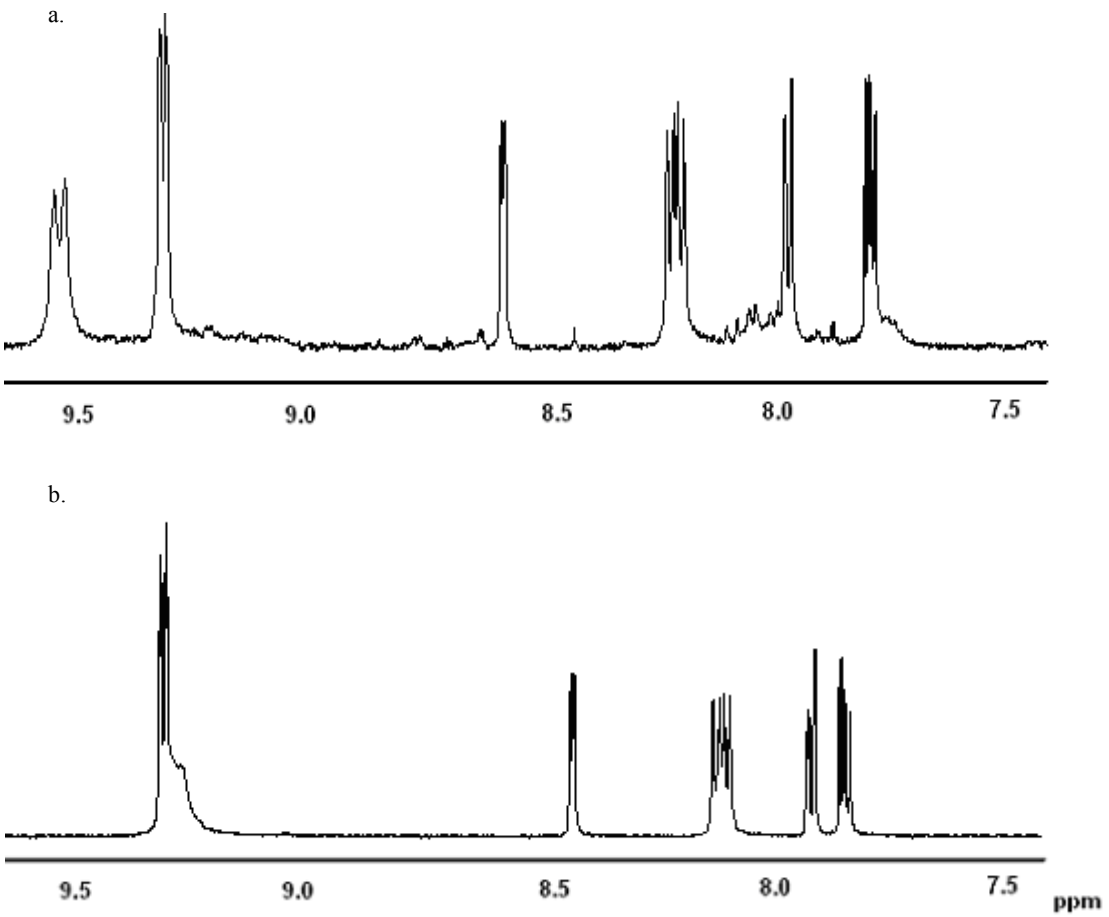

Figure 5.10: ^1H NMR spectrum for (a) the yellow solid obtained by addition of Et_2O to $[Ru(thimphen)_2Cl_2]$ reaction mixture using method outlined in reference 12 and (b) the complex $[Ru(thimphen)_3]^{2+}$ as measured in d_6-DMSO

Comparing the two spectra shown above in Figure 5.10 a small amount of discrepancy can be seen in the chemical shift between the two, specifically the peaks shown between 9.0 and 9.5 ppm in both spectra. However, the different manner of precipitation of the two solids may result in slightly different chemical shift by virtue of residual amounts of different solvents in each sample. For that reason it has been concluded that the yellow solid obtained by addition of diethyl ether to the $[Ru(thimphen)_2Cl_2]$ reaction mixture using the method outlined in reference 12 is most likely $[Ru(thimphen)_3]^{2+}$.

Ascorbic Acid Method[14]

Chapter 6 details a method of ruthenium dichloride synthesis in which ascorbic acid is used to reduce the starting material $RuCl_3.2H_2O$ from the III oxidation state to the II oxidation state before addition of the ligand to be coordinated. This method was also

attempted, following the exact procedure as outlined in Chapter 6. One molar equivalent $RuCl_3.2H_2O$ was heated in methanol overnight in the presence of 10 molar equivalents of ascorbic acid. The ensuing reduction step from Ru(III) to Ru(II) was characterised by a colour change from brown to green as described in Chapter 6. Two molar equivalents of the ligand thimphen were then added to the reaction mixture. In Chapter 6, the addition of the tetradentate ligand paen to the green $RuCl_3.2H_2O$ reaction mixture resulted in an immediate colour change from green to purple. In the case of the addition of the ligand thimphen however, no immediate colour change was observed. The reaction mixture was refluxed overnight yielding a black suspension which was filtered hot, and the dark red/black filtrate left to cool to room temperature. As no solid was formed upon cooling of this filtrate, the solvent was removed and the resulting residue sent for ^{1}H NMR analysis. This yielded a broad spectrum similar to that shown in Figure 5.7. The black solid collected by filtration of the hot reaction solution was also sent for ^{1}H NMR analysis, yielding the spectrum shown below in Figure 5.11.

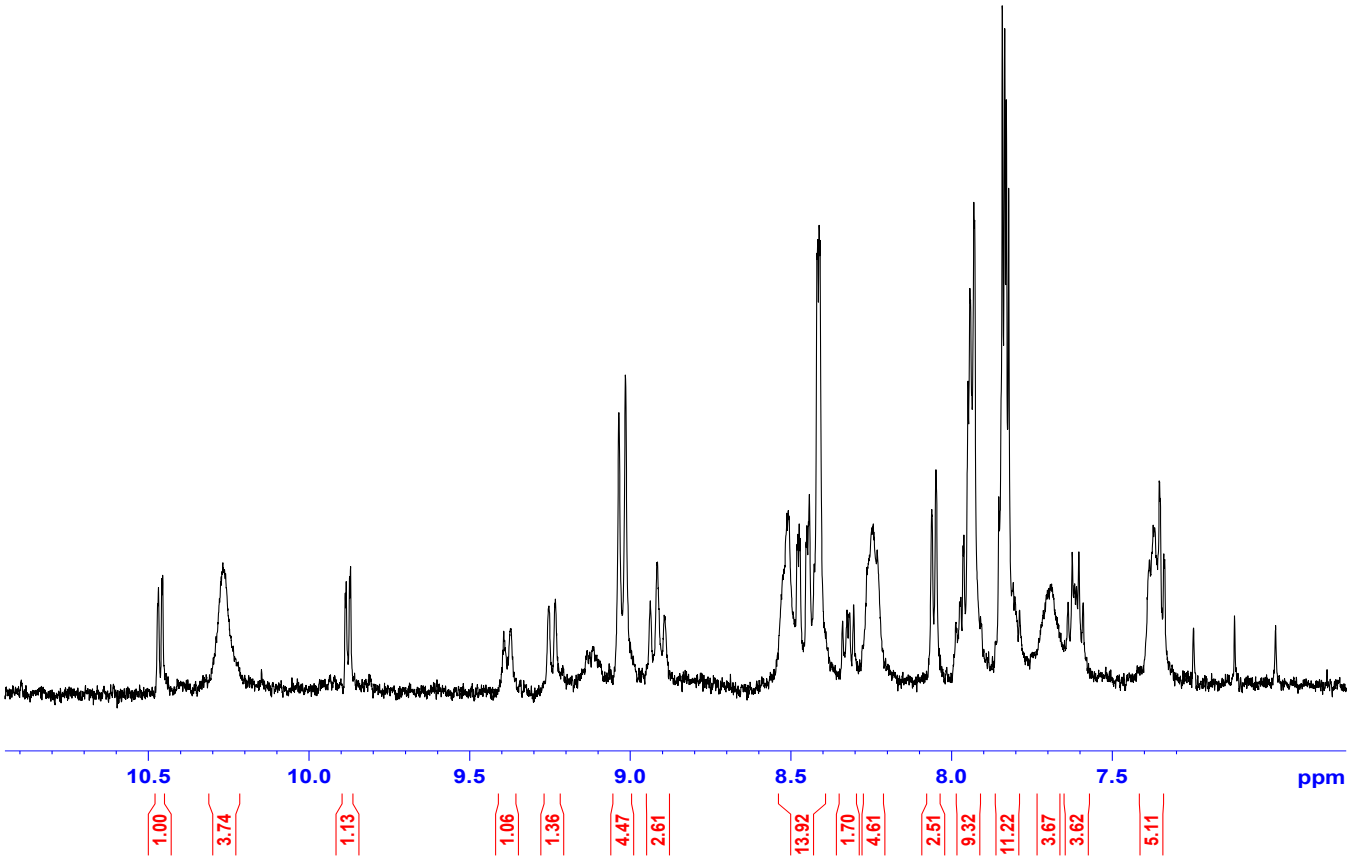

Figure 5.11: ^{1}H NMR spectrum as measured in d_6-DMSO of black precipitate collected from attempted $[Ru(thimphen)_2Cl_2]$ reaction mixture containing ascorbic acid

The ^{1}H NMR spectrum shown in Figure 5.11 displays a number of well defined, sharp peaks as well as some broadening. In order to establish how many (if any) different components were present, the sample was submitted for HPLC analysis. The resulting HPLC chromatogram is shown below in Figure 5.12.

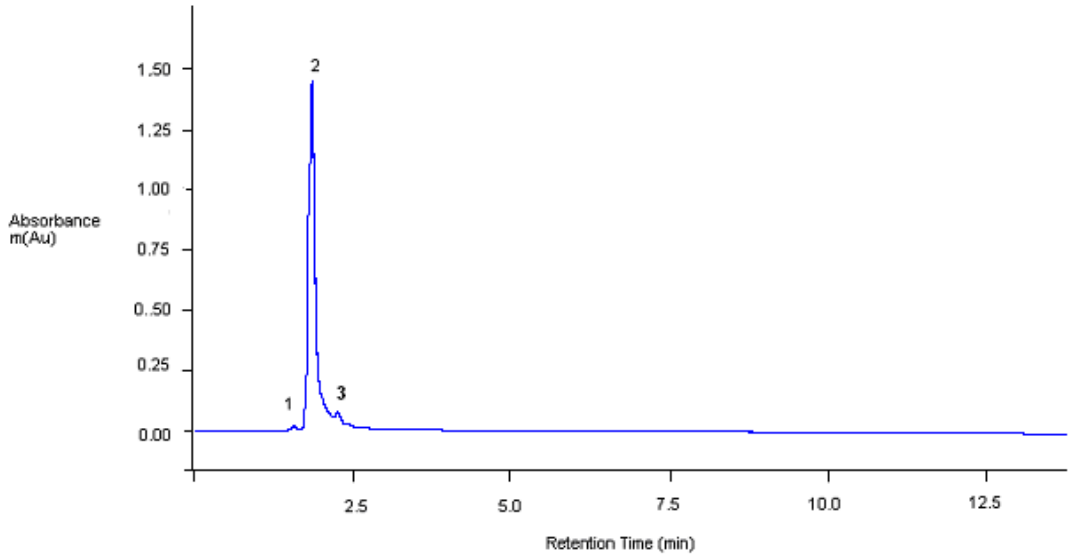

Figure 5.12: HPLC chromatogram obtained for Ru(thimphen)$_2$Cl$_2$ sample obtained from reaction incorporating excess ascorbic acid

This chromatogram shows three main peaks, the first exhibiting a retention time of 1.56 min, the second, most intense peak exhibiting a retention time of 1.83 min and the final peak exhibiting a retention time of 2.26 min. The first two bands when examined by UV/vis spectroscopy exhibited spectra consisting of one intense band at a wavelength >300 nm. As discussed in Chapter 6 this is indicative of a purely organic species, perhaps excess thimphen ligand or remaining ascorbic acid. Due to the quantities of these respective compounds in the reaction it may be inferred that the first, low intensity band is applicable to thimphen while the second, much more intense band refers to the excess of ascorbic acid used in the reaction. The third band however, while exhibiting a strong absorbance band at 300 nm, also exhibits further, albeit lower intensity absorption at 520 nm, which is indicative of the presence of a metal complex. This absorption spectrum is shown below in Figure 5.12.

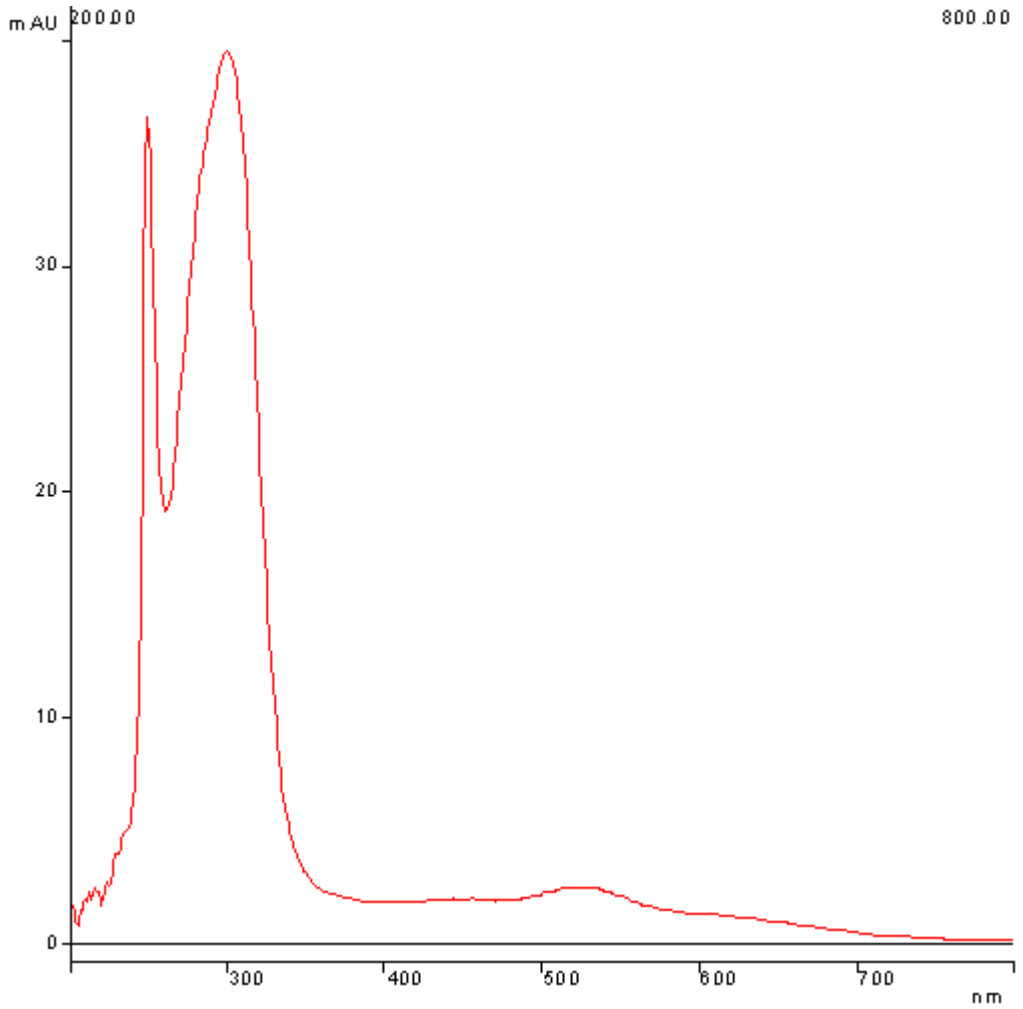

Figure 5.13: UV/vis spectrum of the third eluting band visible in the HPLC chromatogram shown in Figure 5.12

As in chapter 6, the HPLC system in use was found to be very similar to a column chromatography system involving silica stationary phase and a mobile phase of 80: 20 acetonitrile: water 0.05 M KNO_3. The sample obtained was therefore purified using this system, from which three coloured fractions were obtained. The solvent was removed from all three, revealing a reduction in quantity from crude sample to purified product in the order of 80%. From this information it can be assumed that the 'lost' 80% of the sample remained on the column, and could not be removed by any mobile phase substitution implemented. The fractions obtained were sent for ^1H NMR analysis, with one fraction yielding a signal. The spectrum obtained contained a large amount of background noise and so was re-examined under increased scans (~1000 scans). The resulting spectrum is shown below in Figure 5.14.

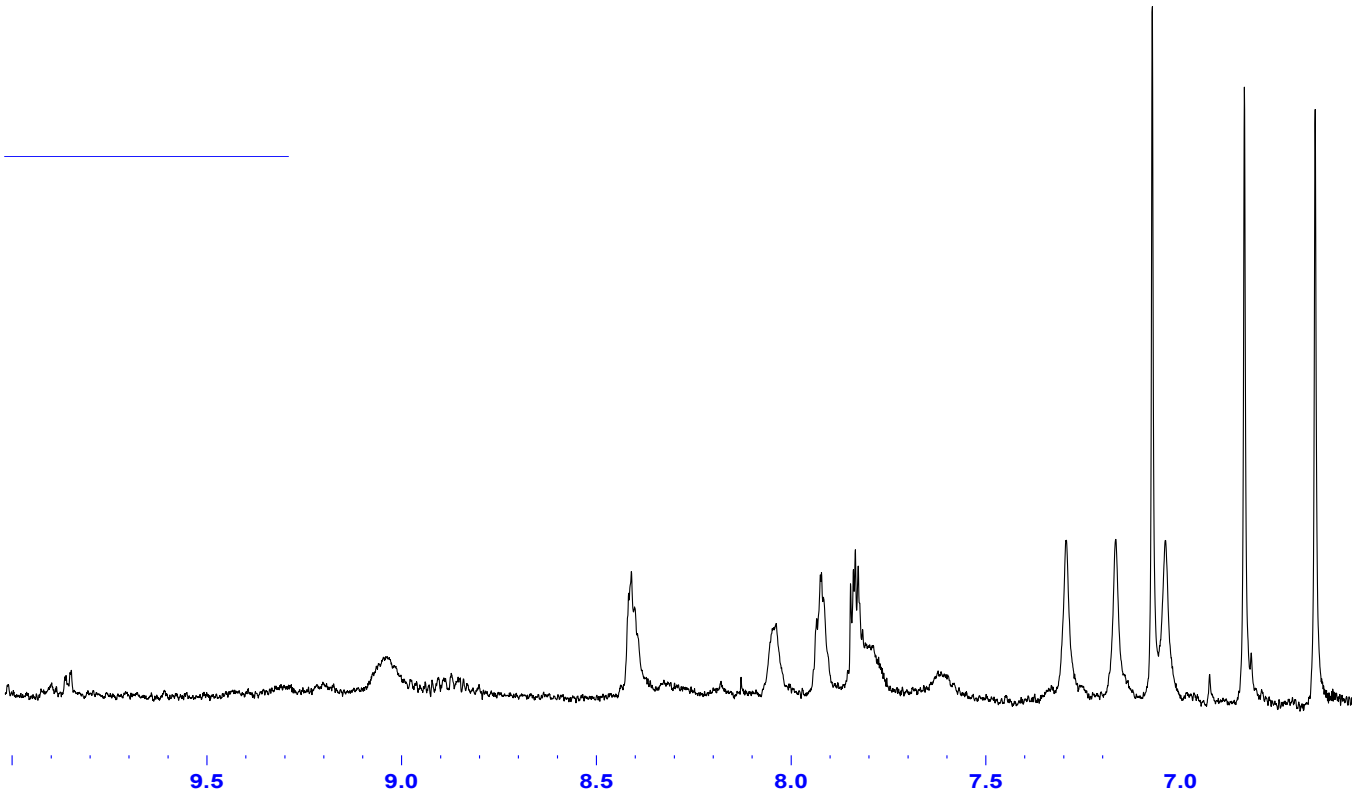

Figure 5.14: ^1H NMR spectrum (1000 scan) as measured in d_6-DMSO of the third fraction of purified solid represented by the spectrum shown in Figure 5.11 as purified by column chromatography on silica using 80: 20 acetonitrile: water 0.05 M KNO_3 as eluent

This broad spectrum bears resemblances to both the ^{1}H NMR spectrum obtained (shown above in Figure 5.7) for the product obtained in the attempted [Ru(thimphen)$_2$Cl$_2$] reaction incorporating LiCl, carried out in DMF as well as to the ^{1}H NMR spectrum of the uncoordinated ligand thimphen. A comparison between these spectra is shown below in Figure 5.15.

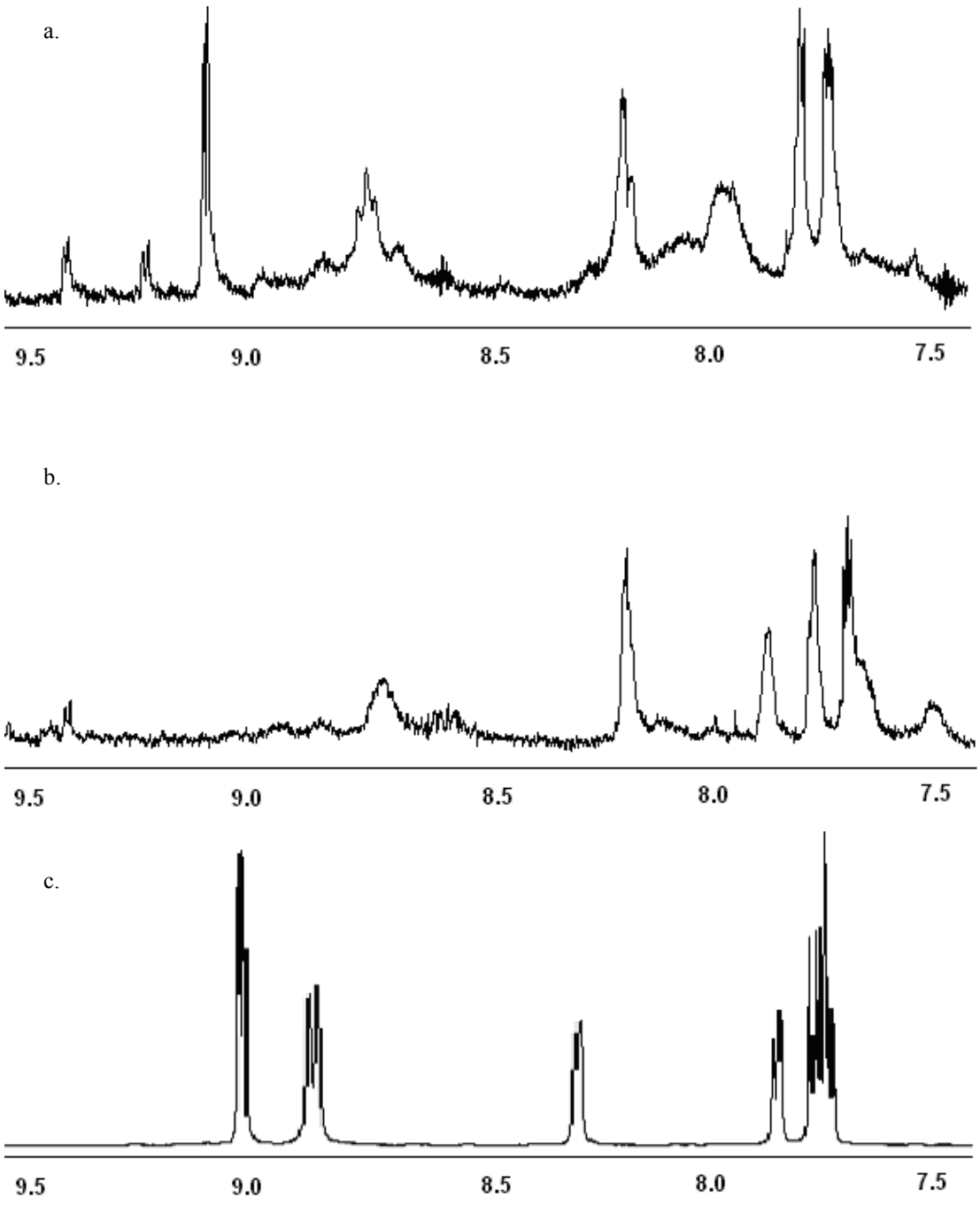

Figure 5.15: ^1H NMR spectra of (a) product from DMF/LiCl $Ru(thimphen)_2Cl_2$ attempted reaction (b) purified product from MeOH/ascorbic acid $Ru(thimphen)_2Cl_2$ attempted reaction and (c) pure thimphen as measured in d_6-DMSO

The spectra shown in Figure 5.15 (b) and (c) both display five peaks with the signals present in Figure 5.15 (b) appearing at slightly upfield chemical shift values compared to the corresponding signals present in the spectrum of the pure, uncoordinated ligand shown in Figure 5.15 (c). This information indicates that the 'purified' product

obtained from the attempted $Ru(thimphen)_2Cl_2$ reaction incorporating ascorbic acid and carried out in methanol consists of uncoordinated ligand only. The upfield shift observed in the spectrum of this product may be attributed to residual ascorbic acid present in the sample.

The spectrum shown in Figure 5.15 (a), corresponding to the product obtained from the attempted synthesis of $[Ru(thimphen)_2Cl_2]$ using DMF and LiCl, shows six signals as opposed to the five observed in Figure 5.15 (b) and (c). It is possible that the extra signal observed in Figure 5.15 (a) is due to the resolution of the overlapping signals present at 7.55 ppm in the spectrum of uncoordinated thimphen (Figure 5.15 c) into two distinct signals, or it is possible that a new species has been formed.

In order to investigate whether the solid corresponding to the ^1H NMR spectrum shown in Figure 5.15 (a) contained the desired dichloride starting material $[Ru(thimphen)_2Cl_2]$ (any further mention of $[Ru(thimphen)_2Cl_2]$ shall refer to this solid), synthesis of the metal complex $[Ru(thimphen)_2(bpy)]^{2+}$ (encountered previously in Chapter 4) was attempted using $[Ru(thimphen)_2Cl_2]$ as a starting material.

5.2.1.2 Attempted synthesis of $[Ru(thimphen)_2(bpy)]^{2+}$

In this attempted synthesis 100 mg $[Ru(thimphen)_2Cl_2]$ (0.13 mmol) was refluxed at 120^0C with 25 mg bpy (0.15 mmol) in 10 cm^3 2:1 ethanol: water for 3 hr. The resulting dark orange suspension was filtered to remove a small amount of brown solid. A saturated aqueous solution of KPF_6 was added to the orange filtrate to precipitate an orange/brown solid, which was removed by vacuum filtration. Both solids collected were sent for ^1H NMR analysis. The brown solid obtained directly from the reaction mixture yielded a spectrum displaying no visible peaks. The orange/brown $–PF_6$ salt precipitated from the reaction solution yielded a noisy, but relatively coherent spectrum. Following column chromatography on neutral alumina using acetonitrile as eluent the cleaner spectrum shown below in Figure 5.16 (a) was obtained.

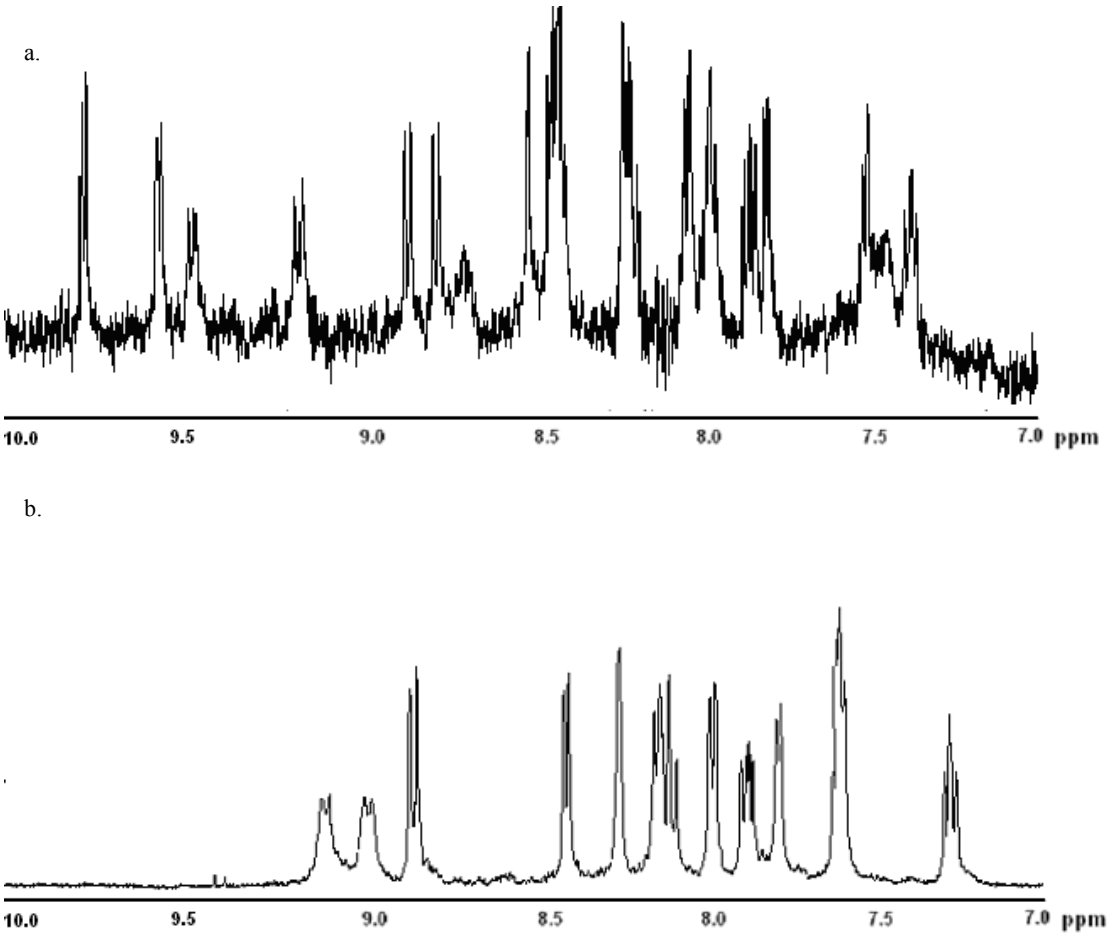

Figure 5.16: ^{1}H NMR spectra in d_6-acetone of (a) $[Ru(thimphen)_2(bpy)]^{2+}$ synthesised by reaction between $[Ru(thimphen)_2Cl_2]$ and 2,2'-bipyridyl and (b) $[Ru(thimphen)_2(bpy)]^{2+}$ as synthesised by modification of the precursor complex $[Ru(phen)_2(bpy)]^{2+}$ (c.f. *Chapter 4)*

Figure 5.16 displays a comparison between two $[Ru(thimphen)_2(bpy)]^{2+}$spectra, one of which (Figure 5.16 a) is the result of the reaction between $[Ru(thimphen)_2Cl_2]^{2+}$ and 2,2'-bipyridyl as described in this chapter, the other resulting from modification of $[Ru(phen)_2(bpy)]^{2+}$ as discussed in chapter 4. Though Figure 5.16 (a) displays much more background noise than Figure 5.16 (b) and a sizeable shift is visible in a number of peaks going from one spectrum to the other, a large amount of similarity is also visible. Figure 5.16 (a) displays 17 discernable peaks while Figure 5.16 (b) displays 12. As Figure 5.16 (b) contains a number of overlapping signals the appearance of 'extra' signals in Figure 5.16 (a) does not necessarily imply that the correct complex is not present. It is possible that due to the different reaction medium a certain element of asymmetry is present in the spectrum shown in Figure 5.16 (a) that is not evident in Figure 5.16 (b). This may be confirmed by comparing the peaks

present in Figure 5.16 a between 10.00 ppm and 8.70 ppm to the peaks present in Figure 5.16 (b) between 9.30 ppm and 8.70 ppm. Instead of two doublets and a broad doublet of doublets visible between 9.30 ppm and 8.70 ppm as seen in Figure 5.16 (b) each integrating for two protons, Figure 5.16 (a) displays six distinct doublets between 10.00 ppm and 8.70 ppm each integrating for one proton. A distinctive singlet is also present in Figure 5.16 (a) at 8.48 ppm which is characteristic of the ligand thimphen (*c.f.* Chapter 3). However, the integration values for Figure 5.16 (a) total 22 which does not correspond with the 26 protons present in the $[Ru(thimphen)_2(bpy)]^{2+}$ molecule. It is possible however that the correct integration for the signals shown in Figure 5.16 (a) cannot be measured accurately on account of the background noise evident in the sample. Also the sample analysed was too weak or impure to obtain a readable COSY spectrum and so the signals evident in Figure 5.16 (a) have not been definitively assigned. However, the result obtained from the reaction of $[Ru(thimphen)_2Cl_2]$ with 2,2'-bipyridyl yielded encouraging results indicating the possibility of a successful synthesis of $[Ru(thimphen)_2Cl_2]$ by the method decided on previously.

Simultaneous to these $[Ru(thimphen)_2(bpy)]^{2+}$ reactions an attempt was made to construct a dinuclear complex using $[Ru(thimphen)_2Cl_2]$ as a reactant. These reactions shall be discussed in section 6.2.1.3 below.

5.2.1.3 Attempted synthesis of dinuclear species containing the group [Ru(thimphen)$_2$-]

As shown in Figure 5.2 the reaction of a dichloride metal complex starting material with a second metal complex containing a free chelating site will yield a dinuclear metal complex. This complex may be homodinuclear (when the metal centres present in the dinuclear metal complex are identical) or heterodinuclear (when the metal centres present in the dinuclear metal complex are different). For the purposes of this project (as outlined in chapter 1) osmium polypyridyl type complexes are the best theoretical candidates for molecular diode synthesis and so the osmium bis-bipyridyl complex $[Os(bpy)_2(bpt)]^{2+}$ was used for reaction with $[Ru(thimphen)_2Cl_2]$ to construct a heterodinuclear complex. As the purity of the dichloride starting material

$[Ru(thimphen)_2Cl_2]$ was unknown, the mononuclear complex $[Os(bpy)_2(bpt)](PF_6)$ was synthesised and purified using effective and well documented methods of synthesis and purification. [19] As a result any large impurity may be attributed to the dichloride sample used, with no interference resulting from the bpt monomer used in the reaction.

The dimer reactions attempted followed a previously published procedure.[15] The dichloride starting material $[Ru(thimphen)_2Cl_2]$ was refluxed with the metal complex $[Os(bpy)_2(bpt)](PF_6)$ in 1:1 ethylene glycol: water overnight. The resulting metal complex was precipitated as the PF_6 salt. Purification by column chromatography was carried out using a silica stationary phase and 80: 20 acetonitrile: water 0.05M KNO_3 as eluent; a system used previously for the purification of dinuclear species.[19] However, when these 'post column' samples were analysed by ^1H NMR, a large amount of residual impurity was evident. Following a second purification by the same method, a slightly cleaner spectrum was obtained, but impurity was still apparent. An example of this is shown below in Figure 5.17.

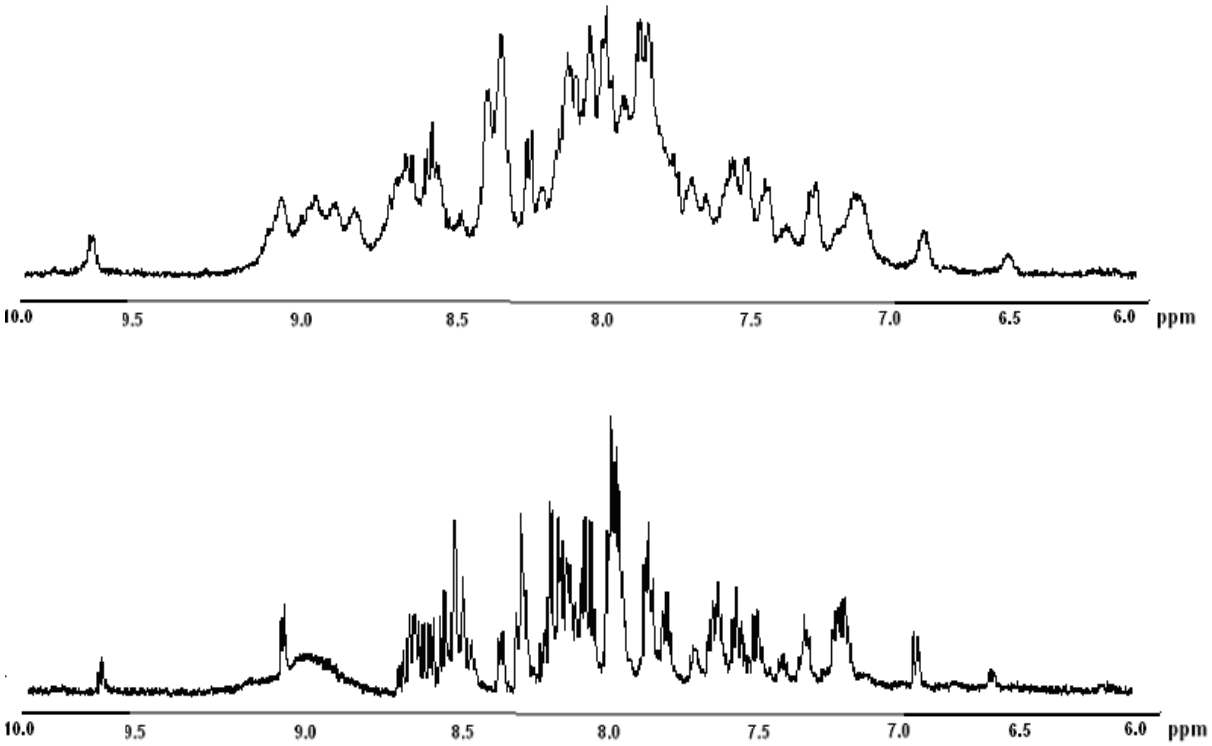

Figure 5.17: ^1H NMR spectrum in d_3-acetonitrile of (a) $[Ru(thimphen)_2(bpt)Os(bpy)_2]^{3+}$ after one column on silica using 80:20 acetonitrile: water 0.05M KNO_3 and (b) $[Ru(thimphen)_2(bpt)Os(bpy)_2]^{3+}$ after two columns using the same system.

Comparing the sharper spectrum shown in Figure 5.17 (b) to the published[16] ^{1}H NMR spectrum for the heterodinuclear complex $[Ru(bpy)_2(bpt)Os(bpy)_2]^{3+}$ on the same scale, certain similarities may be identified.

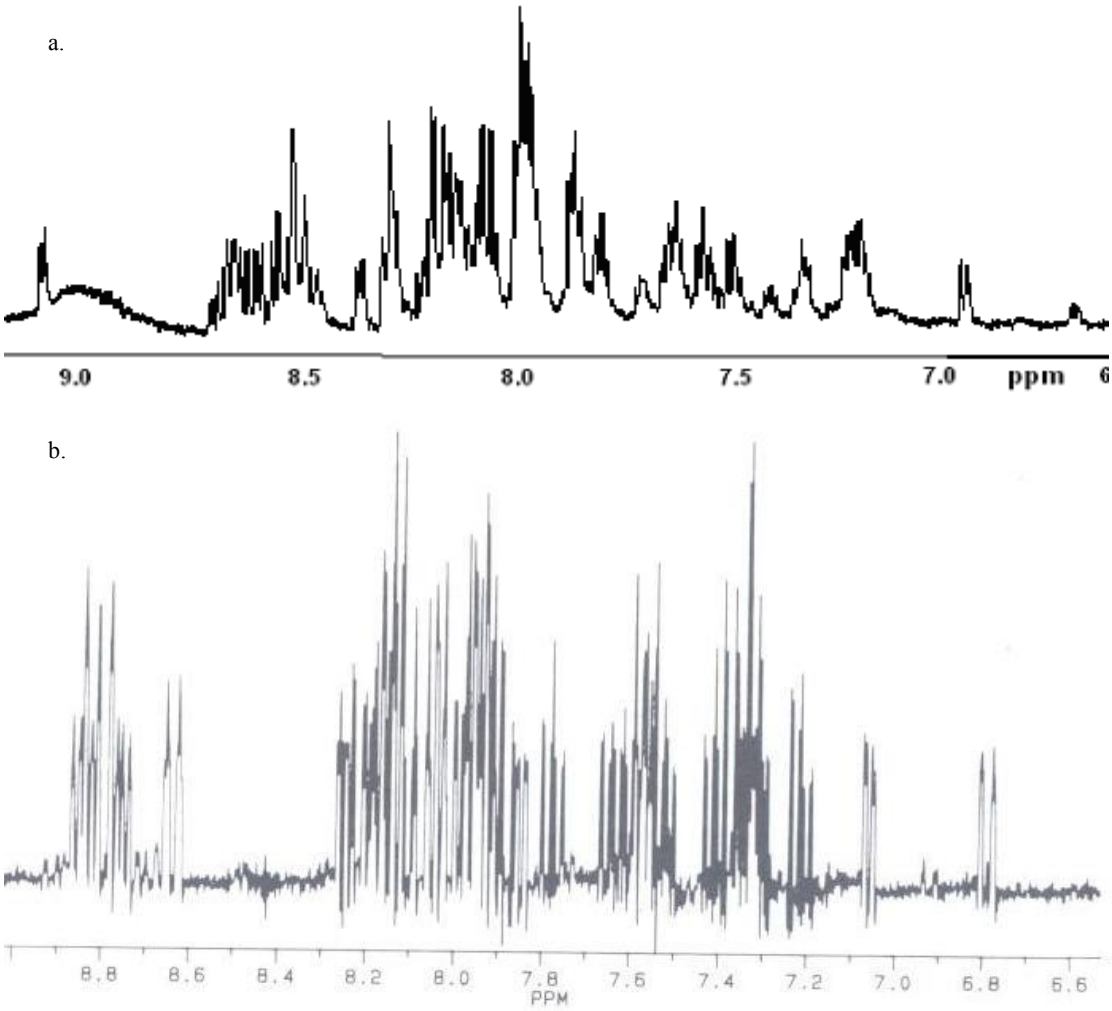

Figure 5.18: ^{1}H NMR spectrum of (a) $[Ru(thimphen)_2(bpt)Os(bpy)_2]^{3+}$ after two columns on silica using 80:20 acetonitrile: water 0.05M KNO_3 as eluent in d_3-acetonitrile and (b) $[Ru(bpy)_2(bpt)Os(bpy)_2]^{3+}$ as measured in d_6-acetone

A definite similarity can be seen between the spectra shown in Figure 5.18 regardless of the spectra being measured in different solvents. However, the broadness apparent at approximately 9.0 ppm in Figure 5.18 (a) does imply that there is still some impurity present in the $[Ru(thimphen)_2(bpt)Os(bpy)_2]^{3+}$ sample synthesised.

Further column chromatography was deemed unfeazible due to dwindling amounts of compound, and so in order to better examine the system the compounds obtained thus far were examined by HPLC using the same system as used in chapter 4/6. The HPLC

chromatogram for $[Ru(thimphen)_2(bpt)Os(bpy)_2]^{3+}$ purified once by column chromatography.

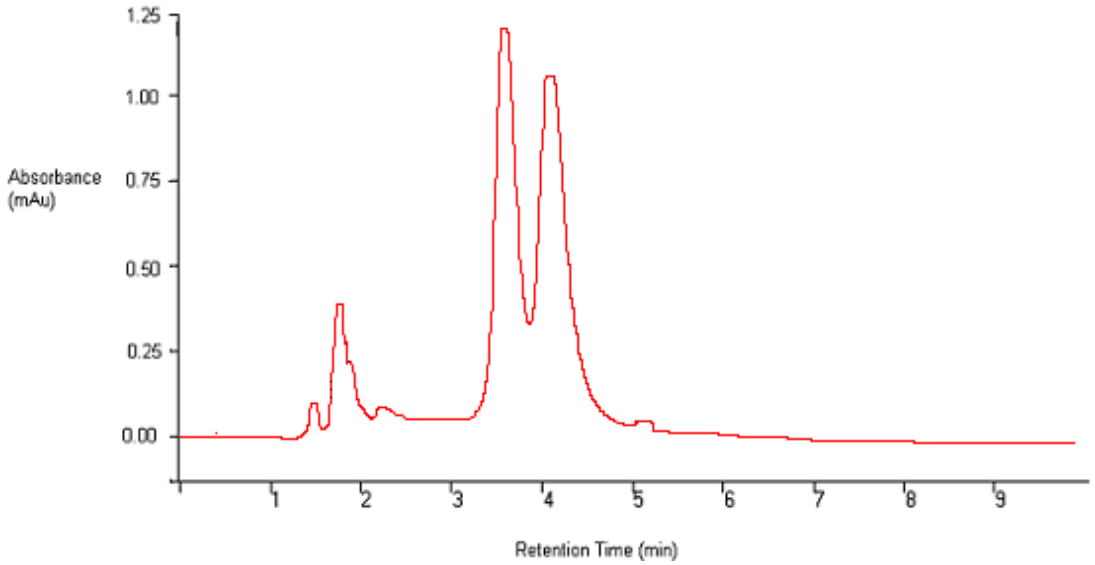

Figure 5.19: HPLC chromatogram for $[Ru(pyrphen)_2(bpt)Os(bpy)_2]^{3+}$ purified once by column chromatography

The chromatogram shown above in Figure 5.19 shows three main components in the sample analysed, one occurring at a retention time of 1.81 min, the next at 3.37 min and the last at 3.80 min. The small peaks at approximately 1.5 min, 2.1 min and 4.6 min all show organic type absorbance spectra, similar to that pictured below in Figure 5.20. As a reult it has been assumed that these peaks relate to species consisting of (a) solvent, (b) organic matter such as free ligand or (c) contain a miniscule amount of inorganic matter and so is of no concern.

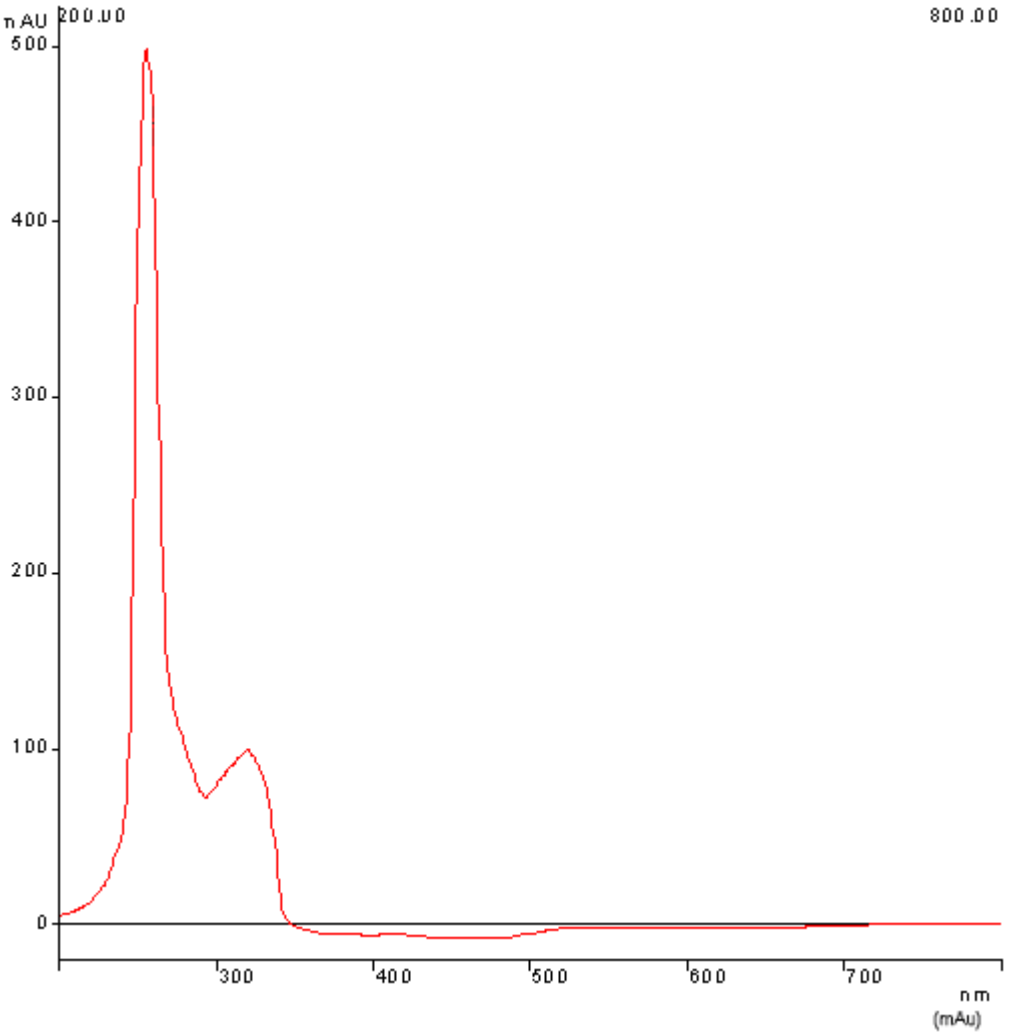

Figure 5.20: UV/vis spectrum of the peak appearing at 1.58 min retention time in Figure 5.19.

The peak appearing at a retention time of 1.81 min in Figure 5.19 yields the UV/vis spectrum shown below in Figure 5.21.

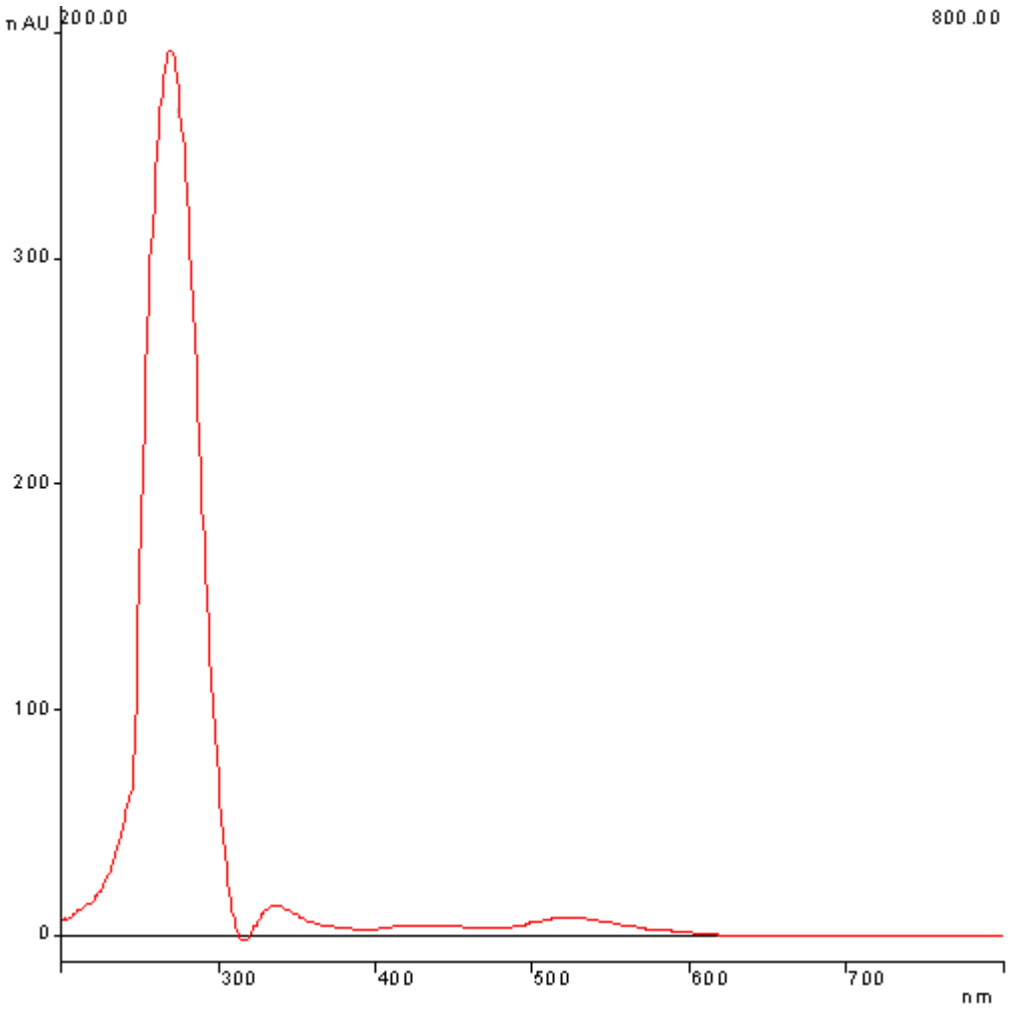

Figure 5.21: UV/vis spectrum of the peak appearing at 1.81 min retention time in Figure 5.19.

This spectrum despicts two organic type bands, one at 269 nm (most likely due to solvent) and 336 nm (most likely due to ligand). The second band at 336 nm has been attributed to a ligand species as it is comparable in intensity to the third band appearing at 530 nm. This band at 530 nm is indicative of an osmium type complex. The maximum absorbance (λ_{max}) of $[Os(bpy)_3]^{2+}$ is 486 nm, and for $[Os(bpy)_2(bpt)]^{+}$ is 486 nm with a ^{3}MLCT band visible at 610 nm[19]. Here, the band visible at 530 nm in Figure 5.21 is much closer in value to the expected λ_{max} value of 486 nm for $[Os(bpy)_2(bpt)]^{+}$ than the expected λ_{max} value of 450 nm attributable to a ruthenium polypyridyl type complex[19]. It is therefore assumed that this peak relates to unreacted $[Os(bpy)_2(bpt)]^{+}$.

The UV/vis spectrum of the peak visible at 3.37 nm is shown below in Figure 5.22.

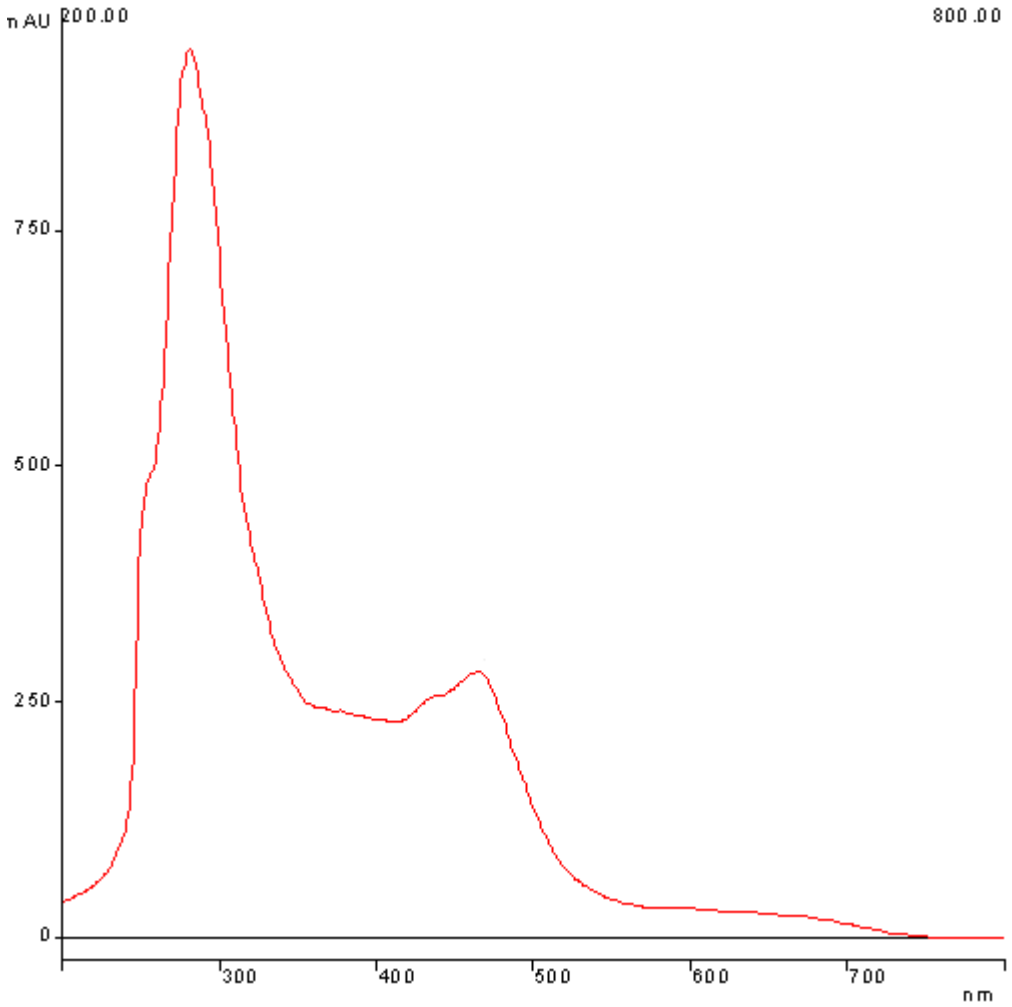

Figure 5.22: UV/vis spectrum of the peak appearing at 3.37 min retention time in Figure 5.19.

The spectrum above displays an organic type band at 291 nm, attributable to solvent or ligand type species, as well as two other main bands at 464 nm with a shoulder at 430 nm and 605 nm. These values are indicative of a ruthenium-osmium dinuclear complex. Similar UV/vis spectra have been recorded for the similar heterodinuclear complex $[Ru(bpy)_2(pytr\text{-}bpy)Os(bpy)_2]^{3+}$.[19] This dinuclear complex also contains as triazole group and so is highly comparable to the dinuclear complex $[Ru(pyrphen)_2(bpt)Os(bpy)_2]^{3+}$ whose synthesis is being attempted here.

The UV/vis spectrum for $[Ru(bpy)_2(pytr\text{-}bpy)Os(bpy)_2]^{3+}$ as measured in acetonitrile is shown below in Figure 5.23.

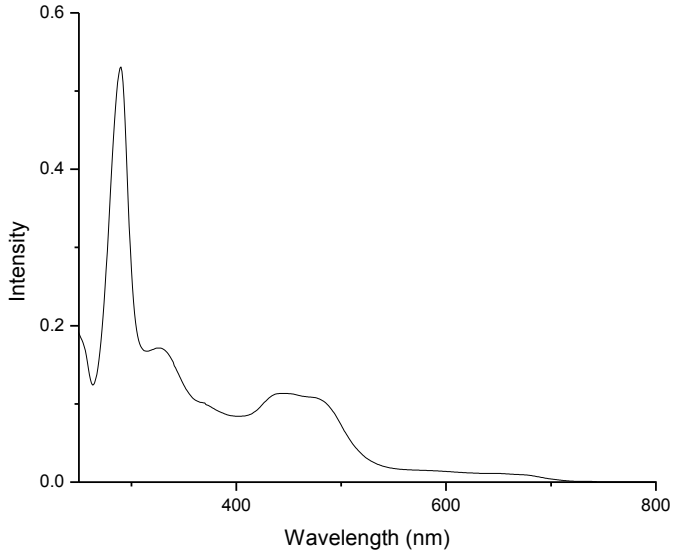

Figure 5.23: UV/vis spectrum of the heterodinuclear metal complex $[Ru(bpy)_2(pytr\text{-}bpy)Os(bpy)_2]^{3+}$ [19]

The UV/vis spectrum shown in Figure 5.23 also displays an intense organic type absorbance at 295 nm, as well as two inorganic type absorbances present at 445 nm and 622 nm. The more intense of the two bands at 445 nm may be attributable to ^{1}MLCT transitions while the band of lower intensity at 622 nm is attributable to formally forbidden ^{3}MLCT transitions which are allowed in this case by increased spin orbit coupling due to the presence of an osmium centre in the complex. The fact that this spectrum corresponds so well with that of the sample component shown in Figure 5.22 implies that a dinuclear complex *has* infact been formed, but has not, at this stage, been sufficiently purified.

The UV/vis spectrum of the peak appearing at 3.80 min retention time in Figure 5.19 is shown below in Figure 5.24.

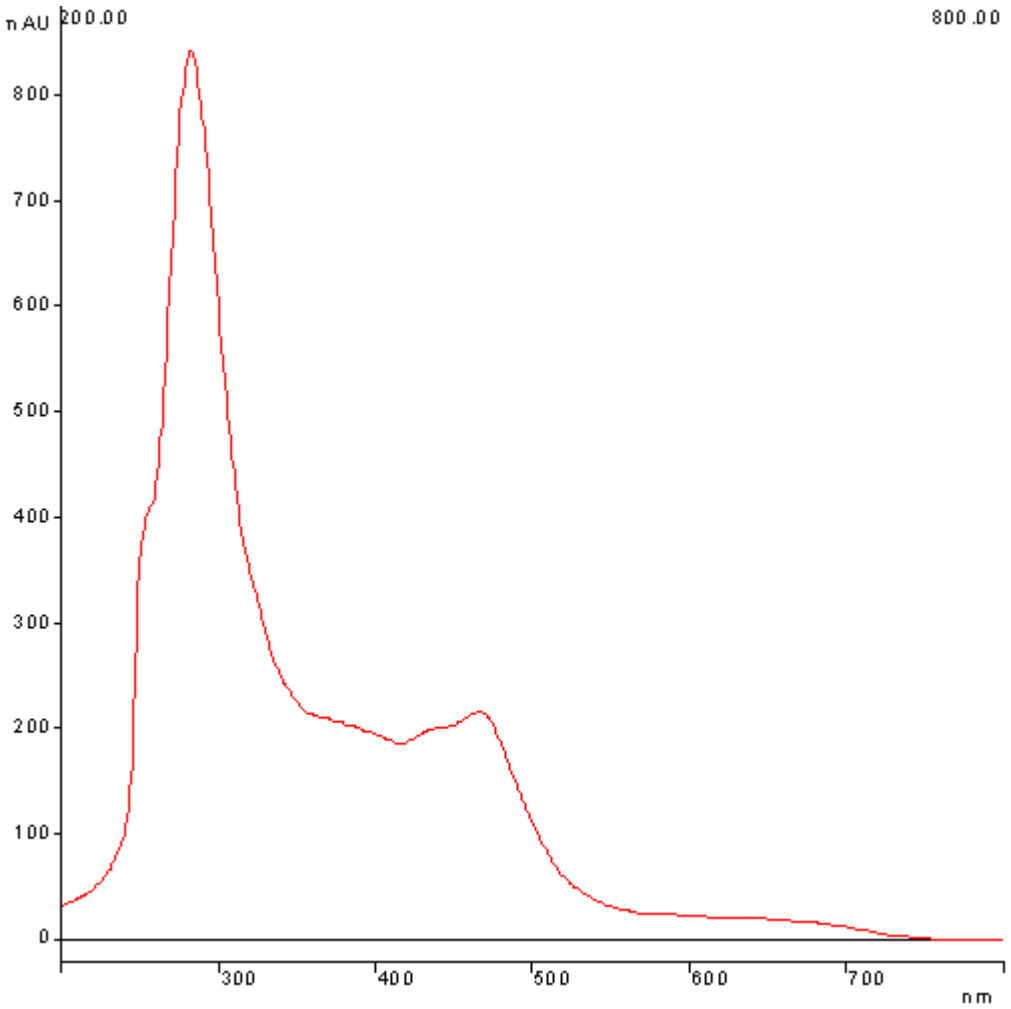

Figure 5.24: UV/vis spectrum of the peak appearing at 3.80 min retention time in Figure 5.19.

The spectrum shown above in Figure 5.24 is very similar to that shown in Figure 5.22, with a main ^{1}MLCT absorbance visible at 466 nm with a shoulder at 425 nm and a second lower intensity ^{3}MLCT band visible at 620 nm. This component must also consist of a heterodinuclear complex given its resemblance to the UV/vis spectrum of $[Ru(bpy)_2(pytr\text{-}bpy)Os(bpy)_2]^{3+}$ as shown in Figure 5.23. It must also be very similar in structure to the component eluting at 3.37 min given their similarity in both retention time and the overall shape of their absorbance spectra. It stands to reason that the compounds corresponding to the peaks at 3.37 min and 3.80 min retention time in Figure 5.19 may be the N_2 and N_4 isomers of the metal complex $[Ru(phen)_2(bpt)Os(bpy)_2]^{3+}$. Formation of these isomers is dependant on the point at which metal atoms coordinate to the bpt triazole ring, the nitrogen labelled N_2 or the

nitrogen labelled N_4. The structure of both isomers is shown diagrammatically in Figure 5.25.

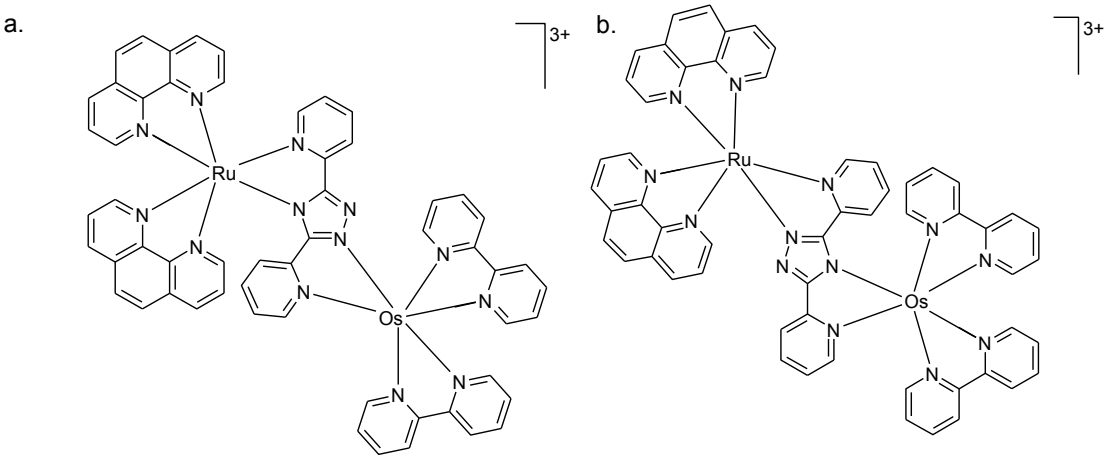

Figure 5.25: Diagrammatical representation of (a) the N_2 isomer and (b) the N_4 isomer of the heterodinuclear metal complex $[Ru(phen)_2(bpt)Os(bpy)_2]^{3+}$

The sample analysed above (i.e. for which the analysis shown in Figure 5.19 relates to) was purified a second time by column chromatography and analysed by HPLC analysis. The HPLC chromatogram obtained for this repurified sample is shown below in Figure 5.26.

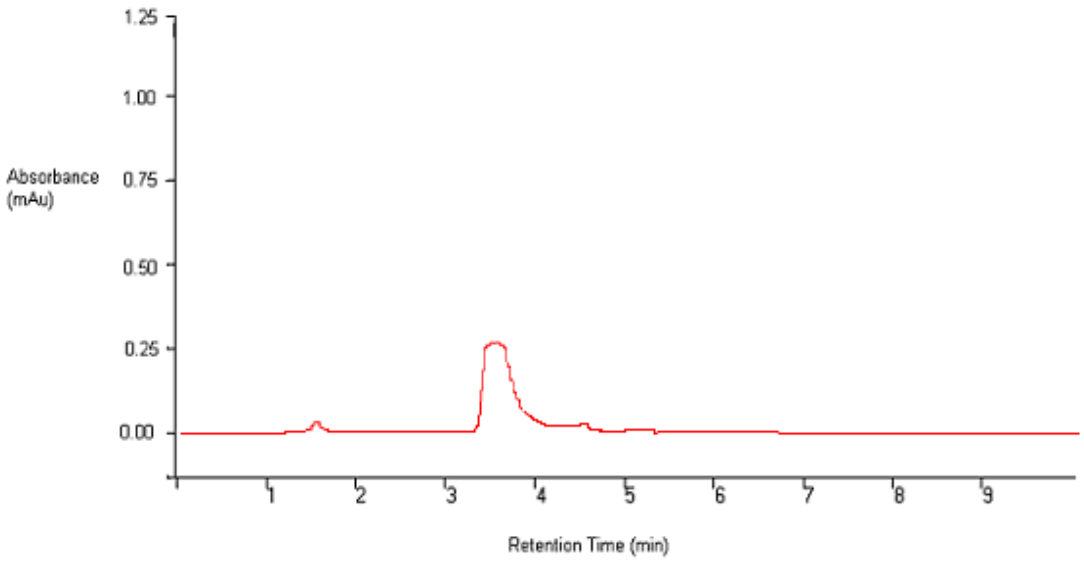

Figure 5.26: HPLC chromatogram for $[Ru(pyrphen)_2(bpt)Os(bpy)_2]^{3+}$ purified twice by column chromatography

The chromatogram shown in Figure 5.26 displays one main peak at retention time 3.44 min as well as a small peak at 1.81 min retention time. As before this early

eluting peak displays no inorganic matter in its UV/vis spectrum (shown below in Figure 5.27) only an organic type absorbance at 269 nm, most likely due to solvent.

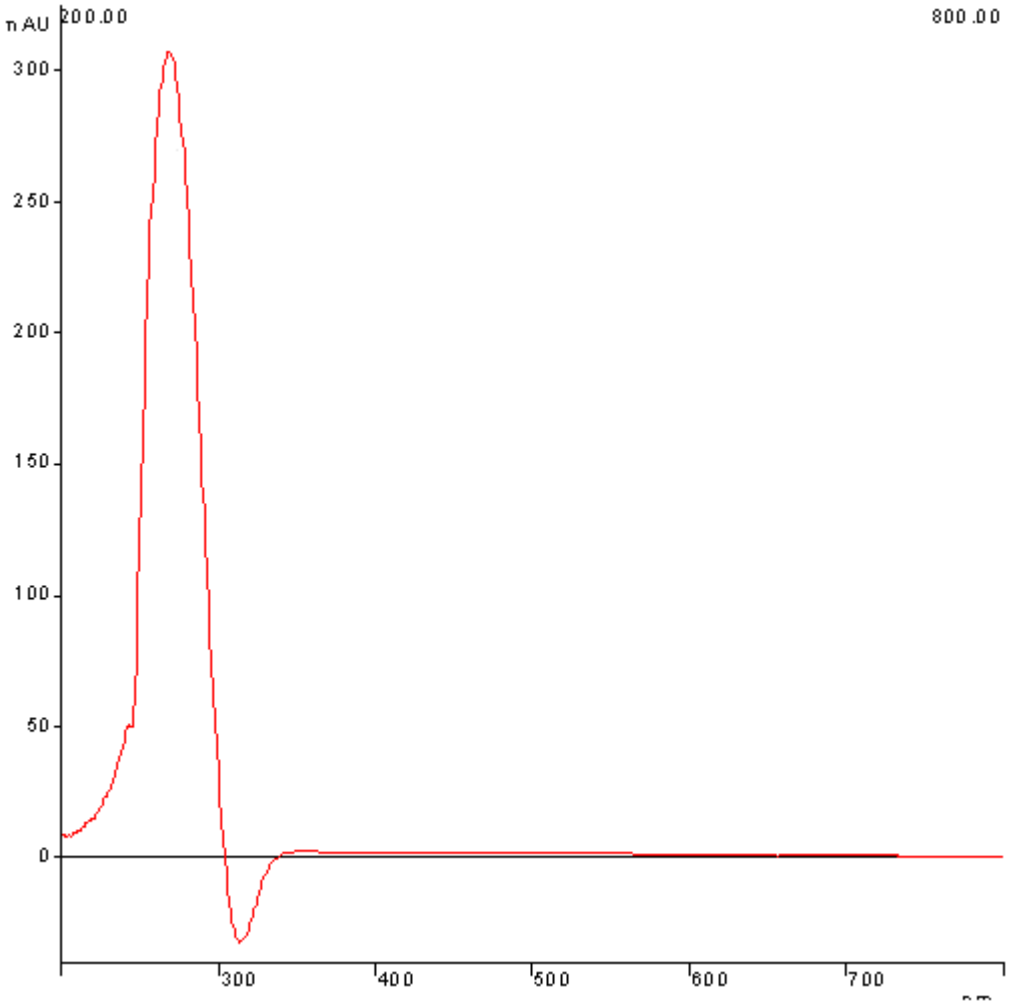

Figure 5.27: UV/vis spectrum of the peak appearing at 1.81 min retention time in Figure 5.26

The later eluting peak displays quite a different absorbance spectrum, shown below in Figure 5.28.

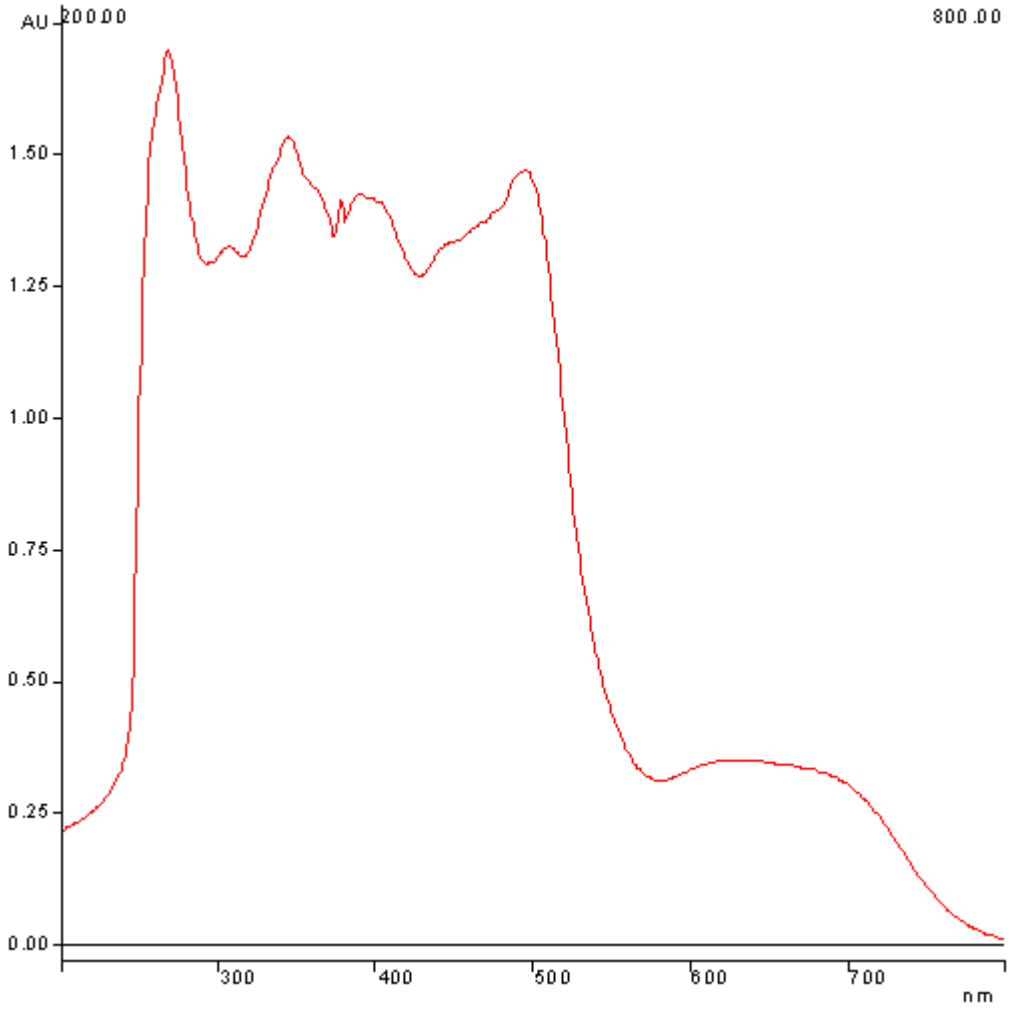

Figure 5.28: UV/vis spectrum of the peak appearing at 3.44 min retention time in Figure 5.26

Examining Figure 5.28 it can be seen that a dinuclear complex is present. An intense band at 495 nm is present as well as a pronounced, though less intense band at 650 nm. This compares very well with the data discussed above for Figure 5.22 and Figure 5.24. However, a flurry of other absorbance activity is visible between 268 nm and 495 nm, with two visible peaks at 345 nm and 398 nm. This does not compare well with the UV/vis spectrum of the purified dinuclear complex shown in Figure 5.23 and so it is highly possible that the sample is still not completely pure. This is in agreement with the ^{1}H NMR data discussed previously in this chapter and the spectrum shown in Figure 5.17.

In order to confirm the presence of a dinuclear ruthenium-osmium complex, the emission properties of the twice columned $[Ru(thimphen)_2(bpt)Os(bpy)_2]^{3+}$ were measured. In a ruthenium-osmium dinuclear complex in which a bridging ligand

allowing electronic communication is employed, excitation of the ruthenium centre will result in emission from the osmium centre. This is due to electron/energy transfer from the ruthenium centre following light absorption to the osmium via the bridging ligand. An electron is promoted to a higher energy level within the osmium centre by the transferred energy and then returns to its ground state, emitting a photon displaying a wavelength charateristic of osmium emission instead of ruthenium emission. The emission spectrum of $[Ru(thimphen)_2(bpt)Os(bpy)_2]^{3+}$ when excited at 490 nm is shown below in Figure 5.29

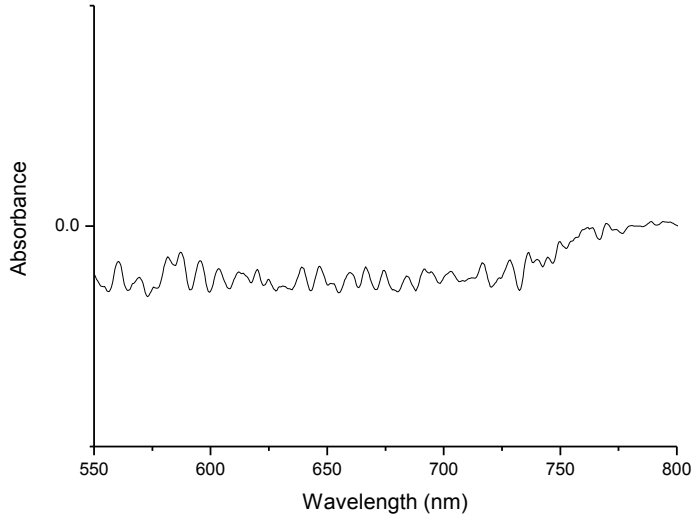

Figure 5.29: Emission spectrum for $[Ru(thimphen)_2(bpt)Os(bpy)_2]^{3+}$ as measured in acetonitrile using 490 nm as an excitation wavelength

A slight emission present at 788 nm is visible in Figure 5.29. This wavelength is characteristic of osmium, with the emission value for the model complex $[Os(bpy)_3]^{2+}$ occurring at 732 nm. The low intensity of the emission observed here may be due to a low concentration of actual pure sample as a result of present impurity or excess counterion salt (in this case KPF_6). The excitation wavelength of 490 nm may also not be the wavelength of maximum absorbance, it is difficult to discern a suitable λ_{max} value in the UV/vis spectrum shown in Figure 5.28 attributable to the ruthenium centre of the molecule.

The fact that there is no emission present at approximately 600 nm implies that the ruthenium centre displays no emission properties in this molecule. This information coupled with the HPLC data shown in Figure 5.26 does imply that the metal complex $[Ru(thimphen)_2(bpt)Os(bpy)_2]^{3+}$ has been synthesised.

5.3 Conclusion

Chapter 6 discusses the attempted synthesis of dinuclear complexes incorporating two novel surface active ligands. The approach employed here involved the synthesis of a ruthenium dichloride type starting material containing two novel 'thimphen' ligands. A number of different approaches were taken when attempting to synthesise this complex including the widely used LiCl reaction in DMF as used for $[Ru(bpy)_2Cl_2]$[17] as well as the method outlined in Chapter 6 for dichloride synthesis incorporating ascorbic acid. The most effective method was found to be reflux of $RuCl_3$ and thimphen in DMF with LiCl. However, a completely pure $[Ru(thimphen)_2Cl_2]$ sample was not obtained. The most encouraging sample was taken and used to attempt the synthesis of the mononuclear complex $[Ru(thimphen)_2(bpy)]^{2+}$ (*c.f.* Chapter 4) as well as a ruthenium-osmium linked dinuclear metal complex. Both reactions yielded encouraging results. The mononuclear complex $[Ru(thimphen)_2(bpy)]^{2+}$ yielded a ^1H NMR spectrum very similar to that obtained for the same compound synthesised by a different pathway in Chapter 4. Although more purification is needed, the dinuclear complex $[Ru(thimphen)_2(bpt)Os(bpy)_2]^{3+}$ displays a ^1H NMR spectrum very similar to that of the previously published dinuclear complex $[Ru(bpy)_2(bpt)Os(bpy)_2]^{3+}$. The HPLC, UV/vis and emission data obtained for this complex also indicate that a ruthenium-osmium heterodinuclear complex has been synthesised. However, in order to obtain coherent spectral data for this dinuclear species lengthy purification was required and full purification of the sample was not achieved. It is the opinion of the researcher that if a slightly more effective method for synthesis and purification of the dichloride starting material $[Ru(thimphen)_2Cl_2]$ was developed the methods detailed in this chapter would most likely provide an elegant method for the construction of dinuclear complexes containin two surface active ligands.

5.4 Experimental

Materials

$[Ru(bpy)_2Cl_2].2H_2O$[17], $[Os(bpy)_2Cl_2].2H_2O$[18] $[Ru(bpy)_2(bpt)]PF_6$' [19], $[Ru(d_8\text{-}bpy)_2(bpt)]PF_6$'[19], $[Os(bpy)_2(bpt)]PF_6$' [19]and $[Os(d_8\text{-}bpy)_2(bpt)]PF_6$'[19] were synthesised according to established literature procedures. Thimphen was synthesised as described in Chapter 3 of this thesis. All other chemicals were purchased from Sigma-Aldrich and used without further purification. All synthetic solvents used were of reagent grade. All solvents used for spectroscopic measurements were of HPLC grade.

5.4.1 Synthesis of Mononuclear starting materials

$Ru(thimphen)_2Cl_2$ (DMF/LiCl Method)

This complex was synthesised in the same manner as for $[Ru(bpy)_2Cl_2].2H_2O$[17]. 5 cm^3 DMF was degassed for 10 min. 68 mg (0.33 mmol) $RuCl_3.3H_2O$, 200 mg (0.66 mmol) thimphen and 60 mg (1.58 mmol) LiCl were placed in the solvent and the mixture was further degassed for 20 min. The resulting green mixture was refluxed for 8 hr under N_2 flow. The purple solution was cooled to room temperature and 25 cm^3 acetone was added. The mixture was left at 0 ^{0}C overnight. The resulting purple/black suspension was vacuum filtered and the black solid collected was washed with deionised water until a colourless filtrate was obtained.

Yield: 54% (138 mg)

Attempted Synthesis: $Ru(thimphen)_2Cl_2$ (ascorbic acid method)

This attempted synthesis follows the same method as for synthesis of the complex $[Ru(paen)Cl_2]$ (*c.f.* Chapter 6). 85 mg (0.41 mmol) $[RuCl_3].2H_2O$ was refluxed with 1.46 g (8.27 mmol) ascorbic acid in 30 cm^3 methanol for one hour after which a colour change from brown to green was observed. 250 mg (0.83 mmol) thimphen was added to the reaction mixture which was then refluxed overnight. The resulting dark suspension was filtered yielding a black residue. This solid was purified by column chromatography on silica using 80: 20 acetonitrile: water 0.05M KNO_3 buffer as eluent.

Yield: 13% (40 mg)

Attempted Synthesis: $Ru(thimphen)_2Cl_2$ (ethanol reflux method)

This attempted synthesis follows a published procedure[12]. 68 mg $[RuCl_3].2H_2O$ (0.33 mmol) and 200 mg thimphen (0.66 mmol) were refluxed in ethanol under N_2 atmosphere for 3 days. The resulting brown suspension was filtered and both residue and filtrate were retained. Diethyl ether was added to the orange filtrate to yield a yellow solid which was collected by filtration. Both solids obtained were analysed by ^1H NMR with the brown solid obtained directly from the reaction solution was identified as a possible dichloride material

Yield: 10 % (51 mg)

5.3.2 Attempted Syntheses of Dinuclear Species

$[Ru(thimphen)_2(bpy)](PF_6)_3$

100 mg (0.13 mmol) $Ru(thimphen)_2Cl_2$ and 25 mg (0.15 mmol) bpy were placed in 10 cm^3 1:1 ethanol: water and refluxed for 3 hr.. The reaction mixture was cooled to room temperature and the ethanol removed in vacuo. A saturated solution $_{(aq)}$ KPF_6 was added to the solution to precipitate the product. The orange/ brown solid was collected and purified by column chromatography on neutral alumina using acetonitrile as eluent.

Yield: 10% (15 mg) (slightly impure)

$[Ru(thimphen)_2(bpt)Os(bpy)_2](PF_6)_3$

31 mg (0.03 mmol) $[Os(bpy)_2(bpt)]PF_6$ and 21 mg (0.03 mmol) $Ru(thimphen)_2Cl_2$ were placed in 5 cm^3 1:1 ethylene glycol: water and heated to reflux overnight. The reaction mixture was cooled to room temperature and a saturated solution $_{(aq)}$ of KPF_6 was added to the reaction mixture to precipitate the product. The dark orange/brown solid was collected by vacuum filtration and purified twice by column chromatography on silica using 80:20 acetonitrile: water 0.05M KNO_3 as eluent.

Yield: 24% (11 mg) (slightly impure)

5.5 Bibliography

[1] P.J. Low *Dalton Trans.* (2005) 2821-2824

[2] J.M. Tour *Acc. Chem. Res.* **33**, (2000) 791-804

[3] T. Albrecht, K. Moth-Poulsen, J.B. Christensen, A. Guckian, T. Bjørnholm, J.G. Vos, J. Ulstrup, *Faraday Discuss.* **131**, (2006) 265-279

[4] V. Balzani, A, Juris, M, Venturi, S. Campagna, S. Serroni; *Chem. Rev.*; **96**; (1996); 759-833

[5] W-J. Mei, J. Liu, H. Chao, L-N. Ji, A-X. Li, J-Z. Liu, *Transition Metal Chemistry,* **28**, (2003) 852.

[6] J. Liu, J-W. Huang, H. Shen, H. Wang, H-C. Yu, L-N. Ji, *Dyes and Pigments,* **77** (2008) 374

[7] C-W. Jiang, H. Chao, R-H. Li, H. Li, L-N. Ji, *Polyhedron*, **20** (2001) 2187

[8] G. Denti, S. Campagna, S. Serroni, M. Ciano, V. Balzani, *J. Am. Chem. Soc*. **114,** (1992), 2944.

[9] G. Denti, S. Serroni, S. Campagna, A. Juris, M. Ciano, V. Balzani, *In Perspectives in Coordination Chemistry*; Ed: A. F. Williams, C. Floriani, A. E. Merbach, VCH: Basel, Switzerland, (1992), 53

[10] J. P. Sauvage, J.P. Collin, J.C. Chambron, S. Guillerez, C. Coudret, V. Balzani, F. Barigelletti, L. De Cola, L. Flamigini, *Chem. Rev*. **94**, (1994), 993.

[11] F. H. Kohnke, J.P Mathias, J. F. Stoddart, *Agnew. Chem. Int. Ed. Engl.*, **28** (1989**),** 1103.

[12] Y-J. Hou, P-H. Xie, B-W. Zhang, Y. Cao, X-R. Xiao, W-B. Wang, *Inorg. Chem.* **38**, (1999), 6320

[13] L. D. Field, S. Sternhell, J. R. Kalman, *Organic Structures from Spectra,* Chichester, West Sussex, England ; New York : J. Wiley & Sons, 2002

[14] S. Pal, S. Pal; *Polyhedron*, **22**, (2003) 867

[15] A. L. Guckian, *PhD Thesis,* Dublin City University (2002)

[16] R. Hage, *PhD Thesis*, Leiden University, (1991)

[17] B. P. Sullivan, D. J. Salmon, T. Meyer, *Inorg. Chem.* **17**, (1978) 3334

[18] D. A. Buckingham, F. P. Dwyer, H. A. Goodwin, A. M. Sargeson, *Aust. J. Chem.* **17**, (1964) 325

[19] L. Cassidy, *PhD Thesis,* Dublin City University (2008)

Chapter 6: Synthesis and Characterisation of Novel $[M(P0P)_2(pa\text{-}R\text{-}n]^{2+}$ Type Metal Complexes

Abstract

Chapter 6 describes the synthesis of novel mononuclear metal complexes containing a tetradendate polypyridyl type ligand. Previously used methods for the synthesis of the ruthenium dichloride starting material have been investigated and modified. These starting materials have then been further reacted to include a surface active group, allowing for monolayer formation on electrode surfaces. The resulting complexes are therefore candidates for molecular electronics prototypes.

The chapter includes characterization of the complexes synthesized using nuclear magnetic resonance and HPLC methods as well as UV/vis and emission spectroscopy.

6.1 Introduction

As explained in Chapter 1, it has emerged that a class of transition metal complexes are capable of acting as molecular electronics devices. A series of osmium polypyridine metal complexes have been reported which display transistor-like behaviour.[1] These systems, consisting of a monolayer of the complex in question on a gold or platinum surface[2] display redox switching and amplification properties at room temperature and under condensed matter conditions. As a result these are perfect model compounds for synthesis of novel molecular electronics prototypes. (For diagrams of these molecules see Figure 1.11, page 12)

Osmium bipyridyl complexes are used due to their low oxidation potentials, rendering the complex viable for use as a realistic transistor prototype[1]. However, osmium comes with many attached synthetic problems, the most prominent of which being the harsh reaction conditions it requires when used in successful synthetic reactions. This rules out the use of any delicate or easily degradable ligands for coordination to an osmium centre.

Ruthenium is a much easier metal to work with synthetically, but the redox potential of usual ruthenium bipyridyl compounds is too high for practical use in monolayers on gold or platinum. However, the use of a tetradentate ligand in place of the conventional bis-bipyridyl model could possibly sufficiently lower the oxidation potential of the resulting complex so as to allow for use of aqueous electrolyte.

As described in Chapter 1, $[Ru(bpy)_3]^{2+}$ has acted as a template for much of the research surrounding ruthenium and osmium chemistry in recent years.[3] As a result a great deal of recent synthetic ruthenium and osmium chemistry has been centred around tris-diimine complexes of these two metals.[4] Although complexes of this type exhibit rich photo- and electrochemistry, tris-diimine complexes of ruthenium and osmium inevitably give rise to stereoisomerism at six-coordinated centres due to their bidentate nature. A $M(bpy)_3^{2+}$ complex exists in two enantiomeric forms and if one or more bpy ligand(s) bears a single substituent, two geometrical forms with *facial* and *meridional* arrangements ensue. Each of these isomers then has two associated enantiomeric forms leading to a huge range of conformational variety within one chemically uniform sample, as shown below in Figure 6.1.[5] Also, if a metal tris-diimine type complex is used in building a supramolecular array, supramolecular

organisation occurs with no control over isomer formation, leading to a mixture of systems in which an indeterminate number of components may occupy a *trans* or *cis* arrangement.[6]

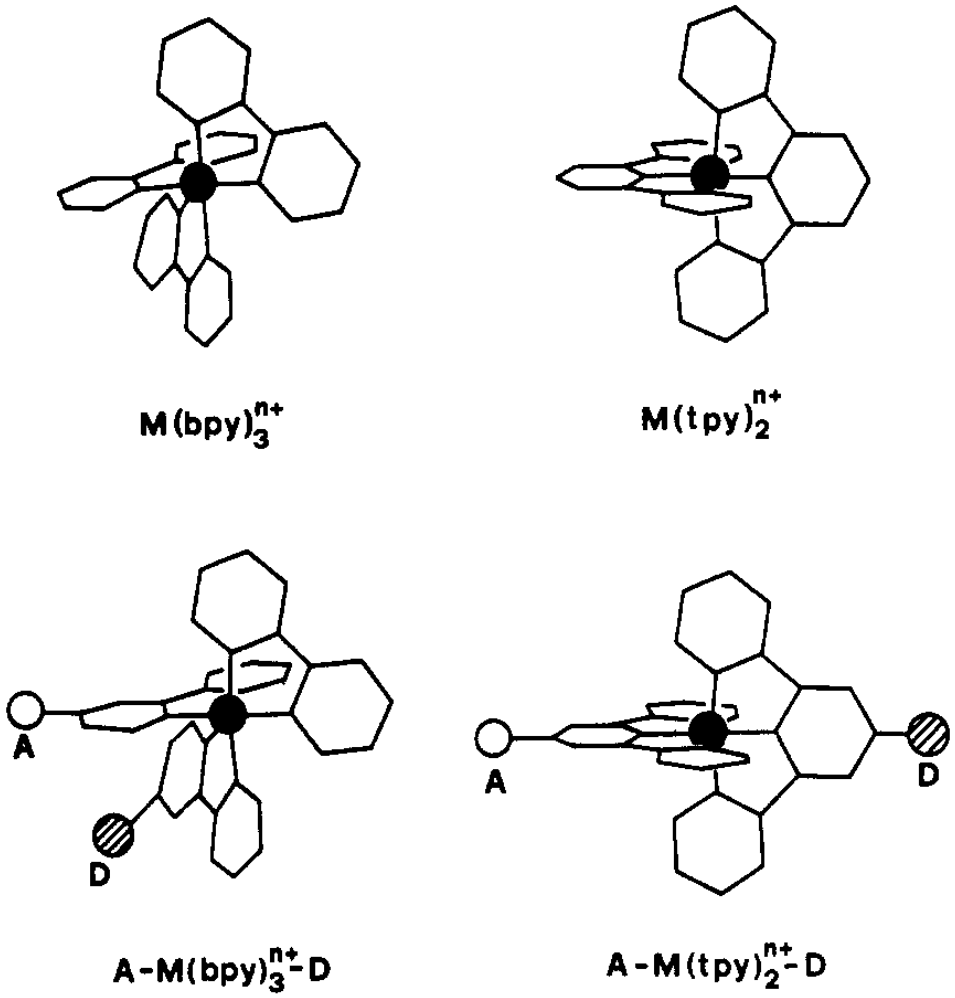

Figure 6.1: Schematic representation of the respective substituted and unsubstituted chiral structures $[M(bpy)_3]^{n+}$ and A-$[M(bpy)_3]^{n+}$-D as compared to the respective substituted and unsubstituted achiral structures $[M(tpy)_2]^{n+}$ and A-$[M(tpy)_2]^{n+}$-D [5]

Attempting to surmount these stereochemical issues a number of research groups have turned to the achiral ruthenium complex $[Ru(tpy)_2]^{2+}$ as a template for novel ruthenium and osmium complexes[5, 7] Complexes of this type however provide more synthetic challenges than the conventional $[Ru(bpy)_3]^{2+}$ model[8, 9] as well as possessing much more limited photochemistry[7]. Again, use of a tetradentate ligand in place of the conventional bis-bipyridyl model should theoretically surmount the stereochemical issues associated with the tris-bipyridyl template while possibly keeping its photo- and electrochemical properties intact. The proposed metal

complexes for synthesis are ruthenium bipyridyl complexes of the tetradentate ligands bis(2-pyridylmethyl)diiminoethane) (paen) and bis(2-pyridylmethyl)diiminopropane) (papn).

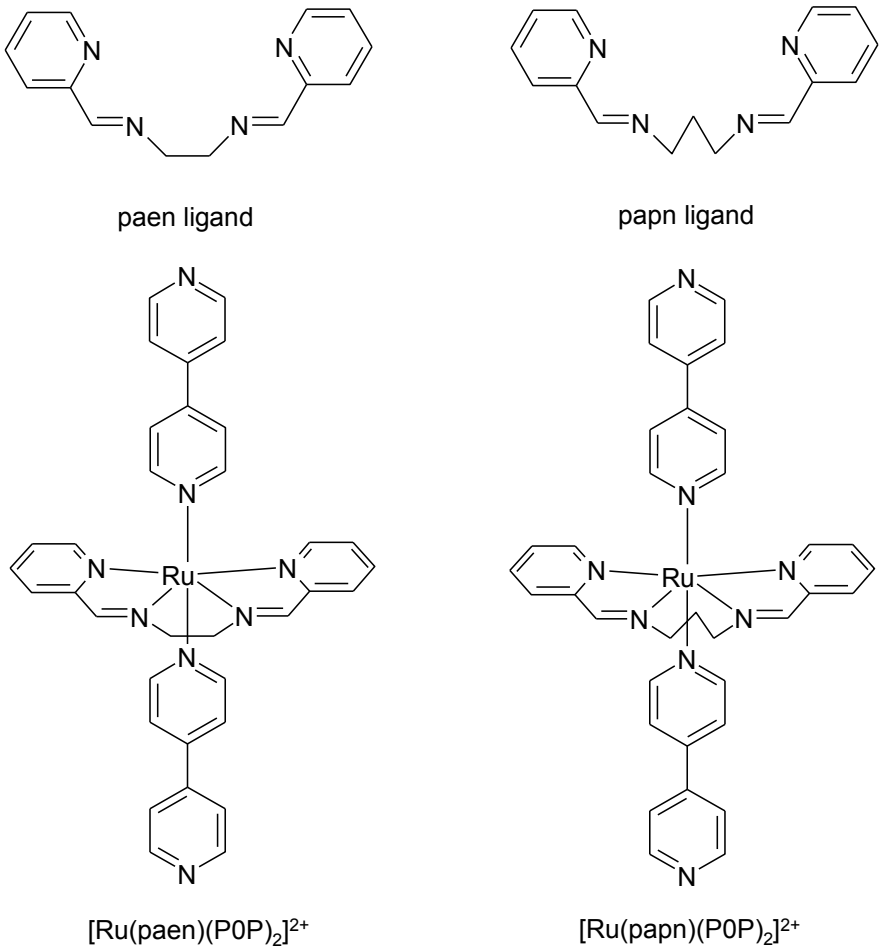

Figure 6.2: Structures of the ligands paen and papn and their respective Ru(P0P)$_2$ complexes

The synthesis of the ligands paen and papn was first published over fifty years ago by Busch and Bailar[10] with a more recent method of preparation being published by Pal *et al.* in 2003[28] Coordination of the ligands to transition metals followed soon after their initial discovery, with one of the first fully characterised complexes consisting of a dinuclear species containing two copper atoms, prepared by Harris and MacKenzie in 1969[11]. This species is shown below in Figure 6.3.

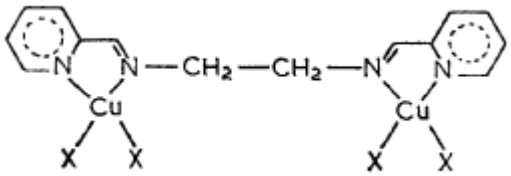

Figure 6.3: Structural representation of the dimeric Cu(II) species prepared by Harris and MacKenzie[11], where X is a monodentate ligand

There have since been reports of Cu(I) and Ag(I) complexes that have double-stranded helical structures[12] as well as Ni(II)[13], heavy metal[14], noble metal[15], and lanthanide metal complexes[16] all containing the ligands paen and papn.

Recently, Ebralidze *et al*. have used paen and papn to construct metallosalen derivatives containing manganese[17] in an attempt to mimic the hydroxyphenyl metallosalen analogues which have found potential uses as efficient oxidation catalysts[18] and as single molecule magnetic building blocks[19]

Brooker *et al* have also used similar Schiff base type ligands for coordination to cobalt[20, 21] and iron[22, 23] but no attempts have been made heretofore to synthesise any such metal complex using the reflux type synthetic methods described in this thesis.

Aydemir *et. al.* have synthesized a bis-ruthenium complex using a bis-bidentate Schiff base type ligand[24]. This method however is carried out at room temperature between $[Ru(p\text{-cymene})Cl_2]_2$ and the ligand in question to yield the bi-metallic product shown in Figure 6.4.

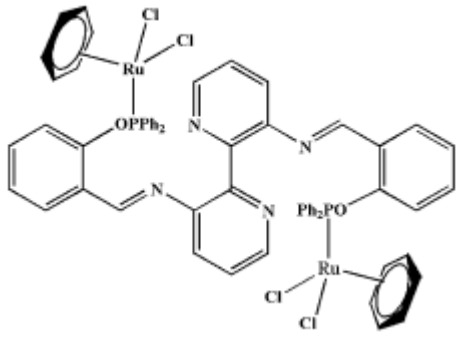

Figure 6.4: Structure for the bimetallic ruthenium Schiff base complex synthesised by Aydemir et. al[24]

A number of Ru(III) Schiff base complexes have been synthesised[25, 26, 27] however as yet there has been no attempt (outside of Pal et al's dichloride[28]) to synthesise a

ruthenium(II) metal complex containing the ligands paen and papn. This chapter details the attempted synthesis of the metal complexes $[Ru(paen)(P0P)_2](PF_6)_2$ and $[Ru(papn)(P0P)_2](PF_6)_2$ as shown previously in Figure 6.2.

6.2 Synthetic Study

6.2.1 Synthesis of Starting Material $Ru(L)Cl_2$

The synthesis of the dichloride starting material $Ru(L)Cl_2$ (where L=paen or papn), to be later implemented as for the ubiquitous $[Ru(bpy)_2Cl_2]$ was attempted using the established method as published by Pal et al[28]. According to this method $Ru(III)Cl_3$ is refluxed in methanol until reduction of the metal to the Ru(II) oxidation state is observed, the appropriate ligand is then added and the resulting mixture is refluxed for one hour. The solvent is removed and the crude product purified by column chromatography.

In the synthesis for $[Ru(paen)Cl_2]$ the first problem encountered was the conversion of Ru(III) to Ru(II). The published method details a reflux of approximately one hour in methanol to yield a colour change from brown to green signalling the desired reduction process. This is identical to the colour change observed for the synthesis of the fundamental ruthenium dichloride $RuCl_2$, in which a colour change in aqueous or methanolic solution from brown through green to blue is observed[29]. The green colour is a result of a mixture of the red and blue species, but does not represent an intermediate[30, 31]. However, the resulting blue solution will undergo rapid atmospheric oxidation to yield a dark green solution[32]

In practice the reduction of $[Ru(III)Cl_3].2H_2O$ as published by Pal *et al* did not yield a green solution after one hour, only after overnight reflux was the desired colour change observed, if indeed it occurred at all. After addition of the ligand (paen or papn) the expected colour change from green to purple was almost instantaneous. However, upon purification by column chromatography and recrystallisation[28] the yield of pure product was found to be extremely low (~ 3mg).

In an attempt to increase the reaction yield, the starting material $[Ru(DMSO)_4Cl_2]$[33] which exists in the +2 oxidation state, was used as an alternative to $RuCl_3$, thus eliminating the need for a reduction step in the synthetic method.

The method used involved refluxing the metal and ligand starting materials together in chloroform for thirty minutes during which time the reaction mixture displayed a colour change from yellow to purple. The solvent was then removed and the dichloride was purified by column chromatography as before. The yield was, unfortunately, identical to previous attempts using $[Ru(III)Cl_3],2H_2O$.

Attempts at other methods of purification were also attempted in order to avoid product unnecessarily lost during the column chromatography process. Recrystallisation was attempted on the solid residue obtained upon removing the solvent from the reaction mixture *in vacuo*. The range of solvents used for these recrystallisation systems is tablulated below in Table 6.1.

Solvent Used	**Result**
Hot CH_2Cl_2	Unsuccessful
Hot MeOH	Unsuccessful
Hot EtOH	Unsuccessful
Acetone: H_2O	Unsuccessful
Acetone: toluene	Unsuccessful
Acetone: hexane	Unsuccessful
Acetone: Ethyl Acetate	Unsuccessful
CH_2Cl_2: hexane	Unsuccessful

Table 6.1: Solvent mixtures used to recrystallise the solid residue from the $Ru(paen)_2Cl_2$ reaction mixture

The attempted recrystallisation using hot ethanol did not dissolve any part of the solid residue. Those using acetone: toluene, acetone: hexane and acetone: ethyl acetate only dissolved a small part of the reaction mixture. The acetone in the solvent mixture was found to dissolve a certain amount of the solid, yielding a purple solution. This suggested that acetone could be used to extract the dichloride (ruthenium dichlorides often being purple in colour), however upon extended stirring and/or reflux in acetone, only ~2 mg dichloride was obtained.

Attempted recrystallisations using CH_2Cl_2 also exhibited a similar 'extraction' property, with a blue solution being yielded (matching the pure fraction obtained

following the literature column chromatography purification). Again, however, after extended stirring and/or reflux in CH_2Cl_2, only ~2mg pure dichloride was obtained. The other recrystallisations involving water and MeOH were also unsuccessful. This was found to be due to the reaction mixture's high solubility in each of these solvents. As a result no single component of the reaction residue crystallised at any particular stage, rather the residue recrystallised as a mixture.

A number of TLC systems were also investigated. The systems and their respective R_f values are shown below in Table 6.2. The purple/blue spot observed was identified by column chromatography (using the literature chromatography system 10:1 dichloromethane: acetone on neutral alumina[28]) as the pure metal dichloride complex $[Ru(paen)Cl_2]$. A red substance remains at the top of the column using this system and only one moving blue band is identified. It has been assumed that this red substance corresponds directly with the red spot observed in the TLC systems shown in Table 6.2 and Figure 6.5. The red complex present at the top of the alumina column during column chromatography would not elute regardless of the solvent used. As a result this compound was not identified.

Mobile Phase	**Stationary Phase**	**Number of Spots**	**R_f value(s)**
Acetonitrile	Silica	2 (one red, one purple)	0.55, 0.24
Acetone	Silica	2 (one red, one purple)	0.61, 0.36
Acetonitrile:H_2O 50 : 50	Silica	1 (streaked, red)	0.74
CH_2Cl_2	Silica	No movement	N/A
THF	Silica	2 (one red, one purple)	0.41, 0.14
Acetone	Neutral Alumina	2 (streaked, not well resolved) (one purple, one red)	0.75, 0.33
CH_2Cl_2	Neutral Alumina	2 (well resolved, one red, one blue)	0.39, 0.26
CH_2Cl_2:acetone 10 : 1	Neutral Alumina	2 (well resolved, one red, one blue)	0.67, 0.42
Acetonitrile	Neutral Alumina	2 (streaked, not well resolved, one red, one purple)	0.59, 0.34
CH_3Cl	Neutral Alumina	2 (well resolved, one red, one blue)	0.26, 0.20

Table 6.2: TLC systems investigated as a method of purification of $[Ru(paen)Cl_2]$

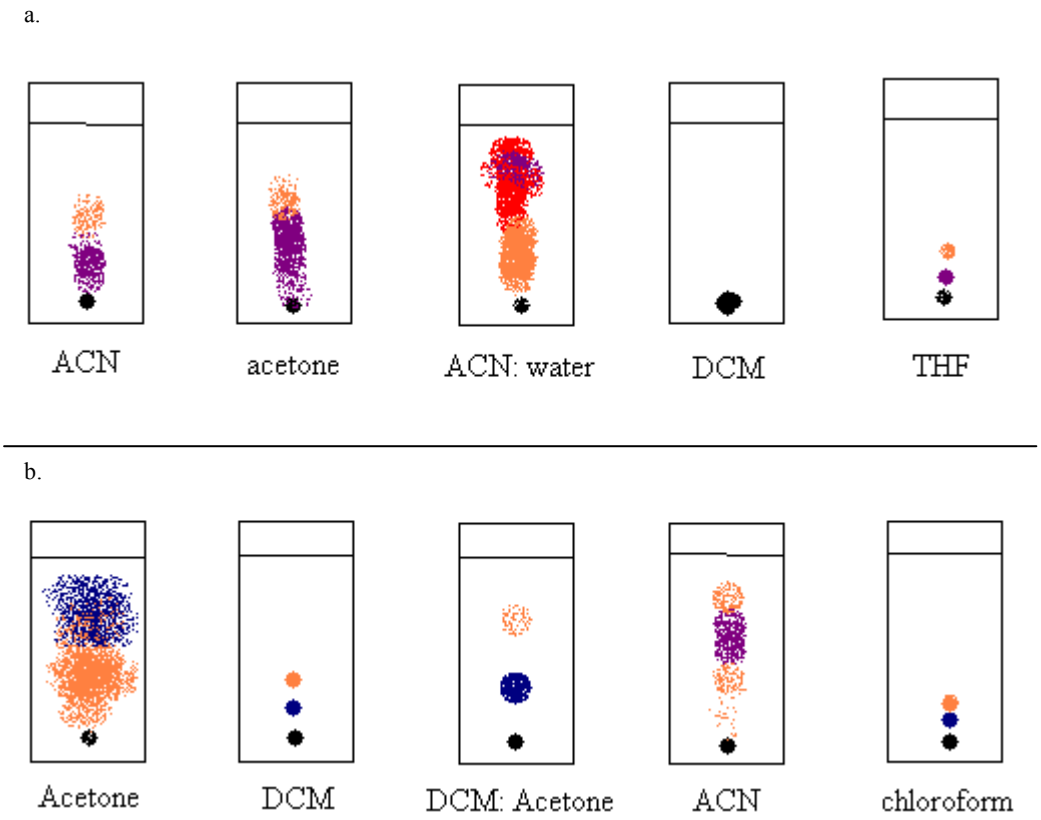

Figure 6.5: Diagrammatic representation of TLC systems investigated on (a) silica and (b) alumina as a method of purification of $[Ru(paen)Cl_2]$

As can be seen from the information shown in Table 6.2 and Figure 6.5, the method of purification published previously[28] consisting of column chromatography on neutral alumina with 10:1 dichloromethane: acetone followed by recrystallisation from dichloromethane: hexane 50: 50 is by far the most effective. Due to the low yields of dichloride obtained using this method of isolation prior to further reaction, it was necessary to devise a different method of dichloride synthesis.

Ascorbic acid is a well known reducing agent.[34] It was found that addition of excess ascorbic acid to the $Ru(III)Cl_3.2H_2O$/methanol reaction mixture shortened the reaction time of the initial reduction step to approximately one hour. $RuCl_3(III).2H_2O$ (1.65 mmol) was placed in 20 cm^3 methanol with a ten-fold excess of ascorbic acid. This mixture was heated to reflux with the progress of the reaction being monitored by UV-vis spectroscopy at ten-minute intervals.

After forty minutes a visible colour change from brown to green had occurred, implying of the starting material had occurred[28] with the change in UV/vis spectrum as shown in Figure 6.6 being displayed.

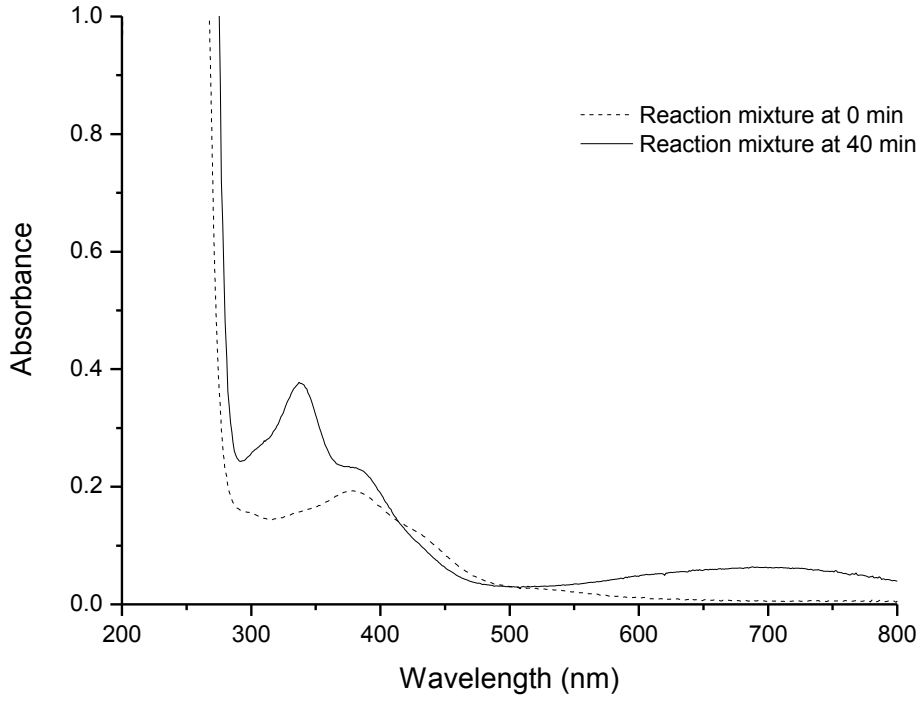

Figure 6.6: Illustration of the reduction from Ru(III) to Ru(II) carried out via reflux with ascorbic acid in methanol as monitored by UV/vis spectroscopy

At this point the ligand paen (1.98 mmol) was added to the reaction mixture in 5 cm^3 methanol. An instant colour change from green to purple was observed. This was accompanied by an instant change in the UV spectrum of the reaction mixture (see Figure 6.7). The reaction was allowed to run for a further 20 minutes but no further change was seen.

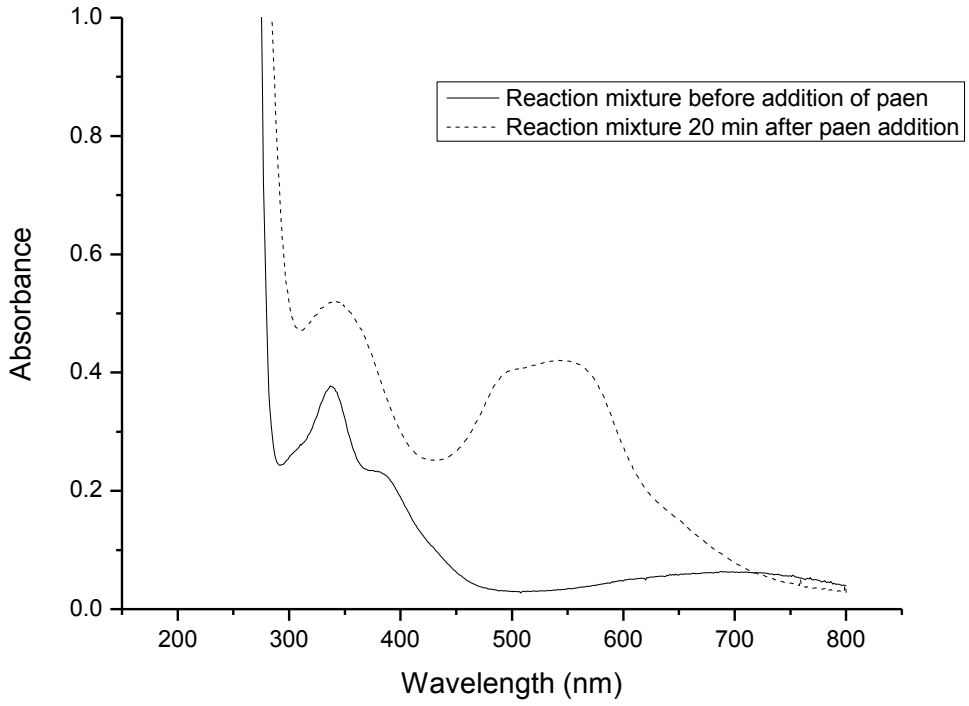

Figure 6.7: Reaction of $Ru(II)Cl_3$ with the ligand paen as monitored by UV/vis spectroscopy

The reaction product was isolated from the mother liquor as previously but the yield was found to be > 1%. Upon reexamination of the spectra shown in Figure 6.6 and Figure 6.7 it was observed that full conversion of the starting materials to their respective products may not have occurred. This is shown diagrammatically below in Figure 6.8.

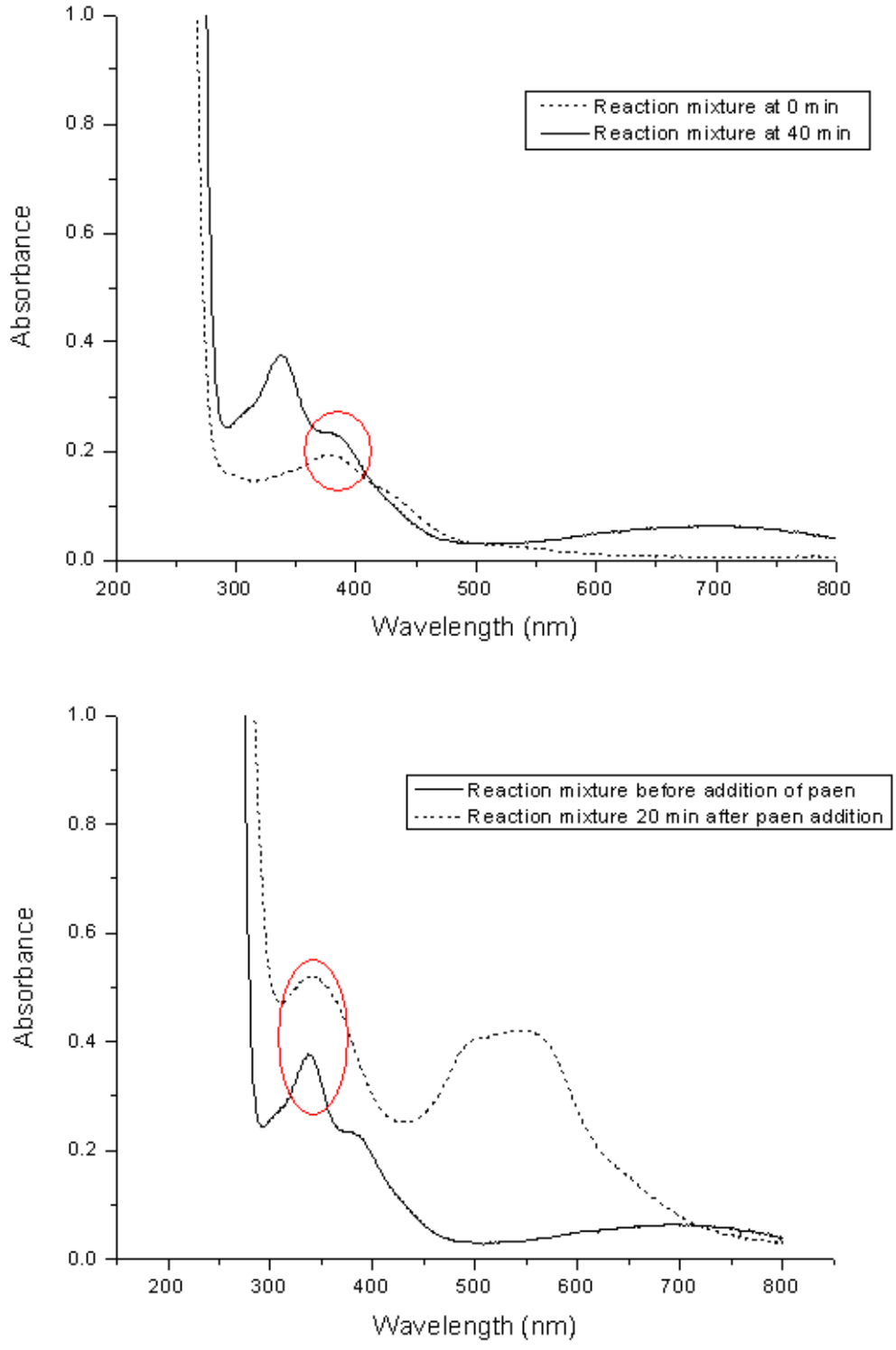

Figure 6.8: UV-vis spectra illustrating (a) the conversion of Ru(III) to Ru(II) in the presence of ascorbic acid and (b) the reaction of Ru(II) with paen to form $[Ru(paen)Cl_2]$. The areas of overlap between the spectra which indicate that full conversion was not achieved are highlighted.

In order to ascertain if a longer reaction time was needed for the reaction to reach completion a second reaction was attempted, this time monitoring the reaction progress by HPLC analysis. As before, $Ru(III)Cl_3$ was refluxed with 10 equivalents ascorbic acid. Samples were taken from the reaction mixture at 1 hour intervals and analysed by HPLC using a cation exchange column and 75: 20: 5 acetonitrile: water: methanol with 0.1 M KNO_3 buffer as mobile phase. The detection wavelength employed was 280 nm, which is a standard wavelength employed for HPLC analysis of ruthenium-N_6 type complexes[35]. The first sample was taken at approximately 10 minutes after the reaction mixture was heated to 120 ^{0}C, and every hour thereafter. The chromatogram shown below in shows the HPLC data for this (10 minute) sample.

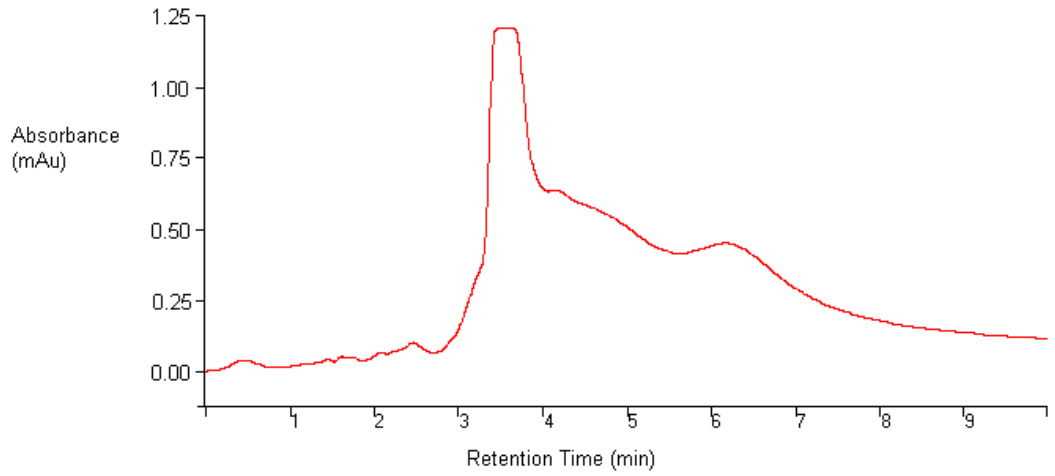

Figure 6.9: HPLC chromatogram obtained for reaction mixture at 10 min for reaction between $RuCl_3.2H_2O$ and excess ascorbic acid

The chromatogram shown in Figure 6.9 is extremely noisy, implying that even at this stage of the reaction a number of different components are present in the reaction mixture. In spite of this a few discernable peaks may be identified. A large signal is visible at 3.5 min in the chromatogram shown above. Judging from the UV/vis spectrum shown below in Figure 6.10, corresponding to this peak, this signal is organic in nature. It stands to reason that this peak therefore relates to the excess of ascorbic acid present in the reaction mixture as this is the only organic substance present in the reaction mixture at this stage in the reaction. In order to ascertain whether this peak may be attributable to solvent, solvent blanks of methanol (the reaction solvent employed) and acetonitrile (the HPLC sample diluent) were run, yielding chromatographs showing no signals. Therefore it may be assumed that

Name: Ru(III) Ru(II) THF
Instrument: Varian Star #2
Method: test.mth
Operator:
Run Date: 26/02/2010 13:37
Scan Rate: 10.000 Hz Bunch: 1 Data Rate: 10.000 Hz
Detector Range: 200.000->800.000 nm Valid Range: 200.000->800.000 nm
Spectrum Type: Within Correction Type: Start
Channel Range: 200.00 to 800.00 nm Absorbance Range: -0.6006 to 1.4401 AU
Max Wavelength(nm): 266.20
Percent of Max Abs.: 100.0%

ascorbic acid is the only organic substance visible in the chromatograph. This assumption is compounded by the huge difference in peak area between the peak occurring at 3.55 min all other peaks present in the chromatogram.

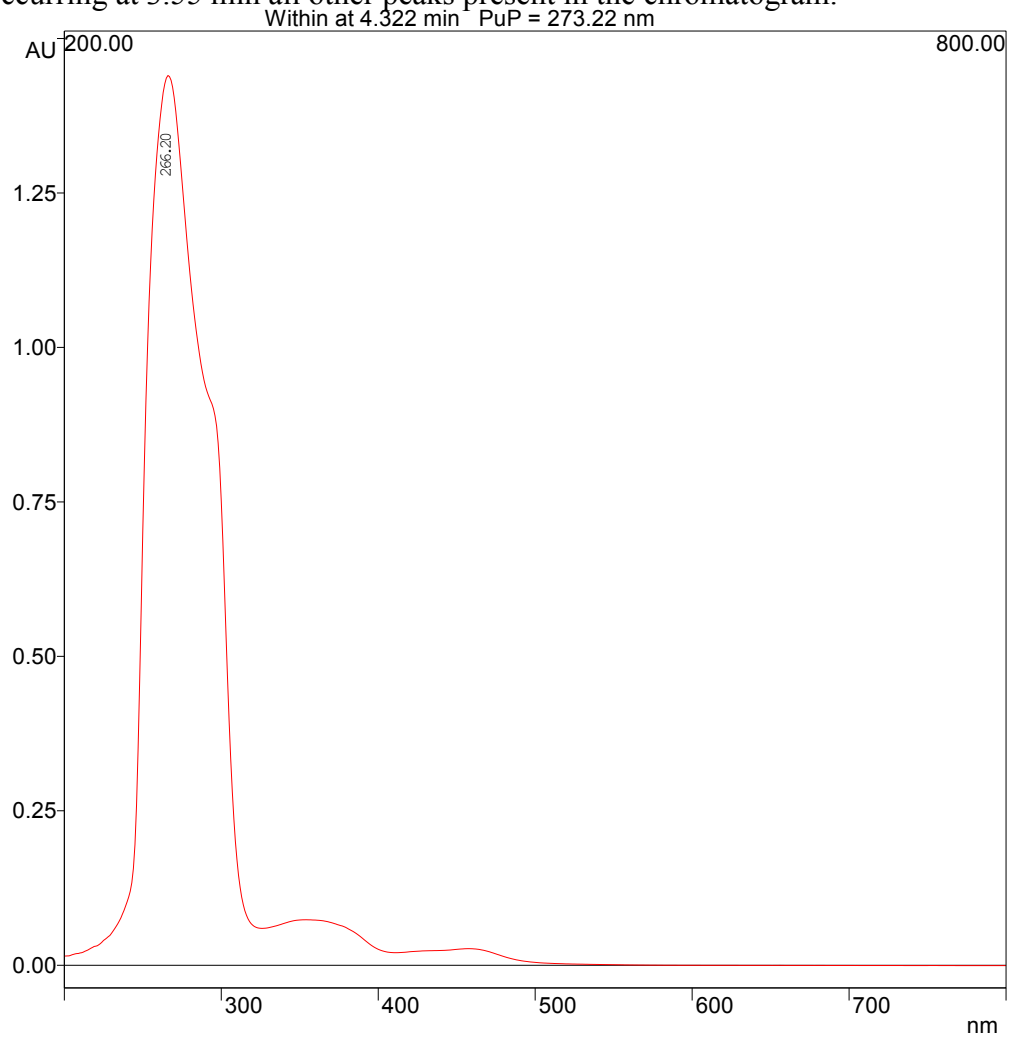

Figure 6.10: UV/vis spectrum of ascorbic acid peak present at 3.5 min in chromatogram shown in Figure 6.14

A weak absorbance that may be attributed to a transition metal at approximately 460 nm is visible in Figure 6.10 as well as the intense organic absorbance visible at 266 nm. This may be due to a small amount of the desired Ru(II) metal being formed at this early stage in the reaction, appearing at a similar retention time to the intense peak attributable to ascorbic acid. The broad peak visible at 6.1 min in the chromatogram shown in Figure 6.9 yielded the UV/vis spectrum shown below in Figure 6.11.

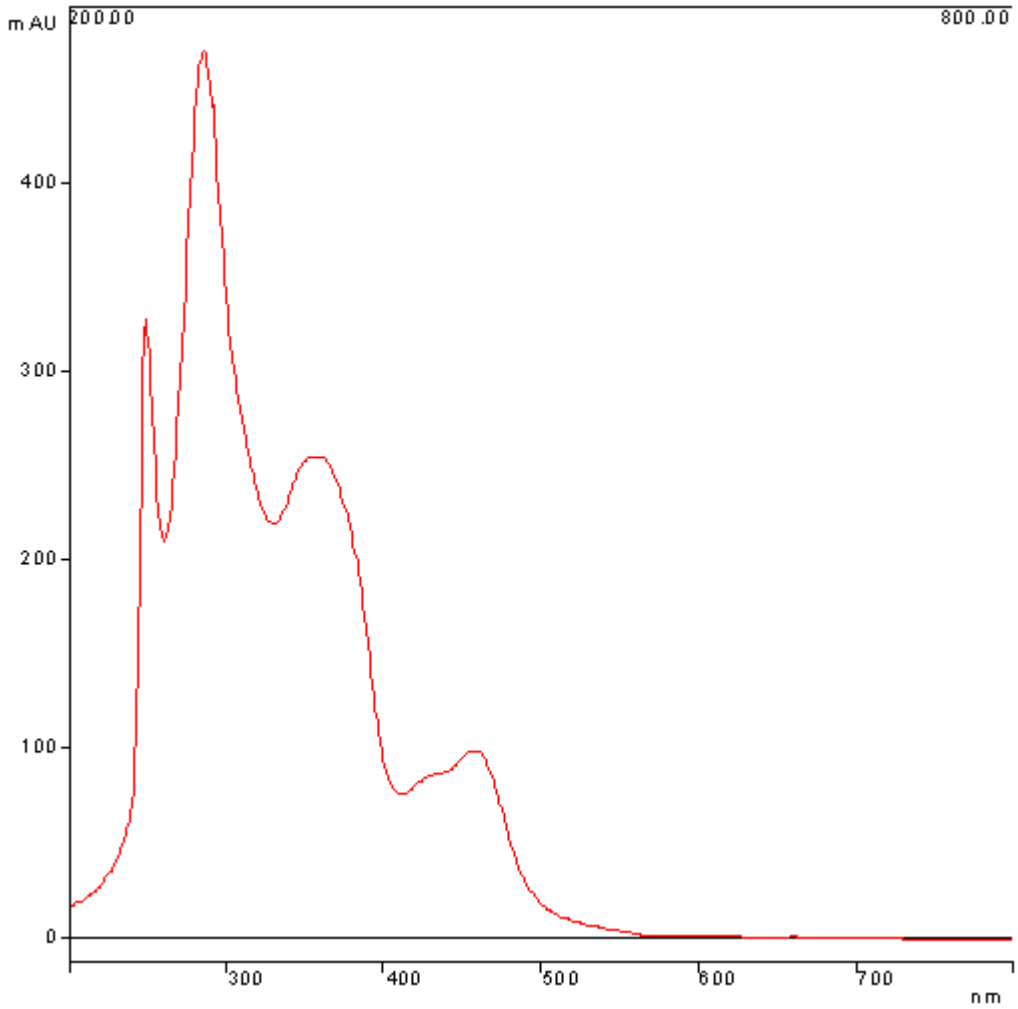

Figure 6.11: UV/vis spectrum for broad peak visible at 6.1 min in the chromatogram shown in Figure 6.9

The UV/vis spectrum displays a peak at 458 nm, implying that a ruthenium metal complex is present. The only transition metal material present in the reaction mixture is Ru(III)Cl_3. In order to confirm if the substance appearing at 6.1 min in Figure 6.9 is due to this material, a sample of $[RuCl_3].2H_2O$ was run yielding the chromatogram shown below in Figure 6.12.

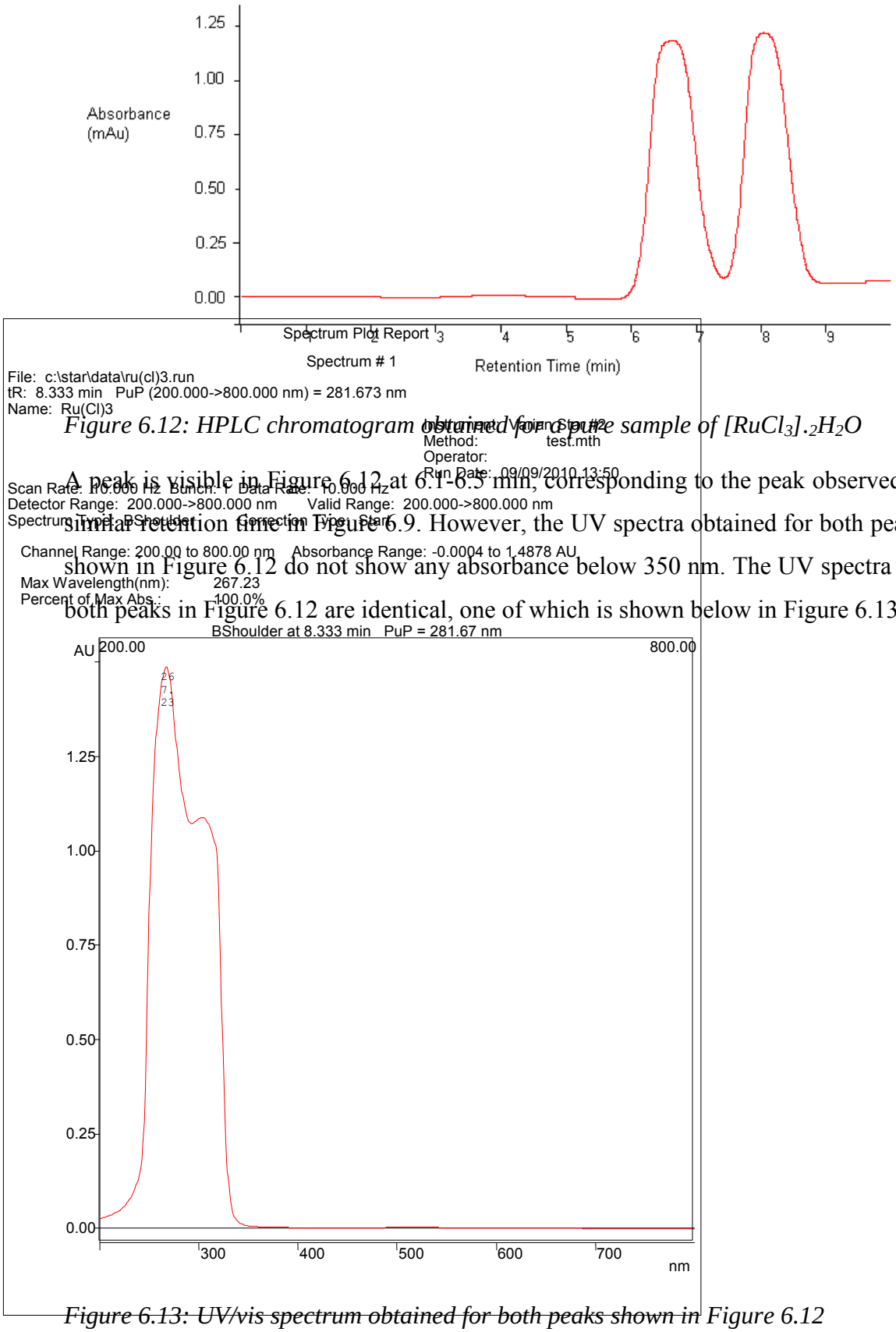

Figure 6.12: HPLC chromatogram obtained for crude sample of $[RuCl_3].{}_2H_2O$

A peak is visible in Figure 6.12 at 6.1-6.5 min, corresponding to the peak observed at similar retention time in Figure 6.9. However, the UV spectra obtained for both peaks shown in Figure 6.12 do not show any absorbance below 350 nm. The UV spectra for both peaks in Figure 6.12 are identical, one of which is shown below in Figure 6.13.

Figure 6.13: UV/vis spectrum obtained for both peaks shown in Figure 6.12

The fact that there are two peaks visible in Figure 6.12 implies that there are two different substances present, one of which is $[RuCl_3].2H_2O$. The other may be a photochemical product in which one or more chloride atoms have been replaced by monodentate acetonitrile ligands. However, there is no absorbance present at ~450 nm in Figure 6.13 and the substance appearing at 6.1 min in Figure 6.9 exhibits a metal based absorbance at approximately 460 nm, and so it may be an intermediate complex in which solvent molecules (perhaps methanol) have coordinated to the ruthenium centre. This suggestion is compounded by the absence of a peak at 6.1 min after 2 hr reflux and an associated colour change from brown to green. The chromatogram for the reaction solution at this stage is shown below in Figure 6.14.

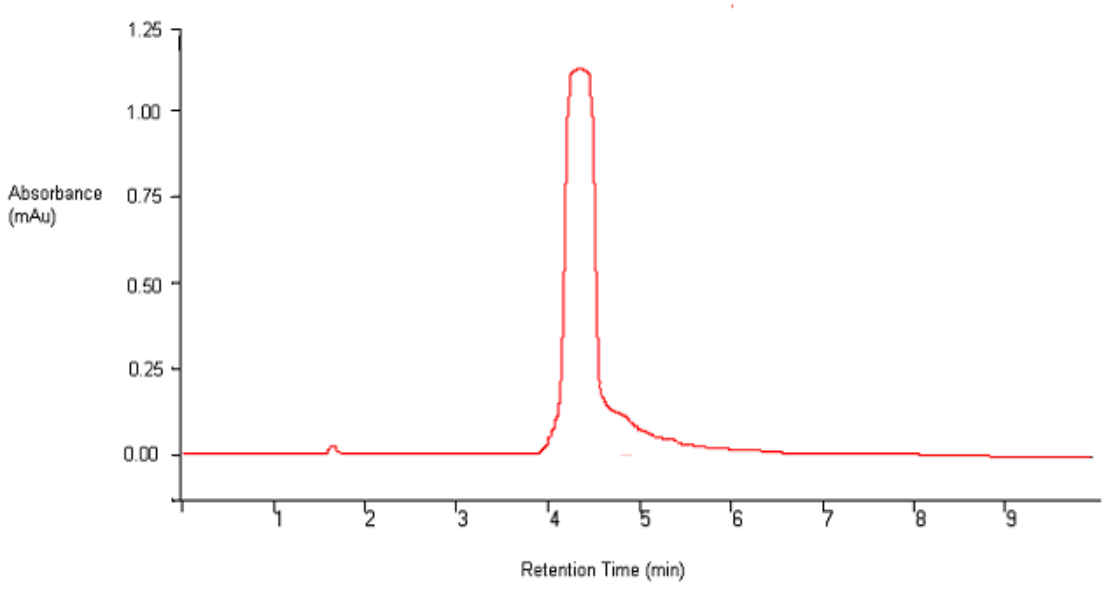

Figure 6.14: HPLC chromatogram obtained following 2 hr reaction between RuCl3.2H2O and excess ascorbic acid

The peak present at 1.8 min yields the UV/vis spectrum shown below in Figure 6.15 (b) as compared to the UV/vis spectrum of the Ru(III) intermediate material identified in Figure 6.14.

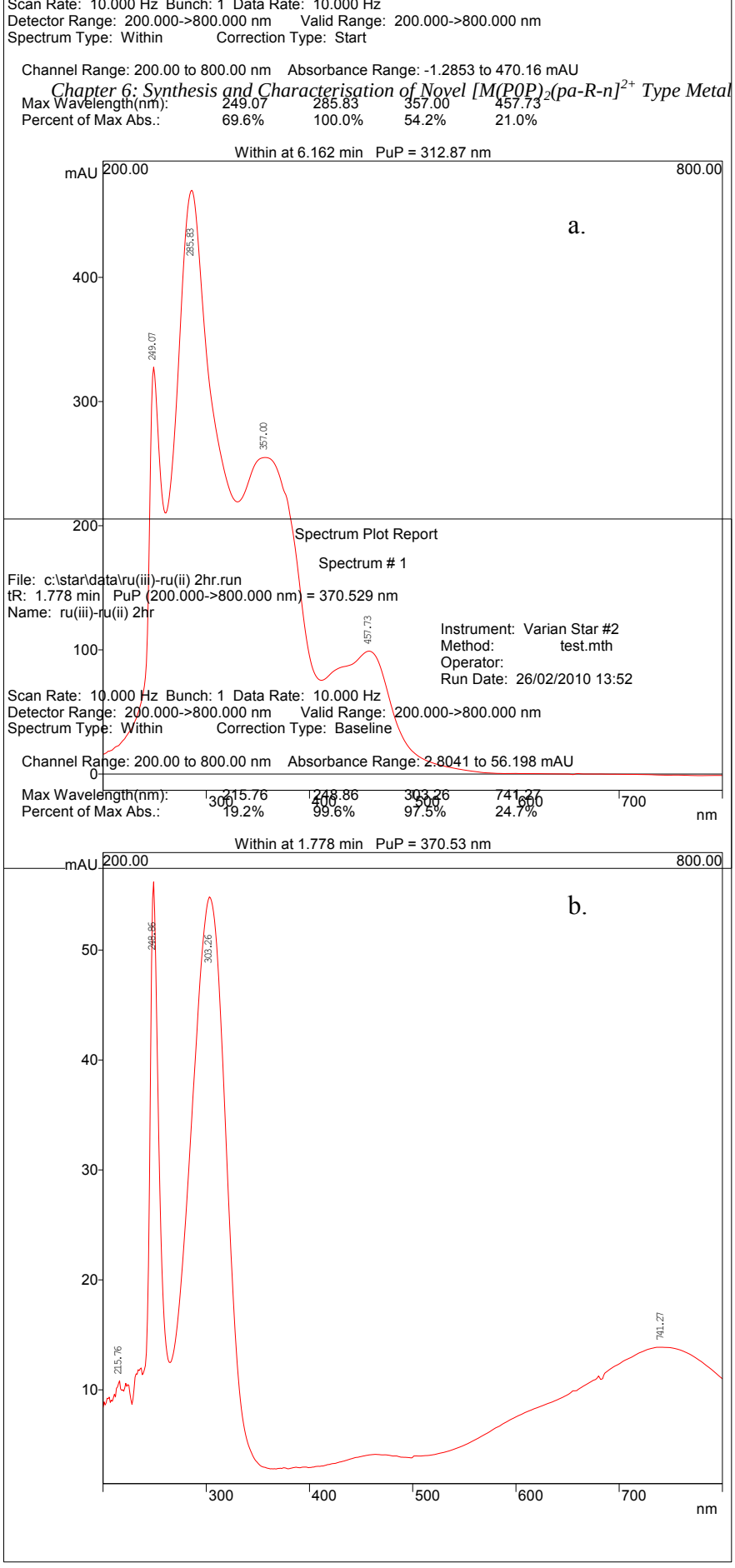

Figure 6.15: UV/vis spectrum of Ru(III)-Ru(II) reaction mixture at (a) 0 hr and (b) 2 hr

It can be seen from Figure 6.15 that there is a clear difference in the UV spectra of these peaks. Both spectra appear to correspond to transition metal complexes with the assumed ^{1}MLCT (metal to ligand charge transfer) band present in Figure 6.15 (a) appearing at 458 nm and the associated ^{1}MLCT band present in Figure 6.15 (b) appearing at 741 nm. There is no evidence of a peak at 6.1 min in Figure 6.14 indicating that the Ru(III) intermediate present in the reaction solution at 0 hr reflux between Ru(III)Cl_3 and ascorbic acid in methanol (the UV/vis spec for which is shown in Figure 6.11) has been consumed. There is also a slight bump visible at approximately 460 nm in the UV/vis spectrum shown in Figure 6.15 (b), implying that there is a trace of Ru(III) intermediate present in the sample eluting at 1.8 min possibly present as a metal based impurity. Also, again, the intense peak visible in this spectrum at 4.3 min is attributable to an organic material, in this case excess ascorbic acid. From this information it may be inferred that the metal complex material present in the reaction mixture after 2 hr reflux (appearing in Figure 6.14 at 1.8 min) is the desired Ru(II) complex Ru(II)Cl_2.

At this point 1.2 equivalents of the ligand paen were added to the reaction mixture. An immediate colour change from green to purple was observed. After 30 minutes a sample of the reaction mixture was taken and analysed by HPLC. The chromatogram shown below in was obtained.

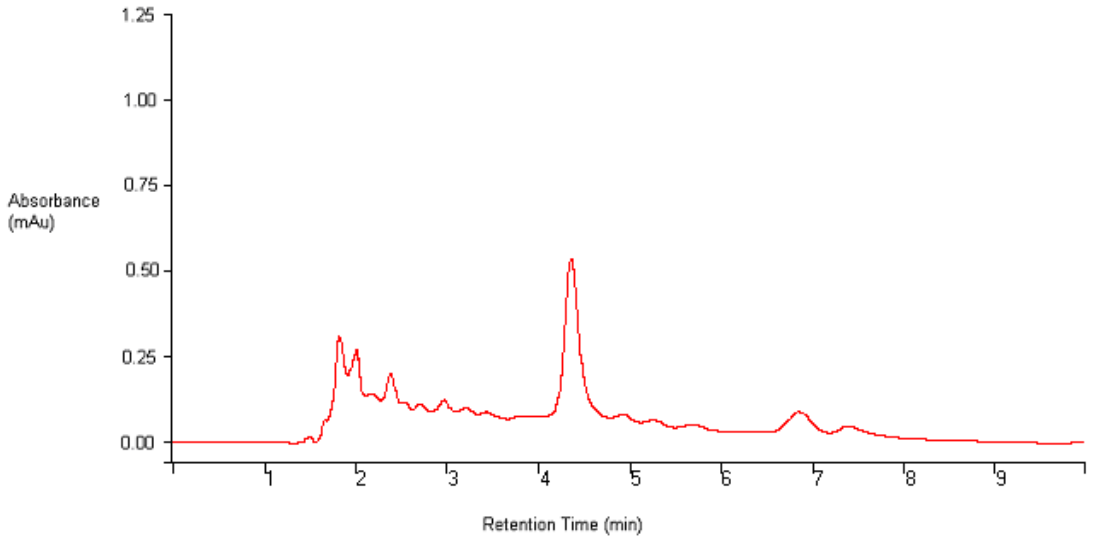

Figure 6.16: Chromatogram for Ru(paen)Cl_2 reaction mixture after 30 min

It can be seen in Figure 6.16 that in spite of the instantaneous colour change observed from green to purple when paen is added to the reaction mixture as described by Pal *et al*[28], many different products are present in the reaction mixture. The reaction was monitored by HPLC, with the chromatogram shown in Figure 6.17 being obtained after an overnight reflux.

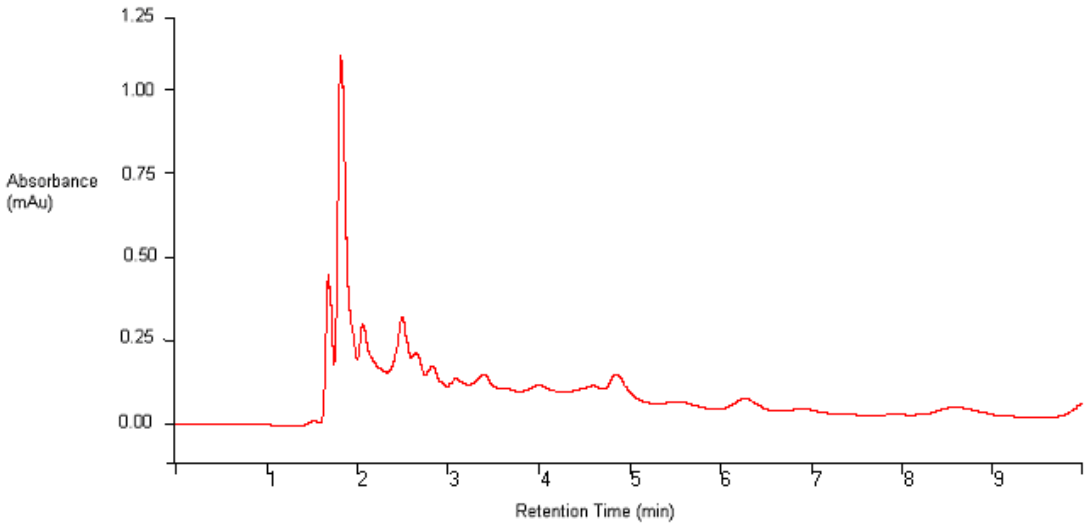

Figure 6.17: HPLC chromatogram for $[Ru(paen)Cl_2]$ reaction mixture after overnight reflux.

As can be seen from Figure 6.17 many different products are still present in the reaction mixture after overnight reflux, but the peaks present at 1.6 min and 1.8 min have increased in intensity to dwarf the other peaks present in the chromatogram.

The UV/vis spectrum corresponding to the peak at 1.6 min displays one peak at 270 nm, and is assumed to be organic in character as a result. The only compounds present in the reaction mixture other than solvent that are organic in character are paen and residual ascorbic acid and so the peak present at 1.6 min must correspond to one of these compounds. The UV/vis spectrum corresponding to the peak at 1.8 nm displays a peak at approximately 480 nm and is shown below in Figure 6.18.

Spectrum Type: Within Correction Type: Start

Channel Range: 200.00 to 800.00 nm Absorbance Range: 0.4203 to 858.60 mAU

Max Wavelength (nm): 258.94
Percent of Max Abs.: 100.0%

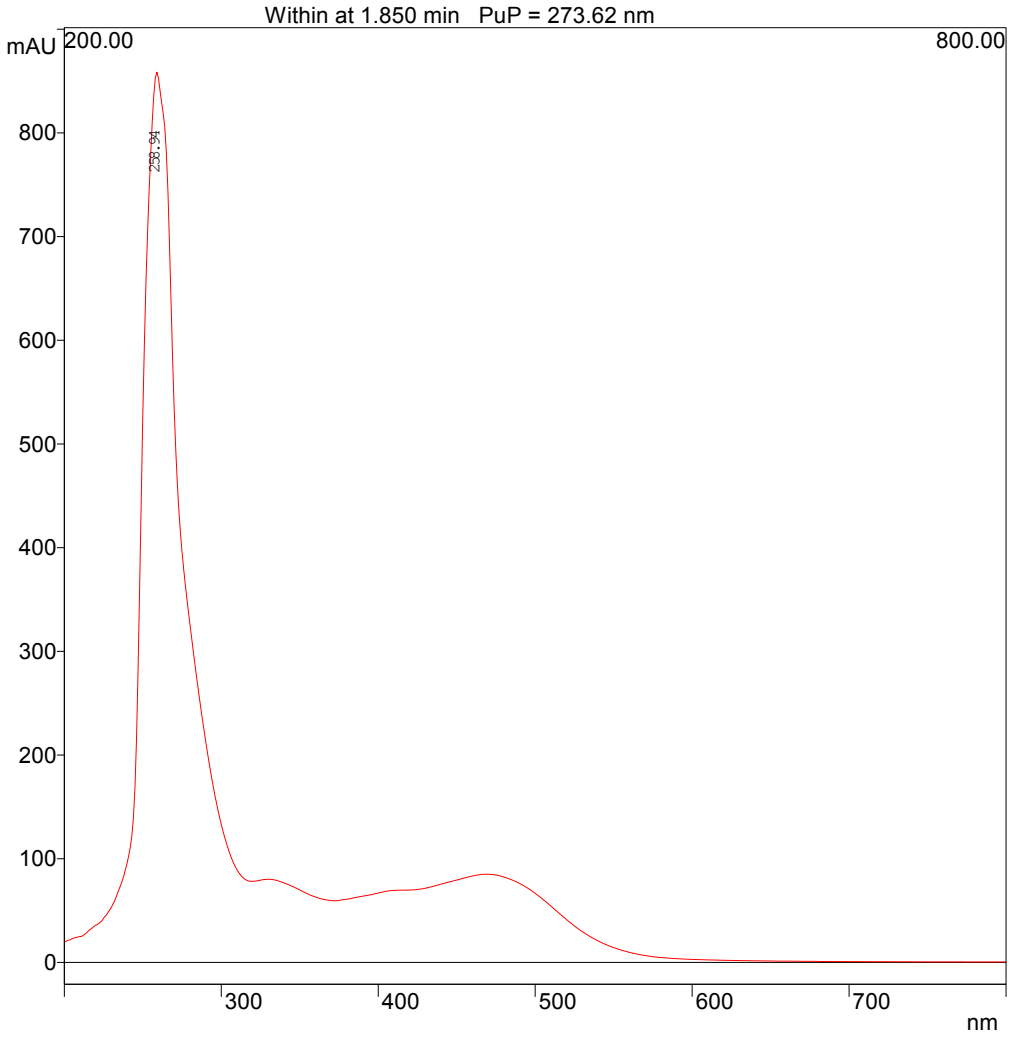

Figure 6.18: UV/vis spectrum corresponding to the peak visible at 1.8 min in Figure 6.17

This reaction solution was then worked up and purified as described previously in this section (i.e. by column chromatography and recrystallisation). This purified solid (7.8% yield) when analysed by HPLC analysis yielded the chromatogram shown below in Figure 6.19.

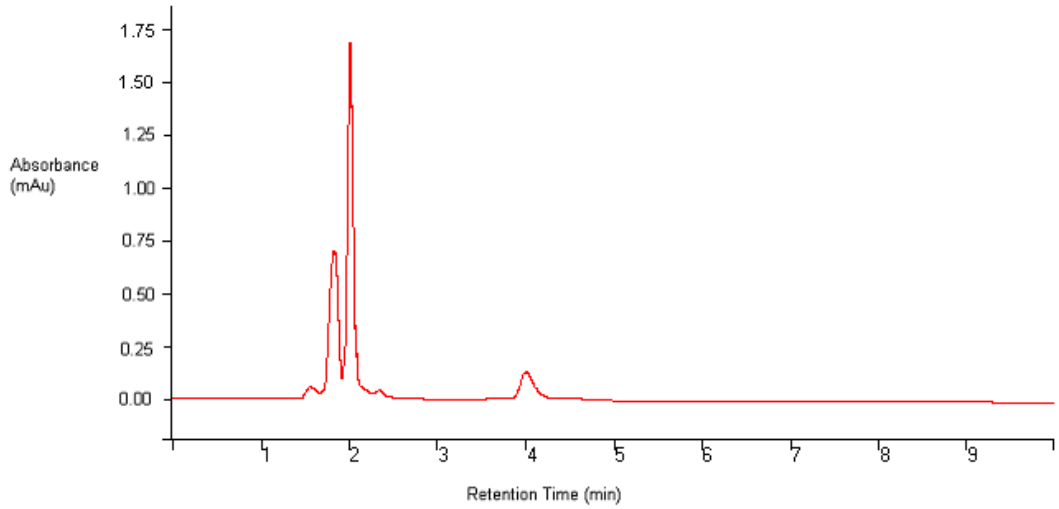

Figure 6.19: HPLC chromatogram relating to purified $[Ru(paen)Cl_2]$

The peak visible at 1.8 min displays the same UV/vis spectra as shown above in Figure 6.18 confirming that this peak corresponds to $[Ru(paen)Cl_2]$. The peak present at 2.05 min displays one peak at 270 nm indicating an organic material, most likely excess ligand. The one remaining peak at 4.00 min also displays a ruthenium based absorbance in its UV/vis spectrum, shown below in Figure 6.20.

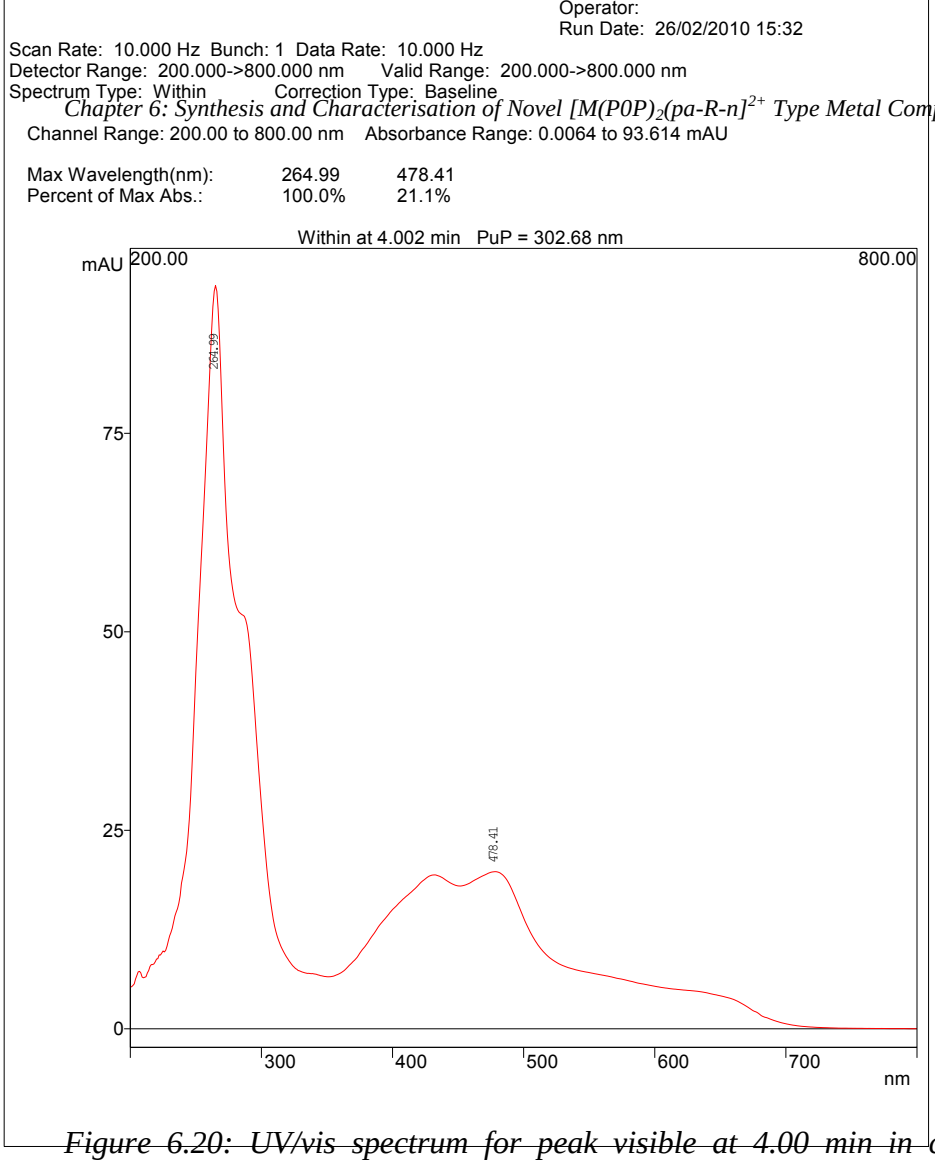

Figure 6.20: UV/vis spectrum for peak visible at 4.00 min in chromatogram for purified Ru(paen)Cl_2 sample

The spectrum shown above in Figure 6.20 displays an absorbance almost identical to that of the dimeric metal complex $[Ru(bpy)_2(pytr\text{-}bpy)Os(bpy)_2]^{3+}$ the UV/vis spectrum for which is shown below in Figure 6.21 [8] As a result it has been postulated that the peak eluting at 4.0 min in Figure 6.19 may relate to a dimeric by-product, a possible structure for which is shown below in Figure 6.22.

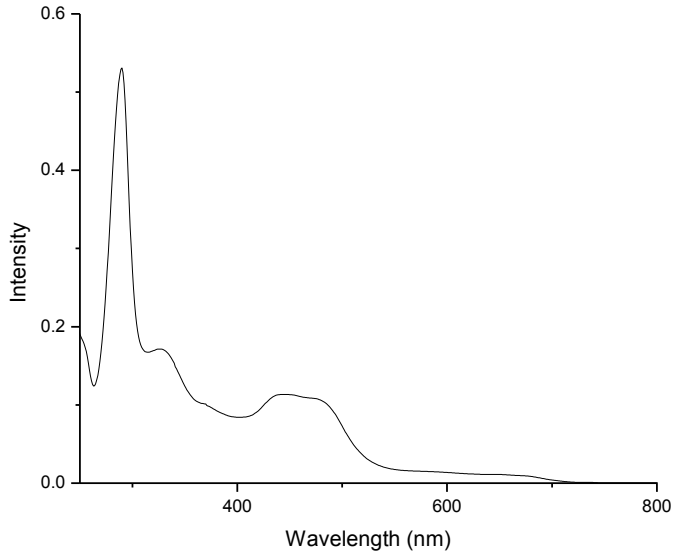

Figure 6.21: UV/vis spectrum of the heterodinuclear metal complex $[Ru(bpy)_2(pytr\text{-}bpy)Os(bpy)_2]^{3+}$ [8]

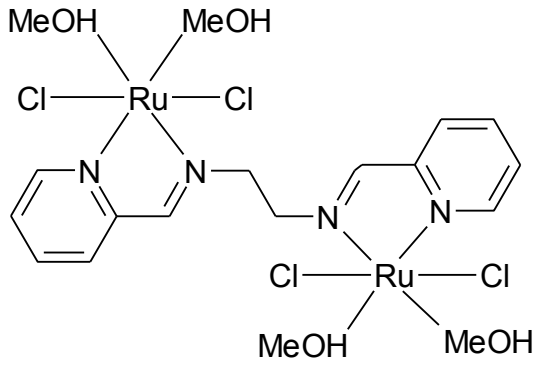

Figure 6.22: Possible dimeric product appearing at 4.0 min in chromatograph shown in Figure 6.19

The purified sample of $[Ru(paen)Cl_2]$ the UV/vis spectrum for which is shown above in Figure 6.20 was also sent for ^1H NMR analysis (which shall be discussed in full later in section 4.3). The ^1H NMR spectrum showed only the expected compound with little to no impurity intimating that there is a negligible amount of the dimeric by-product shown present in the sample. In terms of yield, this reaction produced 28 mg of pure product, signifying a yield of 7.8%. Although still extremely low in terms

of percentage yield, this reaction at last yields an amount of solid suitable for use in subsequent reactions, and so this method was deemed a success.

With a satisfactory synthetic method for the dichloride starting material $[Ru(paen)Cl_2]$ established, synthesis of the metal complex $[Ru(paen)(P0P)_2](PF_6)_2$ was attempted. A number of different approaches were used, all of which shall be discussed in the sections that follow.

6.2.2 'One-Pot Reaction' Approach

Upon ascertaining that the desired dichloride was formed, a one-pot approach was adopted for the synthesis of the complex $[Ru(paen)(P0P)_2](PF_6)_2$, with an excess of P0P ligand being added to the reaction mixture directly following the formation of the dichloride starting material $[Ru(paen)Cl_2]$

As before $[Ru(paen)Cl_2]$ was synthesised by refluxing $RuCl_3.2H_2O$ overnight in methanol the presence of an excess of ascorbic acid, after which a suitable amount of paen was added and the resulting solution refluxed overnight. To the resulting purple solution a 10-fold excess of 4,4'-bipyridyl (P0P) was added. The resulting mixture was refluxed overnight resulting in a colour change from purple to red, indicative of a ruthenium N6 type complex[29].

The solvent was then removed and purification of the resulting crude product was attempted using column chromatography. A silica column was implemented using 80:20 acetonitrile:water with 0.05 KNO_3 buffer as eluent, as this system is used for the purification of the analogous $[Ru(bpy)_2(P0P)_2]^{2+}$ type complexes[36]. The resulting ^1H NMR spectrum indicated the possible formation of a metal complex but a large excess of 4,4'-bipyridyl was still present in the sample. A comparison between the ^1H NMR spectrum obtained for this sample and the spectrum for 4,4'-bipyridyl alone is shown below in Figure 6.23 in order to confirm the identity of the two dominant doublet peaks in the metal complex spectrum as excess P0P ligand.

The similarity between Figure 6.23 (a) and (b) is clear, confirming that the two doublets dominating the spectrum at approximately 8.6 ppm and 7.6 ppm in Figure 6.23 (b) are due to an excess of 4,4'-bipyridyl present in the sample. There is less similarity between Figure 6.23 (b) and (c). The doublet present at approximately 8.65 ppm is present in both spectra, with many others appearing at a shifted chemical shift (δ) value in the complex (Figure 6.23 b) from the free ligand (Figure 6.23 c). The doublet of doublets present at 7.45 ppm in Figure 6.23 (c) appears to be shifted to

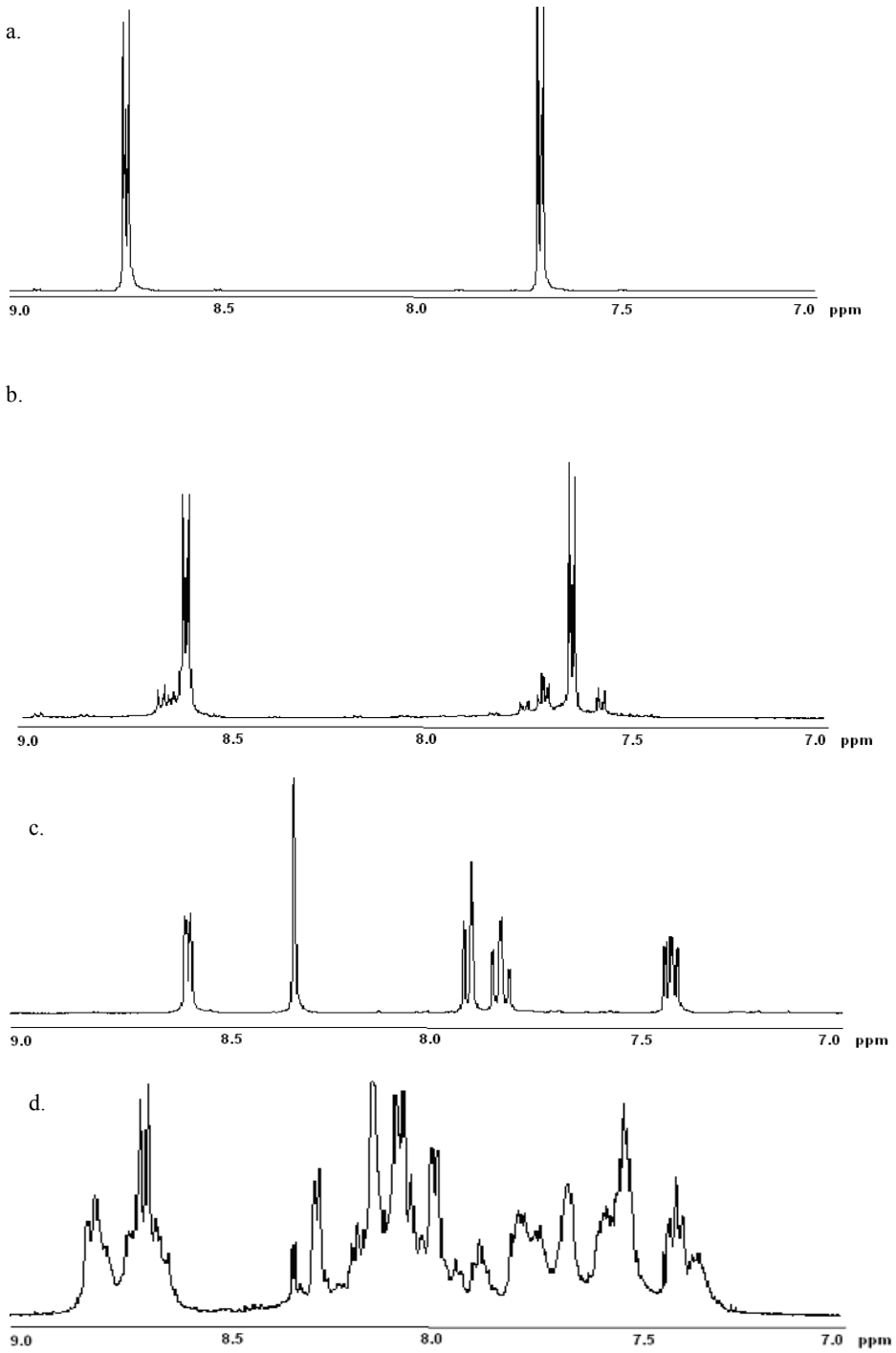

Figure 6.23: ^1H NMR spectra of (a) 4,4'-bipyridyl (P0P) (b) crude $[Ru(paen)(P0P)_2]^{2+}$ after overnight reflux and purification on Si with ACN: H_2O 80:20 0.05M KNO_3 and (c) the free ligand paen after purification by column chromatography, as measured in d_6-acetone (d) crude $[Ru(paen)(P0P)_2]^{2+}$ following overnight reflux purification by column chromatography and precipitation from diethyl ether, as measured in d_6-acetone

7.59 ppm in Figure 6.23 (b). Likewise the doublet present at 7.90 ppm and the triplet present at 7.85 ppm in Figure 6.23 (c) appear at 7.75 ppm and 7.67 ppm respectively in Figure 6.23 (b). The singlet appearing at 8.37 ppm in Figure 6.23 (c) is not apparent in Figure 6.23 (b), but it is possible that the peak has been shifted and is masked by one of the over-powering 4,4'-bipyridyl signals.

Due to the encouraging nature of the spectrum shown in Figure 6.23 (b), further endeavours were made to remove the residual uncoordinated 4,4'-bipyridyl from the sample. The solid obtained was redissolved in acetone and added to a large amount of diethyl ether with vigorous stirring. The precipitate formed was collected and analysed by ^{1}H NMR. The spectrum obtained was free of excess ligand but still displayed a possible range of products as shown in Figure 6.23 (d). Similarities can be seen between the spectrum for the free ligand paen (the ^{1}H NMR spectrum for which is shown in Figure 6.23 (c)) and the further purified crude $[Ru(paen)(P0P)_2](PF_6)_2$ material (the ^{1}H NMR spectrum for which is shown in Figure 6.23 (d)) however, the spectrum is far from clean. Four P0P signals are expected to appear in the spectrum as seen for the analoguos $[Ru(bpy)_2(P0P)_2]^{2+}$ complexes[36] as well as the five distinct paen signals seen in Figure 6.23 (c), However, instead of the predicted nine peaks, eleven discernable signals can be identified in Figure 6.23 (d), and due to the broad nature of the spectrum it is possible that a number of these signals may be amalgamations of two or more overlapping peaks.

It is possible that di- or tri-nuclear materials were formed during the reaction as well as the desired mononuclear complex. Examples of these possible by-products are shown below in Figure 6.24.

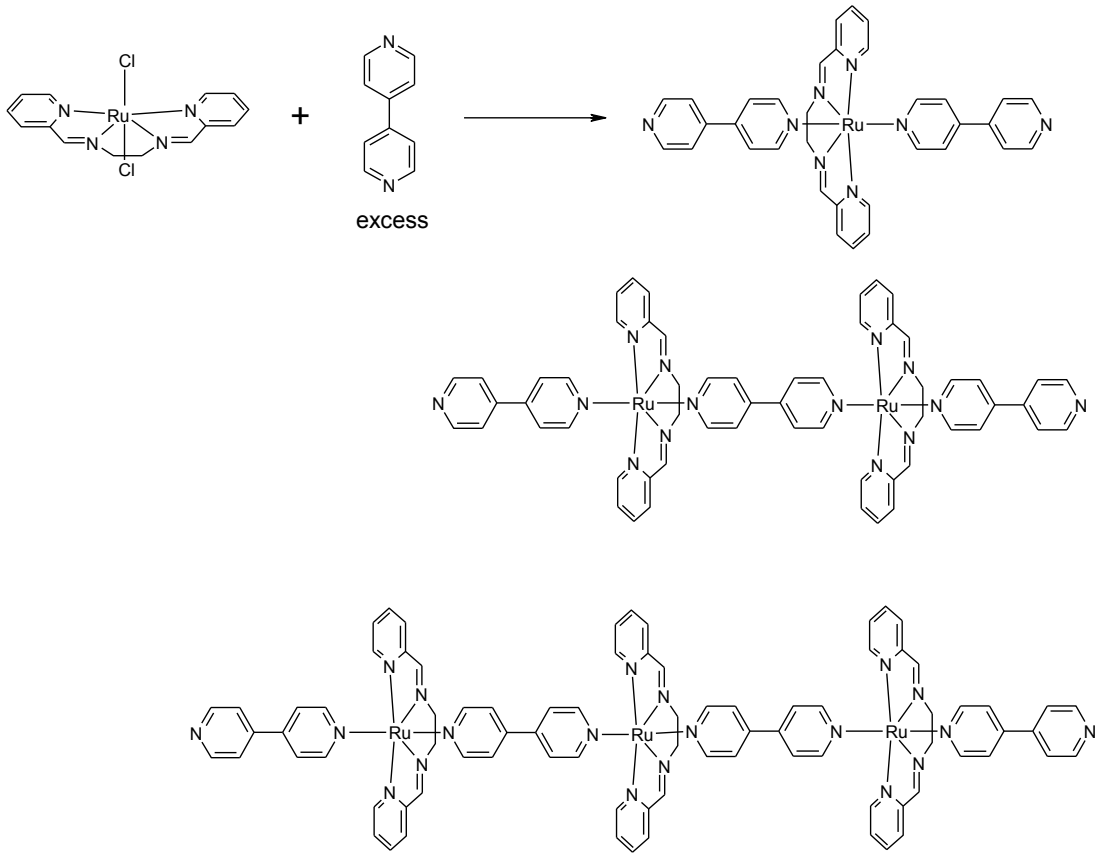

Figure 6.24: Reaction scheme for the formation of $[Ru(paen)(P0P)_2](PF_6)_2$ showing possible dinuclear and trinuclear by-products

The sample corresponding to the ^{1}H NMR spectrum in Figure 6.23 (d) was purified a second time by column chromatography on silica using 80:20 acetonitrile:water with 0.05 KNO_3 buffer as eluent. The resulting yield of >1 mg, however, was not large enough to obtain a readable ^{1}H NMR spectrum.

The reaction was re-attempted, this time removing the solvent from the reaction mixture when the desired dichloride had been formed and redissolving this solid in a 2:1 ethanol:water mixture. The resulting solution was added slowly to a refluxing solution of excess P0P in the same solvent. This reaction mixture was then refluxed overnight, yielding the same red colour as before. The ethanol was removed from this mixture in vacuo and the remaining aqueous fraction was extracted with dichloromethane to remove excess ligand. However, it was found that the complex formed was also soluble in dichloromethane, and so diethyl ether was used to remove excess ligand from this organic extract as before. The resulting precipitate yielded the following encouraging ^{1}H NMR spectrum shown in Figure 6.25.

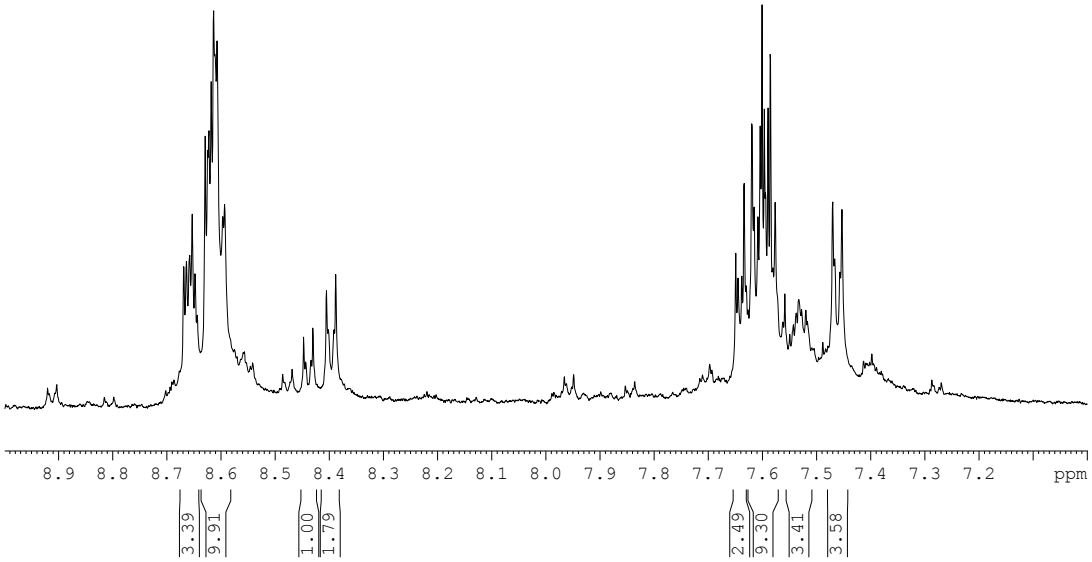

Figure 6.25: ^1H NMR spectrum of $[Ru(paen)(P0P)_2]^{2+}$ reaction product following DCM extraction as measured in d_3-acetonitrile

This sample was then columned on silica using 80:20 acetonitrile: water 0.05M KNO_3 as eluent, yielding the cleaner spectrum shown below in Figure 6.26.

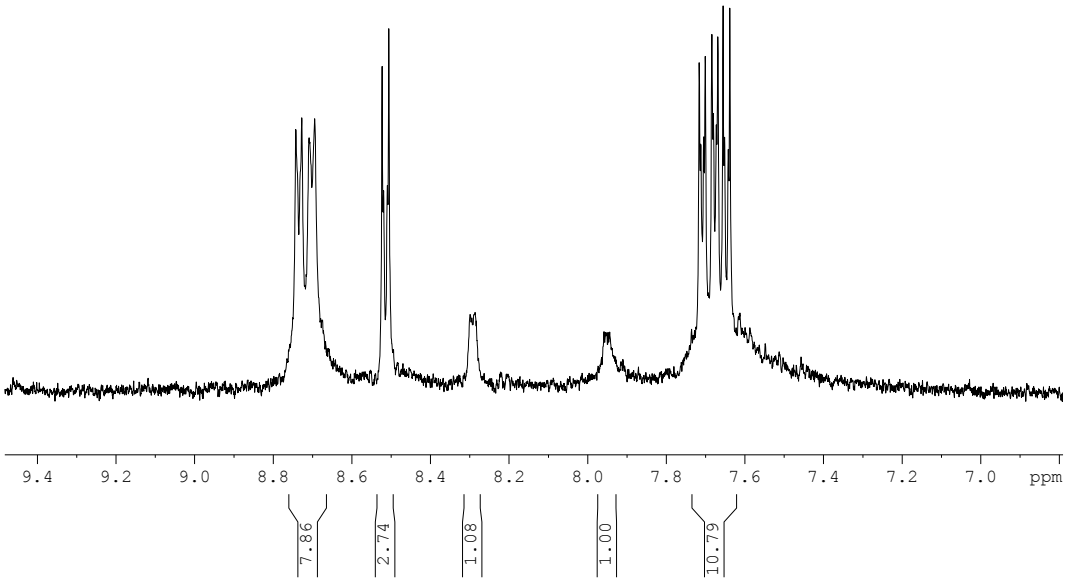

Figure 6.26: ^1H NMR spectrum of $[Ru(paen)(P0P)_2]^{2+}$ sample (corresponding to Figure 6.25) following DCM extraction and column chromatography in d_3-ACN

The spectrum shown in Figure 6.26 is certainly the cleanest obtained for any product of an attempted $[Ru(paen)(P0P)_2]^{2+}$ reaction discussed so far. The spectrum displays eight peaks as opposed to the expected nine, explicable by the possibility of overlapping signals. The expected integration of twenty-four is also very close to the integration of twenty-five displayed in Figure 6.26. However in spite of these

encouraging results, the fact remains that this is not enough conclusive information to definitively term this substance $[Ru(paen)(P0P)_2]^{2+}$.

In order to gain a better understanding of the progress of the reaction and therefore to maximise the amount of mononuclear product formed and obtain information as to how best to purify it, the reaction was reattempted and monitored by HPLC analysis.

6.2.3 HPLC monitored synthesis of $[Ru(paen)(P0P)_2](PF_6)_2$

A reflux reaction using purified $[Ru(paen)Cl_2]$ and 4,4'-bipyridyl as the only two reactants in an ethanol:water 2:1 mixture was attempted and monitored by HPLC. As $[Ru(paen)Cl_2]$ and 4,4'-bipyridyl are the only reactants used it can be assumed that any side products formed during the reaction are formed from these two compounds. The metal dichloride was added to a refluxing ethanolic solution of excess 4,4'-bipyridyl over 30 min. This solution was maintained at reflux and monitored by photodiode array HPLC using 75:20:5 acetonitrile:water:methanol 0.1M KNO_3. The reaction was also kept under a nitrogen atmosphere so as to minimise oxidation of the metal back to Ru(III) from Ru(II) as employed for $[Ru(bpy)_2Cl_2].2H_2O$ (see chapter 2)

Upon first addition of the metal dichloride to the reaction mixture, the mixture turned blue and remained that colour for approximately 10 min, after which the colour changed to purple.

The chromatogram for the reaction mixture at 0 min is shown below in Figure 6.27.

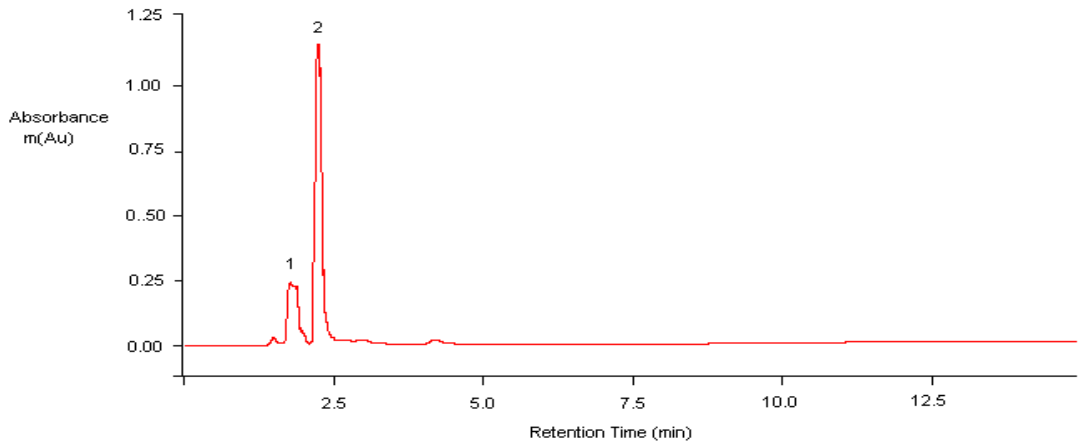

Figure 6.27: HPLC chromatogram for $[Ru(paen)Cl_2]$+4,4'-bipyridyl reaction mixture at 0 min

As expected, only two peaks are visible for at this stage of the reaction. The UV/vis spectrum of both of these peaks is shown in Figure 6.28 below.

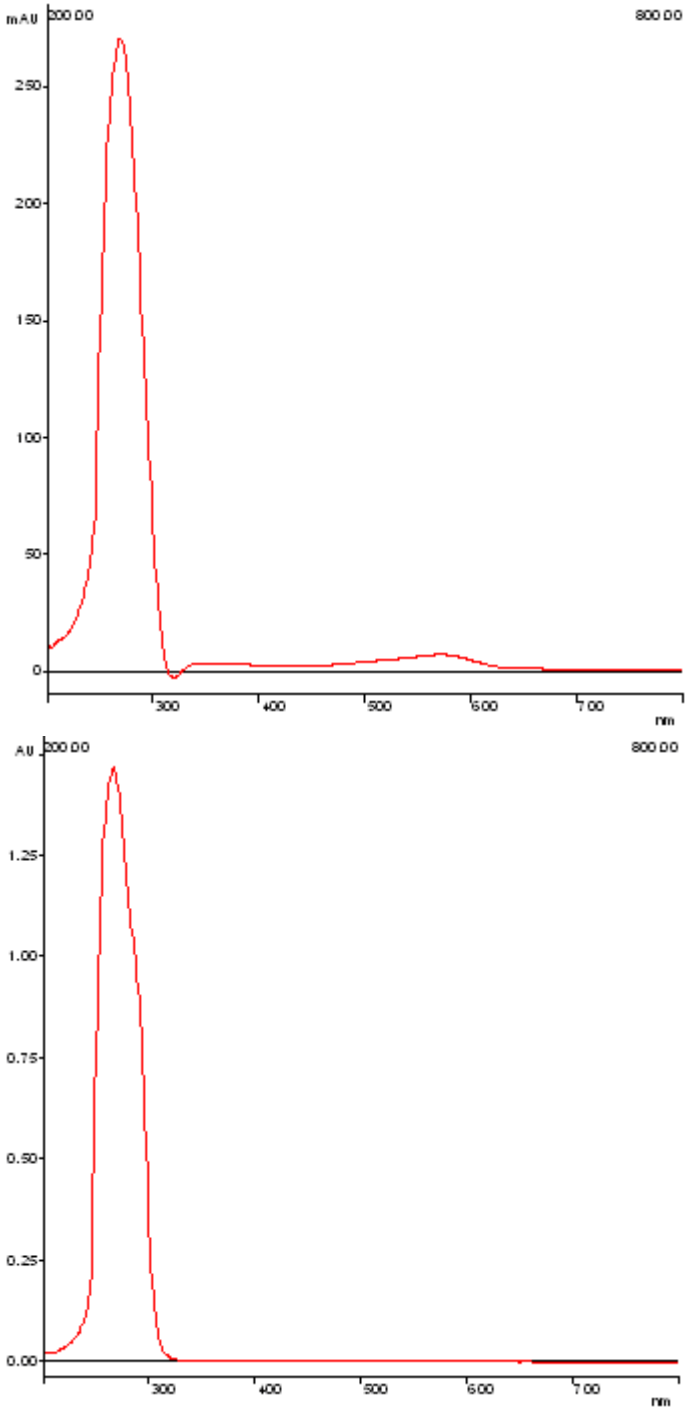

Figure 6.28: UV/vis spectra for (a) Peak 1 and (b) Peak 2 as shown in the HPLC chromatogram in Figure 6.27

The UV/vis spectrum relating to peak 1 as shown in Figure 6.28 a displays a ligand based absorbance at 270 nm as well as a characteristic ruthenium absorbance at 574

nm which implies that this peak relates to $[Ru(paen)Cl_2]$. The UV/vis relating to peak 2, on the other hand, shown in Figure 6.28 b displays only one ligand based absorbance at 270 nm, confirming that this peak relates to 4,4'-bipyridyl. This is compounded by the fact that the first eluting component is greatly dwarfed in amount by the second as shown in Figure 6.27, since the ligand P0P is present in 10 fold excess to the metal dichloride $Ru(paen)Cl_2$.

Samples were then taken at one-hour intervals for the next six hours. The HPLC chromatograms obtained at each of these intervals displayed five distinct peaks at identical retention times for all six samples. Therefore, the chromatograph corresponding to the reaction mixture following a six-hour reflux in ethanol is shown below in Figure 6.29.

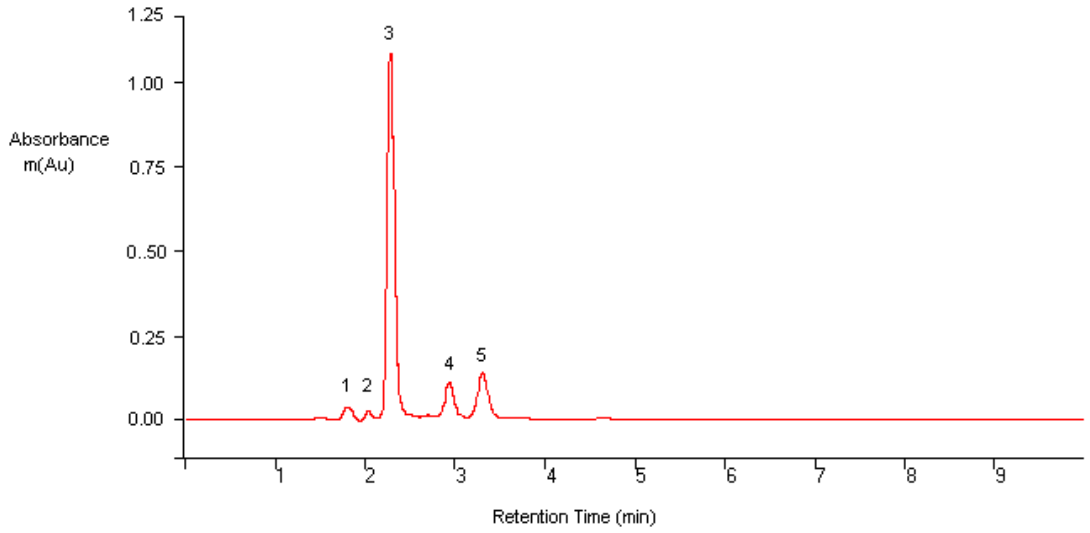

Figure 6.29: HPLC chromatogram for $[Ru(paen)Cl_2]$+4,4'-bipyridyl reaction mixture at 6 hr

The peaks labelled 2 and 3 in Figure 6.29 have identical retention times and UV/vis spectra to peaks 1 and 2 in Figure 6.27 respectively. Therefore peak 2 as shown in Figure 6.29 corresponds to unreacted $Ru(paen)Cl_2$ while peak 3 in the same chromatogram relates to excess 4,4'-bipyridyl present in the sample. Peaks 1, 4 and 5 as shown in Figure 6.29 may then be identified by their UV/vis spectra.

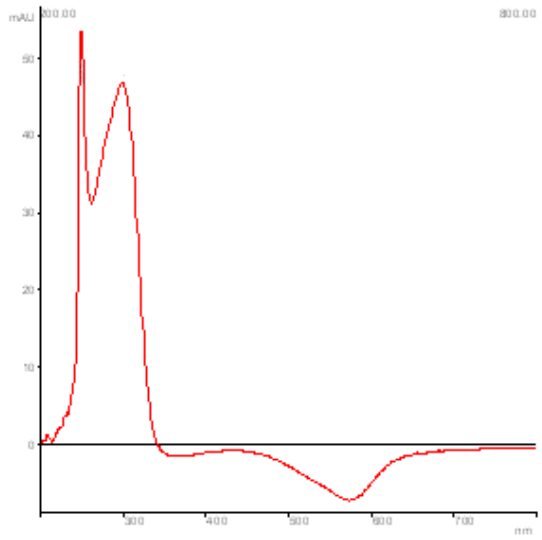

a.

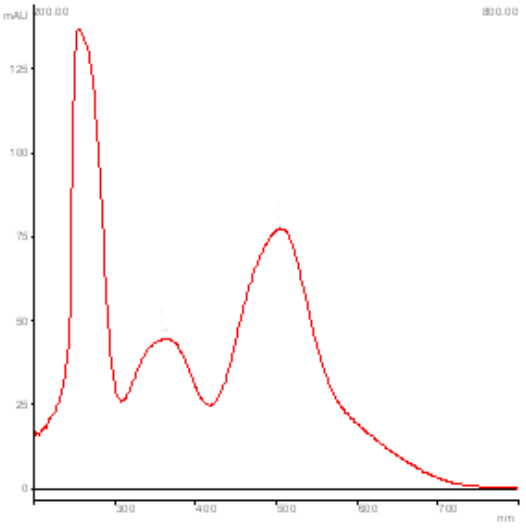

b.

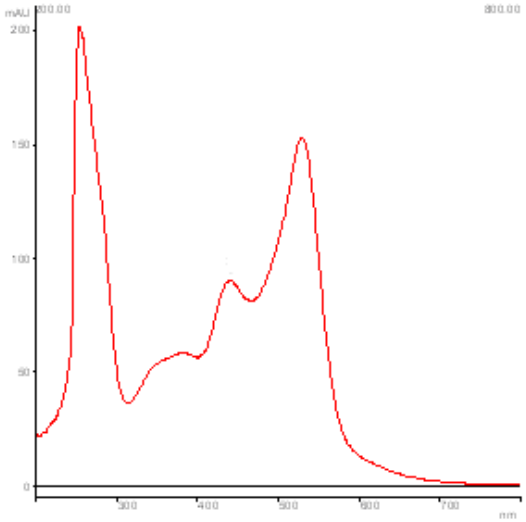

c.

Figure 6.30: UV/vis spectra for (a) Peak 1, (b) Peak 4 and (c) Peak 5 as shown in the HPLC chromatogram in Figure 6.29

The UV/vis spectrum displayed in Figure 6.30(a) corresponding to Peak 1 in Figure 6.29 consists of two ligand based peaks, one at 249 nm and another at 299 nm. As 4,4'-bipyridyl has been defined previously in this report as having an approximate retention time of 2.20 min in this system, this peak (present here at 1.79 min retention time) corresponds to a different ligand type molecule. The only organic species available in the reaction mixture is paen, which in this case may have dissociated from its ruthenium complex.

Both of the remaining UV/vis spectra (shown in Figure 6.30 b and c, relating to Figure 6.29's peaks 4 and 5 respectively) relate to ruthenium metal complexes. Both spectra display a ligand based peak at approximately 260 nm implying that both of these substances contain the ligand 4,4'-bipyridyl. The other absorbencies displayed (367 nm and 505 nm for Peak 4 and 439 nm and 529 nm for Peak 5) are indicative of a ruthenium metal complex. At this point it was postulated that one peak corresponded to an intermediate complex $[Ru(paen)(P0P)Cl]^{+}$ while the other corresponded to the desired product $[Ru(paen)(P0P)_2]^{2+}$.

The reaction mixture was then left overnight, and for a further 6 hr the next day, totalling the overall reaction time as 30 hr. The HPLC chromatogram of the final (30 hr) sample, shown below in Figure 6.31 shows the same mixture of components displayed in Figure 6.29.

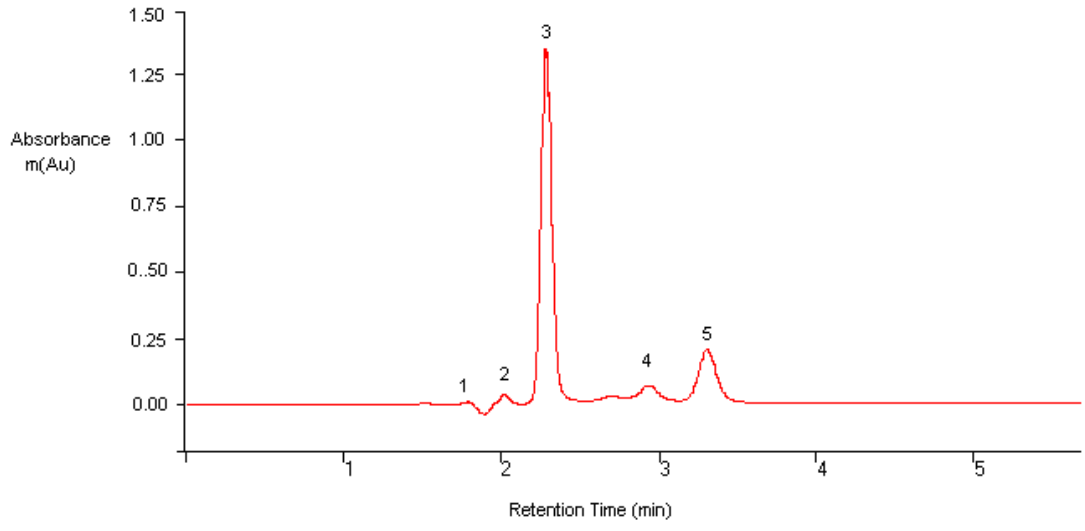

Figure 6.31: HPLC chromatogram for $[Ru(paen)Cl_2]$+4,4'-bipyridyl reaction mixture at 30 hr

The UV/vis spectrum of each respective peak was identical to those discussed for Figure 6.29. Examining peak 4 and peak 5 as shown in Figure 6.31 it can be seen that peak 5 has grown to approximately 4 times the intensity of peak 4, leading to the assumption that peak 5 relates to the final product $[Ru(paen)(P0P)_2]^{2+}$ while peak 4 relates to the intermediate $[Ru(paen)(P0P)Cl]^{+}$.

In order to prove or disprove this assumption, the cooled reaction mixture was separated using column chromatography. The system used for this separation (80:20 acetonitrile: water 0.05M KNO_3 on silica) is very similar to that used in the HPLC separation shown in Figure 6.29. Therefore it was assumed that the components of the mixture would elute in the same order as shown in the chromatograph. As expected a purple band (relating to residual $[Ru(paen)Cl_2]$ corresponding to peak one in Figure 6.31) eluted first, followed by a colourless UV active fraction, with two red bands eluting last, one after the other. The acetonitrile was removed from both of the red fractions and a saturated aqueous solution of KPF_6 was added. Red precipitate immediately formed in both fractions which were then filtered and sent for ^1H NMR analysis.

The solid obtained from the third column fraction (the first red band) yielded a spectrum displaying a huge excess of 4,4'-bipyridyl, identical to the spectrum shown in Figure 6.23 (b). The spectrum shown below in Figure 6.32 relates to the fourth band (the second red band) eluted during the column chromatography detailed above. When analysed by HPLC this purified fraction yielded a retention time identical to that of peak 5 as shown in Figure 6.31. The total integration of this spectrum equal an overall value of 18 as opposed to the expected value of 26 for the aromatic region of $[Ru(paen)(P0P)_2](PF_6)_2$. This integration value may be reconciled by assuming that one of the P0P ligands is not present in the molecule. If this is indeed the case of the metal complex $[Ru(paen)(POP)Cl](PF_6)$ which has a total of 18 protons is present. More thorough interpretation of the spectrum shown in Figure 6.32, confirming that it is in fact the metal complex $[Ru(paen)(P0P)Cl](PF_6)$ is shown in section 6.3

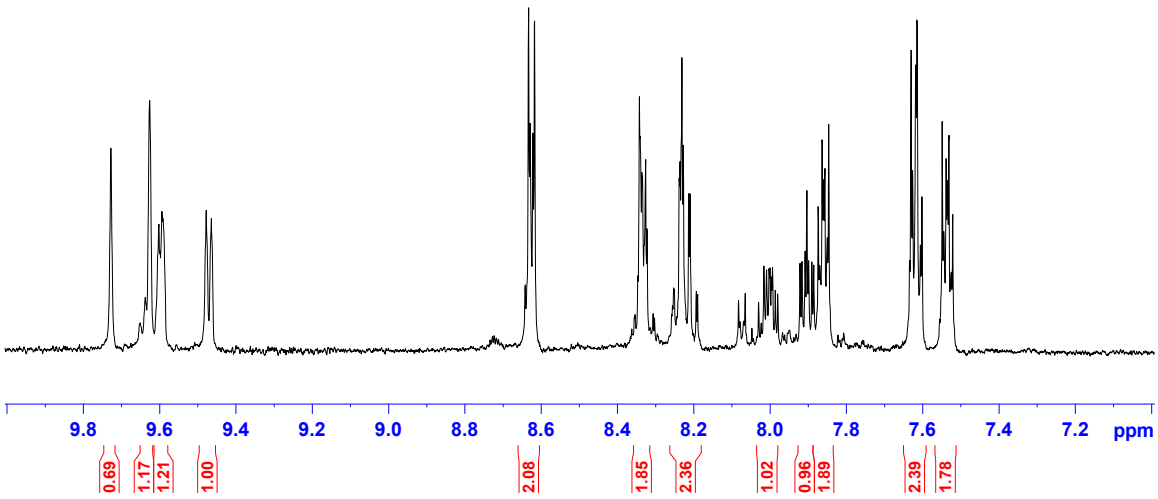

Figure 6.32: ^1H NMR spectrum of [Ru(paen)(P0P)Cl](PF$_6$) as measured in d_6-acetone

In order to investigate whether the bis-4,4'-bipyridyl analogue of the above complex may be formed with increased reaction time a reaction was monitored by HPLC and left at reflux until the starting material [Ru(paen)Cl$_2$] was completely consumed. After 120 hr the HPLC chromatogram shown below in Figure 4.19 was obtained.

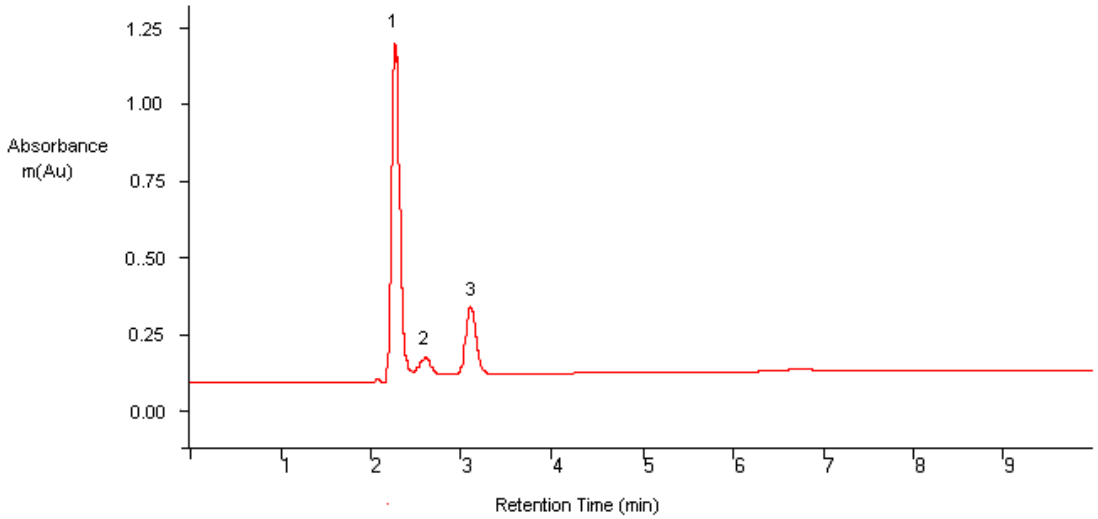

Figure 6.33: HPLC chromatogram for [Ru(paen)Cl$_2$] +4,4'-bipyridyl reaction mixture at 120 hr

It can be seen in Figure 6.33 that two main products are formed (peaks 2 and 3) in addition to the excess of 4,4'-bipyridyl (peak 1). The UV/vis spectra of the two products seen here in Figure 4.31 are shown below in Figure 6.34 and Figure 6.35.

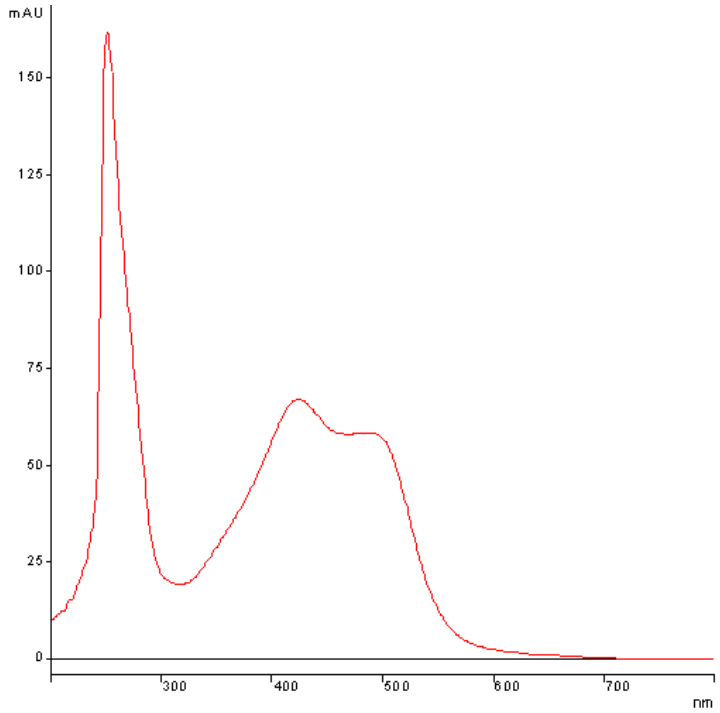

Figure 6.34: UV/vis spectrum for peak 2 as shown in Figure 6.33

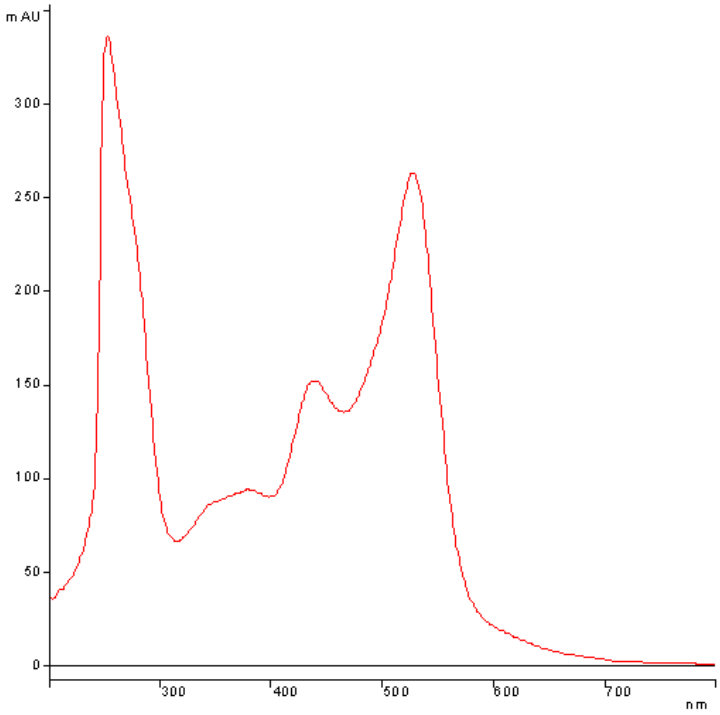

Figure 6.35: UV/vis spectrum for peak 3as shown in Figure 6.33

In order to fully identify these components they were isolated as before. The reaction mixture was reduced in volume to approximately 5 cm^3 and loaded onto a silica column packed with acetonitrile and eluted with 80:20 acetonitrile: water 0.05M

KNO_3. A main red band was observed and collected. When sent for ^1H NMR the same spectrum as shown in Figure 6.32 was observed, implying that the product present is $[Ru(paen)(P0P)Cl]^+$. A late eluting band was observed and collected. Injecting this column fraction onto the HPLC system, the following chromatograph shown below in Figure 6.36 was observed.

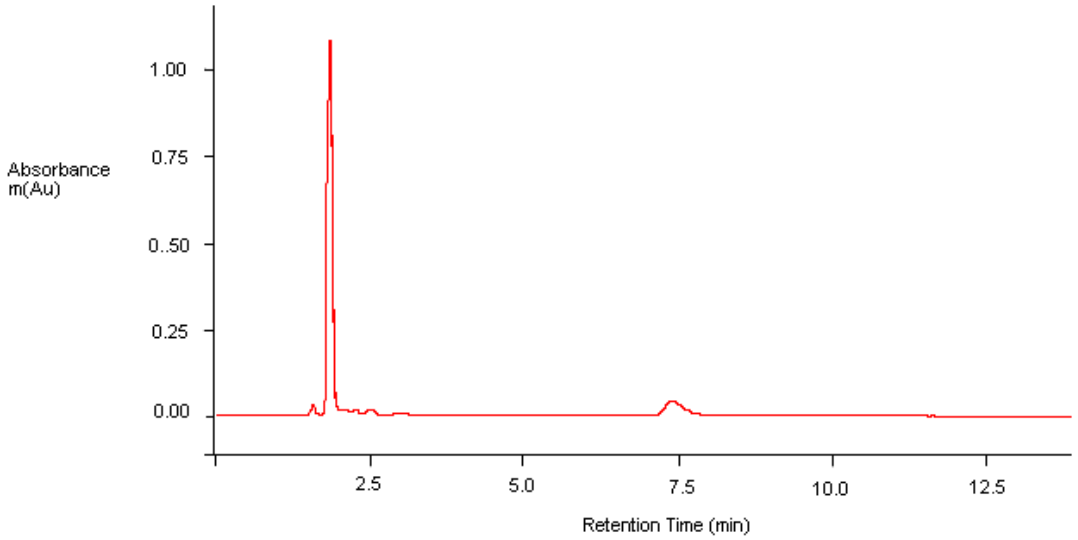

Figure 6.36: HPLC chromatogram for last eluting column fraction obtained from $[Ru(paen)(P0P)_2](PF_6)_2$ 120 hr reflux

As before, the peak appearing at 1.8 min relates to excess 4,4'-bipyridyl present in the HPLC sample. However, the peak appearing at approximately 7.5 min has not been seen before in the reaction mixture chromatographs and therefore must exist within the reaction mixture in very low concentration. The UV/vis spectrum of this compound is shown below in Figure 6.37.

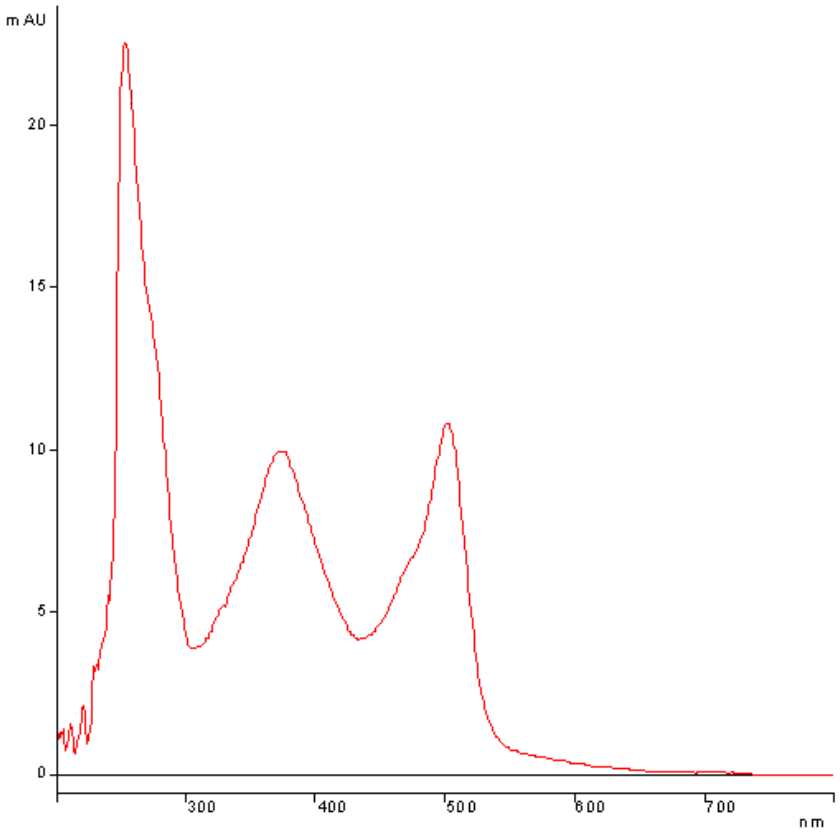

Figure 6.37: UV/vis spectrum for peak at 7.5 min retention time in Figure 6.36

This sample was later sent for ^{1}H NMR, yielding the following spectrum shown in Figure 6.38.

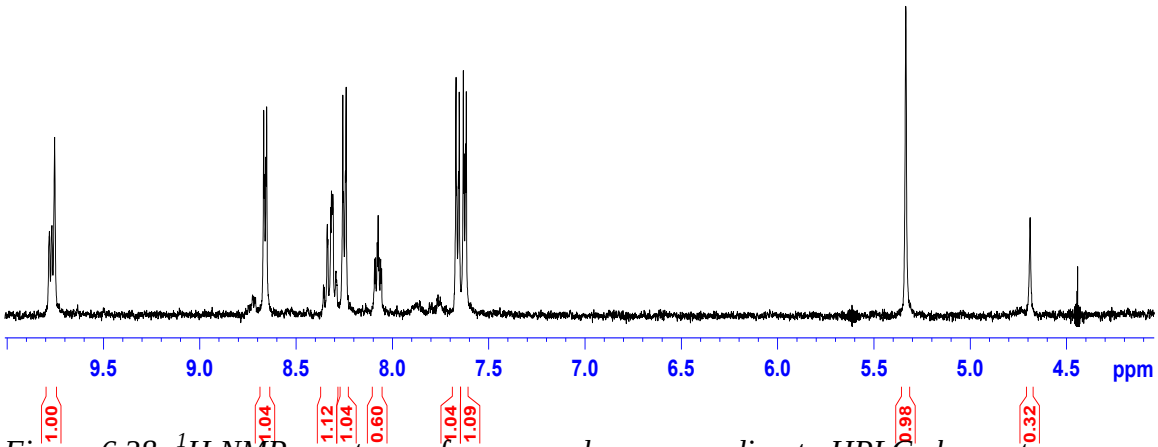

Figure 6.38: ^{1}H NMR spectrum of compound corresponding to HPLC chromatogram shown in Figure 6.37.

This spectrum displays signals at 9.76 ppm, 8.32 ppm and 8.07 ppm relating to the aromatic protons of the paen ligand, and the ethyl protons appearing at 5.42 ppm. The spectrum also displays the expected 4 doublets relating to the two appended P0P groups, implying that this compound is the desired product $[Ru(paen)(P0P)_2]^{2+}$. The fact that this complex forms after such a long reaction time and remains intact,

suggests that paen is not susceptible to the kind of thermal degredation usually associated with imine ligands. However, the reaction time of 120 hr is not ideal and in this case only yielded a small amount of product. In the formation of the bis-bidentate metal complex $[Ru(bpy)_2(P0P)_2](PF_6)_2$ where bpy is 2,2'-bipyridyl and P0P is 4,4'-bipyridyl, $AgNO_3$ may be used to remove the chloride ions from the ruthenium starting material $Ru(bpy)_2Cl_2$[36] The use of this method in an attempt to reduce the reaction time of 120 hr described above, is described below in Section 6.2.4.

6.2.4 $AgNO_3$ Approach

Following the method exactly as previously published[36], 1 equivalent of $Ru(paen)Cl_2$ was refluxed with 20 equivalents of $AgNO_3$ until a suspension was formed. The grey solid formed was removed by filtration and the filtrate was transferred back to reflux and 10 equivalents 4,4'-bipyridyl was added to the reaction vessel. At this point a dense white/grey precipitate formed. This precipitate was removed by filtration and sent for ^1H NMR, but no spectrum was obtained. It was surmised that this material was the polymer $[Ag(P0P)_2]_n$ shown below in Figure 6.39. Polymeric materials, due to their intrinsic insolubility very rarely yield ^1H NMR spectra, and due to the large excesses of both Ag^{2+} and 4,4'-bipyridyl in the reaction mixture it is valid to assume that this is the material formed.

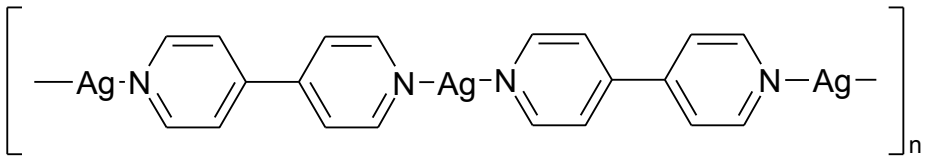

Figure 6.39: Structural representation of the polymer $[Ag(P0P)_2]_n$

In order to avoid the formation of this material, the reaction was repeated, this time incorporating 2 equivalents of $AgNO_3$ instead of 20. As expected a grey precipitate was formed after refluxing $[Ru(paen)Cl_2]$ with 2 equivalents $AgNO_3$ for approximately 1 hr. After removing this precipitate by filtration, the orange filtrate was returned to the reaction vessel. Upon reaching reflux, 10 equivalents 4,4'-bipyridyl were added and the resulting mixture was kept at reflux overnight. The orange/brown solution formed was reduced to approximately 5 cm^3 in vacuo and a saturated solution $KPF_{6\ (aq)}$ was added. The resulting suspension was filtered and the

obtained orange solid washed with water. This solid was dissolved in acetone and purified by column chromatography on a silica column using 80: 20 ACN: H_2O 0.05 M KNO_3. The main orange band was collected and the acetonitrile removed in vacuo. The purified product was isolated by adding a $KPF_{6\ (aq)}$ saturated solution and filtering the resulting suspension. The collected orange solid was dried at the pump and sent for ^1H NMR analysis. In order to obtain a readable spectrum the sample was analysed at a rate of 1000 scans. The spectrum obtained is shown below in Figure 6.40.

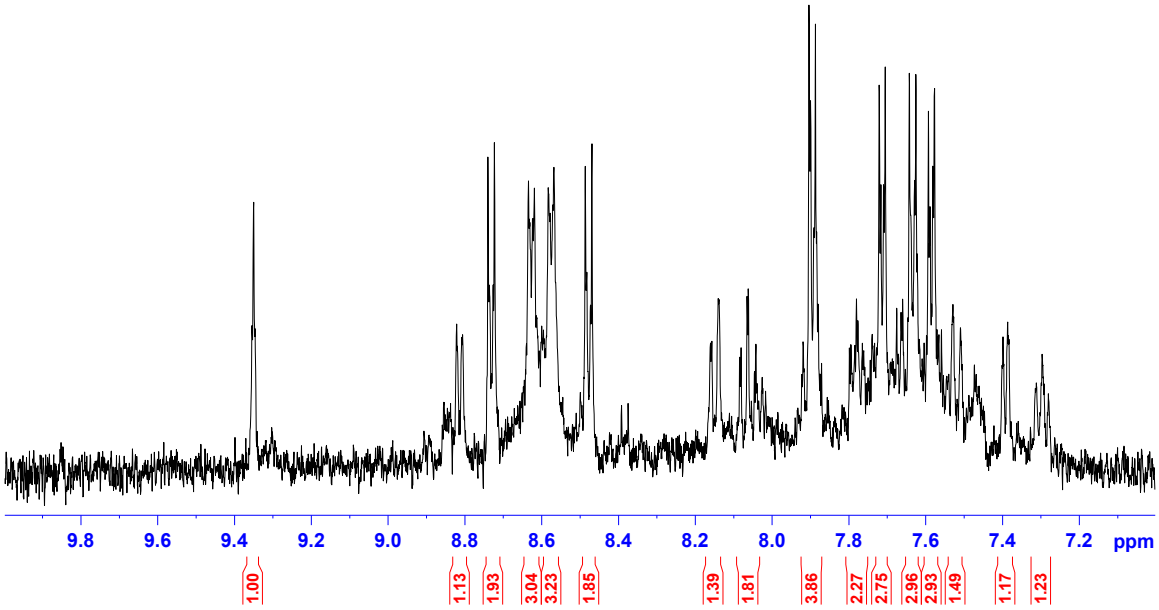

Figure 6.40: ^1H NMR spectrum as measured in d_6-acetone for the PF_6 salt formed from the attempted preparation of $[Ru(paen)(P0P)_2](PF_6)_2$ using $AgNO_3$ as a reactant

Further column chromatography was attempted as well as recrystallisation, but no purification was observed.

As a result of this, extended reflux (120 hr) between purified $[Ru(paen)Cl_2]$ and 4,4'-bipyridyl followed by purification by column chromatography using silica and 80:20 acetonitrile: water 0.05M KNO_3 was deemed to be the most effective method of preparation of the desired $[Ru(paen)(P0P)_2](PF_6)_2$. With this information, preparation of the related complex $[Ru(papn)(P0P)_2](PF_6)_2$ was attempted.

6.2.5.Preparation of $[Ru(papn)(P0P)_2](PF_6)_2$

The same type of successful reaction as detailed above for $[Ru(paen)(P0P)_2](PF_6)_2$ was attempted using the propyl analogue of paen, papn (see Figure 6.2). 333 mg (1.65 mmol) $RuCl_3.2H_2O$ was refluxed in 15 cm^3 MeOH with 2.9 g (16.5 eq) ascorbic acid overnight. 500 mg (1.98 mmol) papn was added to the green reaction mixture and refluxed overnight. The dark purple reaction mixture was reduced to 5 cm^3 in vacuo and loaded onto a neutral alumina column packed with dichloromethane, and the column was then run using 10:1 dichloromethane: acetone as mobile phase. The first eluting blue band was collected and the solvent removed. The resulting blue-black solid was recrystallised from dichloromethane: hexane. 54.5 mg solid was formed, signifying a 7.8% yield of the dichloride $[Ru(papn)Cl_2]$. A clear ^1H NMR spectrum of this solid was not obtained, but as the product matched the analogous $[Ru(paen)Cl_2]$ in preparation, appearance and yield, this solid was used to progress to the next step of the synthesis.

This solid was placed in 20 cm^3 refluxing MeOH with 3.09 g (19.8 mmol) 4,4'-bpy and refluxed overnight. The reaction mixture was reduced in volume to approximately 5 cm^3 in vacuo in a beaker and left at 5^0C overnight after which excess ligand crystallised and was filtered off. Solvent was removed from the dark red filtrate which was redissolved in acetonitrile and columned on silica with 80: 20 acetonitrile: H_2O 0.05 KNO_3. The main orange fraction was collected and sent for ^1H NMR. The resulting spectrum though encourageing showed a sizeable level of impurity still present. A TLC on alumina with acetonitrile showed one orange spot, and so the product was columned using this system. The resulting solid was sent for ^1H NMR analysis and yielded the following spectrum.

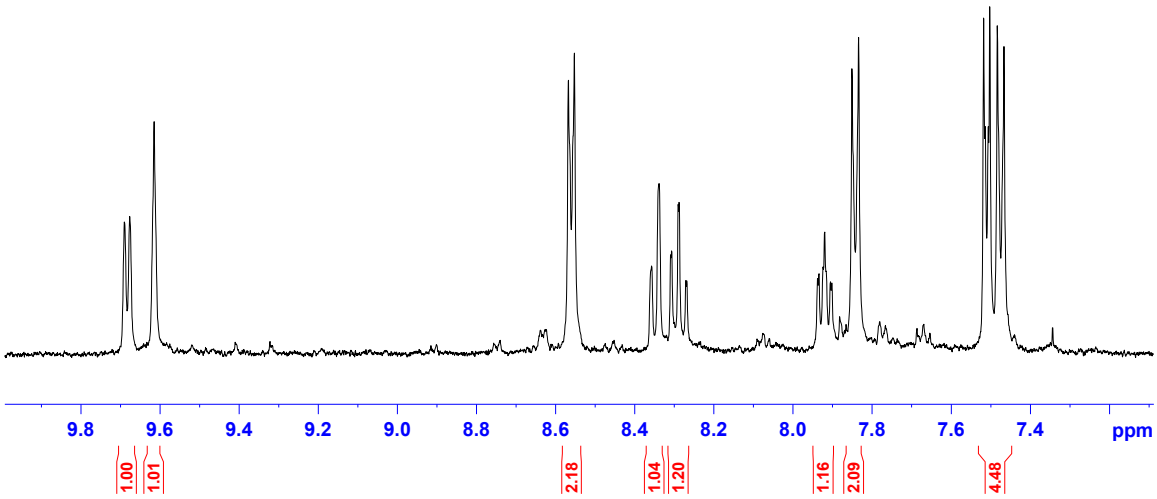

Figure 6.41: ^1H NMR spectrum of $[Ru(papn)(POP)_2]^{2+}$ following purification on silica using 80:20 acetonitrile: water 0.05M KNO_3 followed by further purification on alumina using acetonitrile as eluent

This spectrum is very similar to that of the pure $[Ru(paen)(P0P)_2](PF_6)_2$ shown in Figure 6.38. Again, the signals appearing at 9.69 ppm, 9.61 ppm, 8.33 ppm, 8.28 ppm and 7.92 ppm relate to the aromatic portion of the papn ligand while the doublets present at 8.57 ppm, 7.81 ppm, 7.49 ppm and 7.44 ppm relate to the P0P portion of the molecule.

Through this synthetic study, aided by HPLC analysis methods, it can be seen that the metal complexes $[Ru(paen)(P0P)_2](PF_6)_2$ and $[Ru(papn)(P0P)_2](PF_6)_2$ as well as the additional metal complex $[Ru(paen)(P0P)Cl](PF_6)$ may be synthesised, through a straightforward reflux reaction between the ligand 4,4'-bipyridyl (P0P) and the appropriate metal dichloride starting material, $[Ru(paen)Cl_2]$ or $[Ru(papn)Cl_2]$[28]. The final products however are synthesised in very low yield, though the apparent resilience of the imine ligands paen and papn under reflux may allow for further study into increased reaction times and/or harsher reaction conditions.

6.3 ^{1}H NMR Analysis

The ^{1}H NMR spectrum for $[Ru(paen)Cl_2]$ is shown below in Figure 6.42. This ^{1}H NMR data has not been published previously[28] and so shall be discussed in detail below.

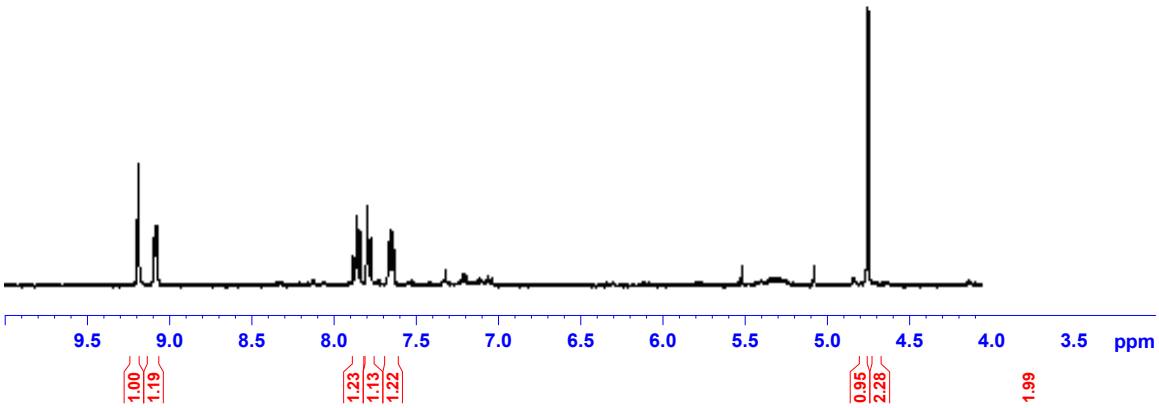

Figure 6.42: ^{1}H NMR spectrum of $Ru(paen)Cl_2$ as measured in CD_2Cl_2

In order to examine the aromatic portion of the molecule more closely, an expanded view of the aromatic region of the spectrum (i.e. from 9.5 ppm-7.0 ppm) is shown below in Figure 6.43.

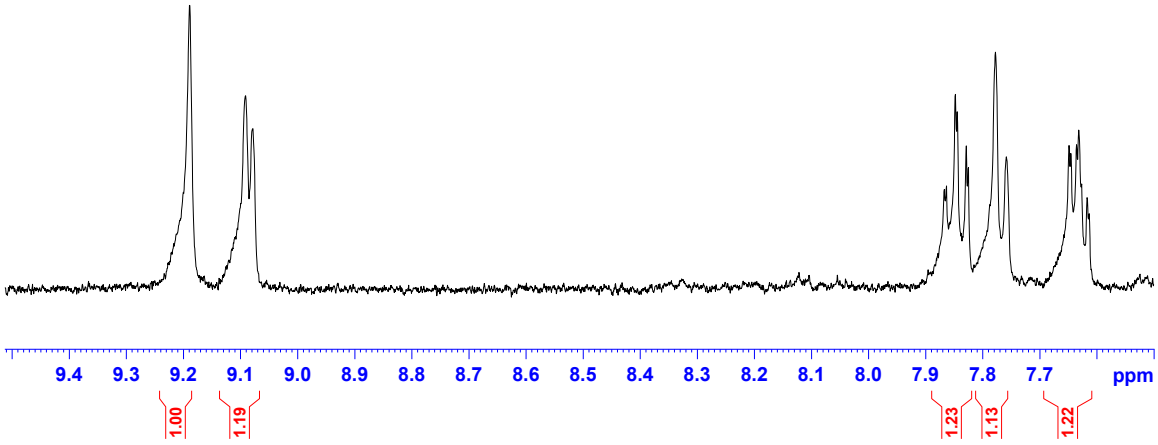

Figure 6.43: Magnified view of the aromatic region of the spectrum shown in Figure 6.42

Due to the symmetrical nature of this molecule, six signals are observed in Figure 6.42 corresponding to the fourteen protons present in the molecule. The fact that only six signals are observed confirms that the molecule is formed in the highly symmetrical *trans* conformation as shown in Figure 6.44.

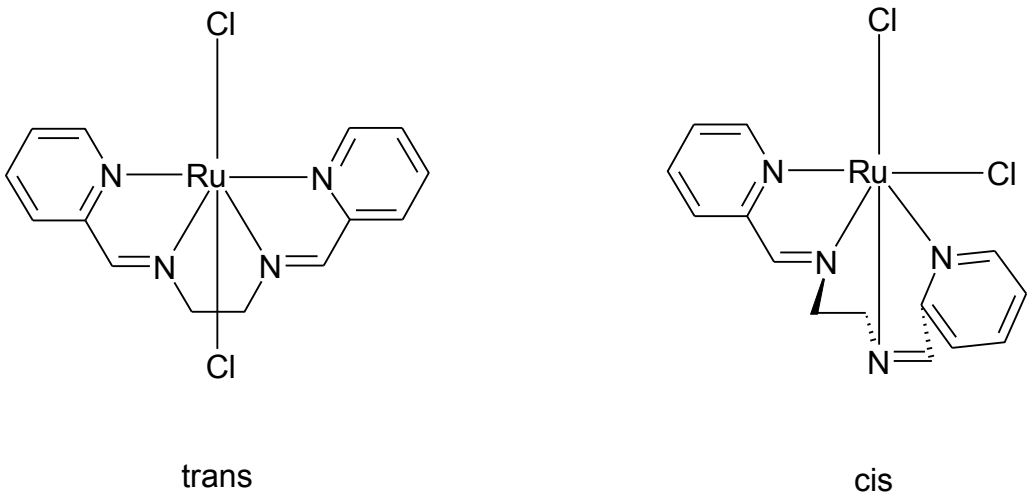

Figure 6.44: Cis and trans conformations of $[Ru(paen)Cl_2]$

In the asymmetric *cis* conformation the aromatic rings and imine groups present in the molecule are not chemically equivalent, and so would produce ten distinct ^1H NMR signals, as opposed to the five aromatic and imine peaks visible in Figure 6.43. This information confirms that the $[Ru(paen)Cl_2]$ material obtained is in the *trans* conformation.

Ten of these protons appear as the five signals present in the aromatic region of the spectrum, shown in Figure 6.43. These protons are shown in the numbering scheme for the molecule illustrated in Figure 6.45 (a) below. The remaining four protons are aliphatic in nature and all exist in an identical environment to each other and so appear as a singlet in the aliphatic region of the spectrum shown in Figure 6.42 (i.e. 5ppm-0 ppm). The ^1H COSY spectrum for this complex is shown below in Figure 6.45 along with the numbering system for this complex.

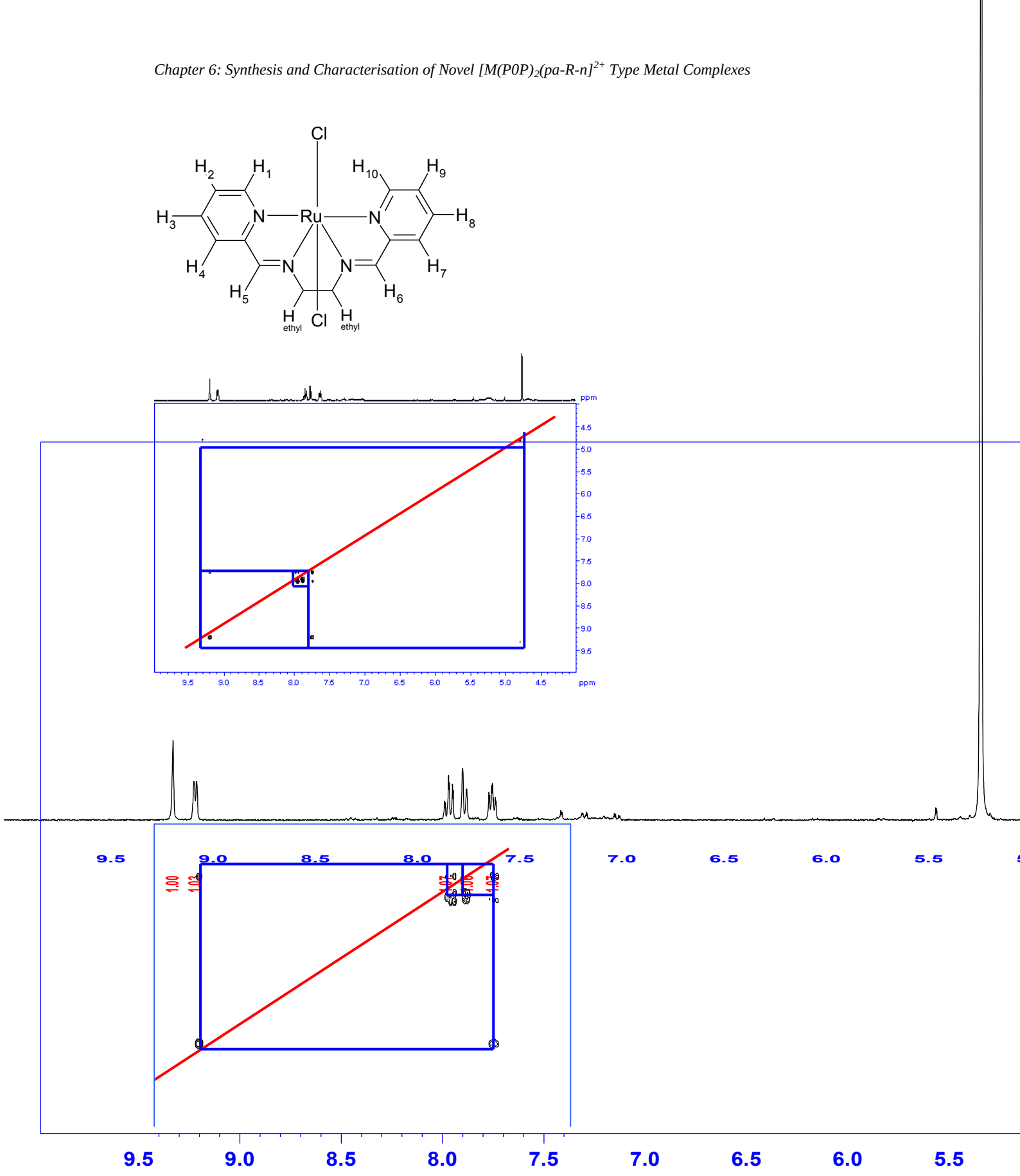

Figure 6.45: (a) Numbering system for the metal complex $[Ru(paen)Cl_2]$ (b) ^1H COSY of the metal complex $[Ru(paen)Cl_2]$ highlighting coupling paen protons and (c) a magnified view of the aromatic region in Figure 4.42 (b) highlighting the coupling paen protons

It can be seen from the spectrum shown in Figure 6.45 (b) that the singlet visible at 9.21 ppm interacts with the singlet present in the aliphatic region of the spectrum at 4.74 ppm. This interaction, along with the fact that both peaks appear as singlets implies that they correspond to the imine protons H_5 and H_6 and the aliphatic CH_2 groups respectively. The interaction between these two signals must be based on long range coupling as both groups have no adjacent protons within the molecule, a fact confirmed by the singlet nature of both peaks which is unaffected by the (weak) interaction between the two protons.

The remaining aromatic protons may be assigned based on their appearance and coupling characteristics. The remaining signals consist of two doublets and two triplets. The most downfield of these signals is a doublet occurring at 9.09 ppm. As this doublet appears in a very similar position to that of the imine protons, it may be inferred that the proton corresponding to the doublet in question exists in a similar environment to H_5 and H_6. This implies that this doublet corresponds to the pyridyl proton H_4 and H_7, which is situated adjacent to the imine groups.

This signal couples with a triplet occurring at 7.63 ppm. This implies that this triplet corresponds to H_4 and H_7's adjacent protons H_3 and H_8. These protons in turn also couple to a second triplet visible at 7.85 ppm indicating that this signal corresponds to H_2 and H_9 which are situated adjacent to H_3 and H_8.

H_2 and H_9 couple also to the one remaining signal: a doublet present at 7.77 ppm, confirming that this signal relates to H_1 and H_{10}.

These values are tabulated below in Table 6.3

Proton	**Chemical Shift (ppm)**	**Integration**	**Coupling Constant (Hz)**
H_1/H_{10}	7.77 (d)	1.06 (2H)	7.6
H_2/H_9	7.63 (t)	1.07 (2H)	4
H_3/H_8	7.84 (t)	1.07 (2H)	6
H_4/H_7	9.09 (d)	1.00 (2H)	5.6
H_5/H_6	9.20 (s)	1.00 (2H)	-
H_{ethyl}	5.32 (s-broad)	1.09 (4H)	-

Table 6.3: Chemical shift and integration for assigned protons in the ^1H NMR spectrum of $[Ru(paen)Cl_2]$

The ^{1}H NMR spectrum for $[Ru(paen)(POP)Cl]^+$ is shown below in Figure 6.46.

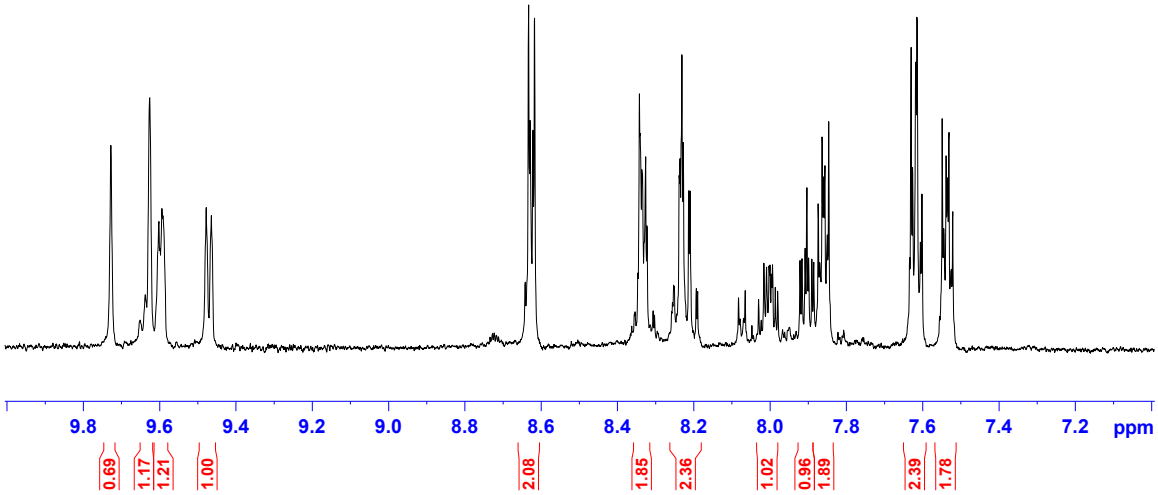

Figure 6.46: ^1H NMR spectrum of $[Ru(paen)(P0P)Cl](PF_6)$ as measured in d_6-acetone

The ^{1}H COSY spectrum for this complex is shown below in Figure 6.47 along with the numbering system for this complex. Initially, it can be seen that the doublet present at 8.62 ppm and the peak present at 7.63 ppm couple only to each other. This implies that these peaks relate to the 4,4'-bipyridyl group present in the molecule. The peak present at 7.63 ppm appears to overlap with a slight impurity in the sample, which results in this peak appearing as a multiplet as opposed to the expected doublet. The two peaks present at 7.86 ppm and 7.53 ppm also only couple to each other and therefore can also be identified as 4,4'-bipyridyl protons. The singlets present at 9.73 ppm and 9.63 ppm relate to the imine protons H_5 and H_6 respectively. The doublets

present at 9.59 ppm and 9.47 ppm therefore relate to H_4 and H_7 respectively. The doublet at 9.59 ppm couples to the multiplet present at 8.00 ppm, indicating that this triplet relates to H_3. This peak relating to H_3 couples also to the multiplet present at 8.33 ppm. This multiplet integrates for a value of 2 and so it can be assumed that both signals for H_2 and H_1 overlap at this point. The doublet relating to H_7 couples with the triplet present at 7.90 ppm. This peak therefore relates to H_8. The peak relating to H_8 couples to the multiplet at 8.22 ppm. As before this indicates that the signals for H_9 and H_{10} overlap at this point.

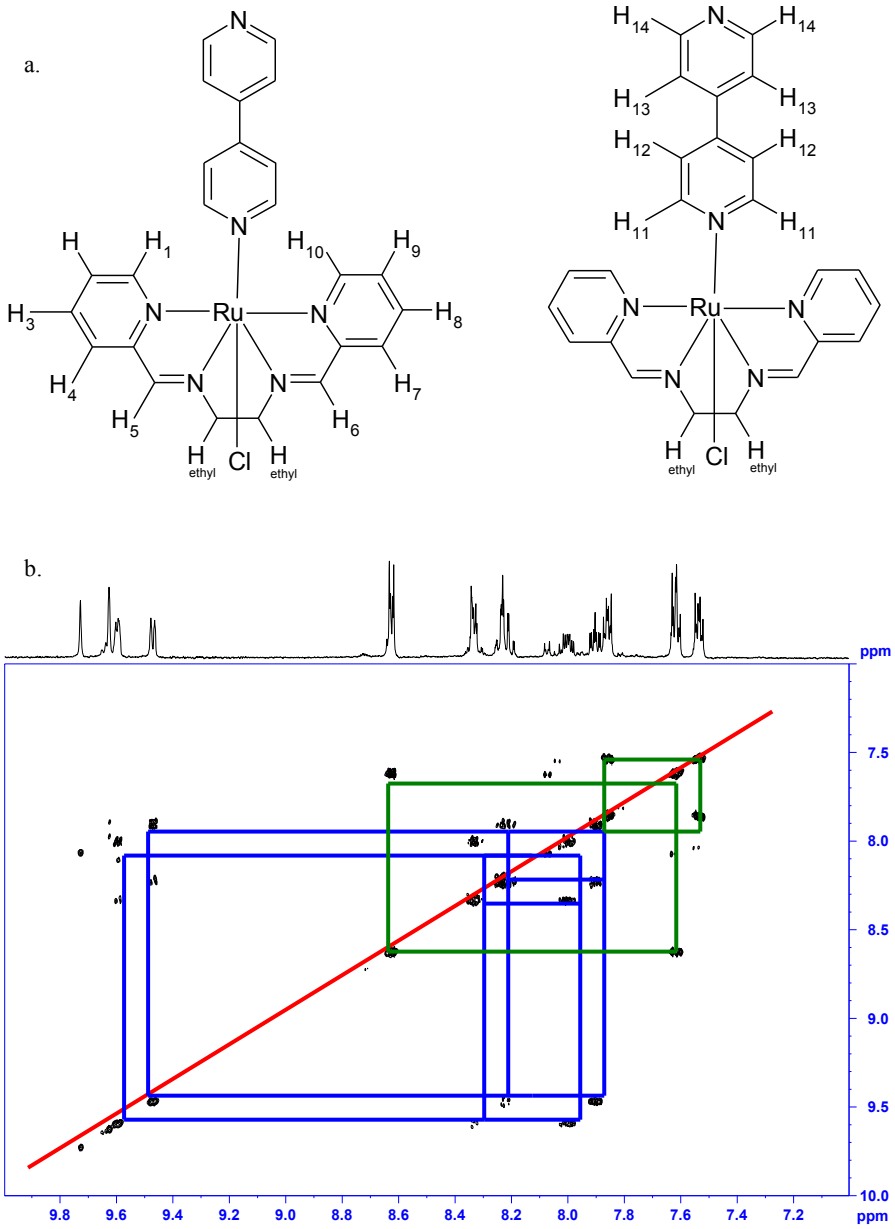

Figure 6.47: (a) Numbering system for the metal complex [Ru(paen)(P0P)Cl](PF$_6$) and (b) 1H COSY of the metal complex [Ru(paen)(P0P)Cl](PF$_6$) highlighting coupling paen protons (blue) and P0P protons (green)

It can be seen from the above spectra that there are two separate singlets present at 9.72 ppm and 9.61 ppm corresponding to the imine proton of the paen ligand (H_5 and H_6 as shown in Figure 6.47 a) and two separate doublets present at 9.59 ppm and 9.47 ppm corresponding to the pyridyl paen protons H_4 and H_7. This information suggests that the metal complex [Ru(paen)(P0P)Cl](PF_6) is not of a symmetrical *trans* geometry as shown in Figure 6.47 (a), but is instead of assymetric *cis* type geometry as shown below in Figure 6.48.

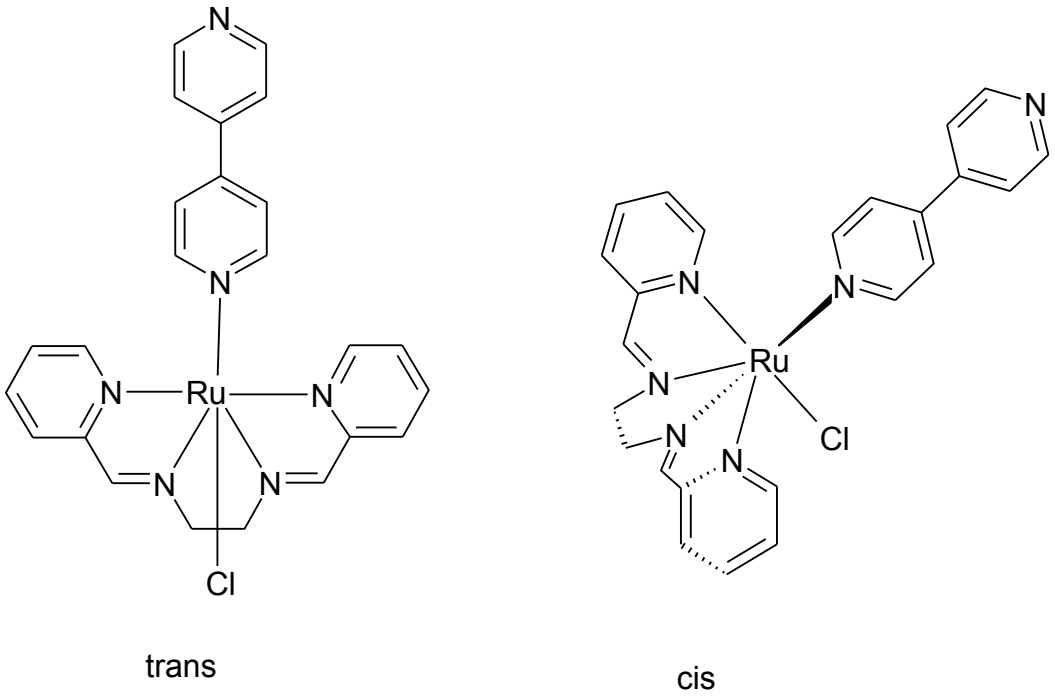

Figure 6.48: Diagrammatical representation of the trans and cis arrangement for the metal complex [Ru(paen)(P0P)Cl](PF_6)

Proton	**Chemical Shift (ppm)**	**Integration**	**Coupling Constant (Hz)**
H_1	8.33 (m)	1.89 (2H)	-
H_2	8.33 (m)	1.89 (2H)	-
H_3	8.00 (m)	1.02 (1H)	-
H_4	9.59 (s br)	1.21 (1H)	-
H_5	9.73 (s)	0.69 (1H)	-
H_6	9.63 (s)	1.17 (1H)	-
H_7	9.47 (d)	1.00 (1H)	-
H_8	7.90 (t)	0.96 (1H)	5.2
H_9	8.22 (m)	2.36 (2H)	-
H_{10}	8.22 (m)	2.36 (2H)	-
H_{11}	8.62 (d)	2.08 (2H)	7
H_{12}	7.63 (d)	2.39 (2H)	6.4
H_{13}	7.53 (d)	1.78 (2H)	7
H_{14}	7.86 (d)	1.89 (2H)	6.8
$H_{ethy;}$	4.78 (s-broad)	3.77 (4H)	-

Table 6.4: Chemical shift and integration for assigned protons in the ^1H NMR spectrum of $[Ru(paen)(P0P)Cl]^+$

The ^{1}H NMR spectrum for $[Ru(paen)(POP)_2](PF_6)_2$ is shown below in Figure 6.49.

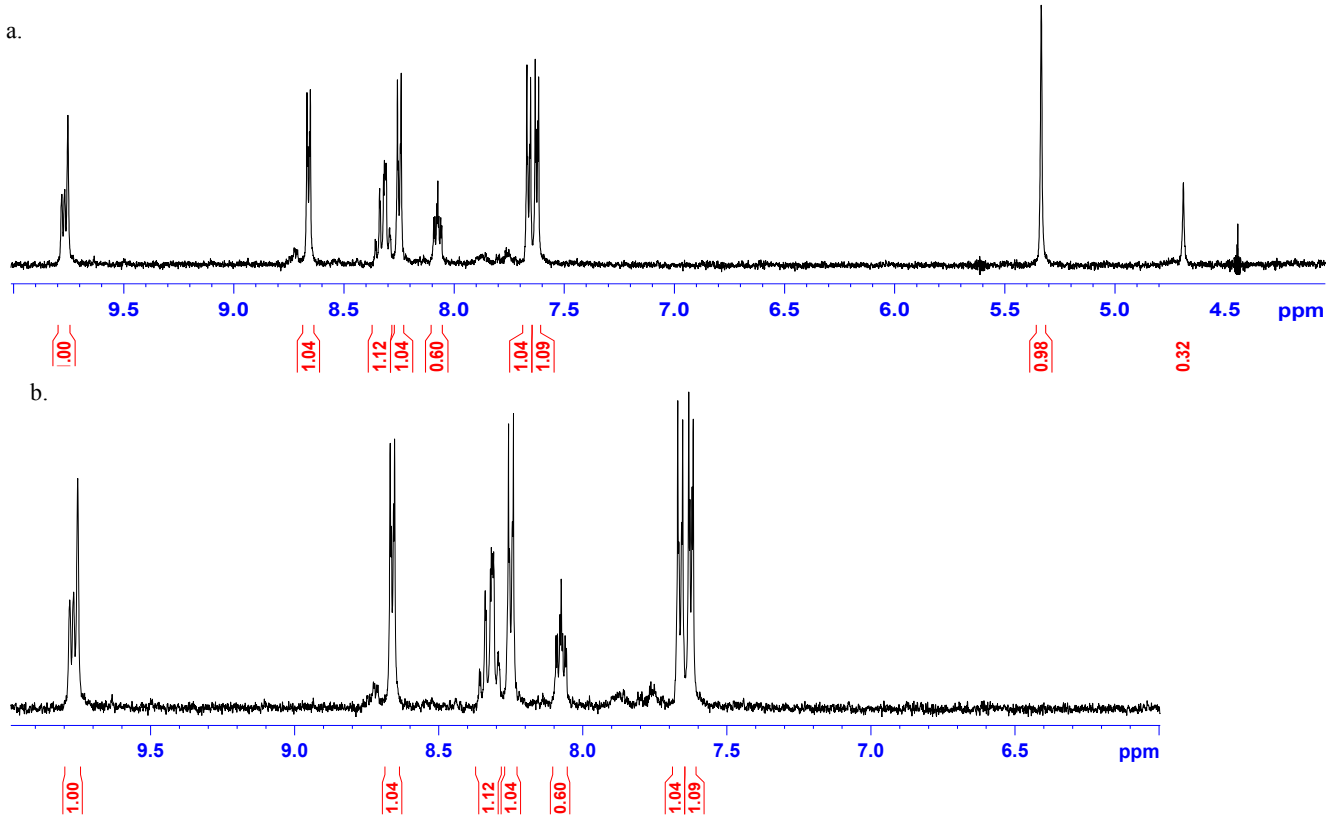

Figure 6.49: ^{1}H NMR spectrum of $[Ru(paen)(P0P)_2](PF_6)_2$ as measured in d_6-acetone. Diagram (a) shows the full scale of the complex and diagram (b) shows the aromatic portion of the spectrum only

The COSY spectrum of $[Ru(paen)(P0P)_2](PF_6)_2$ is shown below in Figure 6.50. As this spectrum is much less complex than that of $[Ru(paen)(P0P)Cl](PF_6)$ it may be inferred that the metal complex $[Ru(paen)(P0P)_2](PF_6)_2$ is symmetrical in character. H_5 and H_6 are signified by a singlet which overlaps with the doublet corresponding to H_4 and H_7 at 9.76 ppm. This signal couples with a singlet at 5.32 ppm (signifying the ethyl protons present in paen) and a triplet at 8.07 ppm corresponding to H_3/H_8. Due to their similar chemical environments, the doublet representing H_1/H_{10} overlaps the triplet representing H_2/H_9, the overall signal appearing as a multiplet at 8.33 ppm.

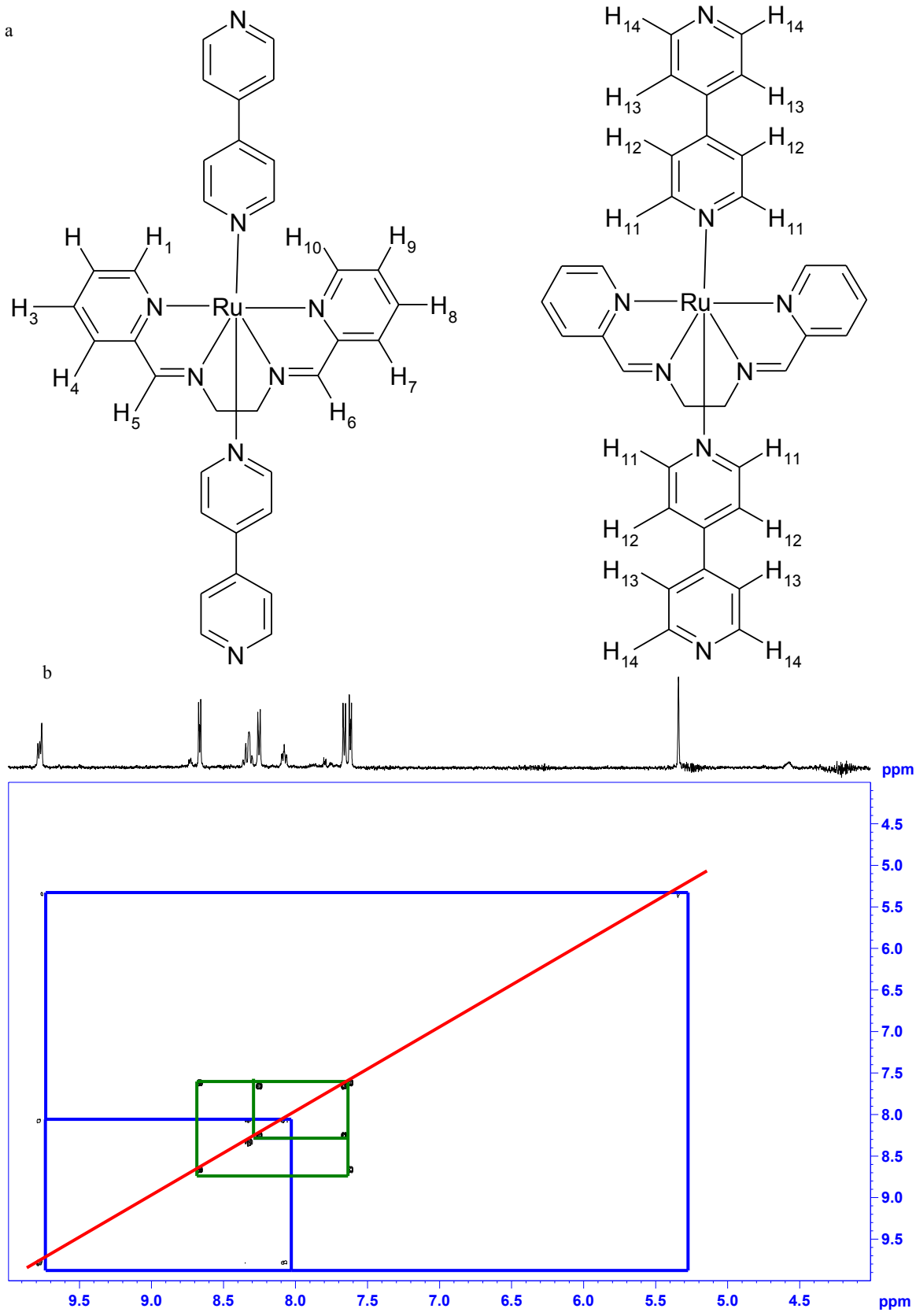

Figure 6.50: (a) Numbering system for the metal complex $[Ru(paen)(P0P)_2](PF_6)_2$ and (b) ^1H COSY of the metal complex $[Ru(paen)(P0P)_2](PF_6)_2$ highlighting coupling paen protons (blue) and P0P protons (green)

Proton	**Chemical Shift (ppm)**	**Integration**	**Coupling Constant (Hz)**
H_1/H_{10}	8.33 (m)	1.12 (4H)	-
H_2/H_9	8.33 (m)	1.12 (4H)	-
H_3/H_8	8.07 (t)	0.60 (2H)	5.6
H_4/H_7	9.76 (m)	1.00 (4H)	-
H_5/H_6	9.63 (m)	1.00 (4H)	-
H_{11}	8.66 (d)	1.04 (4H)	6.4
H_{12}	7.67 (d)	1.04 (4H)	6.8
H_{13}	7.62 (d)	1.09 (4H)	6.4
H_{14}	8.24 (d)	1.04 (4H)	6.8
H_{ethyl}	5.32 (s-broad)	0.98 (4H)	-

Table 6.5: Chemical shift, integration and coupling constants for assigned protons in the ^1H NMR spectrum of $[Ru(paen)(P0P)_2]^{2+}$

The ^1H NMR analysis of the metal complex $[Ru(papn)(P0P)_2]^{2+}$ is discussed below. The numbering system that shall be used for the assignment of proton signals in this section is shown below in Figure 6.51.

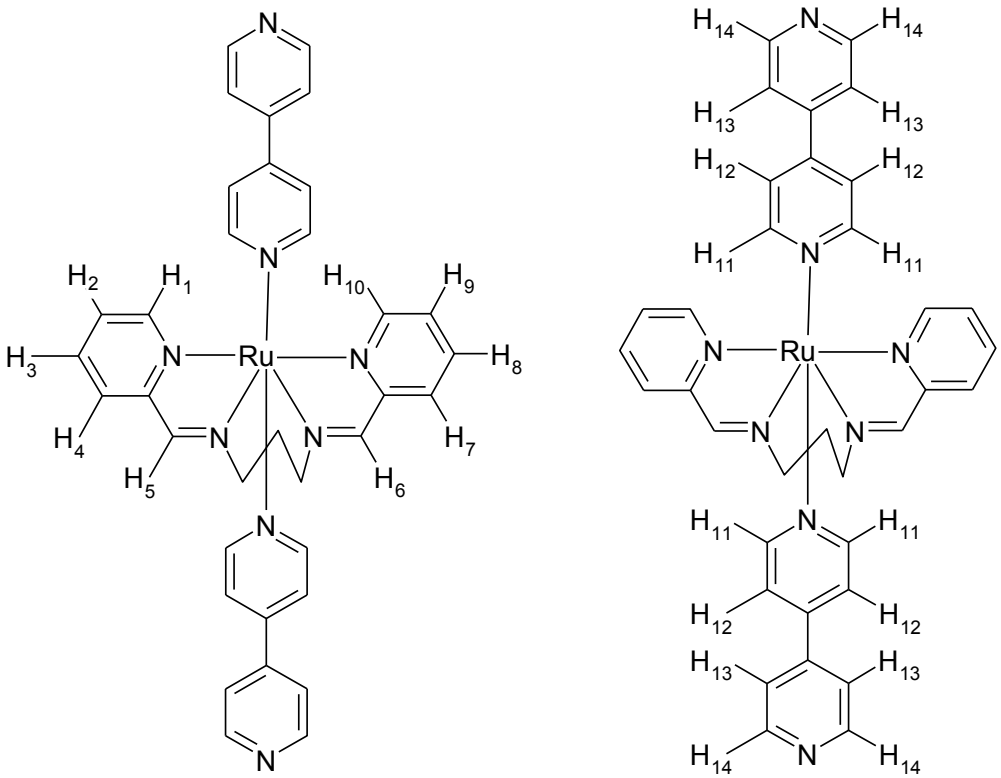

Figure 6.51: Numbering system used for assignment of ^1H NMR signals in this report for the metal complex $[Ru(papn)(P0P)_2]^{2+}$

The chemical shift and integration of each of these protons as they appear in the ^1H NMR spectrum of $[Ru(papn)(P0P)_2]^{2+}$ is shown below in Table 6.6.

Proton	**Chemical Shift (ppm)**	**Integration**	**Coupling Constant (Hz)**
H_1/H_{10}	8.34 (d)	1.20 (2H)	7.2
H_2/H_9	8.29 (t)	1.16 (2H)	8
H_3/H_8	7.94 (t)	1.00 (2H)	6.6
H_4/H_7	9.70 (d)	1.01 (2H)	5.2
H_5/H_6	9.63 (s)	1.04 (2H)	-
H_{11}	8.56 (d)	2.09 (4H)	6.2
H_{12}	7.86 (d)	2.18 (4H)	6.6
H_{13}	7.52-7.49 (m)	4.48 (8H)	-
H_{14}	7.52-7.49 (m)	4.48 (8H)	-
H_{propyl}	4.78 (s-broad)	2.02 (4H)	-
H_{propyl}	2.34 (s-broad)	1.09 (2H)	-

Table 6.6: Chemical shift and integration for assigned protons in the ^1H NMR spectrum of $[Ru(papn)(P0P)_2]^{2+}$

The ^1H NMR spectrum of $[Ru(papn)(P0P_2)]^{2+}$ is shown below in Figure 6.52. Two separate ranges are shown, the first spectrum displaying the full scale of the spectrum from 10-1.5 ppm, the second showing a clearer view of the range between 10 and 7 ppm which contains the majority of the signals pertaining to the extensive aromatic system of the molecule.

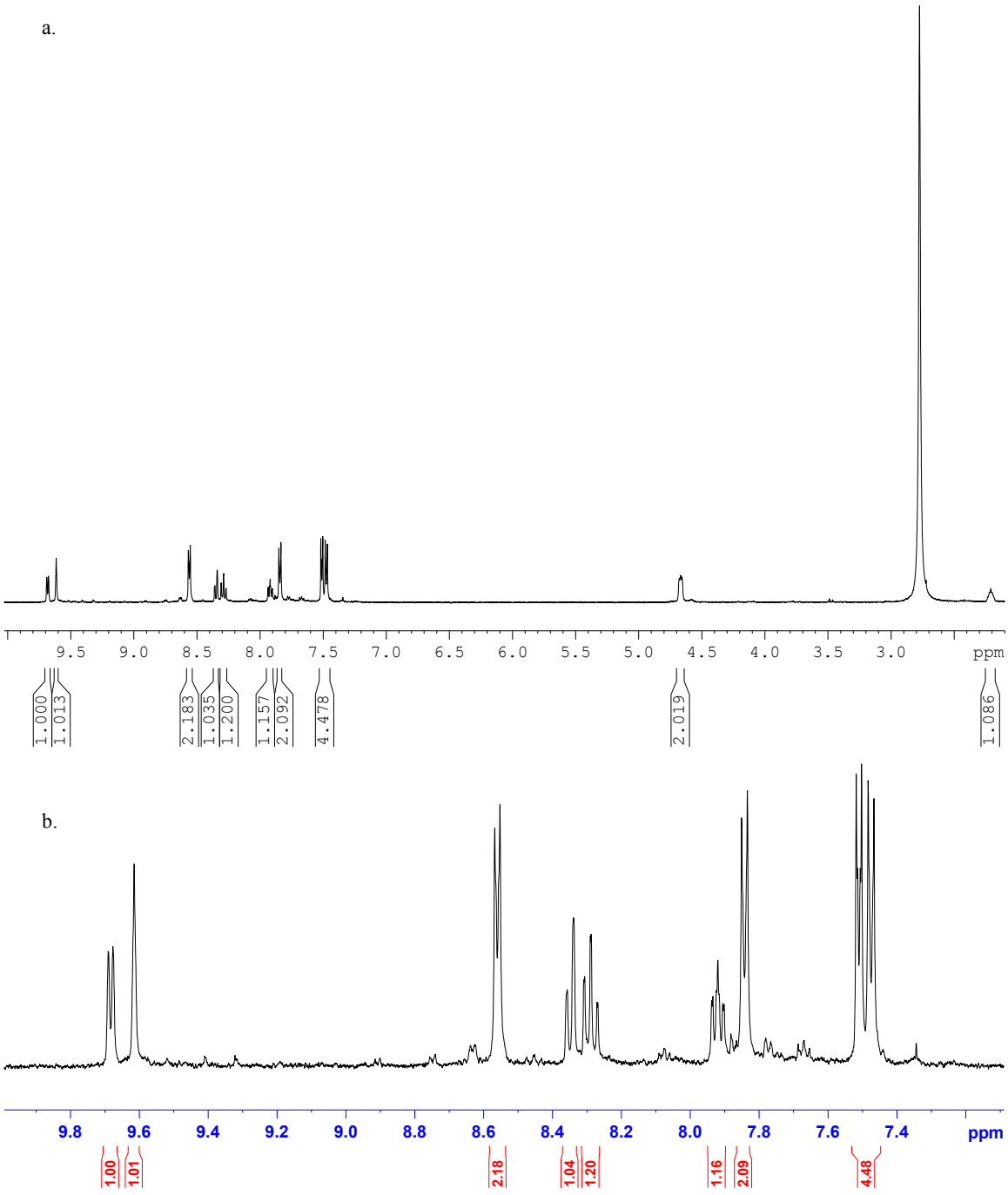

Figure 6.52: ^1H NMR spectrum of $[Ru(papn)(P0P)_2]^{2+}$ between (a) 10 and 1.5 ppm and (b) between 10 and 6 ppm as measured in d-acetone

Examination of the COSY spectrum of the above compound is invaluable in the assignment process. The COSY spectrum of $[Ru(papn)(P0P)_2]^{2+}$ is shown below in within the same ranges as shown for the 1D ^1H NMR spectra in Figure 6.52.

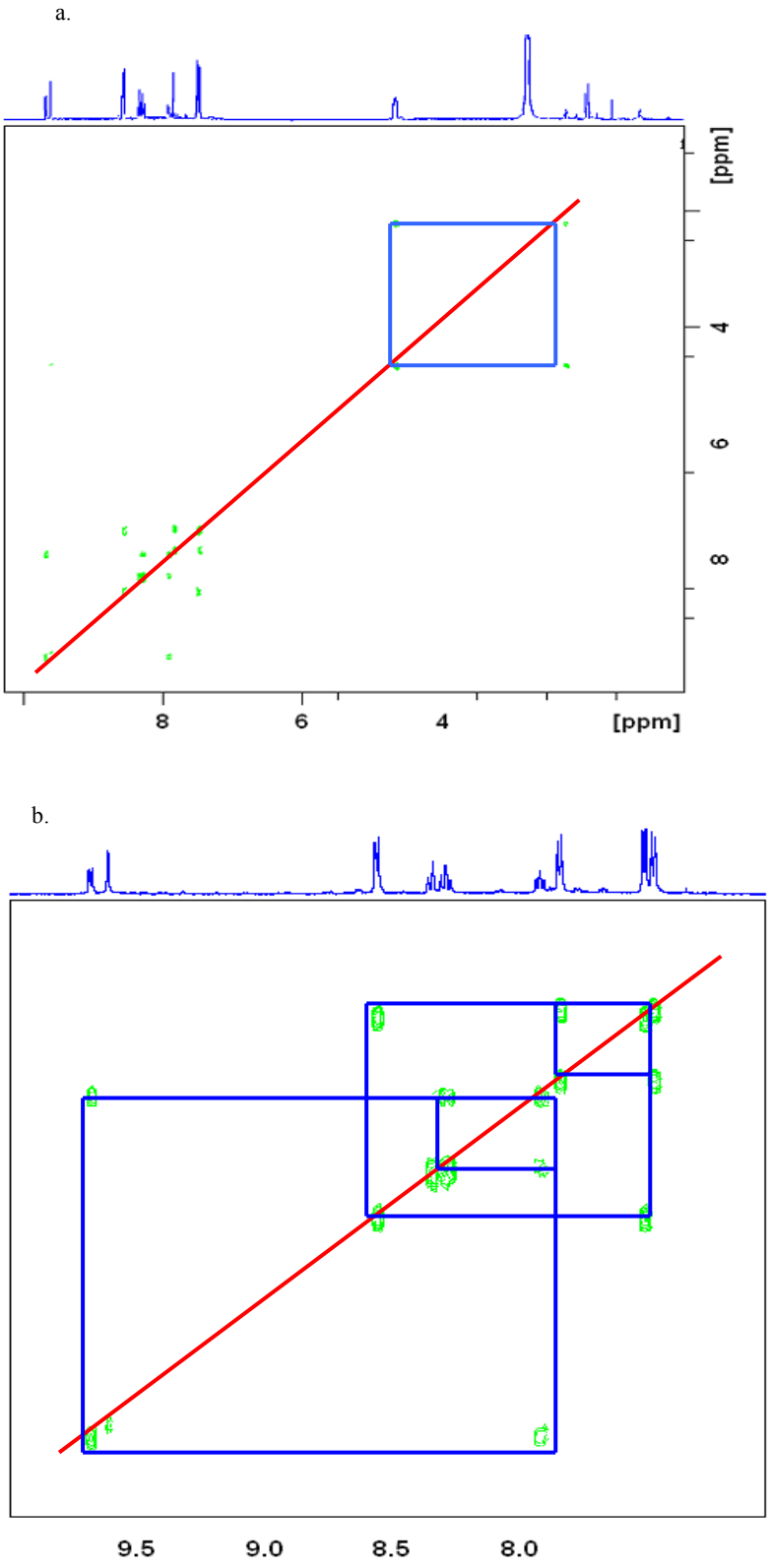

Figure 6.53: 2D COSY spectrum for the complex $[Ru(paen)(P0P)_2]^{2+}$ between the ranges (a) 10 and 1.5 ppm and (b) 10 and 7.5 ppm as measured in d-acetone

As can be seen clearly in Figure 6.53 (a), the only signals to couple with each other in the aliphatic region of the spectrum are the slightly broad singlets present at 4.78 ppm

and 2.23 ppm. These relate to the propyl protons shown in Figure 6.51. Examining the aromatic region of the ^{1}H NMR spectrum as shown in Figure 6.53 (b) the signals corresponding to the appended 4,4'bipyridyl protons are clearly the four similar doublets of identical integration present at 8.56 ppm, 7.86 ppm, 7.52 ppm and 7.49 ppm. These signals switch from appearing as two identical doublets in the spectrum of the free ligand to four identical doublets upon complexation. The furthest downfield of these signals (visible in Figure 6.53 b as a doublet at 8.56 ppm) corresponds to H_{11} as shown in Figure 6.51. The inductive electron withdrawing effect of the complexed metal atom as well as the inherent electronegativity of the adjacent complexed nitrogen results in a large amount of electron density being pulled from the environment surrounding H_{11} and as such explains the signal's high ppm value. This signal couples strongly with the doublet appearing at 7.52 ppm, intimating that this peak coerresponds to H_{12}, again the inductive effect originating from the complexed metal resulting in a minor dowfield shift as compared to the neighbouring doublet at 7.49 ppm which must correspond to H_{13}. The doublet visible at 7.86 ppm is attributable to H_{14} as the electronegative effect of the neighbouring nitrogen atom will cause a downfield shift resulting in the relatively high chemical shift value of this signal. However, the environment of this proton will be slightly more electron rich than that of H_{11} due the unbound nature of H_{14}'s neighbouring nitrogen.

The remaining five signals consist of one singlet, two doublets and two triplets. The signal corresponding to H_5/H_6 appears as a singlet at 9.63 ppm similar to the Ru(paen) complexes discussed above.

The peaks relating to H_1/H_{10} and H_4/H_7 as doublets at 9.70 ppm and 8.34 ppm respectively. The coupling shown in Figure 6.53 compounds this in addition to the similarity of these protons in their chemical shift to the metal complex $[Ru(paen)(P0P)_2](PF_6)_2$ dicussed above. The same can be said of the remaining triplet signals relating to H_2/H_9 and H_3/H_8. Upon inspection of the COSY spectrum shown in Figure 6.53 (b) it can be seen that the doublet present at the higher chemical shift value of 9.70 ppm couples with the triplet of lowest chemical shift present at 7.94 ppm. The doublet present at 8.34 ppm couples with the triplet present at the very similar chemical shift value of 8.29 ppm. Therefore the triplet at 8.29 ppm corresponds to H_3/H_8 while the triplet present at 7.94 ppm corresponds to H_3/H_9.

6.4 UV/vis Analysis

The UV/vis spectrum for [Ru(paen)(P0P)Cl](PF_6) is shown below in Figure 6.54. This UV/vis data for these complexes has not been published previously[28] and so shall be discussed in detail below.

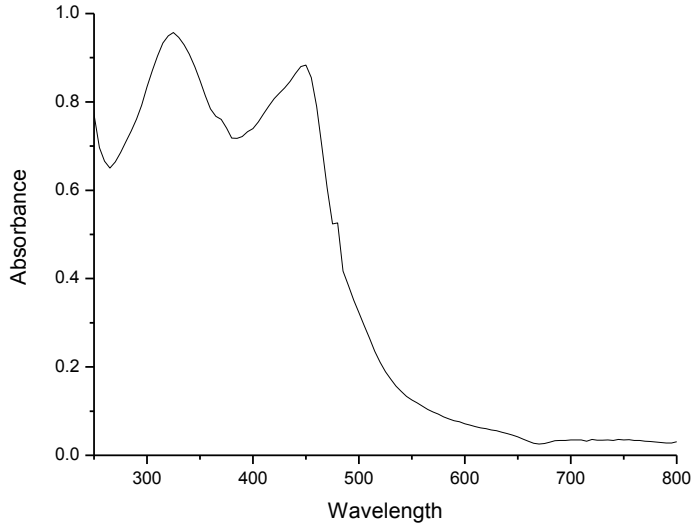

Figure 6.54: UV/vis spectrum for [Ru(paen)(P0P)Cl](PF_6) (0.2 mM) as measured in acetonitrile at 278 K

The UV-vis spectra shown above in Figure 6.54 is dominated by two absorption bands in the visible region at 324 nm (ε=1077) and 455 nm (ε=1275).

The band present at 455 nm may be attributed to dπ-π* metal to ligand charge transfer (^{1}MLCT) transitions within the molecule as this absorbance is comparable to the ^{1}MLCT absorbances seen for $[Ru(bpy)_3]^{2+}$ discussed in Chapter 1. This band is comparable to the maximum absorbance of 450 nm attributed to the widely studied metal complex $[Ru(bpy)_3]^{2+}$.

The presence of a second band in close to 300 nm (i.e. the band visible at 324 nm) is unusual, as ruthenium based absorbencies rarely, if ever, occur at this sort of wavelength. It is possible that this absorbance is attributable to the ligands present in the complex, perhaps the tetradendate paen ligand, as tetradentate ligands may lead to spectral features that do not appear in the more widely studied ruthenium bis-bipyridyl type systems.

The UV/vis spectrum for [Ru(paen)(P0P)$_2$](PF$_6$)$_2$ is shown below in Figure 6.55.

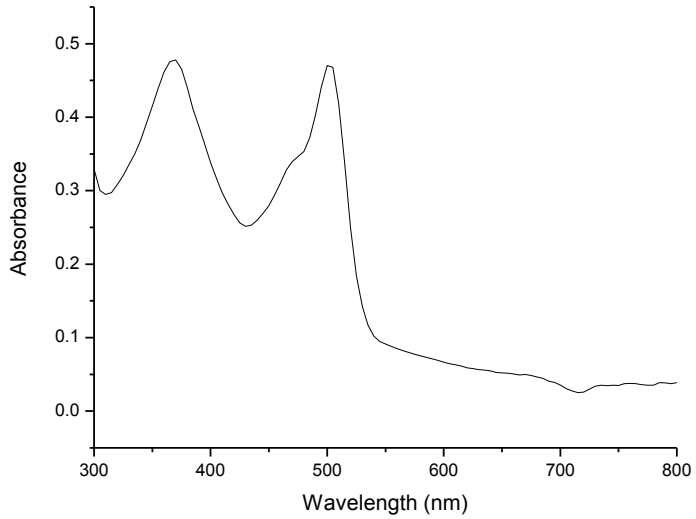

Figure 6.55: UV-vis spectrum of [Ru(paen)(P0P)$_2$](PF$_6$)$_2$ (0.2 mM) as measured in acetonitrile at 278 K

The UV-vis spectra shown above in Figure 6.55 is again dominated by two absorption bands in the visible region at 367 nm (ε=1110) and 502 nm (ε=1191).

The band present at 502 nm may be attributed to dπ-π* metal to ligand charge transfer (^{1}MLCT) transitions within the molecule similar to those seen for [Ru(paen)(P0P)Cl]$^+$. This band constitutes a red shift of 52 nm when compared to the widely studied metal complex [Ru(bpy)$_3$]$^{2+}$, which displays a maximum absorbance at 450 nm, as well as a similar shift of 57 nm when compared to its precursor compound [Ru(paen)(P0P)Cl]PF$_6$ discussed above.

Any changes in the wavelength at which the ^{1}MLCT absorption occur when compared to [Ru(bpy)$_3$]$^{2+}$ is attributable to the coordinated ligand(s). π-acceptor ligands will cause a red shift (i.e. a shift to longer wavelength) as its interaction with the metal dπ orbitals (through backbonding) stabilises the metal orbitals resulting in a greater energy difference between the t$_2$g and π* energy levels. However, introduction of ζ-donor ligands will cause a blue shift as ligands of this type will donate electron density to the metal, destabilising the t$_2$g and decreasing the energy gap between the t$_2$g and π* energy levels.

The absorbance maximum of 502 nm displayed here for [Ru(paen)(P0P)$_2$](PF$_6$)$_2$ is in fact closer to the λ_{max} value of the literature compound [Os(bpy)$_3$]$^{2+}$ (λ_{max}=468 nm) than that of [Ru(bpy)$_3$]$^{2+}$. This is an encouraging result, as osmium bipyridyl

complexes have shown potential as molecular transistor prototypes, while their ruthenium analogues have proven unsuitable[36]. Therefore if the absorption properties of $[Ru(paen)(P0P)_2]^{2+}$ prove to be closer in nature to the osmium tris bipyridyl standard than the ruthenium, it stands to reason that the electrochemical properties of the molecule should be close to the osmium standard also.

As for [Ru(paen)(P0P)Cl a second band is visible, further into the blue end of the spectrum. In Figure 6.55, the band visible at 367 nm may again be attributed to ligand based interactions in the molecule.

It may be noted that the extinction coefficient values obtained for these complexes are quite low with respect to that of $[Ru(bpy)_3]^{2+}$ (~1200 $M^{-1}cm^{-1}$ for $[Ru(paen)(P0P)_2]^{2+}$ vs. 11500 $M^{-1}cm^{-1}$ for $[Ru(bpy)_3]^{2+}$)[8]. This may be a result of the structural differences between the complexes being discussed and $[Ru(bpy)_3]^{2+}$. However it is also possible that there is a large margin of error associated with the exctinction coefficient values calculated for these complexes as there was only a small amount of solid complex available for measurement. Due to the low yield and length of the reaction and work up as well as time constraints, a duplicate measurement was not carried out.

4.5 Emission Analysis

The emission spectrum recorded for a 0.2 mM solution of [Ru(paen)(P0P)Cl](PF_6) in acetonitrile is shown below in Figure 4.56.

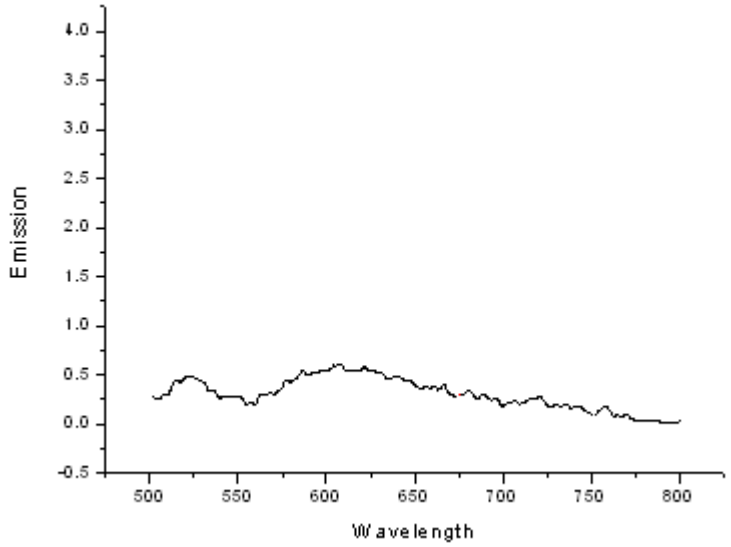

Figure 6.56: Emission spectra for [Ru(paen)(P0P)Cl](PF_6) 455 nm as an excitation wavelength

When excited at 455 nm [Ru(paen)(P0P)Cl](PF_6) exhibits a very low intensity band at 605 nm. This value, much like its associated absorbance value, is comparable to the characteristic emission maximum of 615 nm attributable to the widely studied $[Ru(bpy)_3]^{2+}$.[8] The concentration of the sample analysed here is identical to the sample concentration corresponding to the UV/vis spectrum shown in Figure 6.54. The UV/vis spectrum shown in Figure 6.54 is well defined and relatively intense while the emission spectrum shown in Figure 6.56 is ill-defined and noisy. The emission data shown in Chapter 3 for the bis-bipyridyl complexes $[Ru(bpy)_2(pyrphen)]^{2+}$ and $[Ru(bpy)_2(thimphen)]^{2+}$ display much more intense emission, with an intensity value of ~55 applicable to a 0.2mM sample of either of these complexes. This value dwarfs the emission of ~0.5 observed for the 0.2 mM sample corresponding to Figure 6.56. This information implies that the metal complex $[Ru(paen)(P0P)Cl]^{+}$ does not emit as the model complex $[Ru(bpy)_3]^{2+}$ does. Instead after the excited state is generated, a non-emissive deactivation pathway is followed for the molecule to energetically return to its ground state. Two such deactivation pathways are shown in Figure 6.57 below.

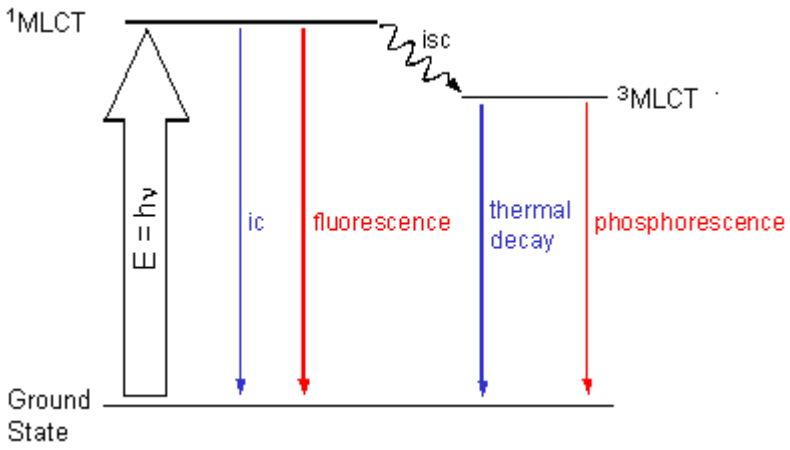

Figure 6.57: Decay paths available to a metal complex from both the singlet (^{1}MLCT) and triplet (^{3}MLCT) states. Decay paths in blue represent non-radiative decay whereas those in red represent radiative decay.

Upon excitation an electron is promoted to the singlet ^{1}MLCT energy level. Following this, the electron may return to the ground state radiatively by fluorescence (thereby emitting a photon) or non-radiatively by internal conversion (IC). If there is a lower lying triplet ^{3}MLCT energy level the promoted electron will be transferred there by intersystem crossing (ISC) after which the electron may return to the ground state radiatively by phosphorescence or nonradiatively by thermal decay. $[Ru(paen)(P0P)Cl]^+$ returns to its ground state following excitation therefore by *non-radiative* internal conversion or thermal decay. As there is only one absorbance visible at 455 nm in the UV/vis absorbance spectrum for this complex it is inferred that its excited state is singlet in character. A second absorbance at ~600 nm is characteristic of population of the triplet ^{3}MLCT excited state (as seen for the osmium bis-bipyridyl complexes seen in Chapter 3), the absence of which in Figure 6.54 confirms that in this case only the ^{1}MLCT energy level is populated following excitation. Therefore the deactivation pathway for the $[Ru(paen)(P0P)Cl]^+$ excited state is assumed to be internal conversion.

A similar lack of emission activity can be seen in the emission spectrum for a 0.2 mM sample of $[Ru(paen)(P0P)_2](PF_6)_2$ shown below in Figure 6.58.

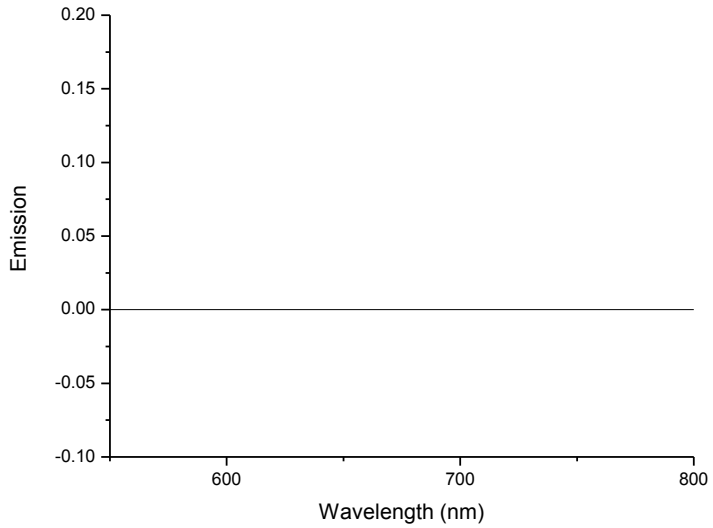

Figure 6.58: Emission spectrum for $[Ru(paen)(P0P)_2](PF_6)_2$ in acetonitrile at 278 K using 500 nm (black) and 365 nm (red) as an excitation wavelength

Here there is no emission activity at all observed for $[Ru(paen)(P0P)_2](PF_6)_2$. This compounds the assumption outlined above for $[Ru(paen)(P0P)Cl](PF_6)$ that these complexes are non-emissive. Again, it has been inferred from the spectrum shown in Figure 6.58 that the molecule returns to its ground state following excitation by non-radiative internal conversion.

6.6 Conclusion

Chapter 6 has detailed the synthesis of the published compounds $[Ru(paen)Cl_2]$ and $[Ru(papn)Cl_2]$[28] as well as the novel metal complexes $[Ru(paen)(P0P)Cl](PF_6)$, $[Ru(paen)(P0P)_2](PF_6)_2$ and $[Ru(papn)(P0P)_2](PF_6)_2$. It was found that the previously published synthetic method for the preparation of the dichloride starting materials $[Ru(paen)Cl_2]$ and $[Ru(papn)Cl_2]$ yielded an impractically low amount of product. Therefore a new method including excess ascorbic acid as a reducing agent was developed, resulting in a higher, more readily employable yield of approximately 8%. The synthesis of the metal complex $[Ru(papn)(P0P)_2](PF_6)_2$ was readily achieved through overnight reflux of the purified dichloride $[Ru(papn)Cl_2]$ followed by column chromatography on silica using 80:20 acetonitrile: water 0.05 M KNO_3 as eluent and a second column on alumina using acetonitrile as eluent.

The paen analogue of this complex on the other hand, was not so easily attained. Following a lengthy HPLC study of the reaction in progress, the desired product $[Ru(paen)(P0P)_2](PF_6)_2$ was successfully synthesised following 120 hr reflux of the reaction mixture and lengthy purification on silica using 80:20 acetonitrile: water 0.05 M KNO_3. The intermediate type complex $[Ru(paen)(P0P)Cl](PF_6)$ was also isolated during the $[Ru(paen)(P0P)_2](PF_6)_2$ synthetic study. In spite of the fact that these three novel complexes were successfully synthesised, all yields obtained were less than 10% and so further research in this area is envisioned in order to increase reaction efficiency. As the ligands paen and papn have been found to withstand extended reflux and purification it is possible that longer reaction times and/or use of catalysts may be employed in order to improve the yield of these reactions.

All complexes successfully synthesised were characterised by ^1H NMR spectroscopy and UV/vis spectroscopy. Examination by emission spectroscopy has found these complexes to be non-emissive, unlike the associated literature complex $[Ru(bpy)_3]^{2+}$ and the ruthenium bis-bipyridyl complexes discussed heretofore.

6.7 Experimental

Materials

The ligands paen and papn were kindly provided by Sally Brooker and workers, University of Otago, NZ. All other chemicals were purchased from Sigma-Aldrich and used without further purification. All synthetic solvents used were of reagent grade. All solvents used for spectroscopic measurements were of HPLC grade.

6.7.1 Synthesis of Metal Complexes

$Ru(paen)Cl_2$

This metal complex was synthesised using a modified literature procedure[28].
200 mg (0.96 mmol) $RuCl_3.2H_2O$ was refluxed in 30 cm^3 methanol with 1.69 g (9.64 mmol) ascorbic acid overnight. 269 mg (1.16 mmol) paen was added to the green reaction mixture, eliciting an immediate colour change from green to purple. The reaction mixture was refluxed for one hour, after which the mixture was reduced in volume to 5 cm^3 and purified by column chromatography using a neutral alumina column and 10:1 dichloromethane: acetone as eluent. The first eluting blue band was

collected and the solvent removed in vacuo. The resulting solid was recrystallised from 1:1 dichloromethane: hexane to yield the product as dark blue crystals.

Yield: 28mg (7.8%)

^{1}H NMR: CD_2Cl_2 ^{1}H δ: 9.20 (2H, s, H_5+H_6), 9.09 (2H, d, H_4+H_7, J= Hz), 7.84 (2H, t, H_3+H_8, J= Hz), 7.77 (2H, d, H_1+H_{10}, J= Hz), 7.63 (2H, t, H_2+H_9, J= Hz), 5.32 (4H, s-br, H_{ethyl}),

Ru(papn)Cl_2

This metal complex was synthesised using a modified litereature appraoch[28]. 333 mg (1.65 mmol) $RuCl_3.2H_2O$ was refluxed in 15 cm^3 methanol with 2.9 g ascorbic acid overnight. 500 mg (1.98 mmol) papn was added to the green reaction mixture, eliciting an immediate colour change from green to purple. The reaction mixture was refluxed for one hour, after which the mixture was reduced in volume to 5 cm^3 and purified by column chromatography using a neutral alumina column and 10:1 dichloromethane: acetone as eluent. The first eluting blue band was collected and the solvent removed in vacuo. The resulting solid was recrystallised from 1:1 dichloromethane: hexane to yield the product as dark blue crystals.

Yield: 54.5 mg (7.8%)

[Ru(paen)(P0P)Cl](PF$_6$)

This metal complex was synthesised using a modified literature procedure[36].

155 mg 4,4'-bipyridyl (P0P) was placed in 25 cm^3 ethanol and heated to reflux. 31 mg (0.10 mmol) Ru(paen)Cl_2, dissolved in 5 cm^3 ethanol was added dropwise to the mixture. The resulting mixture was refluxed overnight and the solvent subsequently reduced to 5 cm^3 in vacuo. The dark red sample was loaded onto a silica column and eluted with 80:20 acetonitrile:H_2O 0.05 KNO_3. The principal red band was collected, and the acetonitrile removed in vacuo. A saturated aqueous solution of KPF_6 was added to the red solution to isolate the complex as a PF_6 salt. The resulting precipitate was collected by vacuum filtration and recrystallised from 1:1 acetone: H_2O, yielding the product as a sticky red solid. This solid was dissolved in acetone and transferred to a preweighed sample tube, yielding the product as a red solid following evaporation of the solvent

Yield: 15mg (26%)

^{1}H NMR: d_6-acetone 1H δ: 9.73 (1H, s, H_5), 9.63 (1H, s, H_6), 9.59 (1H, s-br, H_4), 9.47 (1H, d, H_7), 8.62 (2H, t, H_{11}, J=7 Hz), 8.33 (2H, m, H_1+H_2), 8.22 (2H, m, H_9+H_{10}), 8.00 (1H, m, H_3), 7.90 (1H, t, H_8, J=5.2 Hz), 7.86 (2H, d, H_{14}, J=6.8 Hz), 7.63 (2H, d, H_{12}, J=6.4 Hz), 7.53 (2H, d, H_{13}, J=7 Hz), 4.78 (4H, s-br, H_{ethyl})

[Ru(paen)(P0P)$_2$](PF$_6$)

This metal complex was synthesised using a modified literature procedure[36].

215 mg (1.38 mmol) 4,4'-bipyridyl (P0P) was placed in 25 cm^3 ethanol and heated to reflux. 43 mg (0.14 mmol) Ru(paen)Cl_2, dissolved in 5 cm^3 ethanol was added dropwise to the mixture. The resulting mixture was refluxed for 120 hr and the solvent subsequently reduced to 5 cm^3 in vacuo. The dark red sample was loaded onto a silica column and eluted with 80:20 acetonitrile:H_2O 0.05 KNO_3. The last eluting orange band was collected, and the acetonitrile removed in vacuo. A saturated aqueous solution of KPF_6 was added to the red solution to isolate the complex as a PF_6 salt. The resulting precipitate was collected by vacuum filtration and recrystallised from 1:1 acetone: H_2O, yielding the product as a sticky red solid. This solid was dissolved in acetone and transferred to a preweighed sample tube, yielding the product as a red solid following evaporation of the solvent

Yield: 6 mg (5.2%)

^{1}H NMR: d_6-acetone 1H δ: 9.76 (2H, m, H_4+H_7), 9.63 (2H, m, H_5+H_6), 8.66 (4H, d, H_{11}, J=6.4 Hz), 8.33 (4H, m, H_1+H_{10}+H_2+H_9), 8.24 (4H, d, H_{14}, J= 6.8Hz), 8.07 (2H, t, H_3+H_8, J=5.6 Hz), 7.67 (4H, d, H_{12}, J=6.8 Hz), 7.62 (4H, d, H_{13}, J=6.4), 5.32 (4H, s-br, H_{ethyl})

[Ru(papn)(P0P)$_2$](PF$_6$)

This metal complex was synthesised using a modified literature procedure[36].

3.09 g (19.8 mmol) 4,4'-bipyridyl (P0P) was placed in 20 cm^3 methanol and heated to reflux. 54.5 mg (0.17 mmol) Ru(papn)Cl_2, dissolved in 5 cm^3 methanol was added dropwise to the mixture. The resulting mixture was refluxed for 1 hr and the solvent subsequently reduced to 5 cm^3 in vacuo and 20 cm^3 water added. This mixture was left at 5 ^{0}C overnight, after which excess ligand crystallised and was filtered off. The dark red filtrate was extracted with dichloromethane and the organic layer retained. The solvent was removed and the resulting solid purified by column chromatography

using a silica column and eluted with 80:20 acetonitrile:H_2O 0.05 KNO_3 followed by a second column on neutral alumina using acetonitrile as eluent. The principal red band was taken from both columns. The solid obtained from the second column was dissolved in water and precipitated as the PF_6 salt by addition of a saturated solution of $KPF_{6\ (aq)}$. The resulting precipitate was collected by vacuum filtration and recrystallised from 1:1 acetone: H_2O, yielding the product as a sticky red solid. This solid was dissolved in acetone and transferred to a preweighed sample tube, yielding the product as a red solid following evaporation of the solvent

Yield: 10 mg (6.9%)

^{1}H NMR: d_6-acetone 1H δ: 9.70 (2H, d, H_4+H_7, J=5.2 Hz), 9.63 (2H, s, H_5+H_6), 8.56 (2H, d, H_{11}, J=6.2 Hz), 8.34 (2H, d, H_1+H_{10}, J= 7.2 Hz), 8.29 (2H, t, H_2+H_9, J=8 Hz), 7.86 (4H, d, H_{12}, J=6.6 Hz) 7.52-7.49 (8H, m, $H_{13+}H_{14}$), 4.78 (4H, s-br, H_{propyl}), 2.34 (2H, s-br, H_{propyl})

6.8 Bibliography

[1] T. Albrecht, K. Moth-Poulsen, J. B. Christensen, A. Guckian, T. Bjørnholm, J. G. Vos, J. Ulstrup, *Faraday Discuss.* 2006, **131**, 265

[2] T. Albrecht, A. Guckian, J. Ulstrup, J. G. Vos, *Nano Lett.* 2006 **5**, 7, 1451

[3] J.G. Vos, J. M. Kelly, *Dalton Trans.*, 2006, 4869

[4] V. Balzani, A, Juris, M, Venturi, S. Campagna, S. Serroni; *Chem. Rev.*, 1996, **96,** 759

[5] J.-P. Sauvage, J.-P. Collin, J. C. Chambron, S. Guillerez, C. Coudret, V. Balzani, F. Barigelletti, L. De Cola, L. Flamigni, *Chem. Rev*., 1994, **94**, 993.

[6] E. Danielson, C. M. Elliot, J. W. Merckert, T. J. Meyer, *J. Am. Chem. Soc.* 1987 **,109.** 2519**.**

[7] E. A. Medlycott, G. S. Hanan, *Chem. Soc. Rev*., 2005, **34**, 133

[8] L. Cassidy, *PhD Thesis,* 2008, Dublin City University

[9] S. Tasca, *PhD Thesis,* 2006, Dublin City University

[10] D. H. Busch, J. C. Bailar, *J. Am. Chem. Soc.* 1956, **78**, 1137

[11] C. M. Harris, E. D. MacKenzie, *J. Chem. Soc. A* 1969 746

[12] (a) P.K. Pal, S. Chowdhury, P. Purkayastha, D.A. Tocherm, D. Datta, *Inorg. Chem. Commun.* 2000, **3** 2000, 585.(b)V. Amendola, L. Fabbrizzi, L. Gianelli, C. Maggi, C. Mangano, P. Pallavicini, M. Zema, *Inorg. Chem.* 2001, **40**, 3579.

[13] S. Banerjee, J. Gangopadhyay, C.-Z. Lu, J.-T. Chen and A. Ghosh, *Eur. J. Inorg. Chem.* 2004, 2533

[14] J.R.da.S. Maia, R.C.R. Chaga, V.P. Ferraz and M.I. Yoshida, *Main Met. Group Chem.* 2006, **29**, 321.

[15] C.R. Baar, M.C. Jennings, J.J. Vittal and R.J. Puddephatt, *Organometallics* 2000, **19**, 4150.

[16] M.G.B. Drew, M.R.S. Foreman, M.J. Hudson and K.F. Kennedy, *Inorg. Chim. Acta* 2004, 4102

[17] I. I. Ebralidze, G. Leitus, L. Shimon, Y. Wang, S. Shaik, R. Neumann, *Inorg. Chim Acta,*2009, **362**, 4713

[18] J. F. Larrow, E. N. Jacobsen, *Topics Organiomet. Chem.,* 2004, **6**. 123

[19] C. Boskovic, H. V. Guedel, G. Labat, A. Neels, W. Wernsdorfer, B. Moubaraki, K. S. Murray, *Inorg. Chem.* 2005, **44,** 3181

[20] J. A. Kitchen, S. Brooker, *Dalton Trans.* 2010, **39**, 14, 3358

[21] R. W. Handel , H. Willms, G. B. Jameson, K. J. Berry, B. Moubaraki, K. S. Murray, S. Brooker, *Eur. J. Inorg. Chem.*, 2010, **21**, 3317

[22] J. A. Kitchen , G. N. L. Jameson, J. L. Tallon, S. Brooker, Source: *Chem. Comm.*, 2010, **46**, 18, 3200

[23] A. Noble, J. Olguin , R. Clerac, S. Brooker, *Inorg. Chem.*, 2010, **49**, 10, 4560

[24] M. Aydemira, F. Durapa, A. Baysala, N. Merica, A. Buldaga ,B. Gümgüma, S. Özkarb, L. T. Yıldırımc, *J. Mol. Cat. A*: Chemical 2010, **326**, 75

[25] A. Manimaran, C. Jayabalakrishnan, *Synth. React. Inorg. Metal-Org. Nano-Metal Chem.*, 2010, **40**, 2, 116

[26] S. Arunachalan, N. P. Priya, C. Saravanakumar, C. Jayabalakrishnan, V. Chinnusamy, *J. Coord. Chem.*, 2010, **63,** 10, 1795

[27] S. Arunachalam,N. P. Priya, K. Boopathi,C. Jayabalakrishnan, V. Chinnusamy, *Appl. Organnomet. Chem.,* 2010, **24,** 7, 491

[28] S. Pal, S. Pal; *Polyhedron*, 2003, **22**, 867

[29] E. A. Seddon, K. R. Seddon, *The Chemistry of Ruthenium; Topics in Inorganic and General Chemistry: A Collection of Monographs*, ed: R. J. H. Clark, Elsevier 1984.

[30] D. Rose, G. Wilkinson, *J. Chem. Soc. A.* 1970, 1791

[31] I. E. Starik, Y. A. Barbanel, *Russ. J. Inorg. Chem,* 1961, **6**, 109

[32] E. A. Seddon, K. R. Seddon, *The Chemistry of Ruthenium; Topics in Inorganic and General Chemistry: A Collection of Monographs*, ed: R. J. H. Clark, Elsevier 1984.

[*33*] I. P. Evans, A. Spencer, G. Wilkinson, *J. Chem Soc*., *Dalton* Trans. 1973, 204

[34] K. Min, H. Gao, K. Matyjaszewski *Macromolecules*, 2007, **40,** 6, 1789

[35] H. Ahmed, *PhD Thesis*, Dublin City University, in press

[36] A. Guckian, *PhD Thesis*, Dublin City University, 2004

Chapter 7: Conclusions and Future Work

Abstract:

The work carried out over the duration of this project has been discussed in chapters 1 through 6. Chapter 7 shall summarise all relevant conclusions as well as proposing future experimental or analytical work to further research in this area.

7.1 Conclusions and Future Work

As outlined previously, the main aim of this thesis has been the synthesis of novel mono-and dinuclear transition metal complexes as suitable prototypes for molecular transistors and diodes. Metal complexes containing the novel phenanthroline-imidazo ligands thimphen and pyrphen were chosen as suitable candidates for this purpose (see Chapter 1). Over the course of this research project two synthetic approaches have been revealed as particularly suitable for synthesis of metal complexes of this type. In retrospect, this thesis acts as somewhat of a comparison between the efficacy and applicability of these two methods: ***Direct*** and ***Indirect*** synthesis.

The genesis of this comparison is observed first in Chapter 3, in which the synthesis of ruthenium and osmium bis-bipyridyl complexes containing the novel ligands thimphen and pyrphen is detailed. The ligand 'thimphen' was synthesised using the established Schiff base formation method first used by Steck and Day[1]. Its related mononuclear ruthenium and osmium complexes were then synthesised successfully using the often encountered *"complexes as metals / complexes as ligands"* method (***Direct Synthesis***)[2]. The same 'direct' method of synthesis was attempted for the preparation of the ligand 'pyrphen' and its related ruthenium and osmium complexes, but was found to be unsuitable. Instead an *"on-the-complex"* or ***Indirect*** method was used, with the pyrphen ligand being built from a ruthenium bis-bipyridyl phenanthroline starting material. This method was found to be successful for the synthesis of the mononuclear complexes $[Ru(bpy)_2(pyrphen)]^{2+}$ and $[Os(bpy)_2(pyrphen)]^{2+}$. The osmium complexes $[Os(bpy)_2(thimphen)]^{2+}$ and $[Os(bpy)_2(pyrphen)]^{2+}$ were used in a separate research project in which their electrochemical properties were measured.[3] Both complexes were found to form well ordered monolayers on gold and platinum respectively and may therefore be considered suitable candidates for molecular transistor prototypes. In an effort to better understand the electronic properties of the metal complexes synthesised in Chapter 3, spectroscopic titration experiments were carried out on the ruthenium complexes of thimphen and pyrphen. The results of these experiments are reported but there has been no work to date to relate these findings to the electrochemical behaviour of the metal complexes.

The ligands thimphen and pyrphen are also encountered in Chapter 4. This chapter details the successful synthesis of six mononuclear ruthenium complexes including

two deuterated bipyridyl type analogues as prototypes for molecular transistors. The method used for the synthesis of these complexes is identical to the indirect synthetic method used for construction of the metal complexes $[Ru(bpy)_2(pyrphen)]^{2+}$ and $[Os(bpy)_2(pyrphen)]^{2+}$ as outlined in Chapter 3. This method of synthesis, involving the modification of a bis-phenanthroline precursor to append surface active groups, was found to be effective for the attachment of both a pyridine and thiophene group in the case of the novel metal complexes $[Ru(pyrphen)_2(bpy)]^{2+}$ and $[Ru(thimphen)_2(bpy)]^{2+}$ as well as their deuterated bipyridyl analogues. However in the case of the precursor complex $[Ru(phen)_2(dmbpy)]^{2+}$ only a pyridine group could be successfully appended. These complexes were characterised by ^1H NMR and CHN analysis, with their absorbance and emission properties being recorded also. These reactions were however rather low yielding although this may have resulted from the small scales (~100 mg) these reactions were attempted on. Therefore it is possible that increasing the scale on which these reactions are carried out shall increase the yield also. The synthesis of the novel metal complexes $[Ru(pyrphen)_2(mepytr)]^{2+}$, $[Ru(thimphen)_2(mepytr)]^{2+}$, $[Ru(pyrphen)_2(ppytr)]^{2+}$ and $[Ru(pyrphen)_2(ppytr)]^{2+}$ (complexes 7, 8, 9 and 10 in figure 4.10 in chapter 4) were also attempted, but all reactions were unsuccessful. Synthesis of the metal complexes $[Ru(pyrphen)_2)(bpt)]^{2+}$ and $[Ru(thimphen)_2)(bpt)]^{2+}$ were also attempted, yielding encouraging, though not conclusive results. The reasons for this difference in reactivity between compounds which contain very similar reactive groups have not yet been uncovered. It possible that the presence of a centre of negative charge in the form of the 1,2,4-triazole may affect the reactive points in the phenanthroline moieties exploited to append the desired thiophene or pyridine groups. However, this triazole group is present in the metal complex $[Ru(pyrphen)_2(bpt)]^{2+}$ for which a sample has been synthesised by this method showing encouraging results. It is obvious that further synthetic research is needed in this area in order to ascertain the reasons for this apparent difference in reactivity. It may be possible that longer reaction time may be needed in order to ensure the conversion of the bis-phenanthroline starting materials $[Ru(phen)_2(bpt)]^{+}$, $[Ru(phen)_2(mepytr)]^{2+}$ and $[Ru(phen)_2(ppytr)]^{2+}$ to their related bis-phenanthroline-dione derivatives. It is also possible that the 5 and 6 positions on the phenanthroline ring (on which dione group is situated) may require stronger activation during the reaction, perhaps through incorporation of a stronger acid than the currently used glacial acetic acid as the reaction solvent.

The synthesis of the ligands thimphen and pyrphen on the metal complex via this method may be extended to premade dinuclear metal complexes, allowing for appending of surface active groups to known complexes rendering them novel. This is shown schematically below in Figure 7.1.

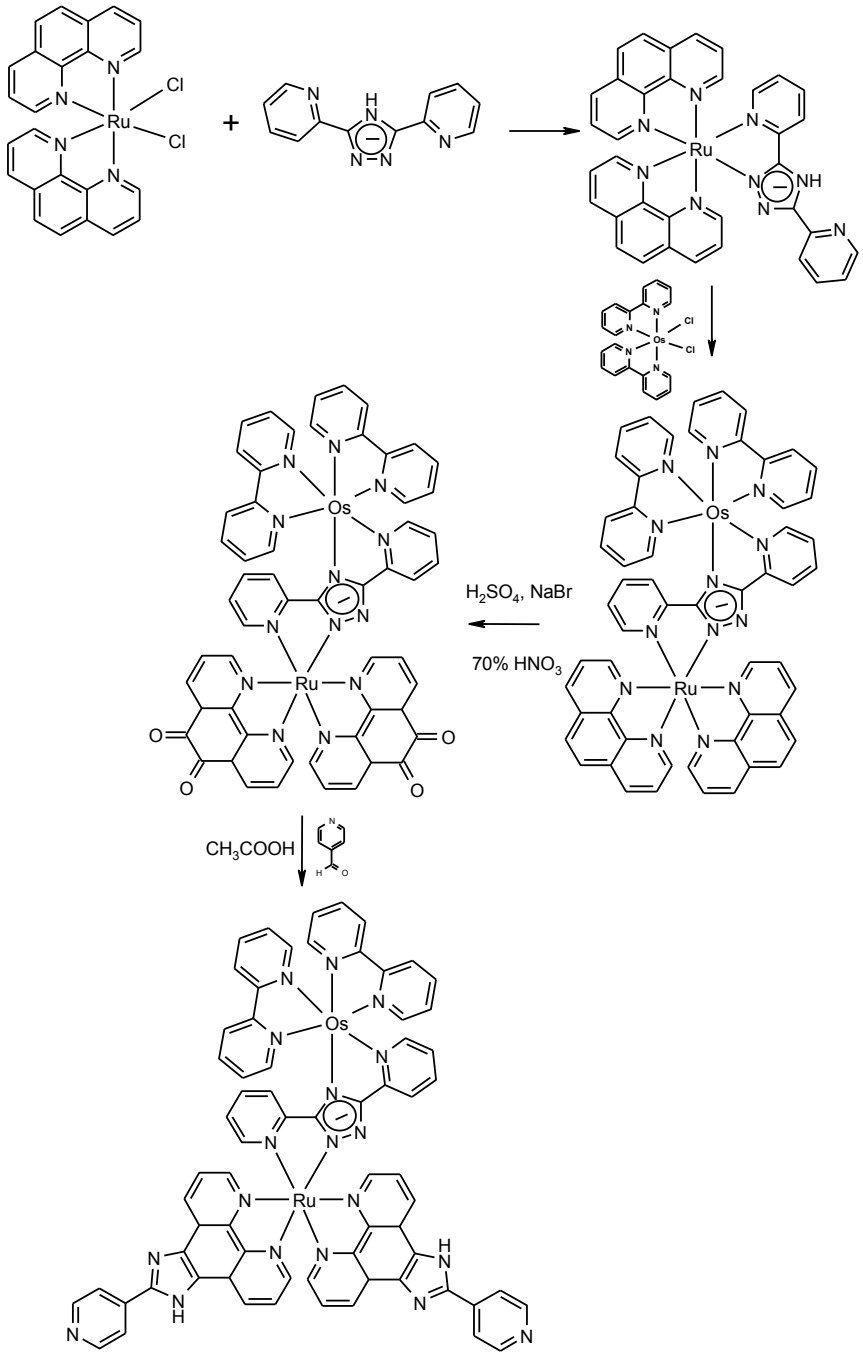

Figure 7.1: Synthesis of a dinuclear Ru-Os complex using hbpt[4] as a bridging ligand and containing 2 pyrphen ligands as a point of coordination to a surface

It has been inferred from the results obtained from Chapter 4 that synthesis of the ligand thimphen on the complex via the indirect synthetic method described is much

more difficult to achieve than synthesis of the ligand pyrphen by the same means. As a result an alternative, ***direct*** synthetic route is described in Chapter 5. The approach employed in Chapter 5 involved the synthesis of a ruthenium dichloride type starting material containing two novel 'thimphen' ligands. A number of different approaches were taken when attempting to synthesise this complex including the widely used LiCl reaction in DMF as used for $[Ru(bpy)_2Cl_2]$[5] as well as the method outlined in Chapter 6 for dichloride synthesis incorporating ascorbic acid. The most effective method was found to be reflux of $RuCl_3$ and thimphen in DMF with LiCl. However, a completely pure $[Ru(thimphen)_2Cl_2]$ sample was not obtained. The most encouraging sample was taken and used to attempt the synthesis of the mononuclear complex $[Ru(thimphen)_2(bpy)]^{2+}$ (*c.f.* Chapter 4) as well as a ruthenium-osmium linked dinuclear metal complex. Both reactions yielded incomplete though encouraging results. The mononuclear complex $[Ru(thimphen)_2(bpy)]^{2+}$ yielded a ^1H NMR spectrum similar to that obtained for the same compound synthesised by a different pathway in Chapter 4. The product obtained from the attempted reaction to form the dinuclear complex $[Ru(thimphen)_2(bpt)Os(bpy)_2]^{3+}$ displays a ^1H NMR spectrum very similar to that of the previously published dinuclear complex $[Ru(bpy)_2(bpt)Os(bpy)_2]^{3+}$. The HPLC, UV/vis and emission data obtained for this complex also indicate that a ruthenium-osmium heterodinuclear complex has been synthesised. However, in order to obtain coherent spectral data for this dinuclear species lengthy purification was required and full purification of the sample was not achieved. Therefore further research into a more effective method for synthesis and purification of the dichloride starting material $[Ru(thimphen)_2Cl_2]$ would most likely alleviate these problems resulting in an elegant method for the construction of dinuclear complexes containin two surface active ligands.

Chapters 4 and 5 have therefore shown that, at least in theory, both Direct and Indirect synthetic methods as described in this thesis may be used to construct homo- and heterodinuclear metal complexes containing surface active groups. Direct synthesis has been shown to be suitable only for ligands which may be synthesised in their pure form and are stable in the high temperature conditions necessary for complexation to a metal centre. In the case of ligands which cannot be synthesised as a pure free ligand or which cannot withstand the harsh conditions of ruthenium and osmium complexation reactions, indirect synthesis has revealed itself as a viable alternative to the ubiquitous *"Complexes as Metals/Complexes as ligands"* strategy.

Chapter 6 deals with a slightly different system, undertaken in collaboration with the University of Otago, NZ. The synthesis of the published compounds $[Ru(paen)Cl_2]$ and $[Ru(papn)Cl_2]$[6] is detailed as well as the novel metal complexes $[Ru(paen)(P0P)Cl](PF_6)$, $[Ru(paen)(P0P)_2](PF_6)_2$ and $[Ru(papn)(P0P)_2](PF_6)_2$. It was found that the previously published synthetic method for the preparation of the dichloride starting materials $[Ru(paen)Cl_2]$ and $[Ru(papn)Cl_2]$ yielded an impractically low amount of product. Therefore a new method including excess ascorbic acid as a reducing agent was developed, resulting in a higher, more readily employable yield. The synthesis of the metal complex $[Ru(papn)(P0P)_2](PF_6)_2$ was readily achieved, but the paen analogue of this complex was not so easily attained. Following a lengthy HPLC study of the reaction in progress, the desired product $[Ru(paen)(P0P)_2](PF_6)_2$ was successfully synthesised via a 120 hr reflux and purification by column chromatography with the intermediate type complex $[Ru(paen)(P0P)Cl](PF_6)$ being isolated also as a by product. Though these three complexes have been successfully synthesised using the methods outlined in this thesis, the yields obtained for each successful reaction described in Chapter 6 are extremely low. Therefore, further synthetic research is needed in this area to improve the efficiency of the reactions described. One such possibility is the option of using longer reaction times as the ligands used have exhibited thermal stability usually not exhibited for Schiff base type complexes[7, 8].

In conclusion, this thesis has provided a thorough, though not exhaustive comparison between two methods of preparation for ruthenium and osmium metal complexes: ***Direct*** and ***Indirect*** synthesis. Both methods have proved both applicable and useful when applied to suitable systems. However, both approaches are in need of further synthetic study: in the case of Direct synthesis a method by which a non-bpy type ligand my be used to construct a pure metal-dichloride type complex of formula $[M(L)_2Cl_2]$ where M is ruthenium or osmium and L is a bidentate polypyridyl type ligand. Also further synthetic study is needed for the synthesis of pure samples in higher yield of the compounds described in Chapter 6 by direct methods. This may be achieved by increasing the reaction time used, as the ligands paen and papn have exhibited good thermal stability during overnight reflux. Also more rigorous purification methods, such as semi-prep HPLC may yield better purified samples than the those obtained using the column chromatography methods detailed in Chapter 6.

In the case of Indirect synthesis, further research has been deemed necessary regarding the modification of phenanthroline containing molecules also containing a 1,2,4-triazole group. Through further study it may be established if this group affects the reactivity of the targeted phenanthroline group in the synthetic methods described in this thesis and if so, whether or not the targeted group may be activated during the imidazole formation reaction.

7.2 Bibliography

[1] E. Steck, A. Day, *J. Am. Chem. Soc.* 1943, **65**, 452

[2] V. Balzani, A, Juris, M.Venturi, *Chem. Rev.* 1996, **2**, 759

[3] Y. Halpin, *PhD Thesis*, Dublin City University, 2010

[4] R. Hage, PhD Thesis, Leiden University, 1991

[5] B. P. Sullivan, D. J. Salmon, T. Meyer, *Inorg. Chem.* **17**, (1978) 3334

[6] S. Pal, S. Pal; *Polyhedron*, 2003, **22**, 867

[7] M. Aydemira, F. Durapa, A. Baysala, N. Merica, A. Buldaga ,B. Gümgüma, S. Özkarb, L. T. Yıldırımc, *J. Mol. Cat. A*: Chemical 2010, **326**, 75

[8] C. M. Harris, E. D. MacKenzie, *J. Chem. Soc. A* 1969 746

Appendix A

Interpretation of ^{1}H NMR data not included in Chapter 4

Interpretation of ^{1}H NMR data for $[Ru(phen)_2(dmbpy)](PF_6)_2$

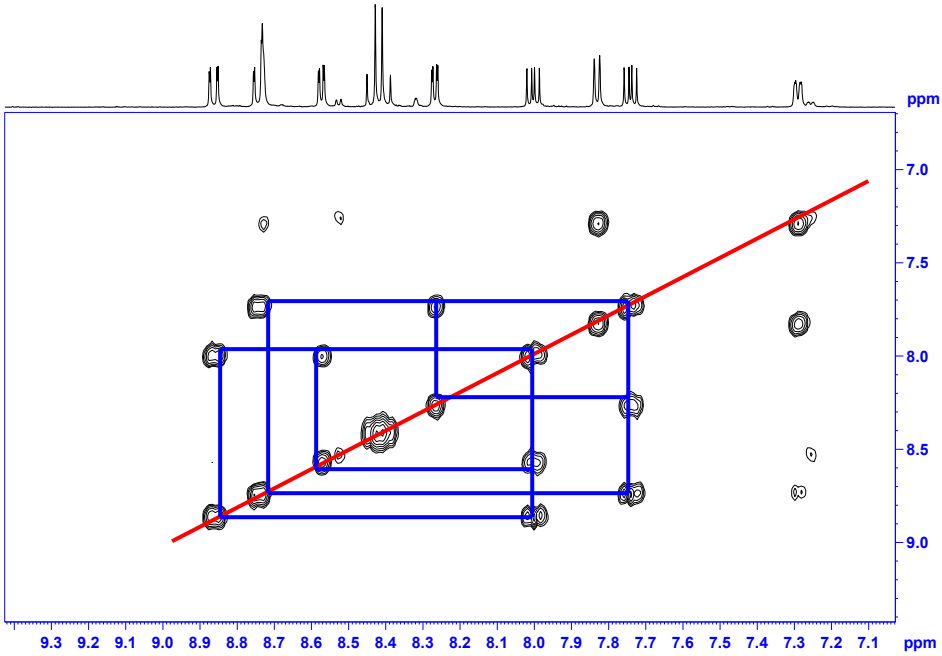

Figure 4.1: COSY spectrum of $[Ru(phen)_2(dmbpy)](PF_6)_2$ highlighting coupling phenanthroline (blue) as measured in d_6-acetone

As in the case of $[Ru(phen)_2(bpy)](PF_6)_2$, the simplest proton signals to identify are those relating to the dmbpy portion of the molecule. An intense singlet appears in the spectrum shown in Figure 4.1 (a) at 2.57 ppm relating to the six CH_{methyl} protons present in the molecule. These aliphatic type protons couple weakly with the multiplet present at 8.74 ppm, indicating that the singlet peak expected for H_{3b} is contained within this multiplet. This is confirmed by the further weak coupling observed between this signal and a broad doublet appearing at 7.29 ppm, corresponding to H_{5b}. This signal in turn couples strongly to the doublet visible at 7.83 ppm, which corresponds to H_{6b}.

The coupling phenanthroline protons, shown in Figure 4.1 (b) also follow the same pattern as for $[Ru(phen)_2(bpy)](PF_6)_2$ (as shown in Chapter 5). The triplet of lowest chemical shift (appearing here at 7.74 ppm) is attributed to H_{3p} on account of its triplet nature and upfield position, caused by the shielding effects described in

Chapter 4. This peak couples with a doublet at 8.27 ppm, attributable to H_{1p} (its upfield chemical shift value a direct result of the same shielding encountered by H_{3b}), as well as the multiplet present at 8.74 ppm, indicating that this multiplet also contains the signal representing H_{5p}.

The only remaining triplet in the spectrum, present at 8.00 ppm therefore represents H_{4p}. This triplet couples with a doublet present at 8.57 ppm corresponding to H_{2p} (its relatively upfield chemical shift value attributable to electronic shielding provided by the adjacent dmbpy ligand) as well as a final doublet present at 8.86 ppm, corresponding to H_{6p}. As before, H_{7p} and H_{8p} appear as a multiplet coupling only to itself at 8.45-8.39 ppm.

As in the case of $[Ru(phen)_2(bpy)](PF_6)_2$ the next complex synthesised was the bis-phenantrholine dione complex $[Ru(phendione)_2(dmbpy)](PF_6)_2$, the ^{1}H-NMR spectrum for which is shown below in Figure 4.2.

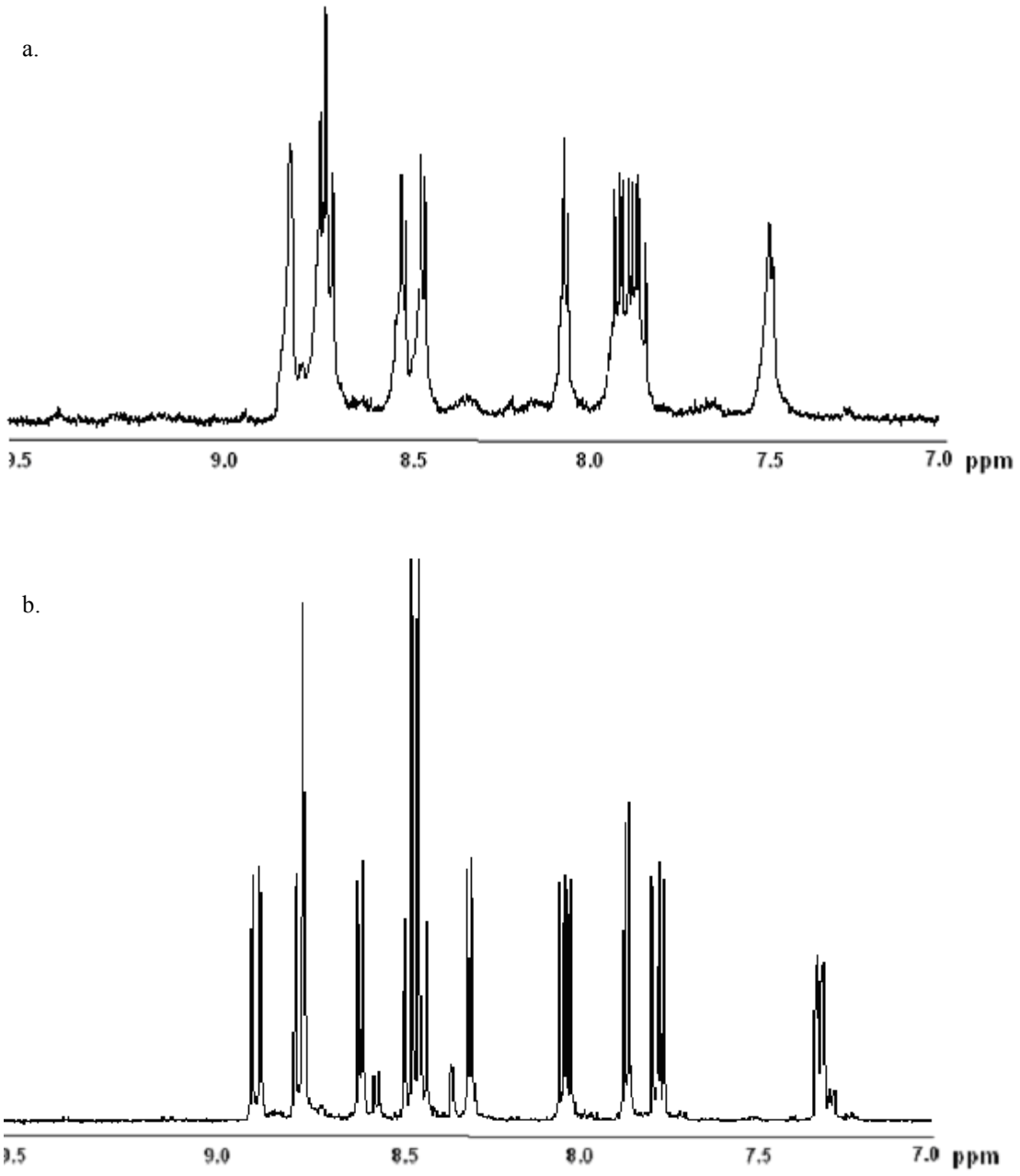

Figure 4.2: ^{1}H NMR spectrum for (a) [Ru(phendione)$_2$(dmbpy)](PF$_6$)$_2$ and (b) [Ru(phen)$_2$(dmbpy)](PF$_6$)$_2$ as measured in d$_6$-acetone

As for [Ru(phendione)$_2$(bpy)](PF$_6$)$_2$ the spectrum shown in Figure 4.2 (a) for [Ru(phendione)$_2$(dmbpy)](PF$_6$)$_2$ displays a conspicuous absence of the multiplet shown for [Ru(phen)$_2$(bpy)](PF$_6$)$_2$ (see Chapter 4) corresponding to H_{7p} and H_{8p} indicating that these protons have been replaced by the desired dione moiety. The remaining signals have shifted somewhat with respect to their original position in the

$[Ru(phendione)_2(dmbpy)](PF_6)_2$ spectrum shown in Figure 4.2 (b). This is most likely due to residual acid in the sample arising from the reaction conditions used. These signals may be accurately assigned by examining the COSY spectrum for the molecule, shown below in Figure 4.3.

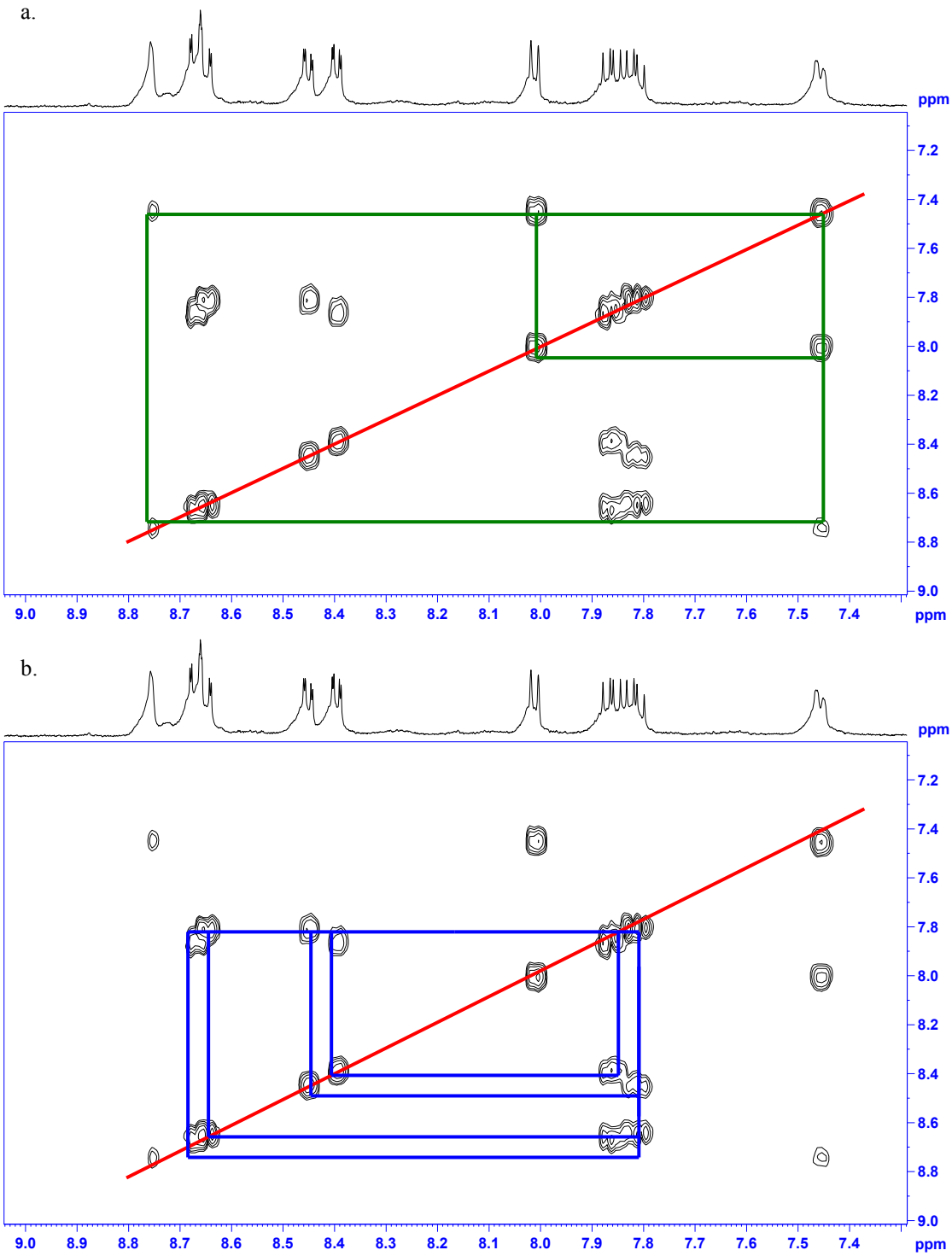

Figure 4.3: ^1H COSY spectrum for $[Ru(phendione)(dmbpy)](PF_6)_2$ as measured in d_6-acetone showing (a) coupling dmbpy protons and (b) coupling phenanthroline protons

The COSY spectrum for $[Ru(phendione)_2(dmbpy)](PF_6)_2$ shown in Figure 4.3 (a) highlighting the coupling dmbpy protons present in the molecule displays these protons as two doublets and a singlet identical to the corresponding signals shown for $[Ru(phen)_2(dmbpy)](PF_6)_2$. This implies that H_{5b} (present at 7.46 ppm) couples to H_{6b} (present at 8.01 ppm) as before and H_{3b} (8.88 ppm) remains a singlet due to its lack of adjacent protons. interacting with H_{3b} via long range coupling. The slight downfield shift of these protons with respect to their position in the spectrum shown $[Ru(phen)_2(dmbpy)](PF_6)_2$ is most likely due to residual acid present in the sample arising from the acidic conditions the reaction was carried out in.

Figure 4.3 (b) shows the COSY spectrum for $[Ru(phendione)_2(dmbpy)](PF_6)_2$ highlighting the coupling between the phenanthroline protons present in the molecule. The furthest upfield signal, a multiplet integrating for four protons, as in the parent complex $[Ru(phen)_2(dmbpy)](PF_6)_2$ may be termed H_{3p} and H_{4p}. This multiplet at 7.89-7.75 ppm couples with each of the remaining four unidentified signals present in the spectrum. As for $[Ru(phendione)_2(bpy)](PF_6)_2$ H_{1p} and H_{2p} may be assigned as the more downfield of these signals, two doublets: H_{1p} at 8.39 ppm, H_{2p} at 8.45 ppm. The one remaining signal, a multiplet at 8.76-8.66 ppm integrating for four protons therefore corresponds to H_{5p} and H_{6p}.

$[Ru(pyrphen)_2(dmbpy)](PF_6)_2$

The numbering scheme for the assignment of the protons present in this molecule is shown below in Figure 4.4.

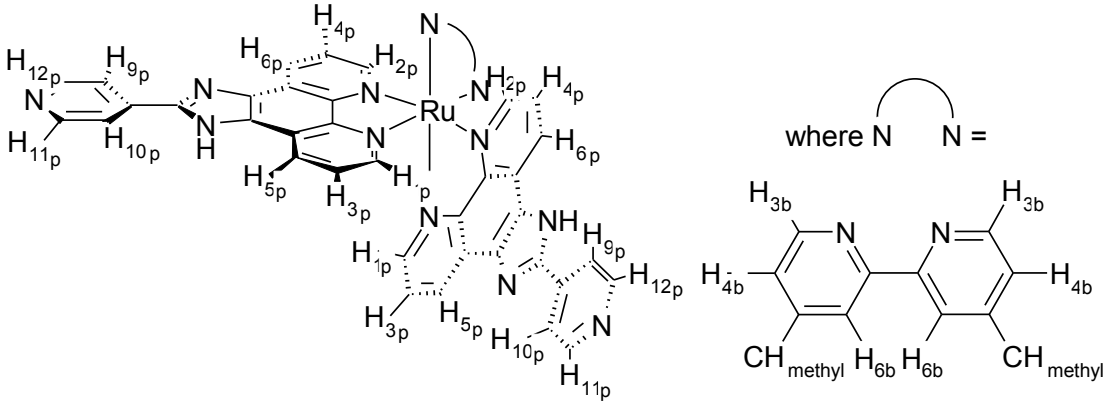

Figure 4.4: Numbering system for the assignment of protons in the ^1H NMR analysis of $[Ru(pyrphen)_2(dmbpy)](PF_6)_2$

The ^{1}H NMR spectra for the metal complexes $[Ru(pyrphen)_2(dmbpy)](PF_6)_2$ and $[Ru(pyrphen)_2(d_8\text{-}bpy)](PF_6)_2$ are shown below in Figure 4.5.

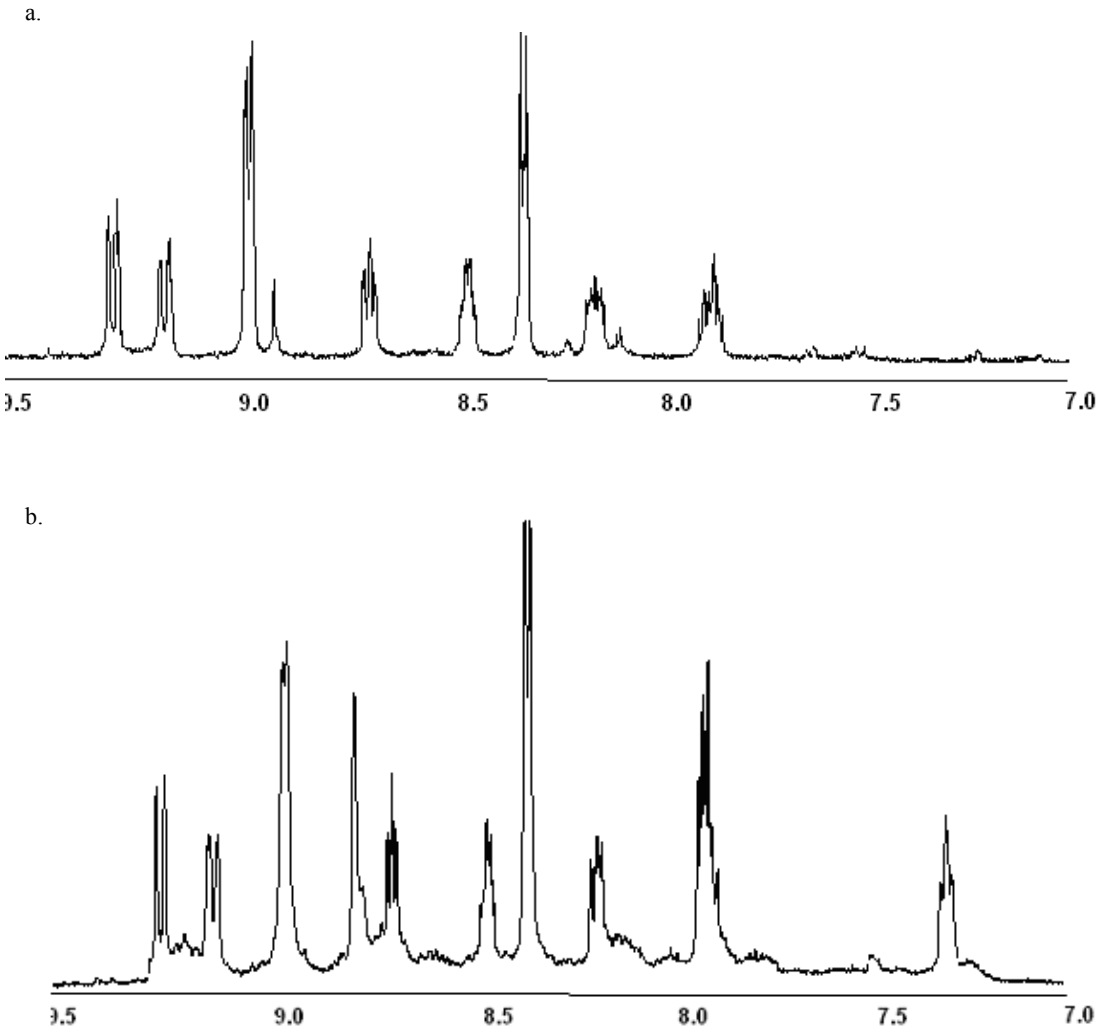

Figure 4.5: ^{1}H NMR spectra of (a) $[Ru(pyrphen)_2(d_8\text{-}bpy)](PF_6)_2$ and (b) $[Ru(pyrphen)_2(dmbpy)](PF_6)_2$ as measured in d_6-acetone

It can be seen from a comparison between the two above spectra that the peaks present in Figure 4.5 (b) at 7.30 ppm, 8.79 ppm as well as part of the multiplet present between 7.91-7.86 ppm. Are attributable to the bipyridyl protons present in the molecule as they are not present in the deuteriated-bipyridyl spectrum shown in Figure 4.5 (a). In order to assign these and the remaining signals in the spectrum shown in Figure 4.5 (b), the COSY spectrum for $[Ru(pyrphen)_2(dmbpy)](PF_6)_2$ is shown below in Figure 4.6.

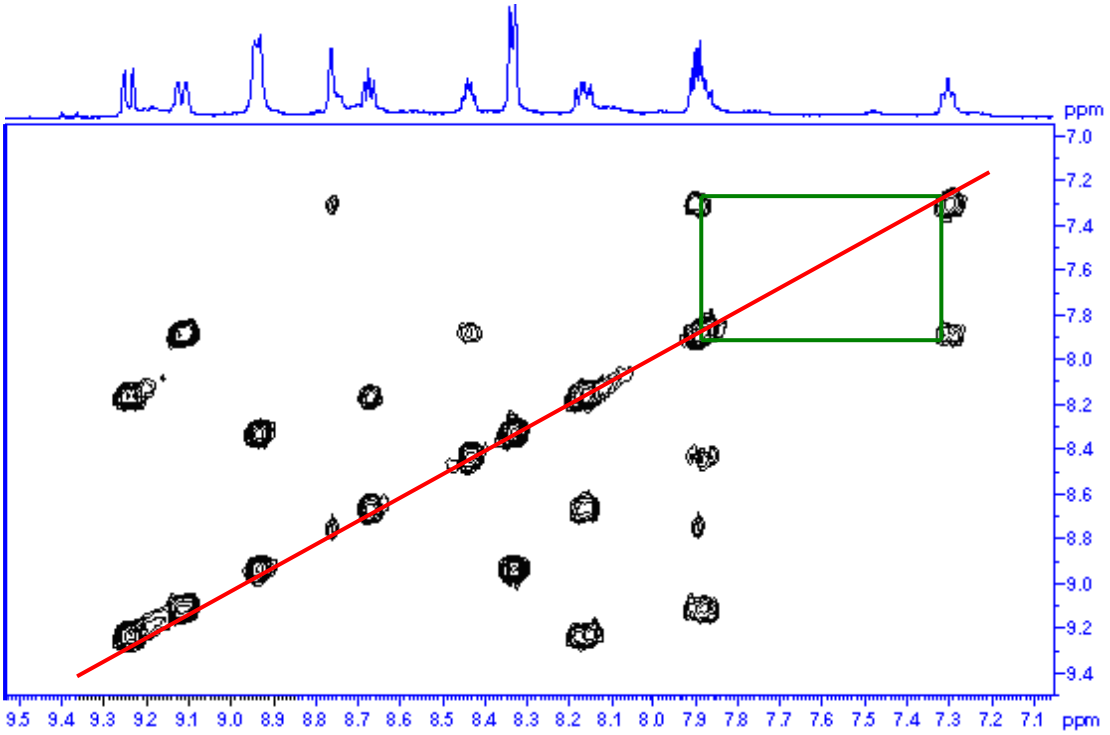

Figure 4.6: COSY spectrum for [Ru(pyrphen)$_2$(dmbpy)](PF$_6$)$_2$ as measured in d_6-acetone with coupling dmbpy protons highlighted

It can be seen from the COSY spectrum shown in Figure 4.6 that the dmbpy signals present in the molecule display a very similar coupling pattern to that observed for the parent complex [Ru(phen)$_2$(dmbpy)](PF$_6$)$_2$. The triplet present at 7.35 ppm couples to the multiplet between 7.99 ppm and 7.89 ppm. The more upfield of these signals corresponds to H_{5b} as in the case of [Ru(phen)$_2$(dmbpy)](PF$_6$)$_2$, and by virtue of the coupling evidence observed the signal corresponding to H_{6b} is contained in the multiplet between 7.99 ppm and 7.89 ppm. The one remaining bipyridyl signal present at 8.82 ppm therefore corresponds to H_{3b}. As for the parent complex [Ru(phen)$_2$(dmbpy)](PF$_6$)$_2$ the H_{3b} signal is singlet in character, coupling to no other peak in the spectrum by virtue of the position of H_{3b} in the [Ru(dmbpy)(pyrphen)$_2$](PF$_6$)$_2$ molecule. There are no protons directly adjacent to H_{3b} in the molecule, explaining why the peak signifying it is singlet in character, however, it is possible that long-range coupling occurs between H_{3b} and H_{5b}, accounting for the triplet nature of the peak corresponding to H_{5b}.

In order to assign the phenanthroline signals in the spectrum, the COSY spectrum for [Ru(pyrphen)$_2$(dmbpy)](PF$_6$)$_2$ is shown again below, this time highlighting the coupling pyrphen signals.

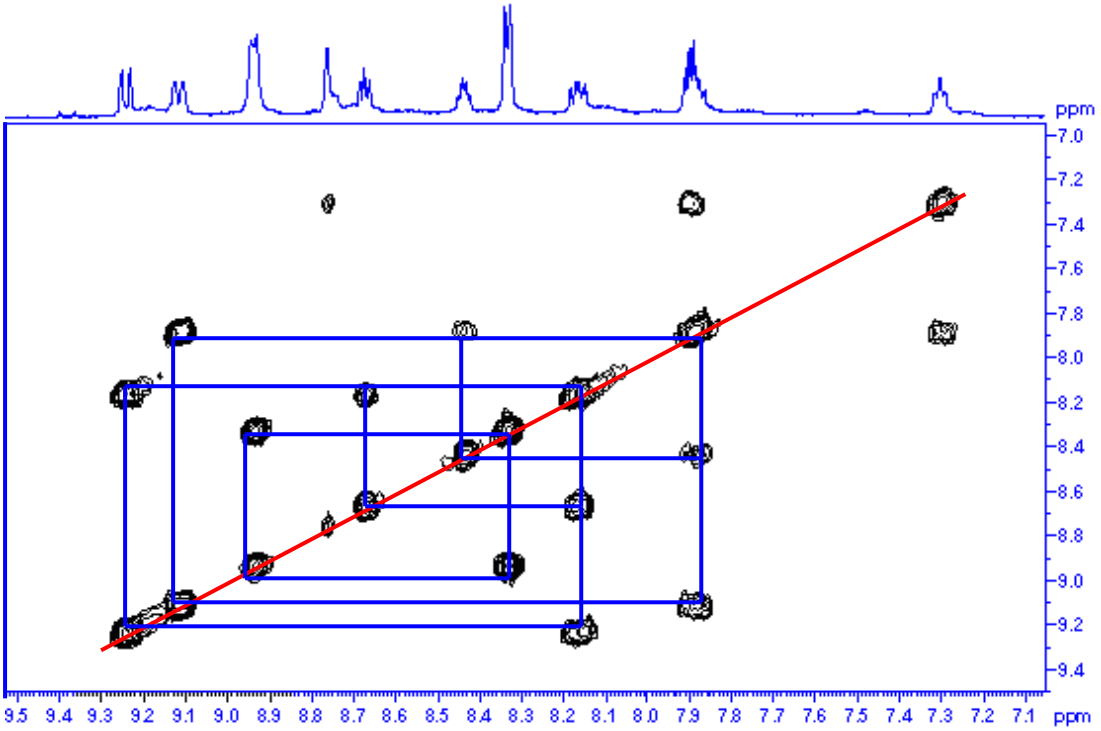

Figure 4.7: COSY spectrum for [Ru(pyrphen)$_2$(dmbpy)](PF$_6$)$_2$ as measured in d_6-acetone with coupling pyrphen protons highlighted

As for [Ru(pyrphen)$_2$(bpy)](PF$_6$)$_2$, two doublets dominate the spectrum shown in Figure 4.7, one at 8.33 ppm and one at 8.94 ppm. As before, these signals couple strongly with each other and to no other peak present in the spectrum, implying that these peaks relate to the pyridine protons H_{9p}, H_{10p}, H_{11p}, and H_{12p}. The further downfield of these signals, appearing at 8.94 ppm correspond to the pyridyl protons H_{12p} and H_{11p}. The downfield position of this peak with respect to the other pyridine peak present at 8.33 ppm (corresponding to H_{9p} and H_{10p}) is a result of the position of the protons H_{11p} and H_{12p} adjacent to the electronegative pyridine nitrogen atom.

As for [Ru(pyrphen)$_2$(bpy)](PF$_6$)$_2$ there are six distinct signals integrating for two protons apiece present in Figure 4.7 corresponding to the phenanthroline base of the two pyrphen ligands. Therefore there is an individual peak corresponding to each phenanthroline proton: H_{1p}, H_{2p}, H_{3p}, H_{4p}, H_{5p} and H_{6p}. These peaks follow an identical coupling pattern to that observed for [Ru(pyrphen)$_2$(bpy)](PF$_6$)$_2$. H_{3p} and H_{4p} are the only protons in the phenanthroline moiety situated adjacent to two chemically distinct CH groups and so shall be the only two signals to couple with two other peaks in the spectrum. These two such peaks appear in the spectrum shown in Figure 4.7 at 8.18-8.15 ppm and as part of the multiplet visible between 7.91 ppm and 7.86 ppm.

As before the further upfield of these signals is attributed to H_{3p}, for the electronic shielding reasons discussed previously.

The signal corresponding to H_{3p} contained within the multiplet between 7.91 ppm and 7.86 ppm couples to the multiplet present at 8.46-8.42 ppm as well as the doublet visible at 9.11 ppm. The further upfield of these signals is attributed to H_{1p} (it's upfield position a direct result of aromatic shielding) while the doublet appearing further downfield may be assigned as H_{5p}.

The peak corresponding to H_{4p} also couples with two distinct signals, a multiplet at 8.68 ppm and a doublet present at 9.23 ppm. As before the multiplet appearing further upfield at 8.68 ppm is attributable to H_{2p} while the further downfield signal present at 9.23 ppm corresponds to H_{6p}. The chemical shifts for the complexes $[Ru(phen)_2(dmbpy)](PF_6)_2$ and $[Ru(phendione)_2(dmbpy)](PF_6)_2$ are tabulated below in Table 4.1.

Proton	**Chemical shift δ (ppm) [Ru(phen)$_2$(dmbpy)](PF$_6$)$_2$**	**Chemical shift δ (ppm) [Ru(phendione)$_2$(dmbpy)](PF$_6$)$_2$**	**Chemical shift δ (ppm) [Ru(pyrphen)$_2$(dmbpy)](PF$_6$)$_2$**
H_{1p}	8.27 (d)	8.39 (d)	8.46-8.42 (m)
H_{2p}	8.57 (d)	8.49 (d)	8.67 (m)
H_{3p}	7.74 (dd)	7.89-7.75 (dd)	7.91-8.86 (m)
H_{4p}	8.00 (t)	7.89-7.75 (dd)	8.19-8.15 (m)
H_{5p}	8.74 (m)	8.76-8.66 (d)	9.11 (d)
H_{6p}	8.86 (dd)	8.76-8.66 (d)	9.23 (d)
H_{7p}	8.45-8.39 (m)	-	-
H_{8p}	8.45-8.39 (m)	-	-
H_{9p}	-	-	8.33 (d)
H_{10p}	-	-	8.33 (d)
H_{11p}	-	-	8.94 (d)
H_{12p}	-	-	8.94 (d)
H_{3b}	8.74 (m)	8.88 (s)	8.79 (s)
H_{5b}	7.29 (t)	7.46 (dd)	7.30 (t)
H_{6b}	7.83 (d)	8.01 (d)	7.91-7.86 (m)
CH_{methyl}	2.57 (s)	3.01 (s)	2.57 (s)

Table 4.1: Chemical shifts for the complexes [Ru(phen)$_2$(dmbpy)](PF$_6$)$_2$, [Ru(phendione)$_2$(dmbpy)](PF$_6$)$_2$ and [Ru(pyrphen)$_2$(dmbpy)](PF$_6$)$_2$

Appendix B: Refereed Publications

This paper is published as part of a *Dalton Transactions* themed issue on:

Supramolecular photochemistry

Guest Editors Michael D. Ward and Julia Weinstein
University of Sheffield, UK

Published in issue 20, 2009 of *Dalton Transactions*

Synthesis of asymmetric supramolecular compounds using a Ni(0) catalysed homo-coupling approach

Lynda Cassidy,[a] Sabine Horn,†[a] Laura Cleary,[a] Yvonne Halpin,[a] Wesley R. Browne[b] and Johannes G. Vos*[a]

Received 13th October 2008, Accepted 4th December 2008
First published as an Advance Article on the web 11th February 2009
DOI: 10.1039/b817896h

Spectroelectrochemical properties of homo- and heteroleptic ruthenium and osmium binuclear complexes: intercomponent communication as a function of energy differences between HOMO levels of bridge and metal centres†

Yvonne Halpin,[a] Laura Cleary,[a] Lynda Cassidy,[a] Sabine Horne,‡[a] Danilo Dini,[a] Wesley R. Browne[b] and Johannes G. Vos*[a]

Received 24th December 2008, Accepted 10th March 2009
First published as an Advance Article on the web 2nd April 2009
DOI: 10.1039/b823104d

